Università degli Studi di Ferrara

DOTTORATO DI RICERCA IN

"SCIENZE CHIMICHE"

CICLO XXXIII

COORDINATORE Prof. Cavazzini Alberto

Oxidative Potential of Atmospheric Particulate Matter: determination with acellular assays and relationship with samples chemical composition

Settore Scientifico Disciplinare CHIM/01

Dottoranda

Dott. Russo Mara

Tutore

Prof. Pietrogrande Maria Chiara

Anni 2018/2020

1. Introduction

1.1 Atmospheric Pollution

According to the World Health Organization, air pollution is the contamination of the indoor or outdoor environment by any chemical, physical or biological agent that modifies the natural characteristics of the atmosphere (World Health Organization, 2016). Air pollution is a problem for all of us, considering that the average adult breathes over 11.5 m^3 of air per day. Numerous studies in the past decades have observed associations between elevated air pollution levels and various health outcomes, including mortality, hospitalization for respiratory and cardiovascular diseases, aggravation of asthma attacks, and adverse lung functions. (Valavanidis et al., 2008).

WHO reports that in 2012, 7 million premature annual deaths are linked to air pollution, which is one eighth of the total global deaths.

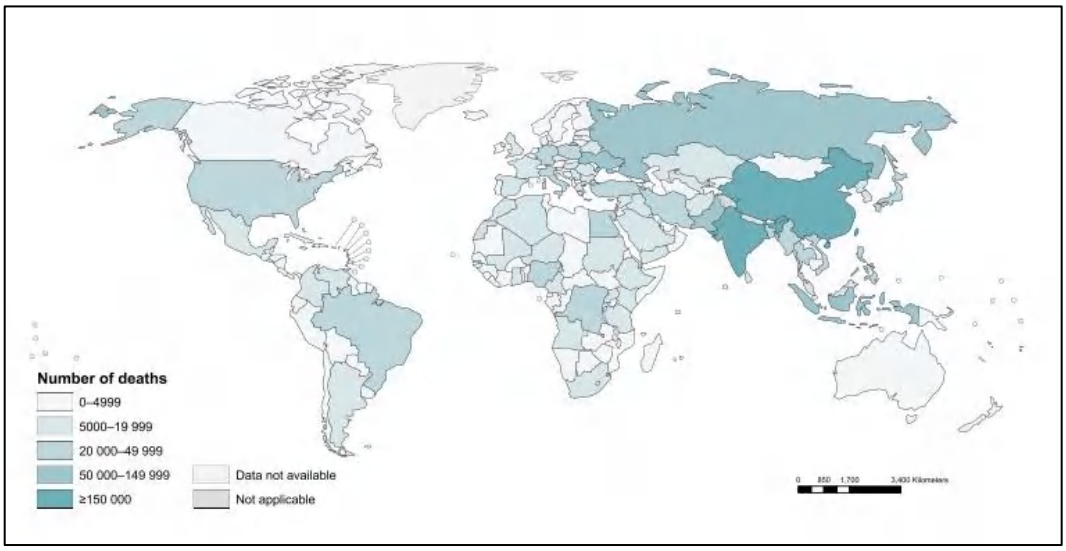

Figure 1. Deaths attributable to Ambient Air Pollution in 2012, by country (World Health Organization, 2016).

This finding more than doubles previous estimates and confirms that air pollution is now the world's largest single environmental health risk (World Health Organization, 2014).

1.1.1 Levels of air pollution

Three types of air pollution are distinguished based on the scale of study: the local, the regional, and the global (Akimoto, 2003)(Craig et al., 2008).

Local air pollution is encountered in the immediate vicinity of emission sources. This form of pollution is mainly due to human activities and occurs close to the emission sources such

as domestic heating, industrial waste, gases associated with transport, waste incineration, etc. The emissions of these sources reach a distance less than few kilometres. In this type of pollution, the most characteristic pollutants are: suspended particulate matter (PM), sulphur dioxide (SO_2), carbon monoxide (CO), nitrogen oxides (NOx), volatile organic compounds (VOCs), polycyclic aromatic hydrocarbons compounds (PAHs), elemental carbon or carbon soot, and metals.

The regional pollution covers larger territories; it affects places distant few kilometres to hundred kilometres from the emission source of pollutants. This regional pollution results in the physico-chemical transformation of primary pollutants to secondary pollutants. The ozone (O_3) is one of these secondary pollutants that are formed by the presence of NOx and VOCs.

The global scale is related to phenomena that may affect the balance of the Earth's ecosystem as a whole. It contributes to climate change and the global warming caused by the accumulation of greenhouse gas emissions (particularly carbon dioxide). It affects the stratospheric ozone layer due to the carbon dioxide (CO_2), methane, nitrous oxide (N_2O), and halogenated gases from domestic activities. This reduction of the ozone layer can cause damage in the human body such as skin cancer.

1.1.2 Main air components

Air pollution is dominated by a few major components whose levels fairly reflect the overall status of air pollution and the various emission sources. These factors are considered as air pollutants because they do not naturally exist in the air or they are present at very low concentration, and they are harmful to the health and the environment.

Air pollutants can be encountered in two forms: gases and particles. Their composition includes CO, NOx, SO_2, O_3, heavy metals, PAHs, VOCs, polychlorinated dibenzo-para-dioxins (PCDDs), polychlorinated dibenzo-furans (PCDFs), polychlorinated biphenyls (PCBs), and PM. Once pollutants are released into the air, they can interact with each other and with the environment in complex ways depending on temperature, humidity, photochemistry, and other environmental conditions.

Pollutants can be categorized into: i) primary pollutants and ii) secondary pollutants which are produced from the interaction of primary pollutants. The presence of all these pollutants modifies the physicochemical characteristics of the atmosphere.

In the atmosphere, all gaseous or particulate components will be diluted, transported and processed, depending on weather conditions (De Sario et al., 2013).

Many atmospheric factors influence the way how air pollution is dispersed, including wind direction and wind speed, type of terrain and heating effects. Lack of rainfall and wind are adverse weather conditions preventing the dispersion of primary pollutants and can lead to episodes of intense pollution often summarized under the term “high pollution”. Dispersion and transport of air pollutants are carried out in a slice of altitude ranging between 1 and 2 km. The latter is indeed the most disturbed layer, constantly agitated by turbulent motions both horizontal and vertical. In this layer, pollutants may also undergo chemical transformations more or less complex. Some pollutants have a lifetime which is high enough to promote their displacement in the layers of a higher altitude even in the stratosphere (air layer between 8 and 40 km in altitude).

1.2 Atmospheric Particles

Among the air pollutant, particulate matter (PM) or atmospheric aerosol is one of the most studied and controlled parameters in the last years, due to the increasing awareness of public opinion and institutions on environmental problems.

Airborne PM consists of a heterogeneous mixture of solid and liquid particles suspended in air that varies continuously in size and chemical composition in space and time.

According to their forming process, airborne particles can be classified as primary or secondary aerosols. Primary aerosols are emitted directly from the emission sources into the atmosphere in particulate form. Whereas secondary aerosols refer to particles generated in the atmosphere, formed by the conversion mode gas-particle due to the condensation of natural and anthropogenic vapours, or generated by the evolution of a primary particle (Kim et al., 2015).

Due to their irregular shapes, particle size is described using the equivalent aerodynamic diameter: it is defined as the diameter of a sphere of density unit that has aerodynamic behaviour identical to the one of the particle in question.

Using this classification, atmospheric aerosol can be divided in three main classes: ultrafine particles ($D_{ae} < 0.1$ μm), fine particles ($0.1 < D_{ae} < 2.5$μm) and coarse particles ($D_{ae} > 2.5$μm) (Brauer et al., 2001)(World Health Organization, 2013).

The sources of fine particles and coarse particles are different and include a wide range of natural phenomena and human activities.

Coarse particles are mechanically produced by the break-up of larger solid particles. These can include wind-blown dust from agricultural processes, uncovered soil, unpaved roads or

mining operations, near coasts and evaporation of sea spray; it can also include pollen grains, mould spores, and plant and insect parts.

Because of their relatively large size, coarse particles settle out of the atmosphere in a reasonably short time by sedimentation, except on windy days, when fallout is balanced by re-entrainment.

Fine particles consist of particles generated by industrial and urban activity but also biogenic particles. This class of particles can be divided into an accumulation mode ($0.1 < D_{ae} < 2.5$ μm) and a nucleation mode ($D_{ae} < 0.1$ μm) (Aitken mode).

Particles with diameters between 0.1 and 2.5 μm are formed due to the coagulation of particles smaller than 0.1 μm and from the condensation of vapours onto existing particles. They can also be introduced directly into the atmosphere, mainly through the incomplete combustion of wood, oil, coal, gasoline, and other fuels.

The accumulation mode is named so because the particle removal mechanisms are less efficient in this regime, particles accumulate there until they are ultimately lost through rain or other forms of wet deposition.

The ultrafine particles are generated directly by combustion and photochemical activity. These particles act as nuclei for the condensation of low vapour pressure gaseous species, causing them to grow into the accumulation range.

The lifetime of smaller size particles ($PM_{2.5}$ and $PM_{0.1}$) can range from days to weeks, while bigger particles (PM_{10}) have a lifetime of hours to days (Pope III et al., 2006) (Valavanidis et al., 2008)(Gugamsetty et al., 2012).

Most of the suspended PM consists of 90% to 95% of coarse particles, whereas smaller particles are only 1% to 8% of the total mass. However, ultrafine and fine particles are very high in numbers, have greater total surface area than the larger particles, and because of their porous surface, can adsorb and retain toxic substances (Valavanidis et al., 2008)(Meng et al., 2013). High concentrations of PM can cause both health and environmental problems.

Both epidemiological and clinical studies have demonstrated strong links between atmospheric aerosol and adverse health effects, including premature deaths and respiratory and cardiovascular diseases (Schwartz et al., 2002)(Perrone, Gualtieri, et al., 2013).

In fact, PM can easily penetrate in the respiratory system and ultrafine particles can reach the alveolus and, from here, the circulatory system.

Epidemiological studies highlight that both physical (surface area, dimension) and chemical (absorbed substances) characteristics of inhaled particles are involved in toxic and carcinogenic effects concerning especially the respiratory tract (Harrison et al., 2000).

The mechanisms through which PM elicits toxic effects are not clearly understood but some transition metals, polycyclic aromatic hydrocarbons (PAHs) and oxoPAHs seem to be the main substances responsible for health problems (Kelly, 2003)(Janssen et al., 2014).
Regarding the environment, PM has other adverse impacts. Fine particles are the main cause of haze, which reduces visibility in urban areas. Due to the influence of long-range transport, haze can also affect otherwise pristine areas such as national parks and wilderness.
When deposited on the surface, PM can change the acidity and the nutrient balance in soil and surface waters, damage vegetation and affect the diversity of ecosystems.
Particle pollution can also cause aesthetic damage to buildings and culturally important objects, and it contributes to climate change by altering the radiation balance of the Earth's atmosphere (Olaguer, 2017).

1.2.1 Emission sources

The origin of airborne particulate matter can be divided into two broad categories: primary and secondary.
Primary PM sources are derived from both human (anthropogenic) and natural (non-anthropogenic or biogenic) activities.
Main natural sources are soil and rock debris (terrestrial dust), volcanic eruption, sea spray, biomass burning, forest fires, biological sources (pollen, bacteria, fungal spores, etc) and reactions between natural gaseous emissions.
Anthropogenic primary emissions of particles result mainly from the transportation sector (cars, trains, ships, and aircraft), industrial waste (metallurgy, foundries, refineries, and mining), petroleum products (housing, industrial, commercial), incineration sites and agricultural activities. Road transport contributes to particulate emissions not only through the exhaust gas but also by the wear of tires and brakes, as well as the resuspension of dust covering the roads (Srimuruganandam et al., 2012).
The particles emitted from these primary sources may undergo photochemical processing in the presence of various atmospheric oxidants (such as ozone, radical OH and NO_3) to yield secondary particles.
Global natural emissions of PM account for about 90% of the PM mass emitted yearly in the atmosphere, whereas anthropogenic PM accounts for the remaining 10%. At the local level, given the presence of many emission sources, anthropogenic sources are often actually more important than natural ones; this is particularly the case in urban areas and heavily industrialized sites.

The origin determines the chemical composition of aerosols, while the production mechanisms are responsible for their size and shape characteristics.

1.3 PM composition

There is a great scientific interest in the chemical composition of atmospheric particulate matter, which may vary largely depending on the sources of particles, the season of the year, the prevailing weather conditions and the chance for dispersion (Terzi et al., 2010)(Lodovici et al., 2011).

Atmospheric aerosols are very complex mixtures consisting of various organic and inorganic compounds such as ions, organic carbon and elemental carbon, trace elements, polycyclic aromatic hydrocarbon, n-alkanes, dicarboxylic acids, water-soluble compounds, etc. (Alves, 2008)(Cheung et al., 2011).

Figure 2. PM composition in urban site (Scotto et al., 2018).

1.3.1 Inorganic Components

1.3.1.1 Inorganic Ions

The main secondary inorganic aerosols are sulphate (SO_4^{2-}), nitrate (NO_3^-) and ammonium (NH_4^+) which are formed from the gas-phase precursors SO_2, NO_x and NH_3.

Sulphate derives predominantly from sulphur dioxide oxidation in the atmosphere and follows three different pathways:

- Oxidation of SO_2 by the hydroxyl radical in gas phase;
- Dissolution of SO_2 in cloud, fog and rainwater followed by aqueous-phase oxidation;

- Oxidation of SO_2 in reactions in the water of the aerosol particles themselves (QUARG, 1996).

Nitrates are formed by the oxidation of NO and NO_2 (NO_x) both in daytime (reaction with OH) and during the night (reaction with ozone and water) (Song et al., 2011).

Nitric acid is continuously transferred between the gas and the condensed phases (condensation and evaporation) in the atmosphere.

Sulfuric and nitric acids formed in the atmosphere, are progressively neutralised by atmospheric ammonia forming ammonium salts. The formation of these salts is favoured by low temperatures and high relative humidity (Harrison et al., 2000).

1.3.1.2 Metal Ions

Besides ammonium, sulphate and nitrate, various other water-soluble inorganic ions are also present in atmospheric aerosols.

Although these ions are often only responsible for a minor fraction of the PM mass, these inorganic species are important for the aerosol mass closure balance and as tracers for source apportionment (Terzi et al., 2010)(Voutsa et al., 2014).

Sea spray is a major source of Cl^-, Na^+ and Mg^{2+}, and Ca^{2+} as contribution from marine aerosols. In continental aerosols, Ca^{2+} and coarse K^+ have often important contributions from mineral dust disposal. Fine K^+ is a good indicator for biomass burning and mineral incinerators as its strongly enriched in biomass smoke.

1.3.1.3 Trace Elements

Trace elements, introduced into the atmosphere from various natural and anthropogenic sources, are adsorbed or condensed on the surface of the particles and may play an important role in the toxicity of the aerosol.

The trace metals of natural origin have a concentration that varies greatly over time because events that spread them are usually sporadic and brief.

These elements are related to the geological composition of the Earth's crust and their re-suspension in the air is in agreement with chemical, physical, biological and meteorological factors, such as resuspension of soil particles by the action of wind, volcanic emissions, sea spray and forest fires. The major trace elements classified as natural are: Na, Mg, K, Ca, Si, Al, Cl, Fe, Ti (Wang et al., 2006).

The concentration of man-made elements, on the other hand, is more consistent over time, since it is based on continuous operations throughout the year.

The anthropogenic sources result mainly from industrial waste (metallurgy, foundries, refineries, and mining), transportation sector (cars, trains, ships, and aircraft), petroleum products (housing, industrial, commercial), incineration sites and agricultural activities.

Industries are responsible for the issuance of a vast majority of heavy metals. However, the nature of the metals emitted depends on the type of industry, for example, arsenic (As) is derived from the raw materials used in the production of certain glasses; cadmium (Cd) is issued by the sectors of steel, non-ferrous metallurgy and production of ceramics; chromium (Cr) is mainly due to the production of ferrous metals, in particular, steel mill and foundry; mercury (Hg) is mainly produced by the chemical industry, by ferrous metallurgy, and non-metallic minerals and materials construction; nickel (Ni) of industrial origin is associated with steel plants; selenium (Se) is emitted by glass production and construction materials; lead (Pb) and zinc (Zn) mainly comes from the ferrous metallurgy.

Heavy metals can have different sources other than the industries, also for example Pb, Cu, and Zn are related to the abrasion of the mobile part of motor vehicles (brakes, tires …). Tire rubber is rich in Zn, Cu, Pb, Mn, Co, Ni and Cd as well as antimony (Sb) which is identified as coming almost exclusively from the excessive use of the vehicle brakes.

The main sources of nickel (Ni) and vanadium (V) are the burning of fossil fuels and oils. Lead, used to be added to petrol, was the source of high levels of lead in the air of major cities. As a result of EPA's regulatory efforts to remove lead from on-road motor vehicle gasoline, emissions from the transportation sector has dramatically declined and levels of emissions to the air today are mainly originated from ore and metals processing and piston-engine aircraft operating on leaded aviation gasoline (Calvo et al., 2013)(Hjortenkrans et al., 2006)(Lee et al., 2011).

From various epidemiological studies, high concentration and/or long exposure of metals may cause harmful effects on human health (Singh et al., 2011)(Di Vaio et al., 2018) because they tend to bioaccumulate in the human body.

Bioaccumulation means an increase in the concentration of a chemical in a biological organism over time, compared to the chemical concentration in the environment. Compounds accumulate in the organisms any time they are taken in and stored faster than they are broken down (metabolized) or excreted (Kampa et al., 2008)(Ali et al., 2019).

1.3.2 Organic Components

Carbonaceous compounds are an important fraction of atmospheric aerosols, contributing annually 20-45% of $PM_{2.5}$ and 20-35% of PM_{10} (Putaud et al., 2010)(Yttri et al., 2007).

In European urban areas, carbonaceous compounds account for 30-50% to $PM_{2.5}$ (Putaud et al., 2004). In recent years, scientists all over the world have paid much attention to carbonaceous particulate matter because it has a great influence on the global radiation budget, cloud microphysics, global climate change (Roeckner et al., 2006) and human health (Toro Araya et al., 2014).

The carbonaceous aerosol is broadly classified into two main fractions: elemental carbon (EC) and organic carbon (OC) (Pietrogrande et al., 2016).

EC is essentially a primary pollutant emitted during incomplete combustion of fossil and biomass carbonaceous fuels.

In urban areas, diesel emissions are one of the main sources of black carbon which is often used as an indicator of urban pollution (Fermo et al., 2005); furthermore, its temporal pattern could be related to traffic intensity. (Bautista VII et al., 2014).

OC has both primary and secondary origin. Primary OC is mainly formed during combustion processes such as unleaded gasoline combustion in urban areas or biomass and field agricultural burning (Cabada et al., 2002). It is also directly emitted as plant spores, pollens and soil organic matter.

Secondary OC can originate from different processes such as gas to particle conversion of low vapour pressure volatile organic compounds, condensation and physical and chemical adsorption (Fermo et al., 2005)(Pio et al., 2011).

OC includes thousands of organic compounds (such as aliphatic, aromatic compounds, carboxylic acids and carboxylic compounds with polar substituents, etc.) with widely varying chemical and physical properties (Jedynska et al., 2014).

The quantification of the contribution of primary and secondary organic carbon is quite difficult through direct chemical analysis since OC is a complex mixture of many compounds. Several indirect methods have been used to estimate secondary organic carbon. Among them, EC tracer method is a widely accepted technique where EC is used as a tracer of primary organic carbon (POC) (Yin et al., 2008).

1.3.2.1 Polycyclic Aromatic Hydrocarbons (PAHs)

Among the organic compounds, the polycyclic aromatic hydrocarbons (PAHs), are ubiquitous organic pollutants (Fang et al., 2002) of relevant health concern, as they were the first atmospheric pollutants to have been identified as suspected carcinogen.

Although PAHs represent a small part of the particulate matter, they are widely distributed in the atmosphere.

They are produced during incomplete combustion and pyrolysis of organic substances and can be emitted from human activities such as industry, vehicles emissions, incineration of waste and wood burning, domestic heating, oil refining, asphalt production, agricultural burning of biomass, shipping and flying (Abbas et al., 2018).

PAHs can be transported over long distances before deposition through atmospheric precipitation onto soils, vegetation, or water.

Polycyclic aromatic hydrocarbons are complex organic chemicals, consisting of two or more fused benzene rings containing only hydrogen and carbon. The best known PAH is benzo[a]pyrene (B[a]P), which contains 5 rings (Ravindra et al., 2008a).

Because of their low vapour pressure, some PAHs are present at ambient temperature in the air, both as gas and associated with particles. The lighter PAHs, such as phenanthrene, are found almost exclusively in the gas phase whereas the heavier PAHs, such as B[a]P, are almost totally adsorbed onto particles (Masiol et al., 2012).

As molecular weight increases, the carcinogenicity of PAHs also increases, and acute toxicity decreases (Ravindra et al., 2008b).

Many hundreds of PAHs exist in the environment, 16 of them are listed as priority pollutants by the US Environmental Protection Agency (USEPA) and of these, some are categorized as human carcinogens (class 1) and probable (class 2A) or possible human carcinogens (class 2B) by the International Agency for Research on Cancer (IARC, 2012).

In the directive 2004/107/EC (Fourth Daughter Directive), the EU has set a target value for polycyclic aromatic hydrocarbons for the protection of human health (Sosa et al., 2017).

The target is defined in terms of concentration of benzo[a]pyrene which is used generally as a marker substance for PAHs: the B[a]P annual mean value may not exceed 1 nanogram per cubic meter (ng/m^3)(Belis et al., 2011).

In order to exert their carcinogenic potential, PAHs require metabolic activation (Valavanidis et al., 2008). The most generally accepted mechanism for activation of PAHs involves the formation of diol-epoxides that can interact with tissue nucleophiles, giving rise to the alkylation of DNA. (Mechanism detailed in paragraph 1.5.2.3)

Over the last years, attention has been redirected also to PAH derivatives formed through atmospheric reactions with oxidative species such as ozone, hydroxyl and nitrate radicals as well as UV-induced photo-reactions (Vione et al., 2006). These PAHs oxidation products are typically found in the intermediate polarity PM fractions and include a wide range of compounds that can be classified in nitro-PAHs and oxygenated PAHs (Walgraeve et al., 2010).

Some of these derivatives are more toxic, posing a greater threat to human health than some PAHs, because of their direct-acting mutagenicity and carcinogenicity (Idowu et al., 2019), and thus they could be significant contributors to the high toxicity of particles at extremely low concentrations (Alves et al., 2017).

1.3.2.3 Oxy-PAHs

Oxy-PAHs are semivolatile compounds with high molecular weights, low vapour pressures and might be as abundant and persistent in the environment as their parent PAHs (Lundstedt et al., 2007).

In contrast to PAHs which are emitted directly from combustion processes, the sources of oxygenated PAHs emission in the atmosphere can be both by direct introduction (combustion processes) and by tropospheric conversion of PAHs (Walgraeve et al., 2010).

Besides direct formation, oxygenated PAHs can be formed from PAHs via photochemical reactions and reactions with hydroxyl radicals, nitrate radicals and ozone. Given the partitioning of PAHs between the gas phase and PM, transformation processes can take place in both phases. Reactions involving hydroxyl radicals (during the day) and nitrate radicals (during the night) are considered to play a major role in gas phase reactions whereas ozone and photolysis are expected to play only a secondary role (Vione et al., 2004)(María Del Rosario Sienra, 2006).

Toxicological studies showed that OPAHs might be more potently mutagenic or carcinogenic than the parent PAHs.

Some oxy-PAHs, such as the quinones, may be converted to electrophilic intermediates that may form adducts with essential macromolecules such as proteins and DNA, causing oxidative damage (Chung et al., 2006)(Wang et al., 2016).

This may lead to genotoxic effects through DNA adduct formation and possibly also cytotoxic effects via the depletion of reduced glutathione.

They can undergo enzymatic and non-enzymatic redox cycling with their corresponding semiquinone radical, leading to the formation of ROS, including superoxide, hydrogen

peroxide and the hydroxyl radical. Production of ROS can cause severe oxidative stress within cells through the formation of oxidized cellular macromolecules, including lipids, proteins and DNA (Benigni et al., 2011)(Idowu et al., 2019).

Furthermore, reactive oxygen species can activate several signalling pathways and cellular events that may be involved in or be responsible for several of the toxic effects associated with oxy-PAHs.

The most abundant oxy-PAHs found in ambient air are 9-fluorenone, 9,10 anthraquinone, benzanthrone and benz[a]anthracene-7,12-dione (Shen et al., 2013)(Viteri et al., 2019).

1.4 General regulation of air pollution

Composition, origin and abatement of atmospheric aerosol are topics of a large number of studies in order to extend the knowledge about this environmental matrix and to limit the problems linked to it.

In light of these results, the legal limit for PM_{10}, $PM_{2.5}$ and some chemical species in PM_{10} fraction have been set by Directive 2008/50/CE of the European Parliament and the Council (Table 1), the most recent directive regarding air pollution.

	Average Period	**Value**	**From**	**Comments**
PM_{10} limit value	One day	50 μg/m^3	From 2010	not to be exceeded more than 35 times a calendar year
PM_{10} limit value	Calendar year	40 μg/m^3	From 2010	
$PM_{2.5}$ limit value	Calendar year	25μg/m^3	From 2015	
Lead	Calendar year	0,5 ng/m^3	2010	In PM_{10} fraction
Arsenic	Calendar year	6 ng/m^3	2013	In PM_{10} fraction
Cadmium	Calendar year	5 ng/m^3	2013	In PM_{10} fraction
Nickel	Calendar year	20 ng/m^3	2013	In PM_{10} fraction
Benzo(a)pyrene	Calendar year	1 ng/m^3	2013	In PM_{10} fraction

Table 1. Directive 2008/50/CE legal limit for some pollutants.

To notice that these limits are higher than the guideline values suggested by World Health Organization (WHO) to reduce cardiopulmonary and lung cancer mortality (20 and 10 μg/m^3 annual average for PM_{10} and $PM_{2.5}$ respectively and 50 and 25 μg/m^3 daily average for PM_{10} and $PM_{2.5}$ respectively).

1.5 Atmospheric particles and their impact on health

1.5.1 General health impacts of air pollution

Observational epidemiology, controlled human exposures to pollutants, animal toxicology and in vitro mechanistic studies can be performed to evaluate or explain the impact on health of air particles.

Each of these approaches has its strengths and weaknesses. Epidemiology is valuable because it generally deals with the full spectrum of susceptibility in human populations. The results obtained in epidemiological studies are relevant for morbidity criteria such as hospitalizations, medical visits, medication use and symptoms. These studies provide the basis for experimental researches.

Most evidence linking the various human health effects to ambient levels of air pollution comes from the fields of epidemiology by short-term studies, which relate day-to-day variations in air pollution and health, and long-term studies, which have followed cohorts of exposed individuals over time (Brunekreef et al., 2002).

Research into the biological mechanisms, through which some air pollutants exert their effects on health, has focused mainly on inflammatory and oxidative stress-related processes that could promote chronic diseases.

Data showed that adverse health effects are dependent on both exposure concentrations and length of exposure, long-term exposures in PM have larger, more persistent, and cumulative effects than short-term ones (Pope III, 2007).

The effects attributed to short-term exposure: daily mortality, respiratory and cardiovascular hospital admissions, days of restricted activity and acute symptoms (wheezing, coughing, phlegm production, respiratory infections)(World Health Organization, 2005).

The effects attributed to long-term exposure: mortality due to cardiovascular and respiratory disease, chronic respiratory disease incidence and prevalence (asthma, chronic pathological changes), lung cancer, chronic cardiovascular disease (Pope III et al., 2002).

In the presence of exposure, the proportion of the population affected by less severe outcomes is much larger than that affected by the more severe outcomes (Figure 3).

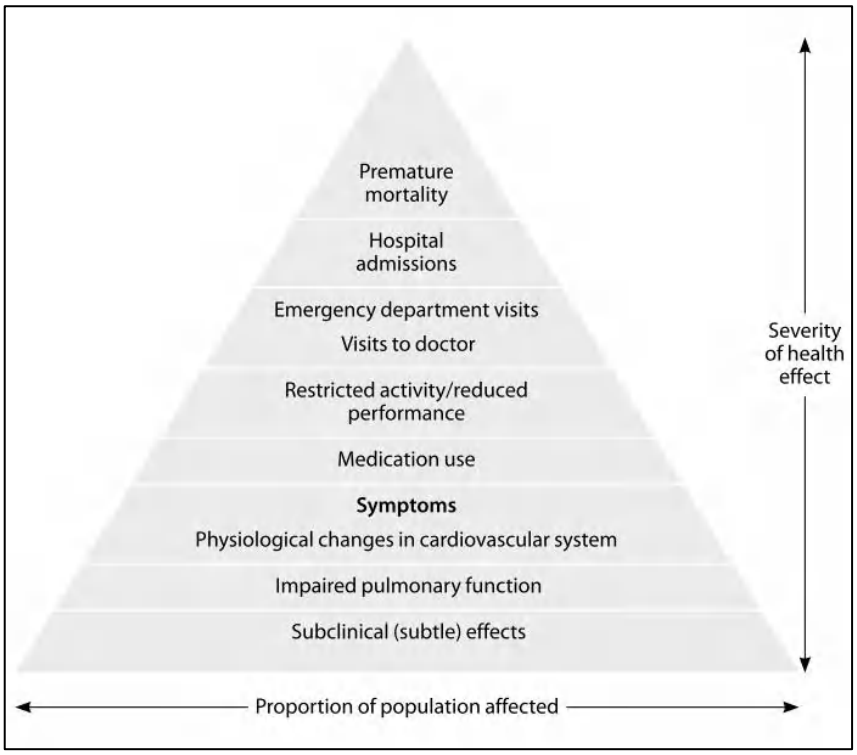

Figure 3. Pyramid of health effects associated with air pollution (American Thoracic Society, 2000).

Subclinical or subtle effects, such as temporary deficits in lung function or pulmonary inflammation, may occur in most of those exposed while mortality may occur in a few.

It is usually the more susceptible who suffer more severe effects. Mortality is advanced by days, weeks or even longer periods in those already ill, and those with a pre-existing medical condition are more likely to be admitted to hospital or to visit an emergency department.

The broad array of health effects associated with air pollution is partly explained by differential susceptibilities to pollutants, depending on both host and environmental factors. Identifying the contribution of susceptibility to the occurrence of health effects from air pollution is key in determining who is most likely to develop adverse effects. Host factors include age, health status, diet and genetics (Sacks et al., 2011). Environmental factors include exposure characteristics as well as the individual's housing and neighbourhood conditions.

Young children are among the most susceptible to the effects of air pollution, they have higher breathing rates than adults and therefore a higher intake of air pollutants per unit of body weight. The developing lung may have a limited metabolic capacity to address toxic insults (Favarato et al., 2014).

1.5.2 The respiratory system, main target of atmospheric particles

The main route of entry for ambient PM to the body is via inhalation. Humans breathe an average of 15 m^3 of air per day and the gas exchange area of the respiratory system has a surface area up to 100 m^2. Thus, the lung constitutes the most important interface between the external medium and the body, which gives it a particular interest in toxicology studies. Therefore, it is a prime target for various toxic agents and pollutants likely to be found in the air we breathe.

1.5.2.1 Penetration, deposition and clearance of airborne particles

The particle deposition in the human respiratory tract is determined by biological factors such as lung morphology and breathing patterns, physical factors such as fluid dynamics, particle properties (shape, charge, density, hygroscopicity and size), and deposition mechanisms (Hofmann, 2011).

These factors determine three deposit areas: the nasal-pharyngeal, tracheobronchial and alveolar regions. Depending on the particle size and mass, the deposition rate varies between these regions.

PM_{10} penetrates through the upper airways (nose, mouth, nasopharynx and larynx) and can be settled in conducting airways (bronchi and upper part of the lungs).

$PM_{2.5}$ can be deposited in the gas-exchange part (deep) of the lung, whereas ultrafine particles (<100 nanometres) deposit in alveoli and may penetrate through the lungs to infect other organs (Churg et al., 2000).

Approximately 40% of the ultrafine particles ($PM_{0.1}$, particles with a diameter up to 0.1 μm) are able to reach the alveoli, carrying along the adsorbed potentially toxic compounds (Figure 4).

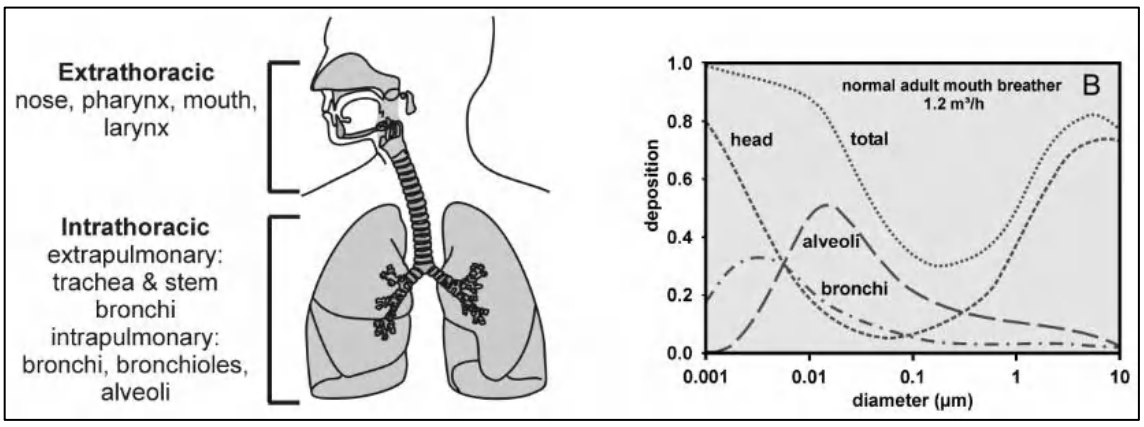

Figure 4. The respiratory tract (A) and particle deposition in a normal adult mouth breathing male human subject at rest, as a function of particle size (Geiser et al., 2010).

After deposition, the body tries to reduce the retention of inhaled particles by clearing them from the lung. The term "clearance" was introduced to describe the translocation, transformation and removal of deposited particles from the various regions of the respiratory tract (Anderson et al., 2012).

In the upper respiratory tract mainly PM_{10} is deposited and in this part of the lung, the clearance is performed by coughing. $PM_{2.5-10}$ deposited onto ciliated surfaces are removed by the "mucociliary escalator" (rapid elimination in 24 hours). The fine and ultrafine fraction of PM mainly deposits in the alveolar region.

After deposition, the particles could be phagocytosed by macrophages and transported to upper lung regions for mucociliary clearance or the particle-loaded phagocytes enter the lymphatic system (slow clearance).

Depending on the inhaled concentrations of particles, a considerable part of the particles are taken up by alveolar epithelial cells, which act in addition to macrophages as initiators of inflammatory responses.

Ultrafine particles taken up by epithelial cells are considered to escape from the clearance done by alveolar macrophages. A fraction of these particles is also able to reach the systemic circulation (Baeza-Squiban et al., 1999)(Squadrito et al., 2001)(Donaldson et al., 2002).

1.5.2.2 ROS, Oxidative Stress and Health Endpoint

Understanding of the biological mechanisms through which air pollution exerts its effects has evolved quite rapidly over the last decade, and several mechanisms are being proposed. Current evidence suggests that the effects of PM may be manifested through several, probably interrelated, biochemical pathways involving oxidative stress and inflammation. (World Health Organization, 2005)(Wessels et al., 2010).

The most important pathophysiological mechanism that has been proposed to explain the association of PM exposure and the occurrence of respiratory infections, lung cancer, and chronic cardiopulmonary diseases are oxidative stress through the generation of ROS (Valavanidis et al., 2008).

Reactive oxygen species (ROS) are species, having an unpaired electron in their valence shell, react with other molecules close to their place of production.

Some are free radicals, such as superoxide anion O^{2-} and hydroxyl radical OH, while others are pro-oxidant non-radical species, such as hydrogen peroxide H_2O_2.

The lifespan of these species is an important issue and ranges from minutes (H_2O_2) to seconds (peroxide radical) to about a nanosecond, in the case of the hydroxyl radical.

ROS may be generated by free radicals present on particle surfaces, by the chemical reaction of specific PM constituents (Squadrito et al., 2001), or through PM-mediated activation of mitochondria or NAD(P)H-oxidase enzymes and immune cells. Intracellular and extracellular production of ROS can activate several redox-sensitive signalling cascades that could, in turn, induce inflammatory responses (Kelly, 2003)(Li et al., 2008).

The nature and degree of oxidative stress induced by particulate air pollution can depend on the chemical reactivity of the PM and the responses that they induce in specific cell populations (Akhtar et al., 2010).

The extent of damage is closely related to the availability of neutralizing enzymatic and non-enzymatic antioxidant defences in the respiratory tract.

After entering the lung, particles first face the extracellular antioxidant mechanisms present in the respiratory tract lining fluid (RTLF).

The RTLF represents the first physical interface encountered by inhaled materials and contains enzymatic antioxidants such as superoxide dismutase (SOD) (it catalyses the dismutation of O^{2-} to H_2O_2 and O_2), catalase (CAT) (it decomposes H_2O_2 to H_2O) and glutathione peroxidase (GPx) (reduces H_2O_2 by oxidizing glutathione (GSH to GSSG)) (Toriba et al., 2016).

Also, low molecular mass non-enzymatic antioxidants, including ascorbate, uric acid, glutathione (GSH) and α-tocopherol are constituent parts of the fluid (Kelly, 2003).

In the alveolar region of the lung, GSH is the major antioxidant and it depends on the activity of gamma-glutamyl-cysteine synthetase (γ-GCS) which is the rate-limiting step. Metal-chelating proteins such as ferritin or transferrin are also present in the RTLF and are part of the protection against oxidative stress by binding of free transition metals.

A three-phase response model has been developed to explain the process of oxidative stress in inducing cellular damage and subsequently adverse health effects.

Initially, when oxidative stress is relatively low, various transcription factors, such as the nuclear factor erythroid-2 (Nrf2), induce a series of antioxidant and detoxification enzymes (e.g., catalase, superoxide dismutase, and glutathione S-transferase) that counteract ROS formation protecting from adverse biological outcomes.

In the second phase, if the protective antioxidant response fails or is inadequate to deal with increasing ROS production, the result is a proinflammatory situation with various cytotoxic effects. These effects are mediated by the redox-sensitive mitogen-activated protein kinase (MAPK) and NF-κB cascades that are responsible for the expression of cytokines, chemokines, and adhesion molecules, which are involved in inflammatory processes.

At high levels of oxidative stress (in the third phase), the antioxidant defences have been overwhelmed and cytotoxic effects ensue (Figure 5) (Lodovici et al., 2011)(Novo et al., 2008).

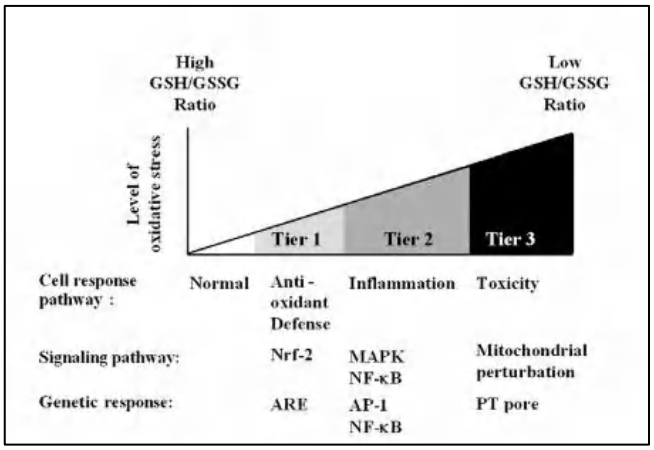

Figure 5. Hierarchical oxidative stress responses. At a low level of oxidative stress (Tier 1), intermediate level (Tier 2), and at a high level of oxidative stress (Tier 3) (Li et al., 2008).

If cellular antioxidant defence systems are overwhelmed, one consequence of oxidative stress is the oxidation of DNA.

1.5.2.3 Oxidative Potential

Recognizing the importance of this ROS generation step, oxidative potential (OP) has been defined, as the capability of particles to deplete physiological antioxidants (reductants) and generate ROS.

The oxidative potential is an attractive measure because it integrates various biologically relevant properties, including size, surface and chemical composition (Janssen et al., 2014) (Pietrogrande et al., 2018a).

The composition of air pollution particles is considered to be a determinant of their capacity for oxidant generation. The components that have been associated with ROS generation in biological systems include organic compounds and metals.

Organic compounds are considered the major source of oxidative stress, specifically PAHs and quinones, that produce oxidative stress in cells and contributed to cellular injury.

PAHs are highly mutagenic and are responsible for increased risk of malignant neoplasms, especially lung cancer.

The principal pathways of metabolic activation of PAHs are:

- Generation of diol epoxides catalysed by cytochrome P450, leading to DNA adduct formation, considered to be essential to PAH mechanism of carcinogenesis;
- Formation of radical cations catalysed by cytochrome P450 peroxidases;

- formation of redox-active quinones catalysed by dihydrodiol dehydrogenases, contributing to PAH carcinogenesis and tumour promotion (Xia et al., 2004).

Quinones and their reduction products are of toxicological interest because of their ability to form covalent bonds with tissue macromolecules and generate reactive oxygen species (ROS), especially the superoxide anion ($\bullet O_2^-$) and the reactive hydroxyl radical (•HO), leading to pulmonary oxidative damage.

The redox recycling of quinones is possible without enzymes, owing to the electron transfer (Chung et al., 2006)(Valavanidis et al., 2006).

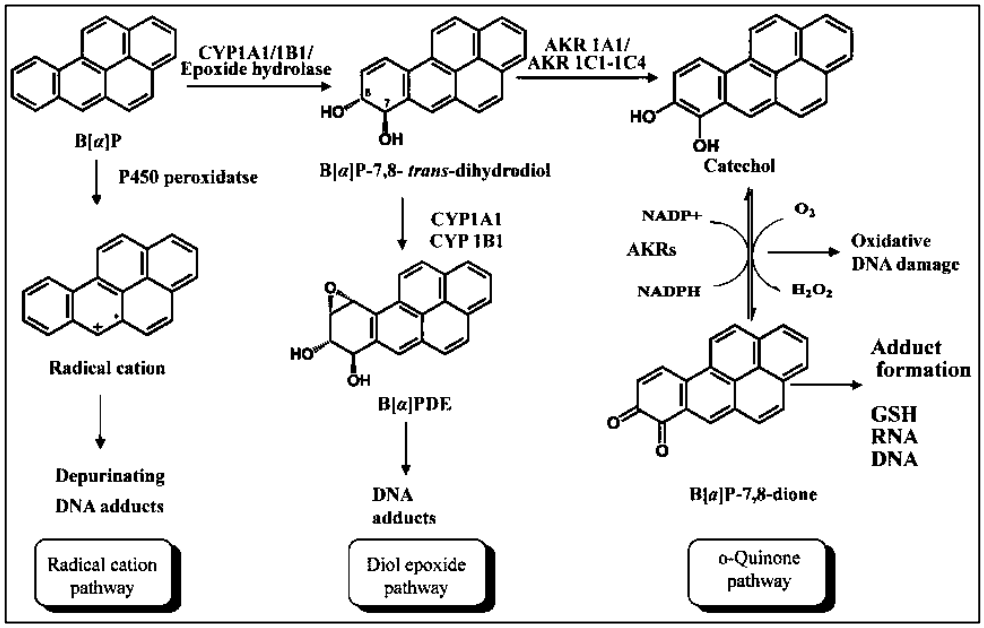

Figure 6. Three pathways of metabolic activation of PAH (B[a]P is used as the representative PAH) (Zhang et al., 2012).

PM oxidative potential may also be largely related to the PM content of soluble species, particularly transition metals.

Metals can initiate ROS formation both directly and indirectly through redox-mediated mechanisms (Daher et al., 2014).

In atmospheric particulate, quantities of Fe can regularly be found in concentrations higher than all other metals. Also, concentrations of copper (Cu), chromium (Cr), manganese (Mn) and nickel (Ni) were significantly present in particles sequestered on filters, while levels of cobalt (Co) approached zero (Ghio et al., 2012).

Iron release from the airborne PM or other redox metals can stimulate the generation of hydroxyl radicals (HO•) by Fenton-type reactions, causing extensive oxidative damage to cellular macromolecules.

In the Fenton reaction, the reduced form of iron, Fe(II), reacts with HOOH to produce the oxidized form of iron and hydroxyl radical.

$$Fe\ (II) + H_2O_2 \rightarrow Fe\ (III) + \cdot OH + OH^-$$

Similar reactions can occur with Cu, Cr, and Ni. Furthermore, biological chelators and reductants can greatly enhance the production of ROS.

For example, in the presence of ascorbate (Asc), a biological reductant, the oxidized form of the transition metal produced by the Fenton reaction can be reactivated, thus allowing additional ROS to be produced.

$$Fe\ (III) + Asc^n \rightarrow Fe\ (II) + Asc^{n+1}$$

$$Cu\ (II) + Asc^n \rightarrow Cu(I) + Asc^{n+1}$$

The reduced forms of transition metals can react with dissolved oxygen to produce superoxide, which can, in turn, react with another reduced metal atom to produce HOOH (Vidrio et al., 2008).

$$Fe\ (II) + O_2 \rightarrow Fe\ (III) + \cdot O_2^-$$

$$Fe\ (II) + \cdot O_2^- \rightarrow Fe\ (III) + H_2O_2$$

The only analytical method that provides direct quantification of radical species in the samples is electron spin resonance (ESR).

However, ESR is an expensive and complicated instrument that has low sensitivity due to low steady-state concentration and short radicals lifetimes (Hedayat et al., 2015).

Thus, to provide the rapid readout of the oxidative potential of PM, acellular assays are employed due to their low price and practicality, when compared to cellular assays.

Acellular assays are based on the capacity of particle suspensions to oxidise antioxidants from models of human respiratory tract lining fluids (RTLFs)(Visentin et al., 2016)(Ayres et al., 2008). A simplified RTLFs model uses only ascorbate (Janssen et al., 2014).

Another common method for the determination of OP of particulate matter measures the oxidation of dithiothreitol (DTT), a strong reducing agent that simulates cellular reducing species in the biological systems (Charrier et al., 2012).

Some studies on oxidative potential of atmospheric aerosol utilize of fluorescent (2',7'-dichlorofluorescein diacetate, profluorescent nitroxide probes, dihydrorhodamine) or chemiluminescent (acridinium ester) reagents which emit after chemical reactions with ROS (Yang et al., 2014).

2. Thesis objectives and outline

The main topic of the present work concerns the PM oxidative properties and their relationship with its chemical composition.
In recent years, there was an increasing consensus on the use of oxidative potential as a biologically relevant metric to be associated with several health endpoints.
This study used two of the most common acellular assays for measuring OP, based on ascorbic acid and dithiothreitol (DTT) as target molecules miming the PM-lung interface.
The aim was to highlight different sensitivity to the ROS generating compounds and better understand the effects of redox-active chemical species in ambient PM.
A critical investigation was carried out of the different experimental protocols generally used in OP assays, with the aim to provide useful information to design a standardized analytical protocol for increasing the reliability and overall quality of data derived from OP assays.
With this purpose, the effects of two important operating conditions were investigated, namely the solvent used for the extraction of the PM samples and the different compositions of antioxidants in the AA assay.
Additional studies were performed to highlight the possible associations of OP responses with cellular endpoints, in order to provide evidence of the usefulness of PM oxidative properties to represent the proinflammatory effects of some PM components.

The second step of the current study was to assess the oxidative potential of real PM samples collected in various locations across Italy to investigate the variation of the OP activity with the particle size and chemical composition.
The responses allowed to identify the specific contribution of the various chemical species and/or sources of pollution, due to the peculiarity of the study site.
Furthermore, the seasonal dependence of the relationships between OP values and chemical element concentrations was studied, showing the difference between winter samples and summer samples caused by different weather conditions.

The last part of this thesis work was devoted to the PM chemical components related to sources and processes that can give important information on the toxicological impact.

The chemical characterization is mainly focused on some specific molecules recognized as dangerous to human health, such as Polycyclic Aromatic Hydrocarbons (PAHs), which have carcinogenic and mutagenic properties.
Due to the large complexity of inorganic and organic PM components, analytical methods have been developed for the treatment of PM samples before analysis, in particular extraction and pre-treatment/purification procedures, which allow to identify and quantify analytes more easily.

Finally, in the frame of the "Piano Lauree Scientifiche" project, the topic of Indoor Air Quality (IAQ) monitoring was investigated in school classrooms and laboratories in the Emilia-Romagna region (Northern Italy).
The monitoring of Indoor Air Quality (IAQ) is essential to provide a picture of the long-term adverse effects on human health, as most of the air exposure occurs indoors, where people spend a large fraction of their lives.
In each school environment, the IAQ parameters were on-site measured using monitoring sensors operating 24 h continuously, investigating temperature, relative humidity (RH%), concentration of fine particle matter ($PM_{2.5}$), concentration of volatile organic compounds (VOCs), and CO_2.

3. Materials and Methods

3.1 Study of Oxidative Potential

In order to provide a rapid screening test to assess the oxidative potential of PM, several quantitative acellular tests have been developed. Their advantage is that they are cheaper and less time consuming and can be applied outdoors. Furthermore, they do not need ethical approval. These assays reflect the chemical properties of PM that are leading to oxidative stress under biological conditions.

Dithiothreitol (DTT) and Ascorbic Acid (AA) are among the most commonly used methods. The goal of this work is to better understand the chemical species in PM that are able to oxidize DTT and Ascorbic Acid and to quantify their redox activity with respect to the two reagents. Thus, the two assays were tested on standard solutions of compounds commonly present in ambient PM.

3.1.1 Standards and reagents

Five compounds representative of different chemical classes were considered for this study: three quinones namely 9,10-phenantrenequinone (9,10-PQN), 1,2-naphthoquinone (1,2-NPQ), 1,4-naphthoquinone (1,4-NPQ), and two metals (copper and iron (II)).

Individual standard stock solutions were prepared for each analyte by weighting pure standards (Acros Organics, Sigma Aldrich, Dr. Ehrenstorfer, Carlo Erba Reagenti) at a concentration of 10^{-2} M in acetonitrile for quinones and MilliQ water for metal ions. The solutions were stored in amber glass vials in the dark at -20°C.

DTT, reduced L-glutathione and uric acid solutions were made at a concentration of 10 mM in a 0.1 M phosphate buffer (Na_2HPO_4 and NaH_2PO_4) at pH 7.4, while ascorbic acid and citric acid solutions were made at the same concentration as DTT but in MilliQ water.

Aqueous solutions of the reagents are unstable at room temperature and DTT solutions are also sensitive to light, thus they were preserved in amber glass vials in the dark and at -20°C. Each antioxidant stock solution was made fresh each day and added to the buffer at the start of the reaction.

Phosphate buffer was treated with Chelex 100 resin (Sigma Aldrich), a cation exchange resin, to remove trace metals. The resin was poured into an acid-rinsed glass chromatographic column that had a permanent glass frit to contain the resin. The phosphate

solution was allowed to drip through the resin at 4°C and the resulting treated phosphate buffer was collected into a clean, acid washed, PTFE bottle.

3.2 DTT assay

DTT can be considered a chemical surrogate of the cellular reductants, such as NADH or NADPH, which reduce O_2 to superoxide anion ($^{\bullet}O^{2-}$) and induces oxidative stress (Kumagai et al., 2002).

It is commonly used as a surrogate of cysteine residues in proteins present in the respiratory tract that can be oxidized when exposed to ROS (Jiang et al., 2019).

The dithiothreitol (DTT) assay is an acellular technique developed to quantify particle OP by monitoring the consumption of DTT in the presence of particle components under physiologically relevant conditions.

The biological relevance of this technique, as the consumption rate of DTT also known as DTT activity (OP^{DTT}), has been linked with the expression of cellular markers of oxidative stress and inflammation, as well as cellular cytotoxic responses (Wong et al., 2019).

Often, the DTT consumption can be attributed to the presence of transition metals and quinones in PM as they can catalyze the oxidation of DTT through catalytic redox reactions (Ayres et al., 2008).

However, the DTT consumption by non-catalytic PM components has not been fully investigated (Charrier et al., 2012). Moreover, weak correlations between DTT consumption, ROS generation, and cellular responses have been observed in several studies, which also reveal the knowledge gaps between DTT-based OP measurements and their implication on health effects (Jiang et al., 2019).

The assay is based on a two-step reaction. In the first step, redox-active chemicals in particulate matter oxidize DTT to its disulphide form and then donate an electron to dissolved molecular oxygen, forming superoxide (Kumagai et al., 2002), which can subsequently form other reactive oxygen species (ROS) such as hydrogen peroxide and, in the presence of metals, hydroxyl radicals (Figure 7).

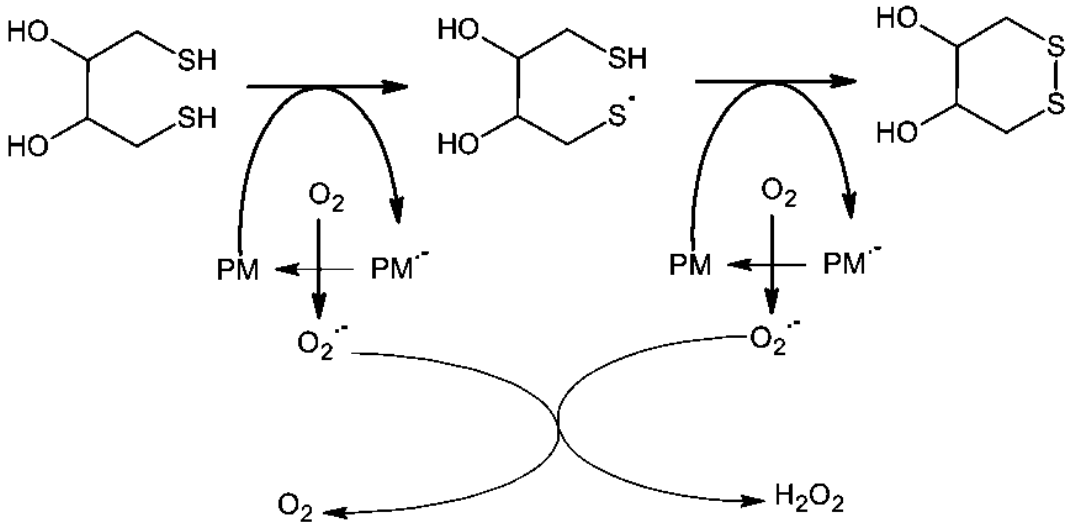

Figure 7. Dithiothreitol (DTT) oxidation by redox-active species in PM with subsequently ROS formation.

When this reaction is monitored under conditions of excess DTT, the rate of DTT consumption is proportional to the concentration of the catalytically active redox-active species in the sample (Velali et al., 2016).

The redox cycle catalysed by PM species is similar to cycles that occur in living cells. Typically, ROS are formed in cells through the reduction of oxygen by biological reducing agents such as NADH and NADPH, with the catalytic assistance of electron transfer enzymes and redox-active chemicals (Cho et al., 2005).

A diagram of the redox cycling of quinones generating ROS in vivo is shown in Figure 8.

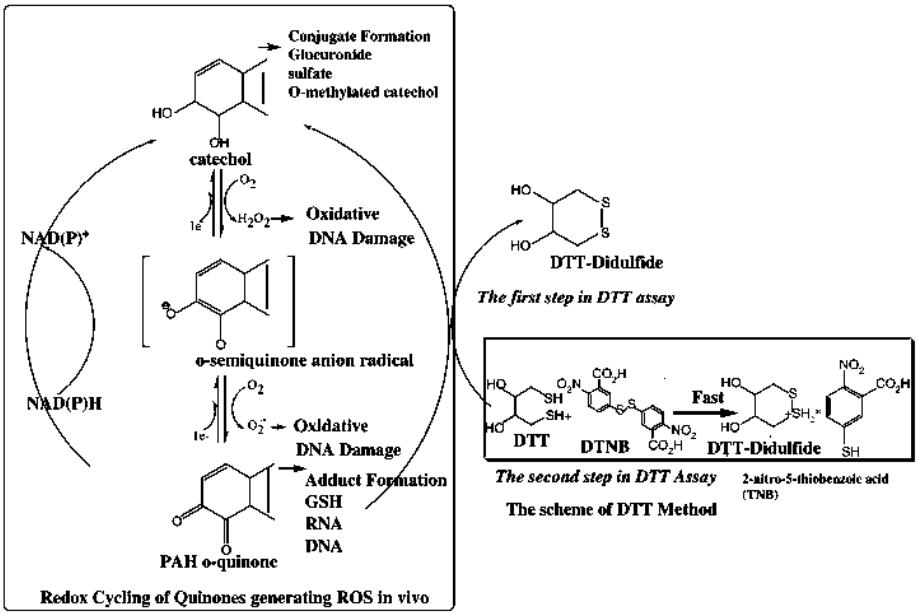

Figure 8. The redox cycling of quinones generating ROS in vivo, and the similar cycling in DTT assay.

Comparing the cycling of the DTT method with the redox cycling of quinones generating ROS in vivo shows that they share elements of the same mechanism of ROS generation (Cho et al., 2005).

In the second step (Figure 9), the remaining DTT is reacted with DTNB (Ellman's Reagent) to generate DTT-Disulfide and 2-nitro-5-thiobenzoic (TNB).

TNB is the "coloured" species produced in this reaction and has a high molar extinction coefficient (14150 M^{-1} cm^{-1} at 412 nm) in the visible range.

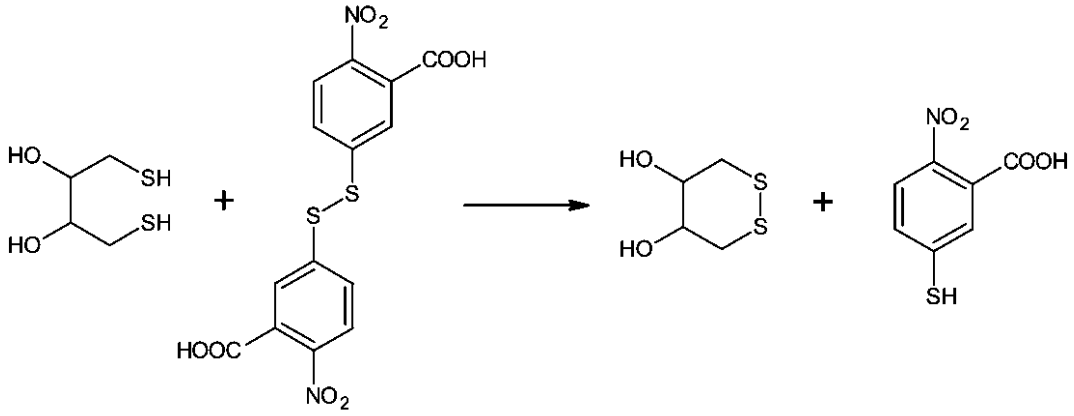

Figure 9. DTT reaction with 5,5 -dithiobis (2-nitrobenzoic acid) (DTNB).

While the DTT assay provides a quantitative measure of oxidation, it does not measure the production of specific ROS, which is significant since the different ROS have very different reactivity (Charrier et al., 2012).

The particulate species responsible for DTT oxidation are typically examined by correlating DTT activity with PM composition. These analyses often identify carbonaceous species, i.e., elemental carbon, water-soluble organic carbon and/or polycyclic aromatic hydrocarbons (PAHs), as most strongly correlated with DTT loss. However, correlations do not show causation, especially since particulate species are often highly covariate. For example, PAHs levels often strongly correlate with DTT loss from particles, but PAHs are not redox-active. Typically compounds which react in this assay are organic species, mainly quinones (Cho et al., 2005)(Xiong et al., 2017), even if some studies have shown that transition metals can also oxidize DTT (Fang et al., 2016)(Gao et al., 2019).

3.2.1 Procedure of DTT Assay

For DTT, the method proposed by Charrier (Charrier et al., 2012) was followed. A small volume (< 30 μL) of stock solution of the compound of interest was added to an amber vial containing 3.0 mL of phosphate buffer at pH 7.4 and the obtained solution was heated at 37°C using a dry bath.

Once the temperature reached 37°C, at time zero 30 μL of the DTT solution 10 mM were added to the vial. At known times, a 500 μL aliquot of the reaction mixture was removed and added to 500 μL of 10% trichloroacetic acid to stop the reaction.

When all time points were quenched, 50 μL of 10 mM DTNB in phosphate buffer at pH 7.4 were added, mixed well, and let them to react for 2 minutes. Then 2.0 mL of 0.40 M Tris-HCl buffer at pH 8.9 with 20 mM of EDTA was added.

It is important to increase pH value because the protonated form of TNB shows only a slight absorbance in contrast with the mercaptide ion (TNB^{2-}, thiol group pKa = 4.53 at 25°C) which has a higher absorbance (ε =14150 M^{-1} cm^{-1} at 412 nm)(Li et al., 2009).

Charrier suggests to add the DTNB before the Tris buffer to ensure the sample remains quenched until DTT has reacted with DTNB, even if the DTNB and DTT reaction is very fast (Li et al., 2009)(Charrier et al., 2012).

Because both DTT and TNB are sensitive to light, the reactions were performed in dark vials covered with aluminium foil and store in the dark when not in use.

TNB was quantified using a 1 cm path length PS cell in a Jasco V-730 UV-Vis spectrophotometer.

The reactions were performed at pH 7.4 and 37°C to simulate biological conditions that normally occur in a human body.

3.3 AA assay

The respiratory tract lining fluid (RTLF), represents the first physical interface encountered by inhaled materials and has been shown to contain high concentrations of antioxidants as urate, reduced glutathione, and ascorbate (vitamin C) which is a physiological antioxidant that prevents the oxidation of lipids and proteins (Ayres et al., 2008).

The oxidative capacity of PM samples has been determined by their ability to oxidize a range of protective antioxidant molecules present at the surface of the lung using a validated in vitro model (Zielinski et al., 1999).

The AA assay is a simplified version of the synthetic respiratory tract lining fluid (RTLF) assay, where only ascorbic acid is used. The reaction mechanism is similar to the first step of DTT reaction: ascorbic acid is oxidized to dehydroascorbic acid while redox-active species in PM are reduced (Figure 10).

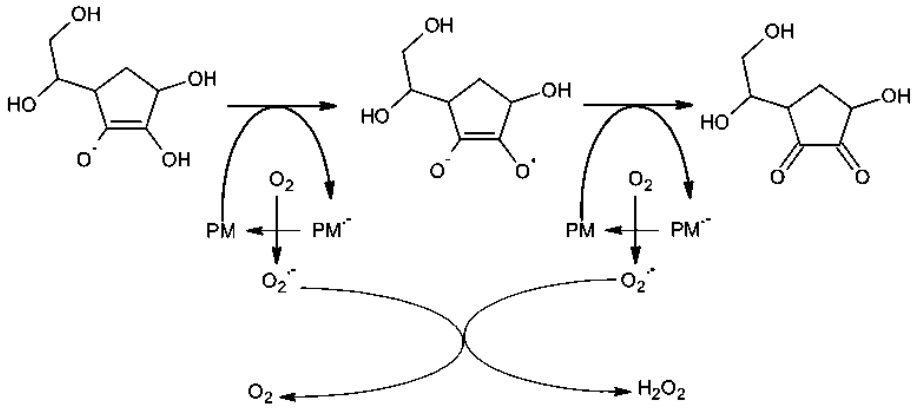

Figure 10. Chemical reaction between ascorbic acid and oxygen with PM as a catalyst.

These reduced species can then transfer an electron to oxygen molecules promoting the formation of ROS. The depletion of ascorbate by PM in acellular assays has been linked to metals, especially copper and iron (Lin et al., 2020), but has also shown to be sensitive to quinones (Roginsky et al., 1999).

3.3.1 Procedure of AA Assay

Most of the ascorbate assay studies in the literature are performed in a 96 well plates equipped with a plate reader (Yang et al., 2014)(Janssen et al., 2014)(Calas et al., 2018).

In this study, the method was adapted to a classical spectrophotometer and the reaction occurred directly into the spectrophotometric quartz cuvette (Yang et al., 2014). The procedure is similar to that used for DTT assay.

Briefly, an aliquot of stock solutions of analytes was diluted in 3.0 mL phosphate buffer and heated at 37°C.

At time zero, 30 µL of ascorbic acid solution were added to the cuvette and at known time the absorbance of the solution was read for 1 h at 265 nm.

At pH 7.4, vitamin C is present almost totally as ascorbate ion that has a molar extinction coefficient of about 14500 M^{-1} cm^{-1} at the considered wavelength.

3.4 Data Analysis

OP response is measured as the antioxidant depletion rate of known quantity of DTT and AA, following the experimental procedure.

The kinetics of DTT or AA oxidation was followed by measuring the decrease of DTT or AA concentrations added to the sample (100 nmol) over the reaction course.

The rate of DTT or AA depletion (nmol min^{-1}) was determined by linearly fitting the experimental points of the reagent's concentration versus time (5, 10, 15, 25, 40 minutes) and then blank corrected by subtracting the average blank rate.

The linear regression was considered acceptable when $R^2 > 0.98$ and when less than 70% of the initial amount of DTT and AA had been oxidized (Q. Li et al., 2009)(Visentin et al., 2016).

For the real PM samples, the obtained OP responses were then normalized by the volume of sampled air (OP^{DTT}_V and OP^{AA}_V expressed as nmol min^{-1} m^{-3}) as an exposure metrics accounting for inhaled air and by the PM mass (OP^{DTT}_m and OP^{AA}_m expressed as nmol min^{-1} μg^{-1}) to point out the intrinsic ability of the particles to deplete physically relevant antioxidants. The response of blank filters was determined and subtracted from the data of real PM samples.

4. Effect of filter extraction solvents and different setups of AA a-cellular assay for measuring oxidative stress

Part of this chapter summarizes the content of the study published in Atmospheric Environment (2019), 211, 103– 112. DOI: https://doi.org/10.1016/j.atmosenv.2019.05.012.

4.1 Effect of filter extraction solvents

Among several in vitro cellular and acellular assays proposed to quantify OP, cell-free assays, besides being non-invasive, have the advantages of being fast, inexpensive, easy to organize, and suitable for automation (Visentin et al., 2016)(Gao et al., 2017)(Calas et al., 2018)(Bates et al., 2019).

They all require a preliminary solvent extraction to retrieve the PM components from the loaded filter, still conserving, as much as possible, the physical and chemical properties of the complex mixtures present in the atmosphere. This is a critical step, as the major contributors to PM toxicity are trace components that contribute little to PM mass and might be a potential loss during the extraction process or contaminated by interfering compounds. (Bein et al., 2015)(Roper et al., 2015)(Roper et al., 2017)(Simonetti et al., 2018b).

Toxicological studies suggest that the biological response of particle-bound species is strongly affected by different extraction protocols since it is strongly influenced the degree of bioaccessibility of the biologically active compounds.

Although several extraction procedures are currently in use, to date, no real consensus has emerged towards standardized protocols, including the type of filters used to collect atmospheric PM, solvent and extraction procedures, OP assay media, and others (Wiseman, 2015)(Roper et al., 2017)(Bates et al., 2019)(Luo et al., 2019)(Molina et al., 2020).

This may generate discrepancies in assay responses reducing the reliability of OP data and, hence, lessen formation of a robust consensus on the use of OP as an exposure metric for ambient air PM in epidemiological studies.

This motivates the present study, which investigates the impact of the filter solvent extraction on responses of two acellular OP assays, in order to guide the selection of an extraction method that is best suited for OP assessments of ambient PM samples.

4.1.1 Extraction Solvents

The study was performed by extracting equal portions of a single PM filter with different solutions, to investigate the combination of different solvent solubility towards the redox-active species and also the reactivity of such components in different solution media of OP assays. The three tested solvents are useful for DTT and AA assays, to generate comparable OP responses.

Phosphate buffer (PB), is the most common aqueous buffer employed and methanol (Me), is already frequently used in $PM_{2.5}$ toxicology studies, due to its ability to extract hydrophobic and hydrophilic compounds (Yang et al., 2014)(Verma et al., 2015)(Gao et al., 2017).

Besides, the Gamble's solution was investigated, as a lung fluid surrogate mixture, that may closely mimic bio-accessibility of particle-bound species in the physiological fluids encountered during PM exposition (De Meringo et al., 1994)(Charrier et al., 2011)(Charrier et al., 2015)(Kastury et al., 2018)(Calas et al., 2018)(Zeng et al., 2019)(Luo et al., 2019).

Gamble's solution is complex artificial biological media that simulate different interstitial conditions in the lung, in particular, is prepared with Magnesium Chloride Hexahydrate 10^{-3} M, Sodium Chloride 0,1 M, Potassium chloride $4 \cdot 10^{-3}$ M, Disodium hydrogen phosphate $0{,}9 \cdot 10^{-3}$ M, Sodium Sulfate $0{,}4 \cdot 10^{-3}$ M, Calcium Chloride dehydrate $2{,}5 \cdot 10^{-3}$ M, Sodium Acetate $7 \cdot 10^{-3}$ M, Sodium hydrogen carbonate 0,03 M, Sodium citrate dehydrate $0{,}3 \cdot 10^{-3}$ M in ultrapure water.

4.1.2 Extraction procedure of real PM samples

The impact of solvent extraction on PM OP or toxicity has been studied by comparing aqueous solutions, organic solvents and simulated lung fluid surrogate (Bein et al., 2015)(Leclercq et al., 2017)(Roper et al., 2019).

Samples of PM were extracted with different extraction methods: water-based and methanol extractions.

Three different quarters of filter were extracted for 15 min in an ultrasonic bath using 10 mL of phosphate buffer 0.1 M at pH 7.4, Gamble's solution, and methanol.

The extracts were then filtered to remove the suspended solid particles with a regenerated cellulose syringe filter (13 mm, 0.22 mm, Kinesis) for the water-based extracts, and with a PTFE syringe filter (25 mm, 0.22 mm, Kinesis) for the organic extract.

The methanol filtrate was then transferred to a rounded glass flask and reduced in volume using the evaporator (miVac, Genevac Inc, USA) at 30°C until dryness and finally, was

reconstituted by adding 10 mL of phosphate buffer 0.1 M at pH 7.4. Then, 3 mL of each solution were submitted to each OP assays (Yang et al., 2014)(Verma et al., 2015)(Gao et al., 2017).

The response of blank filters was determined to take into account the effect of reagents and sampling support on sample DTT and AA loss.

4.1.3 OP^{DTT} and OP^{AA} responses of individual redox-active specie

The effect of the assay media was investigated by measuring OP^{DTT} and OP^{AA} of blank filter spiked with standard solutions of redox-active species after the extraction in phosphate buffer, Gamble's solution, or Methanol.

Different concentrations of standard compounds were tested to represent the range of atmospheric concentrations and obtain comparable OP responses with those from real PM samples.

Two quinones (9,10-PQN and 1,2-NPQ) and two metals (Cu^{2+} and Fe^{2+}) were used to conduct preliminary tests on OP responses.

9,10-phenantrenequinone (9,10-PQN) has been found by far the most reactive quinone to DDT assay, respect the 1,2-naphthoquinone (1,2-NPQ) and high activity in AA oxidation was shown by Cu as the most reactive metal, followed by Fe, that is the most abundant metal in PM (Table 2).

Spiked blank filters	OP^{DTT} (nmol min^{-1})			OP^{AA} (nmol min^{-1})		
	PB	GS	MeOH	PB	GS	MeOH
Cu^{2+}	1.84±0.11	1.21±0.09*	0.23±0.02*	4.76±0.28	4.35±0.26	n.d.
Fe^{2+}	0.55±0.04	0.38±0.03	n.d.	1.29±0.09	1.12±0.06	n.d.
1,2 NPQ	1.17±0.08*	0.75±0.05	1.41±0.11*	3.62±0.23	2.95±0.15	4.87±0.38*
9,10 PQN	1.06±0.09	0.95±0.04	1.65±0.12*	0.78±0.05*	0.53±0.01	1.38±0.08*

Table 2. OP^{DTT} and OP^{AA} responses (depletion rate nmol min^{-1}) of standard solutions of redox-active species after extraction with different solvents on spiked blank quartz filters. For each species, measurements were repeated at least 3 times (mean and standard deviation, n ≥ 3). n.d. not detected.

Overall, the obtained results show that Gamble's solution generated lower responses of both assays compared with phosphate buffer.

The OP^{DTT} trend was ascribed to the presence in Gamble's solution of complexing anions (orthophosphates, carbonates, acetates) and functional groups (carboxyl from glycine, citrate, and amines from glycine) that may chelate metals and thus reduce their redox reactivity (Calas et al., 2017).

Calas et al. 2017 also found a similar Gamble's solution decreasing effect on quinones, which was unexpected, as organic compounds do not form strong complexes with chelating species.

As likely explanation, they suggested that the Gamble's medium may be less favourable to electron transfer than phosphate buffer and/or that quinones may be transformed during the extraction step and storage (Calas et al., 2017).

The trend of OP^{AA} responses, with lower values in Gamble's solution than in phosphate buffer, shows that OP^{AA} values decrease by adding further components to the phosphate buffer (Pietrogrande et al., 2019b).

Besides, the AA assay is more sensitive to the possible larger metal content extracted by Gamble's solution.

The use of methanol generated lower OP responses for Cu and Fe, that is consistent with the decreased solubility of metal ions in MeOH compared with buffer solutions while, for 9,10-PQN and 1,2-NPQ, methanol extraction yielded significantly higher DTT and AA responses compared with other aqueous solvents (Roper et al., 2019)(Wei et al., 2019)(Xing et al., 2019).

Although all the tested solvents are useful for OP^{DTT} and OP^{AA} assessment, the phosphate buffer provided the most sensible measure (nearly double values) compared with other extractions.

4.1.4 Application of extraction solvents on $PM_{2.5}$ samples

The investigated assays were applied to real environmental $PM_{2.5}$ samples collected in March 2018 at an urban and rural site in the Po Valley (northern Italy), applying the different operating conditions previously tested.

Sampling took place at two sites in the Emilia Romagna region, in the eastern part of the Po Valley (northern Italy): an urban background site (URB) located in the middle of the city of Bologna (~400,000 inhabitants) and a rural background station (RUR) located at San Pietro Capofiume about 30 km northeast from the city.

4.1.4.1 Effect of extracting solutions on OP_V response

The effect of the assay media was investigated by measuring OP^{DTT} and OP^{AA} for each filter in phosphate buffer, Gamble's solution and methanol (Appendix, Table A1 and Table A2).

The obtained results show that the OP^{DTT}_V and OP^{AA}_V values of MeOH extracts of real samples were lower than those of phosphate buffer extracts and similar to those of Gamble's solution extracts, with magnified differences for the urban samples.

This result resembles the pattern obtained with the standard solutions of metals, suggesting that the oxidative properties of our real samples are mainly driven by transition metals, among the redox-active species.

Such a conclusion is also consistent with the overall higher responses obtained from the AA assay than those from DDT, as AA is more sensible to metals than to organics (Fang et al., 2016)(Visentin et al., 2016)(Calas et al., 2018)(Simonetti et al., 2018b)(Bates et al., 2019).

Overall, the OP responses measured with Gamble's solution procedure are lower than those with Phosphate Buffer.

This may be ascribed to the dominant role of the inhibition of DTT and AA depletion by the presence of chelating agents in Gamble's solution medium (Calas et al., 2017)(Pietrogrande et al., 2019b).

Otherwise, it must be underlined that an opposite effect is given by the same Gamble's solution complexing components, as they are able to extract larger fractions of metal content from the filter, according to their chelating strengths (Collins et al., 2015)(Wiseman, 2015)(Leclercq et al., 2017)(Luo et al., 2019).

Therefore, the overall variation may be ascribed to the combination of two contrasting contributions, namely solvent extraction efficiency to retrieve redox-active components into solution and reactivity of individual species in the two assay media.

The phosphate buffer, confirming the results obtained with the standard solutions, provided the most sensible measure compared with other extractions for both assays.

4.1.4.2 OP^{DTT} and OP^{AA} responses for ambient PM samples in the three extracting solutions

From the individual volume-normalized OP^{DTT}_V and OP^{AA}_V data measured for each sample, the mean values (Appendix, Table A3) were computed for each investigated solvent and compared in Figures 11a,b.

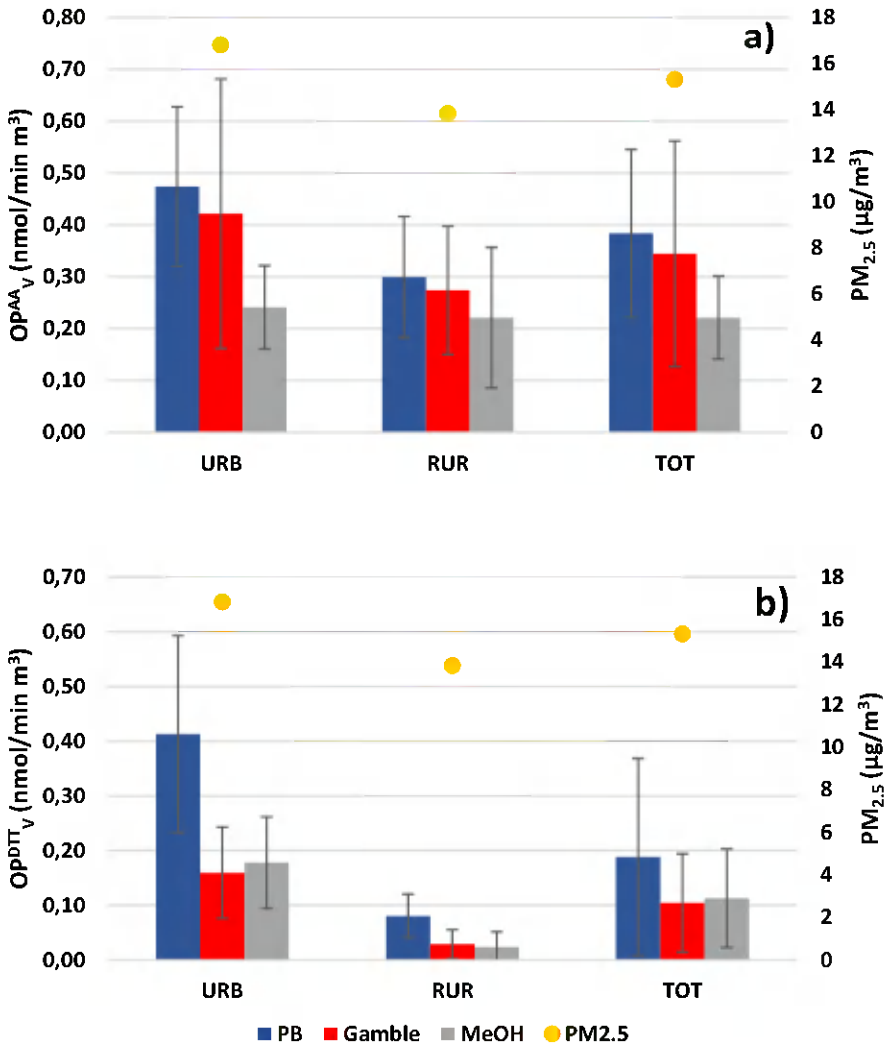

Figure 11. Comparison among OP_V responses using different extraction solvents. Mean values were computed on all the investigated $PM_{2.5}$ samples, as well as on urban and rural samples, separately. Blue bars: phosphate buffer; red bars: Gamble's solution; light grey bars: methanol. 11a) comparison among $OP^{AA}{}_V$ responses; 11b) comparison among $OP^{DTT}{}_V$ responses.

Similar OP values were measured from the different extracts, with total mean $OP^{DTT}{}_V$ values ranging from 0.10±0.09 nmol min^{-1} m^{-3} to 0.19±0.18 nmol min^{-1} m^{-3} and total mean $OP^{AA}{}_V$ from 0.22± 0.08 nmol min^{-1} m^{-3} to 0.38±0.16 nmol min^{-1} m^{-3}.

A deeper insight into the data highlights that the OP responses varied for different extraction methods, since methanol extraction generated the lowest values and phosphate buffer the highest, following the same increasing order for both $OP^{DTT}{}_V$ and $OP^{AA}{}_V$ responses:

$$MeOH < Gamble's\ solution < Phosphate\ Buffer$$

4.1.4.3 *Correlations between OP responses: in different extraction solutions and different assays*

To highlight the effect of the extraction solvent on OP responses of different samples, the intercorrelation between OP data measured after each extraction procedure was explored (Pearson correlation coefficients in Appendix, Table A4).

OP^{DTT}_V responses showed a significant Pearson coefficient ($p \leq 0.01$) among the data obtained with the different solvents, suggesting that the effect of the various extraction solvents on DTT reactivity is similar for all the samples.

The obtained data highlight that the use of phosphate buffer generates higher OP^{DTT}_V responses with a larger variation range, therefore, it is possible to conclude that, among the instigated solvents, the extraction with phosphate buffer provides the most sensible measures.

Otherwise, OP^{AA}_V responses showed weaker correlations among the data with different solvents, with no significant correlation between Gamble and MeOH extraction.

This suggests that the extraction solvent has a different impact on AA reactivity of the various PM samples, that may be likely related to variation in concentrations of components mostly effective towards the AA assay.

Furthermore, to investigate the specific role of the extraction procedure on each OP assay, the intercorrelation between OP^{DTT}_V and OP^{AA}_V responses was explored for each extraction procedure (Appendix, Table A4).

Overall, no significant correlation was found between the responses of the two assays, even by separately investigating URB and RUR samples (Appendix, Tables A5 and A6). This confirms the finding that the two OP assays display different sensitivity towards the redox-active species present in PM because they capture the redox reactions of different species (Charrier et al., 2015)(Fang et al., 2016)(Calas et al., 2018)(Simonetti et al., 2018b)(Bates et al., 2019).

4.1.4.4 *Correlation between OP responses in different extraction solutions and PM chemical constituents*

In addition to OP responses, $PM_{2.5}$ mass concentrations and some chemical components were measured for each $PM_{2.5}$ sample, i.e., Organic and Elemental Carbon, secondary ions and soluble transition metals.

The correlation analysis was performed to associate OP_V response with $PM_{2.5}$ chemical composition with the aim to single out the components that drive PM oxidative properties and also to highlight if such associations vary with the extraction conditions.

Overall, the obtained results show similar behaviour for the three investigated solvents, suggesting no major impact of extraction solvent on these correlations (Appendix, Table A3).

In general, OP^{DTT}_V data resulted more widely correlated with several PM components, including $PM_{2.5}$ mass concentration, compared with OP^{AA}_V.

OP^{DTT}_V responses are also affected by traffic-related metals, mainly non-exhaust traffic emissions, such as Fe, Mn, Zn and Pb ($p<0.01$), by organic compounds, traced by OC and EC ($p<0.01$), that represent fuel vehicular (EC) and biomass burning emissions (Levoglucosan, $p<0.05$), and also secondary atmospheric processes, traced by NH_4^+, NO_3^- and SO_4^{2-} ions ($p<0.05$).

Concerning OP^{AA}_V responses, significant associations ($p<0.01$) were found only with EC after phosphate buffer and Gamble's solution extraction and none with other investigated parameters (Appendix, Table A4).

By separating URB and RUR samples, we can observe that OP^{DTT}_V values of the URB site are more strongly associated with metals, while those at the RUR site with OC and EC (Appendix, Tables A5 and A6).

This is consistent with the predominant role of secondary organic carbon, OC, and biomass burning at the rural site, as it is less impacted by traffic emission (metals) (Pietrogrande et al., 2019a).

Among the extraction solvents, Gamble's solution generates OP^{DTT}_V values better correlated with metal concentration, that is consistent with its higher extraction power towards water-soluble components.

Such results are consistent with the lack of intercorrelation between OP^{DTT}_V and OP^{AA}_V responses, as they are differently correlated with the same redox-active PM components (Fang et al., 2016)(Visentin et al., 2016)(Calas et al., 2018)(Bates et al., 2019).

Based on these results, we can confirm that the OP of the investigated $PM_{2.5}$ samples depends on both transition metals and organics, with a stronger association of DTT reactivity with chemical components.

Overall, it must be pointed out that it is difficult to identify the relative contribution of the two classes of compounds, as it is given by the combination of the specific reactivity of each individual component, associated with its concentration level in PM.

4.1.4.5 Comparison between urban and rural PM samples

The data from filters collected at the urban (URB, n = 16) and rural (RUR, n = 16) site were separated and investigated in detail. The objective was to explore the effect of solvent extraction on OP of PM samples with different chemical compositions.

The mean and SD values of volume- and mass-based OP^{DTT} and OP^{AA} responses computed on the two groups are reported in Appendix Table A3 and, $OP^{DTT}{}_V$ and $OP^{AA}{}_V$ have shown in Figures 11a,b for comparison.

Both groups showed the same general solvent extraction effects, with even magnified differences for the URB samples.

Otherwise, the RUR group showed almost constant $OP^{DTT}{}_V$ and $OP^{AA}{}_V$ data, nearly independent of the extraction conditions.

$OP^{DTT}{}_V$ responses were significantly higher ($p \leq 0.05$) for phosphate buffer, which yielded $OP^{DTT}{}_V$ values nearly double that of those with other solvents.

Methanol extraction generated $OP_V{}^{AA}$ values nearly 50% ($p \leq 0.05$) of those with phosphate buffer and Gamble's solution procedures.

Moreover, can be explained the differences in intrinsic oxidative properties, quantified as mass-related OP_m parameter, as the relation with the variation in sample chemical composition.

The measured $OP^{DTT}{}_m$ values are significantly higher ($p<0.05$) at URB (from 0.010 ± 0.006 nmol min^{-1} μg^{-1} to 0.023 ± 0.018 nmol min^{-1} μg^{-1}) compared with RUR site (from 0.001 ± 0.001 nmol min^{-1} μg^{-1} to 0.002 ± 0.002 nmol min^{-1} μg^{-1}).

Such an increase at the urban site can be explained by increasing the concentration of redox-active components (Pietrogrande et al., 2018b)(Pietrogrande et al., 2019b)(Pietrogrande et al., 2019a)(Simonetti et al., 2018b)(Visentin et al., 2016).

On the contrary, mass related $OP^{AA}{}_m$ responses were not significantly ($p<0.05$) different between the two sites (mean values from 0.012 ± 0.009 nmol min^{-1} μg^{-1} to 0.031 ± 0.016 nmol min^{-1} μg^{-1}), suggesting a weak dependence of the AA assay reactivity on PM chemical composition, as found by other Authors (Bates et al., 2019)(Calas et al., 2018)(Perrone et al., 2019a)(Pietrogrande et al., 2019a).

4.2 Effect of different setups of AA a-cellular assay

To accurately estimate the inhalation risks of airborne elements, there is the need of designing the experimental set-up of any a-cellular assay that most closely simulates the physiological conditions effectively encountered in the air interaction with the human body.

In fact, the harmful effects of $PM_{2.5}$ are determined not only by its concentrations and hazardous components from diverse sources but more by their bioavailable fractions absorbed by the human body.

For this reason, we used different synthetic simulated lung fluids (SLFs) as solution media in AA a-cellular assay and investigated the role of their different composition on AA assay response.

It is difficult to closely represent the physiological condition, as RTLF has unique features that vary in different levels of the respiratory tract, as shown by discrepant quantitative compositions of antioxidants reported in literature (Kumar et al., 2017)(Marques et al., 2011)(Van Der Vliet et al., 1999).

Among the different compositions of synthetic SLFs, the investigated composite RTLF surrogates were obtained by adding GSH and urate, which are antioxidants naturally occurring in the lung fluid to compensate ROS production, and possibly to modulate ROS release (Godri et al., 2011)(Weichenthal et al., 2016)(Kumar et al., 2017).

Also, citrate (Cit) was added, to represent proteins able to mobilize iron that can be found in the lung lining fluid (Marques et al., 2011).

4.2.1 OP^{AA} of standard solutions of redox-active species in different synthetic RTLFs

The experimental setups were applied to standard solutions of redox-active species, namely Cu^{2+} and Fe^{2+}, 1,2-naphthoquinone (1,2-NPQ), 1,4-naphthoquinone (1,4-NPQ) and 9,10-phenantrenequinone (9,10-PQN) (Charrier et al., 2014)(Antiñolo et al., 2015)(Charrier and Anastasio, 2015)(Tuet et al., 2017a)(Lyu et al., 2018).

The standard solutions of the investigated species were prepared at a concentration of 1 μM to represent the order of magnitude that ambient PM could produce in lung fluid (e.g., (Vidrio et al., 2008)).

In the experiments, standard solutions of Cu^{2+} and 1,2-NPQ solutions were diluted to 0.1 μM and 0.2 μM, respectively, to obtain comparable OP^{AA} responses and guarantee the response linearity of the AA assay (Charrier et al., 2015)(Visentin et al., 2016).

All the investigated species show that in general OP^{AA} significantly decreases with the increasing complexity of the synthetic RTLFs, as well as $PM_{2.5}$ samples, but each redox-active species displays a different variation pattern (Appendix, Table A7 and Table A8).

Developed based on the composition of human RTLF, solutions of endogenous antioxidants were added individually or in combination at a concentration of 100 μM for ascorbate, 150 μM for citrate and 50 μM glutathione and urate.

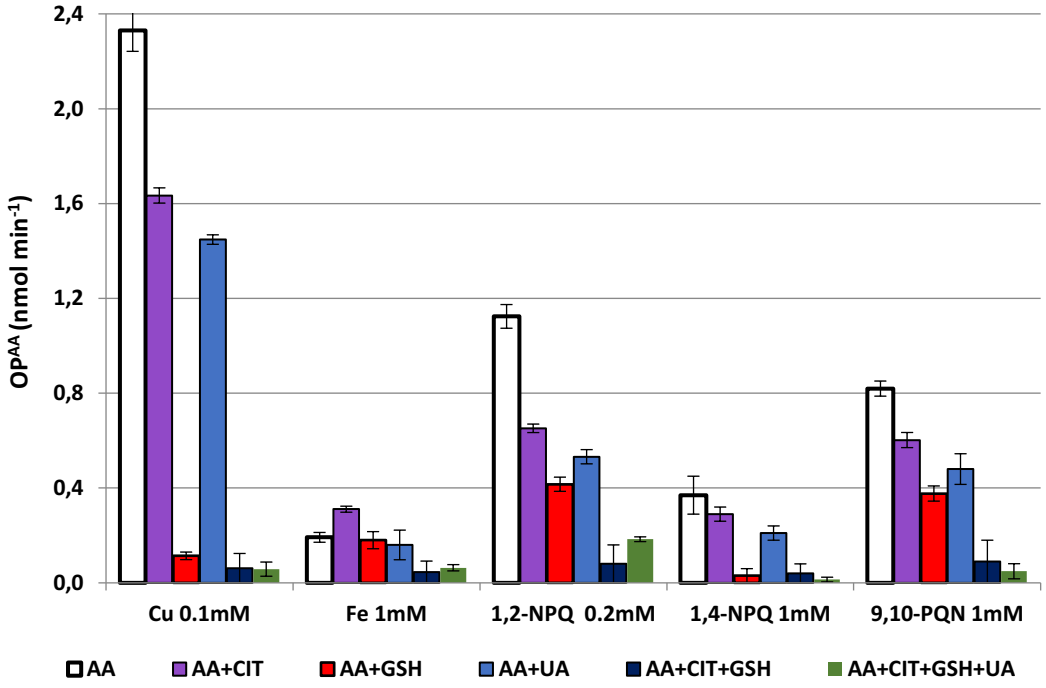

Figure 12. OP^{AA} responses (nmol min^{-1} m^{-3}) of standard solutions in six different RTLF surrogates.

Concerning Cu^{2+}, the individual addition of citrate and urate reduces OP^{AA} by 30% compared to Asc.

This may be explained by the dominant presence under these conditions of the Cu-citrate and Cu-urate complexes, which have been found less reactive than the free Cu^{2+} (Vidrio et al., 2008)(Charrier et al., 2011).

OP^{AA} reduction is the strongest by adding glutathione (about 93%), independent of the further addition of other AOs.

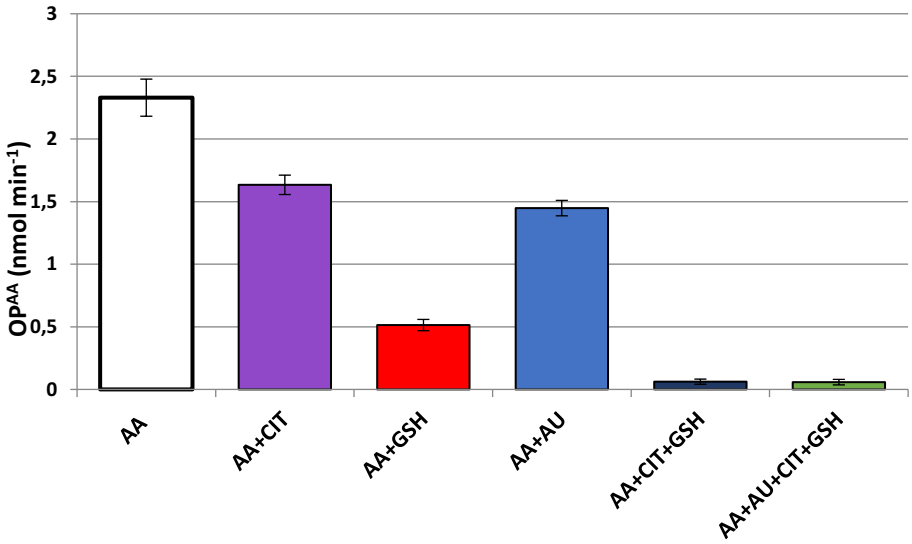

Figure 13. OP^{AA} responses (nmol min^{-1} m^{-3}) of Cu^{2+} in the different RTLF surrogates: in six different RTLF surrogates.

Such an effect is likely due to the GSH ability of binding Cu^{2+} to form a Cu-GSH complex with reduced reactivity.

This is the underlying mechanism of Cu^{2+} storage and transport as well as its antioxidant activity (Aliaga et al., 2010).

Fe^{2+} shows different behaviour, as the addition of Cit to the Asc solution strongly enhanced OP^{AA} response by 62%.

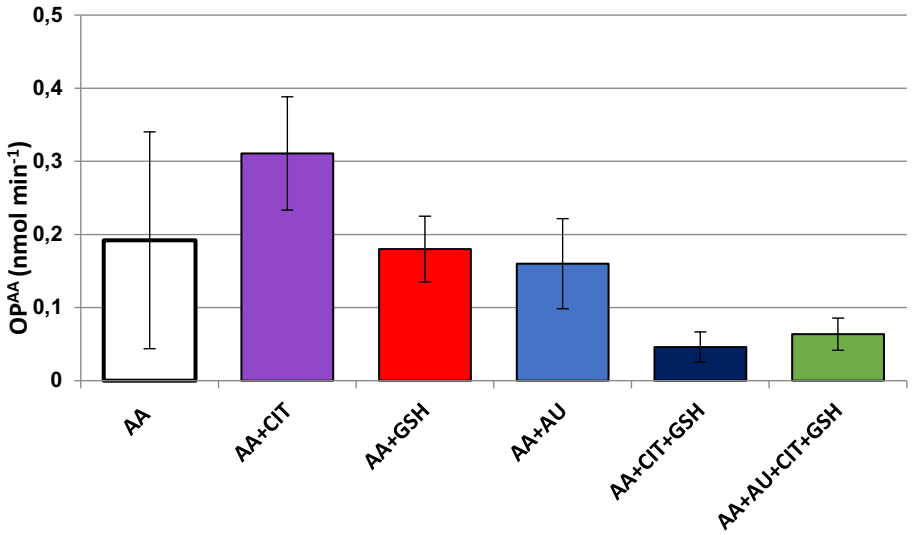

Figure 14. OP^{AA} responses (nmol min^{-1} m^{-3}) of Fe^{2+} in six different RTLF surrogates.

This may be ascribed to the dominant presence of the Fe-Citrate complex, which has been found to increase the Fe^{2+} reactivity and effectively promote the Fenton reaction.

GSH doesn't significantly change OP^{AA}, which is consistent with the fact that GSH doesn't change the Fe speciation (Vidrio et al., 2008).

Otherwise, uric acid leads to a decrease of OP^{AA} by 17%. It can be explained by the formation of stable coordination complexes Fe-urate that inhibits the catalyzed ascorbate oxidation (Charrier et al., 2011).

The concomitant addition of one or two more AOs further inhibits the Asc oxidation generating lower OP^{AA} (~70%).

Also for the three investigated quinones we found that the change of the antioxidant mixture affects the OP^{AA} responses: compared to Asc solution, the addition of citrate or urate significantly ($p<0.05$) decreases OP^{AA} of about 40%, while increased GSH of 70%.

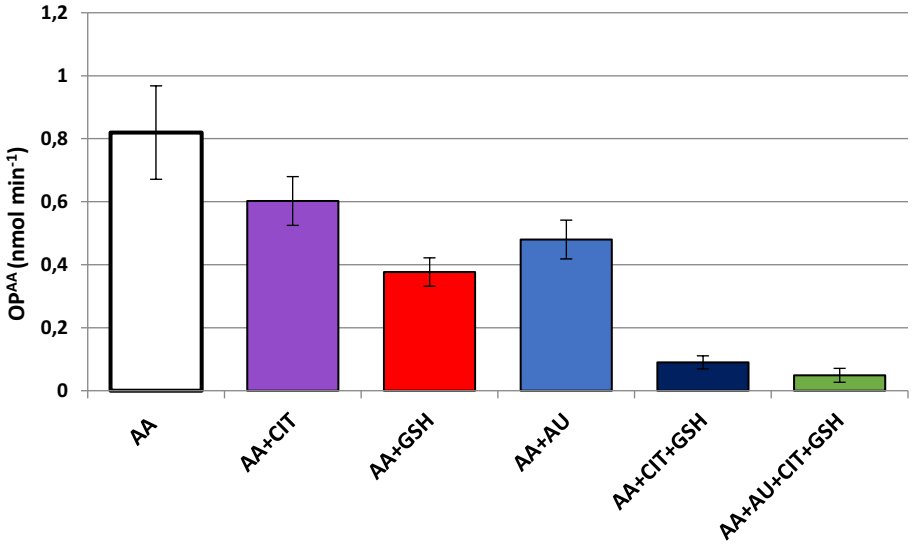

Figure 15. OP^{AA} responses (nmol min^{-1} m^{-3}) of 9,10-PQN in six different RTLF surrogates.

The combination of Cit and GSH generates a drastic OP^{AA} reduction close to 90%, nearly independently of the presence of UA.

In addition to the general explanation of the concomitant contribution of GSH and UA antioxidants to increase RTLF antioxidant strength, it is difficult to understand the reason of such a surprisingly strong effect on quinones, in comparison with that on metals, where additional mechanisms involving the formation of metal complexes can be invoked (Charrier et al., 2014).

Inside such variations, the reactivity hierarchy of the individual compounds is kept constant in all the investigated assay setups, as follows:

$$Cu^{2+} > 1{,}2\ NPQ \gg 9{,}10\ PQN > 1{,}4\ NPQ \sim Fe^{2+}$$

4.2.2 Effect of different setups of Ascorbic Acid a-cellular assay on $PM_{2.5}$ samples

As an initial step, the OP^{AA} values were measured for each $PM_{2.5}$ extract using the simple Asc solution as the reductant.

The measured AA activity is inside the typical range observed for fine particles collected at sites with different source characteristics, i.e., ~0.2–2.0 nmol min^{-1} m^{-3}.

From the obtained data, the mean and S.D. values were computed for all samples and grouping urban (URB, n=10) and rural (RUR, n=10) samples, separately.

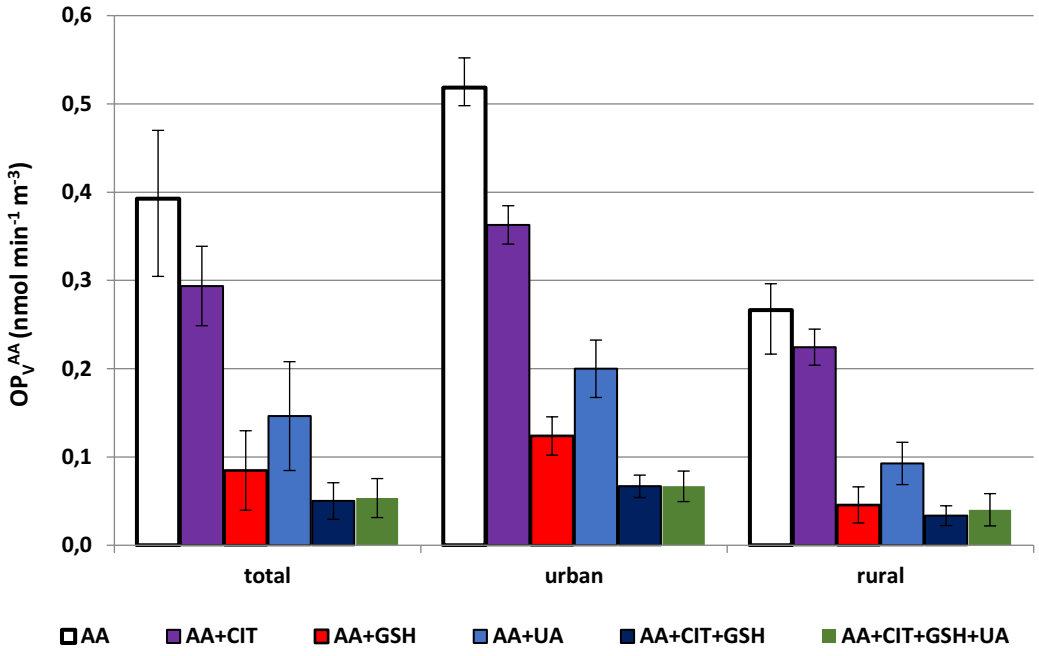

Figure 16. OP^{AA} response (nmol min^{-1} m^{-3}) measured in different RTLF surrogates of PM$_{2.5}$ real samples: bars represent the mean values, error bars are one standard deviation computed from 20 investigated samples (total), from 10 samples at urban (URB) and 10 samples at rural (RUR).

The Student's t-test showed that the OP^{AA} responses measured in Bologna (0.52 ± 0.09 nmol min^{-1} m^{-3}) are significantly higher than those at the rural site (0.27 ± 0.06 nmol min^{-1} m^{-3}). As values of PM$_{2.5}$ concentration mass are similar at both sites in the sampling period (mean value 15 ± 7 μg m^3), this difference may be explained by the variation of the chemical composition of PM$_{2.5}$.

In the city it can be expected a higher impact from anthropogenic source emissions, yielding pollutant accumulation, as a consequence of the stagnant atmospheric conditions in the cold season. (Perrone, Zhou, et al., 2016)(Pietrogrande et al., 2016).

Then, the complexity of the assay solution was increased by adding individually or in combination three endogenous antioxidants i.e., citrate, urate, glutathione (Charrier et al., 2011)(Charrier et al., 2014).

The data measured in the five different synthetic RTLFs are reported individually for each PM$_{2.5}$ sample in Appendix, Table A9-A10, and summarized in Table A11 (including the filter blank responses, mean values ± S.D., n≥5), and Figure 16 as mean values (total and urban and rural samples, separately).

The obtained results clearly show that the measured OP^{AA} values are significantly changed ($p<0.05$) by the composition of the synthetic RTLFs since they are lower when other antioxidants are added to ascorbate (Figure 16).

The strength of each experimental set up in reducing OP^{AA} response can be quantified by computing the relative percentage decrease of the measured value with respect to that in the simplified AA solution ($\%OP^{AA}$).

These variations were calculated in all RTLFs for each $PM_{2.5}$, from which the mean values were computed for all urban and rural samples, separately (Appendix, Table A11).

Among the investigated components, GSH is the most effective, since it yields a mean OP^{AA} decrease of 79 ± 6%, followed by urate (mean $\%OP^{AA}$: 63 ± 5%) and citrate (mean %OPAA: 20 ± 10%).

Furthermore, the combination of both Cit and GSH antioxidants synergistically inhibits the AA oxidation (87 ± 3%), while the further addition of UA doesn't significantly change OP^{AA} (Figure 16).

The same trend is observed for all the analysed samples so that OP^{AA} response follows the general order:

$$Asc > Asc + Cit > Asc + UA > Asc + GSH > Asc + Cit + GSH \sim Asc + Cit + GSH + UA$$

Inside such variations, in all the different assay conditions OP^{AA} values of URB samples are significantly higher ($p<0.05$) than those at RUR site, except for Asc + Cit + GSH + UA mixture.

To investigate the effects of each synthetic RTLF in detail, for each $PM_{2.5}$ sample the OP^{AA} responses in the different solutions were correlated with those in the Asc solution (Figure 17).

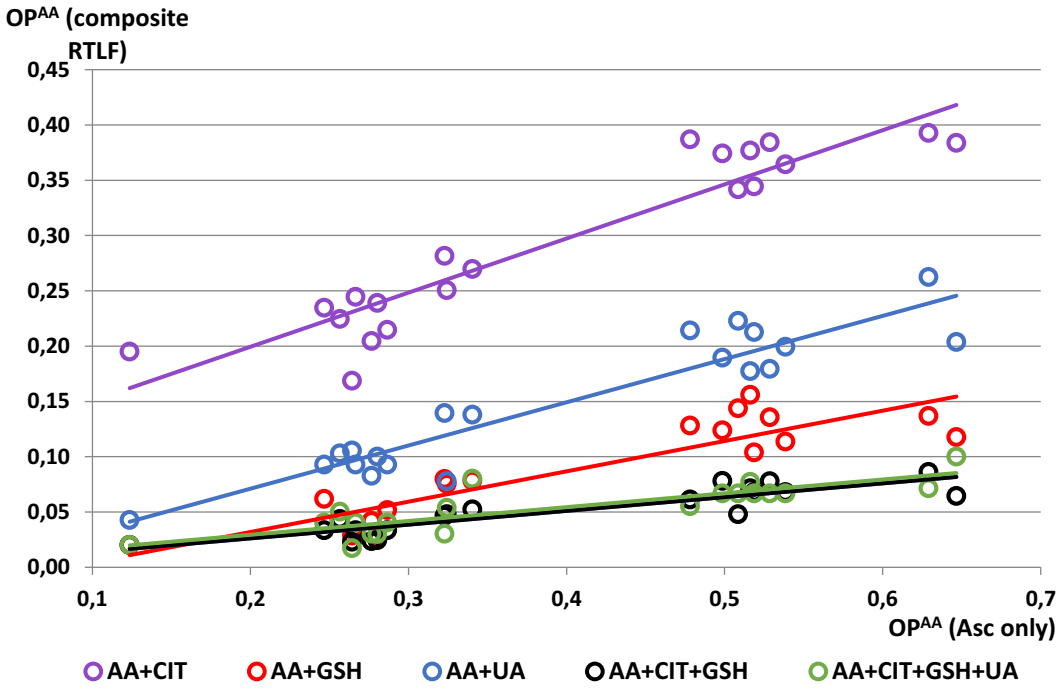

Figure 17. OP^{AA} responses (nmol min^{-1} m^{-3}) of 20 $PM_{2.5}$ real samples: relationship of OP^{AA} values measured in the different RTLF surrogates with those in Asc solution.

In general, a good linear relationship was obtained for each dataset ($R^2 \geq 0.8$), indicating that the effect of the various RTLF surrogates on OP^{AA} responses is similar for all the samples. This suggests that all the tested assay setups are useful for OP^{AA} assessment.

However, for each sample, the use of composite RTLFs generates lower OP^{AA} responses with lower variation range, which means less sensible measurements.

This is indicated by the slopes of the computed straight lines, which are always lower than 1, following the order:

$$Asc + Cit\ (slope: 0.5 \pm 0.2) > Asc + UA\ (slope: 0.4 \pm 0.2) > Asc + GSH\ (slope: 0.3 \pm 0.1)$$
$$> Asc + Cit + GSH \sim Asc + Cit + GSH + UA\ (slope: 0.1 \pm 0.1)$$

This means that, concerning Asc solution, the addition of citrate and urate reduces the assay responses by about two times, while that of GSH of three times.

Furthermore, when two or more AOs are combined, the OP^{AA} responses are decreased even by 10 times. Such a reduction is combined with the decrease of the measurement precision.

Therefore, among the tested RTLF surrogates, the simplified Asc solution provides the most sensible and precise measure of OP^{AA}.

However, such a sensibility may be detrimental to a realistic representation of the particle-lung interactions, as simpler RTLF surrogates are more different from the complex antioxidant mixtures of lung lining fluid.

Also, some differences may be expected in comparison with the simplified assumption of the additive contribution of each antioxidant, as a consequence of concurrent reactions between antioxidants and reductants.

Overall, these results can be explained by the increase of the mixture antioxidant strength due to the concomitant contribution of GSH and UA antioxidants, in addition to Asc. The higher reactivity of GSH is consistent with the lower oxidation-reduction potential for the glutathione/glutathione disulfide system, ranging from −0.17 to −0.27 V under various physiological conditions (Millis et al., 1993), in comparison with the higher values of +0.105 V for the ascorbic/dehydroascorbic acid couple (Merkofer et al., 2006).

Therefore, GSH strongly promotes the AA oxidation, as it likely acts as a sacrificial antioxidant (Charrier et al., 2011)(Charrier et al., 2014)(Weichenthal et al., 2016).

This is consistent with the well known strong antioxidant properties of GSH in vivo, as reported by several toxicological studies (i.e., (Crobeddu et al., 2017)(Hellack et al., 2017)(Maikawa et al., 2016)).

4.2.2.1 *Comparison of OP^{AA} for ambient samples and standards redox-active*

To identify the chemical components of $PM_{2.5}$ samples mainly responsible for the effects of the various antioxidants in RTLF on OP^{AA} responses was compared the relative $\%OP^{AA}$ variation in each synthetic RTLF of ambient $PM_{2.5}$ with that of the species (Appendix, $\%OP^{AA}$ mean values in Table A7-A8 and Table A11).

In general, a good linear correlation ($R^2 \geq 0.75$) was found between $PM_{2.5}$ and all the investigated species, confirming that they all are responsible for OP^{AA} responses of the $PM_{2.5}$ samples (Figure 12).

In particular, Cu^{2+} and quinones appear to display nearly the same dependence on RTLF composition, as proved by the slope of straight lines close to 1, i.e., 0.95 ± 0.1 for Cu^{2+} and 0.89 ± 0.2 to 1.1 ± 0.3 for quinones, respectively.

Otherwise, the Fe^{2+} solution displays a nearly double sensitivity to the variation of RTLF compositions than $PM_{2.5}$ samples, as the best fitting straight line ($R^2=0.85$) has a slope of 1.8 ± 0.2 (orange line in Figure 18).

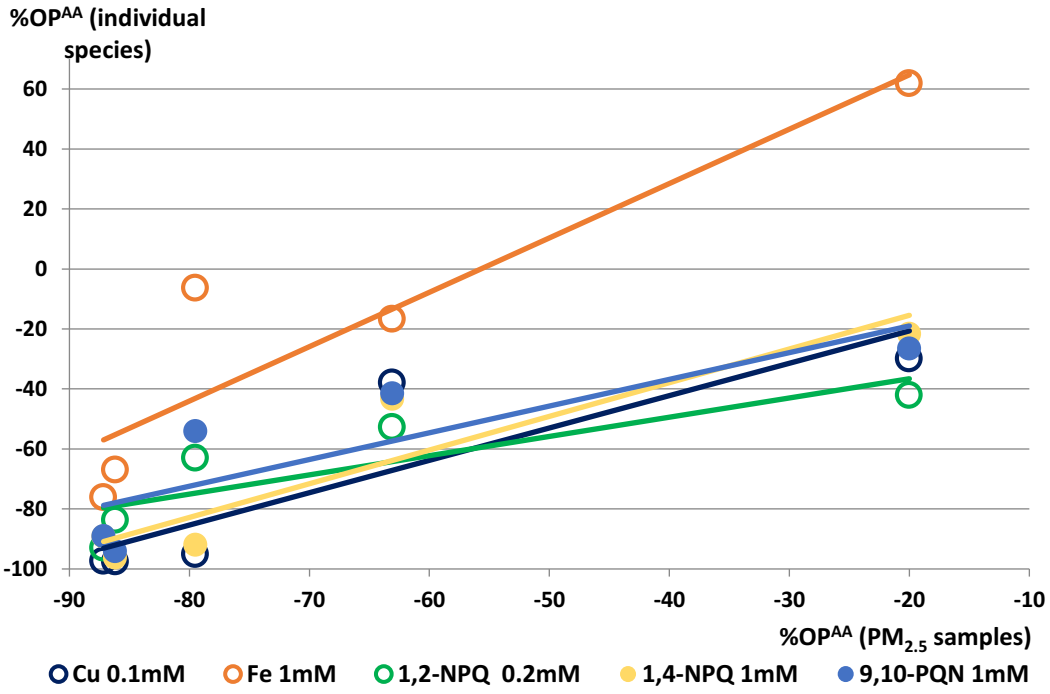

Figure 18. Relative % variation of OP^{AA} responses ($\%OP^{AA}$) measured in different RTLF surrogates concerning those in simplified Asc solution: relationship between $\%OP^{AA}$ of ambient samples (mean value of the 20 $PM_{2.5}$ samples) with those of individual redox-active species.

From these results, the variation of $PM_{2.5}$ OP^{AA} response in the different RTLFs is mainly generated by quinones and copper.

Accordingly, the addition of GSH mostly decreased the OP^{AA} measured values (79% for $PM_{2.5}$ and 95% and 92% for Cu^{2+} and 1,4-NPQ, respectively), followed by urate (63% for

$PM_{2.5}$ and 53% and 43% for 1,2-NPQ, and 1,4-NPQ, respectively) and by citrate (20% for $PM_{2.5}$ and 22% and 27% for 1,4-NPQ and 9,10-PQN, respectively).

Such a predominant contribution of quinones and Cu^{2+} to $PM_{2.5}$ oxidative properties is in agreement with results found in several past studies (Charrier and Anastasio, 2015) (Chung et al., 2006)(Crobeddu et al., 2017)(Janssen et al., 2015)(Jianget al., 2018)(Lyu et al., 2018)(Tuet et al., 2017b)(Shen et al., 2012).

However, this is only an approximated explanation, since it is well known that behaviour of individual species poorly represent the complex chemistry of ambient PM, where components may synergically interact to contribute to ROS production (Yu et al., 2018).

In addition, some studies report that many trace metals and quinones are covariates, which confounds identifying the redox-active species responsible for ROS generation (Charrier et al., 2014).

4.3 Comparison between AA and DTT and in vivo cells oxidation in the presence of PM components

Although these surrogate systems are frequently applied to predict PM biological effects, there is still a gap of knowledge about the associations between the oxidative potential results obtained using these assays and health endpoints (Fang et al., 2016).

In order to assess the possible mechanisms involved in the proinflammatory process, was evaluated the role of oxidative stress in mediating PM-induced skin damage by investigating the effects of specific redox-active species that have been demonstrated mostly responsible for PM-induced ROS generation.

To more fully understand the ROS reactivity of the individual species, we performed two acellular assays (DTT and AA assays) and the responses were compared with the biological responses of human keratinocyte (HaCaT) cells after treatment with these PM components.

In particular, four redox-active chemicals were investigated, such as Cu (II) metal and quinones generated from polycyclic aromatic hydrocarbons (PAHs), i.e., 9,10 phenanthrenequinone and isomers 1,2 and 1,4 naphthoquinone.

Further toxicity tests have confirmed the important role of PM composition, showing contrasting results when acellular oxidative potential (OP) data have correlated with the outcomes of in vitro (or in vivo) toxicological tests.

These results suggest that the health endpoints depend on PM chemical composition and not only on exposure concentrations (Lionetto et al., 2019).

In this thesis, the biological analysis has carried out by Professor Cervellati and Professor Valacchi from the Department of Medical and Surgical Sciences and Neurosciences at the University of Siena.

4.3.1 Responses assays of DTT and AA assays to PM redox-active

In general, the OP responses are proportional to the species concentration, and the slope of each computed regression line is a measure of the species reactivity toward DTT or AA oxidation. The only exception is OP^{DTT} response for 9,10-PQN, as the response-concentration function is linear only in a limited concentration range up to 1 mM, as found by other Authors (Charrier et al., 2012). Although all the investigated quinones and Cu are reactive to both assays, they show different sensitivity.

Based on our results on DTT assay, we can observe that 9,10-PQN is by far the most reactive species, as the slope computed in the 0.25 - 1 mM range is nearly 10 times higher than that of the other species, that display similar reactivity.

Then, the relative reactivities follow the order:

$$9{,}10\ PQN \gg 1{,}2\ NPQ > 1{,}4\ NPQ \sim Cu(II)$$

Otherwise, 1,2-NPQ and Cu are the most active species towards the AA assay, across the entire range of concentrations tested, followed by 1,4-NPQ and 9,10-PQN, which show lower reactivity with similar values.

Then, the relative reactivities of the AA assay are the following:

$$1{,}2\ NPQ \sim Cu(II) \gg 1{,}4\ NPQ \sim 9{,}10\ PQN$$

4.3.2 Association of OP responses with cellular endpoints

In this study, we observed that treating human keratinocytes with Cu (II), 9,10-PQN, 1,2- and 1,4-NPQ stimulates the inflammatory response in HaCaT cells.

The biological responses were evaluated by cellular morphological alterations and the biochemical effects analyzing genic and protein expression (Hedayat et al., 2015).

Since alterations in the cellular inflammatory state can result in oxidative stress, was investigated whether treatment with the PM constituents altered transcript levels of genes involved in the cellular redox balance (Schäfer et al., 2015) and, if could also cause ultrastructural damage to the exposed cells and observed structural alterations of mitochondria (Leni et al., 2020).

Altogether, the results consistently indicate that all of the tested PM components induce inflammation and a redox-imbalance.

In particular, we can observe that 9,10 PQN, which is the species with the highest OP^{DTT} response, is the only one which significantly increased LDH release and also induced dilatation and vacuolization of mitochondria, together with Cu (II), with a high OP^{AA} response, while 1,2 NPQ, with the highest OP^{AA}, induced mitochondrial shrinkage and condensation.

Indeed, these are partial and preliminary results, that require further experimental evidence to highlight the possible associations of the acellular assay responses with biological findings elicited by exposure to redox-active species.

The data showed that, although chemically different, all the investigated redox-active PM components were able to induce a proinflammatory status and the activation of the cellular defensive system, suggesting a common mechanism of action among these species.

In addition, due to the variability of OP responses in relation to biological effects, further studies will be conducted to investigate the different particle characteristics, which may act as critical determinants for different toxicological effects (Øvrevik, 2019), suggesting the existence of a variety of triggering mechanisms.

5. $PM_{2.5}$ and PM_{10} oxidative potential at a Central Mediterranean Site: Contrasts between dithiothreitol- and ascorbic acid-measured values in relation with particle size and chemical composition

This chapter summarizes the content of the study published in Atmospheric Environment (2019), 210, 143-155, DOI: 10.1016/j.atmosenv.2019.04.047.

Inside the research activity devoted to the investigation of real PM samples, this study concerned $PM_{2.5}$ and PM_{10} samples collected in Lecce, a suburban site in the Central Mediterranean, in different seasons.

The oxidative properties were assessed with both DTT and AA assays and the impact of size-distribution and chemical composition on OP^{DTT} and OP^{AA} responses has been investigated.

Relevant information on the specific contribution of the various chemical species and/or the pollution sources could be identified, because of the peculiarity of the study site, which is strongly impacted by long-range-transported particles from different sources, and the monitoring campaign duration all over the year.

In addition, the comparison between the DTT and AA responses clearly highlighted that the two assays contrast in terms of towards individual redox-active species/sources.

5.1 Sampling site and period

$PM_{2.5}$ and PM_{10} samples were simultaneously collected in a suburban site (40.3°N; 18.1°E) of the flat Salento's peninsula, in the Central Mediterranean, which is impacted by different sources, because of the contributions of long-range transported air masses from the surrounding regions (Perrone et al., 2014a)(Perrone et al., 2014b)(Becagli et al., 2017)(Chirizzi et al., 2017).

Thirty-nine $PM_{2.5}$ filters collected from 5th December 2014 until 12th October 2015 have been analysed: more specifically, 24 samples from April to September (Spring-Summer, SS) and 15 in October–March months (Autumn-Winter, AW).

Sampling was performed with a low volume (2.3m^3 h^{-1}) HYDRA-FAI dual-sampler that made it possible to simultaneously collect $PM_{2.5}$ and PM_{10} granulometric fractions using two independent sampling lines.

Note that the PM_{10} samples of this study were included in a more extended study devoted to 53 PM_{10} filters, as previously reported in (Pietrogrande et al., 2018a).

For each sampling day, $PM_{2.5}$ and PM_{10} samples were simultaneously collected and analysed to investigate the variation of the OP activity (DTT and AA assays) with the particle size and chemical composition (Visentin et al., 2016)(Pietrogrande et al., 2018a)(Pietrogrande et al., 2018b).

5.2 $PM_{2.5}$ mass concentration and chemical composition

The $PM_{2.5}$ and PM_{10} loaded filters were divided into four punches for the determination of ions, metals, organic and elemental carbon, and the oxidative potential.

The chemical composition of $PM_{2.5}$ particles was characterized in detail for more than 30 species, including ions − Na^+, NH_4^+, K^+, Mg^{2+}, Ca^{2+}, Cl^-, NO_2^-, NO_3^- and SO_4^{2-} − metals – Al, Ba, Cd, Ce, Co, Cr, Cu, Fe, La, Mn, Mo, Ni, Pb, Sr, Ti, V and Zn – and organic components, – OC and EC, methanesulfonate ion (MS−) and carboxylic ions.

The measured $PM_{2.5}$ mass concentrations are reported in Appendix, Table A12 as the mean values and corresponding standard errors of the mean (SEM) computed for autumn-winter (AW, 15 days) and spring-summer (SS, 24 days) data, separately.

Such a grouping is motivated by the season dependence of the PM mass concentration and chemical composition at the study site, as reported in previous studies (e.g., (Perrone et al., 2014a)(Perrone, Genga, et al., 2016)(Pietrogrande et al., 2018a)).

The two-tail t-test was applied to the mean AW and SS values to assess their statistical difference at $p<0.05$ significance level (values marked by * in Table A12).

The mean $PM_{2.5}$ mass concentration varied weakly with seasons being 26 ± 2 and 20 ± 1 μg m^{-3} in AW and SS, respectively.

This result may be related to the weak dependence on seasons of the planetary boundary layer (PBL) depth in the study area, as reported in previous studies (Perrone, Becagli, et al., 2013)(Perrone et al., 2018).

OC was discriminated between primary (POC) and secondary organic carbon (SOC) by using the OC/EC ratio approach (Pio et al., 2011).

The mass percentages due to metals and to MS− and carboxylic ions have been grouped in Met and Oxi, respectively.

Among the analysed species, the carbonaceous compounds are the major components.

SO_4^{2-}, NO_3^-, NH_4^+ and K^+ are by far the most abundant inorganic ions, while metals are minor components.

The higher levels of EC, POC, NO_3^-, and K^+ in AW than in SS can be related to the stronger contribution from residential heating in the cold season.

The greater mass concentration of Na^+, NH_4^+, Mg^{2+}, Ca^{2+}, SO_4^{2-}, and SOC in SS than in AW may be related to the meteorological conditions occurring in SS over the Mediterranean, mainly the formation of secondary particles favoured by the large solar irradiance and the dust resuspension because of the lack of rainy days (e.g. (Perrone, Becagli et al., 2013)(Perrone et al., 2014a)).

5.3 $PM_{2.5}$ and PM_{10} samples: comparisons between mass concentrations and chemical components

The $PM_{2.5}$ chemical composition was compared with that of the simultaneously collected PM_{10} samples, which are a subset of the overall data reported in (Pietrogrande et al., 2018a).

The mean PM_{10} mass concentration was 34 ± 3 and 28 ± 2 μg m^{-3} in AW and SS (Appendix, Table A12), confirming the prevalent contribution of fine particles at the study site, i.e., $PM_{2.5}$ accounted for 77 and 70% of the PM_{10} mass, in AW and SS, respectively (Perrone, Becagli, et al., 2013)(Perrone et al., 2014a).

Accordingly, the distribution of all the investigated chemical species showed the same seasonal trend in PM_{10} as in $PM_{2.5}$ fractions (Pietrogrande et al., 2018a).

In particular, carbonaceous compounds showed similar concentration in both fractions being accumulated in the fine PM (Jaafar et al., 2014)(Lovett et al., 2018).

Accordingly, the OC/EC ratios computed in both PM fractions were similar in SS and AW, respectively (Table A12) (Waked et al., 2014).

In addition, SO_4^{2-} and organic secondary ions have similar concentrations in both fractions, as they preferentially concentrate in the accumulation mode due to their secondary nature (Daher et al., 2014).

Conversely, the NO_3^- ion showed a size distribution with a higher concentration in PM_{10} than in $PM_{2.5}$, as previously found in most coastal sites of the southern Mediterranean Basin (e.g., (Bardouki et al., 2003)(Pérez et al., 2008)).

Nitrate particles are the result of nitric acid/ammonia reactions with Na^+ (tracers of sea salt aerosol), Mg^{2+} and Ca^{2+} (crustal tracers of soil resuspension), leading to twice concentration

in PM_{10} compared with $PM_{2.5}$, which is consistent with the nature and size of these particles (Hasheminassab et al., 2014).

Looking at the $PM_{2.5}$ fraction, there is a decrease of nitrate contribution during the warm seasons (spring and summer) because of its thermal instability and likely for the lower NOx emissions of traffic and biomass burning during the warm period in most of the Central Mediterranean sites (Querol et al., 2008)(Cesari et al., 2018).

As expected, also metal species are accumulated in the coarse fraction, i.e., Al, Ba, Ce, Cu, Fe, with Fe, Zn and Cu as the dominant metal species (Lyu et al., 2018)(Pant et al., 2015)(Shirmohammadi et al., 2017).

5.4 Oxidative potential of $PM_{2.5}$ samples

Overall, the OP^{DTT}_V responses were higher than the OP^{AA}_V ones in both seasons. More specifically, in AW, the mean OP^{DTT}_V value was 0.29 ± 0.03 nmol min^{-1} m^{-3} and the mean OP^{AA}_V value was 0.21 ± 0.03 nmol min^{-1} m^{-3}.

In SS, the difference was larger, with OP^{DTT}_V responses of 0.19 ± 0.02 nmol min^{-1} m^{-3} and OP^{AA}_V of 0.09 ± 0.01 nmol min^{-1} m^{-3}.

In general, our results are towards the lowest end of the range of values reported in literature for $PM_{2.5}$ particles, being the study site away from large sources of local pollution. This may represent a peculiarity of the results reported, as most of the literature data concern OP at large urban and/or polluted sites.

Oxidative Potential	Autumn-Winter				Spring-Summer			
	PM_{10}		$PM_{2.5}$		PM_{10}		$PM_{2.5}$	
	Mean	SEM	Mean	SEM	Mean	SEM	Mean	SEM
OP^{AA}_V ($nmol^{AA}$ min^{-1} m^{-3})	**0.35**	0.06	**0.21***	0.03	**0.23**	0.04	**0.09***	0.01
OP^{DTT}_V ($nmol^{DTT}min^{-1}$ m^{-3})	0.24	0.04	0.29*	0.03	0.22	0.02	0.19*	0.02
$OP^{AA}m$ ($nmol^{AA}$ min^{-1} μg^{-1})	0.010	0.002	0.008*	0.001	**0.008**	0.001	**0.005***	0.001
$OP^{DTT}m$ ($nmol^{DTT}$ min^{-1} μg^{-1})	**0.007**	0.001	0.011	0.001	0.008	0.001	0.010	0.001

*Table 3. Volume- (OP_V) and mass-normalized (OP_m) Oxidative Potential responses measured for PM_{10} and $PM_{2.5}$ with DTT and AA assays: mean values and standard errors of the mean (SEMs) computed for AW and SS data, separately. Values with significant ($p<0.05$) differences between the seasons are marked by * and those with significant ($p<0.05$) differences between the PM_{10} and $PM_{2.5}$ fractions are reported in bold.*

In general, the two assays displayed similar sensitivity to the studied $PM_{2.5}$ samples (Table 3), as proved by the significant correlation ($p<0.01$) between OP^{DTT}_V and corresponding OP^{AA}_V responses in both seasons ($r = 0.91$ and $r = 0.70$, for AW and SS, Table A13).

This is in agreement with some results reported in literature (e.g., (Janssen et al., 2014)(Mudway et al., 2004)).

But, it is in contrast to other papers reporting different sensitivity of the two assays towards the same redox-active species (Calas et al., 2018)(Fang et al., 2016)(Szigeti et al., 2016)(Weber et al., 2018).

Indeed, the specific sensitivity of OP^{DTT} and OP^{AA} responses is still an open question.

Despite the similarity of the mean OP^{DTT}_V and OP^{AA}_V responses (Table 3) and the overall good correlation between the data, the individual OP^{DTT}_V and OP^{AA}_V values largely varied day-by-day with different behaviour for the same sample.

Such a large variability may be likely ascribed to the day-by-day change of the $PM_{2.5}$ concentration/composition, because of the impact at the study site of long-range transported particles from the surrounding regions.

The comparison of the OP^{DTT}_V and OP^{AA}_V values with the corresponding $PM_{2.5}$ mass concentrations revealed that high OP_V values were associated with high $PM_{2.5}$ mass concentrations, indicating that the OP_V responses were extensive parameters dependent on $PM_{2.5}$ mass concentration.

This is described by the good linear correlation ($p<0.001$) of both the OP^{DTT}_V and OP^{AA}_V values with the $PM_{2.5}$ mass: the Pearson correlation coefficients are 0.79 and 0.63 ($p<0.001$) for OP^{DTT}_V in AW and SS respectively, and 0.82 ($p<0.001$) for OP^{AA}_V in AW.

Consistently, the OP^{DTT}_m response was nearly constant through the investigated period, with a mean value of 0.010 ± 0.001 nmol min^{-1} μg^{-1} (Table 3).

The OP^{AA}_V values were less significantly ($r = 0.47$, $p<0.002$) correlated with the $PM_{2.5}$ mass in SS. Therefore, the mean OP^{AA}_m responses changed through the year, with significantly higher values in AW (0.008 ± 0.001 nmol min^{-1} μg^{-1}) compared with SS (0.005 ± 0.001 nmol min^{-1} μg^{-1}).

As OP responses were measured over a full year, the OP seasonal trend was investigated and related to the particle chemical composition.

Significantly higher OP^{DTT}_V and OP^{AA}_V responses were measured in the cold than in warm seasons, as supported by a two-tail t-test on AW and SS mean values (significant differences at $p<0.05$ level are marked by * in Table 3).

More specifically, the average OP^{DTT}_V and OP^{AA}_V values were 1.5 and 2.3 times higher in the cold period than in the warm period, respectively.

Such a seasonality of OP^{DTT}_V and OP^{AA}_V values has been also observed in other studies for ambient $PM_{2.5}$ samples and related to seasonal changes of the PM chemical composition (Verma et al., 2015)(Weber et al., 2018)(Visentin et al., 2016).

5.4.1 Association of the oxidative potential with chemical components/sources

To identify the $PM_{2.5}$ chemical components, and hence the pollution sources driving ROS activity, the association between the OP^{DTT}_V and OP^{AA}_V responses and the concentrations of chemical species was investigated by correlation analysis.

The Pearson correlation coefficient (r) was computed for each investigated component for AW and SS, separately, and reported in Appendix Table A13 (r values significant at $p<0.05$ level are in bold).

In the cold season, both OP responses were widely correlated with several species, namely, K^+ and NO_3^-, several metals (Ba, Cd, Cu, Fe, Mn, P, V), and carbonaceous species (OC, EC, Acetate, Oxalate and Glycolate). In SS samples OP showed a significant correlation with only a few species, i.e., NO_3^-, Cu, OC and EC.

Besides, the inter-correlation among the analysed species was investigated to highlight the association among common emission sources and/or secondary processes (correlation coefficient r reported in Appendix, Tables A14 and A15 for AW and SS, respectively).

One observes that in AW all the species highly correlated with OP^{DTT}_V and/or OP^{AA}_V also showed a significant inter-correlation.

In SS, the species NO_3^-, Cu, OC and EC were highly inter-correlated, but their correlation with K^+, Ba, Cd, Fe, Mn, P, V, OC, Acetate, Oxalate and Glycolate was rather weak (Table A15).

These results are consistent with several literature data on $PM_{2.5}$, that report the dominant contribution to OP_V of carbon components from biomass combustion (Mugica et al., 2009)(Zhang et al., 2017)(Styszko et al., 2017) as well as of traffic-related metals, such as road dust components, vehicular abrasion metals and fuel oil combustion emissions (Crobeddu et al., 2017)(Moreno et al., 2017)(Lyu et al., 2018)(Shafer et al., 2016).

5.4.2 OP^{DTT} and OP^{AA} responses for $PM_{2.5}$ and PM_{10} fractions

The variation of the OP activity in $PM_{2.5}$ and PM_{10} fractions was investigated about the PM chemical composition/source.

The $PM_{2.5}$ results were compared with the PM_{10} data obtained from the previous work of (Pietrogrande et al., 2018a). Table A12 reports the mean ± SEM concentration values for the same data subset.

The DTT assay produced similar responses for both size fractions, i.e., 0.24 ± 0.04 and 0.29 ± 0.03 nmol min^{-1} m^{-3} in AW, and 0.22 ± 0.02 and 0.19 ± 0.02 nmol min^{-1} m^{-3} in SS, for PM_{10} and $PM_{2.5}$ particles, respectively.

This likely suggests that this assay is mainly associated with redox-active species accumulated in the fine fraction.

Otherwise, the AA assay exhibited a clear particle-size dependence, as OP^{AA}_V responses were significantly higher for PM_{10} than for $PM_{2.5}$, i.e., 0.35 ± 0.06 vs. 0.21 ± 0.03 nmol min^{-1} m^{-3} in AW and 0.23 ± 0.04 vs. 0.09 ± 0.01 in SS (Table 3, bold values).

This suggests that AA depletion is more affected by species present in coarse particles, especially by those generated by vehicular traffic, such as brake abrasion and re-suspended dust (Simonetti et al., 2018b).

Concerning the association of OP^{DTT}_V and OP^{AA}_V responses with PM_{10} components, data in Table A13 show that in AW both responses were significantly correlated with K^+, Ba, Cd, Fe, OC, and EC, which are markers of the "mixed anthropogenic" source, as found for $PM_{2.5}$ particles.

Besides, OP^{AA}_V responses were also significantly correlated with metals − Cr, Cu, Mn, V – and some organic compounds − MS−, acetate, glycolate, propionate, formate, and pyruvate − that are components of the "heavy oils/secondary marine" source.

In SS, the association of OP_V responses with chemical components significantly varied with both the OP assay and PM fraction, as shown in Table A13, because of the changes with seasons of the pollution source contributions.

In PM_{10}, the OP^{DTT}_V responses were correlated with NH_4^+, Cu, OC, EC, oxalate, and glycolate, which species were mainly associated with the biomass-burning component of the "mixed anthropogenic" source.

Note that in SS the Mediterranean basin is a worldwide wildfire hotspot due to the occurrence of a huge number of wildfires. The PM_{10} OP^{DTT}_V response was also associated in SS with the "sulphate" source of which NH_4^+ is a maker.

Otherwise, the PM_{10} OP^{AA}_V responses were correlated with more species, namely NH_4^+, K^+, Ca^{2+}, SO_4^{2-}, MS−, Mn, Ni, P, Ti, V, oxalate, and glycolate.

The dominant species of the "sulphate" source were NH_4^+ and SO_4^{2-}, while V, Ni and MS− were the main components of the "heavy oil/secondary marine" source, and Ca^{2+}, Mn, and Ti contributed to the "soil dust" source.

Therefore, the PM_{10} OP^{AA}_V responses were likely associated with the above-mentioned sources, whose contribution has almost doubled from AW to SS (Appendix, Table A12).

The negligible correlation of the OP^{AA}_V responses with OC and EC was likely responsible for the significant OP^{AA}_V decrease from 0.35 ± 0.06 to 0.23 ± 0.04 nmol min^{-1} m^{-3} from AW to SS (Table 3), being OC and EC the main species contributing to the PM_{10} mass.

5.4.3 Regression analysis of the OP^{DTT} and OP^{AA} responses with individual species

To further highlight the sensitivity of the two OP assays to various PM components, regression analysis was applied to describe OP^{DTT}_V and OP^{AA}_V responses as a function of the chemical species.

Linear regressions were computed for species in the $PM_{2.5}$ and PM_{10} samples for AW and SS data, separately. Among the obtained equations, the parameters of those of the most abundant and/or well correlated ($R^2 \geq 0.4$) components are reported in Table 4 (intercept, slope, linear correlation coefficient, R^2, and chi-square (χ^2) values to test the goodness of the fit). Therefore, the results of the linear regressions will be discussed in the following.

Species	OP^{AA}_V			OP^{DTT}_V		
	Intercept	Slope	$R^2(\chi^2)$	Intercept	Slope	R^2
PM^{10} AW						
EC	0.11±0.08	0.07±0.02	0.50 (0.31)	0.08±0.04	0.05±0.01	0.59 (0.11)
POC	0.11±0.09	0.03±0.02	0.50 (0.31)	0.08±0.04	0.02±0.01	0.59 (0.11)
K^+	0.10±0.09	0.45±0.02	0.41 (0.37)	0.08±0.05	0.31±0.09	0.49 (0.11)
Cu	0.02±0.07	31±6	0.71 (0.18)	-	-	-
Fe	0.03±0.05	1.7±0.4	0.58 (0.27)	-	-	-
$PM_{2.5}$ AW						
EC	0.04±0.03	0.05±0.01	0.74 (0.06)	0.14±0.03	0.05±0.01	0.71 (0.06)
POC	0.04±0.04	0.025±0.004	0.74 (0.06)	0.14±0.05	0.022±0.004	0.69 (0.06)
K^+	0.04±0.04	0.30±0.07	0.62 (0.09)	0.14±0.04	0.25±0.06	0.53 (0.09)
NO_2^-	-	-	-	0.15±0.05	0.13±0.04	0.44 (0.11)
Cu	0.13±0.04	10±3	0.41 (0.13)	-	-	-
Fe	0.01±0.01	1.4±0.3	0.58 (0.11)	0.12±0.04	1.6±0.3	0.74 (0.07)
PM_{10} SS						
EC	-	-	-	0.07±0.04	0.09±0.02	0.40 (0.13)
POC	-	-	-	0.07±0.04	0.04±0.01	0.38 (0.13)
Cu	-	-	-	0.09±0.04	18±7	0.27 (0.13)
Ca^{2+}	0.00±0.09	0.24±0.08	0.27 (0.67)	-	-	-
SO_4^{2-}	-0.11±0.08	0.09±0.02	0.71 (0.45)	-	-	-
$PM_{2.5}$ SS						
EC	-0.03±0.03	0.08±0.02	0.56 (0.04)	0.03±0.02	0.10±0.01	0.53 (0.07)
POC	-0.03±0.02	0.04±0.01	0.53 (0.04)	0.03±0.03	0.05±0.01	0.50 (0.07)
NO_2^-	0.05±0.02	0.08±0.03	0.26 (0.07)	-	-	-
Cu	0.00±0.03	26±7	0.40 (0.06)	-	-	-

Table 4. Parameters of the linear regression equations linking the OP^{AA}_V and OP^{DTT}_V responses with the tracer concentrations measured in PM_{10} and $PM_{2.5}$ samples, in Autumn-Winter (AW, October–March, 15 samples) and in Spring-Summer (SS, April–September, 24 samples). The squared correlation coefficient (R^2) and the chi-square (χ^2) value provide a measure of the corresponding linear correlation and the goodness of the fit, respectively. Note that only the linear regression lines related to chemical species significantly correlated with OPV with a p-level<0.01 have been reported.

Overall, in AW, similar regressions were computed for the OP^{DTT}_V and OP^{AA}_V responses with OC, EC, POC, K^+ and Fe in both fractions.

In particular, close slopes of the regression lines were computed, as a measure of the assay sensitivity to the investigated species (Table 4).

An exception is K^+ in PM_{10}, as the slope of the OP^{AA}_V regression line is nearly 1.5 greater than that of OP^{DTT}_V (0.45 ± 0.15 and 0.31 ± 0.09 nmol min^{-1} μg^{-1}, respectively).

This likely explained the higher OP^{AA}_V than OP^{DTT}_V responses measured in PM_{10} samples (Table 3).

By comparing the different particle sizes, we can observe that the sensitivity of the OP^{AA}_V responses toward POC, EC, K^+, Fe, and Cu decreases from PM_{10} to $PM_{2.5}$ particles in AW (Table 4). This is particularly marked for Cu, as the line slope is three times higher for PM_{10} (31 ± 6 nmol min^{-1} μg^{-1}) than for $PM_{2.5}$ (10 ± 3 nmol min^{-1} μg^{-1}).

Furthermore, the Cu and Fe concentrations are nearly double in PM_{10} compared with $PM_{2.5}$ (Appendix, Table A12). These results clearly account for the higher OP^{AA}_V response in PM_{10} than in $PM_{2.5}$, besides indicating that the transition metals, especially Cu, are significantly driven by OP^{AA}_V responses. Both reasons motivate the higher sensitivity of AA assay to coarse particles.

Otherwise, the OP^{DTT}_V responses display higher sensitivity towards EC, POC and K^+, which have similar concentrations in both fractions (Table A12), supporting the finding that the DTT assay was more sensitive to $PM_{2.5}$ than to PM_{10} particles (Table 3).

In SS, the OP^{DTT}_V values were roughly correlated ($R^2 \geq 0.4$) with POC and EC mass concentration while the OP^{AA}_V values with SO_4^{2-} mass concentration, for PM_{10} (Table 4).

In these samples, SO_4^{2-} and OC were the most abundant species, contributing on average by 14 and 22% to the PM_{10} mass.

Consequently, the OP^{DTT}_V and OP^{AA}_V responses may significantly vary day-by-day depending on the amount of SO_4^{2-} and/or OC in the tested PM_{10} sample.

For $PM_{2.5}$, both OP^{AA}_V and OP^{DTT}_V responses showed significant association with POC and EC mass concentrations, with similar sensitivity of the two assays, i.e., ~0.05 nmol min^{-1} μg^{-1} for POC and ~0.10 nmol min^{-1} μg^{-1} for EC (Table 4).

In conclusion, the contrasts between the AA and DTT assay responses were likely associated with the different sensitivity of both assays towards specific emission sources, such as "sulphate", "heavy oil/secondary marine" and "soil dust" sources.

This is in agreement with results found by other Authors, i.e., (Calzolai et al., 2015)(Jaafar et al., 2014)(Shirmohammadi et al., 2017)(Styszko et al., 2017)(Weber et al., 2018).

6. Comparison between Acellular Assays in different sites across Italy

This chapter summarizes the content of the study published in Atmosphere (2019), 10, 626, DOI:10.3390/atmos10100626.

As a part of the research activity, that has been widely devoted to the topic of PM oxidative properties, a review study has been written to summarize the previous studied to date performed in Italy to give a picture of the spatial and seasonal variability of different contributions to OP in the various geographical areas across Italy.

In particular, the study reviews the association between OP from different assays with several inorganic ad organic components, that affect PM oxidative properties, i.e., metals, ions, and carbonaceous components.

The relevance of such an investigation is based on the large variability in the chemical composition of different PM size fractions in various locations across Italy, as a consequence of the strong differences in the density of anthropogenic sources and the orographic and meteorological characteristics.

An additional outcome is a comparison among the sensitivities of various acellular OP assays to PM composition, emission sources, and particle size.

6.1 Study Overview

The investigated assays were applied to some real samples of PM collected in several sites, located in different regions to cover the main geographical areas across the Italian peninsula, even if their spatial distribution is rather inhomogeneous, with Northern Italy, mainly the Po Valley, quite extensively monitored and other areas, especially Southern Italy, still lacking data (Figure 19).

Figure 19. Location of different studied sites across the Italian peninsula. Symbols indicate different PM size fractions investigated in each site, i.e., black points: PM_{10}; red points: $PM_{2.5}$; blue points: Other PM size fractions.

The monitoring stations include urban, industrial, traffic, and semi-rural sites, so that they may give information on the impact of anthropogenic sources on PM oxidative property.

Different particle size fractions were investigated, including total suspended particles, PM_{10}, $PM_{2.5}$, and size-aggregated fractions, even if most of the studies concerned fine $PM_{2.5}$ fraction.

The Italian sites where the oxidative potential has been investigated are multiple, in this part of the study were specifically compared the OP responses for the sites of Lecce and Bologna, which use the most common assays (DTT and AA) on $PM_{2.5}$.

6.2 Comparison among Different Acellular Assays

6.2.1 Relations between OP responses of different acellular assays and chemical composition in two different sites

The general finding that the various OP assays display different sensitivity towards the same redox-active PM components has been confirmed (Janssen et al., 2015)(Saffari et al., 2014)(Sauvain et al., 2013)(Jiang et al., 2019)(Hedayat et al., 2015)(Hellack et al., 2017).

DTT mainly responded to the organic compounds, as traced by OC, EC, that represent burning sources, including fuel vehicular and biomass burning emissions—and redox-active species such as quinones, associated with other markers of photochemical ageing (SO_4^{2-}, NO_3^-). In addition, OP^{DTT} responses are also affected by traffic-related metals while, OP^{AA} is mostly responsive to metals, mainly related to non-exhaust traffic emissions (Cu, Zn, Cr, Fe, Ni, Mn, Sn, Cd, Pb) (Mihucz et al., 2015)(Visentin et al., 2016)(Simonetti al., 2018a)(Simonetti et al., 2018b).

Both assays showed similar sensitivity to the soluble fractions of K, Ca, Mn, Rb, and WSTC, while AA was six times more sensitive to Zn and Cu compared with DTT (Pietrogrande et al., 2018b).

Overall, it must be pointed out that the association of volume-normalized OP^{DTT} with transition metals should be interpreted with caution, as it may be due to similar variations in metal and PM concentrations, and also a higher concentration of metals compared with that of quinones, that are more efficient than metals to DTT oxidation (Jiang et al., 2016).

Also, Pearson correlation analysis was performed to investigate the significance of correlations among OP responses for different sites as well as associations between OP responses and chemical composition (Table 5).

Site	Correlation	Assay	Chemical Species
Lecce	Pearson p<0.01	DTT	K^+, Ba, Cd, Fe, Mn, OC, EC, POC
		AA	SO_4^{2-}, Ba, Cd, Cu, OC, EC, POC, P, Oxalate
Bologna	Pearson p<0.01	DTT	Mn, Fe, Cu, Cr, Zn, OC, EC
		AA	Mn, Cu, OC, EC

Table 5. Association among the measured OP and chemical composition. Studies are grouped according to site location of PM samples collection, correlation analysis used for association at p level, the acellular assay used for OP measurement, chemical species showing significant correlation to OP.

For $PM_{2.5}$ samples of Lecce, the measured $OP^{DTT}{}_V$ and $OP^{AA}{}_V$ are correlated with several inorganic species, namely ions and metals, and with organic/elemental carbon.

$OP^{DTT}{}_V$ is strongly correlated with K^+ in addition to Ba, Cd, Cu, Fe, and Mn (traffic-related metals) and with EC, OC, and POC associated with the traffic exhaust source and/or with the combustion including biomass-burning source.

As well as Ba, Cd, Cu, Fe, Mn, EC, OC, and POC, which are related to traffic and/or combustion emissions, the $OP^{AA}{}_V$ is also well correlated with SO_4^{2-}, Cu, Mn, P, and oxalate, which are species related to secondary aerosols and resuspended soil from vehicular traffic and/or transported Saharan dust.

Concerning the investigated comparison between OP^{DTT} and OP^{AA} responses on $PM_{2.5}$ at Bologna, no highly significant correlation was found, even if the values obtained with both assays were similarly correlated with metals and carbonaceous components (OC and EC).
To confirm that the major source of PM in urban sites is traffic, by computing the Pearson's coefficient, OP^{DTT} was found correlated with several metals (Cu, Zn, Cr, Fe, Ni, Mn), mainly originating from the wear of vehicle components such as brakes and tires as well as suspension of road dust.
In contrast, OP^{AA} has correlated only moderately with Cu and Mn but no correlation with the other ions as well as the concentration of the total metals (Visentin et al., 2016).
Traffic-related redox-active metals, i.e., Cu, Fe, Mn, play a predominant role in driving ROS production in fact, both assays show positive responses to these components (Shuster-Meiseles et al., 2016)(Charrier et al., 2012)(Perrone, Zhou, et al., 2016)(Daher et al., 2012)(Simonetti et al., 2018a)(Simonetti et al., 2018b)(Calas et al., 2017).
Concerning the seasonal variation, in winter the correlation was higher than in summer, probably due to atmospheric stagnation conditions, typical of the Po Valley.

6.3 Spatial Variability of OP in different Areas across Italy

Although several OP^{DTT} and OP^{AA} values have been up to date measured across Italy, the meaningful comparison among the data has to be restricted to the OP responses obtained with similar experimental assay protocols, to generate reliable and conclusive results within every study. Such a comparison across studies may give a picture of the spatial and seasonal variability of aerosol OP across the Italian peninsula to obtain insight into the contribution of sources, atmospheric processes, and meteorological conditions.

6.3.1 OP Responses of $PM_{2.5}$ Particles

The OP responses were measured for both assays with the same protocol, upon the $PM_{2.5}$ filters collected in Lecce and Bologna in two different seasons.
The values obtained have been related with the mass concentration of $PM_{2.5}$ to provide a picture of the spatial and seasonal variability of OP in two cities with a strong difference in the density of anthropogenic sources and the orographic and meteorological characteristics (Visentin et al., 2016)(Perrone et al., 2019a).
The mean values of OP^{DTT}_V for each sampling campaign and the mean of $PM_{2.5}$ mass concentration are summarized in Figure 20.

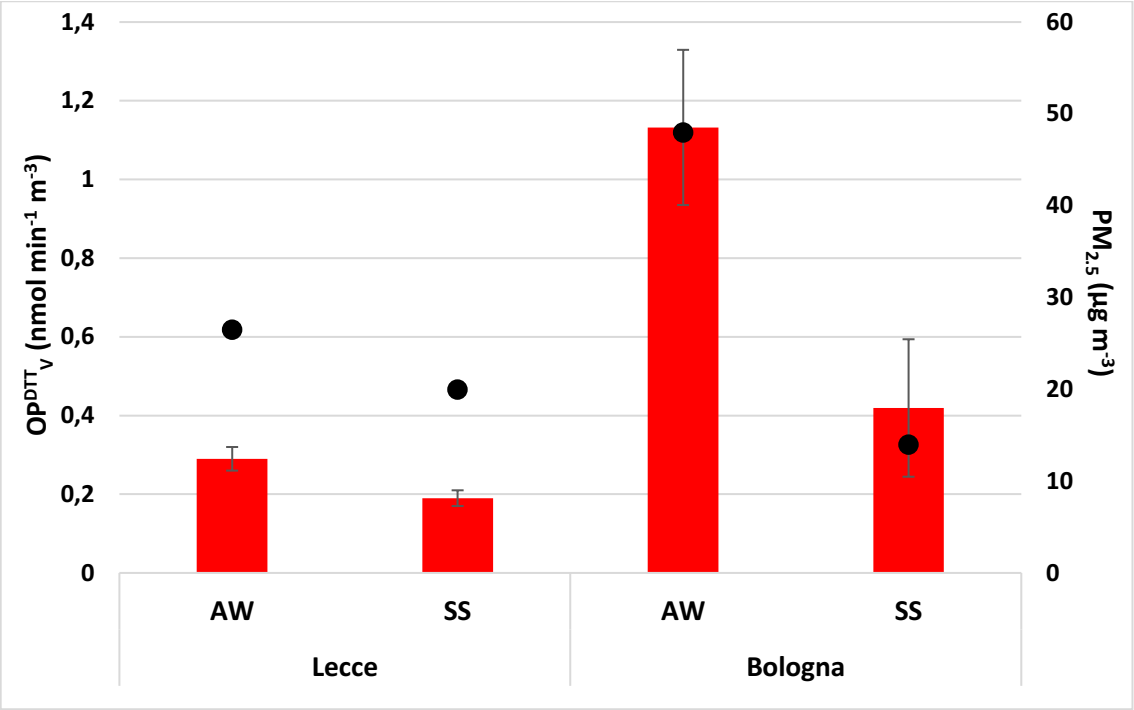

Figure 20. OP_V responses of $PM_{2.5}$ samples measured using the same DTT assay protocols. Mean values of each sampling campaign, standard errors are indicated by the bars. Points: Mean $PM_{2.5}$ mass concentration values of each sampling campaign (right y-axis).

The location-dependence (or source-dependence) of PM oxidative potential is more evident for the $PM_{2.5}$ size, with values nearly 5 times higher at Bologna in AW (1.1 ± 0.2 nmol min^{-1} m^{-3}) than at Lecce in SS (0.2 ± 0.02 nmol min^{-1} m^{-3}).

This variation can be explained by higher $PM_{2.5}$ concentrations at Bologna in wintertime (48 µg m^{-3}) compared to those in all the investigates studies (14 to 25 µg m^{-3}) and also by the intrinsic redox reactivity, measured as mass-normalized OP^{DTT}_m value, that is higher at Bologna compared to Lecce i.e., 0.029 nmol min^{-1} μg^{-1} vs. 0.010 nmol min^{-1} μg^{-1}.

In addition, a clear seasonal trend is shown at both sites, with a larger winter increase at Bologna (4 times higher) compared to Lecce (2 times).

Also, the OP^{AA} values were measured for $PM_{2.5}$ samples collected at Bologna and Lecce in different seasons (data summarized in Figure 21, (Perrone et al., 2019a)(Pietrogrande et al., 2019a)(Visentin et al., 2016)).

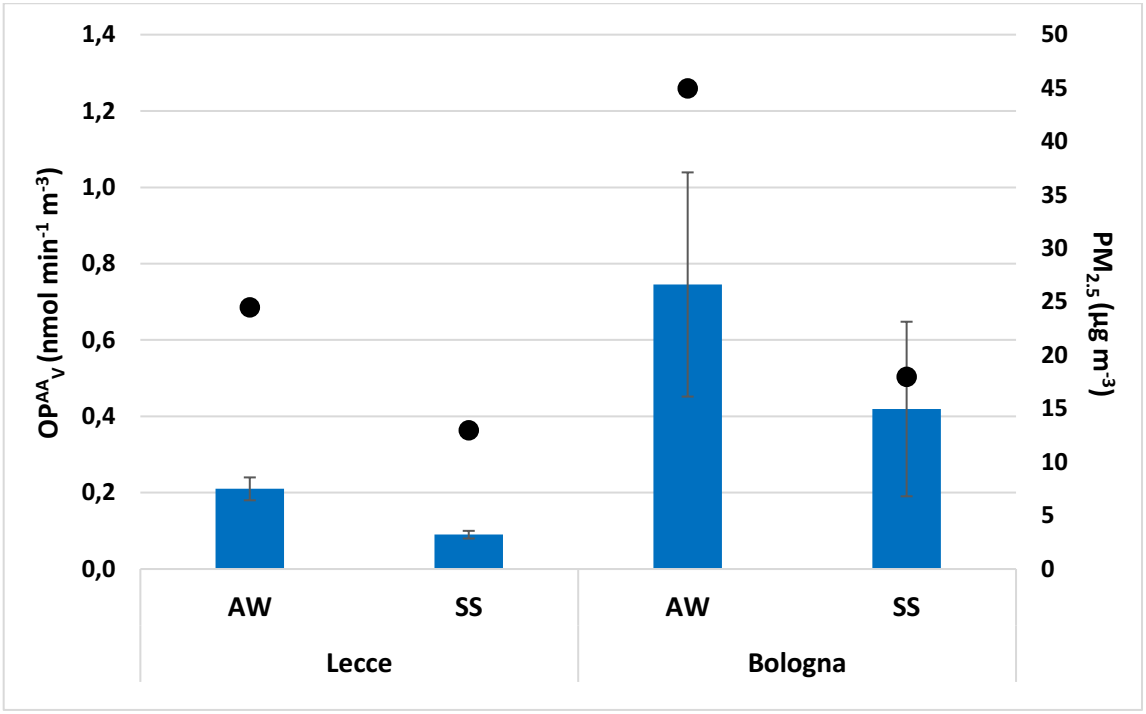

Figure 21. OP_V responses of $PM_{2.5}$ samples measured using the same AA assay protocols. Mean values of each sampling campaign, standard errors are indicated by the bars. Points: Mean $PM_{2.5}$ mass concentration values of each sampling campaign (right y-axis).

The highest OP^{AA}_V responses were measured in Bologna, as their value was nearly triple (0.75 ± 0.2 nmol min^{-1} m^{-3}) compared to Lecce (~0.20 nmol min^{-1} m^{-3}) with a clear increase during the cold season at both sites.

As $PM_{2.5}$ mass concentrations were similar at both sites, the OP^{AA} variations can be mainly explained by differences in the intrinsic redox reactivity, as confirmed by higher OP^{AA}_m measured at Bologna than at Lecce, mainly during the warm season, i.e., 0.03 nmol min^{-1} μg^{-1} vs. 0.005 nmol min^{-1} μg^{-1}, respectively.

Considering that the OP^{DTT} values showed higher spatial and temporal variations, compared to OP^{AA}, and that DDT assay is mostly sensitive to organic species, we can infer that the observed behaviour for $PM_{2.5}$ OP is mainly associated with the contribution of secondary organics, especially highly oxidized organics traced by SOC concentration.

In fact, significantly higher SOC concentrations have been found at Bologna compared to Lecce, mainly in the cold season, both as concentration values (on average, ≈ 3 vs. 1.5 µg m^{-3}) and relative contribution to $PM_{2.5}$ mass (~50% vs. 15%) (Pietrogrande et al., 2016)(Perrone et al., 2019a).

The high contribution of secondary pollutants in the Po Plain has been motivated by the large impact of anthropogenic emissions, mainly wood combustion for domestic heating during winter, combined with the stable atmospheric conditions (Hmix ≈ 300 m), that promote pollutant accumulation in the atmosphere and therefore favour the photochemical ageing of organic aerosol.

In particular, PAHs can be converted into large oxidized aromatic, e.g., DTT-active quinones, as strongly supported by chamber studies (Jiang et al., 2016)(Tuet et al., 2017a).

7. Cleanup and GC/MS determination of Polycyclic Aromatic Hydrocarbons in Atmospheric Aerosol

In addition to the main research topic concerning PM oxidative properties, some research work has been devoted to the analysis of Polycyclic Aromatic Hydrocarbons, as relevant PM components that can provide useful information about the PM origin and processes in the atmosphere.

In particular, special attention must be paid to sixteen PAHs designated as priority pollutants, because of their high carcinogenic and mutagenic potentials.

Thus, they are routinely monitored in ambient particulate matter (PM), as an essential step for better understanding their fate and exposure to humans.

The work described in this chapter has been performed in the framework of the IPA/BC-MONITOR project, supported by the Emilia Romagna Region (POR FESR 2014-2020), which aimed to develop an innovative, compact and stand-alone system for the online measurement of PAHs.

Despite years of effort and the use of the most sophisticated chromatographic techniques available, the accurate PAH determination in PM samples is still a challenging task, because of the very large complexity of inorganic and organic PM components, concerning molecular weight, functional groups and polarity, and also of the low content of PAHs in the sampled air (0.1-2 ng m^{-3}) (Nozière et al., 2015)(Nalin et al., 2018)(Wilson et al., 2018).

The conventional approach for PAH analysis in PM must include processes for isolation of compounds, separation and pre-concentration for multi-component mixtures.

In this study, we investigated the cleanup performance of the MIP-SPE cartridge for the analysis of PAHs in atmospheric aerosol, with the specific concern of selectively removing the mostly interfering n-alkanes.

The method was compared with SPME procedure, by highlighting advantages and disadvantages in terms of extraction efficiency and selectivity towards interferences.

The comparative study was carried out on ambient $PM_{2.5}$ samples collected in an urban polluted site.

7.1 The importance of pretreatment in the PM real sample analysis

Generally, trace analysis of environmental samples needs a pretreatment step in order to reduce matrix interference and enrich the analyte.

The first analytical problem to be solved is the isolation of the analytes from a mixture of organic pollutants, knowing that interfering compounds mainly originate from unburned fuel (alkanes, phenylalkanes, and alkylnaphthalenes) or result from oxidation of PAH during the combustion process. Very efficient clean-up is needed to enable such purification.

A visible example is the GC/MS signal obtained after the extraction procedure of a real PM sample (Figure 22).

Due to the complex matrix, the signal is characterized by a high intensity of interferent components, typically present in the PM composition, making it difficult to quantify the PAHs concentration.

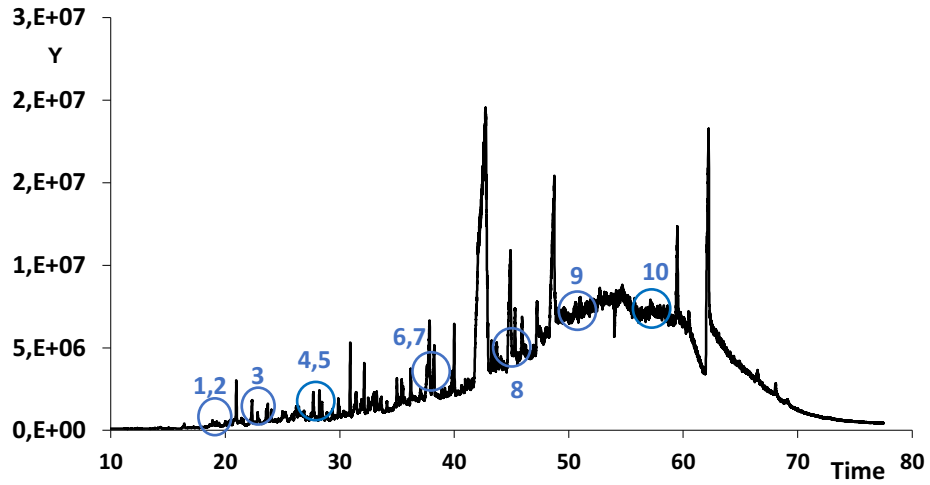

*Figure 22. GC/MS chromatogram of a real $PM_{2.5}$ extract without any cleanup. PAHs are highlighted with blue circles: **1** Acenaphthylene, **2** Ancenaphthene, **3** Fluorene, **4** Phenanthrene, **5** Anthracene, **6** Fluoranthene, 7 Pyrene, **8** Chrysene, **9** Benzo[a]pyrene, **10** Benzo[g,h,i]perylene)*

PAHs are not clearly visible because the saturated hydrocarbons ─ normal and branched alkanes ─, show GC retention properties similar to those of PAHs and are commonly present in urban PM at high concentration levels.

For this reason, there was a need to implement processes, as Solid-Phase Extraction and Solid-Phase Microextraction, for isolation of PAHs, separation and pre-concentration from the complex mixture.

These procedures were investigated in detail, to make the analytes of environmental interest clearly visible and properly quantifiable.

7.1.1 Solid-Phase Extraction (SPE)

Solid-phase extraction (SPE) is a sample pretreatment technique that is commonly utilized to pretreat the analytes, with the advantages that only a small amount of extraction solvent and considerably less time are required, compared with liquid-liquid extraction.

Additionally, the pretreatment is relatively simple, has low detection limits, and can be implemented using conventional instrumentation (Ho et al., 2011).

A new rapidly growing trend in SPE is the design and use of synthetic antibody mimics, for example molecularly imprinted polymers (MIPs).

MIPs are highly cross-linked polymer-based molecular recognition materials engineered to bind one target compound or a class of structurally related target compounds with high selectivity (Krupadam et al., 2010).

In this technique, polymerizable functional monomers are prearranged around a template molecule by noncovalent or covalent interactions before the initiation of polymerization.

A rigid, highly cross-linked macroporous polymer is formed that contains sites complementary to the template molecule both in shape and in the arrangement of functional groups.

After removal of the template molecule by extraction, the MIPs can be used as artificial receptors to selectively rebind the template from a mixture of chemical species (Figure 23) (Martín-Esteban, 2016).

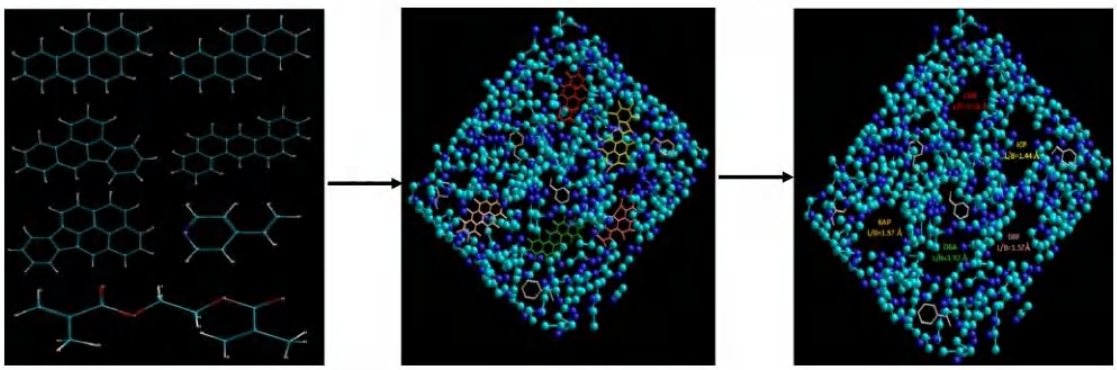

Figure 23. Schematic representation of multiple template molecular imprinting technique (Krupadam et al., 2010).

In particular, a MIP-SPE cartridge has been developed and commercially available for distinctive recognition of PAHs containing 4 and more benzene rings, including highly carcinogenic dibenzo pyrene isomers.

It has been used to extract PAHs from various environmental samples, including ambient particulate matter and showed high selectivity, combined with high capacity and excellent mechanical and thermal stability (Sun et al., 2017).

Optimization of the operative conditions is particularly critical in the MIP-SPE methods in order to achieve the strongest selective interactions with the sorbent, in fact, it requires the use of solvents with varying polarity to separate compounds according to their different properties (Beltran et al., 2010).

7.1.2 Solid-Phase Microextraction (SPME)

As a solvent-free alternative, solid-phase microextraction (SPME) can be used for such a separation, as it is a well-established green technique for extraction and pre-concentration of the compounds from a variety of matrices (Menezes et al., 2011).

Compared with the laborious SPE procedure, it reduces the number of steps, by combining sampling and pre-concentration in one step, as it permits desorption directly into the injector of the chromatographic system (Naing et al., 2020).

This method has been successfully used for quantification of PAHs in different environmental matrices (Ballesteros et al., 2009)**,** including ambient air in both the gas phase and airborne particulate adsorbed fractions (Reyes-Garce et al., 2017).

A critical point is the choice of the fibre coating, as different analytes have different sorption behaviours on the fibre depending on their different physicochemical properties (Pawliszyn, 2000)(Naccarato et al., 2019).

To date, the bipolar PDMS/DVB and the relatively polar PA fibres are recommended as the most appropriate polymeric phases for the extraction of PAHs from various environmental matrices (dos Santos et al., 2019), including PM extracts (Santos et al., 2016)(Ballesteros et al., 2009)(Menezes et al., 2011).

In a previous study, the two fibres were evaluated with the aim of a selective cleanup.

Overall, the obtained results have shown that the more polar PA coating is able to selectively adsorb PAHs in comparison with n-alkanes.

Thus, such selectivity is the basis for choosing the PA fibre for separating PAHs from n-alkanes interfering with the GC/MS signal of the complex PM samples. Therefore, in this study, the PA fibre was chosen for comparison with MIP-SPE.

7.2 Analytical procedure for PAHs

Ambient particulate matter ($PM_{2.5}$) were collected in an urban site in Bologna (Northern Italy) from January to February 2017.

Particles were collected on prewashed and prebaked quartz fibre filter (Pall; 9-cm diameter) by a high-volume air sampler operating at a constant nominal flow rate of 500 L min^{-1} for 24 h, to collect an air volume of 240 m^3.

The 16 investigated US EPA priority PAHs in $PM_{2.5}$ samples are: naphthalene (NaP), acenaphthene (AcP), acenaphthylene (AcPy), fluorene (Flu), phenanthrene (PhA), anthracene (AnT), fluoranthene (FluA), pyrene (Pyr), benz(α)anthracene (BaA), chrysene (Chr), benzo(b)fluoranthene (BbF), benzo(k)fluoranthene (BkF), benzo(α)pyrene (BaP), indeno(1,2,3-cd)pyrene (InP), dibenz(a,h)anthracene (DbA), and benzo(ghi)perylene (BghiP).

A quarter of the filter was extracted for 30 min in an ultrasonic bath with 15 mL of n-hexane:dichloromethane (30:70) solvent mixture.

Then, the extracts were filtered using a syringe filter (PTFE 25 mm, 0,22 µm, Kinesis) to remove insoluble particles and the filtrates were evaporated to dryness in a centrifugal vacuum concentrator (miVac Duo Concentrator, Genevac Ltd, Ipswich, UK) at room temperature.

The samples were reconstituted with 500 µL of the extraction solvent mixture, transferred in 2 mL glass vials and dried under gently nitrogen flow. Then, samples were recovered with 100 µL of n-hexane for direct injection into the GC/MS system or submitted to SPE or SPME cleanup.

Method blanks, comprising filters, were extracted, cleaned with both procedures and analyzed in the same way as the samples.

7.2.1 Clean-up procedures

SPE procedure: The cleanup protocol consisted in preconditioning of the MIP-SPE cartridges (SupelMIP™ SPE-PAHs by Supelco) with 2 mL of cyclohexane before sample loading. Samples loading was performed under vacuum at a flow rate of 3 mL min^{-1}. Then the sorbent was washed with 2 mL of cyclohexane and the retained PAHs were eluted with 3mL of dichloromethane.

Eluate was dried under gently nitrogen flow and reconstituted with 100µL of n-hexane, 2 µL of the extract were automatically injected into the GC/MS instrument for analysis.

SPME procedure: Following the conditioning guidelines, the fibre was conditioned under helium at a flow-rate of nearly 1.0 mL min^{-1} with the split valve open (to reduce the number

of impurities entering the column) in the hot injection port of the gas chromatograph kept for 30 min at 280°C for the PA fibre, prior to use.

SPME fibre was directly immersed in a 20 mL flask containing 2 mL of methanol solution under agitation for 1 h at room temperature.

Then, the fibre was transferred into the GC injection port, where desorption of the analyte occurred for 5 min at 280°C for the PA fibre.

The blanks were tested by thermal desorption (5 min in the injection port) followed by GC analysis to confirm that all compounds were desorbed and prevent the fibre memory effect.

7.2.2 GC/MS analysis

Chromatographic analyses were performed on a Gas Chromatograph Focus GC, (Thermo-Fisher Scientific) coupled with a mass spectrometry detector PolarisQ Ion Trap Mass Spectrometer (Thermo Fisher Scientific, Bellefonte, PA, USA). A Rxi®-5Sil MS capillary column (30 m x 0.25 mm I.D., 0.25 μm film thickness) was purchased from Restek (USA). High purity helium (99.999%) was used as the carrier gas at a constant flow rate of 1.4 mL min^{-1}.

For direct injection, 2 μL of the sample was injected in the split/splitless injector maintained at 280 °C (splitless for 5 min). The oven temperature program started at 40 °C. It was heated up to 275 °C at a rate of 15 °C min^{-1}, increased to 320 °C at a rate of 10 °C min^{-1} and finally held for 10 min. The GC/MS interface and ion source temperatures were kept at 280 °C and 250 °C, respectively.

The MS analysis was performed in electronic impact mode (EI) on positive mode with an energy of 70 eV. The signal acquisition was operated in full-scan mode (40-650 m/z range) and selected ion monitoring (SIM) mode by selecting specific fragments of each target PAH (values of the most abundant characteristic ion).

The tandem MS was operated in single reaction monitoring (SRM) mode, by using transition (precursor ion, product ion and collision energy) reported in literature.

Data acquisition was performed using a Thermo Scientific 1.4 X-Calibur program (WestPalm Beach, USA).

7.3 Application on real samples

The applicability of the MIP-SPE and SPME methods to real-word $PM_{2.5}$ samples was comparatively investigated by analyzing six ambient $PM_{2.5}$ filters collected in an urban site during winter 2017.

Such samples were expected to contain a high concentration of PAHs, mainly related to the major anthropogenic sources typical of urban sites, such as motor vehicle exhaust, industrial activity and biomass combustion for residential heating in the cold season (Masala et al., 2016)(Kim et al., 2019)(Nyiri et al., 2016)(Ramírez et al., 2010).

In addition, a concomitant contribution of alkanes was expected, mainly n-alkanes with $C_{max} \leq C_{26}$ related to anthropogenic sources, in combination with those with $C_{max} > C_{26}$, typically emitted from biogenic sources, and several branched isomers, generating the unresolved carbon mixture band in GC/MS signal (Ding et al., 2012)(Chan et al., 2013)(Wang et al., 2019)(Lyu et al., 2019).

The benefit of both cleanup procedures can be clearly depicted in Figure 24, comparing the total ion chromatograms of a real $PM_{2.5}$ filter (sample 1) without any cleanup (dashed black trace) and after the MIP-SPE and SPME procedures (red and black tracers, respectively).

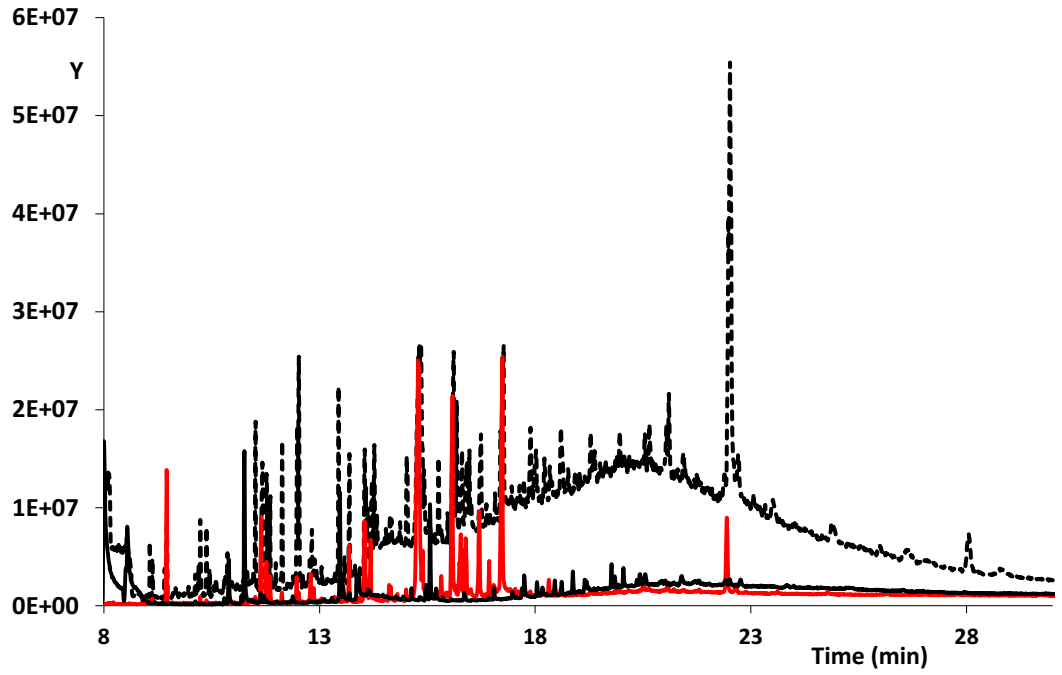

Figure 24. GC–MS traces (total ion detection) of an extract of a real sample (sample 1) without any clean-up (dashed trace), after MIP SPE (red trace) and after SPME (black trace).

The GC/MS signal of the untreated solution (dashed black trace) is very complex, mainly dominated by the unresolved alkane band and several overlapped peaks.

In comparison, the chromatograms of the purified solutions are strongly simplified, in particular, they are nearly lacking the alkane band, so proving the efficiency of the cleanup procedure in selectively retaining interfering hydrocarbons.

Such a result is confirmed by a detailed inspection of the GC/MS signals that are mainly generated by the n-alkanes, by using SIM mode at m/z values 57+71+85 (Figure 25).

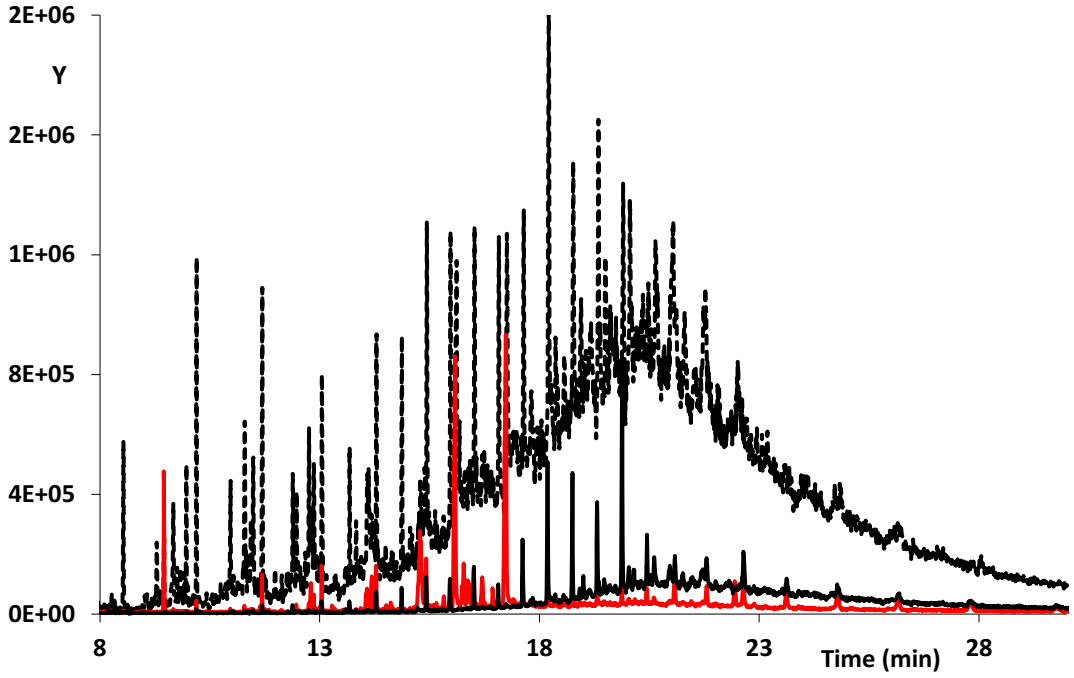

Figure 25. GC–MS traces (SIM mode at m/z values 57+71+85) of an extract of a real sample (sample 1) without any clean-up (dashed trace), after MIP SPE (red trace) and after SPME (black trace).

In comparison with the original extract (dashed black trace), both purified solutions show a strong reduction of the hydrocarbon concentration, so that most of the mixture components can be properly separated and identified in the chromatograms (red and black tracers, respectively). However, the two procedures show different complementary selectivity.

Even if the adsorption on the PA fibre strongly reduces the unresolved carbon mixture band, it is not able to remove the interfering hydrocarbons corresponding to C_{27} - C_{30} terms of n-alkane series, that elute in the same retention region between 17 and 20 mins as 5 rings PAHs (black trace).

On the contrary, SPE on the MIP polymer is able to eliminate the heavier alkanes, so that the unresolved carbon mixture is nearly absent and only lighter C_{21}-C_{25} n-alkanes are still present in the mixture (red trace). Thus, the MIP-SPE procedure appeared more efficient than SPME in removing hydrocarbons that may interfere with high-ring PAH signal.

In order to quantitatively evaluate the recovery of the SPE or SPME procedures, the concentration of each target PAH in real $PM_{2.5}$ samples was quantified by directly submitting each original extract, before cleanup, to the GC analysis using tandem mass spectrometry (GC/MS/MS), under MLR conditions specific for each PAH, as recovered from literature (Kim et al., 2019)(Naing et al., 2020).

Several PAHs were quantified (LOD in Appendix, Table A16), with individual concentrations ranging from <LOQ to 1.20 ng m^{-3} for PAHs and total concentrations ranging from 6.33 up to 11.94 ng m^{-3}, that are comparable values with those observed in other urban

sites in Italy (Pietrogrande et al., 2014)(Masiol et al., 2013) and also in Europe (Abdel-Shafy et al., 2016)(Alves et al., 2017)(Masala et al., 2016).

These measured values can be assumed as the effective PAH concentrations in the real samples, as tandem MS is the most sensible and selective detection mode able to obtain accurate results, independent of interferences in the GC/MS signals (Kim et al., 2019)(Nyiri et al., 2016)(Naing et al., 2020).

Based on these GC/MS/MS values as reference real concentrations, the % recovery of SPE and SPME procedures was computed for each PAHs in 1-6 samples (Tables 5 and 6 for SPE and SPME procedures, respectively).

PAHs	PM 1	PM 2	PM 3	PM 4	PM 5	PM 6	mean
FluA	65	66	69	71	68	66	68
Pyr	67	65	72	70	71	65	68
BaA	68	64	71	74	73	64	69
Chr	83	82	84	86	85	82	84
BbF	82	90	90	89	92	81	87
BkF	81	92	92	89	91	88	89
BaP	94	93	93	95	94	92	94
InP	91	92	94	96	93	92	93
DbA	94	93	95	94	95	92	94
BghiP	93	92	91	96	95	93	93

Table 5. % recovery of the MIP-SPE procedure for target PAHs in the real $PM_{2.5}$ samples.

PAHs	PM 1	PM 2	PM 3	PM 4	PM 5	PM 6	mean
NaP	75	81	81	82	79	83	80
AcPy	80	86	75	78	80	84	81
AcP	86	80	77	75	75	85	80
Flu	80	88	73	82	76	79	80
PhA	75	75	80	77	84	80	79
AnT	80	80	83	79	88	80	82
FluA	86	76	75	80	76	86	80
Pyr	80	87	82	79	78	80	81
BaA	81	79	77	83	81	81	80
Chr	80	86	79	75	81	80	80
BbF	82	82	74	80	87	75	80
BkF	86	87	81	81	79	73	81
BaP	**115**	**110**	**114**	80	75	84	96
InP	**138**	**114**	**112**	83	75	70	99
DbA	**136**	**126**	**122**	75	80	71	102
BghiP	**131**	**111**	**128**	80	74	73	100

Table 6. % recovery of the SPME procedure of target PAHs in the real $PM_{2.5}$ samples. In bold values: overestimated results in the most polluted samples.

Overall, satisfactory recovery results were achieved ranging from 73 to 138% for the target PAHs, indicating that both cleanup methods provide acceptable accuracy in environmental analysis.

However, a detailed inspection of the data points out specific advantages and drawbacks of each of the two procedures. The MIP-SPE method shows acceptable accuracy with R% values above 82% for PAHs heavier than chrysene to achieve the best recovery close to 93% for PAHs with 5 and more benzene rings (Table 5).

In contrast, the SPME shows a homogeneous recovery for all the investigated PAHs, independent of PAH molecular weight, with a mean acceptable value close to 80% (Table 6). However, some overestimated results were obtained for BaP, InP, DbA and BghiP in the most polluted samples, as described by R% values from 110 to 138% (bold values of samples 1 to 3 in Table 6).

Such quantification errors may be due to the positive interference of C_{27} - C_{30} n-hydrocarbons that co-elute with PAHs and generate the same m/z fragment ions in the MS spectra, as shown in the SIM GC/MS signals reported in Figure 25 (black trace).

Specific attention should be paid at this point, as this group also includes the indicator benzo[α]pyrene, overlapped with C_{29} n-alkane.

In conclusion, the reported results demonstrated the potential advantages of the MIP-SPE for sample cleanup for a precise and accurate analysis of PAHs in airborne particles, although limited to PAHs with more than 4 benzene rings.

In particular, using the MIP sorbent magnifies the specificity of SPE cleanup, since it is capable of selective recognition binding with target PAHs.

Thus, undesirable matrix interferences can be removed from the complex sample to improve the specificity and sensitivity of the MS ion-trap detector.

This is the case of high levels of interfering hydrocarbons, commonly present on ambient PM strongly impacted by traffic emission.

In contrast, SPE suffers the drawbacks of requiring pre-concentration by solvent evaporation of the extracted solutions, which increases the run time and can cause a decrease in analytical reproducibility.

SPME procedure is a green alternative since it reduces the number of steps by eliminating the use of solvents to avoid exposure risk and environmental contamination. The current work confirmed the good performance of the polyacrylate SPME fibre in extraction and purification of the PM-associated PAHs, with homogenous recovery for all the target PAHs, having the big benefit of a minimal number of steps.

However, the SPME cleanup can only partially remove heavy hydrocarbons from the PM extract, so that they can interfere in the SIM chromatographic signal of the 5 rings PAHs to generate quantification errors.

Based on the critical comparison between MIP-SPE and SPME methods, we can conclude that both procedures compare in terms of reliability, accuracy and sensibility for PAH analysis in PM samples, but the MIP-SPE exceeds in the specific selectivity towards hydrocarbon components in PM.

Thus, this is the procedure of choice for the preconcentration/separation of PAHs in urban polluted PM samples, although the disadvantages of requiring labour-intensive and time-consuming sample pretreatment.

8. On site-monitoring Indoor Air Quality in Schools

This chapter summarizes the content of the study published in Journal of Chemical Education (2020), 97 (11), 4069-4072, DOI: 10.1021/acs.jchemed.0c00065.

A further activity carried out during the Ph.D. period, concerned the monitoring of air quality in indoor environments, with specific application to school environments.

The activity was performed as part of the "Piano Lauree Scientifiche" project (Italian Educational and Research Minister, MIUR) of Chemistry degree courses involving the University of Ferrara and several secondary schools of the region.

The aim was to provide students with direct knowledge of the quality of the air they breathe and approaching to the modern sensor technology, that is able to collect high-density temporal and spatial data in a border range of households.

The students were actively involved in the teaching−learning activity since they personally used low-cost sensors, to measure the main parameters of the indoor air quality (IAQ) monitoring in classrooms and laboratories of their schools.

In addition, were given instructions to elaborate the IAQ data measured in their own classroom/laboratory, in order to analyze their dependence on different environmental conditions.

Indoor air quality (IAQ) has been a well-known problem since the late 1970s. Its significant impact on human health has been addressed several times by the World Health Organization (WHO). Further studies and researches have highlighted the great importance that IAQ now has in all environments, e.g., houses, schools, banks, post offices, offices, hospitals, and public transport (Settimo et al., 2020).

Exposure to indoor air pollutants may generate long-term adverse effects, as most of the air exposure occurs indoors, where people spend a large fraction of their lives.

This is particularly critical in school buildings, where the permanence of young people is supposed to last for a relatively long period, more than 60% of their time.

The students are very sensitive to indoor pollutants, also including a significant decrease in the efficiency of student learning processes and cognitive performances. The evaluation of the exposure to indoor pollutants is far from being a simple task.

The concentration and chemical composition of indoor air, in fact, depends on the release of contaminants from indoor sources as well as on their penetration from the outdoors (Tofful et al., 2020).

8.1 Monitoring of IAQ Parameters and Data Collection

The activity was performed during February−March 2019 in two secondary schools in the Emilia-Romagna region (Northern Italy) and involved nearly 200 students.

In each school environment, the IAQ parameters were on-site measured using monitoring sensors operating 24 h continuously.

The investigated parameters were temperature, relative humidity (RH%), concentration of fine particle matter ($PM_{2.5}$) of volatile organic compounds (VOCs), ubiquitous compounds with significant impact on the environment and human health, and CO_2, a surrogate for the quality of ventilation in the indoor environment (Becerra et al., 2020)(Bluyssen, 2017)(Schibuola et al., 2020)(Ruggieri et al., 2019).

Measurements were performed with Foobot sensors purchased from Foobot (AirBoxLab, Luxembourg). Although such sensors may suffer from limited sensitivity and specificity, they can provide adequately reliable data for IAQ monitoring, supplying relevant properties for on-site monitoring, in fact, the Foobot device has been found one of the most suitable market low-cost sensor to provide reliable IAQ data in indoor environments (Singer et al., 2018).

Using light scattering technology, the sensor measures particles with an aerodynamic diameter between 0.3 and 2.5 μm, in the concentration range of 0–1300 μg m^{-3}, with a precision of ±4 μg m^{-3}. Total VOCs are measured through a metal-oxide semiconductor (MOX) sensor in a concentration range of 125–1000 ppb, with a precision of ±1.0 ppb.

The Foobot lacks a CO_2 sensor, however, an algorithm converts total VOC concentration into a CO_2 equivalent (range 400–6000 ppm, with precision ±1.0 ppm). The device is also equipped with a temperature and relative humidity sensor.

In each school, the monitors operated in four rooms at the same time. The devices communicated the real-time measurements via Wi-Fi to the manufacturer Web site (https://partner.foobot.io/), from which data can be downloaded using a smartphone application. The sensors were placed at the side of each room in a location that minimized disruption to classroom activities.

The indoor data obtained were compared with the outdoor temperature and $PM_{2.5}$ mass concentration, measured by the Regional Environment Protection Agency of Emilia Romagna (ARPAE) network in air monitoring stations located close to the schools.
At the end of each monitoring campaign, hourly data of each IAQ parameter were discharged and shared with the students for visualization and investigation.

8.2 Classroom Activity on IAQ Parameters of Individual Classroom/Laboratory

The daily profile of the concentration of the indoor pollutant was studied, which was related to the activity inside the school classroom and the opening/closing of windows and doors.
The recorded data show a progressive increase in the concentration of CO_2 from the beginning of the lessons until the opening of the windows, which determines, on the contrary, a significant increase in the concentration of $PM_{2.5}$ introduced from the outside.
As an example, Figure 26 reports the variation of $PM_{2.5}$ mass and CO_2 concentrations in the most crowded classroom Cl3 (occupancy, 0.75 m^{-2}). From the plot, it is clear that the indoor CO_2 and $PM_{2.5}$ values largely changed throughout the occupation hours, mainly depending on windows opening (arrows in the figure).

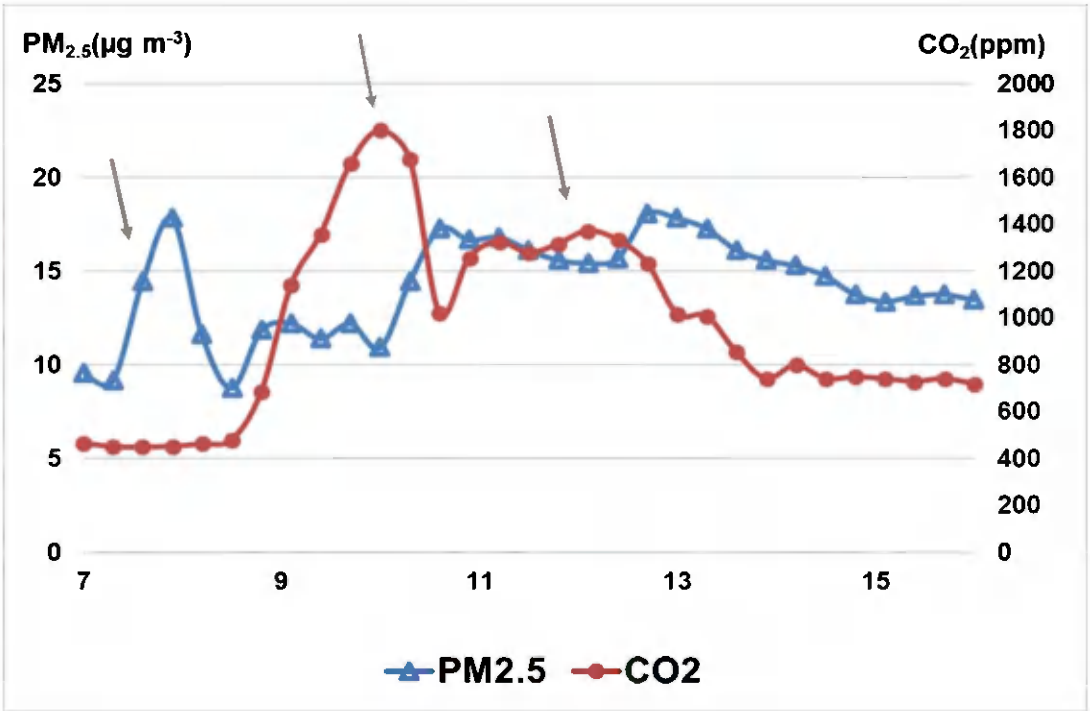

Figure 26. Temporal evolution of the monitored indoor $PM_{2.5}$ and CO_2 concentrations through the occupation hours monitored in classroom Cl3 during Feb. 14, 2019. Red points, indoor CO_2 level; Blue triangles, indoor level. Grey arrows indicate windows opening.

Overall, the mean indoor $PM_{2.5}$ concentrations measured in each room were close to the WHO threshold value (25.0 μg m^{-3}) (Settimo et al., 2020), as they ranged from 20.7 ± 9.8 μg m^{-3} (Lab3) to 25.0 ±17.0 μg m^{-3} (Lab2 and Cl2) (Appendix, Table A18).

This critical situation can be attributed to the high levels of outdoor $PM_{2.5}$, common during the winter in the Po Valley (Pietrogrande et al., 2016).

In fact, a clear dependence was found between indoor and outdoor $PM_{2.5}$ concentrations, with a significant correlation ($p<0.05$) for most of the investigated rooms (Table 7).

Monitoring period		Indoor- outdoor Temperature	Indoor- outdoor $PM_{2.5}$	Indoor $PM_{2.5}$-VOC
11th to 24th Feb 2019	Lab1	0.220	**0.677**	0.479
	Lab2	-0.108	**0.641**	0.206
	Lab3	0.436	**0.797**	0.340
	Lab4	-0.075	**0.804**	-0.156
28th Feb to 17th Mar 2019	Cl1	0.029	0.215	**0.524**
	Cl2	-0.118	**0.692**	0.107
	Cl3	-0.264	0.410	0.485
	Cl4	0.073	0.363	0.459

Table 7. Pearson's coefficients of correlation between the different parameters measured during each monitoring campaign in each investigated room: indoor vs. outdoor Temperature, indoor vs. outdoor $PM_{2.5}$ concentrations, indoor $PM_{2.5}$ vs. VOC concentrations. Bold values: Pearson's coefficient significant at $p<0.05$ level.

This suggests that indoor $PM_{2.5}$ values are mainly dominated by the contribution of outdoor $PM_{2.5}$ (Figure 27), which may enter indoor environments by natural ventilation when windows are opened, by penetration through cracks in building envelopes, and through the operation of mechanical ventilation systems (Abbatt et al., 2020)(Becerra et al., 2020)(Rovelli et al., 2014)(Stabile et al., 2019)(Chen et al., 2020).

To quantify the contribution of particles incoming from outside was computed the indoor to outdoor I/O ratio $PM_{2.5}$ levels.

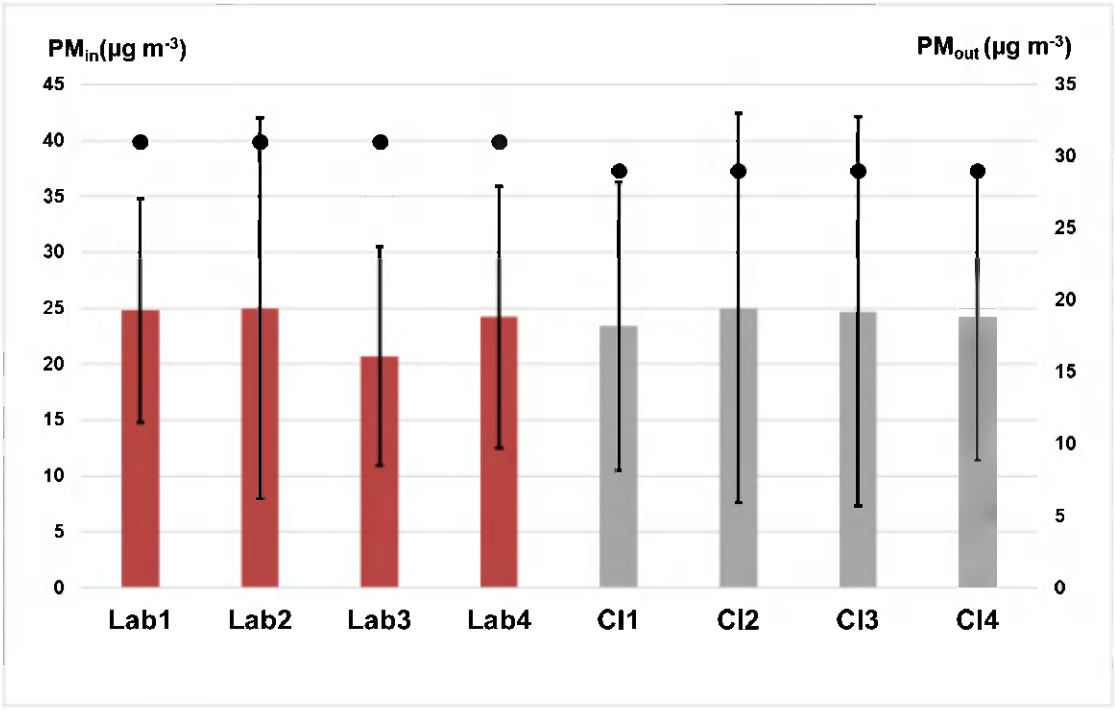

Figure 27. Mean $PM_{2.5}$ concentrations measured in each room in the two monitoring campaigns. Histograms: indoor $PM_{2.5}$ values; error bars represent one standard deviation of the mean; Points (right scale): outdoor $PM_{2.5}$ values.

The computed I/O values were close to 0.8, ranging from 0.67 ±0.17 (Lab3) to 0.86± 0.43 (Cl2) (Appendix, Table A18). These values always below 1 indicate that the penetration through building physical barriers can remove particles so that the particle concentration experienced by persons inside the schools is lower than outdoors.

Another critical IAQ parameter discussed in detail was the indoor CO_2 concentration, as it is of relevant health concern in schools (de Gennaro et al., 2013)(Bluyssen, 2017)(Stabile et al., 2019)(Fisk, 2017).

The mean CO_2 levels measured, pointed out critical situations since half of the surveyed rooms showed CO_2 levels exceeding the limit of 1000 ppm imposed by ASHRAE (American Society of Heating, Refrigerating and Air-Conditioning Engineers).

The measured data showed that the CO_2 concentration is significantly correlated with the student occupancy (Pearson $r=0.72$; $p>0.01$), with a general increase in more densely crowded rooms (Appendix, Tables A17 and A18).

This is consistent with literature that reports that the CO_2 concentration in closed spaces mainly depends on emission from the human body of occupants through breathing and correlates with human metabolic activity (Abbatt et al., 2020)(Becerra et al., 2020)(Schibuola et al., 2020).

Another reason for CO_2 accumulation may be an inadequate air exchange, as the investigated school buildings were lacking mechanical ventilation systems.

8.3 Summary

The main results of this school activity have been highly appreciated and the availability of IAQ monitoring sensors for continuous on-site measurements enabled students to achieve a good awareness of indoor pollution.

The presence of the sensor in the room stimulates healthier and environmentally friendly behaviour, permitting them to identify the most effective strategy to mitigate indoor air pollution.

9. General Conclusions

Although there is an increasing general consensus that the measurement of particulate oxidative potential represents a valuable additional method for assessing the relative toxicity of particulate matter to humans, some questions are still open.
A critical point is to design a standardized procedure to obtain data suitable for inter-comparison of different test methods on identical particle samples.
In particular, this thesis work tried to provide some useful informations regarding the operative conditions, the application on real PM samples and biological responses.

Once PM has been collected, suitable methods are needed to extract the PM from real samples. A substantial part of this thesis work is related to the choice of the extraction solvent, which was chosen for its chemical properties and to simulating more closely the physiological conditions.
The three tested solvents: i) the phosphate buffer, the most common aqueous buffer employed, ii) methanol, frequently used due to its ability to extract organic compounds, and iii) Gamble's solution, a complex artificial biological media that simulate different interstitial conditions in the lung.
The obtained results likely derive from the combination of different solvent solubility towards the redox-active species and also, the reactivity of such components in different solution media of OP assays.
For our research goals, the three tested solvents were useful for DTT and AA assays, as generate comparable OP responses, but the phosphate buffer provides the most sensible measure of OP^{DTT}.
In addition, to represent the first physical interface encountered by inhaled particles, were used different synthetic simulated lung fluids (SLFs), by addition of several antioxidants (i.e., GSH, Urate and Citrate) as solution media in AA a-cellular assay. Among the investigated surrogates, the simplified Asc solution shows the advantage of generating higher OP^{AA}, displaying higher sensitivity of the assay response, in comparison with the composite solutions containing two or more physiological AOs.
However, all the investigated assays can be used to measure OP^{AA} values, since they generate linearly correlated responses. Although our RTLF is a reasonable, simple surrogate for actual lung fluid, it certainly does not represent its full chemical or biological complexity.

Another important part of the studies conducted during the thesis on real PM samples has provided important informations to identify the specific contribution of the various PM chemical species on oxidative potential. By assessing the OP response of real PM samples collected in various locations across Italy, it was possible to investigate the variation of the OP activity with the particle size and chemical composition. They might be explained by variation in PM chemical composition, as a consequence of the different impacts of emission sources and atmospheric conditions.

The study supports the current literature highlighting that both OP assays respond to metals, mainly associated with vehicle traffic emission, and also to organics, from sources like biomass burning. Inside a general similarity among different investigated sites, the OP^{DTT}_V and OP^{AA}_V responses show some differences, in particular between Northern and Southern regions. Furthermore, the seasonal dependence of the relationships between OP values and chemical element concentrations was studied, showing the difference between winter and summer samples caused by different weather conditions.

The conclusions reached clearly confirm that OP is a multipollutant parameter, that integrates the composition effects into just one measurement, rather than speciation of individual components requiring a suite of instrumental measurements.

Further possible development will regard the study of the contribution of specific redox-active components to PM oxidative potential, in particular the oxidized PAHs (mainly quinones), which are able to promote the formation of reactive oxygen species (ROS). Further studies will be carried out to determine their concentration levels, their origin and their seasonal variation, but above all to estimate their potential impact on PM oxidative properties. A better understanding of the formation pathways and the environmental fate of oxy-PAHs will help to develop strategies for targeted mitigation of the atmospheric oxidation potential.

Finally, a minor part of the research studies regarded to the still unclear linkage between particle oxidative potential with adverse human health outcomes, to demonstrate that the OP measurements have biological plausibility. Encouraging results were obtained by exploring links between OP responses from cell-free assays and different oxidative stress-related responses derived from PM-exposed cells. On these were investigated the biochemical effects, analyzing genic and protein expression, and cellular morphological alterations.

There is clearly a need for more studies examining the association between particle oxidative potential with cellular endpoints, in order to provide new evidence of the usefulness of PM oxidative properties to represent the proinflammatory effects of some PM components.

Appendix A

Chapter 4

Table A1. Experimental parameters measured in $PM_{2.5}$ samples collected at the urban site: volume-normalized OP_V^{DTT} and OP_V^{AA} responses measured with different extraction protocols and concentrations of $PM_{2.5}$ mass and chemical components. Concentration of chemical species is in ng m^{-3}, unless differently specified.

Urban	OP_V^{DTT} PB	OP_V^{DTT} G	OP_V^{DTT} MeOH	OP_V^{AA} PB	OP_V^{AA} G	OP_V^{AA} MeOH	$PM_{2.5}$ µg m^{-3}	OC µg m^{-3}	EC µg m^{-3}	Levo	NH_4^+ µg m^{-3}	K^+	Cl^-	NO_3^- µg m^{-3}	SO_4^{2-} µg m^{-3}	Total metals	Fe	Mn	Zn	Pb	V
10/03/2018	0.16	0.07	0.09	0.56	0.34	0.14	17	4.82	1.12	192	1.68	100	230	3.73	1.11	97.85	92.83	1.55	<LOD	1.46	<LOD
11/03/2018	0.72	0.31	0.31	0.56	0.37	0.15	42	8.58	2.20	85.9	0.74	50	140	1.44	0.72	85.54	61.15	1.83	12.21	6.54	<LOD
12/03/2018	0.28	0.12	0.16	0.34	0.21	0.13	16	4.34	1.21	204.8	1.83	90	180	3.67	1.13	65.49	53.73	1.52	7.35	1.54	<LOD
16/03/2018	0.20	0.13	0.07	0.69	0.43	<LOD	17	3.39	0.62	171.8	2.35	60	240	5.44	1.31	67.54	51.24	1.63	11.97	1.52	<LOD
17/03/2018	0.17	0.11	0.06	0.45	0.32	<LOD	12	2.45	0.56	75	1.87	50	130	3.66	1.27	3.33	<LOD	0.66	<LOD	1.01	<LOD
18/03/2018	0.08	0.05	0.03	0.19	0.12	<LOD	7	2.70	0.48	64	1.00	<LOD	190	1.46	0.73	1.41	<LOD	<LOD	<LOD	0.79	<LOD
20/03/2018	1.38	0.23	0.46	0.25	0.20	0.18	20	3.85	0.79	177.3	2.84	110	160	4.58	3.19	59.06	42.56	1.79	10.69	2.56	<LOD
21/03/2018	0.98	0.14	0.42	0.38	0.34	0.27	18	4.01	0.82	120.7	2.16	100	180	3.74	2.68	113.24	96.87	2.29	9.98	2.52	<LOD
22/03/2018	0.66	0.11	0.22	0.69	0.55	0.30	21	5.18	1.38	182.8	2.08	130	130	4.27	1.68	23.34	521.12	4.79	12.63	2.65	<LOD
23/03/2018	0.42	0.18	0.12	0.40	0.60	0.27	18	4.90	1.25	148.1	2.02	120	160	4.61	1.33	248.13	226.45	3.60	13.09	2.98	<LOD
24/03/2018	0.16	0.16	0.16	0.58	0.58	0.30	14	4.15	0.93	104.2	1.52	90	150	2.71	1.03	151.79	136.22	2.50	8.96	2.27	<LOD
25/03/2018	0.33	0.20	0.20	0.47	1.25	0.24	24	6.00	1.52	215.7	2.38	170	160	3.87	2.31	109.07	90.07	2.05	10.90	3.80	<LOD
27/03/2018	0.40	0.28	0.24	0.35	0.28	0.25	21	4.89	1.07	131.6	2.27	130	<LOD	3.99	2.27	668.49	642.47	6.62	13.95	3.29	<LOD
28/03/2018	0.43	0.30	0.26	0.45	0.36	0.34	33	5.55	1.26	166.4	3.88	150	<LOD	8.82	3.22	263.29	239.51	4.22	12.80	3.20	<LOD
29/03/2018	<LOD	0.1	<LOD	0.70	0.47	0.39	11	3.24	0.84	51.2	1.51	80	<LOD	2.50	1.66	90.42	76.20	2.36	8.19	1.13	<LOD
02/04/2018	0.24	0.06	0.06	0.53	0.32	0.19	8	2.61	0.51	71.3	0.72	50	210	1.30	0.82	<LOD	<LOD	<LOD	<LOD	<LOD	<LOD

Table A2. Experimental parameters measured in $PM_{2.5}$ samples collected at the rural site: volume-normalized OP_V^{DTT} and OP_V^{AA} responses measured with different extraction protocols and concentrations of $PM_{2.5}$ mass and chemical components. Concentration of chemical species is in ng m^{-3}, unless differently specified.

Rural	OP_V^{DTT} PB	OP_V^{DTT} G	OP_V^{DTT} MeOH	OP_V^{AA} PB	OP_V^{AA} G	OP_V^{AA} MeOH	$PM_{2.5}$ µg m^{-3}	OC µg m^{-3}	EC µg m^{-3}	Levo	NH_4^+ µg m^{-3}	K^+	Cl^-	NO_3^- µg m^{-3}	SO_4^{2-} µg m^{-3}	Total metals	Fe	Mn	Zn	Pb	V
10/03/2018	0.11	0.03	0.05	0.40	0.49	0.13	16	4.50	0.83	234	1.72	130	< LOD	3.55	1.08	13.44	< LOD	1.28	< LOD	1.85	0.79
13/03/2018	0.06	0.04	0.02	0.60	0.44	0.31	14	3.70	0.81	60.3	0.47	< LOD	< LOD	0.52	< LOD	15.07	< LOD	1.30	< LOD	2.23	0.13
15/03/2018	0.04	< LOD	0.01	0.17	0.13	0.12	12	3.81	0.53	149.9	1.44	90	< LOD	2.85	0.95	3.74	< LOD	1.08	< LOD	1.13	1.35
16/03/2018	0.05	0.01	< LOD	0.23	0.15	0.08	13	2.99	0.40	80.4	1.63	50	< LOD	3.04	1.03	2.76	< LOD	0.80	< LOD	0.99	0.46
20/03/2018	0.12	0.03	0.02	0.26	0.40	0.40	15	3.32	0.55	133.5	2.13	90	< LOD	2.75	2.61	55.02	40.93	2.10	< LOD	2.78	0.28
22/03/2018	0.11	0.03	0.03	0.21	0.35	0.12	15	3.79	0.54	146.3	1.72	110	< LOD	2.99	1.46	37.79	35.50	1.15	< LOD.	0.84	0.13
24/03/2018	0.15	0.06	0.01	0.28	0.22	< LOD	11	3.68	0.52	120.7	1.43	80	< LOD	2.59	0.93	35.98	33.40	1.02	< LOD	1.04	0.32
25/03/2018	0.16	0.09	0.09	0.21	0.27	< LOD	20	6.47	0.85	224.9	2.63	170	< LOD	4.35	2.25	52.92	40.07	1.01	< LOD	2.83	0.47
27/03/2018	0.08	0.04	0.05	0.16	0.17	0.06	20	5.44	0.69	129.8	2.93	140	< LOD	5.02	3.51	80.22	63.86	2.65	< LOD	2.19	0.29
30/03/2018	< LOD	< LOD	< LOD	0.38	0.26	0.33	11	2.46	0.45	75	1.12	60	< LOD	1.46	1.07	5.26	< LOD	1.22	< LOD	1.57	2.30
02/04/2018	< LOD	< LOD	< LOD	0.39	0.41	0.46	7	2.04	0.25	40.2	0.87	< LOD	< LOD	1.39	0.72	2.45	< LOD	1.26	< LOD	0.68	0.41
03/04/2018	0.08	0.02	< LOD	0.33	0.22	0.31	11	2.40	0.39	34.7	1.46	70	< LOD	2.73	1.35	85.43	80.86	1.76	< LOD	0.93	1.38
05/04/2018	0.06	0.01	0.01	0.31	0.15	0.20	17	2.47	0.47	43.9	2.85	60	< LOD	6.39	1.95	61.16	56.12	1.61	< LOD	1.44	1.14
06/04/2018	0.02	< LOD	< LOD	0.27	0.17	0.14	14	2.98	0.57	51.2	2.28	60	< LOD	5.21	1.37	39.24	35.74	1.26	< LOD	0.99	1.01
07/04/2018	0.08	0.04	0.02	< LOD	< LOD	< LOD	11	3.05	0.43	51.2	1.56	50	< LOD	2.58	1.18	44.49	39.87	1.21	< LOD	1.32	1.86
08/04/2018	0.01	< LOD	< LOD	< LOD	< LOD	< LOD	11	2.58	0.37	31.1	1.59	70	< LOD	2.53	1.3	3.85	< LOD	0.62	< LOD	0.68	2.40

Table A3 Experimental parameters measured in $PM_{2.5}$ particles: mean values and standard deviation (SD) computed for all the investigated samples (total, n=32) and the samples collected at the urban (n=16) and rural sites (n=16), separately. OP^{DTT} and OP^{AA} responses were measured after extraction with each investigated solvent and expressed as volume-based OP_V (nmol min^{-1} m^{-3}) and mass-based OP_m (nmol min^{-1} μg^{-1}) values. Concentrations of chemical components are expressed in ng m^{-3}, unless differently specified. * indicates statistically significant difference ($p<0.05$) among the extraction solvents; †indicates statistically significant difference between urban and rural samples.

	Total (n=32)		Urban(n=16)		Rural (n=16)	
	Mean	SD	Mean	SD	Mean	SD
OP_V^{DTT} PB (nmol min^{-1} m^{-3})	0.19	0.18	0.41*	0.18	0.08†	0.04
OP_V^{DTT} G (nmol min^{-1} m^{-3})	0.10	0.09	0.16	0.08	0.03†	0.03
OP_V^{DTT} MeOH (nmol min^{-1} m^{-3})	0.11	0.09	0.18	0.08	0.02†	0.03
OP_V^{AA} PB (nmol min^{-1} m^{-3})	0.38	0.16	0.47	0.15	0.30	0.12
OP_V^{AA} G (nmol min^{-1} m^{-3})	0.34	0.22	0.42	0.26	0.27	0.12
OP_V^{AA} MeOH (nmol min^{-1} m^{-3})	0.22*	0.08	0.24*	0.08	0.22	0.14
OP_m^{DTT} PB (nmol min^{-1} μg^{-1})	0.014	0.008	0.023	0.018	0.002†	0.002
OP_m^{DTT} G (nmol min^{-1} μg^{-1})	0.006	0.004	0.009	0.003	0.002†	0.002
OP_m^{DTT} MeOH (nmol min^{-1} μg^{-1})	0.006	0.005	0.010	0.006	0.001†	0.001
OP_m^{AA} PB (nmol min^{-1} μg^{-1})	0.027	0.015	0.031	0.016	0.024	0.013
OP_m^{AA} Gamble (nmol min^{-1} μg^{-1})	0.023	0.013	0.026	0.013	0.021	0.013
OP_m^{AA} MeOH (nmol min^{-1} μg^{-1})	0.013	0.012	0.012	0.009	0.016	0.015
$PM_{2.5}$ (μg m^{-3})	15.32	4.67	16.81	5.19	13.83†	3.66
OC (μg m^{-3})	3.95	1.41	4.42	1.49	3.48	1.14
EC (μg m^{-3})	0.79	0.41	1.04	0.43	0.54†	0.17
Levoglucosan	117.81	60.69	135.18	52.75	100.44	63.10
NH_4^+ (μg m^{-3})	1.83	0.72	1.93	0.77	1.74	0.66
K^+	84.69	43.87	92.50	42.20	76.88	44.12
Cl^-	70.63	88.14	141.25	74.57	< LOD†	-
NO_3^- (μg m^{-3})	3.43	1.65	3.74	1.76	3.12	1.46
SO_4^{2-} (μg m^{-3})	1.54	0.81	1.65	0.81	1.42	0.80
Metals	91.89	144.16	166.46	82.56	26.65†	16.14
Fe	80.84	123.03	128	58.38	33.68†	27.24
Mn	1.89	1.32	2.49	1.63	1.33	0.48
Zn	0.46	0.69	< LOD	-	0.92	0.73
Pb	4.58	5.60	10.21	3.52	< LOD†	-
V	1.89	1.23	2.33	1.48	1.47†	0.69

Table A4. Pearson inter-correlation matrix of OP_V (nmol min^{-1} m^{-3}) responses with concentration of $PM_{2.5}$ mass and chemical components for all $PM_{2.5}$ samples. OP_V were measured after extraction with phosphate buffer, Gamble's solution and methanol. Concentrations of chemical components are expressed in ng m^{-3}, unless differently specified. Significant r values based on a two-tailed t-test (n=32) are reported in **bold (at p-level < 0.01**) and in *italic (at p-level < 0.05*).

	OP_V^{DTT} PB	OP_V^{DTT} G	OP_V^{DTT} MeOH	OP_V^{AA} PB	OP_V^{AA} G	OP_V^{AA} MeOH
OP_V^{DTT} PB (nmol min^{-1} m^{-3})	1.00					
OP_V^{DTT} G (nmol min^{-1} m^{-3})	**0.683**	1.00				
OP_V^{DTT} MeOH (nmol min^{-1} m^{-3})	**0.945**	**0.807**	1.00			
OP_V^{AA} PB (nmol min^{-1} m^{-3})	0.175	*0.382*	0.226	1.00		
OP_V^{AA} G (nmol min^{-1} m^{-3})	0.162	*0.387*	0.255	**0.605**	1.00	
OP_V^{AA} MeOH (nmol min^{-1} m^{-3})	0.113	0.148	0.155	**0.4 56**	*0.431*	1.00
$PM_{2.5}$ (µg m^{-3})	**0.541**	**0.770**	**0.651**	0.253	0.305	0.075
OC (µg m^{-3})	*0.423*	**0.674**	**0.554**	0.227	*0.390*	-0.045
EC (µg m^{-3})	**0.507**	**0.781**	**0.631**	**0.486**	**0.532**	0.161
Levoglucosan	0.359	*0.376*	0.427	0.161	*0.430*	-0.118
NH_4^+ (µg m^{-3})	0.307	*0.361*	0.371	-0.136	0.059	-0.051
K^+	0.319	*0.419*	0.421	-0.012	*0.387*	0.011
Cl^-	**0.471**	*0.402*	**0.472**	**0.454**	0.324	-0.137
NO_3^- (µg m^{-3})	0.240	*0.360*	0.305	0.002	0.045	-0.065
SO_4^{2-} (µg m^{-3})	**0.452**	*0.379*	**0.496**	-0.186	0.076	0.114
Metals	0.239	**0.643**	*0.399*	0.114	0.156	0.245
Fe	0.335	**0.539**	*0.423*	0.280	0.222	0.296
Mn	0.363	**0.609**	**0.473**	0.293	0.290	*0.442*
Zn	0.083	*0.442*	0.232	*0.428*	*0.420*	0.264
Pb	0.268	**0.871**	**0.755**	**0.498**	**0.480**	0.292
V	*0.432*	**0.473**	**0.675**	-0.033	0.025	0.050

Table A5. Pearson inter-correlation matrix of volume normalized OP_V (nmol min^{-1} m^{-3}) responses with concentration of $PM_{2.5}$ mass and chemical components for $PM_{2.5}$ samples collected at the urban site. OP_V were measured after extraction with phosphate buffer, Gamble's solution and methanol. Significant r values based on a two-tailed t-test (n=16) are reported in **bold (at p-level < 0.01**) and in *italic (at p-level < 0.05*).

Urban	OP_V^{DTT} PB	OP_V^{DTT} Gamble	OP_V^{DTT} MeOH	OP_V^{AA} PB	OP_V^{AA} Gamble	OP_V^{AA} MeOH
OP_V^{DTT} PB (nmol min^{-1} m^{-3})	1.00					
OP_V^{DTT} G (nmol min^{-1} m^{-3})	0.468	1.00				
OP_V^{DTT} MeOH (nmol min^{-1} m^{-3})	**0.929**	**0.634**	1.00			
OP_V^{AA} PB (nmol min^{-1} m^{-3})	-0.319	-0.141	-0.328	1.00		
OP_V^{AA} G (nmol min^{-1} m^{-3})	-0.123	0.137	-0.036	0.363	1.00	
OP_V^{AA} MeOH (nmol min^{-1} m^{-3})	-0.158	0.321	0.275	0.278	0.358	1.00
$PM_{2.5}$ (µg m^{-3})	0.448	**0.846**	*0.586*	0.098	-0.036	0.237
OC (µg m^{-3})	0.317	**0.715**	0.468	0.148	0.352	0.296
EC (µg m^{-3})	0.248	*0.626*	0.379	0.196	0.391	0.327
Levoglucosan	0.283	0.207	0.345	-0.034	0.353	0.059
NH_4^+ (µg m^{-3})	0.340	0.476	0.430	-0.138	0.147	0.285
K^+	0.312	0.488	0.445	0.072	0.579	0.655
Cl^-	0.040	-0.521	-0.097	-0.044	-0.003	-0.612
NO_3^- (µg m^{-3})	0.194	0.428	0.276	0.002	0.095	0.230
SO_4^{2-} (µg m^{-3})	0.600	0.518	*0.676*	-0.260	0.119	0.449
Metals	0.020	0.594	0.212	-0.186	0.011	0.373
Fe	0.125	0.377	0.220	0.092	0.088	0.465
Mn	0.201	0.572	0.338	0.107	0.162	*0.607*
Zn	0.451	**0.735**	*0.547*	0.144	0.333	*0.512*
Pb	0.795	0.428	**0.684**	-0.218	-0.136	0.023

Table A6. Pearson inter-correlation matrix of volume normalized OP_V (nmol min^{-1} m^{-3}) responses with concentration of $PM_{2.5}$ mass and chemical components for $PM_{2.5}$ samples collected at the rural site. OP_V were measured after extraction with phosphate buffer, Gamble's solution and methanol. Significant r values based on a two-tailed t-test (n=16) are reported in **bold (at p-level < 0.01**) and in *italic (at p-level < 0.05*).

Rural	OP_V^{DTT} PB	OP_V^{DTT} Gamble	OP_V^{DTT} MeOH	OP_V^{AA} PB	OP_V^{AA} Gamble	OP_V^{AA} MeOH
OP_V^{DTT} PB (nmol min^{-1} m^{-3})	1.00					
OP_V^{DTT} G (nmol min^{-1} m^{-3})	**0.859**	1.00				
OP_V^{DTT} MeOH (nmol min^{-1} m^{-3})	**0.679**	**0.818**	1.00			
OP_V^{AA} PB (nmol min^{-1} m^{-3})	-0.044	-0.045	-0.092	1.00		
OP_V^{AA} G (nmol min^{-1} m^{-3})	0.265	0.166	0.243	**0.782**	1.00	
OP_V^{AA} MeOH (nmol min^{-1} m^{-3})	-0.348	-0.406	-0.401	**0.662**	*0.597*	1.00
$PM_{2.5}$ (µg m^{-3})	*0.521*	*0.538*	**0.753**	-0.039	0.116	-0.343
OC (µg m^{-3})	*0.653*	**0.770**	**0.930**	-0.099	0.179	-0.489
EC (µg m^{-3})	*0.552*	*0.622*	**0.765**	0.297	0.430	-0.248
Levoglucosan	**0.672**	*0.570*	**0.792**	0.013	0.424	-0.301
NH_4^+ (µg m^{-3})	0.339	0.294	0.473	-0.419	-0.278	-0.391
K^+	**0.628**	0.546	**0.781**	-0.360	0.007	-0.513
NO_3^- (µg m^{-3})	0.206	0.125	0.312	-0.306	-0.308	-0.394
SO_4^{2-} (µg m^{-3})	0.335	0.307	0.466	-0.415	-0.153	-0.179
Metals	0.493	0.425	0.323	-0.142	-0.107	-0.064
Fe	0.438	0.350	0.215	-0.203	-0.199	-0.084
Mn	0.174	0.099	0.160	0.127	0.200	0.333
Pb	*0.507*	*0.617*	**0.677**	0.217	0.393	0.082
V	-0.530	-0.451	-0.373	-0.403	-0.607	-0.123

Table A7. OP^{AA} responses (nmol min^{-1} m^{-3}) of 5 standard solutions of redox-active species measured in different compositions of surrogate RTLF by adding citrate, urate and glutathione to Ascorbic acid.

RTLF	STD	OP^{AA} (nmol min^{-1} m^{-3})	S.D.	$\%OP^{AA}$
Asc 100 µM	Cu^{2+} (0.1 µM)	2.33	0.09	
	Fe^{2+} (1 µM)	0.19	0.02	
	1,2 NPQ (0.2 µM)	1.12	0.05	
	1,4 NPQ (1 µM)	0.37	0.08	
	9,10 PQN (1 µM)	0.82	0.03	
	Reagent blank	0.59	0.01	
Asc + citrate 100:150 µM	Cu^{2+} (0.1 µM)	1.63	0.03	30
	Fe^{2+} (1 µM)	0.31	0.01	+ 62 (increase)
	1,2 NPQ (0.2 µM)	0.65	0.02	42
	1,4 NPQ (1 µM)	0.29	0.03	22
	9,10 PQN (1 µM)	0.60	0.03	27
	Reagent blank	0.48	0.10	
Asc + glutathione 100:50 µM	Cu^{2+} (0.1 µM)	0.11	0.02	95
	Fe^{2+} (1 µM)	0.18	0.04	6
	1,2 NPQ (0.2 µM)	0.42	0.03	63
	1,4 NPQ (1 µM)	0.03	0.03	92
	9,10 PQN (1 µM)	0.38	0.03	54
	Reagent blank	0.40	0.03	
Asc + urate 100:50 µM	Cu^{2+} (0.1 µM)	1.45	0.02	38
	Fe^{2+} (1 µM)	0.16	0.06	17
	1,2 NPQ (0.2 µM)	0.53	0.03	53
	1,4 NPQ (1 µM)	0.21	0.03	43
	9,10 PQN (1 µM)	0.48	0.06	41
	Reagent blank	0.38	0.32	

Table A8. OP^{AA} responses (nmol min^{-1} m^{-3}) of 5 standard solutions of redox-active species measured in different compositions of surrogate RTLF by adding citrate, urate and glutathione to Ascorbic acid.

RTLF	STD	OP^{AA} (nmol min^{-1} m^{-3})	S.D.	$\%OP^{AA}$
Asc + citrate + glutathione 100:150:50 µM	Cu^{2+} (0.1 µM)	0.06	0.03	97
	Fe^{2+} (1 µM)	0.05	0.02	76
	1,2 NPQ (0.2 µM)	0.08	0.02	93
	1,4 NPQ (1 µM)	0.04	0.02	89
	9,10 PQN (1 µM)	0.09	0.02	89
	Reagent blank	0.28	0.01	
Asc + citrate + glutathione + urate 100:150:50:50 µM	Cu^{2+} (0.1 µM)	0.02	0.01	98
	Fe^{2+} (1 µM)	0.05	0.02	67
	1,2 NPQ (0.2 µM)	0.08	0.03	84
	1,4 NPQ (1 µM)	0.00	0.01	96
	9,10 PQN (1 µM)	0.04	0.02	94
	Reagent blank	0.18	0.01	
Asc + citrate + glutathione + urate 100:100:100:100 µM	Cu^{2+} (0.1 µM)	0.02	0.01	99
	Fe^{2+} (1 µM)	0.05	0.02	72
	1,2 NPQ (0.2 µM)	0.08	0.03	94
	1,4 NPQ (1 µM)	0.00	0.01	96
	9,10 PQN (1 µM)	0.04	0.02	98
	Reagent blank	0.11	0.02	

Table A9. OP^{AA} responses of 20 $PM_{2.5}$ samples measured in different compositions of surrogate RTLF by adding citrate, urate and glutathione to Ascorbic acid. For each sample, measurements were repeated 5 times (mean and standard deviation).

RTLF	Samples	OP^{AA} (nmol min^{-1} m^{-3})	SD	Samples	OP^{AA} (nmol min^{-1} m^{-3})	SD
Asc 100µM	URB1	0.63	0.17	RUR1	0.29	0.09
	URB2	0.32	0.05	RUR2	0.28	0.09
	URB3	0.48	0.09	RUR3	0.25	0.09
	URB4	0.52	0.17	RUR4	0.26	0.09
	URB5	0.65	0.17	RUR5	0.27	0.09
	URB6	0.51	0.13	RUR6	0.34	0.05
	URB7	0.53	0.13	RUR7	0.26	0.05
	URB8	0.54	0.13	RUR8	0.12	0.04
	URB9	0.50	0.13	RUR9	0.32	0.05
	URB10	0.52	0.13	RUR10	0.28	0.05
Asc + citrate 100:150 µM	URB1	0.14	0.09	RUR1	0.21	0.04
	URB2	0.08	0.05	RUR2	0.20	0.04
	URB3	0.13	0.09	RUR3	0.23	0.04
	URB4	0.16	0.09	RUR4	0.22	0.04
	URB5	0.12	0.09	RUR5	0.2	0.04
	URB6	0.14	0.05	RUR6	0.27	0.04
	URB7	0.14	0.05	RUR7	0.17	0.03
	URB8	0.11	0.05	RUR8	0.19	0.04
	URB9	0.12	0.05	RUR9	0.25	0.05
	URB10	0.10	0.05	RUR10	0.24	0.05
Asc + glutathione 100:50 µM	URB1	0.26	0.03	RUR1	0.05	0.03
	URB2	0.14	0.03	RUR2	0.04	0.03
	URB3	0.21	0.03	RUR3	0.06	0.03
	URB4	0.18	0.03	RUR4	0.04	0.03
	URB5	0.20	0.03	RUR5	0.03	0.03
	URB6	0.22	0.03	RUR6	0.08	0.03
	URB7	0.18	0.03	RUR7	0.03	0.03
	URB8	0.20	0.03	RUR8	0.02	0.03
	URB9	0.19	0.03	RUR9	0.08	0.03
	URB10	0.21	0.03	RUR10	0.10	0.02
Asc + urate 100:50 µM	URB1	0.09	0.05	RUR1	0.09	0.04
	URB2	0.05	0.03	RUR2	0.08	0.04
	URB3	0.06	0.05	RUR3	0.09	0.04
	URB4	0.07	0.05	RUR4	0.10	0.04
	URB5	0.06	0.05	RUR5	0.09	0.04
	URB6	0.05	0.05	RUR6	0.14	0.03
	URB7	0.08	0.05	RUR7	0.11	0.03
	URB8	0.07	0.05	RUR8	0.04	0.02
	URB9	0.08	0.05	RUR9	0.08	0.03
	URB10	0.07	0.05	RUR10	0.10	0.05

Table A10. OP^{AA} responses of 20 $PM_{2.5}$ samples measured in different compositions of surrogate RTLF by adding citrate, urate and glutathione to Ascorbic acid. For each sample, measurements were repeated 5 times (mean and standard deviation).

RTLF	Samples	OP^{AA} (nmol min^{-1} m^{-3})	SD	Samples	OP^{AA} (nmol min^{-1} m^{-3})	SD
Asc + citrate + glutathione 100:150:50 µM	URB1	0.09	0.03	RUR1	0.03	0.02
	URB2	0.05	0.03	RUR2	0.02	0.02
	URB3	0.06	0.03	RUR3	0.03	0.02
	URB4	0.07	0.03	RUR4	0.04	0.02
	URB5	0.06	0.03	RUR5	0.03	0.02
	URB6	0.05	0.01	RUR6	0.05	0.03
	URB7	0.08	0.02	RUR7	0.02	0.03
	URB8	0.07	0.02	RUR8	0.02	0.03
	URB9	0.08	0.02	RUR9	0.05	0.03
	URB10	0.07	0.02	RUR10	0.02	0.03
Asc + citrate + glutathione + urate 100:150:50:50 µM	URB1	0.07	0.03	RUR1	0.04	0.03
	URB2	0.03	0.03	RUR2	0.03	0.03
	URB3	0.06	0.03	RUR3	0.04	0.03
	URB4	0.08	0.02	RUR4	0.05	0.03
	URB5	0.10	0.03	RUR5	0.04	0.03
	URB6	0.07	0.03	RUR6	0.08	0.04
	URB7	0.07	0.04	RUR7	0.02	0.03
	URB8	0.07	0.03	RUR8	0.02	0.03
	URB9	0.07	0.02	RUR9	0.05	0.03
	URB10	0.07	0.03	RUR10	0.03	0.03

Table A11. OP^{AA} responses (nmol min^{-1} m^{-3}) of 20 $PM_{2.5}$ samples measured in different compositions of surrogate RTLF by adding citrate, urate and glutathione to Ascorbic acid. Filter responses are reported as mean and standard deviation values computed from quintuplicate measurements. $\%OP^{AA}$ represents the relative % decrease of OP^{AA} response in each surrogate RTLF with respect to that in the simplified Asc solution.

For $PM_{2.5}$ samples mean and standard deviation values were computed on all samples and from urban and rural sites, separately.

RTLF	Samples	OP^{AA} (nmol min^{-1} m^{-3})	SD	$\%OP^{AA}$	SD
Asc 100µM	All $PM_{2.5}$	0.39	0.15		
	Urban	0.52	0.09		
	Rural	0.27	0.06		
	Filter Blank	0.81	0.07		
Asc + citrate 100:150 µM	All $PM_{2.5}$	0.29	0.08	20	10
	Urban	0.36	0.03	29	8
	Rural	0.22	0.08	11	10
	Filter Blank	0.69	0.10		
Asc + glutathione 100:50 µM	All $PM_{2.5}$	0.08	0.05	79	6
	Urban	0.12	0.02	76	4
	Rural	0.05	0.03	83	5
	Filter Blank	0.59	0.06		
Asc + urate 100:50 µM	All $PM_{2.5}$	0.15	0.06	63	5
	Urban	0.20	0.03	61	5
	Rural	0.09	0.02	65	5
	Filter Blank	0.53	0.03		
Asc + citrate + glutathione 100:150:50 µM	All $PM_{2.5}$	0.05	0.02	87	3
	Urban	0.07	0.01	87	2
	Rural	0.03	0.02	87	3
	Filter Blank	0.39	0.02		
Asc + citrate + glutathione + urate 100:150:50:50 µM	All $PM_{2.5}$	0.05	0.02	86	4
	Urban	0.07	0.02	87	2
	Rural	0.04	0.02	85	5
	Filter Blank	0.22	0.03		

Chapter 5

Table A12. Concentrations of chemical components measured in PM_{10} and $PM_{2.5}$ particles: mean values and standard errors of the mean (SEMs) computed for AW and SS data, separately. Mass concentration of chemical species is in ng m^3, unless differently specified. Species with significant ($p<0.05$) differences between the seasons are marked by *. For each species, the mean mass percentage with respect to the total PM mass is reported in the brackets.

Species	PM_{10} (ng m^{-3})				$PM_{2.5}$ (ng m^{-3})			
	AW (N=15)		SS (N=24)		AW (N=15)		SS (N=24)	
	Mean	SEM	Mean	SEM	Mean	SEM	Mean	SEM
PM	34500	2600	28500	2000	26500	2500	20000	1500
$PM_{2.5}/PM_{10}$	0.8	0.1	0.7	0.1				
Na^+	606 (1.8)	81	688 (2.4)	58	156* (0.6)	23	237* (1.2)	20
NH_4^+	482 (1.4)	87	514 (1.8)	54	543* (2.0)	94	719* (3.6)	66
K^+	566* (1.6)	78	283* (1.0)	29	559* (2.1)	88	272* (1.4)	31
Mg^{2+}	113* (0.3)	12	177* (0.6)	15	35* (0.1)	5	81* (0.4)	10
Ca^{2+}	345* (1.0)	38	972* (3.4)	89	135* (0.5)	20	461* (2.3)	51
Cl^-	380 (1.1)	130	212 (0.7)	50	109 (0.4)	28	64 (0.3)	4
NO_3^-	2370 (7)	300	2150 (8)	380	1090* (4.1)	150	534* (2.7)	84
SO_4^{2-}	2590* (8)	370	3980* (14)	330	2410* (9)	370	3760* (19)	340
MS^-	7* (0.02)	1	51* (0.2)	7	6* (0.02)	1	45* (0.2)	6
Al	46* (0.1)	16	199* (0.7)	25	17* (0.06)	8	100* (0.5)	11
Ba	6 (0.02)	1	4.9 (0.02)	0.3	2.9 (0.01)	0.4	2.4 (0.01)	0.2
Cd	0.33 (0.001)	0.01	0.09 ($3\cdot10^{-4}$)	0.03	0.33 (0.001)	0.03	0.06 ($3\cdot10^{-4}$)	0.01
Ce	0.03 ($1\cdot10^{-4}$)	0.02	0.08 ($3\cdot10^{-4}$)	0.02	0.01 ($4\cdot10^{-5}$)	0.01	0.04 ($2\cdot10^{-4}$)	0.02
Co	0.20 (0.001)	0.01	0.4 (0.001)	0.1	0.18 (0.001)	0.01	0.14 (0.001)	0.01
Cr	1.5 (0.004)	0.1	2.2 (0.01)	0.1	1.3 (0.005)	0.2	1.7 (0.01)	0.1
Cu	10 (0.03)	1	7 (0.02)	1	7 (0.03)	2	3.5 (0.02)	0.3
Fe	241 (0.7)	30	270 (0.9)	20	107 (0.4)	15	134 (1)	10
La	0.01 ($3\cdot10^{-5}$)	0.01	0.03 ($1\cdot10^{-4}$)	0.01	0.01 ($4\cdot10^{-5}$)	0.01	0.01 ($1\cdot10^{-4}$)	0.01
Mn	3.2* (0.01)	0.3	5.6* (0.02)	0.5	1.7* (0.01)	0.2	3.0* (0.02)	0.3
Mo	3.2 (0.01)	0.5	2.3 (0.01)	0.3	2.6 (0.01)	0.4	2.3 (0.01)	0.4
Ni	2.4* (0.01)	0.2	3.8* (0.01)	0.4	2.2* (0.01)	0.3	3.1* (0.02)	0.4
P	20* (0.1)	2	37* (0.1)	2	13* (0.05)	1	23* (0.1)	2
Pb	8 (0.02)	1	8 (0.03)	2	6 (0.02)	1	4 (0.02)	1
Sr	1.7 (0.005)	0.2	2.2 (0.01)	0.3	0.7 (0.003)	0.1	0.9 (0.005)	0.1
Ti	1.7* (0.005)	0.4	7* (0.02)	1	0.7* (0.003)	0.2	6* (0.03)	3
V	1.6* (0.005)	0.1	6* (0.02)	1	1.4* (0.005)	0.1	6* (0.03)	1
Zn	63 (0.2)	9	46 (0.2)	4	40 (0.2)	4	45 (0.2)	6
OC	8800 (26)	300	6200 (22)	200	8400 (32)	300	5100 (26)	100
EC	3500* (10)	200	1700* (6)	100	3400* (13)	200	1600* (8)	100
OC/EC	2.5	0.5	3.6	0.9	2.5	0.5	3.2	1.2
SOC	1800 (5)	100	2800 (10)	100	1500 (6)	100	2000 (10)	100
POC	7000* (20)	300	3400* (12)	100	6900* (26)	300	3100* (16)	100
Oxalate	171* (0.5)	17	269* (1)	20	159* (0.6)	13	204* (1)	14
Acetate	24* (0.1)	3	11* (0.04)	1	24* (0.1)	2	9* (0.05)	1
Glycolate	18 (0.1)	2	25 (0.1)	2	14 (0.1)	2	11 (0.1)	1
Propionate	1.9 (0.01)	0.5	0.3 (0.001)	0.3	1.2 (0.004)	0.2	0.2 (0.001)	0.1
Formate	33* (0.1)	3	21* (0.1)	2	25 (0.1)	2	20 (0.1)	4
Pyruvate	7* (0.02)	1	3* (0.01)	1	2 (0.01)	1	2 (0.01)	1

Table A13. Pearson correlation coefficients (r) between OP^{DTT}_V and OP^{AA}_V responses and chemical components in PM_{10} and $PM_{2.5}$ particles computed for autumn-winter (AW, 15 days) and spring-summer (SS, 24 days) data, separately. Statistically significant correlations are marked by *** at p<0.01 level, ** at p<0.02 level, and * at p<0.05 level.

Parameter	Autumn-Winter				Spring-Summer			
	PM_{10}		$PM_{2.5}$		PM_{10}		$PM_{2.5}$	
	OP_V^{AA}	OP_V^{DTT}	OP_V^{AA}	OP_V^{DTT}	OP_V^{AA}	OP_V^{DTT}	OP_V^{AA}	OP_V^{DTT}
PM_{10} OP_V^{AA}	**1.00**	0.50	**0.61****	**0.75*****	**1.00**	**0.45***	0.20	0.29
PM_{10} OP_V^{DTT}	0.50	**1.00**	**0.70*****	**0.65*****	**0.45***	**1.00**	**0.42***	**0.57*****
$PM_{2.5}$ OP_V^{AA}	**0.61****	**0.70*****	**1.00**	**0.91*****	0.20	**0.42***	**1.00**	**0.70*****
$PM_{2.5}$ OP_V^{DTT}	**0.75*****	**0.65*****	**0.91*****	**1.00**	**0.29**	**0.57*****	**0.70*****	**1.00**
PM_{10} mass	0.47	**0.70*****	**0.84*****	**0.81*****	0.24	0.30	**0.50*****	**0.72*****
$PM_{2.5}$ mass	0.46	**0.59****	**0.82*****	**0.79*****	0.18	0.24	**0.47****	**0.63*****
Na^+	**-0.64*****	-0.49	-0.32	-0.43	**-0.40***	-0.18	**0.41***	0.29
NH_4^+	-0.32	-0.05	-0.07	-0.05	**0.63*****	**0.43***	-0.25	0.00
K^+	**0.64*****	**0.70*****	**0.79*****	**0.73*****	**0.44***	0.25	0.19	0.26
Mg^{2+}	-0.41	-0.23	-0.06	-0.09	0.17	0.14	0.01	0.13
Ca^{2+}	0.18	0.32	0.23	0.27	**0.52*****	0.27	0.02	0.14
Cl^-	-0.46	-0.23	-0.14	-0.20	**-0.53*****	**-0.49****	0.08	-0.03
NO_3^-	0.13	0.46	**0.60****	**0.66*****	-0.00	0.39	**0.51*****	**0.45***
SO_4^{2-}	-0.36	-0.15	-0.05	-0.04	**0.71*****	0.34	-0.22	0.01
MS^-	**0.62*****	0.12	0.21	0.26	**0.52*****	0.00	-0.35	-0.05
Al	0.13	0.02	-0.01	0.04	0.37	-0.00	-0.06	0.20
Ba	**0.89*****	**0.57***	**0.67*****	**0.62*****	0.22	0.30	0.45	0.34
Cd	**0.67*****	**0.55***	**0.75*****	**0.73*****	-0.11	0.02	0.18	0.31
Ce	0.27	0.38	**0.53***	0.40	0.07	-0.18	-0.26	-0.14
Co	-0.06	0.22	0.28	0.32	-0.08	-0.32	0.09	-0.18
Cr	**0.61****	0.23	0.37	0.35	0.09	0.27	0.14	0.02
Cu	**0.84*****	0.50	**0.64*****	**0.56***	0.21	**0.52*****	**0.63*****	**0.47****
Fe	**0.76*****	**0.53***	**0.76*****	**0.80*****	0.38	0.26	0.17	0.34
La	0.19	0.22	0.24	0.10	0.21	-0.18	-0.38	-0.06
Mn	**0.57***	0.38	**0.58****	**0.66*****	**0.46****	0.13	0.15	0.32
Mo	0.19	0.21	-0.47	-0.44	0.14	-0.08	**-0.43***	-0.33
Ni	0.29	0.16	0.27	0.04	**0.48****	-0.08	-0.25	-0.10
P	0.17	0.29	**0.76*****	**0.72*****	**0.56*****	0.15	0.04	0.07
Pb	-0.28	0.00	0.49	0.44	0.16	0.14	0.34	0.29
Sr	-0.03	-0.15	0.24	0.18	0.34	-0.06	-0.05	0.18
Ti	0.17	0.06	0.14	0.21	**0.44***	0.07	0.06	-0.21
V	**0.63*****	0.42	**0.73*****	**0.77*****	**0.59*****	0.13	-0.21	0.02
Zn	-0.44	-0.43	**0.64*****	0.41	0.38	-0.13	-0.09	-0.03
OC	**0.65*****	**0.76*****	**0.83*****	**0.80*****	0.02	**0.52*****	**0.64*****	**0.65*****
EC	**0.71*****	**0.77*****	**0.86*****	**0.84*****	0.22	**0.63*****	**0.75*****	**0.73*****
POC	**0.71*****	**0.77*****	**0.86*****	**0.83*****	0.22	**0.62*****	**0.73*****	**0.71*****
SOC	-0.27	-0.04	-0.32	-0.39	-0.11	0.38	**0.40***	**0.43***
Oxalate	0.19	0.29	**0.55***	**0.52***	**0.53*****	**0.41***	0.25	0.39
Acetate	**0.66*****	0.35	**0.67*****	**0.58****	-0.06	-0.01	0.24	0.26
Glycolate	**0.58****	0.44	**0.60****	**0.59****	**0.41***	0.13	0.29	0.34
Propionate	**0.78*****	0.38	0.35	0.31	-0.00	**0.44***	-0.12	0.04
Formate	**0.65*****	0.37	0.37	0.33	0.36	0.03	0.28	0.23
Pyruvate	**0.63*****	0.19	-0.05	0.04	**-0.50*****	-0.05	-0.09	-0.36

Table A14. Pearson inter-correlation matrix among the analyzed species in the $PM_{2.5}$ samples for Autumn-Winter (October-March, 15 days). Positive r values significant at p-level < 0.05 based on a two-tailed t-test are reported in bold.

	OP^{AA}_V	OP^{DTT}_V	Na^+	NH_4^+	K^+	Mg^{2+}	Ca^{2+}	Cl^-	NO_3^-	SO_4^{2-}	Ox	Ac	Gl	Fo	MS^-	Al	Ba	Cd	Ce	Co	Cr	Cu	Fe	P	Pb	Zn	OC	EC	SOC	POC
OP^{AA}_V	1.00																													
OP^{DTT}_V	**0.91**	1.00																												
Na^+	-0.32	-0.43	1.00																											
NH_4^+	-0.07	-0.05	-0.32	1.00																										
K^+	**0.79**	**0.74**	-0.45	-0.31	1.00																									
Mg^{2+}	0.15	0.19	0.20	-0.34	0.14	1.00																								
Ca^{2+}	0.24	0.29	0.36	-0.44	0.20	**0.90**	1.00																							
Cl^-	-0.14	-0.20	**0.81**	-0.38	-0.05	0.21	0.41	1.00																						
NO_3^-	**0.60**	**0.66**	-0.17	-0.35	**0.63**	0.26	**0.49**	-0.06	1.00																					
SO_4^{2-}	-0.04	-0.04	-0.30	**0.99**	-0.30	-0.25	-0.37	-0.36	-0.38	1.00																				
Ox	**0.55**	**0.52**	-0.56	**0.64**	0.43	-0.18	-0.24	-0.33	0.06	**0.65**	1.00																			
Ac	**0.67**	**0.58**	-0.45	-0.01	**0.76**	0.25	0.18	-0.06	0.23	0.05	**0.51**	1.00																		
Gl	**0.60**	**0.59**	-0.63	0.48	**0.60**	-0.20	-0.23	-0.28	0.10	**0.49**	**0.84**	**0.75**	1.00																	
Fo	0.37	0.33	-0.48	**0.70**	0.27	-0.26	-0.39	-0.23	-0.28	**0.72**	**0.84**	**0.54**	**0.89**	1.00																
MS^-	0.21	0.26	-0.64	0.26	0.34	-0.20	-0.27	-0.55	0.29	0.23	**0.46**	0.17	0.25	0.15	1.00															
Al	-0.01	0.04	0.38	-0.37	-0.25	0.38	**0.59**	0.10	0.38	-0.37	-0.57	-0.36	-0.51	-0.64	-0.42	1.00														
Ba	**0.67**	**0.62**	-0.07	-0.64	**0.73**	0.00	0.21	0.11	**0.70**	-0.66	0.01	0.32	0.07	-0.26	0.24	0.11	1.00													
Cd	**0.75**	**0.73**	-0.31	-0.15	**0.66**	0.19	0.41	-0.14	**0.75**	-0.15	0.25	0.44	0.42	0.10	0.14	**0.41**	**0.56**	1.00												
Ce	**0.53**	0.40	-0.02	-0.11	**0.55**	0.40	**0.46**	0.16	**0.47**	-0.06	0.41	0.44	0.19	0.04	0.41	-0.10	**0.45**	0.38	1.00											
Co	0.28	0.32	0.09	-0.44	0.12	0.40	**0.56**	-0.04	**0.45**	-0.40	-0.23	-0.06	-0.29	-0.51	0.10	**0.67**	**0.46**	**0.51**	0.38	1.00										
Cr	0.37	0.35	-0.10	-0.15	0.22	**0.53**	0.35	-0.14	-0.03	-0.07	0.06	0.22	0.10	0.15	-0.14	0.13	0.06	0.26	0.14	0.33	1.00									
Cu	**0.64**	**0.56**	-0.15	-0.35	**0.81**	0.42	**0.51**	0.18	**0.65**	-0.32	0.33	**0.58**	0.27	0.00	0.38	-0.08	**0.67**	**0.57**	**0.90**	0.38	0.21	1.00								
Fe	**0.76**	**0.80**	-0.25	-0.35	**0.69**	0.33	**0.54**	-0.07	**0.84**	-0.34	0.21	0.37	0.23	-0.10	0.24	0.40	**0.73**	**0.87**	**0.60**	**0.66**	0.29	**0.75**	1.00							
P	**0.76**	**0.72**	-0.01	-0.38	**0.64**	0.16	0.43	0.17	**0.79**	-0.39	0.12	0.31	0.13	-0.14	0.16	0.31	**0.81**	**0.74**	**0.57**	**0.46**	0.13	**0.70**	**0.88**	1.00						
Pb	**0.49**	0.44	0.13	0.18	0.30	0.21	0.28	0.32	0.05	0.24	0.28	**0.57**	**0.49**	0.45	-0.16	-0.07	0.09	0.32	0.24	0.07	0.32	0.24	0.18	0.27	1.00					
Zn	**0.64**	0.41	0.10	-0.06	**0.62**	0.14	0.30	0.29	0.44	-0.03	0.36	**0.53**	**0.44**	0.24	-0.05	-0.02	**0.44**	**0.58**	**0.62**	0.14	0.13	**0.66**	**0.48**	**0.56**	**0.54**	1.00				
OC	**0.83**	**0.80**	-0.43	-0.27	**0.98**	0.15	0.24	-0.03	**0.65**	-0.26	**0.49**	**0.76**	**0.63**	0.29	0.29	-0.19	**0.74**	**0.70**	**0.59**	0.19	0.20	**0.82**	**0.75**	**0.68**	0.33	**0.65**	1.00			
EC	**0.86**	**0.84**	-0.42	-0.25	**0.94**	0.17	0.29	-0.07	**0.71**	-0.24	**0.52**	**0.68**	**0.57**	0.24	0.36	-0.11	**0.77**	**0.74**	**0.66**	0.31	0.22	**0.85**	**0.84**	**0.75**	0.27	**0.63**	**0.98**	1.00		
SOC	-0.32	-0.39	0.09	-0.04	-0.03	-0.16	-0.29	0.23	-0.43	-0.03	-0.25	0.22	0.14	0.21	-0.38	-0.36	-0.30	-0.34	-0.46	-0.64	-0.12	-0.34	-0.58	-0.46	0.22	-0.04	-0.12	-0.32	1.00	
POC	**0.86**	**0.83**	-0.42	-0.25	**0.95**	0.17	0.29	-0.08	0.71	-0.25	0.52	**0.69**	**0.57**	0.23	0.36	-0.12	**0.77**	**0.75**	**0.66**	0.32	0.22	**0.85**	**0.83**	**0.75**	0.26	**0.64**	**0.98**	**1.00**	-0.32	1.00

Table A15. Pearson inter-correlation matrix among the analyzed species in the $PM_{2.5}$ samples for Spring-Summer (April-September, 24 days). Positive r values significant at p-level < 0.05 based on a two-tailed t-test are reported in bold.

	OP^{AA}_V	OP^{DTT}_V	Na^+	NH_4^+	K^+	Mg^{2+}	Ca^{2+}	Cl^-	NO_3^-	SO_4^{2-}	Ox	Ac	Gl	Fo	MS^-	Al	Ba	Cd	Ce	Co	Cr	Cu	Fe	P	Pb	Zn	OC	EC	SOC	POC
OP^{AA}_V	1.00																													
OP^{DTT}_V	**0.70**	1.00																												
Na^+	0.41	0.29	1.00																											
NH_4^+	-0.25	0.00	-0.58	1.00																										
K^+	0.18	0.25	-0.03	0.36	1.00																									
Mg^{2+}	-0.09	0.06	-0.09	0.35	0.39	1.00																								
Ca^{2+}	0.02	0.14	-0.09	**0.45**	**0.47**	0.89	1.00																							
Cl^-	0.08	-0.03	**0.83**	-0.53	-0.29	-0.18	-0.25	1.00																						
NO_3^-	**0.51**	0.45	**0.45**	-0.30	0.05	0.05	0.04	0.23	1.00																					
SO_4^{2-}	-0.22	0.00	-0.60	**0.97**	0.43	**0.43**	**0.55**	-0.60	-0.37	1.00																				
Ox	0.25	0.39	-0.18	**0.63**	**0.67**	**0.63**	**0.76**	-0.38	-0.04	**0.70**	1.00																			
Ac	0.24	0.26	0.07	-0.17	0.20	0.18	0.07	0.10	0.19	-0.11	0.17	1.00																		
Gl	0.29	0.34	-0.21	**0.61**	**0.62**	**0.48**	**0.69**	-0.44	-0.14	**0.69**	**0.90**	-0.01	1.00																	
Fo	0.28	0.23	0.17	0.22	**0.51**	0.23	0.32	-0.09	-0.01	0.28	0.33	0.08	0.39	1.00																
MS^-	-0.35	-0.05	-0.43	**0.52**	**0.46**	**0.46**	**0.60**	-0.48	-0.18	**0.58**	**0.57**	-0.16	**0.47**	-0.12	1.00															
Al	-0.06	0.20	-0.11	0.40	**0.63**	**0.67**	**0.79**	-0.37	-0.01	**0.52**	**0.62**	0.08	**0.55**	**0.56**	**0.61**	1.00														
Ba	**0.45**	0.34	-0.13	-0.01	0.27	0.09	0.17	-0.51	0.30	0.04	0.24	0.04	0.23	0.19	0.21	0.26	1.00													
Cd	0.18	0.31	-0.42	**0.47**	**0.59**	**0.57**	**0.63**	-0.57	0.03	**0.57**	**0.73**	0.16	**0.58**	0.22	**0.59**	**0.61**	0.40	1.00												
Ce	-0.26	-0.14	0.13	0.38	0.18	**0.57**	**0.60**	0.06	0.02	0.40	0.25	-0.11	0.19	**0.51**	0.29	**0.58**	-0.02	0.11	1.00											
Co	0.09	-0.18	-0.45	0.09	0.24	0.21	0.24	-0.49	-0.13	0.19	0.12	0.21	0.23	0.02	0.17	0.20	0.35	0.36	-0.07	1.00										
Cr	0.14	0.02	0.14	-0.15	-0.47	-0.12	-0.18	0.32	-0.05	-0.14	-0.32	0.16	-0.26	-0.03	-0.54	-0.32	-0.15	-0.23	0.03	-0.04	1.00									
Cu	**0.63**	**0.47**	0.12	0.20	**0.56**	0.32	**0.45**	-0.27	0.29	0.25	**0.68**	0.07	**0.65**	**0.52**	0.09	0.39	**0.47**	**0.56**	0.08	0.10	-0.36	1.00								
Fe	0.17	0.34	-0.12	0.26	**0.64**	**0.60**	**0.72**	-0.45	0.09	0.40	**0.59**	0.18	**0.54**	**0.49**	**0.51**	**0.92**	**0.45**	**0.68**	0.35	**0.43**	-0.31	**0.48**	1.00							
P	0.04	0.07	-0.33	**0.46**	**0.62**	**0.72**	**0.81**	-0.60	-0.02	**0.57**	**0.68**	0.07	**0.66**	0.38	**0.60**	**0.81**	0.39	**0.66**	0.40	**0.58**	-0.42	**0.51**	**0.86**	1.00						
Pb	0.34	0.29	-0.19	0.15	0.17	0.40	**0.45**	-0.30	-0.05	0.26	**0.56**	0.07	**0.43**	0.11	0.37	0.33	0.41	**0.67**	0.08	0.12	-0.12	**0.51**	0.39	0.39	1.00					
Zn	-0.09	-0.03	0.00	-0.27	-0.02	-0.03	-0.17	0.11	-0.18	-0.20	-0.13	0.18	-0.15	-0.13	-0.20	-0.13	-0.08	-0.03	-0.21	0.11	0.27	-0.11	-0.07	-0.13	0.08	1.00				
OC	**0.64**	**0.65**	0.33	-0.21	0.09	-0.21	-0.17	0.14	**0.72**	-0.28	0.02	0.24	0.04	0.02	-0.27	-0.17	0.31	-0.10	-0.23	-0.04	0.04	0.17	-0.01	-0.13	-0.12	-0.05	1.00			
EC	**0.75**	**0.73**	0.21	-0.08	0.30	-0.12	-0.05	-0.14	**0.74**	-0.11	0.19	0.27	0.16	0.16	-0.14	0.01	**0.53**	0.23	-0.23	0.08	-0.11	**0.48**	0.23	0.09	0.07	-0.14	**0.85**	1.00		
SOC	0.40	0.43	0.36	-0.27	-0.11	-0.23	-0.24	0.33	**0.53**	-0.36	-0.13	0.16	-0.06	-0.10	-0.31	-0.28	0.05	-0.35	-0.18	-0.13	0.16	-0.11	-0.21	-0.29	-0.25	0.04	**0.90**	**0.53**	1.00	
POC	**0.73**	**0.71**	0.21	-0.09	0.30	-0.13	-0.06	-0.14	**0.75**	-0.12	0.19	0.28	0.16	0.18	-0.14	0.00	0.53	0.22	-0.23	0.09	-0.11	**0.49**	0.23	0.11	0.07	-0.15	**0.84**	1.00	**0.53**	1.00

Chapter 7

Table A16. Quantitative results of the MIP-SPE procedure of PAHs under optimized conditions: linearity (expressed as correlation coefficient R^2), sensitivity (expressed as slope of the calibration curve for the calibration range listed), limit of detection (LOD), limit of quantification (LOQ) and precision (RSD %, relative standard deviations from five replicate measurements). Both LOD and LOQ values are listed in ng mL^{-1} as well as in ng m^{-3} units.

PAH	Calibration range (ng mL^{-1}) [a]	R^2	sensitivity	LOD (ng mL^{-1})	LOD (ng m^{-3})	LOQ (ng mL^{-1})	LOQ (ng m^{-3})	Intra-day RSD%[b]
FluA	35 - 300	0.995	7.9	**11.4**	**0.09**	**38.1**	**0.33**	3.6
Pyr	15 - 300	0.992	14.5	4.8	0.03	15.9	0.12	4.9
BaA	18 - 300	0.996	12.5	5.4	0.06	18.3	0.15	3.8
Chr	13 - 300	0.999	14.7	**3.9**	**0.03**	**13.5**	**0.12**	2.5
BbF	16 - 300	0.995	13.1	5.1	0.03	16.5	0.15	3.2
BkF	21 - 300	0.995	12.7	6.3	0.06	21.3	0.18	3.3
BaP	15 - 300	0.997	13	4.5	0.03	15.6	0.12	3.7
InP	25 - 300	0.992	8.1	7.5	0.06	25.2	0.21	4.6
DbA	24 - 300	0.998	6.7	7.5	0.06	24.6	0.21	5.7
BghiP	14 - 300	0.991	11.1	4.2	0.03	14.4	0.12	5.9

[a]The range of calibration corresponds to the linear range. The lowest concentration corresponds to the LOQ value.

[b]Calculated from standard solution containing 100 ng mL^{-1} of each PAH.

Chapter 8

Table A17. Characteristics of meteorological parameters and investigated rooms: outdoor temperature and $PM_{2.5}$ mass concentration measured during each monitoring campaign (mean ± standard deviation values); surface, volume and student occupancy of each investigated laboratory and classroom.

Monitoring period	Outdoor T (C°)	Outdoor $PM_{2.5}$ ($\mu g\ m^{-3}$)		Surface (m^2)	Volume (m^3)	Occupancy (n° m^{-2})
Cento secondary school						
11th to 24th Feb 2019	7 ± 1°C	31 ± 19	Lab1	225	1013	0.08
			Lab2	93.2	307	0.32
			Lab3	97.3	321	0.20
			Lab4	97.3	321	0.20
Ferrara secondary school						
28th Feb to 17th Mar 2019	11 ± 2°C	29 ± 16	Cl1	40.8	122	0.49
			Cl2	40.6	122	0.59
			Cl3	36.4	115	0.75
			Cl4	45.2	144	0.60

Table A18. Indoor parameters measured during each monitoring campaign in each investigated room (campaign mean ± standard deviation values).

	Indoor T (C°)	Indoor $PM_{2.5}$ ($\mu g\ m^{-3}$)	$PM_{2.5}$ I/O ratio	VOC (ppb)	CO_2 (ppm)	Relative Humidity (%)
Lab1	22.6 ± 0.9	24.8 ± 10.0	0.80 ± 0.16	206 ± 34	742± 124	32.0 ± 3.1
Lab2	20.9 ± 1.5	25.0 ± 17.0	0.81 ± 0.26	318 ± 110	1152 ± 402	40.7 ± 3.5
Lab3	22.1 ± 0.6	20.7 ± 9.8	0.67 ± 0.17	227 ± 74	822± 268	36.8 ± 3.2
Lab4	22.9 ± 1.0	24.2 ± 11.7	0.78 ± 0.17	254± 79	919 ± 285	35.4 ± 3.0
Cl1	22.1± 1.1	23.4 ± 12.9	0.81 ± 0.48	244 ± 69	885± 249	39.5 ± 3.0
Cl2	23.1 ± 1.6	25.0 ± 17.4	0.86 ± 0.43	319± 98	1152± 355	38.5 ± 4.3
Cl3	20.9 ± 0.6	24.7 ± 17.4	0.85 ± 0.77	301 ± 109	1089 ± 397	46.0 ± 3.2
Cl4	22.6 ± 0.9	24.8 ± 10.0	0.80 ± 0.16	206 ± 34	742± 124	32.0 ± 3.1

References

Abbas, I., Badran, G., Verdin, A., Ledoux, F., Roumié, M., Courcot, D., Garçon, G. (2018). Polycyclic aromatic hydrocarbon derivatives in airborne particulate matter: sources, analysis and toxicity. *Environmental Chemistry Letters* 16(2), 439–475. https://doi.org/10.1007/s10311-017-0697-0

Abbatt, J.P.D., Wang, C. (2020). The atmospheric chemistry of indoor environments. *Environmental Science: Processes and Impacts* 22(1), 25–48. https://doi.org/10.1039/c9em00386j

Abdel-Shafy, H.I., Mansour, M.S.M. (2016). A review on polycyclic aromatic hydrocarbons: Source, environmental impact, effect on human health and remediation. *Egyptian Journal of Petroleum* 25(1), 107–123. https://doi.org/10.1016/j.ejpe.2015.03.011

Akhtar, U.S., Mcwhinney, R.D., Rastogi, N., Abbatt, J.P.D., Evans, G.J., Scott, J.A. (2010). Cytotoxic and proinflammatory effects of ambient and source-related particulate matter (PM) in relation to the production of reactive oxygen species (ROS) and cytokine adsorption by particles. *Inhalation Toxicology* 22, 37–47. https://doi.org/10.3109/08958378.2010.518377

Akimoto, H. (2003). Global Air Quality and Pollution. *Science* 302(5651), 1716–1719. https://doi.org/10.1126/science.1092666

Ali, H., Khan, E., Ilahi, I. (2019). Environmental chemistry and ecotoxicology of hazardous heavy metals: Environmental persistence, toxicity, and bioaccumulation. *Journal of Chemistry* 2019. https://doi.org/10.1155/2019/6730305

Aliaga, M.E., Carrasco-Pozo, C., López-Alarcón C., Speisky, H. (2010). The Cu(I)-glutathione complex: factors affecting its formation and capacity to generate reactive oxygen species. *Transition Met Chem*, 35, 321–329. https://doi.org/10.1007/s11243-010-9330-9

Alves, C.A. (2008). Characterisation of solvent extractable organic constituents in atmospheric particulate matter: An overview. *Anais da Academia Brasileira de Ciencias* 80(1), 21–82. https://doi.org/10.1590/s0001-37652008000100003

Alves, C.A., Vicente, A.M., Custódio, D., Cerqueira, M., Nunes, T., Pio, C., Lucarelli, F., Calzolai, G., Nava, S., Diapouli, E., Eleftheriadis, K., Querol, X., Musa Bandowe, B. A. (2017). Polycyclic aromatic hydrocarbons and their derivatives (nitro-PAHs, oxygenated PAHs, and azaarenes) in PM 2.5 from Southern European cities. *Science of The Total Environment* 595, 494–504. https://doi.org/10.1016/j.scitotenv.2017.03.256

American Thoracic Society. (2000). What constitutes an adverse health effect of air pollution? Official statement of the American Thoracic Society. *American Journal of Respiratory and Critical Care Medicine* 161, 665–673. https://doi.org/10.1164/ajrccm.161.2.ats4-00

Anderson, J.O., Thundiyil, J.G., Stolbach, A. (2012). Clearing the Air: A Review of the

Effects of Particulate Matter Air Pollution on Human Health. *Journal of Medical Toxicology* 8(2), 166–175. https://doi.org/10.1007/s13181-011-0203-1

Antiñolo, M., Willis, M.D., Zhou, S., Abbatt, J.P.D. (2015). Connecting the oxidation of soot to its redox cycling abilities. *Nature Communications*, 6(6812). https://doi.org/10.1038/ncomms7812

Ayres, J.G., Borm, P., Cassee, F.R., Castranova, V., Donaldson, K., Ghio, A., Harrison, R. M., Hider, R., Kelly, F., Kooter, I.M., Marano, F., Maynard, R.L., Mudway, I., Nel, A., Sioutas, C., Smith, S., Baeza-Squiban, A., Cho, A., Duggan, S., Froines, J. (2008). Evaluating the toxicity of airborne particulate matter and nanoparticles by measuring oxidative stress potential - A workshop report and consensus statement. *Inhalation Toxicology* 20(1), 75–99. https://doi.org/10.1080/08958370701665517

Baeza-Squiban, A., Bonvallot, V., Boland, S., Marano, F. (1999). Airborne particles evoke an inflammatory response in human airway epithelium. Activation of transcription factors. *Cell Biology and Toxicology* 15(6), 375–380. https://doi.org/10.1023/A:1007653900063

Ballesteros, R., Hernández, J.J., Lyons, L.L. (2009). Determination of PAHs in diesel particulate matter using thermal extraction and solid phase micro-extraction. *Atmospheric Environment* 43(3), 655–662. https://doi.org/10.1016/j.atmosenv.2008.10.015

Bardouki, H., Liakakou, H., Economou, C., Sciare, J., Smolík, J., Ždímal, V., Eleftheriadis, K., Lazaridis, M., Dye, C., Mihalopoulos, N. (2003). Chemical composition of size-resolved atmospheric aerosols in the eastern Mediterranean during summer and winter. *Atmospheric Environment* 37(2), 195–208. https://doi.org/10.1016/S1352-2310(02)00859-2

Bates, J.T., Fang, T., Verma, V., Zeng, L., Weber, R.J., Tolbert, P.E., Abrams, J.Y., Sarnat, S.E., Klein, M., Mulholland, J.A., Russell, A.G. (2019). Review of Acellular Assays of Ambient Particulate Matter Oxidative Potential: Methods and Relationships with Composition, Sources, and Health Effects. *Environmental Science and Technology* 53(8), 4003–4019. https://doi.org/10.1021/acs.est.8b03430

Bautista VII, A.T., Pabroa, P.C.B., Santos, F.L., Racho, J.M.D., Quirit, L.L. (2014). Carbonaceous particulate matter characterization in an urban and a rural site in the Philippines. *Atmospheric Pollution Research* 5(2), 245–252. https://doi.org/10.5094/APR.2014.030

Becagli, S., Anello, F., Bommarito, C., Cassola, F., Calzolai, G., Di Iorio, T., di Sarra, A., Gómez-Amo, J.-L., Lucarelli, F., Marconi, M., Meloni, D., Monteleone, F., Nava, S., Pace, G., Severi, M., Sferlazzo, D.M., Traversi, R., Udisti, R. (2017). Constraining the ship contribution to the aerosol of the central Mediterranean. *Atmospheric Chemistry and Physics* 17(3), 2067–2084. https://doi.org/10.5194/acp-17-2067-2017

Becerra, J.A., Lizana, J., Gil, M., Barrios-Padura, A., Blondeau, P., Chacartegui, R. (2020). Identification of potential indoor air pollutants in schools. *Journal of Cleaner Production*, 242, 118420. https://doi.org/10.1016/j.jclepro.2019.118420

Bein, K.J., Wexler, A.S. (2015). Compositional variance in extracted particulate matter using different filter extraction techniques. *Atmospheric Environment* 107, 24–34.

https://doi.org/10.1016/j.atmosenv.2015.02.026

Belis, C.A., Cancelinha, J., Duane, M., Forcina, V., Pedroni, V., Passarella, R., Tanet, G., Douglas, K., Piazzalunga, A., Bolzacchini, E., Sangiorgi, G., Perrone, M.G., Ferrero, L., Fermo, P., Larsen, B.R. (2011). Sources for PM air pollution in the Po Plain, Italy: I. Critical comparison of methods for estimating biomass burning contributions to benzo(a)pyrene. *Atmospheric Environment* 45(39), 7266–7275. https://doi.org/10.1016/j.atmosenv.2011.08.061

Beltran, A., Borrull, F., Marcé, R.M., Cormack, P.A.G. (2010). Molecularly-imprinted polymers: Useful sorbents for selective extractions. *TrAC - Trends in Analytical Chemistry* 29(11), 1363–1375. https://doi.org/10.1016/j.trac.2010.07.020

Benigni, R., Bossa, C. (2011). Mechanisms of chemical carcinogenicity and mutagenicity: A review with implications for predictive toxicology. *Chemical Reviews* 111(4), 2507–2536. https://doi.org/10.1021/cr100222q

Bluyssen, P.M. (2017). Health, comfort and performance of children in classrooms – New directions for research. *Indoor and Built Environment* 26(8), 1040–1050. https://doi.org/10.1177/1420326X16661866

Brauer, M., Avila-Casado, C., Fortoul, T.I., Vedal, S., Stevens, B., Churg, A. (2001). Air pollution and retained particles in the lung. *Environmental Health Perspectives* 109(10), 1039–1043. https://doi.org/10.1289/ehp.011091039

Brunekreef, B., Holgate, S.T. (2002). Air pollution and health. *Lancet* 360(9341), 1233–1242). https://doi.org/10.1016/S0140-6736(02)11274-8

Cabada, J.C., Pandis, S.N., Robinson, A.L. (2002). Sources of Atmospheric Carbonaceous Particulate Matter in Pittsburgh, Pennsylvania. *Journal of the Air & Waste Management Association* 52(6), 732–741. https://doi.org/10.1080/10473289.2002.10470811

Calas, A., Uzu, G., Kelly, F.J., Houdier, S., Martins, J.M.F., Thomas, F., Molton, F., Charron, A., Dunster, C., Oliete, A., Jacob, V., Besombes, J.-L., Chevrier, F., Jaffrezo, J.-L. (2018). Comparison between five acellular oxidative potential measurement assays performed with detailed chemistry on PM 10 samples from the city of Chamonix (France). *Atmos. Chem. Phys* 18, 7863–7875. https://doi.org/10.5194/acp-18-7863-2018

Calas, A., Uzu, G., Martins, J.M.F., Voisin, D., Spadini, L., Lacroix, T., Jaffrezo, J. (2017). The importance of simulated lung fluid (SLF) extractions for a more relevant evaluation of the oxidative potential of particulate matter. *Scientific Reports* 7(11617). https://doi.org/10.1038/s41598-017-11979-3

Calvo, A.I., Alves, C., Castro, A., Pont, V., Vicente, A.M., Fraile, R. (2013). Research on aerosol sources and chemical composition: Past, current and emerging issues. *Atmospheric Research* 120–121, 1–28. https://doi.org/10.1016/j.atmosres.2012.09.021

Calzolai, G., Nava, S., Lucarelli, F., Chiari, M., Giannoni, M., Becagli, S., Traversi, R., Marconi, M., Frosini, D., Severi, M., Udisti, R., di Sarra, A., Pace, G., Meloni, D., Bommarito, C., Monteleone, F., Anello, F., Sferlazzo, D.M. (2015). Characterization of PM10 sources in the central Mediterranean. *Atmospheric Chemistry and Physics 15*(24), 13939–13955. https://doi.org/10.5194/acp-15-13939-2015

Cesari, D., De Benedetto, G.E., Bonasoni, P., Busetto, M., Dinoi, A., Merico, E., Chirizzi, D., Cristofanelli, P., Donateo, A., Grasso, F.M., Marinoni, A., Pennetta, A., Contini, D. (2018). Science of the Total Environment Seasonal variability of PM 2.5 and PM10 composition and sources in an urban background site in Southern Italy. *Science of the Total Environment* 612, 202–213. https://doi.org/10.1016/j.scitotenv.2017.08.230

Chan, A.W.H., Isaacman, G., Wilson, K.R., Worton, D.R., Ruehl, C.R., Nah, T., Gentner, D.R., Dallmann, T.R., Kirchstetter, T.W., Harley, R.A., Gilman, J.B., Kuster, W.C., de Gouw, J.A., Offenberg, J.H., Kleindienst, T.E., Lin, Y.H., Rubitschun, C.L., Surratt, J.D., Hayes, P.L., Jimenez, J.L., Goldstein, A.H. (2013). Detailed chemical characterization of unresolved complex mixtures in atmospheric organics: Insights into emission sources, atmospheric processing, and secondary organic aerosol formation. *Journal of Geophysical Research: Atmospheres* 118(12), 6783–6796. https://doi.org/10.1002/jgrd.50533

Charrier, J.G., Anastasio, C. (2012). On dithiothreitol (DTT) as a measure of oxidative potential for ambient particles: Evidence for the importance of soluble \newline transition metals. *Atmospheric Chemistry and Physics* 12(19), 9321–9333. https://doi.org/10.5194/acp-12-9321-2012

Charrier, J.G., Richards-Henderson, N.K., Bein, K.J., McFall, A.S., Wexler, A.S., Anastasio, C. (2015). Oxidant production from source-oriented particulate matter - Part 1: Oxidative potential using the dithiothreitol (DTT) assay. *Atmospheric Chemistry and Physics* 15(5), 2327–2340. https://doi.org/10.5194/acp-15-2327-2015

Charrier, J.G., Mcfall, A.S., Richards-Henderson, N.K., Anastasio, C. (2014). Hydrogen Peroxide Formation in a Surrogate Lung Fluid by Transition Metals and Quinones Present in Particulate Matter. *Environ. Sci. Technol*, 48. https://doi.org/10.1021/es501011w

Charrier, J.G., Anastasio, C. (2011). Impacts of antioxidants on hydroxyl radical production from individual and mixed transition metals in a surrogate lung fluid. *Atmospheric Environment* 45(40), 7555–7562. https://doi.org/10.1016/j.atmosenv.2010.12.021

Charrier, J.G., Anastasio, C. (2015). Rates of Hydroxyl Radical Production from Transition Metals and Quinones in a Surrogate Lung Fluid. *Environ. Sci. Technol.* 49, 9317−9325. https://doi.org/10.1021/acs.est.5b01606

Chen, L.W.A., Olawepo, J.O., Bonanno, F., Gebreselassie, A., Zhang, M. (2020). Schoolchildren's exposure to PM2.5: a student club–based air quality monitoring campaign using low-cost sensors. *Air Quality, Atmosphere and Health* 13(5), 543–551. https://doi.org/10.1007/s11869-020-00815-9

Cheung, K., Daher, N., Kam, W., Shafer, M.M., Ning, Z., Schauer, J.J., Sioutas, C. (2011). Spatial and temporal variation of chemical composition and mass closure of ambient coarse particulate matter (PM10-2.5) in the Los Angeles area. *Atmospheric Environment* 45(16), 2651–2662. https://doi.org/10.1016/j.atmosenv.2011.02.066

Chirizzi, D., Cesari, D., Guascito, M.R., Dinoi, A., Giotta, L., Donateo, A., Contini, D. (2017). Influence of Saharan dust outbreaks and carbon content on oxidative potential of water-soluble fractions of PM2.5 and PM10. *Atmospheric Environment* 163, 1–8. https://doi.org/10.1016/j.atmosenv.2017.05.021

Cho, A.K., Sioutas, C., Miguel, A.H., Kumagai, Y., Schmitz, D.A., Singh, M., Eiguren-Fernandez, A., Froines, J.R. (2005). Redox activity of airborne particulate matter at different sites in the Los Angeles Basin. *Environmental Research* 99(1), 40–47. https://doi.org/10.1016/j.envres.2005.01.003

Chung, M.Y., Lazaro, R.A., Lim, D., Jackson, J., Lyon, J., Rendulic, D., Hasson, A.S. (2006). Aerosol-borne quinones and reactive oxygen species generation by particulate matter extracts. *Environmental Science and Technology*, 40(16), 4880–4886. https://doi.org/10.1021/es0515957

Churg, A., Brauer, M. (2000). Ambient atmospheric particles in the airways of human lungs. *Ultrastructural Pathology*, 24(6), 353–361. https://doi.org/10.1080/019131200750060014

Collins, C.D., Craggs, M., Garcia-Alcega, S., Kademoglou, K., Lowe, S. (2015). Towards a unified approach for the determination of the bioaccessibility of organic pollutants. *Environment International* 78, 24–31. https://doi.org/10.1016/j.envint.2015.02.005

Craig, L., Brook, J.R., Chiotti, Q., Croes, B., Gower, S., Hedley, A., Krewski, D., Krupnick, A., Krzyzanowski, M., Moran, M.D., Pennell, W., Samet, J.M., Schneider, J., Shortreed, J., Williams, M. (2008). Air pollution and public health: A guidance document for risk managers. *Journal of Toxicology and Environmental Health - Part A: Current Issues* 71(9–10), 588–698. https://doi.org/10.1080/15287390801997732

Crobeddu, B., Aragao-Santiago, L., Bui, L.C., Boland, S., Baeza Squiban, A. (2017). Oxidative potential of particulate matter 2.5 as predictive indicator of cellular stress. *Environmental Pollution*, 230, 125–133. https://doi.org/10.1016/j.envpol.2017.06.051

Daher, N., Ruprecht, A., Invernizzi, G., De Marco, C., Miller-Schulze, J., Heo, J.B., Shafer, M.M., Shelton, B.R., Schauer, J.J., Sioutas, C. (2012). Characterization, sources and redox activity of fine and coarse particulate matter in Milan, Italy. *Atmospheric Environment* 49, 130–141. https://doi.org/10.1016/j.atmosenv.2011.12.011

Daher, N., Saliba, N.A., Shihadeh, A.L., Jaafar, M., Baalbaki, R., Shafer, M.M., Schauer, J.J., Sioutas, C. (2014). Oxidative potential and chemical speciation of size-resolved particulate matter (PM) at near-freeway and urban background sites in the greater Beirut area. *Science of the Total Environment*, *470–471*, 417–426. https://doi.org/10.1016/j.scitotenv.2013.09.104

de Gennaro, G., Farella, G., Marzocca, A., Mazzone, A., Tutino, M. (2013). Indoor and Outdoor Monitoring of Volatile Organic Compounds in School Buildings: Indicators Based on Health Risk Assessment to Single out Critical Issues. *International Journal of Environmental Research and Public Health* 10(12), 6273–6291. https://doi.org/10.3390/ijerph10126273

De Meringo, A., Morscheidt, C., Thelohan, S., Tiesler, H. (1994). In vitro assessment of biodurability: Acellular systems. *Environmental Health Perspectives*, *102*(Suppl.5), 47–53. https://doi.org/10.1289/ehp.94102s547

De Sario, M., Katsouyanni, K., Michelozzi, P. (2013). Climate change, extreme weather events, air pollution and respiratory health in Europe. *European Respiratory Journal* 42(3), 826–843. https://doi.org/10.1183/09031936.00074712

Di Vaio, P., Magli, E., Caliendo, G., Corvino, A., Fiorino, F., Frecentese, F., Saccone, I., Santagada, V., Severino, B., Onorati, G., Freda, O., Manzo, C., Perissutti, E. (2018). Heavy Metals Size Distribution in PM 10 and Environmental-Sanitary Risk Analysis in Acerra (Italy). *Atmophere* 9, 58. https://doi.org/10.3390/atmos9020058

Ding, J., Zhong, J., Yang, Y., Li, B., Shen, G., Su, Y., Wang, C., Li, W., Shen, H., Wang, B., Wang, R., Huang, Y., Zhang, Y., Cao, H., Zhu, Y., Simonich, S.L.M., Tao, S. (2012). Occurrence and exposure to polycyclic aromatic hydrocarbons and their derivatives in a rural Chinese home through biomass fuelled cooking. *Environmental Pollution* 169, 160–166. https://doi.org/10.1016/j.envpol.2011.10.008

Donaldson, K., Brown, D., Clouter, A., Duffin, R., MacNee, W., Renwick, L., Tran, L., Stone, V. (2002). The pulmonary toxicology of ultrafine particles. *Journal of Aerosol Medicine* 15(2), 213–220. https://doi.org/10.1089/089426802320282338

dos Santos, R.R., Vidotti Leal, L.D., de Lourdes Cardeal, Z., Menezes, H.C. (2019). Determination of polycyclic aromatic hydrocarbons and their nitrated and oxygenated derivatives in coffee brews using an efficient cold fiber-solid phase microextraction and gas chromatography mass spectrometry method. *Journal of Chromatography A*, 1584, 64–71. https://doi.org/10.1016/j.chroma.2018.11.046

Fang, G.C., Chang, K.F., Lu, C., Bai, H. (2002). Toxic equivalency factors study of polycyclic aromatic hydrocarbons (PAHs) in Taichung City, Taiwan. *Toxicology and Industrial Health*, 18(6), 279–288. https://doi.org/10.1191/0748233702th151oa

Fang, T., Verma, V., Bates, J.T., Abrams, J., Klein, M., Strickland, J.M., Sarnat, E.S., Chang, H.H., Mulholland, A.J., Tolbert, E.P., Russell, G.A., Weber, J.R. (2016). Oxidative potential of ambient water-soluble PM2.5 in the southeastern United States: Contrasts in sources and health associations between ascorbic acid (AA) and dithiothreitol (DTT) assays. *Atmospheric Chemistry and Physics* 16(6), 3865–3879. https://doi.org/10.5194/acp-16-3865-2016

Favarato, G., Anderson, R.H., Atkinson, R., Fuller, G., Mills, I., Walton, H. (2014). Traffic-related pollution and asthma prevalence in children. Quantification of associations with nitrogen dioxide. *Air Quality, Atmosphere, & Health* 7, 459–466. https://doi.org/10.1007/s11869-014-0265-8

Fermo, P., Piazzalunga, A., Vecchi, R., Valli, G., Ceriani, M. (2005). A TGA/FT-IR study for OC and EC quantification applied to carbonaceous aerosol collected in Milan (Italy). *Atmos. Chem. Phys. Discuss* 5. www.atmos-chem-phys.org/acpd/5/4335/SRef-ID:1680-7375/acpd/2005-5-4335EuropeanGeosciencesUnion

Fisk, W.J. (2017). The ventilation problem in schools: literature review. *Indoor Air*, 27(6), 1039–1051. https://doi.org/10.1111/ina.12403

Gao, D., Fang, T., Verma, V., Zeng, L., Weber, R.J. (2017). A method for measuring total aerosol oxidative potential (OP) with the dithiothreitol (DTT) assay and comparisons between an urban and roadside site of water-soluble and total OP. *Atmospheric Measurement Techniques*, 10(8), 2821–2835. https://doi.org/10.5194/amt-10-2821-2017

Gao, D., Pollitt, K.J.G., Mulholland, J.A., Russell, A.G., Rodney, J. (2020). Characterization and comparison of PM2.5 oxidative potential assessed by two acellular assays. *Atmos.*

Chem. Phys. 20, 5197–5210. https://doi.org/10.5194/acp-20-5197-2020

Geiser, M., Kreyling, W.G. (2010). Deposition and biokinetics of inhaled nanoparticles. *Particle and Fibre Toxicology* 7(2). https://doi.org/10.1186/1743-8977-7-2

Ghio, A.J., Carraway, M.S., Madden, M.C. (2012). Composition of Air Pollution Particles and Oxidative Stress in Cells , Tissues , and Living Systems. *Journal of Toxicology and Environmental Health , Part B : Critical Reviews* 15(1), 1–21. https://doi.org/10.1080/10937404.2012.632359

Godri, K.J., Harrison, R.M., Evans, T., Baker, T., Dunster, C., Mudway, I.S., Kelly, F.J. (2011). Increased oxidative burden associated with traffic component of ambient particulate matter at roadside and Urban background schools sites in London. *PLoS ONE*, *6*(7), e21961. https://doi.org/10.1371/journal.pone.0021961

Gugamsetty, B., Wei, H., Liu, C. N., Awasthi, A., Tsai, C.J., Roam, G.D., Wu, Y.C., Chen, C.F. (2012). Source Characterization and Apportionment of PM10, PM2.5 and PM0.1 by Using Positive Matrix Factorization. *Aerosol and Air Quality Research* 12(4), 476–491. https://doi.org/10.4209/aaqr.2012.04.0084

Harrison, R.M., Yin, J. (2000). Particulate matter in the atmosphere: Which particle properties are important for its effects on health? *Science of the Total Environment*, 249(1–3), 85–101. https://doi.org/10.1016/S0048-9697(99)00513-6

Hasheminassab, S., Daher, N., Saffari, A., Wang, D., Ostro, B. D., Sioutas, C. (2014). Spatial and temporal variability of sources of ambient fine particulate matter (PM2.5) in California. *Atmospheric Chemistry and Physics*, 14(22), 12085–12097. https://doi.org/10.5194/acp-14-12085-2014

Hedayat, F., Stevanovic, S., Miljevic, B., Bottle, S., Ristovski, Z.D. (2015). Review – Evaluating the molecular assays for measuring the oxidative potential of particulate matter. *Chemical Industry and Chemical Engineering Quarterly* 21(1–2), 201–210. https://doi.org/10.2298/CICEQ140228031H

Hellack, B., Nickel, C., Albrecht, C., Kuhlbusch, T.A.J., Boland, S., Baeza-Squiban, A., Wohlleben, W., Schins, R.P.F. (2017). Analytical methods to assess the oxidative potential of nanoparticles: A review. *Environmental Science: Nano* 4(10), 1920–1934. https://doi.org/10.1039/c7en00346c

Hjortenkrans, D., Bergbäck, B., Aggerud, A.H. (2006). NEW METAL EMISSION PATTERNS IN ROAD TRAFFIC ENVIRONMENTS. *Environmental Monitoring and Assessment* 117, 85–98. https://doi.org/10.1007/s10661-006-7706-2

Ho, W.L., Liu, Y.Y., Lin, T.C. (2011). Development of molecular imprinted polymer for selective adsorption of benz[a]pyrene among airborne polycyclic aromatic hydrocarbon compounds. *Environmental Engineering Science* 28(6), 421–434. https://doi.org/10.1089/ees.2010.0268

Hofmann, W. (2011). Modelling inhaled particle deposition in the human lung-A review. *Journal of Aerosol Science* 42(10), 693–724. https://doi.org/10.1016/j.jaerosci.2011.05.007

IARC (2012). *Agents Classified by the IARC Monographs*. *1–105*(026148), 1–36.

Idowu, O., Semple, K.T., Ramadass, K., O'Connor, W., Hansbro, P., Thavamani, P. (2019). Beyond the obvious: Environmental health implications of polar polycyclic aromatic hydrocarbons. *Environment International* 123, 543–557. https://doi.org/10.1016/j.envint.2018.12.051

Jaafar, M., Baalbaki, R., Mrad, R., Daher, N., Shihadeh, A., Sioutas, C., Saliba, N.A. (2014). Dust episodes in Beirut and their effect on the chemical composition of coarse and fine particulate matter. *Science of the Total Environment* 496, 75–83. https://doi.org/10.1016/j.scitotenv.2014.07.018

Janssen, N.A.H., Strak, M., Yang, A., Hellack, B., Kelly, F.J., Kuhlbusch, T.A.J., Harrison, R.M., Brunekreef, B., Cassee, F.R., Steenhof, M., Hoek, G. (2015). Associations between three specific a-cellular measures of the oxidative potential of particulate matter and markers of acute airway and nasal inflammation in healthy volunteers. *Occupational and Environmental Medicine* 72(1), 49–56. https://doi.org/10.1136/oemed-2014-102303

Janssen, N.A.H., Yang, A., Strak, M., Steenhof, M., Hellack, B., Gerlofs-Nijland, M.E., Kuhlbusch, T., Kelly, F., Harrison, R., Brunekreef, B., Hoek, G., Cassee, F. (2014). Oxidative potential of particulate matter collected at sites with different source characteristics. *Science of the Total Environment* 472, 572–581. https://doi.org/10.1016/j.scitotenv.2013.11.099

Jedynska, A., Hoek, G., Eeftens, M., Cyrys, J., Keuken, M., Ampe, C., Beelen, R., Cesaroni, G., Forastiere, F., Cirach, M., de Hoogh, K., De Nazelle, A., Madsen, C., Declercq, C., Eriksen, K. T., Katsouyanni, K., Akhlaghi, H. M., Lanki, T., Meliefste, K., Nieuwenhuijsen, M., Oldenwening, M., Pennanen, A., Raaschou-Nielsen, O., Brunekreef, B., Kooter, I.M. (2014). Spatial variations of PAH, hopanes/steranes and EC/OC concentrations within and between European study areas. *Atmospheric Environment* 87(2), 239–248. https://doi.org/10.1016/j.atmosenv.2014.01.026

Jiang, H., Ahmed, C.M.S., Canchola, A., Chen, J.Y., Lin, Y.-H. (2019). Use of Dithiothreitol Assay to Evaluate the Oxidative Potential of Atmospheric Aerosols. *Atmosphere* 10(10), 571. https://doi.org/10.3390/atmos10100571

Jiang, H., Jang, M. (2018). Dynamic Oxidative Potential of Atmospheric Organic Aerosol under Ambient Sunlight. *Environmental Science and Technology* 52(13), 7496–7504. https://doi.org/10.1021/acs.est.8b00148

Jiang, H., Jang, M., Sabo-Attwood, T., Robinson, S.E. (2016). Oxidative potential of secondary organic aerosols produced from photooxidation of different hydrocarbons using outdoor chamber under ambient sunlight. *Atmospheric Environment* 131, 382–389. https://doi.org/10.1016/j.atmosenv.2016.02.016

Kampa, M., Castanas, E. (2008). Human health effects of air pollution. *Environmental Pollution* 151(2), 362–367. https://doi.org/10.1016/j.envpol.2007.06.012

Kastury, F., Smith, E., Karna, R.R., Scheckel, K.G., Juhasz, A.L. (2018). An inhalation-ingestion bioaccessibility assay (IIBA) for the assessment of exposure to metal(loid)s in PM10. *Science of the Total Environment* 631–632, 92–104. https://doi.org/10.1016/j.scitotenv.2018.02.337

Kelly, F.J. (2003). Oxidative stress: Its role in air pollution and adverse health effects.

Occupational and Environmental Medicine 60(8), 612–616. https://doi.org/10.1136/oem.60.8.612

Kim, I., Lee, S., Kim, S.D. (2019). Determination of toxic organic pollutants in fine particulate matter using selective pressurized liquid extraction and gas chromatography–tandem mass spectrometry. *Journal of Chromatography A* 1590, 39–46. https://doi.org/10.1016/j.chroma.2019.01.009

Kim, K.H., Kabir, E., Kabir, S. (2015). A review on the human health impact of airborne particulate matter. *Environment International* 74, 136–143. https://doi.org/10.1016/j.envint.2014.10.005

Krupadam, R.J., Bhagat, B., Khan, M.S. (2010). Highly sensitive determination of polycyclic aromatic hydrocarbons in ambient air dust by gas chromatography-mass spectrometry after molecularly imprinted polymer extraction. *Analytical and Bioanalytical Chemistry* 397(7), 3097–3106. https://doi.org/10.1007/s00216-010-3858-6

Kumagai, Y., Koide, S., Taguchi, K., Endo, A., Nakai, Y., Yoshikawa, T., Shimojo, N. (2002). Oxidation of proximal protein sulfhydryls by phenanthraquinone, a component of diesel exhaust particles. *Chemical Research in Toxicology* 15(4), 483–489. https://doi.org/10.1021/tx0100993

Kumar, A., Terakosolphan, W., Hassoun, M., Vandera, K.K., Novicky, A., Harvey, R., Royall, P.G., Bicer, E.M., Eriksson, J., Edwards, K., Valkenborg, D., Nelissen, I., Hassall, D., Mudway, I.S., Forbes, B. (2017). A Biocompatible Synthetic Lung Fluid Based on Human Respiratory Tract Lining Fluid Composition. *Pharmaceutical Research* 34(12), 2454–2465. https://doi.org/10.1007/s11095-017-2169-4

Leclercq, B., Alleman, L.Y., Perdrix, E., Riffault, V., Happillon, M., Strecker, A., Lo-Guidice, J.M., Garçon, G., Coddeville, P. (2017). Particulate metal bioaccessibility in physiological fluids and cell culture media: Toxicological perspectives. *Environmental Research* 156, 148–157. https://doi.org/10.1016/j.envres.2017.03.029

Lee, B.-K., Thi Hieu, N. (2011). Seasonal Variation and Sources of Heavy Metals in Atmospheric Aerosols in a Residential Area of Ulsan, Korea. *Aerosol and Air Quality Research* 11, 679–688. https://doi.org/10.4209/aaqr.2010.10.0089

Leni, Z., Künzi, L., Geiser, M. (2020). Air pollution causing oxidative stress. *Current Opinion in Toxicology*, 20–21, 1–8. https://doi.org/10.1016/j.cotox.2020.02.006

Li, N., Xia, T., Nel, A.E. (2008). The role of oxidative stress in ambient particulate matter-induced lung diseases and its implications in the toxicity of engineered nanoparticles. *Free Radical Biology and Medicine* 44(9), 1689–1699. https://doi.org/10.1016/j.freeradbiomed.2008.01.028

Li, Q., Wyatt, A., Kamens, R.M. (2009). Oxidant generation and toxicity enhancement of aged-diesel exhaust. *Atmospheric Environment* 43(5), 1037–1042. https://doi.org/10.1016/j.atmosenv.2008.11.018

Lin, M., Yu, J.Z. (2020). Assessment of interactions between transition metals and atmospheric organics: ascorbic acid depletion and hydroxyl radical formation in organic-metal mixtures. *Environmental Science and Technology* 54(3), 1431–1442.

https://doi.org/10.1021/acs.est.9b07478

Lionetto, M.G., Guascito, M.R., Caricato, R., Giordano, M.E., De Bartolomeo, A.R., Romano, M.P., Conte, M., Dinoi, A., Contini, D. (2019). Correlation of oxidative potential with ecotoxicological and cytotoxicological potential of PM10 at an urban background site in Italy. *Atmosphere* 10(12). https://doi.org/10.3390/ATMOS10120733

Lodovici, M., Bigagli, E. (2011). Oxidative stress and air pollution exposure. *Journal of Toxicology* 2011. https://doi.org/10.1155/2011/487074

Lovett, C., Sowlat, M.H., Saliba, N.A., Shihadeh, A.L., Sioutas, C. (2018). Oxidative potential of ambient particulate matter in Beirut during Saharan and Arabian dust events. *Atmospheric Environment* 188, 34–42. https://doi.org/10.1016/j.atmosenv.2018.06.016

Lundstedt, S., White, P.A., Lemieux, C.L., Lynes, K.D., Lambert, I.B., Öberg, L., Haglund, P., Tysklind, M. (2007). Sources, fate, and toxic hazards of oxygenated Polycyclic Aromatic Hydrocarbons (PAHs) at PAH-contaminated sites. *Ambio* 36(6), 475–485. https://doi.org/10.1579/0044-7447(2007)36[475:SFATHO]2.0.CO;2

Luo, X., Zhao, Z., Xie, J., Luo, J., Chen, Y., Li, H., Jin, L. (2019). Pulmonary bioaccessibility of trace metals in PM2.5 from different megacities simulated by lung fluid extraction and DGT method. *Chemosphere* 218, 915–921. https://doi.org/10.1016/j.chemosphere.2018.11.079

Lyu, R., Shi, Z., Salim Alam, M., Wu, X., Liu, D., Vu, T.V., Stark, C., Fu, P., Feng, Y., Harrison, R.M. (2019). Insight into the composition of organic compounds (≥C6) in PM2.5 in wintertime in Beijing, China. *Atmospheric Chemistry and Physics* 19(16), 10865–10881. https://doi.org/10.5194/acp-19-10865-2019

Lyu, Y., Guo, H., Cheng, T., Li, X. (2018). Particle Size Distributions of Oxidative Potential of Lung-Deposited Particles: Assessing Contributions from Quinones and Water-Soluble Metals. *Environ. Sci. Technol*. 52, 6592–6600. https://doi.org/10.1021/acs.est.7b06686

Maikawa, C.L., Weichenthal, S., Wheeler, A.J., Dobbin, N.A., Smargiassi, A., Evans, G., Liu, L., Goldberg, M.S., Pollitt, K.J.G. (2016). Particulate Oxidative Burden as a Predictor of Exhaled Nitric Oxide in Children with Asthma. *Environmental Health Perspectives* 124(10), 1616–1622. https://doi.org/10.1289/EHP175

María Del Rosario Sienra, M. (2006). Oxygenated polycyclic aromatic hydrocarbons in urban air particulate matter. *Atmospheric Environment* 40(13), 2374–2384. https://doi.org/10.1016/j.atmosenv.2005.12.009

Marques, M.R.C., Loebenberg, R., Almukainzi, M. (2011). Simulated Biological Fluids with Possible Application in Dissolution Testing. *Dissolution Technologies* 18, 15–28. https://doi.org/10.14227/DT180311P15

Martín-Esteban, A. (2016). Recent molecularly imprinted polymer-based sample preparation techniques in environmental analysis. *Trends in Environmental Analytical Chemistry* 9, 8–14. https://doi.org/10.1016/j.teac.2016.01.001

Masala, S., Lim, H., Bergvall, C., Johansson, C., Westerholm, R. (2016). Determination of

semi-volatile and particle-associated polycyclic aromatic hydrocarbons in Stockholm air with emphasis on the highly carcinogenic dibenzopyrene isomers. *Atmospheric Environment* 140, 370–380. https://doi.org/10.1016/j.atmosenv.2016.06.007

Masiol, M., Formenton, G., Pasqualetto, A., Pavoni, B. (2013). Seasonal trends and spatial variations of PM10-bounded polycyclic aromatic hydrocarbons in Veneto Region, Northeast Italy. *Atmospheric Environment* 79, 811–821. https://doi.org/10.1016/j.atmosenv.2013.07.025

Masiol, M., Hofer, A., Squizzato, S., Piazza, R., Rampazzo, G., Pavoni, B. (2012). Carcinogenic and mutagenic risk associated to airborne particle-phase polycyclic aromatic hydrocarbons: A source apportionment. *Atmospheric Environment* 60, 375–382. https://doi.org/10.1016/j.atmosenv.2012.06.073

Menezes, H.C., De Lourdes Cardeal, Z. (2011). Determination of polycyclic aromatic hydrocarbons from ambient air particulate matter using a cold fiber solid phase microextraction gas chromatography-mass spectrometry method. *Journal of Chromatography A* 1218(21), 3300–3305. https://doi.org/10.1016/j.chroma.2010.10.105

Meng, X., Ma, Y., Chen, R., Zhou, Z., Chen, B., Kan, H. (2013). Size-Fractionated Particle Number Concentrations and Daily Mortality in a Chinese City. *Environmental Health Perspectives* 1174(10), 1174–1179.

Merkofer, M., Kissner, R., Hider, R.C., Brunk, U.T., Koppenol, W.H. (2006). Fenton chemistry and iron chelation under physiologically relevant conditions: Electrochemistry and kinetics. *Chemical Research in Toxicology* 19(10), 1263–1269. https://doi.org/10.1021/tx060101w

Mihucz, V.G., Szigeti, T., Dunster, C., Giannoni, M., de Kluizenaar, Y., Cattaneo, A., Mandin, C., Bartzis, J.G., Lucarelli, F., Kelly, F.J., Záray, G. (2015). An integrated approach for the chemical characterization and oxidative potential assessment of indoor PM2.5. *Microchemical Journal* 119, 22–29. https://doi.org/10.1016/j.microc.2014.10.006

Millis, K.K., Weaver, K.H., Rabenstein, D.L. (1993). Oxidation/Reduction Potential of Glutathione. *Journal of Organic Chemistry* 58(15), 4144–4146. https://doi.org/10.1021/jo00067a060

Molina, C., Andrade, C., Manzano, C.A., Richard Toro, A., Verma, V., Leiva-Guzmán, M. A. (2020). Dithiothreitol-based oxidative potential for airborne particulate matter: an estimation of the associated uncertainty. *Environmental Science and Pollution Research* 27(23), 29672–29680. https://doi.org/10.1007/s11356-020-09508-3

Moreno, T., Kelly, F.J., Dunster, C., Oliete, A., Martins, V., Reche, C., Minguillón, M.C., Amato, F., Capdevila, M., de Miguel, E., Querol, X. (2017). Oxidative potential of subway PM2.5. *Atmospheric Environment* 148, 230–238. https://doi.org/10.1016/j.atmosenv.2016.10.045

Mudway, I.S., Stenfors, N., Duggan, S.T., Roxborough, H., Zielinski, H., Marklund, S.L., Blomberg, A., Frew, A.J., Sandström, T., Kelly, F.J. (2004). An in vitro and in vivo investigation of the effects of diesel exhaust on human airway lining fluid antioxidants. *Archives of Biochemistry and Biophysics* 423(1), 200–212.

https://doi.org/10.1016/j.abb.2003.12.018

Mugica, V., Ortiz, E., Molina, L., De Vizcaya-Ruiz, A., Nebot, A., Quintana, R., Aguilar, J., Alcántara, E. (2009). PM composition and source reconciliation in Mexico City. *Atmospheric Environment* 43(32), 5068–5074. https://doi.org/10.1016/j.atmosenv.2009.06.051

Naccarato, A., Tagarelli, A. (2019). Recent Applications and Newly Developed Strategies of Solid-Phase Microextraction in Contaminant Analysis: Through the Environment to Humans. *Separations* 6, 54. https://doi.org/10.3390/separations6040054

Naing, N.N., Yeo, K. Bin, Lee, H.K. (2020). A combined microextraction procedure for isolation of polycyclic aromatic hydrocarbons in ambient fine air particulate matter with determination by gas chromatography-tandem mass spectrometry. *Journal of Chromatography A* 1612, 460646. https://doi.org/10.1016/j.chroma.2019.460646

Nalin, F., Sander, L.C., Wilson, W.B., Wise, S.A. (2018). Gas chromatographic retention behavior of polycyclic aromatic hydrocarbons (PAHs) and alkyl-substituted PAHs on two stationary phases of different selectivity. *Analytical and Bioanalytical Chemistry* 410(3), 1123–1137. https://doi.org/10.1007/s00216-017-0700-4

Novo, E., Parola, M. (2008). Redox mechanisms in hepatic chronic wound healing and fibrogenesis. *Fibrogenesis and Tissue Repair* 1(1), 5. https://doi.org/10.1186/1755-1536-1-5

Nozière, B., Kalberer, M., Claeys, M., Allan, J., D'Anna, B., Decesari, S., Finessi, E., Glasius, M., Grgić, I., Hamilton, J. F., Hoffmann, T., Iinuma, Y., Jaoui, M., Kahnt, A., Kampf, C. J., Kourtchev, I., Maenhaut, W., Marsden, N., Saarikoski, S., Schnelle-Kreis, J., Surratt, J.D., Szidat, S., Szmigielski, R., Wisthaler, A. (2015). The Molecular Identification of Organic Compounds in the Atmosphere: State of the Art and Challenges. *Chemical Reviews* 115(10), 3919–3983. https://doi.org/10.1021/cr5003485

Nyiri, Z., Novák, M., Bodai, Z., Szabó, B.S., Eke, Z., Záray, G., Szigeti, T. (2016). Determination of particulate phase polycyclic aromatic hydrocarbons and their nitrated and oxygenated derivatives using gas chromatography–mass spectrometry and liquid chromatography–tandem mass spectrometry. *Journal of Chromatography A* 1472, 88–98. https://doi.org/10.1016/j.chroma.2016.10.021

Olaguer, E.P. (2017). Particulate Matter and Surface Deposition. *Atmospheric Impacts of the Oil and Gas Industry*, 47–53. https://doi.org/10.1016/b978-0-12-801883-5.00005-x

Øvrevik, J. (2019). Oxidative Potential Versus Biological Effects: A Review on the Relevance of Cell-Free/Abiotic Assays as Predictors of Toxicity from Airborne Particulate Matter. *International Journal of Molecular Sciences* 20, 4772. https://doi.org/10.3390/ijms20194772

Pant, P., Baker, S.J., Shukla, A., Maikawa, C., Godri Pollitt, K.J., Harrison, R.M. (2015). The PM10 fraction of road dust in the UK and India: Characterization, source profiles and oxidative potential. *Science of the Total Environment* 530–531, 445–452. https://doi.org/10.1016/j.scitotenv.2015.05.084

Pawliszyn, J. (2000). Theory of Solid-Phase Microextraction. *Journal of Chromatographic*

Science 38, 270–278. https://academic.oup.com/chromsci/article/38/7/270/371966

Pérez, N., Pey, J., Castillo, S., Viana, M., Alastuey, A., Querol, X. (2008). Interpretation of the variability of levels of regional background aerosols in the Western Mediterranean. *Science of the Total Environment* 407(1), 527–540. https://doi.org/10.1016/j.scitotenv.2008.09.006

Perrone, M.G., Gualtieri, M., Consonni, V., Ferrero, L., Sangiorgi, G., Longhin, E., Ballabio, D., Bolzacchini, E., Camatini, M. (2013). Particle size, chemical composition, seasons of the year and urban, rural or remote site origins as determinants of biological effects of particulate matter on pulmonary cells. *Environmental Pollution* 176, 215–227. https://doi.org/10.1016/j.envpol.2013.01.012

Perrone, M.R., Becagli, S., Garcia Orza, J.A., Vecchi, R., Dinoi, A., Udisti, R., Cabello, M. (2013). The impact of long-range-transport on PM1 and PM2.5 at a Central Mediterranean site. *Atmospheric Environment* 71, 176–186. https://doi.org/10.1016/j.atmosenv.2013.02.006

Perrone, M.R., Genga, A., Siciliano, M., Siciliano, T., Paladini, F., Burlizzi, P. (2016). Saharan dust impact on the chemical composition of PM10 and PM1 samples over south-eastern Italy. *Arabian Journal of Geosciences* 9(2), 1–11. https://doi.org/10.1007/s12517-015-2227-3

Perrone, M.R., Romano, S. (2018). Relationship between the planetary boundary layer height and the particle scattering coefficient at the surface. *Atmospheric Research* 213, 57–69. https://doi.org/10.1016/j.atmosres.2018.04.017

Perrone, M.R., Romano, S., Orza, J.A.G. (2014a). Particle optical properties at a Central Mediterranean site: Impact of advection routes and local meteorology. *Atmospheric Research* 145–146, 152–167. https://doi.org/10.1016/j.atmosres.2014.03.029

Perrone, M.G., Zhou, J., Malandrino, M., Sangiorgi, G., Rizzi, C., Ferrero, L., Dommen, J., Bolzacchini, E. (2016). PM chemical composition and oxidative potential of the soluble fraction of particles at two sites in the urban area of Milan, Northern Italy. *Atmospheric Environment* 128, 104–113. https://doi.org/10.1016/j.atmosenv.2015.12.040

Perrone, M.R., Bertoli, I., Romano, S., Russo, M., Rispoli, G., Pietrogrande, M.C. (2019a). PM2.5 and PM10 oxidative potential at a Central Mediterranean Site: Contrasts between dithiothreitol- and ascorbic acid-measured values in relation with particle size and chemical composition. *Atmospheric Environment* 210, 143–155. https://doi.org/10.1016/j.atmosenv.2019.04.047

Perrone, M.R., Dinoi, A., Becagli, S., Udisti, R. (2014b). Chemical composition of PM1 and PM2.5 at a suburban site in southern Italy. *International Journal of Environmental Analytical Chemistry* 94(2), 127–150. https://doi.org/10.1080/03067319.2013.791978

Perrone, M.R., Vecchi, R., Romano, S., Becagli, S., Traversi, R., Paladini, F. (2019b). Weekly cycle assessment of PM mass concentrations and sources, and impacts on temperature and wind speed in Southern Italy. *Atmospheric Research* 218, 129–144. https://doi.org/10.1016/j.atmosres.2018.11.013

Pietrogrande, M.C., Perrone, M.G., Sangiorgi, G., Ferrero, L., Bolzacchini, E. (2014). Data handling of GC/MS signals for characterization of PAH sources in Northern Italy

aerosols. *Talanta* 120, 283–288. https://doi.org/10.1016/j.talanta.2013.12.010

Pietrogrande, M.C., Bacco, D., Ferrari, S., Ricciardelli, I., Scotto, F., Trentini, A., Visentin, M. (2016). Characteristics and major sources of carbonaceous aerosols in PM2.5 in Emilia Romagna Region (Northern Italy) from four-year observations. *Science of the Total Environment* 553, 172–183. https://doi.org/10.1016/j.scitotenv.2016.02.074

Pietrogrande, M.C., Bertoli, I., Manarini, F., Russo, M. (2019a). Ascorbate assay as a measure of oxidative potential for ambient particles: Evidence for the importance of cell-free surrogate lung fluid composition. *Atmospheric Environment* 211, 103–112. https://doi.org/10.1016/j.atmosenv.2019.05.012

Pietrogrande, M.C., Dalpiaz, C., Dell'Anna, R., Lazzeri, P., Manarini, F., Visentin, M., Tonidandel, G. (2018b). Chemical composition and oxidative potential of atmospheric coarse particles at an industrial and urban background site in the alpine region of northern Italy. *Atmospheric Environment* 191, 340–350. https://doi.org/10.1016/j.atmosenv.2018.08.022

Pietrogrande, M.C., Perrone, M.R., Manarini, F., Romano, S., Udisti, R., Becagli, S. (2018a). PM 10 oxidative potential at a Central Mediterranean Site: Association with chemical composition and meteorological parameters. *Atmospheric Environment* 188, 97–111. https://doi.org/10.1016/j.atmosenv.2018.06.013

Pietrogrande, M.C., Russo, M., Zagatti, E. (2019b). Review of PM oxidative potential measured with acellular assays in urban and rural sites across Italy. *Atmosphere* 10(10), 8–11. https://doi.org/10.3390/atmos10100626

Pio, C., Cerqueira, M., Harrison, R.M., Nunes, T., Mirante, F., Alves, C., Oliveira, C., Sanchez de la Campa, A., Artíñano, B., Matos, M. (2011). OC/EC ratio observations in Europe: Re-thinking the approach for apportionment between primary and secondary organic carbon. *Atmospheric Environment* 45(34), 6121–6132. https://doi.org/10.1016/j.atmosenv.2011.08.045

Pope III, C.A. (2007). Mortality effects of longer term exposures to fine particulate air pollution: Review of recent epidemiological evidence. *Inhalation Toxicology* 19(Suppl. 1), 33–38. https://doi.org/10.1080/08958370701492961

Pope III, C.A., Dockery, D.W. (2006). Health effects of fine particulate air pollution: Lines that connect. *Journal of the Air and Waste Management Association* 56(6), 709–742. https://doi.org/10.1080/10473289.2006.10464485

Pope III, C.A., Burnett, R.T., Thun, M.J., Calle, E.E., Krewski, D., Thurston, G.D. (2002). to Fine Particulate Air Pollution. *The Journal of the American Medical Association* 287(9), 1132–1141. http://jama.jamanetwork.com/article.aspx?doi=10.1001/jama.287.9.1132

Putaud, J.P., Van Dingenen, R., Alastuey, A., Bauer, H., Birmili, W., Cyrys, J., Flentje, H., Fuzzi, S., Gehrig, R., Hansson, H.C., Harrison, R.M., Herrmann, H., Hitzenberger, R., Hüglin, C., Jones, A.M., Kasper-Giebl, A., Kiss, G., Kousa, A., Kuhlbusch, T.A.J., Löschau, G., Maenhaut, W., Molnar, A., Moreno, T., Pekkanen, J., Perrino, C., Pitz, M., Puxbaum, H., Querol, X., Rodriguez, S., Salma, I., Schwarz, J., Smolik, J., Schneider, J., Spindler, G., ten Brink, H., Tursic, J., Viana, M., Wiedensohler, A., Raes, F. (2010). A European aerosol phenomenology - 3: Physical and chemical

characteristics of particulate matter from 60 rural, urban, and kerbside sites across Europe. *Atmospheric Environment* 44(10), 1308–1320. https://doi.org/10.1016/j.atmosenv.2009.12.011

Putaud, J.P., Raes, F., Van Dingenen, R., Brüggemann, E., Facchini, M.C., Decesari, S., Fuzzi, S., Gehrig, R., Hüglin, C., Laj, P., Lorbeer, G., Maenhaut, W., Mihalopoulos, N., Müller, K., Querol, X., Rodriguez, S., Schneider, J., Spindler, G., Ten Brink, H., Tørseth, K., Wiedensohler, A. (2004). A European aerosol phenomenology - 2: Chemical characteristics of particulate matter at kerbside, urban, rural and background sites in Europe. *Atmospheric Environment* 38(16), 2579–2595. https://doi.org/10.1016/j.atmosenv.2004.01.041

QUARG, Quality of Urban Air Review Group (1996). Airborne Particulate Matter in the United Kingdom Third Report of the Quality of Urban Air Review Group Prepared at the request of the Department of the Environment. pp.1-175.

Querol, X., Alastuey, A., Moreno, T., Viana, M.M., Castillo, S., Pey, J., Rodríguez, S., Artiñano, B., Salvador, P., Sánchez, M., Garcia Dos Santos, S., Herce Garraleta, M.D., Fernandez-Patier, R., Moreno-Grau, S., Negral, L., Minguillón, M.C., Monfort, E., Sanz, M.J., Palomo-Marín, R., Pinilla-Gil, E., Cuevas, E., de la Rosa, J., Sánchez de la Campa, A. (2008). Spatial and temporal variations in airborne particulate matter (PM10 and PM2.5) across Spain 1999-2005. *Atmospheric Environment* 42(17), 3964–3979. https://doi.org/10.1016/j.atmosenv.2006.10.071

Ramírez, N., Cuadras, A., Rovira, E., Borrull, F., Marcé, R. M. (2010). Comparative study of solvent extraction and thermal desorption methods for determining a wide range of volatile organic compounds in ambient air. *Talanta* 82(2), 719–727. https://doi.org/10.1016/j.talanta.2010.05.038

Ravindra, K., Sokhi, R., Van Grieken, R. (2008a). Atmospheric polycyclic aromatic hydrocarbons: Source attribution, emission factors and regulation. *Atmospheric Environment* 42(13), 2895–2921. https://doi.org/10.1016/j.atmosenv.2007.12.010

Ravindra, K., Wauters, E., Van Grieken, R. (2008b). Variation in particulate PAHs levels and their relation with the transboundary movement of the air masses. *Science of the Total Environment* 396(2–3), 100–110. https://doi.org/10.1016/j.scitotenv.2008.02.018

Reyes-Garce, N., Gionfriddo, E., Gómez-Ríos, G.A., Nazmul Alam, M., Boyacı, E., Bojko, B., Singh, V., Grandy, J., Pawliszyn, J. (2017). Advances in Solid Phase Microextraction and Perspective on Future Directions. *Anal. Chem*. 90, 302−360. https://doi.org/10.1021/acs.analchem.7b04502

Roeckner, E., Stier, P., Feichter, J., Kloster, S., Esch, M., Fischer-Bruns, I. (2006). Impact of carbonaceous aerosol emissions on regional climate change. *Climate Dynamics* 27(6), 553–571. https://doi.org/10.1007/s00382-006-0147-3

Roginsky, V.A., Barsukova, T.K., Stegmann, H.B. (1999). Kinetics of redox interaction between substituted quinones and ascorbate under aerobic conditions. *Chemico-Biological Interactions* 121(2), 177–197. https://doi.org/10.1016/S0009-2797(99)00099-X

Roper, C., Chubb, L.G., Cambal, L., Tunno, B., Clougherty, J.E., Fattman, C., Mischler, S. E. (2017). Association of IL-6 with PM2.5Components: Importance of Characterizing

Filter-Based PM2.5 Following Extraction. *Water, Air, and Soil Pollution* 228(1). https://doi.org/10.1007/s11270-016-3219-y

Roper, C., Chubb, L.G., Cambal, L., Tunno, B., Clougherty, J.E., Mischler, S.E. (2015). Characterization of ambient and extracted PM2.5 collected on filters for toxicology applications. *Inhalation Toxicology* 27(13), 673–681. https://doi.org/10.3109/08958378.2015.1092185

Roper, C., Delgado, L.S., Barrett, D., Massey Simonich, S.L., Tanguay, R.L. (2019). PM 2.5 Filter Extraction Methods: Implications for Chemical and Toxicological Analyses. *Environmental Science and Technology* 53(1), 434–442. https://doi.org/10.1021/acs.est.8b04308

Rovelli, S., Cattaneo, A., Nuzzi, C., Spinazzè, A., Piazza, S., Carrer, P., Cavallo, D. (2014). Airborne Particulate Matter in School Classrooms of Northern Italy. *International Journal of Environmental Research and Public Health* 11(2), 1398–1421. https://doi.org/10.3390/ijerph110201398

Ruggieri, S., Longo, V., Perrino, C., Canepari, S., Drago, G., L'Abbate, L., Balzan, M., Cuttitta, G., Scaccianoce, G., Minardi, R., Viegi, G., Cibella, F., Bilocca, D., Borg, C., Montefort, S., Zammit, C., Bucchieri, S., Colombo, P., Ferrante, G., La Grutta, S., Melis, M.R., Piva, G., Ristagno, R., Rizzo, G. (2019). Indoor air quality in schools of a highly polluted south Mediterranean area. *Indoor Air* 29(2), 276–290. https://doi.org/10.1111/ina.12529

Sacks, J.D., Stanek, L.W., Luben, T.J., Johns, D.O., Buckley, B.J., Brown, J.S., Ross, M. (2011). Particulate matter-induced health effects: Who is susceptible? *Environmental Health Perspectives* 119(4), 446–454. https://doi.org/10.1289/ehp.1002255

Saffari, A., Daher, N., Shafer, M.M., Schauer, J.J., Sioutas, C. (2014). Global perspective on the oxidative potential of airborne particulate matter: A synthesis of research findings. *Environmental Science and Technology* 48(13), 7576–7583. https://doi.org/10.1021/es500937x

Santos, A.G., Regis, A.C.D., da Rocha, G.O., Bezerra, M. de A., de Jesus, R.M., de Andrade, J.B. (2016). A simple, comprehensive, and miniaturized solvent extraction method for determination of particulate-phase polycyclic aromatic compounds in air. *Journal of Chromatography A* 1435, 6–17. https://doi.org/10.1016/j.chroma.2016.01.018

Sauvain, J.J., Rossi, M.J., Riediker, M. (2013). Comparison of three acellular tests for assessing the oxidation potential of nanomaterials. *Aerosol Science and Technology* 47(2), 218–227. https://doi.org/10.1080/02786826.2012.742951

Schäfer, M., Werner, S. (2015). Nrf2 - A regulator of keratinocyte redox signaling. *Free Radical Biology and Medicine* 88(Part B), 243–252. https://doi.org/10.1016/j.freeradbiomed.2015.04.018

Schibuola, L., Tambani, C. (2020). Indoor environmental quality classification of school environments by monitoring PM and CO2 concentration levels. *Atmospheric Pollution Research* 11(2), 332–342. https://doi.org/10.1016/j.apr.2019.11.006

Schwartz, J., Laden, F., Zanobetti, A. (2002). The concentration-response relation between PM2.5 and daily deaths. *Environmental Health Perspectives* 110(10), 1025–1029.

https://doi.org/10.1289/ehp.021101025

Scotto, F., Bacco, D., Trentini, A., Poluzzi, V. (2018). Ecoscienza - Sostenibilità e Controllo Ambientale. *Ecoscienza*, *2*, 69–75.

Settimo, G., Manigrasso, M., Avino, P. (2020). Indoor air quality: A focus on the european legislation and state-of-the-art research in Italy. *Atmosphere* 11(4), 1–19. https://doi.org/10.3390/ATMOS11040370

Shafer, M.M., Hemming, J.D.C., Antkiewicz, D.S., Schauer, J.J. (2016). Oxidative potential of size-fractionated atmospheric aerosol in urban and rural sites across Europe. *Faraday Discussions* 189, 381–405. https://doi.org/10.1039/c5fd00196j

Shen, G., Wei, S., Zhang, Y., Wang, B., Wang, R., Shen, H., Li, W., Huang, Y., Chen, Y., Chen, H., Tao, S. (2013). Emission and size distribution of particle-bound polycyclic aromatic hydrocarbons from residential wood combustion in rural China. *Biomass and Bioenergy* 55, 141–147. https://doi.org/10.1016/j.biombioe.2013.01.031

Shen, H., Anastasio, C. (2012). A comparison of hydroxyl radical and hydrogen peroxide generation in ambient particle extracts and laboratory metal solutions. *Atmospheric Environment* 46, 665–668. https://doi.org/10.1016/j.atmosenv.2011.10.006

Shirmohammadi, F., Wang, D., Hasheminassab, S., Verma, V., Schauer, J.J., Shafer, M.M., Sioutas, C. (2017). Oxidative potential of on-road fine particulate matter (PM2.5) measured on major freeways of Los Angeles, CA, and a 10-year comparison with earlier roadside studies. *Atmospheric Environment* 148, 102–114. https://doi.org/10.1016/j.atmosenv.2016.10.042

Shuster-Meiseles, T., Shafer, M.M., Heo, J., Pardo, M., Antkiewicz, D.S., Schauer, J.J., Rudich, A., Rudich, Y. (2016). ROS-generating/ARE-activating capacity of metals in roadway particulate matter deposited in urban environment. *Environmental Research* 146, 252–262. https://doi.org/10.1016/j.envres.2016.01.009

Simonetti, G., Conte, E., Massimi, L., Frasca, D., Perrino, C., Canepari, S. (2018a). Oxidative potential of particulate matter components generated by specific emission sources. *Journal of Aerosol Science* 126, 99–109. https://doi.org/10.1016/j.jaerosci.2018.08.011

Simonetti, G., Conte, E., Perrino, C., Canepari, S. (2018b). Oxidative potential of size-segregated PM in an urban and an industrial area of Italy. *Atmospheric Environment* 187, 292–300. https://doi.org/10.1016/j.atmosenv.2018.05.051

Singer, B.C., Delp, W.W. (2018). Response of consumer and research grade indoor air quality monitors to residential sources of fine particles. *Indoor Air* 28(4), 624–639. https://doi.org/10.1111/ina.12463

Singh, R., Gautam, N., Mishra, A., Gupta, R. (2011). Heavy metals and living systems: An overview. *Indian Journal of Pharmacology* 43(3), 246–253. https://doi.org/10.4103/0253-7613.81505

Song, F., Shin, J.Y., Jusino-Atresino, R., Gao, Y. (2011). Relationships among the springtime ground-level NOX, O3 and NO3 in the vicinity of highways in the US East Coast. *Atmospheric Pollution Research* 2(3), 374–383. https://doi.org/10.5094/APR.2011.042

Sosa, B.S., Porta, A., Colman Lerner, J.E., Banda Noriega, R., Massolo, L. (2017). Human health risk due to variations in PM10-PM2.5 and associated PAHs levels. *Atmospheric Environment* 160, 27–35. https://doi.org/10.1016/j.atmosenv.2017.04.004

Squadrito, G.L., Cueto, R., Dellinger, B., Pryor, W.A. (2001). Quinoid redox cycling as a mechanism for sustained free radical generation by inhaled airborne particulate matter. *Free Radical Biology and Medicine* 31(9), 1132–1138. https://doi.org/10.1016/S0891-5849(01)00703-1

Srimuruganandam, B., Shiva Nagendra, S.M. (2012). Source characterization of PM 10 and PM 2.5 mass using a chemical mass balance model at urban roadside. *Science of the Total Environment* 433, 8–19. https://doi.org/10.1016/j.scitotenv.2012.05.082

Stabile, L., Massimo, A., Canale, L., Russi, A., Andrade, A., Dell'Isola, M. (2019). The Effect of Ventilation Strategies on Indoor Air Quality and Energy Consumptions in Classrooms. *Buildings* 9(5), 110. https://doi.org/10.3390/buildings9050110

Styszko, K., Samek, L., Szramowiat, K., Korzeniewska, A., Kubisty, K., Rakoczy-Lelek, R., Kistler, M., Giebl, A.K. (2017). Oxidative potential of PM10 and PM2.5 collected at high air pollution site related to chemical composition: Krakow case study. *Air Quality, Atmosphere and Health* 10(9), 1123–1137. https://doi.org/10.1007/s11869-017-0499-3

Sun, Y., Pang, Y., Zhang, J., Li, Z., Liu, J., Wang, B. (2017). Application of molecularly imprinted polymers for the analysis of polycyclic aromatic hydrocarbons in lipid matrix-based biological samples. *Analytical and Bioanalytical Chemistry* 409(29), 6851–6860. https://doi.org/10.1007/s00216-017-0646-6

Szigeti, T., Dunster, C., Cattaneo, A., Cavallo, D., Spinazzè, A., Saraga, D. E., Sakellaris, I. A., de Kluizenaar, Y., Cornelissen, E.J.M., Hänninen, O., Peltonen, M., Calzolai, G., Lucarelli, F., Mandin, C., Bartzis, J.G., Záray, G., Kelly, F.J. (2016). Oxidative potential and chemical composition of PM2.5 in office buildings across Europe - The OFFICAIR study. *Environment International* 92–93, 324–333. https://doi.org/10.1016/j.envint.2016.04.015

Terzi, E., Argyropoulos, G., Bougatioti, A., Mihalopoulos, N., Nikolaou, K., Samara, C. (2010). Chemical composition and mass closure of ambient PM10 at urban sites. *Atmospheric Environment* 44(18), 2231–2239. https://doi.org/10.1016/j.atmosenv.2010.02.019

Tofful, L., Perrino, C., Canepari, S. (2020). Comparison study between indoor and outdoor chemical composition of PM2.5 in two Italian areas. *Atmosphere* 11(4), 1–27. https://doi.org/10.3390/ATMOS11040368

Toriba, A., Homma, C., Kita, M., Uozaki, W., Boongla, Y., Orakij, W., Tang, N., Kameda, T., Hayakawa, K. (2016). Simultaneous determination of polycyclic aromatic hydrocarbon quinones by gas chromatography-tandem mass spectrometry, following a one-pot reductive trimethylsilyl derivatization. *Journal of Chromatography A* 1459, 89–100. https://doi.org/10.1016/j.chroma.2016.06.034

Toro Araya, R., Flocchini, R., Morales Segura, R.G.E., Guzmán, M.A.L. (2014). Carbonaceous Aerosols in Fine Particulate Matter of Santiago Metropolitan Area, Chile. The Scientific World Journal 2014. https://doi.org/10.1155/2014/794590

Tuet, W.Y., Chen, Y., Fok, S., Gao, D., Weber, R.J., Champion, J.A., Ng, N.L. (2017a). Chemical and cellular oxidant production induced by naphthalene secondary organic aerosol (SOA): Effect of redox-active metals and photochemical aging. *Scientific Reports* 7(1), 15157. https://doi.org/10.1038/s41598-017-15071-8

Tuet, W.Y., Chen, Y., Xu, L., Fok, S., Gao, D., Weber, R.J., Ng, N.L. (2017b). Chemical oxidative potential of secondary organic aerosol (SOA) generated from the photooxidation of biogenic and anthropogenic volatile organic compounds. *Atmospheric Chemistry and Physics* 17(2), 839–853. https://doi.org/10.5194/acp-17-839-2017

Valavanidis, A., Fiotakis, K., Vlachogianni, T. (2008). Airborne particulate matter and human health: Toxicological assessment and importance of size and composition of particles for oxidative damage and carcinogenic mechanisms. *Journal of Environmental Science and Health - Part C* 26(4), 339–362. https://doi.org/10.1080/10590500802494538

Valavanidis, A., Fiotakis, K., Vlachogianni, T., Papadimitriou, V., Pantikaki, V. (2006). Determination of selective quinones and quinoid radicals in airborne particulate matter and vehicular exhaust particles. *Environmental Chemistry* 3(3), 118–123. https://doi.org/10.1071/EN05089

Van Der Vliet, A., O'Neill, C.A., Cross, C.E., Koostra, J.M., Volz, W.G., Halliwell, B., Louie, S. (1999). Determination of low-molecular-mass antioxidant concentrations in human respiratory tract lining fluids. *American Journal of Physiology - Lung Cellular and Molecular Physiology 276*(2), L289-296. https://doi.org/10.1152/ajplung.1999.276.2.l289

Velali, E., Papachristou, E., Pantazaki, A., Choli-Papadopoulou, T., Planou, S., Kouras, A., Manoli, E., Besis, A., Voutsa, D., Samara, C. (2016). Redox activity and in vitro bioactivity of the water-soluble fraction of urban particulate matter in relation to particle size and chemical composition. *Environmental Pollution* 208, 774–786. https://doi.org/10.1016/j.envpol.2015.10.058

Verma, V., Fang, T., Xu, L., Peltier, R.E., Russell, A.G., Ng, N.L., Weber, R.J. (2015). Organic aerosols associated with the generation of reactive oxygen species (ROS) by water-soluble PM2.5. *Environmental Science and Technology* 49(7), 4646–4656. https://doi.org/10.1021/es505577w

Vidrio, E., Jung, H., Anastasio, C. (2008). Generation of hydroxyl radicals from dissolved transition metals in surrogate lung fluid solutions. *Atmospheric Environment* 42 4369–4379. https://doi.org/10.1016/j.atmosenv.2008.01.004

Vione, D., Barra, S., De Gennaro, G., De Rienzo, M., Gilardoni, S., Perrone, M. G., Pozzoli, L. (2004). Polycyclic aromatic hydrocarbons in the atmosphere: Monitoring, sources, sinks and fate. II: Sinks and fate. *Annali di Chimica* 94(4), 257–268. https://doi.org/10.1002/adic.200490031

Vione, D., Maurino, V., Minero, C., Pelizzetti, E., Harrison, M.A.J., Olariu, R.I., Arsenec, C. (2006). Photochemical reactions in the tropospheric aqueous phase and on particulate matter. *Chemical Society Reviews* 35(5), 441–453. https://doi.org/10.1039/b510796m

Visentin, M., Pagnoni, A., Sarti, E., Pietrogrande, M.C. (2016). Urban PM2.5 oxidative potential: Importance of chemical species and comparison of two spectrophotometric cell-free assays. *Environmental Pollution* 219, 72–79. https://doi.org/10.1016/j.envpol.2016.09.047

Viteri, F., Pezo, D., Millera, Á., Bilbao, R., Alzueta, M.U. (2019). Joint quantification of PAH and oxy-PAH from standard reference materials (urban dust and diesel particulate matter) and diesel soot surrogate by GC-MS. *International Journal of Environmental Analytical Chemistry*. https://doi.org/10.1080/03067319.2019.1691177

Voutsa, D., Samara, C., Manoli, E., Lazarou, D., Tzoumaka, P. (2014). Ionic composition of PM 2.5 at urban sites of northern Greece: secondary inorganic aerosol formation. *Environmental Science and Pollution Research* 21, 4995–5006. https://doi.org/10.1007/s11356-013-2445-8

Waked, A., Favez, O., Alleman, L.Y., Piot, C., Petit, J.-E., Delaunay, T., Verlinden, E., Golly, B., Besombes, J.-L., Jaffrezo, J.-L., Leoz-Garziandia, E. (2014). Source apportionment of PM10 in a north-western Europe regional urban background site (Lens, France) using positive matrix factorization and including primary biogenic emissions. *Atmospheric Chemistry and Physics* 14(7), 3325–3346. https://doi.org/10.5194/acp-14-3325-2014

Walgraeve, C., Demeestere, K., Dewulf, J., Zimmermann, R., Van Langenhove, H. (2010). Oxygenated polycyclic aromatic hydrocarbons in atmospheric particulate matter: Molecular characterization and occurrence. *Atmospheric Environment* 44(15), 1831–1846. https://doi.org/10.1016/j.atmosenv.2009.12.004

Wang, J., Hang Ho, S.S., Huang, R., Gao, M., Liu, S., Zhao, S., Cao, J., Wang, G., Shen, Z., Han, Y. (2016). Characterization of parent and oxygenated-polycyclic aromatic hydrocarbons (PAHs) in Xi'an, China during heating period: An investigation of spatial distribution and transformation. *Chemosphere* 159, 367–377. https://doi.org/10.1016/j.chemosphere.2016.06.033

Wang, M., Huang, R.-J., Cao, J., Dai, W., Zhou, J., Lin, C., Ni, H., Duan, J., Wang, T., Chen, Y., Li, Y., Chen, Q., Haddad, I. El, Hoffmann, T. (2019). Determination of n-alkanes, polycyclic aromatic hydrocarbons and hopanes in atmospheric aerosol: evaluation and comparison of thermal desorption GC-MS and solvent extraction GC-MS approaches. *Atmos. Meas. Tech*. 12, 4779–4789. https://doi.org/10.5194/amt-12-4779-2019

Wang, X., Sato, T., Xing, B. (2006). Size distribution and anthropogenic sources apportionment of airborne trace metals in Kanazawa, Japan. *Chemosphere* 65(11), 2440–2448. https://doi.org/10.1016/j.chemosphere.2006.04.050

Weber, S., Uzu, G., Calas, A., Chevrier, F., Besombes, J.-L., Charron, A., Salameh, D., Ježek, I., Močnik, G., Jaffrezo, J.-L. (2018). An apportionment method for the oxidative potential of atmospheric particulate matter sources: application to a one-year study in Chamonix, France. *Atmospheric Chemistry and Physics* 18(13), 9617–9629. https://doi.org/10.5194/acp-18-9617-2018

Wei, J., Yu, H., Wang, Y., Verma, V. (2019). Complexation of Iron and Copper in Ambient Particulate Matter and Its Effect on the Oxidative Potential Measured in a Surrogate Lung Fluid. *Environmental Science and Technology* 53(3), 1661–1671. https://doi.org/10.1021/acs.est.8b05731

Weichenthal, S., Crouse, D.L., Pinault, L., Godri-Pollitt, K., Lavigne, E., Evans, G., van Donkelaar, A., Martin, R.V., Burnett, R.T. (2016). Oxidative burden of fine particulate air pollution and risk of cause-specific mortality in the Canadian Census Health and Environment Cohort (CanCHEC). *Environmental Research* 146, 92–99. https://doi.org/10.1016/j.envres.2015.12.013

Wessels, A., Birmili, W., Albrecht, C., Hellack, B., Jermann, E., Wick, G., Harrison, R.M., Schins, R.P.F. (2010). Oxidant generation and toxicity of size-fractionated ambient particles in human lung epithelial cells. *Environmental Science and Technology* 44(9), 3539–3545. https://doi.org/10.1021/es9036226

Wilson, W.B., Hayes, H.V., Campiglia, A.D., Wise, S.A. (2018). Qualitative characterization of three combustion-related standard reference materials for polycyclic aromatic sulfur heterocycles and their alkyl-substituted derivatives via normal-phase liquid chromatography and gas chromatography/mass spectrometry. *Analytical and Bioanalytical Chemistry* 410(17), 4177–4188. https://doi.org/10.1007/s00216-018-1065-z

Wiseman, C.L.S. (2015). Analytical methods for assessing metal bioaccessibility in airborne particulate matter: A scoping review. *Analytica Chimica Acta* 877, 9–18. https://doi.org/10.1016/j.aca.2015.01.024

Wong, J.P.S., Tsagkaraki, M., Tsiodra, I., Mihalopoulos, N., Violaki, K., Kanakidou, M., Sciare, J., Nenes, A., Weber, R.J. (2019). Effects of Atmospheric Processing on the Oxidative Potential of Biomass Burning Organic Aerosols. *Environmental Science and Technology* 53(12), 6747–6756. https://doi.org/10.1021/acs.est.9b01034

World Health Organization. (2013). Health Effects of Particulate Matter. *The Korean Journal of Medicine*, 91(2), 106–113. https://doi.org/10.3904/kjm.2016.91.2.106

World Health Organization. (2014). *Burden of disease from Household Air Pollution for 2012*. https://doi.org/10.1146/annurev-publhealth-032013-182356

World Health Organization. (2016). *Ambient air pollution: A global assessment of exposure and burden of disease*.

World Health Organization, W. (2005). *WHO Air quality guidelines for particulate matter, ozone, nitrogen dioxide and sulfur dioxide: Global update 2005*. 1–21. https://doi.org/10.1016/0004-6981(88)90109-6

Xia, T., Korge, P., Weiss, J.N., Li, N., Venkatesen, M. I., Sioutas, C., Nel, A. (2004). Quinones and aromatic chemical compounds in particulate matter induce mitochondrial dysfunction: Implications for ultrafine particle toxicity. *Environmental Health Perspectives*, *112*(14), 1347–1358. https://doi.org/10.1289/ehp.7167

Xing, W., Zhao, Q., Scheckel, K.G., Zheng, L., Li, L. (2019). Inhalation bioaccessibility of Cd, Cu, Pb and Zn and speciation of Pb in particulate matter fractions from areas with different pollution characteristics in Henan Province, China. *Ecotoxicology and Environmental Safety*, 175, 192–200. https://doi.org/10.1016/j.ecoenv.2019.03.062

Xiong, Q., Yu, H., Wang, R., Wei, J., Verma, V. (2017). Rethinking Dithiothreitol-Based Particulate Matter Oxidative Potential: Measuring Dithiothreitol Consumption versus Reactive Oxygen Species Generation. *Environmental Science & Technology* 51(11).

https://doi.org/10.1021/acs.est.7b01272

Yang, A., Jedynska, A., Hellack, B., Kooter, I., Hoek, G., Brunekreef, B., Kuhlbusch, T.A. J., Cassee, F.R., Janssen, N.A.H. (2014). Measurement of the oxidative potential of PM2.5 and its constituents: The effect of extraction solvent and filter type. *Atmospheric Environment* 83, 35–42. https://doi.org/10.1016/j.atmosenv.2013.10.049

Yin, J., Harrison, R.M. (2008). Pragmatic mass closure study for PM1.0, PM2.5 and PM10 at roadside, urban background and rural sites. *Atmospheric Environment* 42(5), 980–988. https://doi.org/10.1016/j.atmosenv.2007.10.005

Yttri, K.E., Aas, W., Bjerke, A., Cape, J.N., Cavalli, F., Ceburnis, D., Dye, C., Emblico, L., Facchini, M.C., Forster, C., Hanssen, J.E., Hansson, H.C., Jennings, S.G., Maenhaut, W., Putaud, J.P., Torseth, K. (2007). Elemental and organic carbon in PM10: A one year measurement campaign within the European Monitoring and Evaluation Programme EMEP. *Atmospheric Chemistry and Physics* 7(22), 5711–5725. https://doi.org/10.5194/acp-7-5711-2007

Yu, H., Wei, J., Cheng, Y., Subedi, K., Verma, V. (2018). Synergistic and Antagonistic Interactions among the Particulate Matter Components in Generating Reactive Oxygen Species Based on the Dithiothreitol Assay. *Environmental Science and Technology* 52(4), 2261–2270. https://doi.org/10.1021/acs.est.7b04261

Zeng, Y., Fan, Y., Yan, X., Zheng, J., Chen, S.-J., & Mai, B.-X. (2019). In vitro oral and inhalation bioaccessibility of hydrophobic organic contaminants (HOCs) in airborne particles and influence of relevant parameters. *Environmental Research* 170, 134–140. https://doi.org/10.1016/j.envres.2018.12.025

Zhang, L., Jin, Y., Huang, M., Penning, T.M. (2012). The role of human aldo-keto reductases in the metabolic activation and detoxication of polycyclic aromatic hydrocarbons: Interconversion of PAH catechols and PAH o-quinones. *Frontiers in Pharmacology* 3. https://doi.org/10.3389/fphar.2012.00193

Zhang, Z., Gao, J., Zhang, L., Wang, H., Tao, J., Qiu, X., Chai, F., Li, Y., Wang, S. (2017). Observations of biomass burning tracers in PM2.5 at two megacities in North China during 2014 APEC summit. *Atmospheric Environment* 169, 54–64. https://doi.org/10.1016/j.atmosenv.2017.09.011

Zielinski, H., Mudway, I.S., Bé Rubé, K.A., Murphy, S., Richards, R., Kelly, F.J. (1999). Modeling the interactions of particulates with epithelial lining fluid antioxidants. *Lung Cell. Mol. Physiol* 227(4), L719-726. https://doi.org/10.1152/ajplung.1999.277.4.L719

Publications

Atmospheric Environment 210 (2019) 143–155

Contents lists available at ScienceDirect

Atmospheric Environment

journal homepage: www.elsevier.com/locate/atmosenv

$PM_{2.5}$ and PM_{10} oxidative potential at a Central Mediterranean Site: Contrasts between dithiothreitol- and ascorbic acid-measured values in relation with particle size and chemical composition

Maria Rita Perrone[a], Ilaria Bertoli[b], Salvatore Romano[a], Mara Russo[b], Gennaro Rispoli[a], Maria Chiara Pietrogrande[b,*]

[a] Department of Mathematics and Physics, University of Salento, Via per Arnesano, 73100, Lecce, Italy
[b] Department of Chemical and Pharmaceutical Sciences, University of Ferrara, Via Fossato di Mortara 17/19, 44121, Ferrara, Italy

GRAPHICAL ABSTRACT

ARTICLE INFO

Keywords:
Oxidative potential
$PM_{2.5}$ particulate matter
$PM_{2.5}$ and PM_{10} size distribution
Dithiothreitol assay
Ascorbic acid assay
$PM_{2.5}$ and PM_{10} chemical composition

ABSTRACT

In this study, $PM_{2.5}$ airborne particulate matter was collected over a full year at a costal site of the Central Mediterranean Sea and analysed for its chemical composition and oxidative potential (OP), determined by the dithiothreitol (DTT) and the ascorbic acid (AA) assays. In autumn-winter, the volume normalized oxidative OP (OP_V) were 0.29 ± 0.03 nmol min^{-1} m^{-3} and 0.21 ± 0.03 nmol min^{-1} m^{-3} for the DTT (OP_V^{DTT}) and AA (OP_V^{AA}) assay, respectively. In spring-summer the OP_V^{DTT} values were higher than OP_V^{AA} responses, i.e., 0.19 ± 0.02 nmol min^{-1} m^{-3} vs. 0.09 ± 0.01 nmol min^{-1} m^{-3}. Overall, marked seasonality was observed with higher values in Autumn-Winter (AW) than in Spring-Summer (SS), i.e., 1.5 and 2.3 times increase for OP_V^{DTT} and OP_V^{AA}, respectively.

In the cold season, the OP_V activity was broadly correlated with metals and carbon species, such as K^+, NO_3^-, Ba, Cd, Cu, Fe, Mn, P, V, OC, EC, Acetate, Oxalate and Glycolate ($p < 0.05$). This suggested the main contribution of a "mixed anthropogenic" source, consisting of the biomass burning (K^+, OC and EC) and traffic (Ba, Cu, Fe, Mn, V, EC) emissions. In SS, OP_V was significantly correlated with only few species i.e., OC, EC, Cu, and NO_3^-, suggesting main association with the "mixed anthropogenic" and the "reacted dust" sources.

For each sampling day, $PM_{2.5}$ and PM_{10} samples were simultaneously collected and analysed to investigate the variation of the OP activity in relation with the particle size and chemical composition.

OP_V^{DTT} values exhibited a poor particle-size dependence, with similar values close to 0.20 ± 0.04 nmol min^{-1} m^{-3} in both fractions. This could be explained by the association of OP_V^{DTT} with species mainly accumulated in the fine fraction, i.e., OC, POC and EC and K^+. Otherwise, the OP_V^{AA} responses exhibited a clear particle-size dependence, with significantly higher values for PM_{10} than for $PM_{2.5}$, i.e., 0.35 ± 0.06 vs. 0.21 ± 0.03 nmol min^{-1} m^{-3} in AW and 0.23 ± 0.04 vs. 0.09 ± 0.01 in SS. This may be supported by the strong correlation of OP_V^{AA} with Cu and Fe, which were most abundant metals in the PM_{10} fraction.

* Corresponding author.
E-mail address: mpc@unife.it (M.C. Pietrogrande).

https://doi.org/10.1016/j.atmosenv.2019.04.047
Received 11 December 2018; Received in revised form 25 March 2019; Accepted 21 April 2019
Available online 26 April 2019

The data of specific monitoring days were investigated in detail to better highlight the impact of some individual redox active species on the OP_V^{DTT} and OP_V^{AA} responses.The oxidative potential of $PM_{2.5}$ and PM_{10} samples was assessed with Dithiothreitol and Ascorbic Acid assays: the variation of OP responses was related with the PM size and chemical composition.

1. Introduction

The interest on the health effects associated with the air particulate matter (PM) has been growing over the last few decades. In fact, the exposure to PM has been linked to adverse health effects, such as respiratory and cardiovascular diseases, through the production of reactive oxygen species (ROS) in the human respiratory tract (Bates et al., 2015; Kelly, 2003; Mittal et al., 2014; Samara, 2017 and references therein; Venkatachari and Hopke, 2008). These ROS could be carried either by the PM themselves or generated via interactions between particle-bound redox-active components and lung lining fluid (Poschl and Shiraiwa, 2015). Therefore, the oxidative potential (OP), defined as the capacity of PM to cause damaging oxidative reactions, has been suggested as an additional PM indicator, that would encompass the PM toxicological response (Pietrogrande et al., 2018a and references therein). The compounds likely implicated in the ROS formation include organic carbon, polycyclic aromatic hydrocarbons, quinones (Cho et al., 2005; Janssen et al., 2015; Lyu et al., 2018; Verma et al., 2015), and also soluble species, particularly transition metals such as iron, copper, and vanadium (Charrier and Anastasio, 2012; Crobeddu et al., 2017; Fang et al., 2017; Shuster-Meiseles et al., 2016; Valko et al., 2005). Among the most used acellular methods for assessing PM OP, the dithiothreitol (OP^{DTT}, Charrier and Anastasio, 2012) and the ascorbic acid (OP^{AA}, Mudway et al., 2004) depletion assays display the advantage of using low-cost spectrophotometric UV–Vis measurements (Calas et al., 2018; Crobeddu et al., 2017). These assays have been found to display different sensitivity towards the redox-active species present in PM (Calas et al., 2018; Fang et al., 2016; Janssen et al., 2015; Visentin et al., 2016; Weber et al., 2018; Yang et al., 2014). Using these assays, some authors of this study assessed the OP^{DTT} and OP^{AA} activity of $PM_{2.5}$ and PM_{10} samples collected at different sites across Italy (Visentin et al., 2016; Pietrogrande et al., 2018a, 2018b).

Additionally, particle-size has been found critical in mediating PM toxicity, with particular attention to $PM_{2.5}$ and PM_{10} particles, for which the European Union has defined target values of mass concentrations in the Air Quality Directives in order to improve air quality (CEC; 2008). $PM_{2.5}$ has been found more potent than larger PM_{10}, because of its increased number, large surface area and high pulmonary deposition efficiency (Chalupa et al., 2004). The dependence of the OP responses on the PM size has been investigated, mainly for PM_{10} and $PM_{2.5}$ (Boogaard et al., 2012; Chirizzi et al., 2017; Daher et al., 2014; Fang et al., 2017; Jaafar et al., 2014; Janssen et al., 2014; Lyu et al., 2018; Shafer et al., 2016; Simonetti et al., 2018).

This paper assesses OP of $PM_{2.5}$ and PM_{10} samples simultaneously collected at a peninsular site of the Central Mediterranean basin, which is impacted by different sources, because of the contributions of long-range-transported air masses from the surrounding regions (Perrone et al., 2013, 2014a; 2014b, 2016; Becagli et al., 2017; Chirizzi et al., 2017).

In this study, the responses from the DTT and AA assays are investigated and compared in order to associate the variation in the OP activity with the particle size and distribution of the redox-active species in $PM_{2.5}$ and PM_{10} fractions. Therefore, the findings of this work would provide relevant insight in identifying the PM sources that mostly influence the oxidative properties of the PM size fractions.

2. Materials and methods

2.1. Sampling site and period

The study site is located in a suburban site (40.3°N; 18.1°E) of the flat Salento's peninsula, in the Central Mediterranean. Thirty-nine $PM_{2.5}$ filters collected from 5th December 2014 until 12th October 2015 have been analysed: more specifically, 24 samples from April to September (Spring-Summer, SS) and 15 in October–March months (Autumn-Winter, AW). Sampling was performed with a low volume (2.3 $m^3\,h^{-1}$) HYDRA-FAI dual-sampler that made it possible to simultaneously collect $PM_{2.5}$ and PM_{10} granulometric fractions using two independent sampling lines. Note that the PM_{10} samples of this study were included in a more extended study devoted to 53 PM_{10} filters, as previously reported in Pietrogrande et al. (2018a).

The sampler was located at the Mathematics and Physics Department of the University of Salento (~10 m above ground level) to collect 24-h $PM_{2.5}$ and PM_{10} samples on 47-mm-diameter preheated filters (PALLFLEX, Tissuquartz). The filters were conditioned for 48 h (25 °C and 50% humidity) before and after sampling and the PM mass concentrations were determined by the gravimetric method. Uncertainties on mass concentrations are lower than 5%. The $PM_{2.5}$ and PM_{10} loaded filters were divided in four punches for the determination of ions, metals, organic and elemental carbon, and the oxidative potential.

2.2. Ions, metals, and organic and elemental carbon analyses in the PM samples

Loaded as well as blank $PM_{2.5}$ filters were submitted to different analyses to characterize their chemical composition by using the methods described in detail in Perrone et al. (2014a) and Pietrogrande et al. (2018a). In particular, anions (Cl^-, NO_2^-, NO_3^-, SO_4^{2-}, MSA^-, oxalate, acetate, glycolate, proponiate, formate, and pyruvate) and cations (Na^+, NH_4^+, K^+, Mg^{2+}, Ca^{2+}) mass concentrations were determined by a Flow Analysis Ion Chromatography (FA-IC). An Inductively Coupled Plasma Atomic Emission Spectrometer was used to determine the mass concentration of Al, Ba, Cd, Ce, Co, Cr, Cu, Fe, La, Mn, Mo, Ni, P, Pb, Sr, Ti, V, and Zn. Ion and metal analyses were performed at the Chemistry Department of the University of Florence. The Sunset Carbon Analyzer Instrument with the EUSAAR-2 temperature program protocol (Cavalli et al., 2010) was used to determine the organic and elemental carbon (OC and EC, respectively) mass concentrations.

2.3. Assessment of the PM oxidative potential

The OP of the collected $PM_{2.5}$ samples was assessed with the DTT and AA acellular methods. The OP response was measured as the antioxidant depletion rate of known quantity of DTT and AA, following the experimental procedure described in Pietrogrande et al. (2018a, b).

The DTT and AA depletion rates (nmol min^{-1}) were determined by linear fitting of the reagent concentration versus time relationship (five

experimental points at 5, 10, 15, 25, 40 min) plot. In general, a good linearity was found with correlation coefficient $R^2 \geq 0.98$ (Visentin et al., 2016). For both methods, the DTT or AA depletion rates were determined for blank quartz filters and subtracted from response of each real PM sample. Sample and blank assays were run in duplicate.

3. Results

3.1. $PM_{2.5}$ mass concentration and chemical composition

The chemical composition of $PM_{2.5}$ particles was characterized in detail for more than 30 species, including ions – Na^+, NH_4^+, K^+, Mg^{2+}, Ca^{2+}, Cl^-, NO_2^-, NO_3^- and SO_4^{2-} – metals – Al, Ba, Cd, Ce, Co, Cr, Cu, Fe, La, Mn, Mo, Ni, Pb, Sr, Ti, V and Zn – and organic components, – OC and EC, methanesulfonate ion (MS^-) and carboxylic ions. The measured $PM_{2.5}$ mass concentrations are reported in Table S1 of the Supplementary Information (SI), as the mean values and corresponding standard errors of the mean (SEM) computed for AW and SS period, separately. Such a grouping is motivated by the season dependence of the PM mass concentration and chemical composition at the study site, as reported in previous studies (e.g., Perrone et al., 2014a, 2016; Pietrogrande et al., 2018a). The two-tail *t*-test was applied to the mean AW and SS values to assess their statistical difference at $p < 0.05$ significance level (values marked by * in Table S1).

The mean $PM_{2.5}$ mass concentration varied weakly with seasons being 26 ± 2 and $20 \pm 1\ \mu g\ m^{-3}$ in AW and SS, respectively. This result may be related to the weak dependence on seasons of the planetary boundary layer (PBL) depth in the study area, as reported in previous studies (Perrone et al., 2013, 2014b, 2016; Perrone and Romano, 2018). The percentage contribution of the investigated species to the total $PM_{2.5}$ and PM_{10} mass are summarized in Fig. 1 for AW and SS data (Fig. 1a–c and 1b-d, respectively). OC was discriminated between primary (POC) and secondary organic carbon (SOC) by using the OC/EC ratio approach (Pio et al., 2011). The mass percentages due to metals and to MS^- and carboxylic ions have been grouped in Met and Oxi, respectively. Among the analysed species, the carbonaceous

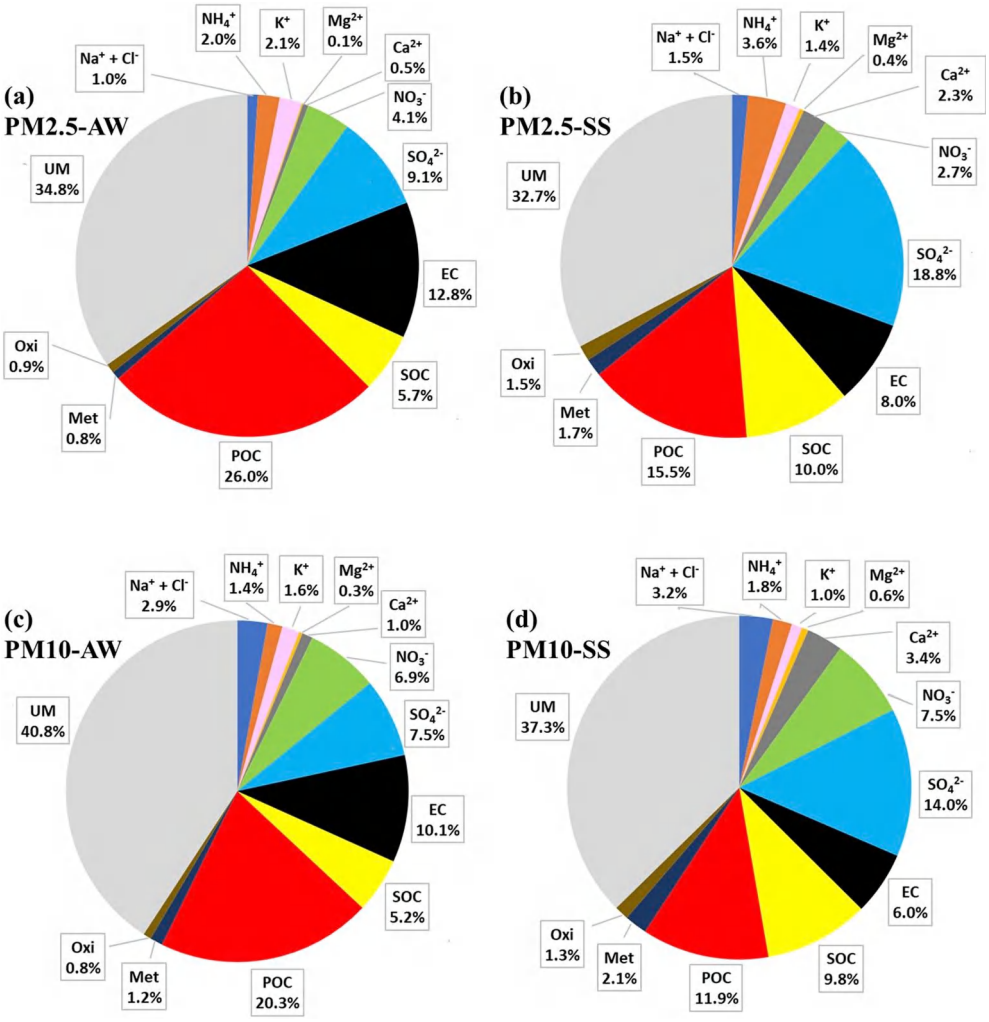

Fig. 1. Mean mass percentage distribution of the tested chemical species for the $PM_{2.5}$ samples collected in (a) AW (Autumn-Winter) and in (b) SS (Spring-Summer) and the PM_{10} samples collected in (c) AW and in (d) SS. Al, Ba, Cd, Ce, Co, Cr, Cu, Fe, La, Mn, Mo, Ni, P, Pb, Sr, Ti, V, and Zn are represented by Met. MS^-, oxalate, acetate, glycolate, propionate, formate, and pyruvate are indicated by Oxi. The undetermined mass is denoted as UM.

compounds are the major components. SO_4^{2-}, NO_3^-, NH_4^+ and K^+ are by far the most abundant inorganic ions, while metals are minor components.

The higher levels of EC, POC, NO_3^-, and K^+ in AW than in SS can be related to the stronger contribution from residential heating in the cold season. The greater mass concentration of Na^+, NH_4^+, Mg^{2+}, Ca^{2+}, SO_4^{2-}, and SOC in SS than in AW may be related to the meteorological conditions occurring in SS over the Mediterranean, mainly the formation of secondary particles favoured by the large solar irradiance and the dust resuspension because of the lack of rainy days (e.g. Perrone et al., 2013, 2014a).

3.2. $PM_{2.5}$ and PM_{10} samples: comparisons between mass concentrations and chemical components

The $PM_{2.5}$ chemical composition was compared with that of the simultaneously collected PM_{10} samples, which are a subset of the overall data reported in Pietrogrande et al. (2018a). The mean PM_{10} mass concentration was 34 ± 3 and 28 ± 2 μg m^{-3} in AW and SS (Table S1), confirming the prevalent contribution of fine particles at the study site, i.e., $PM_{2.5}$ accounted for 77 and 70% of the PM_{10} mass, in AW and SS, respectively (Perrone et al., 2013, 2014a). Accordingly, the distribution of all the investigated chemical species showed the same seasonal trend in PM_{10} as in $PM_{2.5}$ fractions (e.g., Perrone et al., 2013, 2014a, 2014b; Pietrogrande et al., 2018a), as clearly depicted in Fig. 1 (compare Fig. 1a and b with Fig. 1c and d, respectively). In particular, carbonaceous compounds showed similar concentration in both fractions being accumulated in the fine PM (Jaafar et al., 2014; Lovett et al., 2018). Accordingly, the OC/EC ratios computed in both PM fractions were similar in SS and AW, respectively (Table S1) (Waked et al., 2014). In addition, SO_4^{2-} and organic secondary ions have similar concentrations in both fractions, as they preferentially concentrate in the accumulation mode due to their secondary nature (Daher et al., 2014). Conversely, the NO_3^- ion showed an unexpected size distribution with higher concentration in PM_{10} than in $PM_{2.5}$, as previously found in most coastal sites of the southern Mediterranean Basin (e.g., Bardouki et al., 2003; Perez et al., 2008). It is probably due to the low thermal stability of NH_4NO_3 in SS, when the formation of HNO_3 instead of NH_4NO_3 is favoured under the prevalent warm conditions of most of the Central Mediterranean sites (Querol et al., 2008). The presence of gaseous HNO_3 and the possible interaction of the pollutant with mineral calcium carbonate, K^+, and sea salt may account for the increase of the coarse nitrate proportion (Perrone et al., 2013, 2019). Fine nitrate particles are usually the result of nitric acid/ammonia reactions leading to the formation of ammonium nitrate. The concentrations of Cl^- and Na^+ (tracers of sea salt aerosol) and Mg^{2+} and Ca^{2+} (crustal tracers of soil resuspension) were nearly twice in PM_{10} compared with $PM_{2.5}$, that is consistent with the nature and size of these particles (Hasheminassab et al., 2014). As expected, also metal species are accumulated in the coarse fraction, i.e., Al, Ba, Ce, Cu, Fe, with Fe, Zn and Cu as the dominant metal species (Lyu et al., 2018; Pant et al., 2015; Shirmohammadi et al., 2017; Simonetti et al., 2018; Waked et al., 2014).

3.2.1. Source apportionment of $PM_{2.5}$ and PM_{10} particles

Although the small number of the present $PM_{2.5}$ samples prevents a source apportionment study, to describe the source contribution to PM mass we can use the factors computed from Positive Matrix Factorization (PMF) in a recent study concerning overall 90 $PM_{2.5}$ and PM_{10} samples collected at the study site (Perrone et al., 2019). The present subset of 39 randomly selected samples well represent the whole dataset, as for each investigated species, the computed mean concentrations show a good agreement (within ± 1 SEM) (Table S1) with those of the all dataset (Perrone et al., 2019). For convenience, the PMF results are summarized in Table 1, reporting the 6 identified factors/sources with the corresponding percentage contributions in AW and SS, respectively. The “sulphate” source was associated to the high percentage of SO_4^{2-}, NH_4^+, and Pb. The “mixed anthropogenic” source was related to markers from both traffic (e.g., EC, OC, Cu, Fe, Ba) and biomass burning (e.g., K^+, OC, EC). The “heavy oil/secondary marine” source was dominated by V, Ni, and Cr, likely due to ship emissions, and MS^-. The “reacted dust” factor was related to crustal particles mixed with nitrate and sulphate secondary species. The “sea salt” source was characterized by the main markers Na^+ and Cl^-. The “soil dust” source was mainly associated with soil related species, i.e., Al, Ca^{2+}, Sr, Ti, Fe, Mn.

3.3. Oxidative potential of $PM_{2.5}$ samples

The $PM_{2.5}$ OP responses were measured with both assays (OP^{DTT}: nmol min^{-1} and OP^{AA}: nmol min^{-1}) and normalized by the volume of sampled air (OP_V^{DTT} and OP_V^{AA} expressed as nmol min^{-1} m^{-3}) as an exposure metrics accounting for inhaled air. In addition, OP^{DTT} and OP^{AA} were normalized by the $PM_{2.5}$ mass (OP_m^{DTT} and OP_m^{AA} expressed as nmol min^{-1} μg^{-1}) to point out the intrinsic ability of the particles to deplete physically relevant antioxidants. Fig. 2 reports the time series of the OP_V^{AA} and OP_V^{DTT} activity measured in the different particle size fractions ($PM_{2.5}$: dark grey bars; PM_{10}: light grey bars) during the cold

Table 1
Aerosol sources (and main markers) for $PM_{2.5}$ and PM_{10} particles. The percentage contribution of each source is also provided for AW (Autumn-Winter) and SS (Spring-Summer), extracted from Perrone et al. (2019).

Source	$PM_{2.5}$		PM_{10}	
	AW (%)	SS (%)	AW (%)	SS (%)
Sulphate (SO_4^{2-}, NH_4^+, Pb)	17.5	46.1	13.2	28.8
Heavy Oils/Sec. Marine (V, Ni, Cr, MS^-)	0.1	0.5	0.4	2.1
Mixed Anthropogenic (EC, OC, K^+, Cu, Fe, Ba)	55.3	15.9	59.7	28.1
Soil Dust (Al, Ca^{2+}, Sr, Ti, Fe, Mn)	7.9	9.3	12.1	23.5
Reacted Dust (NO_3^-, SO_4^{2-})	2.9	11.7	6.4	12.5
Sea Salt (Na^+, Cl^-)	16.3	16.6	8.3	5.0

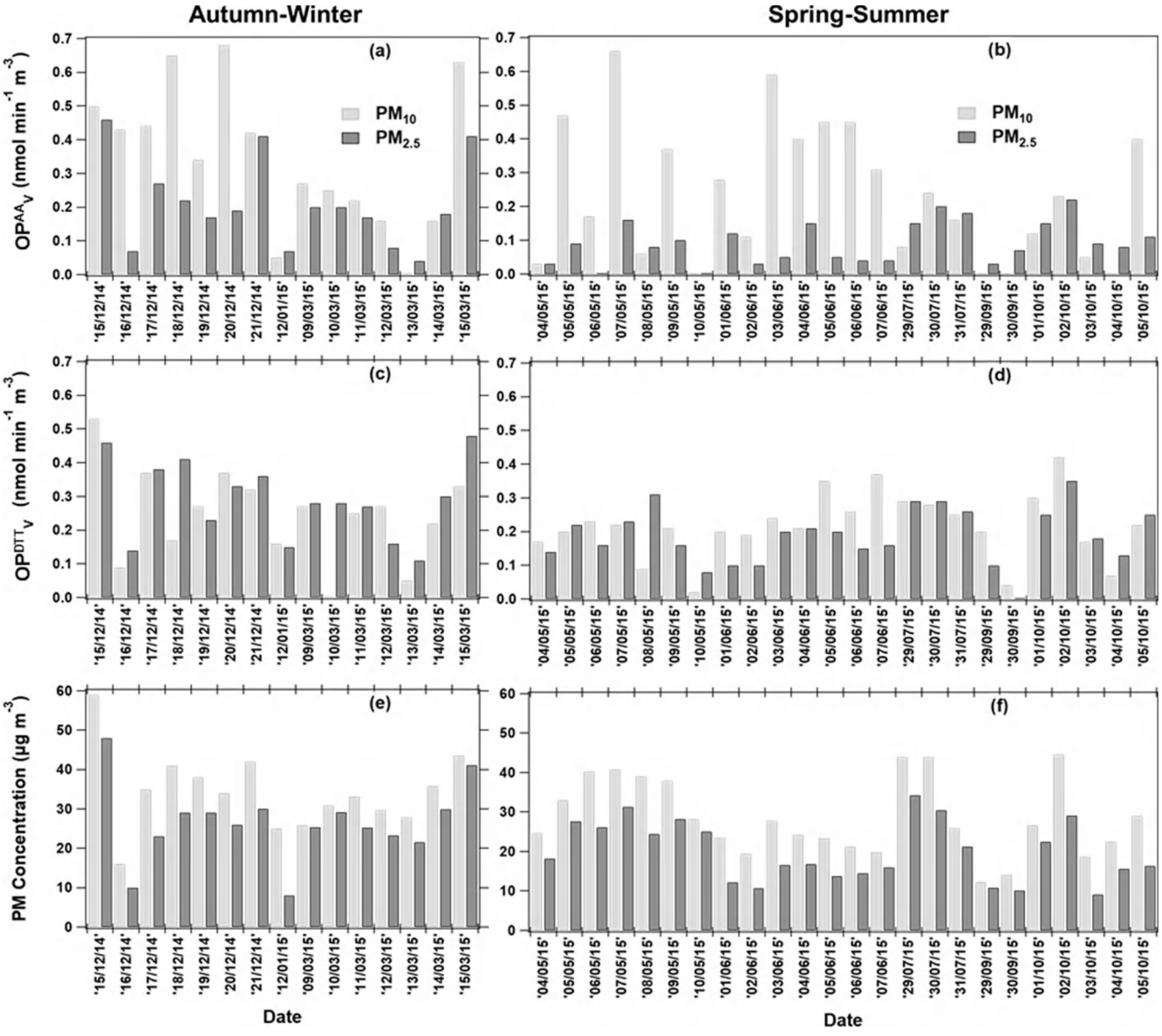

Fig. 2. Daily evolution of the volume-normalized OP_V values in $PM_{2.5}$ and PM_{10} particles (dark and light grey bars, respectively). Figures 1a and 1b: OP_V^{AA} responses measured with AA assay for Autumn-Winter (a) and Spring-Summer (b) periods; Figures 1c and 1d: OP_V^{DTT} responses measured with DTT assay for Autumn-Winter (c) and Spring-Summer (d) periods; Figures 1e and 1f: temporal evolution of the $PM_{2.5}$ and PM_{10} mass concentration in Autumn-Winter (e) and Spring-Summer (f).

(AW, Fig. 2a, c) and the warm period (Fig. 2b, d).

Overall, the OP_V^{DTT} responses were higher than the OP_V^{AA} ones in both seasons. More specifically, in AW, the mean OP_V^{DTT} value was $0.29 \pm 0.03\,nmol\,min^{-1}\,m^{-3}$ and the mean OP_V^{AA} value was $0.21 \pm 0.03\,nmol\,min^{-1}\,m^{-3}$. In SS, the difference was larger, with OP_V^{DTT} responses of $0.19 \pm 0.02\,nmol\,min^{-1}\,m^{-3}$ and OP_V^{AA} of $0.09 \pm 0.01\,nmol\,min^{-1}\,m^{-3}$.

The measured OP_V^{DTT} values are in reasonable agreement with the

Table 2
Volume- (OP_V) and mass-normalized (OP_m) Oxidative Potential responses measured for PM_{10} and $PM_{2.5}$ with DTT (OP^{DTT}) and AA assays (OP^{AA}): mean values and standard errors of the mean (SEMs) computed for autumn-winter (AW, 15 days) and spring-summer (SS, 24 days) data, separately. Values with significant ($p < 0.05$) difference between the seasons are marked by * and those with significant ($p < 0.05$) differences between the PM_{10} and $PM_{2.5}$ fractions are reported in **bold**.

Oxidative Potential	Autumn-Winter				Spring-Summer			
	PM_{10}		$PM_{2.5}$		PM_{10}		$PM_{2.5}$	
	Mean	SEM	Mean	SEM	Mean	SEM	Mean	SEM
OP_V^{AA} ($nmol^{AA}\,min^{-1}\,m^{-3}$)	**0.35**	0.06	**0.21***	0.03	**0.23**	0.04	**0.09***	0.01
OP_V^{DTT} ($nmol^{DTT}\,min^{-1}\,m^{-3}$)	0.24	0.04	0.29*	0.03	0.22	0.02	0.19*	0.02
OP_m^{AA} ($nmol^{AA}\,min^{-1}\,\mu g^{-1}$)	0.010	0.002	0.008*	0.001	**0.008**	0.001	**0.005***	0.001
OP_m^{DTT} ($nmol^{DTT}\,min^{-1}\,\mu g^{-1}$)	**0.007**	0.001	**0.011**	0.001	0.008	0.001	0.010	0.001

Table 3
Pearson correlation coefficients (r) between OP_V^{DTT} and OP_V^{AA} responses and chemical components in PM_{10} and $PM_{2.5}$ particles computed for autumn-winter (AW, 15 days) and spring-summer (SS, 24 days) data, separately. Statistically significant correlations are marked by *** at $p < 0.01$ level, ** at $p < 0.02$ level, and * at $p < 0.05$ level.

Parameter	Autumn-Winter				Spring-Summer			
	PM_{10}		$PM_{2.5}$		PM_{10}		$PM_{2.5}$	
	OP_V^{AA}	OP_V^{DTT}	OP_V^{AA}	OP_V^{DTT}	OP_V^{AA}	OP_V^{DTT}	OP_V^{AA}	OP_V^{DTT}
PM_{10}	**1.00**	0.50	**0.61****	**0.75*****	**1.00**	**0.45***	0.20	0.29
PM_{10} OP_V^{AA}								
PM_{10} OP_V^{DTT}	0.50	**1.00**	**0.70*****	**0.65*****	**0.45***	**1.00**	**0.42***	**0.57*****
$PM_{2.5}$	**0.61****	**0.70*****	**1.00**	**0.91*****	0.20	**0.42***	**1.00**	**0.70*****
$PM_{2.5}$ OP_V^{AA}								
$PM_{2.5}$ OP_V^{DTT}	**0.75*****	**0.65*****	**0.91*****	**1.00**	**0.29**	**0.57*****	**0.70*****	**1.00**
PM_{10} mass	0.47	**0.70*****	**0.84*****	**0.81*****	0.24	0.30	**0.50*****	**0.72*****
$PM_{2.5}$ mass	0.46	**0.59****	**0.82*****	**0.79*****	0.18	0.24	**0.47****	**0.63*****
Na^+	**−0.64*****	−0.49	−0.32	−0.43	**−0.40***	−0.18	**0.41***	0.29
NH_4^+	−0.32	−0.05	−0.07	−0.05	**0.63*****	**0.43***	−0.25	0.00
K^+	**0.64*****	**0.70*****	**0.79*****	**0.73*****	**0.44***	0.25	0.19	0.26
Mg^{2+}	−0.41	−0.23	−0.06	−0.09	0.17	0.14	0.01	0.13
Ca^{2+}	0.18	0.32	0.23	0.27	**0.52*****	0.27	0.02	0.14
Cl^-	−0.46	−0.23	−0.14	−0.20	**−0.53*****	**−0.49****	0.08	−0.03
NO_3^-	0.13	0.46	**0.60****	**0.66*****	−0.00	0.39	**0.51*****	**0.45***
SO_4^{2-}	−0.36	−0.15	−0.05	−0.04	**0.71*****	0.34	−0.22	0.01
MS^-	**0.62*****	0.12	0.21	0.26	**0.52*****	0.00	−0.35	−0.05
Al	0.13	0.02	−0.01	0.04	0.37	−0.00	−0.06	0.20
Ba	**0.89*****	**0.57***	**0.67*****	**0.62*****	0.22	0.30	0.45	0.34
Cd	**0.67*****	**0.55***	**0.75*****	**0.73*****	−0.11	0.02	0.18	0.31
Ce	0.27	0.38	**0.53***	0.40	0.07	−0.18	−0.26	−0.14
Co	−0.06	0.22	0.28	0.32	−0.08	−0.32	0.09	−0.18
Cr	**0.61****	0.23	0.37	0.35	0.09	0.27	0.14	0.02
Cu	**0.84*****	0.50	**0.64*****	**0.56***	0.21	**0.52*****	**0.63*****	**0.47****
Fe	**0.76*****	**0.53***	**0.76*****	**0.80*****	0.38	0.26	0.17	0.34
La	0.19	0.22	0.24	0.10	0.21	−0.18	−0.38	−0.06
Mn	**0.57***	0.38	**0.58****	**0.66*****	**0.46****	0.13	0.15	0.32
Mo	0.19	0.21	−0.47	−0.44	0.14	−0.08	**−0.43***	−0.33
Ni	0.29	0.16	0.27	0.04	**0.48****	−0.08	−0.25	−0.10
P	0.17	0.29	**0.76*****	**0.72*****	**0.56*****	0.15	0.04	0.07
Pb	−0.28	0.00	0.49	0.44	0.16	0.14	0.34	0.29
Sr	−0.03	−0.15	0.24	0.18	0.34	−0.06	−0.05	0.18
Ti	0.17	0.06	0.14	0.21	**0.44***	0.07	0.06	−0.21
V	**0.63*****	0.42	**0.73*****	**0.77*****	**0.59*****	0.13	−0.21	0.02
Zn	−0.44	−0.43	0.64***	0.41	0.38	−0.13	−0.09	−0.03
OC	**0.65*****	**0.76*****	**0.83*****	**0.80*****	0.02	**0.52*****	**0.64*****	**0.65*****
EC	**0.71*****	**0.77*****	**0.86*****	**0.84*****	0.22	**0.63*****	**0.75*****	**0.73*****
POC	**0.71*****	**0.77*****	**0.86*****	**0.83*****	0.22	**0.62*****	**0.73*****	**0.71*****
SOC	−0.27	−0.04	−0.32	−0.39	−0.11	0.38	**0.40***	**0.43***
Oxalate	0.19	0.29	**0.55***	**0.52***	**0.53*****	**0.41***	0.25	0.39
Acetate	**0.66*****	0.35	**0.67*****	**0.58****	−0.06	−0.01	0.24	0.26
Glycolate	**0.58****	0.44	**0.60****	**0.59****	**0.41***	0.13	0.29	0.34
Propionate	**0.78*****	0.38	0.35	0.31	−0.00	**0.44***	−0.12	0.04
Formate	**0.65*****	0.37	0.37	0.33	0.36	0.03	0.28	0.23
Pyruvate	**0.63*****	0.19	−0.05	0.04	**−0.50*****	−0.05	−0.09	−0.36

mean value (0.40 ± 0.26 nmol min^{-1} m^{-3}) reported by Chirizzi et al. (2017) for the same site by analyzing 30 $PM_{2.5}$ samples collected in AW between 2013 and 2016. In general, our results are towards the lowest end of the range of values reported in literature for $PM_{2.5}$ particles, being the study site away from large sources of local pollution. This may represent a peculiarity of the results reported in the paper, as most of the literature data concern OP at large urban and/or polluted sites. Consequently, the OP_V^{DTT} varied from 0.3 nmol min^{-1} m^{-3} in Atlanta to 2.0 nmol min^{-1} m^{-3} in Rotterdam (Janssen et al., 2014; Lyu et al., 2018; Samara, 2017), while the OP_V^{AA} ranged from 0.3 to 20 nmol^{AA} min^{-1} m^{-3} (Fang et al., 2016; Janssen et al., 2014; Weber et al., 2018).

Overall, the two assays displayed similar sensitivity to the studied $PM_{2.5}$ samples (Table 2), as proved by the significant correlation ($p < 0.01$) between OP_V^{DTT} and corresponding OP_V^{AA} responses in both seasons (r = 0.91 and r = 0.70, for AW and SS, Table 3). This is in agreement with some results reported in literature (e.g., Janssen et al., 2014; Mudway et al., 2004). But, it is in contrast to other papers reporting different sensitivity of the two assays towards the same redox-active species (Calas et al., 2018; Fang et al., 2016; Simonetti et al., 2018; Szigeti et al., 2016; Visentin et al., 2016; Weber et al., 2018; Yang et al., 2014). Indeed, the specific sensitivity of OP^{DTT} OP^{AA} responses is still an open question. The results of the present study may likely contribute to elucidate this point.

Despite the similarity of the mean OP_V^{DTT} and OP_V^{AA} responses (Table 2) and the overall good correlation between the data, the individual OP_V^{DTT} and OP_V^{AA} values largely varied day-by-day with different behaviour for the same sample, as shown by the daily trend reported in Fig. 2 a-d (dark grey bars). Such a large variability may be likely ascribed to the day-by-day change of the $PM_{2.5}$ concentration/composition, because of the impact at the study site of long-range transported particles from the surrounding regions. Such an impact has been found by the Authors by investigating the main airflows by using the Hybrid Single-Particle Lagrangian Integrated Trajectory (HYSPLIT) model version 4.8, from NOAA/ARL (Draxler and Hess, 1998) (Perrone et al., 2013, 2014a; 2014b, 2016; Becagli et al., 2017; Chirizzi et al., 2017; Pietrogrande et al., 2018a). This represents an additional

peculiarity of paper's results, as most of the previous studies were mainly devoted to sites mainly impacted by local-pollution sources, e.g. traffic sites, underground train stations, farms, as mentioned (Boogaard et al., 2012; Calas et al., 2018; Jaafar et al., 2014; Janssen et al., 2014; Moreno et al., 2017; Shafer et al., 2016; Shuster-Meiseles et al., 2016; Simonetti et al., 2018; Weber et al., 2018; Zhang et al., 2017).

The comparison of the OP_V^{DTT} and OP_V^{AA} values (Fig. 2a–d, dark grey bars) with the corresponding $PM_{2.5}$ mass concentrations (Fig. 2e and f, dark grey bars) revealed that high OP_V values were associated with high $PM_{2.5}$ mass concentrations, indicating that the OP_V responses were extensive parameters dependent on $PM_{2.5}$ mass concentration. This is described by the good linear correlation ($p < 0.001$) of both the OP_V^{DTT} and OP_V^{AA} values with the $PM_{2.5}$ mass: the Pearson correlation coefficients are 0.79 and 0.63 ($p < 0.001$) for OP_V^{DTT} in AW and SS respectively, and 0.82 ($p < 0.001$) for OP_V^{AA} in AW. Consistently, the OP_m^{DTT} response was nearly constant through the investigated period, with mean value of 0.010 ± 0.001 nmol min^{-1} μg^{-1} (Table 2). The OP_V^{AA} values were less significantly ($r = 0.47$, $p < 0.002$) correlated with the $PM_{2.5}$ mass in SS. Therefore, the mean OP_m^{AA} responses changed through the year, with significantly higher values in AW (0.008 ± 0.001 nmol min^{-1} μg^{-1}) compared with SS (0.005 ± 0.001 nmol min^{-1} μg^{-1}). Janssen et al. (2014) also found significant correlations between the $PM_{2.5}$ mass concentration and OP_V^{DTT}.

As OP responses were measured over a full year, the OP seasonal trend was investigated and related with the particle chemical composition. Significantly higher OP_V^{DTT} and OP_V^{AA} responses were measured in the cold than in warm seasons, as supported by a two-tail *t*-test on AW and SS mean values (significant differences at $p < 0.05$ level are marked by * in Table 2). More specifically, the average OP_V^{DTT} and OP_V^{AA} values were 1.5 and 2.3 times higher in the cold period than in the warm period, respectively. Such a seasonality of OP_V^{DTT} and OP_V^{AA} values has been also observed in other studies for ambient $PM_{2.5}$ samples and related to seasonal changes of the PM chemical composition (Fang et al., 2016; Verma et al., 2015; Visentin et al., 2016; Weber et al., 2018).

3.4. Association of the oxidative potential with chemical components/sources

To identify the $PM_{2.5}$ chemical components, and hence the pollution sources driving ROS activity, the association between the OP_V^{DTT} and OP_V^{AA} responses and the concentrations of chemical species was investigated by correlation analysis. The Pearson correlation coefficient (r) was computed for each investigated component for AW and SS, separately, and reported in Table 3 (r values significant at $p < 0.05$ level are in bold).

In the cold season both OP responses were widely correlated with several species, namely, K^+ and NO_3^-, several metals (Ba, Cd, Cu, Fe, Mn, P, V), and carbonaceous species (OC, EC, Acetate, Oxalate and Glycolate). In SS samples OP showed significant correlation with only few species, i.e., NO_3^-, Cu, OC and EC.

In addition, the inter-correlation among the analysed species was investigated to highlight association among common emission sources and/or secondary processes (correlation coefficient r reported in Tables S2 and S3 of the Supplementary Information for AW and SS, respectively). One observes that in AW all the species highly correlated with OP_V^{DTT} and/or OP_V^{AA} also showed a significant inter-correlation. In SS, the species NO_3^-, Cu, OC and EC were highly inter-correlated, but their correlation with K^+, Ba, Cd, Fe, Mn, P, V, OC, Acetate, Oxalate and Glycolate was rather weak (Table S3).

By combining these data with the PMF results, we can infer that in both seasons OP was mainly associated with the "mixed anthropogenic" source, including traffic and biomass burning, and also with the "reacted dust" factor (Table 1). Therefore, the smaller OP values observed in SS were likely explained by the lower contribution of the "mixed anthropogenic" source, which decreased from 55.3% to 15.9% from AW to SS (Table 1).

These results are consistent with several literature data on $PM_{2.5}$, that report the dominant contribution to OP_v of carbon components from biomass combustion (Fang et al., 2016; Janssen et al., 2014; Muciga et al., 2009; Reid et al., 2005; Styszko et al., 2017; Verma et al., 2015; Zhang et al., 2017), as well as of traffic related metals, such as

Table 4
Parameters of the linear regression equations linking the OP_V^{AA} and OP_V^{DTT} responses with the tracer concentrations measured in PM_{10} and $PM_{2.5}$ samples, in Autumn-Winter (AW, October–March, 15 samples) and in Spring-Summer (SS, April–September, 24 samples). The squared correlation coefficient (R^2) and the chi-square (χ^2) value provide a measure of the corresponding linear correlation and the goodness of the fit, respectively. Note that only the linear regression lines related to chemical species significantly correlated with OP_V with a p-level < 0.01 have been reported.

Species	OP_V^{AA}			OP_V^{DTT}		
	Intercept (nmol min^{-1} m^{-3})	**Slope** (nmol min^{-1} μg^{-1})	**R^2 (χ^2)**	**Intercept** (nmol min^{-1} m^{-3})	**Slope** (nmol min^{-1} μg^{-1})	**R^2 (χ^2)**
PM_{10} AW						
EC	0.11 ± 0.08	0.07 ± 0.02	0.50 (0.31)	0.08 ± 0.04	0.05 ± 0.01	0.59 (0.11)
POC	0.11 ± 0.09	0.03 ± 0.01	0.50 (0.31)	0.08 ± 0.04	0.02 ± 0.01	0.59 (0.11)
K^+	0.10 ± 0.09	0.45 ± 0.15	0.41 (0.37)	0.08 ± 0.05	0.31 ± 0.09	0.49 (0.13)
Cu	0.02 ± 0.07	31 ± 6	0.71 (0.18)	–	–	–
Fe	0.03 ± 0.05	1.7 ± 0.4	0.58 (0.27)	–	–	–
$PM_{2.5}$ AW						
EC	0.04 ± 0.03	0.05 ± 0.01	0.74 (0.06)	0.14 ± 0.03	0.04 ± 0.01	0.71 (0.06)
POC	0.04 ± 0.04	0.025 ± 0.004	0.74 (0.06)	0.14 ± 0.05	0.022 ± 0.004	0.69 (0.06)
K^+	0.04 ± 0.04	0.30 ± 0.07	0.62 (0.09)	0.14 ± 0.04	0.25 ± 0.06	0.53 (0.09)
NO_3^-	–	–	–	0.15 ± 0.05	0.13 ± 0.04	0.44 (0.11)
Cu	0.13 ± 0.04	10 ± 3	0.41 (0.13)	–	–	–
Fe	0.01 ± 0.01	1.4 ± 0.3	0.58 (0.11)	0.12 ± 0.04	1.6 ± 0.3	0.64 (0.07)
PM_{10} SS						
EC	–	–	–	0.07 ± 0.04	0.09 ± 0.02	0.40 (0.13)
POC	–	–	–	0.07 ± 0.04	0.04 ± 0.01	0.38 (0.13)
Cu	–	–	–	0.09 ± 0.04	18 ± 7	0.27 (0.16)
Ca^{2+}	0.00 ± 0.09	0.24 ± 0.08	0.27 (0.67)	–	–	–
SO_4^{2-}	−0.11 ± 0.08	0.09 ± 0.02	0.71 (0.45)	–	–	–
$PM_{2.5}$ SS						
EC	−0.03 ± 0.03	0.08 ± 0.02	0.56 (0.04)	0.03 ± 0.02	0.10 ± 0.01	0.53 (0.07)
POC	−0.03 ± 0.02	0.04 ± 0.01	0.53 (0.04)	0.03 ± 0.03	0.05 ± 0.01	0.50 (0.07)
NO_3^-	0.05 ± 0.02	0.08 ± 0.03	0.26 (0.07)	–	–	–
Cu	0.00 ± 0.03	26 ± 7	0.40 (0.06)	–	–	–

road dust components, vehicular abrasion metals and fuel oil combustion emissions (Crobeddu et al., 2017; Daher et al., 2014; Lyu et al., 2018; Moreno et al., 2017; Shafer et al., 2016; Shirmohammadi et al., 2017; Shuster-Meiseles et al., 2016; Valko et al., 2005; Yang et al., 2014).

3.5. OP^{DTT} and OP^{AA} responses for $PM_{2.5}$ and PM_{10} fractions

The variation of the OP activity in $PM_{2.5}$ and PM_{10} fractions was investigated in relation with the PM chemical composition/source. The $PM_{2.5}$ results were compared with the PM_{10} data obtained from the previous work of Pietrogrande et al. (2018a). Table S1 of SI reports the mean ± SEM concentration values for the same data subset.

The DTT assay produced similar responses for both size fractions, i.e., 0.24 ± 0.04 and 0.29 ± 0.03 nmol min^{-1} m^{-3} in AW, and 0.22 ± 0.02 and 0.19 ± 0.02 nmol min^{-1} in SS, for PM_{10} and $PM_{2.5}$ particles, respectively. This likely suggests that this assay is mainly associated with redox active species accumulated in the fine fraction. Otherwise, the AA assay exhibited a clear particle-size dependence, as OP_V^{AA} responses were significantly higher for PM_{10} than for $PM_{2.5}$, i.e., 0.35 ± 0.06 vs. 0.21 ± 0.03 nmol min^{-1} m^{-3} in AW and 0.23 ± 0.04 vs. 0.09 ± 0.01 in SS (Table 2, bold values). This suggest that AA depletion is more affected by species present in coarse particles, especially by those generated by vehicular traffic, such as brake abrasion and re-suspended dust (Simonetti et al., 2018).

Concerning the association of OP_V^{DTT} and OP_V^{AA} responses with PM_{10} components, data in Table 3 show that in AW both responses were significantly correlated with K^+, Ba, Cd, Fe, OC, and EC, which are markers of the "mixed anthropogenic" source, as found for $PM_{2.5}$ particles. In addition, OP^{AA}v responses were also significantly correlated with metals − Cr, Cu, Mn, V − and some organic compounds − MS^-, acetate, glycolate, propionate, formate, and pyruvate − that are components of the "heavy oils/secondary marine" source (Table 1).

In SS, the association of OP_V responses with chemical components significantly varied with both the OP assay and PM fraction, as shown in Table 3, because of the changes with seasons of the pollution source contributions.

In PM_{10}, the OP^{DTT}v responses were correlated with NH_4^+, Cu, OC, EC, oxalate, and glycolate. These species were mainly associated with the biomass-burning component of the "mixed anthropogenic" source. Note that in SS the Mediterranean basin is a worldwide wildfire hotspot due to the occurrence of a huge number of wildfires. The PM_{10} OP^{DTT}v response was also associated in SS with the "sulphate" source of which NH_4^+ is a maker.

Otherwise, the PM_{10} OP^{AA}v responses were correlated with more species, namely NH_4^+, K^+, Ca^{2+}, SO_4^{2-}, MS^-, Mn, Ni, P, Ti, V, oxalate, and glycolate. The results of the PMF model showed that NH_4^+ and SO_4^{2-} were the dominant species of the "sulphate" source, V, Ni and MS^- were the main components of the "heavy oil/secondary marine" source, and Ca^{2+}, Mn, and Ti contributed to the "soil dust" source. Therefore, the PM_{10} OP^{AA}v responses were likely associated with the above-mentioned sources, whose contribution has almost doubled from AW to SS (Table S1). The negligible correlation of the OP^{AA}v responses with OC and EC was likely responsible for the significant OP^{AA}v decrease from 0.35 ± 0.06 to 0.23 ± 0.04 nmol min^{-1} m^{-3} from AW to SS (Table 2), being OC and EC the main species contributing to the PM_{10} mass (Fig. 2a–b).

3.5.1. Regression analysis of the OP^{DTT} and OP^{AA} responses with individual species

To further highlight the sensitivity of the two OP assays to various PM components, regression analysis was applied to describe OP_V^{DTT} and OP_V^{AA} responses as a function of the chemical species. Linear regressions were computed for species in the $PM_{2.5}$ and PM_{10} samples for AW and SS data, separately. Among the obtained equations, the parameters of those of the most abundant and/or well correlated ($R^2 \geq 0.4$) components are reported in Table 4 (intercept, slope, linear correlation coefficient, R^2, and chi-square (χ^2) values to test goodness of the fit). Also

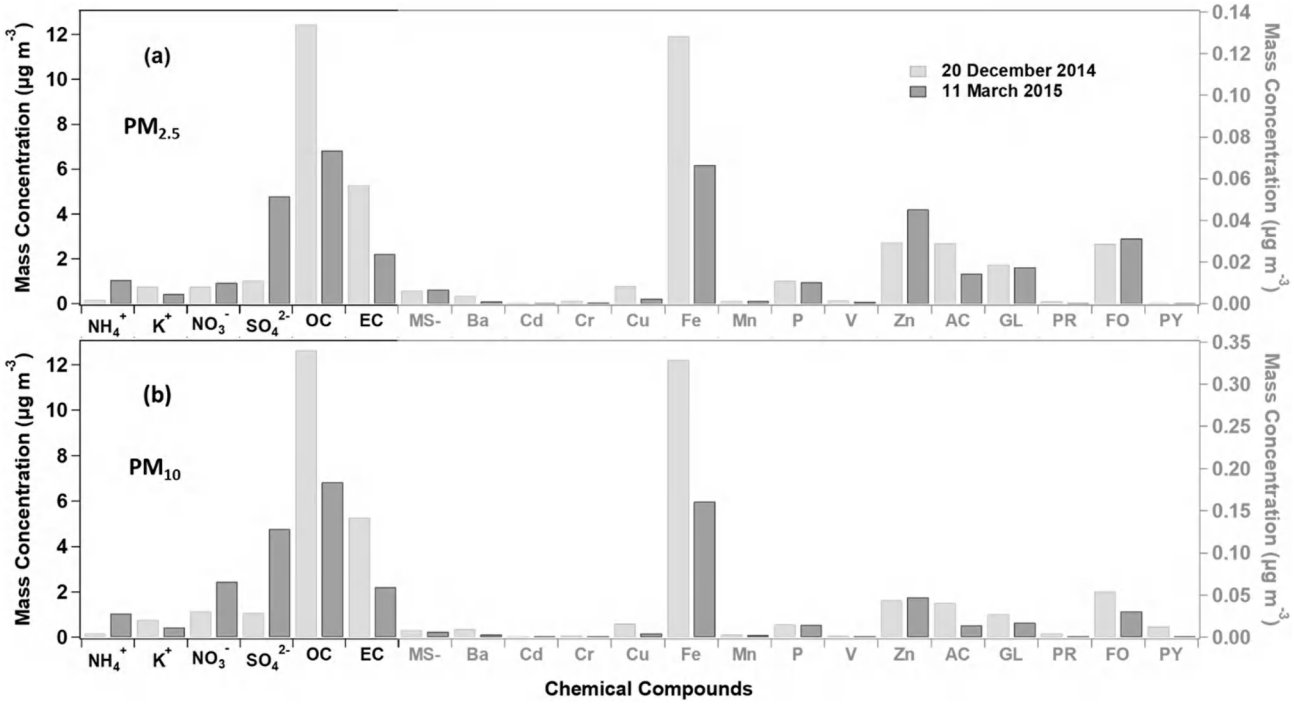

Fig. 3. Mass concentration of the main redox active species monitored in the (a) $PM_{2.5}$ and (b) PM_{10} samples collected on 20 December 2014 and 11 March 2015 (light and dark grey bars, respectively). The chemical compounds marked in black and in grey are referred to the left and right y-axis, respectively. AC, GL, PR, FO, and PY represent the acetate, glycolate, propionate, formate, and pyruvate mass concentration.

multi-linear regressions were computed by including two or three chemical species: the best obtained results are reported in Table S4a (OP_V^{AA}) and S4b (OP_V^{DTT}) of SI, for AW and SS and for $PM_{2.5}$ and PM_{10} particles, respectively. In general, we can observe that the inclusion of two or more variables did not significantly improve the fitting goodness, measured by χ^2 value, in comparison with simple linear model. Therefore, the results of the linear regressions will be discussed in the following.

Overall, in AW, similar regressions were computed for the OP_V^{DTT} and OP_V^{AA} responses with OC, EC, POC, K^+ and Fe in both fractions. In particular, close slopes of the regression lines were computed, as a measure of the assay sensitivity to the investigated species (Table 4). An exception is K^+ in PM_{10}, as the slope of the OP_V^{AA} regression line is nearly 1.5 greater than that of OP_V^{DTT} (0.45 ± 0.15 and 0.31 ± 0.09 nmol min^{-1} μg^{-1}, respectively). This likely explained the higher OP_V^{AA} than OP_V^{DTT} responses measured in PM_{10} samples (Table 2).

By comparing the different particle size, we can observe that the sensitivity of the OP_V^{AA} responses toward POC, EC, K^+, Fe, and Cu decreases from PM_{10} to $PM_{2.5}$ particles in AW (Table 4). This is particularly marked for Cu, as the line slope is three times higher for PM_{10} (31 ± 6 nmol min^{-1} μg^{-1}) than for $PM_{2.5}$ (10 ± 3 nmol min^{-1} μg^{-1}). Furthermore, the Cu and Fe concentrations are nearly double in PM_{10} compared with $PM_{2.5}$ (Table S1). These results clearly account for the higher OP_V^{AA} response in PM_{10} than in $PM_{2.5}$, besides indicating that the transition metals, especially Cu, significantly driven of OP_V^{AA} responses. Both reasons motivate the higher sensitivity of AA assay to coarse particle. Otherwise, the OP_V^{DTT} responses display higher sensitivity towards EC, POC and K^+, that have similar concentrations in both fractions (Table S1 of SI), supporting the finding that the DTT assay was more sensitive to $PM_{2.5}$ than to PM_{10} particles (Table 2).

In SS, the OP_V^{AA} and OP_V^{DTT} values were roughly correlated ($R^2 \geq 0.4$) with POC, EC and SO_4^{2-} mass concentration for PM_{10} (Table 4). In these samples, SO_4^{2-} and OC were the most abundant species, contributing on average by 14 and 22% to the PM_{10} mass (Fig. 1d). Consequently, the OP_V^{DTT} and OP_V^{AA} responses may significantly vary day-by-day depending on the amount of SO_4^{2-} and/or OC in the tested PM_{10} sample, as shown in the study cases described in the following. For $PM_{2.5}$, both OP_V^{AA} and OP_V^{DTT} responses showed significant association with POC and EC mass concentrations, with similar sensitivity of the two assays, i.e., ~0.05 nmol min^{-1} μg^{-1} for POC and ~0.10 nmol min^{-1} μg^{-1} for EC (Table 4).

In conclusion, the contrasts between the AA and DTT assay responses were likely associated with the different sensitivity of both assays towards specific emission sources, such as “sulphate”, “heavy oil/secondary marine” and “soil dust” sources. This is in agreement with results found by other Authors, i.e., Calzolai et al. (2015); Jaafar et al. (2014); Shirmohammadi et al. (2017); Styszko et al. (2017); Verma et al., 2015; Waked et al. (2014); Weber et al. (2018).

3.6. OP_V^{DTT} and OP_V^{AA} responses on selected monitoring days

The data of selected monitoring days were investigated in detail to relate the contrasts between the OP_V^{DTT} and OP_V^{AA} responses in $PM_{2.5}$ and PM_{10} samples with the change of the mass concentration of specific chemical species.

3.6.1. Study cases: 20 December 2014 and 11 March 2015

The days 20 December 2014 and 11 March 2015 showed a different pattern of the OP_V^{AA} and OP_V^{DTT} values (Fig. 2a, c). In fact, on 20 December 2014 the PM_{10} OP_V^{AA} reached the highest value (0.68 nmol min^{-1} m^{-3}), while the $PM_{2.5}$ OP_V^{AA} value (0.19 nmol min^{-1} m^{-3}) was smaller than the mean AW value (0.21 nmol min^{-1} m^{-3}). Otherwise, on 11 March 2015 the OP_V^{AA} values were rather similar for both size fractions (close to 0.20 nmol min^{-1} m^{-3}, Fig. 2a). Concerning OP_V^{DTT}, the PM_{10} value was 0.37 nmol min^{-1} m^{-3} on 20 December and 0.25 nmol min^{-1} m^{-3} on 11 March, while the $PM_{2.5}$ value was 0.33 nmol min^{-1} m^{-3} and 0.27 nmol min^{-1} m^{-3}, respectively (Fig. 2c).

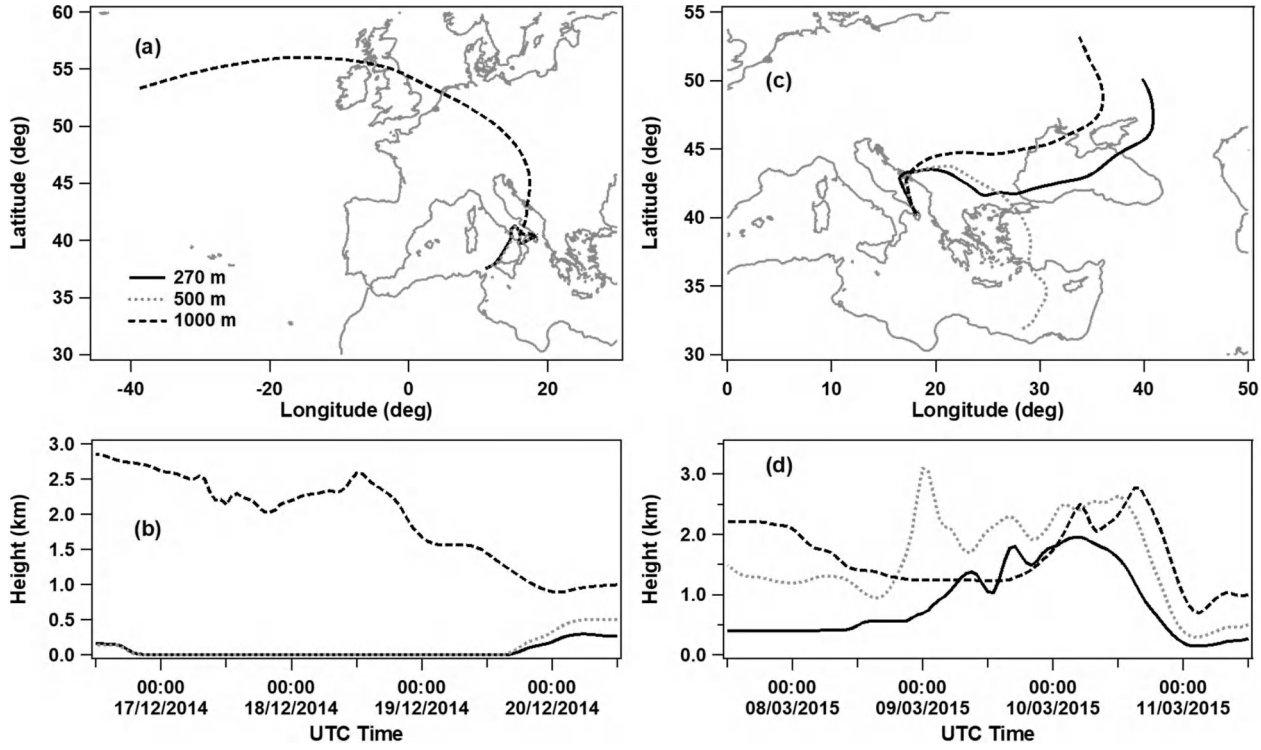

Fig. 4. Four-day analytical back trajectories reaching the monitoring site (Lecce, Italy) at 270 (solid black line), 500 (dashed grey line), and 1000 m (dashed black line) above the ground level, at 12:00 UTC of (a) 20 December 2014 and (c) 11 March 2015. The altitude of each back trajectory as a function of time is reported in (b) and (d) for the back trajectories plotted in (a) and (c), respectively.

The PM mass concentration was very similar in the two days, i.e., 26 and 25 μg/m^3 for $PM_{2.5}$ and 34 and 33 μg/m^3 for PM_{10} on 20 December and 11 March, respectively (Fig. 2e). Therefore, the above outlined contrasts resulting from Fig. 2a and c cannot be ascribed to differences in mass concentrations, but have to be searched in the different PM composition. The mass concentration of the main redox active species on 20 December (light grey bars) and 11 March (dark grey bars) are reported in Fig. 3 for $PM_{2.5}$ (a) and PM_{10} (b) samples. More specifically, the left side axis of Fig. 3 provides the mass concentration of the dominant chemical components, i.e., NH_4^+, K^+, NO_3^-, SO_4^{2-}, OC and EC, being their respective mass percentage ≥1% in the PM_{10} fraction (Table S1 of SI). The right side axis refers to the species characterized by a mass percentage < 1% (MS^-, Ba, Cd, Cr, Cu, Fe, Mn, P, V, Zn, acetate, glycolate, propionate, formate, pyruvate), reported in light grey axis. The OC and EC mass concentrations reached one of the highest values on 20 December, while their mass was almost halved on 11 March. More specifically, OC and EC accounted for 53% and 27% of the PM_{10} mass and for 68% and 36% of the $PM_{2.5}$ mass on 20 December and 11 March 2015, respectively. Therefore, we can infer that the high contrast between the PM_{10} OP_V^{DTT} and OP_V^{AA} values on 20 December was mainly due to the faster rate of change of the OP_V^{AA} with the OC and EC mass concentrations than the OP_V^{DTT} (Table 4). The contrast between the two assay responses decreases on 11 March, likely because of the remarkable decrease of the OC and EC mass contribution to the PM_{10} mass. Note also that the contribution of SOC particles was greater on 11 March than on 20 December, as indicated by the OC/EC mass ratio, which is 3.1 and 2.4 on 11 March and 20 December, respectively. Consequently, the significant decrease of the POC concentration on 11 March contributed to the above result, being the POC particles the main redox active species (Tables 3 and 4). The change in the PM chemical composition on the selected days can be explained by investigating the main airflows at the study site by using the HYSPLIT model (Draxler and Hess, 1998). The 4-day HYSPLIT back trajectories that reached the study site at 12:00 UTC of 20 December (Fig. 4a–b) show that the air masses associated with the 0.27 and 0.5 km arrival-height back trajectories came from the Central Mediterranean Sea and anthropogenic polluted areas in southern Italy. Conversely, on 11 March, back trajectories crossed Eastern Europe and therefore they likely transported aged carbonaceous particles or SOC enriched particles to the study site (Fig. 4c–d).

3.6.2. Study cases: 7 May 2015 and 29 July 2015

In SS period, an opposing trend of the OP_V^{AA} and OP_V^{DTT} values was observed in the days 7 May and 29 July (Fig. 2b, d). On 7 May, OP_V^{AA} reached one of its highest values (0.66 nmol min^{-1} m^{-3}) in PM_{10}, while it was more than 4 times smaller in $PM_{2.5}$ (0.16 nmol min^{-1} m^{-3}, Fig. 2b). In the same day, OP_V^{DTT} showed similar responses for both PM_{10} and $PM_{2.5}$ samples, i.e., close to their SS mean value (Fig. 2d). The PM_{10} ($PM_{2.5}$) mass concentration was equal to 41 (31) and 44 (34) μg/m^3 on 7 May and 29 July 2015, respectively (Fig. 2f). This pattern can be related to the variation in the mass concentration of the main redox active species, as reported in Fig. 5 for (a) $PM_{2.5}$ and (b) PM_{10} on 7 May (light grey bars) and 29 July (dark grey bars). On 7 May, the SO_4^{2-} mass concentration reached one of the highest values, i.e., 5.5 and 5.3 μg/m^3 in PM_{10} and $PM_{2.5}$, respectively. For PM_{10}, the significant association of OP_V^{AA} with SO_4^{2-} (Table 4), may likely accounts for the difference between the PM_{10} OP_V^{DTT} and OP_V^{AA} values on 7 May (Fig. 2b, d).

On 29 July 2015, the OP_V^{AA} and OP_V^{DTT} value was 0.08 and 0.29 nmol min^{-1} m^{-3}, respectively (Fig. 2b, d). In this day, the SO_4^{2-} and OC mass concentration was equal to 3.6 and 8.0 μg/m^3, respectively, in the PM_{10} sample (Fig. 5b). The low SO_4^{2-} and high OC mass concentrations, respectively, have likely been responsible for the observed differences between the OP_V^{AA} and OP_V^{DTT} values. Concerning OP_V^{DTT}, similar responses were measured in $PM_{2.5}$ and PM_{10} samples. In contrast, the OP_V^{AA} value was nearly twice larger in $PM_{2.5}$ than in PM_{10}, likely because of the higher OP_V^{AA} sensitivity toward OC in $PM_{2.5}$ than that in PM_{10}.

Fig. 6a, b show that the 4-day back trajectories crossed north-western Africa and the Mediterranean before reaching the study site at 12:00 UTC of 7 May 2015. Therefore, the rather high concentrations of SO_4^{2-} and oxalate, respectively, are likely due to the prevalent

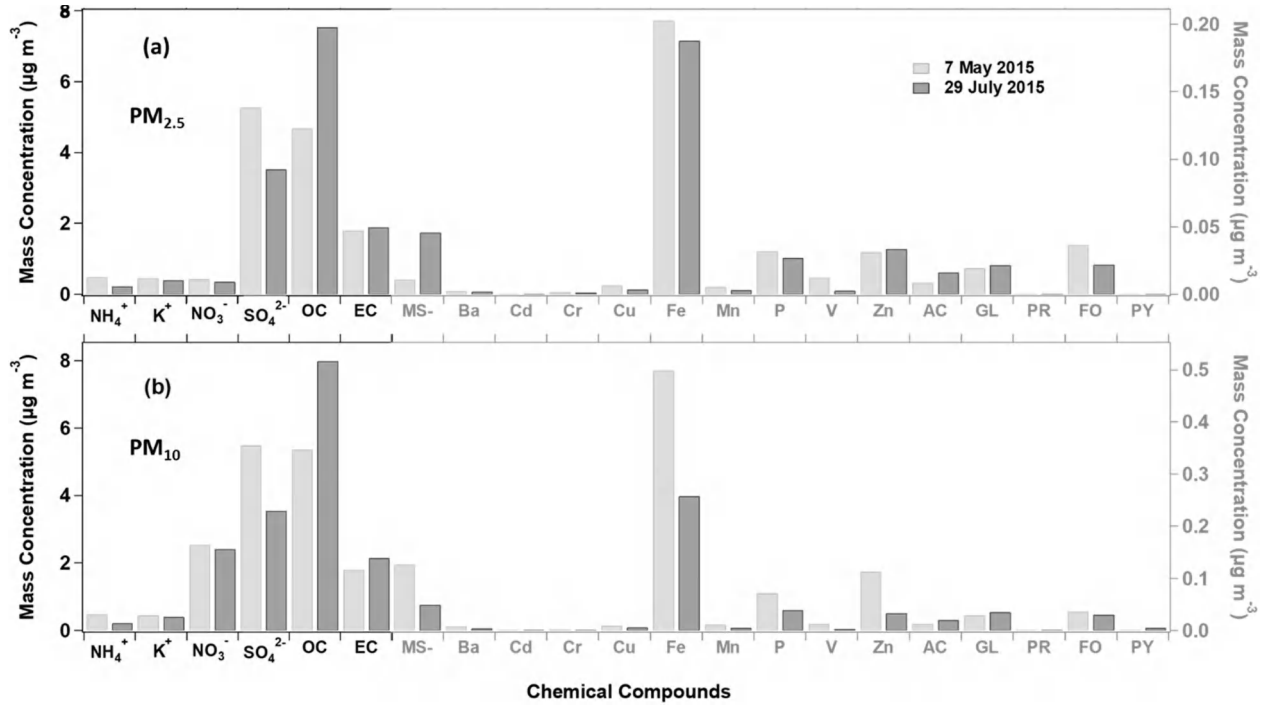

Fig. 5. Mass concentration of the main redox active species monitored in the (a) $PM_{2.5}$ and (b) PM_{10} samples collected on 7 May and 29 July 2015 (light and dark grey bars, respectively). The chemical compounds marked in black and in grey are referred to the left and right y-axis, respectively. AC, GL, PR, FO, and PY represent the acetate, glycolate, propionate, formate, and pyruvate mass concentration.

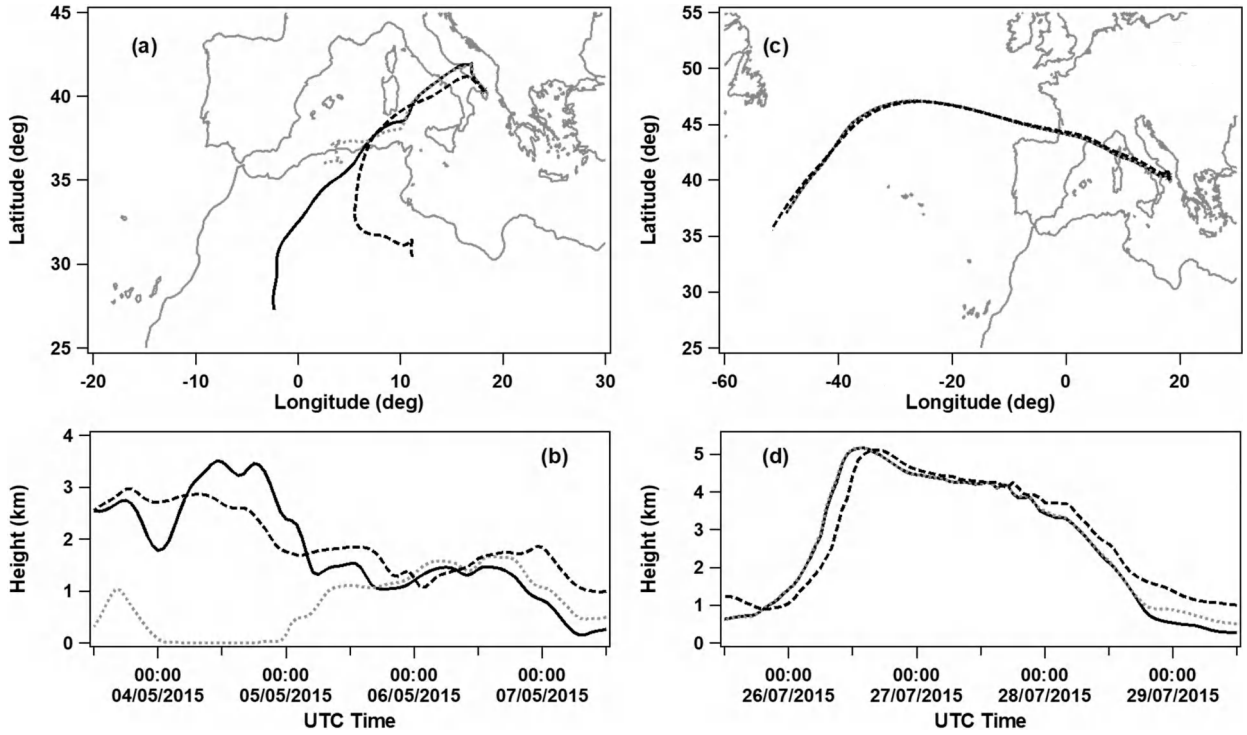

Fig. 6. Four-day analytical back trajectories reaching the monitoring site (Lecce, Italy) at 270 (solid black line), 500 (dashed grey line), and 1000 m (dashed black line) above the ground level, at 12:00 UTC of (a) 7 May and (c) 29 July 2015. The altitude of each back trajectory as a function of time is reported in (b) and (d) for the back trajectories plotted in (a) and (c), respectively.

stagnant conditions occurring in SS over the Mediterranean basin (e.g. Calzolai et al., 2015) and the enhanced photochemistry, which favours the formation of secondary aerosols. Moreover, the rather high Fe mass concentration may be likely due to the transport of dust particles at the study site, according to Perrone et al. (2016). In contrast, the 4-day HYSPLIT back trajectories that reached the study site at 12:00 UTC of 29 May 2015 came from the Atlantic Sea and crossed France and south western Italy before reaching the study site (Fig. 6cd).

4. Summary and conclusion

In summary, we investigated the impact of size-distribution and chemical composition on OP^{DTT} and OP^{AA} responses of $PM_{2.5}$ and PM_{10} samples. We could identify specific contribution of the various chemical species and/or the pollution sources, because of the peculiarity of the study site, which is strongly impacted by long-range-transported particles from different sources, and the monitoring campaign duration all over the year. In addition, the comparison between the DTT and AA responses clearly highlighted that the two assays contrast in sensibility towards individual redox active species/sources.

We observed that in AW, the OP_V^{DTT} and OP_V^{AA} responses were associated with the "mixed anthropogenic" source in both $PM_{2.5}$ and PM_{10} particles. In addition, the PM_{10} $OP^{AA}v$ responses were associated with the "heavy oils/secondary marine" source.

During SS, in $PM_{2.5}$, the ROS activity was associated with the "mixed anthropogenic" and the "reacted dust" sources. In PM_{10}, the $OP^{DTT}v$ responses were mainly associated with the biomass-burning component of the "mixed anthropogenic" source, while the $OP^{AA}v$ responses were likely driven by the "sulphate", "heavy oil/secondary marine", and "soil dust" sources.

Therefore, the variation of the OP_V^{DTT} and OP_V^{AA} responses with season can be explained by combining seasonal changing of $PM_{2.5}$ and PM_{10} chemical composition with the different sensitivity of the DTT and AA assays to the various redox-active species. Overall, the DTT assay was more sensitive to species generated by combustion processes, mostly belonging to the fine mode particles. This last finding merits further investigation, also because of the increasing relevance of this source in the last years. Conversely, the AA assay was particularly sensitive to metals in PM_{10} particles, mainly generated by vehicular traffic, such as brake abrasion and re-suspended road dust.

Therefore, the results of this study should be considered helpful to design regulatory strategies toward establishing more effective and source-specific regulations for mitigating PM toxicity. Such policies could focus on reducing PM emissions from vehicular traffic and biomass burning. In addition, the chemical specificity observed for DTT and AA assays emphasizes the need of a standardized approach for the future studies on epidemiology or toxicology of the PM.

Acknowledgments

S. Romano has carried out this work with the support of a post-doctoral fellowship from the Consorzio Nazionale Interuniversitario per le Scienze Fisiche della Materia (CNISM). The financial support of EARLINET as part of the ACTRIS Research Infrastructure Project by the European Union's Horizon 2020 research and innovation programme under grant agreement no. 654109 and 739530 (previously under grant agreement no. 262254) in the 7th Framework Programme (FP7/2007–2013) is gratefully acknowledged. S. Becagli and R. Traversi are acknowledged for the ion and metal analyses on PM samples. The NOAA Air Resources Laboratory is kindly acknowledged for the provision of the HYSPLIT back trajectories.

Appendix A. Supplementary data

Supplementary data to this article can be found online at https://doi.org/10.1016/j.atmosenv.2019.04.047.

References

Bardouki, H., Liakakou, H., Economou, C., Sciare, J., Smolík, J., Ždímal, V., Eleftheriadis,

K., Lazaridis, M., Dye, C., Mihalopoulos, N., 2003. Chemical composition of size-resolved atmospheric aerosols in the eastern Mediterranean during summer and winter. Atmos. Environ. 37, 195–208.
Bates, J.T., Weber, R.J., Abrams, J., Verma, V., Fang, T., Klein, M., Strickland, M.J., Sarnat, S.E., Chang, H.H., Mulholland, J.A., Tolbert, P.E., Russell, A.G., 2015. Reactive oxygen species generation linked to sources of atmospheric particulate matter and cardiorespiratory effects. Environ. Sci. Technol. 49, 13605–13612.
Becagli, S., Anello, F., Bommarito, C., Cassola, F., Calzolai, G., Di Iorio, T., di Sarra, A., Gómez-Amo, J.-L.-., Lucarelli, F., Marconi, M., Meloni, D., Monteleone, F., Nava, S., Pace, G., Severi, M., Sferlazzo, D.M., Traversi, R., Udisti, R., 2017. Constraining the ship contribution to the aerosol of the central Mediterranean. Atmos. Chem. Phys. 17, 2067–2084.
Boogaard, H., Janssen, N.A.H., Fischer, P.H., Kos, G.P.A., Weijers, E.P., Cassee, F.R., van der Zee, S.C., de Hartog, J.J., Brunekreef, B., Hoek, G., 2012. Contrasts in oxidative potential and other particulate matter characteristics collected near major streets and background locations. Environ. Health Perspect. 120, 185–191.
Calas, A., Uzu, G., Kelly, F.J., Houdier, S., Martins, J.M.F., Thomas, F., Molton, F., Charron, A., Dunster, C., Oliete, A., Jacob, V., Besombes, J.L., Chevrier, F., Jaffrezo, J.L., 2018. Comparison between five acellular oxidative potential measurement assays performed with detailed chemistry on PM_{10} samples from the city of Chamonix (France). Atmos. Chem. Phys. 18, 7863–7875.
Calzolai, G., Nava, S., Lucarelli, F., Chiari, M., Giannoni, M., Becagli, S., Traversi, R., Marconi, M., Frosini, D., Severi, M., Udisti, R., di Sarra, A., Pace, G., Meloni, D., Bommarito, C., Monteleone, F., Anello, F., Sferlazzo, D.M., 2015. Characterization of PM_{10} sources in the central Mediterranean. Atmos. Chem. Phys. 15, 13939–13955.
Cavalli, F., Viana, M., Yttri, K.E., Genberg, J., Putaud, J., 2010. Toward a standardised thermal-optical protocol for measuring atmospheric organic and elemental carbon: the EUSAAR protocol. Atmos. Meas. Tech. 3, 79–89.
CEC (Commission of the European Communities), 2008. Directive 2008/50/EC of the european parliament and of the council of 21 may 2008 on ambient air quality and cleaner air for europe. Off. J. Eur. Union L152, 1–44.
Chalupa, D.C., Morrow, P.E., Oberdorster, G., Utell, M.J., Frampton, M.W., 2004. Ultrafine particle deposition in subjects with asthma. Environ. Health Perspect. 112, 879–882.
Charrier, J.G., Anastasio, C., 2012. On dithiothreitol (DTT) as a measure of oxidative potential for ambient particles: evidence for the importance of soluble transition metals. Atmos. Chem. Phys. 12, 11317–11350.
Chirizzi, D., Cesari, D., Guascito, M.R., Dinoi, A., Giotta, L., Donateo, A., Contini, D., 2017. Influence of Saharan dust outbreaks and carbon content on oxidative potential of water-soluble fractions of $PM_{2.5}$ and PM_{10}. Atmos. Environ. 163, 1–8.
Cho, A.K., Sioutas, C., Miguel, A.H., Kumagai, Y., Schmitz, D.A., Singh, M., Eiguren-Fernandez, A., Froines, J.R., 2005. Redox activity of airborne particulate matter at different sites in the Los Angeles Basin. Environ. Res. 99, 40–47.
Crobeddu, B., Aragao-Santiago, L., Bui, L.C., Boland, S., Baeza Squiban, A., 2017. Oxidative potential of particulate matter 2.5 as predictive indicator of cellular stress. Environ. Pollut. 230, 125–133.
Daher, N., Saliba, N.A., Shihadeh, A.L., Jaafar, M., Baalbaki, R., Shafer, M.M., Schauer, J.J., Sioutas, C., 2014. Oxidative potential and chemical speciation of size-resolved particulate matter (PM) at near-freeway and urban background sites in the greater Beirut area. Sci. Total Environ. 470–471, 417–426.
Draxler, R.R., Hess, G.D., 1998. An overview of the HYSPLIT_4 modeling system of trajectories, dispersion, and deposition. Australian Met. Mag. 47, 295–308.
Fang, T., Verma, V., Bates, J.T., Abrams, J., Klein, M., Strickland, M.J., Sarnat, S.E., Chang, H.H., Mulholland, J.A., Tolbert, P.E., Russell, A.G., Weber, R.J., 2016. Oxidative potential of ambient water-soluble $PM_{2.5}$ in the southeastern United States: contrasts in sources and health associations between ascorbic acid (AA) and dithiothreitol (DTT) assays. Atmos. Chem. Phys. 16, 3865–3879.
Fang, T., Zeng, L., Gao, D., Verma, V., Stefaniak, A.B., Weber, R.J., 2017. Ambient size distributions and lung deposition of aerosol dithiothreitol-measured oxidative potential: contrast between soluble and insoluble particles. Environ. Sci. Technol. 51, 6802–6811.
Hasheminassab, S., Daher, N., Saffari, A., Wang, D., Ostro, B.D., Sioutas, C., 2014. Spatial and temporal variability of sources of ambient fine particulate matter ($PM_{2.5}$) in California. Atmos. Chem. Phys. 14, 12085–12097.
Jaafar, M., Baalbaki, R., Mrad, R., Daher, N., Shihadeh, A., Sioutas, C., Saliba, N.A., 2014. Dust episodes in Beirut and their effect on the chemical composition of coarse and fine particulate matter. Sci. Total Environ. 496, 75–83.
Janssen, N.A.H., Yang, A., Strak, M., Steenhof, M., Hellack, B., Gerlofs-Nijland, M.E., Kuhlbusch, T., Kelly, F., Harrison, R., Brunekreef, B., Hoek, G., Cassee, F., 2014. Oxidative potential of particulate matter collected at sites with different source characteristics. Sci. Total Environ. 472, 572–581.
Janssen, N.A.H., Strak, M., Yang, A., Hellack, B., Kelly, F.J., Kuhlbusch, T.A.J., Harrison, R.M., Brunekreef, B., Cassee, F.R., Steenhof, M., Hoek, G., 2015. Associations between three specific a-cellular measures of the oxidative potential of particulate matter and markers of acute airway and nasal inflammation in healthy volunteers. Occup. Environ. Med. 72, 49–56.
Kelly, F.J., 2003. Oxidative stress: its role in air pollution and adverse health effects. Occup. Environ. Med. 60, 612–616.
Lovett, C., Sowlat, M.H., Saliba, N.A., Shihadeh, A.L., Sioutas, C., 2018. Oxidative potential of ambient particulate matter in Beirut during Saharan and Arabian dust events. Atmos. Environ. 188, 34–42.
Lyu, Y., Guo, H., Cheng, T., Li, X., 2018. Particle size distributions of oxidative potential of lung-deposited particles: assessing contributions from quinones and water-soluble metals. Environ. Sci. Technol. 52, 6592–6600.
Mittal, M., Siddiqui, M.R., Tran, K., Reddy, S.P., Malik, A.B., 2014. Reactive oxygen species in inflammation and tissue injury. Antioxidants Redox Signal. 20, 1126–1167.
Moreno, T., Kelly, F.J., Dunster, C., Oliete, A., Martins, V., Reche, C., Minguillòn, M.C., Amato, F., Capdevila, M., de Miguel, E., Querol, X., 2017. Oxidative potential of subway $PM_{2.5}$. Atmos. Environ. 148, 230–238.
Mudway, I.S., Stenfors, N., Duggan, S.T., Roxborough, H., Zielinski, H., Marklund, S.L., Blomberg, A., Frew, A.J., Sandström, T., Kelly, F.J., 2004. An in vitro and in vivo investigation of the effects of diesel exhaust on human airway lining fluid antioxidants. Arch. Biochem. Biophys. 423, 200–212.
Mugica, V., Ortiz, E., Molina, L., De Vizcaya-Ruiz, A., Nebot, A., Quintana, R., Aguilar, J., Alcántara, E., 2009. PM composition and source reconciliation in Mexico City. Atmos. Environ. 43, 5068–5074.
Perez, N., Pey, J., Castillo, S., Viana, M., Alastuey, A., Querol, X., 2008. Interpretation of the variability of levels of regional background aerosols in the Western Mediterranean. Sci. Total Environ. 407, 527–540.
Pant, P., Baker, S.J., Shukla, A., Maikawa, C., Godri Pollitt, K.J., Harrison, R.M., 2015. The PM_{10} fraction of road dust in the UK and India: characterization, source profiles and oxidative potential. Sci. Total Environ. 530–531, 445–452.
Perrone, M.R., Becagli, S., Garcia Orza, J.A., Vecchi, R., Dinoi, A., Udisti, R., Cabello, M., 2013. The impact of long-range-transport on PM_1 and $PM_{2.5}$ at a Central Mediterranean site. Atmos. Environ. 71, 176–186.
Perrone, M.R., Dinoi, A., Becagli, S., Udisti, R., 2014a. Chemical composition of PM_1 and $PM_{2.5}$ at a suburban site in southern Italy. Int. J. Environ. Anal. Chem. 94, 127–150.
Perrone, M.R., Romano, S., Orza, J.A.G., 2014b. Particle optical properties at a Central Mediterranean site: impact of advection routes and local meteorology. Atmos. Res. 145–146, 152–167.
Perrone, M.R., Genga, A., Siciliano, M., Siciliano, T., Paladini, F., Burlizzi, P., 2016. Saharan dust impact on the chemical composition of PM_{10} and PM_1 samples over south-eastern Italy. Arabian J. Geosc. 9 (2) article 127.
Perrone, M.R., Romano, S., 2018. Relationship between the planetary boundary layer height and the particle scattering coefficient at the surface. Atmos. Res. 213, 57–69.
Perrone, M.R., Vecchi, R., Romano, S., Becagli, S., Traversi, R., Paladini, F., 2019. Weekly cycle assessment of PM mass concentrations and sources, and impacts on temperature and wind speed in Southern Italy. Atmos. Res. 218, 129–144.
Pietrogrande, M.C., Perrone, M.R., Manarini, F., Romano, S., Udisti, R., Becagli, S., 2018a. PM_{10} oxidative potential at a Central Mediterranean Site: association with chemical composition and meteorological parameters. Atmos. Environ. 188, 97–111.
Pietrogrande, M.C., Dalpiaz, C., Dell'Anna, R., Lazzeri, P., Manarini, F., Visentin, M., Tonidandel, G., 2018b. Chemical composition and oxidative potential of atmospheric coarse particles at an industrial and urban background site in the alpine region of northern Italy. Atmos. Environ. 191, 340–350.
Pio, C., Cerqueira, M., Harrison, R.M., Nunes, T., Mirante, F., Alves, C., Oliveira, C., Sanchez de la Campa, A., Artíñano, B., Matos, M., 2011. OC/EC ratio observations in Europe: re-thinking the approach for apportionment between primary and secondary organic carbon. Atmos. Environ. 45, 6121–6132.
Poschl, U., Shiraiwa, M., 2015. Multiphase chemistry at the Atmosphere – Biosphere interface influencing climate and public health in the anthropocene. Chem. Rev. 115, 4440–4475.
Querol, X., Alastuey, A., Moreno, T., Viana, M., Castillo, S., Pey, J., Rodríguez, S., Artiñano, B., Salvador, P., Sánchez, M., Garcia Dos Santos, S., Herce Garraleta, M.D., Fernandez-Patier, R., Moreno-Grau, S., Minguillón, M.C., Monfort, E., Sanz, M.J., Palomo-Marín, R., Pinilla-Gil, E., Cuevas, E., 2008. Spatial and temporal variations in airborne particulate matter (PM_{10} and $PM_{2.5}$) across Spain 1999-2005. Atmos. Environ. 42, 3964–3979.
Reid, J.S., Koppmann, R., Eck, T.F., Eleuterio, D.P., 2005. A review of biomass burning emissions part II: intensive physical properties of biomass burning particles. Atmos. Chem. Phys. 5, 799–825.
Samara, C., 2017. On the redox activity of urban aerosol particles: implications for size distribution and relationships with organic aerosol components. Atmosphere 8, 205.
Shafer, M.M., Hemming, J.D., Antkiewicz, D.S., Schauer, J.J., 2016. Oxidative potential of size-fractionated atmospheric aerosol in urban and rural sites across Europe. Faraday Discuss 189, 381–405.
Shirmohammadi, F., Wang, D., Hasheminassab, S., Verma, V., Schauer, J.J., Shafer, M.M., Sioutas, C., 2017. Oxidative potential of on-road fine particulate matter ($PM_{2.5}$) measured on major freeways of Los Angeles, CA, and a 10-year comparison with earlier roadside studies. Atmos. Environ. 148, 102–114.
Shuster-Meiseles, T., Shafer, M.M., Heo, J., Pardo, M., Antkiewicz, D.S., Schauer, J.J., Rudich, A., Rudich, Y., 2016. ROS-generating/ARE-activating capacity of metals in roadway particulate matter deposited in urban environment. Environ. Res. 146, 252–262.
Simonetti, G., Conte, E., Perrino, C., Canepari, S., 2018. Oxidative potential of size-segregated PM in an urban and an industrial area of Italy. Atmos. Environ. 187, 292–300.
Szigeti, T., Dunster, C., Cattaneo, A., Cavallo, D., Spinazzè, A., Saraga, D.E., Sakellaris, I.A., de Kluizenaar, Y., Cornelissen, E.J.M., Hänninen, O., Peltonen, M., Calzolai, G., Lucarelli, F., Mandin, C., Bartzis, J.G., Záray, G., Kelly, F.J., 2016. Oxidative potential and chemical composition of PM2.5 in office buildings across Europe – the OFFICAIR study. Environ. Int. 92–93, 324–333.
Styszko, K., Samek, L., Szramowiat, K., Korzeniewska, A., Kubisty, K., Rakoczy-Lelek, R., Kistler, M., Giebl, A.K., 2017. Oxidative potential of PM_{10} and $PM_{2.5}$ collected at high air pollution site related to chemical composition: krakow case study. Air Qual. Atmos. Health 10, 1123–1137.
Valko, M., Morris, H., Cronin, M.T., 2005. Metals, toxicity and oxidative stress. Curr. Med. Chem. 12, 1161–1208.
Venkatachari, P., Hopke, P.K., 2008. Development and laboratory testing of an automated monitor for the measurement of atmospheric particle-bound reactive oxygen species (ROS). Aerosol Sci. Technol. 42, 629–635.
Verma, V., Fang, T., Xu, L., Peltier, R.E., Russel, A.G., Ng, N.L., Weber, R.J., 2015. Organic

aerosols associated with the generation of reactive oxygen species (ROS) by water-soluble $PM_{2.5}$. Environ. Sci. Technol. 49, 4646–4656.
Visentin, M., Pagnoni, A., Sarti, E., Pietrogrande, M.C., 2016. Urban $PM_{2.5}$ oxidative potential: importance of chemical species and comparison of two spectrophotometric cell-free assays. Environ. Pollut. 219, 72–79.
Waked, A., Favez, O., Alleman, L.Y., Piot, C., Petit, J.E., Delaunay, T., Verlinden, E., Golly, B., Besombes, J.L., Jaffrezo, J.L., Leoz-Garziandia, E., 2014. Source apportionment of PM_{10} in a north-western Europe regional urban background site (Lens, France) using positive matrix factorization and including primary biogenic emissions. Atmos. Chem. Phys. 14, 3325–3346.
Weber, S., Uzu, G., Calas, A., Chevrier, F., Besombes, J.L., Charron, A., Salameh, D., Jevzek, I., Movcnik, G., Jaffrezo, J.L., 2018. An apportionment method for the oxidative potential of atmospheric particulate matter sources: application to a one-year study in Chamonix. France. Atmos. Chem. Phys. 18, 9617–9629.
Yang, A., Jedynska, A., Hellack, B., Kooter, I., Hoek, G., Brunekreef, B., Kuhlbusch, T.A.J., Cassee, F.R., Janssen, N.A.H., 2014. Measurement of the oxidative potential of $PM_{2.5}$ and its constituents: the effect of extraction solvent and filter type. Atmos. Environ. 83, 35–42.
Zhang, Z., Gao, J., Zhang, L., Wang, H., Tao, J., Qiu, X., Chai, F., Li, Y., Wang, S., 2017. Observations of biomass burning tracers in $PM_{2.5}$ at two megacities in North China during 2014 APEC summit. Atmos. Environ. 169, 54–64.

Atmospheric Environment 211 (2019) 103–112

Contents lists available at ScienceDirect

Atmospheric Environment

journal homepage: www.elsevier.com/locate/atmosenv

Ascorbate assay as a measure of oxidative potential for ambient particles: Evidence for the importance of cell-free surrogate lung fluid composition

Maria Chiara Pietrogrande*, Ilaria Bertoli, Francesco Manarini, Mara Russo

Department of Chemical and Pharmaceutical Sciences, University of Ferrara, Via Fossato di Mortara 17/19, 44121, Ferrara, Italy

GRAPHICAL ABSTRACT

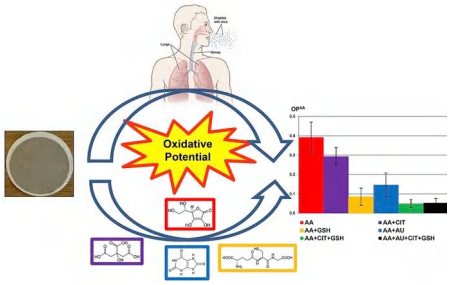

ARTICLE INFO

Keywords:
Particulate matter (PM)
Oxidative potential (OP)
Ascorbic acid assay
Simulated respiratory tract lining fluid

ABSTRACT

In this study, we investigated the cell-free ascorbic acid assay (OP^{AA} response) to quantify the oxidative potential (OP) of particle matter (PM), as a promising metric for studying the association between the chemical properties and toxicological effects of PM.

With the purpose of designing an experimental set-up mostly representative of the intracellular oxidation, the assay was performed in different media, representing an artificial respiratory tract lining fluid (RTLF), i.e., simple ascorbate (Asc) or mixtures of reduced glutathione (GSH), urate (UA) and citrate (Cit).

The study was performed on real $PM_{2.5}$ samples collected at an urban and rural site in the Po Valley (northern Italy). For comparison, standard solutions of redox-active species were investigated, i.e., Cu^{2+}, Fe^{2+}, 1,2-naphthoquinone, 1,4-naphthoquinone and 9,10-phenantrenequinone, that are known to give positive response to the AA assay.

The composition of the synthetic RTLF strongly effected the OP^{AA} responses, as they decreased with increasing the mixture complexity, following the order:

Asc > Asc + Cit > Asc + UA > Asc + GSH > Asc + Cit + GSH ~ Asc + Cit + GSH + UA.

Based on comparison of the dependence of OP^{AA} on RTLF composition, we could infer that Cu^{2+} and quinones were the redox active species most responsible of the OP^{AA} response of the analysed $PM_{2.5}$ samples.

1. Introduction

Many studies have demonstrated that induction of oxidative stress is one likely mechanism involved in adverse health outcomes of exposure to ambient particulate matter (PM). This is related to an imbalance between the generation of reactive oxygen species (ROS) and the antioxidant defenses (Bates et al., 2015; Delfino et al., 2010; Godri et al., 2011; Janssen et al., 2015; Mudway et al., 2004; Shen and Anastasio,

* Corresponding author.
E-mail address: mpc@unife.it (M.C. Pietrogrande).

https://doi.org/10.1016/j.atmosenv.2019.05.012
Received 18 September 2018; Received in revised form 2 May 2019; Accepted 4 May 2019
Available online 08 May 2019
1352-2310/

2012; Shiraiwa et al., 2012; Steenhof et al., 2013).

Therefore, the PM oxidative potential (OP) – defined as the capacity of PM to oxidize target molecules generating ROS – has been proposed as a biologically-relevant exposure metric for attempting to link atmospheric aerosol and health end points (Antiñolo et al., 2015; Ayres et al., 2008; Crobeddu et al., 2017; Fang et al., 2016; Hedayat et al., 2015; Lyu et al., 2018; Orru et al., 2018; Saffari et al., 2014; Strak et al., 2012; Steenhof et al., 2013; Weichenthal et al., 2016; Strak et al., 2012, 2012). Among the variety of methods developed for measuring OP, in vitro cell-free assays, besides being non-invasive, have the advantages of being fast, inexpensive, easy to organize and suitable for automation as compared to cellular tests (Calas et al., 2018; Fang et al., 2016; Janssen et al., 2015; Hedayat et al., 2015; Hellack et al., 2014; Hellack et al., 2017; Visentin et al., 2016; Weber et al., 2018). One of the most common method is the ascorbic acid (AA) assay using ascorbate (Asc), as the most abundant antioxidant found in lung fluids, which has a vital role in oxidant production from redox-active species (Ayres et al., 2008; Charrier and Anastasio, 2011; Crobeddu et al., 2017; Janssen et al., 2014; Fang et al., 2016; Maikawa et al., 2016; Rui-Wen et al., 2018; Weichenthal et al., 2016). This assay simulates the electron-transfer mechanism from AA to oxygen based on the catalytic ability of redox-active species. The assay response, commonly called OP^{AA}, is the Asc oxidation rate measured with a basic cheap laboratory equipment, such as an UV–Visible Spectrophotometer.

To make OP^{AA} a reliable measure of the in vivo capacity of PM to induce ROS, there is the need of designing an assay set up that most closely simulates the interactions of the inhaled particles when come into contact with interstitial macrophages in the lung. This is not an easy task, because the respiratory tract lining fluid (RTLF) has unique features that varies in different levels of the respiratory tract, as shown by discrepant quantitative compositions of antioxidants reported in literature (Kumar et al., 2017; Marques et al., 2011; Van der Vliet et al., 1999). A further difficulty in replicating RTLF in vitro is due to the extremely small amount of aqueous fluid and lung surfactant (Charrier et al., 2014; Hedayat et al., 2015; Van der Vliet et al., 1999).

In this work we investigated the role of different composition of synthetic RTLF on OP^{AA} response of ambient $PM_{2.5}$ samples collected at an urban and rural site in the Po Valley (northern Italy). In comparison to the simplest surrogate containing only ascorbate, composite solutions were used by adding three endogenous lung components at physiological levels, namely reduced glutathione (GSH), urate (UA) and citrate (Cit) (Godri et al., 2011; Kumar et al., 2017; Ma et al., 2015; Marques et al., 2011; Mudway et al., 2004; Pryor, 1994; Szigeti et al., 2016; Weichenthal et al., 2016). The obtained results were compared with the data from individual chemical source markers, chosen for either their known positive response to the AA assay and their abundance in atmospheric aerosol, namely transition metals (Charrier and Anastasio, 2011; Charrier et al., 2014; DiStefano et al., 2009; Fang et al., 2016; Hedayat et al., 2015; Lyu et al., 2018; Shuster-Meiseles et al., 2016; Yang et al., 2015; Yu et al., 2018) and quinones (Charrier and Anastasio, 2015; Chung et al., 2006; Jiang and Jang, 2018; Lyu et al., 2018; McWhinney et al., 2013).

2. Materials and methods

2.1. Study sites and sampling

Sampling took place at two sites in the Emilia Romagna region, in the eastern part of the Po Valley (northern Italy). The urban background site (URB) is located in the in the middle of the city of Bologna (~400,000 inhabitants) in a densely populated area, and the rural background station (RUR) is located at San Pietro Capofiume about 30 km northeast from the city. From 10th to 31st March 2018, 24 h $PM_{2.5}$ samples were collected every day concurrently at the two sites.

A low volume automatic outdoor sampler (Skypost PM, TCRTECORA Instruments, Corsico, Milan, Italy) was used, operating at the standard airflow rate of 38.3 l min^{-1} for 24 h to collect an air volume of 55 m^3 per day. $PM_{2.5}$ samples were collected on 47 mm diameter quartz fiber filters (Whatman® QM-A quartz filters). The procedure outlined in European Standard EN 12341 (EN, 1998) was applied for equilibrating and weighing the quartz fiber filters. They were heated for 3 h at 800 °C in air before use, to reduce their carbon blank, and conditioned for 24 h at 20 °C after sampling, to control the relative humidity. Field blank filters were placed in the sampler equipment and exposed for 24 h without operating the air pump. All details concerning the site and the logistical aspects of the sampling procedure can be found in Authors'papers (Pietrogrande et al., 2016, 2018).

2.2. Standards and reagents

Sodium phosphate (NaH_2PO_4, ACS), potassium phosphate ($KHPO_4$, HPLC grade), Tris base (Mol Bio grade), sodium chloride (NaCl, ACS) and disodium EDTA (ACS) were from Fisher Scientific. L-ascorbic acid sodium salt (Asc, CAS: 50-81-7), citric acid sodium salt (Cit, CAS: 994-36-5), reduced L-glutathione (GSH, CAS: 70-18-8), uric acid sodium salt (UA, CAS 1198-77-2) were from Sigma Aldrich. Standard solutions of these reagents were prepared at 10 mM concentration in ultrapure water (Milli-Q® IQ 7000 water purification system).

Aqueous solutions of the reagents are unstable at room temperature and sensible to light, thus they were preserved in amber glass vials in the dark at −20 °C.

Each antioxidant stock solution was made fresh each day and added to the buffer at the start of the reaction.

2.2.1. Simulated respiratory tract lining fluid

Six simulated RTLFs have been tested. The simplest synthetic RTLF is based on ascorbate-only model (100 μM ascorbate solution), as commonly used in AA assay (Ayres et al., 2008; Fang et al., 2016; Godri et al., 2011; Mudway et al., 2004; Hedayat et al., 2015; Janssen et al., 2014; Pietrogrande et al., 2018; Visentin et al., 2016). The composite RTLF surrogates were obtained by adding GSH and UA, which are antioxidants naturally occurring in the lung fluid to compensate ROS production, and possibly to modulate ROS release (Godri et al., 2011; Kumar et al., 2017; Ma et al., 2015; May et al., 2005; Mudway et al., 2004; Pryor, 1994; Weichenthal et al., 2016). Also citrate (Cit) was added, to represent proteins able to mobilize iron that can be found in lung lining fluid (Marques et al., 2011). The used concentrations were 150 μM citrate, 50 μM reduced L -glutathione and 50 μM urate to represent typical lung concentrations, as widely used in AA assays by Charrier's group (Charrier and Anastasio, 2011, 2015; Charrier et al., 2014).

In addition, an equimolar solution of the four AOs was investigated, i.e., 100 μM, AA, Cit, GSH and UA at pH 7.0, as used by several Authors (Strak et al., 2012; Mudway et al., 2004; Steenhof et al., 2013; Szigeti et al., 2016; Godri et al., 2011).

Finally, two different buffers at pH 7.4 were tested: 0.1 M phosphate buffer (Na_2HPO_4 and NaH_2PO_4) and a phosphate buffered saline (PBS). It contains 114 mM NaCl, 7.8 mM sodium phosphate dibasic, and 2.2 mM potassium phosphate monobasic, pH 7.2–7.4 (Charrier and Anastasio, 2011; Charrier et al., 2014; Ma et al., 2015).

2.2.2. Standard solutions of redox-active species

Copper (II) sulfate (98%), iron (II) chloride (ACS), 1,2-naphthoquinone (1,2-NPQ, 97%), 1,4-naphthoquinone (1,4-NPQ, 97%) and 9,10-phenanthrenequinone (9,10-PNQ, 99%) were from Sigma-Aldrich. Individual standard stock solutions were prepared for each analyte by weighting pure standards with a concentration of 10^{-2} M using MilliQ water for metal ions and acetonitrile for quinones as solvent.

2.3. Determination of oxidative potential

Oxidative Potential of the collected $PM_{2.5}$ samples and standard

solutions were assessed with the ascorbic acid assay, following the experimental procedure described elsewhere (Visentin et al., 2016).

The assay was performed under the biological relevant temperature of 37 °C and pH of 7.4. UV absorbance was measured with a V-730 Jasco UV–Visible Spectrophotometer (JASCO EUROPE s.r.l.). It was a double-beam spectrophotometer with single monochromator, equipped with a with a temperature controller of the 1 cm path length optical cell. The assay was performed directly in the quartz cuvette inside the dark spectrophotometer cell, in order to guarantee the reagent stability during the procedure. Briefly, 30 µl of each simulated RTLF were added to the sample (total volume of 3 mL) and the Asc depletion rate was followed by directly measuring of the ascorbate ion absorbance at 265 nm (ε = 14500 $M^{-1}cm^{-1}$).

2.3.1. Data analysis

The kinetics of the AA oxidation was investigated by following the depletion of the AA concentration (100 nmol initially added to the sample solution) over the reaction course. Five experimental points were measured at different reaction times (5, 10, 15, 20, 25 min). Such values were fitted by a linear equation and the slope of the best fitting straight line represents the AA depletion rate (nmol min^{-1}). In general, a good linearity of the concentration-time relationship was found with correlation coefficient $R^2 \geq 0.98$ (Visentin et al., 2016).

Reagent blank and filter blank responses were determined by measuring the AA depletion rate of buffer solutions and extracts of a quarter of blank quartz filters, respectively. Each sample and blank measurement was run in quintuplicate to calculate the mean and precision of measurements, expressed as standard deviation values (S.D.). For each experimental set up, the procedure limit of detection (LOD) was computed as three times the blank standard deviation. The final OP^{AA} result was obtained from each OP^{AA} response > LOD, by subtracting the reagent or filter blank from the measured value. For $PM_{2.5}$ samples, the OP^{AA} values were then normalized by the volume of sampled air (expressed as nmol min^{-1} m^{-3}) as an exposure metrics accounting for inhaled air.

OP^{AA} of redox-active species was measured in quintuplicate on a volume of 3 mL of individual standard solutions.

2.3.2. PM samples extraction

Briefly, the AA assay was performed on a quarter of each sampled $PM_{2.5}$ filter. It was extracted using 3 mL of 0.1 M buffer at pH 7.4 by sonication for 15 min in an ultrasonic bath (Elmasonic S 100 H, Elma Schmidbauer GmbH) operating at 37 kHz frequency and 150 W power. The extract was then filtered on a regenerate cellulose syringe filter (13 mm, 0.22 µm, Kinesis) to remove the suspended solid particles and then introduced into an amber vial at a constant temperature of 37 °C using a dry bath.

2.4. Statistics

The two-tailed Student's *t*-test was conducted to check statistically significant differences between OP^{AA} responses measured in the different surrogates as well as between filters collected at the two sampling sites. A p value less than 0.05 was regarded as statistically significant.

Moreover, univariate analysis was applied by computing the linear correlation of OP^{AA} responses measured in the different composite RTLFs as well as between OP^{AA} values of $PM_{2.5}$ samples and standard solutions of individual compounds.

3. Results and discussion

3.1. OP^{AA} for ambient PM in six simulated RTLFs

As an initial step, the OP^{AA} values were measured for each $PM_{2.5}$ extract using the simple Asc solution as the reductant (Calas et al.,

Table 1
OP^{AA} responses of 20 $PM_{2.5}$ samples measured in different compositions of surrogate RTLF by adding citrate, urate and glutathione to Ascorbic acid. For each sample, measurements were repeated 5 times (mean and standard deviation).

Samples	OP^{AA} (nmol min^{-1} m^{-3})	S.D.	Samples	OP^{AA} (nmol min^{-1} m^{-3})	S.D.
simplified RTLF: Asc 100 µM					
URB1	0.63	0.17	RUR1	0.29	0.09
URB2	0.32	0.05	RUR2	0.28	0.09
URB3	0.48	0.09	RUR3	0.25	0.09
URB4	0.52	0.17	RUR4	0.26	0.09
URB5	0.65	0.17	RUR5	0.27	0.09
URB5	0.51	0.13	RUR6	0.34	0.05
URB7	0.53	0.13	RUR7	0.26	0.05
URB8	0.54	0.13	RUR8	0.12	0.04
URB9	0.50	0.13	RUR9	0.32	0.05
URB10	0.52	0.13	RUR10	0.28	0.05
RTLF with two AOs: Asc + citrate 100:150 µM					
URB1	0.39	0.09	RUR1	0.21	0.04
URB2	0.28	0.05	RUR2	0.20	0.04
URB3	0.39	0.09	RUR3	0.23	0.04
URB4	0.38	0.09	RUR4	0.22	0.04
URB5	0.38	0.09	RUR5	0.24	0.04
URB5	0.34	0.05	RUR6	0.27	0.04
URB7	0.38	0.05	RUR7	0.17	0.03
URB8	0.36	0.05	RUR8	0.19	0.04
URB9	0.37	0.05	RUR9	0.25	0.05
URB10	0.34	0.05	RUR10	0.24	0.05
RTLF with two AOs: Asc + glutathione 100:50 µM					
URB1	0.14	0.03	RUR1	0.05	0.03
URB2	0.08	0.03	RUR2	0.04	0.03
URB3	0.13	0.03	RUR3	0.06	0.03
URB4	0.16	0.03	RUR4	0.04	0.03
URB5	0.12	0.03	RUR5	0.03	0.03
URB5	0.14	0.03	RUR6	0.08	0.03
URB7	0.14	0.03	RUR7	0.03	0.03
URB8	0.11	0.03	RUR8	0.02	0.03
URB9	0.12	0.03	RUR9	0.08	0.03
URB10	0.10	0.03	RUR10	0.03	0.02
RTLF with two AOs: Asc + urate 100:50 µM					
URB1	0.26	0.05	RUR1	0.09	0.04
URB2	0.14	0.03	RUR2	0.08	0.04
URB3	0.21	0.05	RUR3	0.09	0.04
URB4	0.18	0.05	RUR4	0.10	0.04
URB5	0.20	0.05	RUR5	0.09	0.04
URB6	0.22	0.05	RUR6	0.14	0.03
URB7	0.18	0.05	RUR7	0.11	0.03
URB8	0.20	0.05	RUR8	0.04	0.02
URB9	0.19	0.05	RUR9	0.08	0.03
URB10	0.21	0.05	RUR10	0.10	0.05
RTLF with three AOs: Asc + citrate + glutathione 100:150:50					
URB1	0.09	0.03	RUR1	0.03	0.02
URB2	0.05	0.03	RUR2	0.02	0.02
URB3	0.06	0.03	RUR3	0.03	0.02
URB4	0.07	0.03	RUR4	0.04	0.02
URB5	0.06	0.03	RUR5	0.03	0.02
URB6	0.05	0.01	RUR6	0.05	0.03
URB7	0.08	0.02	RUR7	0.02	0.03
URB8	0.07	0.02	RUR8	0.02	0.03
URB9	0.08	0.02	RUR9	0.05	0.03
URB10	0.07	0.02	RUR10	0.02	0.03
RTLF with four AOs: Asc + citrate + glutathione + urate 100:150:50:50 µM					
URB1	0.07	0.03	RUR1	0.04	0.03
URB2	0.03	0.03	RUR2	0.03	0.03
URB3	0.06	0.03	RUR3	0.04	0.03
URB4	0.08	0.02	RUR4	0.05	0.03
URB5	0.10	0.03	RUR5	0.04	0.03
URB6	0.07	0.03	RUR6	0.08	0.04
URB7	0.07	0.04	RUR7	0.02	0.03
URB8	0.07	0.03	RUR8	0.02	0.03
URB9	0.07	0.02	RUR9	0.05	0.03
URB10	0.07	0.03	RUR10	0.03	0.03

Table 2
OP^{AA} responses (nmol min^{-1} m^{-3}) of 20 $PM_{2.5}$ samples and 5 standard solutions of redox-active species measured in different compositions of surrogate RTLF by adding citrate, urate and glutathione to Ascorbic acid. Reagent and filter responses are reported as mean and standard deviation values computed from quintuplicate measurements. $\%OP^{AA}$ represents the relative % decrease of OP^{AA} response in each surrogate RTLF with respect to that in the simplified Asc solution. For $PM_{2.5}$ samples mean and standard deviation values were computed on all samples and from urban and rural sites, separately.

Samples	OP^{AA} (nmol min^{-1} m^{-3})	S.D.	$\%OP^{AA}$	S.D.
simplified RTLF: Asc 100 μM				
All $PM_{2.5}$	0.39	0.15		
Urban	0.52	0.09		
Rural	0.27	0.06		
Cu^{2+} (0.1 μM)	2.33	0.09		
Fe^{2+} (1 μM)	0.19	0.02		
1,2-NPQ (0.2 μM)	1.12	0.05		
1,4-NPQ (1 μM)	0.37	0.08		
9,10-PQN (1 μM)	0.82	0.03		
Reagent blank	0.59	0.01		
Filter blank	0.81	0.07		
RTLF with two AOs: Asc + citrate 100:150 μM				
All $PM_{2.5}$	0.29	0.08	20	10
Urban	0.36	0.03	29	8
Rural	0.22	0.08	11	10
Cu^{2+} (0.1 μM)	1.63	0.03	30	
Fe^{2+} (1 μM)	0.31	0.01	+62 (increase)	
1,2-NPQ (0.2 μM)	0.65	0.02	42	
1,4-NPQ (1 μM)	0.29	0.03	22	
9,10-PQN (1 μM)	0.60	0.03	27	
Reagent blank	0.48	0.10		
Filter blank	0.69	0.10		
RTLF with two AOs: Asc + glutathione 100:50 μM				
All $PM_{2.5}$	0.08	0.05	79	6
Urban	0.12	0.02	76	4
Rural	0.05	0.03	83	5
Cu^{2+} (0.1 μM)	0.11	0.02	95	
Fe^{2+} (1 μM)	0.18	0.04	6	
1,2-NPQ (0.2 μM)	0.42	0.03	63	
1,4-NPQ (1 μM)	0.03	0.03	92	
9,10-PQN (1 μM)	0.38	0.03	54	
Reagent blank	0.40	0.03		
Filter blank	0.59	0.06		
RTLF with two AOs: Asc + urate 100:50 μM				
All $PM_{2.5}$	0.15	0.06	63	5
Urban	0.20	0.03	61	5
Rural	0.09	0.02	65	5
Cu^{2+} (0.1 μM)	1.45	0.02	38	
Fe^{2+} (1 μM)	0.16	0.06	17	
1,2-NPQ (0.2 μM)	0.53	0.03	53	
1,4-NPQ (1 μM)	0.21	0.03	43	
9,10-PQN (1 μM)	0.48	0.06	41	
Reagent blank	0.38	0.32		
Filter blank	0.53	0.03		
RTLF with three AOs: Asc + citrate + glutathione 100:150:50 μM				
All $PM_{2.5}$	0.05	0.02	87	3
Urban	0.07	0.01	87	2
Rural	0.03	0.02	87	3
Cu^{2+} (0.1 μM)	0.06	0.03	97	
Fe^{2+} (1 μM)	0.05	0.02	76	
1,2-NPQ (0.2 μM)	0.08	0.02	93	
1,4-NPQ (1 μM)	0.04	0.02	89	
9,10-PQN (1 μM)	0.09	0.02	89	
Reagent blank	0.28	0.01		
Filter blank	0.39	0.02		
RTLF with four AOs: Asc + citrate + glutathione + urate 100:150:50:50 μM				
All $PM_{2.5}$	0.05	0.02	86	4
Urban	0.07	0.02	87	2
Rural	0.04	0.02	85	5
Cu^{2+} (0.1 μM)	0.02	0.01	98	
Fe^{2+} (1 μM)	0.05	0.02	67	
1,2-NPQ (0.2 μM)	0.08	0.03	84	
1,4-NPQ (1 μM)	0.00	0.01	96	
9,10-PQN (1 μM)	0.04	0.02	94	
Reagent blank	0.18	0.01		
Filter blank	0.22	0.03		
RTLF with four AOs: Asc + citrate + glutathione + urate 100:100:100:100 μM				
Cu^{2+} (0.1 μM)	0.02	0.01	99	
Fe^{2+} (1 μM)	0.05	0.02	72	
1,2-NPQ (0.2 μM)	0.08	0.03	94	
1,4-NPQ (1 μM)	0.00	0.01	96	
9,10-PQN (1 μM)	0.04	0.02	98	
Reagent blank	0.11	0.02		

2018; Fang et al., 2016; Godri et al., 2011; Mudway et al., 2004; Pietrogrande et al., 2018; Rui-Wen et al., 2018; Visentin et al., 2016; Weber et al., 2018). The individual results obtained for each sample are reported in Table 1 (mean values ± S.D., n ≥ 5). The precision values for most of the quintuplicate measurements were less than 20%, that is consistent with literature data (Ayres et al., 2008; Fang et al., 2016; Janssen et al., 2014; Janssen et al., 2015; Simonetti et al., 2018; Visentin et al., 2016; Yang et al., 2015).

The measured OP^{AA} ranged from a minimum of 0.12 nmol min^{-1} m^{-3} (sample RUR 8) to a maximum 0.65 nmol min^{-1} m^{-3} (sample URB5). Overall, the measured AA activity is inside the typical range observed for fine particles collected at sites with different source characteristics, i.e., ~0.2–2.0 nmol min^{-1} m^{-3} (Calas et al., 2018; Hedayat et al., 2015; Janssen et al., 2014; Perrone et al., 2016; Pietrogrande et al., 2018; Simonetti et al., 2018; Weber et al., 2018).

From the obtained data, the mean and S.D. values were computed for all samples and grouping urban (URB, n = 10) and rural (RUR, n = 10) samples, separately (Table 2, including filter blank responses, and Fig. 1a). The Student's *t*-test showed that the OP^{AA} responses measured in Bologna (0.52 ± 0.09 nmol min^{-1} m^{-3}) are significantly higher than those at the rural site (0.27 ± 0.06 nmol min^{-1} m^{-3}). As values of $PM_{2.5}$ concentration mass are similar at both sites in the sampling period (mean value 15 ± 7 μg m^3), this difference may be explained by variation in chemical composition of $PM_{2.5}$. In the city it can be expected an higher impact from anthropogenic source emissions, yielding pollutant accumulation, as a consequence of the stagnant atmospheric conditions in the cold season (Perrone et al., 2016; Pietrogrande et al., 2016). These results are in agreement with those previously found by the authors in the same sites (Visentin et al., 2016) and by others at urban sites, by using experimental conditions close to those reported in the present Work (Bates et al., 2015; Fang et al., 2016; Janssen et al., 2014; Simonetti et al., 2018).

Then, the complexity of the assay solution was increased with the aim of designing an experimental setup most representative of RTLF. Solutions of endogenous antioxidants were added, i.e., citrate (150 μM), urate (50 μM), glutathione (50 μM), individually or in combination, i.e., citrate and glutathione, and citrate, glutathione and urate (Charrier and Anastasio, 2011; Charrier et al., 2014). The data measured in the five different synthetic RTLFs are reported individually for each $PM_{2.5}$ sample in Table 1, and summarized in Table 2 (including the filter blank responses, mean values ± S.D., n ≥ 5), and Fig. 1a as mean values (total and urban and rural samples, separately).

The obtained results clearly show that the measured OP^{AA} values are significant changed ($p < 0.05$) by the composition of the synthetic RTLFs, since they are lower when other antioxidants are added to ascorbate (indicated by asterisk in Fig. 1a). Consistently, also the precision for most of the quintuplicate measurements decrease (S.D. up to 100%). The strength of each experimental set up in reducing OP^{AA} response can be quantified by computing the relative percentage decrease of the measured value with respect to that in the simplified AA solution ($\%OP^{AA}$). These variations were calculated in all RTLFs for each $PM_{2.5}$, from which the mean values were computed for all samples and for

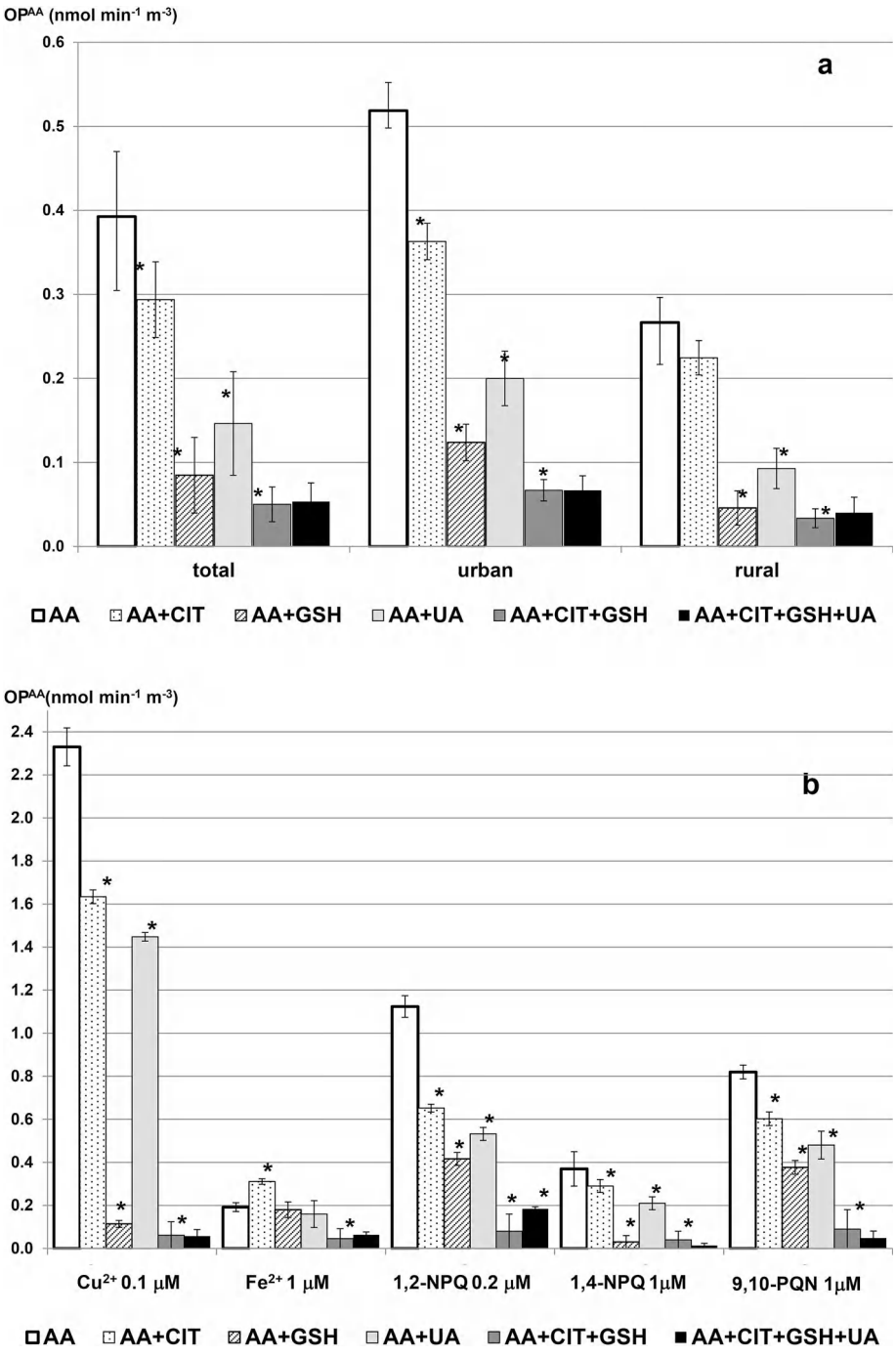

Fig. 1. OP^{AA} response (nmol min^{-1} m^{-3}) measured in different RTLF surrogates: dotted bar: AA + Cit; dashed bar: AA + GSH; light grey bar: AA + UA; dark grey bar: AA + UA + GSH; black bar: AA + UA + GSH + UA. Asterisks (*) indicate OP^{AA} means that are significantly different ($p < 0.05$) from that measured in simplified Asc solution.
1a) OP^{AA} response of $PM_{2.5}$ real samples: bars represent the mean values, error bars are one standard deviations computed from 20 investigated samples (total), from 10 samples at urban (URB) and from 10 samples at rural (RUR).
1b) OP^{AA} response of standard solution of individual redox active species: Cu^{2+}, 0.1 µM solution; Fe^{2+}, 1.0 µM solution; 1,2-naphthoquinone, 0.2 µM solution; 1,4-naphthoquinone, 1.0 µM solution; 9,10-phenanthrenequinone, 1.0 µM solution. Bars represent the mean values, error bars are one S.D. calculated from replicates ($n \geq 5$).

urban and rural filters, separately (Table 2).

Among the investigated components, GSH is the most effective, since it yields a mean OP^{AA} decrease of 79 ± 6%, followed by urate (mean $\%OP^{AA}$: 63 ± 5%) and citrate (mean $\%OP^{AA}$: 20 ± 10%). Furthermore, the combination of both Cit and GSH antioxidants synergistically inhibits the AA oxidation (87 ± 3%), while the further addition of UA doesn't significantly change OP^{AA} (Fig. 1a).

The same trend is observed for all the analysed samples, so that OP^{AA} response follows the general order:

Asc > Asc + Cit > Asc + UA > Asc + GSH > Asc + Cit + GSH ~ Asc + Cit + GSH + UA.

Inside such variations, in all the different assay conditions OP^{AA} values of URB samples are significantly higher ($p < 0.05$) than those at RUR site, with the exception of Asc + Cit + GSH + UA mixture.

To investigate the effects of each synthetic RTLF in detail, for each $PM_{2.5}$ sample the OP^{AA} responses in the different solution were correlated with those in the Asc solution (Fig. 2). In general, a good linear relationship was obtained for each dataset ($R^2 \geq 0.8$), indicating that the effect of the various RTLF surrogates on OP^{AA} responses is similar for all the samples. This suggests that all the tested assay set ups are useful for OP^{AA} assessment.

However, for each sample, the use of composite RTLFs generates lower OP^{AA} responses with lower variation range, that means less sensible measurements. This is indicated by the slopes of the computed straight lines, which are always lower than 1, following the order:

Asc + Cit (slope: 0.5 ± 0.2) > Asc + UA (slope: 0.4 ± 0.2) > Asc + GSH (slope: 0.3 ± 0.1) > Asc + Cit + GSH ~ Asc + Cit + GSH + UA (slope: 0.1 ± 0.1).

This means that, with respect to Asc solution, the addition of citrate and urate reduces the assay responses by about 2 times, while that of

GSH of 3 times. Furthermore, when 2 or more AOs are combined the OP^{AA} responses are decreased even by 10 times. Such a reduction is combined with the decrease of the measurement precision.

Therefore, we can conclude that, among the tested RTLF surrogates, the simplified Asc solution provides the most sensible and precise measure of OP^{AA}. However, such a sensibility may be detrimental to a realistic representation of the particle-lung interactions, as simpler RTLF surrogates are more different from the complex antioxidant mixtures of lung lining fluid. In addition, some differences may be expected in comparison with the simplified assumption of additive contribution of each antioxidant, as a consequence of concurrent reactions between antioxidants and reductants. For example, the consumption rate of GSH was found less than that expected, when RTLF antioxidants were exposed to a range of ambient O_3 concentrations, since oxidized GSH may interact with AA and/or UA to be recycled back to GSH (Pryor, 1994).

Overall, these results can be explained by the increasing of the mixture antioxidant strength due to the concomitant contribution of GSH and UA antioxidants, in addition to Asc. The higher reactivity of GSH is consistent with the lower oxidation-reduction potential for the glutathione/glutathione disulfide system, ranging from −0.17 to −0.27 V under various physiological conditions (Millis et al., 1993), in comparison with the higher values of +0.105 V for the ascorbic/dehydroascorbic acid couple (Merkofer et al., 2006). Therefore, GSH strongly promotes the AA oxidation, as it likely acts as a sacrificial antioxidant (Charrier and Anastasio, 2011; Charrier et al., 2014; Weichenthal et al., 2016). This is consistent with the well known strong antioxidant properties of GSH in vivo, as reported by several toxicological (i.e., Crobeddu, et al., 2017; Hellack et al., 2017; Künzli et al., 2006; Maikawa et al., 2016).

In order to extract information for highlighting the effect of each RTLF component on OP^{AA} responses, we start by screening the AA depletion from individual chemicals in different mixtures of the four antioxidants.

3.2. OP^{AA} for individual redox-active species in simulated RTLFs

The study was performed on standard solutions of some redox active species, that has been found as the mostly responsible of ROS generation in PM ambient sample. Iron and copper have been identified by several studies as the most important transition metals (Charrier and Anastasio, 2015; Charrier et al., 2014; DiStefano et al., 2009; Hellack et al., 2014; Lyu et al., 2018; Shen and Anastasio, 2012; Shirmohammadi et al., 2015; Shuster-Meiseles et al., 2016; Tuet et al., 2017; Vidrio et al., 2008; Wang et al., 2010; Yang et al., 2015). In addition, quinones have been reported highly redox-active compounds, in particular 1,2- and 1,4-naphthoquinone and 9,10-phenanthrenequinone (Antiñolo et al., 2015; Charrier and Anastasio, 2011; Charrier et al., 2014; Chung et al., 2006; Janssen et al., 2014; Jiang and Jang, 2018; Lyu et al., 2018). Quinones can be directly emitted from traffic or formed from secondary oxidation (Charrier et al., 2014; Jiang and Jang, 2018; McWhinney et al., 2013).

The standard solutions of the investigated species were prepared at concentration of 1 μM to represent the order of magnitude that ambient PM could produce in lung fluid (e.g., Vidrio et al., 2008). In the experiments, standard solutions of Cu^{2+} and 1,2-NPQ solutions were diluted to 0.1 μM and 0.2 μM, respectively, to obtain comparable OP^{AA} responses and guarantee the response linearity of the AA assay (Charrier and Anastasio, 2015; Visentin et al., 2016).

The results obtained for each individual species (mean values ± S.D., n ≥ 5) are reported in Table 2, including the reagent blank responses (mean values ± S.D., n ≥ 5) and summarized in Fig. 1b. All the investigated species show that in general OP^{AA} significantly decreases with increasing complexity of the synthetic RTLFs, as well as $PM_{2.5}$ samples, but each redox active species displays a different variation pattern (in Fig. 1b asterisk indicates OP^{AA} means significantly different at $p < 0.05$).

Concerning Cu^{2+}, the individual addition of citrate and urate reduces OP^{AA} by 30% compared to Asc. This may be explained by the dominant presence under these conditions of the Cu-citrate and Cu-urate complexes, which have been found less reactive than the free Cu^{2+} (Charrier and Anastasio, 2011; Vidrio et al., 2008). OP^{AA} reduction is the strongest by adding glutathione (about 93%), independent of the further addition of other AOs (Table 2). Such an effect is likely due to the GSH ability of binding Cu^{2+} to form a Cu-GSH complex with reduced reactivity. This is the underlying mechanism of Cu^{2+} storage and transport as well as its antioxidant activity (Aliaga et al., 2010).

The results of this study may be compared with past papers, that

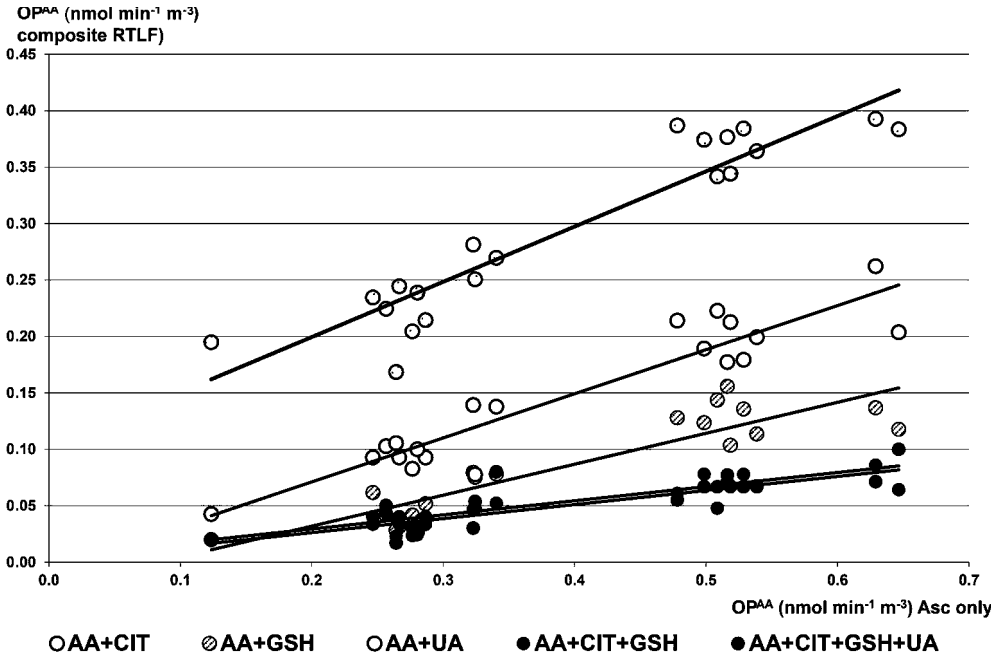

Fig. 2. OP^{AA} responses (nmol min^{-1} m^{-3}) of 20 $PM_{2.5}$ real samples: relationship of OP^{AA} values measured in the different RTLF surrogates with those in Asc solution. Dotted circles: AA + Cit; dashed circles: AA + GSH; light grey circles: AA + UA; dark grey circles: AA + UA + GSH; black circles: AA + UA + GSH + UA.

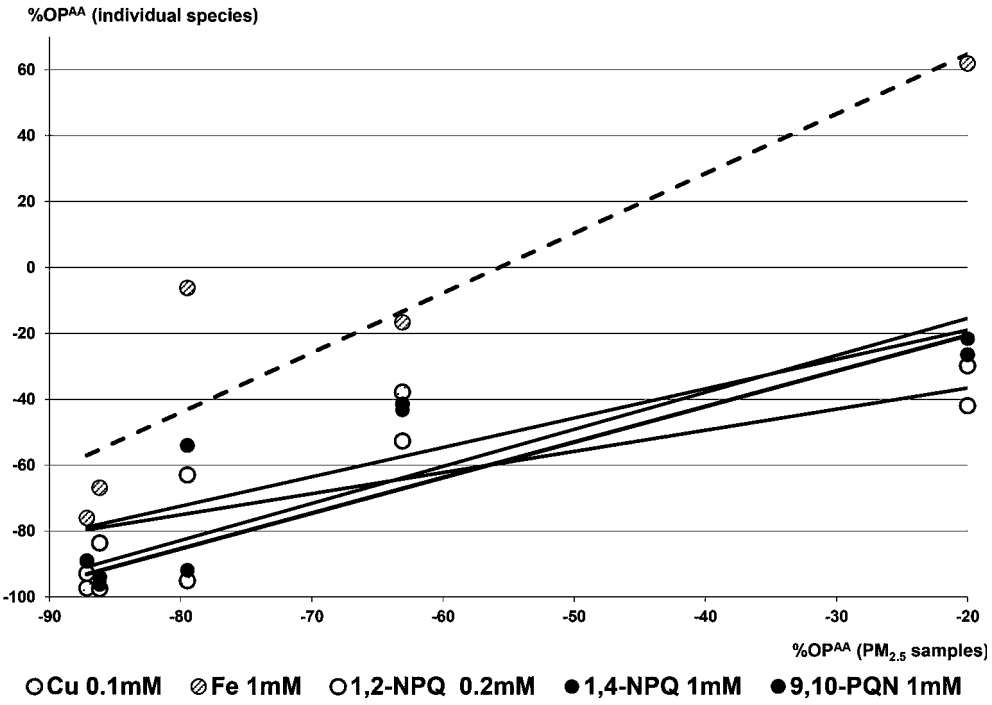

Fig. 3. Relative % variation of OP^{AA} responses ($\%OP^{AA}$) measured in different RTLF surrogates with respect to those in simplified Asc solution: relationship between $\%OP^{AA}$ of ambient samples (mean value of the 20 $PM_{2.5}$ samples) with those of individual redox active species. Dotted circles: AA + Cit; dashed circles: AA + GSH; light grey circles: AA + UA; dark grey circles: AA + UA + GSH; black circles: AA + UA + GSH + UA.

investigated the rate of Asc oxidation for transition metals and quinones in surrogate RTLFs. Indeed, only a qualitative comparison is possible in terms of inhibition/promotion of Asc oxidation as other Authors reported complementary information concerning the product formation, such as hydroxyl radical (Charrier and Anastasio, 2011, 2015; DiStefano et al., 2009; Ma et al., 2015; Shen and Anastasio, 2012; Vidrio et al., 2008) or hydrogen peroxide (Charrier et al., 2014; Wang et al., 2010). In particular, for Cu^{2+} Charrier and Anastasio (2011) observed a similar inhibition effect of citrate, urate and GSH addition on the $^{\bullet}OH$ production, while Charrier found a reduction of H_2O_2 generation by adding urate and GSH (Charrier et al., 2014).

Fe^{2+} shows a different behaviour, as the addition of Cit to the Asc solution strongly enhanced OP^{AA} response by 62%. This may be ascribed to the dominant presence of the Fe-Citrate complex, that has been found to increase the Fe^{2+} reactivity and effectively promote the Fenton reaction (Merkofer et al., 2006; Vidrio et al., 2008). This was confirmed by cyclic voltammograms of Fe-Citrate complexes under physiologically relevant conditions (Engelmann et al., 2003). This result is in agreement with the promotion of •OH production observed in a previous study (Charrier and Anastasio, 2015). GSH doesn't significantly change OP^{AA}, that is consistent with the fact that GSH doesn't change the Fe speciation (Vidrio et al., 2008). Otherwise, uric acid leads to a decrease of OP^{AA} by 17%. It can be explained by the formation of stable co-ordination complexes Fe-urate that inhibits the catalyzed ascorbate oxidation (Charrier and Anastasio, 2011). This is confirmed by polarographic measurements, that revealed that (upon binding) urate decreases the reduction potential for the Fe^{2+}/Fe^{3+} half-reaction from −0.77 V to - 0.67 V (Davies et al., 1987). The concomitant addition of one or two more AOs further inhibits the Asc oxidation generating lower OP^{AA} (~70%).

Also for the three investigated quinones we found that the change of the antioxidant mixture affects the OP^{AA} responses: compared to Asc solution, addition of citrate or urate significantly ($p < 0.05$) decreases OP^{AA} of about 40%, while addition of GSH of 70%. The combination of Cit and GSH generates a drastic OP^{AA} reduction close to 90%, nearly independently of the presence of UA. These last data are consistent with the strong reduction of H_2O_2 formation observed by Charrier for 9,10-PQN (500 nM) and 1,2-NPQ (20 nM) in the composite mixture of four antioxidants (Charrier et al., 2014).

In addition to the general explanation of the concomitant contribution of GSH and UA antioxidants to increase RTLF antioxidant strength, it is difficult to understand the reason of such a surprising strong effect on quinones, in comparison with that on metals, where additional mechanisms involving the formation of metal complexes can be invoked (Charrier and Anastasio, 2015; Charrier et al., 2014; Vidrio et al., 2008).

Inside such variations, the reactivity hierarchy of the individual compounds is kept constant in all the investigated assay setups, as follows:

$Cu^{2+} > 1,2\text{-NPQ} > \ > 9,10\text{-PQN} > 1,4\text{-NPQ} \sim Fe^{2+}$.

3.3. Comparison of OP^{AA} for ambient samples and standards redox-active solutions

Based on these information on individual redox-active species, we tried to identify the chemical components of $PM_{2.5}$ samples mainly responsible of the effects of the various antioxidants in RTLF on OP^{AA} responses. Therefore, we compared the relative $\%OP^{AA}$ variation in each synthetic RTLF of ambient $PM_{2.5}$ with that of the species ($\%OP^{AA}$, mean values in Table 2). In general, a good linear correlation ($R^2 \geq 0.75$) was found between $PM_{2.5}$ and all the investigated species, confirming that they all are responsible of OP^{AA} responses of the $PM_{2.5}$ samples (best fitting lines reported in Fig. 3). In particular, Cu^{2+} and quinones appear to display nearly the same dependence on RTLF composition, as proved by the slope of straight lines close to 1, i.e., 0.95 ± 0.1 for Cu^{2+} and 0.89 ± 0.2 to 1.1 ± 0.3 for quinones, respectively. Otherwise, the Fe^{2+} solution displays a nearly double sensitivity to the variation of RTLF compositions than $PM_{2.5}$ samples, as the best fitting straight line ($R^2 = 0.85$) has a slope of 1.8 ± 0.2 (dashed line in Fig. 3).

From our results we can infer that the variation of $PM_{2.5}$ OP^{AA} response in the different RTLFs is mainly generated by quinones and copper. Accordingly, addition of GSH mostly decreased the OP^{AA} measured values (79% for $PM_{2.5}$ and 95% and 92% for Cu^{2+} and 1,4-NPQ, respectively), followed by urate (63% for $PM_{2.5}$ and 53% and 43% for 1,2-NPQ, and 1,4-NPQ, respectively) and by citrate (20% for $PM_{2.5}$ and 22% and 27% for 1,4-NPQ and 9,10-PQN, respectively). Such a predominant contribution of quinones and Cu^{2+} to $PM_{2.5}$ oxidative

Table 3
OP^{AA} responses (nmol min^{-1} m^{-3}) of standard solutions of redox-active species measured in different compositions of surrogate RTLF with saline PBS buffer, by adding citrate, urate and glutathione to Ascorbic acid. Each OP^{AA} value, also including reagent blanks, is reported as mean and standard deviation values computed from quintuplicate measurements.

Species	OP^{AA} (nmol min^{-1} m^{-3})	S.D.
simplified RTLF: Asc 100 μM		
Cu^{2+} (0.1 μM)	0.57	0.04
Fe^{2+} (1 μM)	0.07	0.01
1,2-NPQ (0.2 μM)	0.38	0.03
1,4-NPQ (1 μM)	0.37	0.04
9,10-PQN (1 μM)	0.82	0.02
Reagent blank	0.28	0.03
RTLF with two AOs: Asc + citrate 100:150 μM		
Cu^{2+} (0.1 μM)	0.40	0.02
Fe^{2+} (1 μM)	0.11	0.02
1,2-NPQ (0.2 μM)	0.22	0.03
1,4-NPQ (1 μM)	0.29	0.03
9,10-PQN (1 μM)	0.30	0.03
Reagent blank	0.23	0.03
RTLF with two AOs: Asc + glutathione 100:50 μM		
Cu^{2+} (0.1 μM)	0.03	0.01
Fe^{2+} (1 μM)	0.06	0.02
1,2-NPQ (0.2 μM)	0.14	0.03
1,4-NPQ (1 μM)	0.03	0.02
9,10-PQN (1 μM)	0.38	0.02
Reagent blank	0.18	0.03
RTLF with two AOs: Asc + urate 100:50 μM		
Cu^{2+} (0.1 μM)	0.33	0.01
Fe^{2+} (1 μM)	0.38	0.03
1,2-NPQ (0.2 μM)	0.07	0.02
1,4-NPQ (1 μM)	0.07	0.02
9,10-PQN (1 μM)	0.48	0.05
Reagent blank	0.11	0.02
RTLF with three AOs: Asc + citrate + glutathione 100:150:50 μM		
Cu^{2+} (0.1 μM)	0.02	0.02
Fe^{2+} (1 μM)	0.02	0.01
1,2-NPQ (0.2 μM)	0.03	0.01
1,4-NPQ (1 μM)	0.04	0.01
9,10-PQN (1 μM)	0.09	0.03
Reagent blank	0.08	0.01
RTLF with four AOs: Asc + citrate + glutathione + urate 100:150:50:50 μM		
Cu^{2+} (0.1 μM)	0.01	0.02
Fe^{2+} (1 μM)	0.03	0.01
1,2-NPQ (0.2 μM)	0.05	0.02
1,4-NPQ (1 μM)	0.01	0.01
9,10-PQN (1 μM)	0.04	0.02
Reagent blank	0.09	0.02
RTLF with four AOs: Asc + citrate + glutathione + urate 100:100:100:100 μM		
Cu^{2+} (0.1 μM)	0.01	0.01
Fe^{2+} (1 μM)	0.02	0.01
1,2-NPQ (0.2 μM)	0.02	0.02
1,4-NPQ (1 μM)	0.00	0.01
9,10-PQN (1 μM)	0.03	0.01
Reagent blank	0.08	0.02

properties is in agreement with results found in several past studies (Charrier and Anastasio, 2015; Charrier et al., 2014; Chung et al., 2006; Crobeddu et al., 2017; Janssen et al., 2015; Jiang and Jang, 2018; Lyu et al., 2018; McWhinney et al., 2013; Shen and Anastasio, 2012; Shuster-Meiseles et al., 2016; Tuet et al., 2017; Wang et al., 2010). However, this is only an approximated explanation, since it is well known that behaviour of individual species poorly represent the complex chemistry of ambient PM, where components may synergically interact to contribute to ROS production (Yu et al., 2018). In addition, some studies report that many trace metals and quinones are covariate, which confounds identifying the redox active species responsible for ROS generation (Charrier et al., 2014). From this work, we cannot deduce more precise information on the mechanism at work, but we plan to explore this in the future by looking at OP^{AA} responses in ambient PM extracts with known chemical composition.

3.4. Effect of different compositions of simulated RTLFs on OP^{AA} for individual redox-active species

Recognizing the influence of the synthetic RTLF composition for assessing OP_{AA} values, the study on standard mixtures was extended to other RTLF surrogates, among those most commonly reported in literature for simulating RTLFs. In particular:

- an equimolar solution of the four AOs i.e., 100 μM, AA, Cit, GSH and UA at pH 7.0, as used by several Authors (Calas et al., 2018; Crobeddu et al., 2017; Godri et al., 2011; Mudway et al., 2004; Strak et al., 2012; Szigeti et al., 2016; Steenhof et al., 2013),
- a phosphate buffered saline (PBS, phosphate and NaCl solution) to represent pH and ionic strength conditions of the cellular environment to the extent possible (Charrier and Anastasio, 2011, 2015; Charrier et al., 2014; Ma et al., 2015).

OP^{AA} of individual metals and quinones solutions was measured for each experimental setup and the obtained data reported in Table 3 (including reagent blank values).

The obtained results show that, compared to the Charrier's composition, OP^{AA} in the equimolar RTLF is further decreased by 50%, on average, as a consequence of higher concentration of GSH (100 vs. 50 μM), which strongly reduces OP_{AA} of Cu^{2+} and quinones and of urate (100 vs. 50 μM), which decreases OP_{AA} of metals (Table 3).

OP^{AA} of individual metals and quinones solutions was measured for each experimental setup and the obtained data reported in Tables 2 and 3 (including reagent blank values).

The obtained results show that, compared to the Charrier's composition, OP^{AA} in the equimolar RTLF is further decreased, as a consequence of higher concentration of GSH (100 vs. 50 μM), which strongly reduces OP^{AA} of Cu^{2+} and quinones and of urate (100 vs. 50 μM), which decreases OP^{AA} of metals (Table 2).

Concerning the effect of the buffer composition, the use of PBS solution reduced to one half OP^{AA} responses compared to those in phosphate buffer, with larger difference for Cu^{2+} and Fe^{2+}, i.e., 75% and 60%, respectively. The reason of such an unexpected behaviour is unclear: it can be tentatively ascribed to the presence of some contaminants, mainly redox-active metals, that is more likely in Na_2HPO_4 and NaH_2PO_4 phosphates than in NaCl salt. This is consistent with the requirement of removing trace metals from phosphate buffer to improve the assay reproducibility and stability, as described in some procedures including elution on a cation exchange resin (Charrier and Anastasio, 2015; Visentin et al., 2016). This reasoning is further supported by the observation that the measured responses from the reagent blank is in general higher in phosphate buffer (OP^{AA} form 0.60 to 0.11 nmol min^{-1}) compared with that in PBS (OP^{AA} form 0.28 to 0.08 nmol min^{-1}) (Tables 2 and 3).

4. Conclusions

As a general conclusion, our results highlight that the response of the acellular AA assay is strongly dependent upon the composition of the synthetic RTLF used. Among the investigated surrogates, the simplified Asc solution shows the advantage of generating higher OP^{AA}, displaying higher sensitivity of the assay response, in comparison with the composite solutions containing two or more physiological AOs. However, all the investigated assays can be used to measure OP^{AA} values, since they generate linearly correlated responses.

Although our RTLF is a reasonable, simple surrogate for actual lung fluid, it certainly does not represent its full chemical or biological complexity. In addition, the investigated assessment of the AA assay based on the measure of the Asc depletion rate does not capture important information on the ROS cascade, i.e., the generation of H_2O_2 and $^{\bullet}OH$. Therefore, further work is needed to search for proper experimental setups that more closely resemble the particle−lung

interactions underlying the intracellular ROS generation. In particular, the concurrent contribution of different antioxidants present in human RTLF has to be investigated in detail on real PM samples.

Finally, in an effort to find physiologically relevant assays to predict health outcomes from PM toxic components, work is in progress for exploring links between OP responses from cell-free assays and different oxidative stress-related responses derived from PM-exposed cells, such as biochemical effects analyzing genic and protein expression, and cellular morphological alterations.

Acknowledgements

ARPAE E-R, the Regional Agency for Environmental Protection of Emilia-Romagna, is acknowledged for an air monitoring campaign for sampling $PM_{2.5}$ filters.

Appendix A. Supplementary data

Supplementary data to this article can be found online at https://doi.org/10.1016/j.atmosenv.2019.05.012.

References

Aliaga, M.E., Carrasco-Pozo, C., Lopez-Alarcon, C., Speisky, H., 2010. The Cu(I)- glutathione complex: factors affecting its formation and capacity to generate reactive oxygen species. Transit. Met. Chem. 35, 321–329. https://doi.org/10.1007/s11243-010-9330-9.

Antiñolo, M., Willis, M.D., Zhou, S., Abbatt, J.P.D., 2015. Connecting the oxidation of soot to its redox cycling abilities. Nat. Commun. 6, 6812. https://www.nature.com/articles/ncomms7812.

Ayres, J.G., Borm, P., Cassee, F.R., Castranova, V., Donaldson, K., Ghio, A., Harrison, R.M., Hider, R., Kelly, F., Kooter, I.M., Marano, F., Maynard, R.L., Mudway, I., Nel, A., Sioutas, C., Smith, S., Baeza-Squiban, A., Cho, A., Duggan, S., Froines, J., 2008. Evaluating the toxicity of airborne particulate matter and nanoparticles by measuring oxidative stress potential— a workshop report and consensus statement. Inhal. Toxicol. 20, 75–99. https://doi.org/10.1080/08958370701665517.

Bates, J.T., Weber, R.J., Abrams, J., Verma, V., Fang, T., Klein, M., Strickland, M.J., Sarnat, S.E., Chang, H.H., Mulholland, J.A., Tolbert, P.E., Russell, A.G., 2015. Reactive oxygen species generation linked to sources of atmospheric particulate matter and cardiorespiratory effects. Environ. Sci. Technol. 49, 13605–13612. https://pubs.acs.org/doi/10.1021/acs.est.5b02967.

Calas, A., Uzu, G., Kelly, F.J., Houdier, S., Martins, J.M.F., Thomas, F., Molton, F., Charron, A., Dunster, C., Oliete, A., Jacob, V., Besombes, J.L., Chevrier, F., Jaffrezo, J.L., 2018. Comparison between five acellular oxidative potential measurement assays performed with detailed chemistry on PM_{10} samples from the city of Chamonix (France). Atmos. Chem. Phys. Atmos. Chem. Phys. 18, 7863–7875. https://doi.org/10.5194/acp-18-7863-2018.

Charrier, J.G., Anastasio, C., 2011. Impacts of antioxidants on hydroxyl radical production from individual and mixed transition metals in a surrogate lung fluid. Atmos. Environ. 45, 7555–7562. https://doi.org/10.1016/j.atmosenv.2010.12.021.

Charrier, J.C., McFall, A.S., Richards-Henderson, N.K., Anastasio, C., 2014. Hydrogen peroxide formation in a surrogate lung fluid by transition metals and quinones present in particulate matter. Environ. Sci. Technol. 48, 7010–7017. https://pubs.acs.org/doi/abs/10.1021/es501011w.

Charrier, J.G., Anastasio, C., 2015. Rates of hydroxyl radical production from transition metals and quinones in a surrogate lung fluid. Environ. Sci. Technol. 49, 9317–9325. https://pubs.acs.org/doi/abs/10.1021/acs.est.5b01606.

Chung, M.Y., Lazaro, R.A., Lim, D., Jackson, J., Lyon, J., Rendulic, D., Hasson, A.S., 2006. Aerosol-borne quinones and reactive oxygen species generation by particulate matter extracts. Environ. Sci. Technol. 40, 4880–4886. https://doi.org/10.1021/es0515957.

Crobeddu, B., Aragao-Santiago, L., Bui, L.C., Boland, S., Baeza-Squiban, A., 2017. Oxidative potential of particulate matter 2.5 as predictive indicator of cellular stress. Environ. Pollut. 230, 125–133. https://doi.org/10.1016/j.envpol.2017.06.051.

Davies, M.I., Donkor, R., Dunster, C.A., Gee, C.A., Jonas, S., Willson, R.L., 1987. Desferrioxamine and superoxide free radicals: formation of an enzymedamaging nitroxide. Biochem. J. 246, 725–729. https://doi.org/10.1042/bj2460725.

Delfino, R.J., Staimer, N., Tjoa, T., Arhami, M., Polidori, A., Gillen, D.L., George, S.C., Shafer, M.M., Schauer, J.J., Sioutas, C., 2010. Associations of primary and secondary organic aerosols with airway and systemic inflammation in an elderly panel cohort. Epidemiology 21, 892–902. https://doi.org/10.1097/EDE.0b013e3181f20e6c.

DiStefano, E., Eiguren-Fernandez, A., Delfino, R.J., Sioutas, C., Froines, J.R., Cho, A.K., 2009. Determination of metal-based hydroxyl radical generating capacity of ambient and diesel exhaust particles. Inhal. Toxicol. 21, 731–738. https://doi.org/10.1080/08958370802491433.

EN 12341, 1998. Determination of the PM10 fraction of suspended particulate matter - Reference method and field test procedure to demonstrate reference equivalence of measurement methods.

Engelmann, M.D., Bobier, R.T., Hiatt, T., Cheng, I.F., 2003. Variability of the Fenton reaction characteristics of the EDTA, DTPA, and citrate complexes of iron. Biometals 16, 519–527. https://doi.org/10.1023/A:1023480617038.

Fang, T., Verma, V., Bates, J.T., Abrams, J., Klein, M., Strickland, M.J., Sarnat, S.E., Chang, H.H., Mulholland, J.A., Tolbert, P.E., Russell, A.G., Weber, R.J., 2016. Oxidative potential of ambient water-soluble $PM_{2.5}$ in the southeastern United States: contrasts in sources and health associations between ascorbic acid (AA) and dithiothreitol (DTT) assays. Atmos. Chem. Phys. 16, 3865–3879. https://doi.org/10.5194/acp-16-3865-2016.

Godri, K.J., Harrison, R.M., Evans, T., Baker, T., Dunster, C., Mudway, I.S., Kelly, F.J., 2011. Increased oxidative burden associated with traffic component of ambient particulate matter at roadside and urban background schools sites in. London PLoS One 6 (7), e21961. https://doi.org/10.1371/journal.pone.0021961.

Hedayat, F., Stevanovic, S., Miljevic, B., Bottle, S., Ristovski, Z.D., 2015. Review evaluating the molecular assays for measuring the oxidative potential of particulate matter. Chem. Ind. Chem. Eng. Q. 21, 201–210. https://doi.org/10.2298/ciceq140228031h.

Hellack, B., Yang, A., Cassee, F.R., Janssen, N.A.H., Schins, R.P.F., Kuhlbusch, T.A.J., 2014. Intrinsic hydroxyl radical generation measurements directly from sampled filters as a metric for the oxidative potential of ambient particulate matter. J. Aerosol Sci. 72, 47–55.

Hellack, B., Nickel, C., Albrecht, C., Kuhlbusch, T.A.J., Boland, S., Baeza-Squiban, A., Wohlleben, W., Schins, R.P.F., 2017. Analytical methods to assess the oxidative potential of nanoparticles: a review. Environ. Sci.: Nano 4, 1920–1934.

Janssen, N.A.H., Yang, A., Strak, M., Steenhof, M., Hellack, B., Gerlofs-Nijland, M.E., Kuhlbusch, T., Kelly, F., Harrison, R., Brunekreef, B., Hoek, G., Cassee, F., 2014. Oxidative potential of particulate matter collected at sites with different source characteristics. Sci. Total Environ. 472, 572–581. https://doi.org/10.1016/j.scitotenv.2013.11.099.

Janssen, N.A.H., Strak, M., Yang, A., Hellack, B., Kelly, F.J., Kuhlbusch, T.A.J., Harrison, R.M., Brunekreef, B., Cassee, F.R., Steenhof, M., Hoek, G., 2015. Associations between three specific a-cellular measures of the oxidative potential of particulate matter and markers of acute airway and nasal inflammation in healthy volunteers. Occup. Environ. Med. 72, 49–56. https://doi.org/10.1136/oemed-2014-102303.

Jiang, H., Jang, M., 2018. Dynamic oxidative potential of atmospheric organic aerosol under ambient sunlight. Environ. Sci. Technol. 52, 7496–7504. https://doi.org/10.1021/acs.est.8b00148.

Kumar, A., Terakosolphan, W., Hassoun, M., Vandera, K.K., Novicky, A., Harvey, R., Royall, P.G., Bicer, E.M., Eriksson, J., Edwards, K., Valkenborg, D., Nelissen, I., Hassall, D., Mudway, I.S., Forbes, B., 2017. A biocompatible synthetic lung fluid based on human respiratory tract lining fluid composition. Pharma Res. 34, 2454–2465. https://doi.org/10.1007/s11095-017-2169-4.

Künzli, N., Mudway, I.S., Götschi, T., Shi, T., Kelly, F.J., Cook, S., Burney, P., Forsberg, B., Gauderman, J.W., Hazenkamp, M.E., Heinrich, J., Jarvis, D., Norbäck, D., Payo-Losa, F., Poli, A., Sunyer, J., Borm, P.J., 2006. Comparison of oxidative properties, light absorbance, total and elemental mass concentration of ambient PM2.5 collected at 20 european sites. Environ. Health Perspect. 114, 684–690. https://doi.org/10.1289/ehp.8584.

Lyu, Y., Guo, H., Cheng, T., Li, X., 2018. Particle size distributions of oxidative potential of lung-deposited particles: assessing contributions from quinones and water-soluble metals. Environ. Sci. Technol. 52, 6592–6600. https://doi.org/10.1021/acs.est.7b06686.

Ma, S.X., Ren, K., Liu, X., Chen, L., Li, M., Li, X., Yang, J., Huang, B., Zheng, M., Xu, Z., 2015. Production of hydroxyl radicals from Fe-containing fine particles in Guangzhou, China. Atmos. Environ. Times 123, 72–78. https://doi.org/10.1016/j.atmosenv.2015.10.057.

Maikawa, C.L., Weichenthal, S., Wheeler, A.J., Dobbin, N.A., Smargiassi, A., Evans, G., Liu, L., Goldberg, M.S., Godri-Pollitt, K.J., 2016. Particulate oxidative burden as a predictor of exhaled nitric oxide in children with asthma. Environ. Health Perspect. 124, 1616–1622. https://doi.org/10.1289/EHP175.

Marques, M.R.C., Loebenberg, R., Almukainzi, M., 2011. Simulated biological fluids with possible application in dissolution testing. Dissolution Technol. 18, 15–28. https://doi.org/10.14227/DT180311P15.

May, J.M., Huang, J., Qu, Z., 2005. Macrophage uptake and recycling of ascorbic acid: response to activation by lipopolysaccharide. Free Radic. Biol. Med. 39, 1449–1459. https://doi.org/10.1016/j.freeradbiomed.2005.07.006.

McWhinney, R.D., Zhou, S., Abbatt, J.P.D., 2013. Naphthalene SOA: redox activity and naphthoquinone gas–particle partitioning. Atmos. Chem. Phys. 13, 9731–9744. https://trove.nla.gov.au/version/241959569.

Merkofer, M., Kissner, R., Hider, R.C., Brunk, U.T., Koppenol, W.H., 2006. Fenton chemistry and iron chelation under physiologically relevant conditions: electrochemistry and kinetics. Chem. Res. Toxicol. 19, 1263–1269. https://doi.org/10.1021/tx060101w.

Millis, K.K., Weaver, K.H., Rabenstein, D.L., 1993. Oxidation/reduction potential of glutathione. J. Org. Chem. 58, 4144–4146. https://doi.org/10.1021/jo00067a060.

Mudway, I.S., Stenfors, N., Duggan, S.T., Roxborough, H., Zielinski, H., Marklund, S.L., Blomberg, A., Frew, A.J., Sandström, T., Kelly, F.J., 2004. An in vitro and in vivo investigation of the effects of diesel exhaust on human airway lining fluid antioxidants. Arch. Biochem. Biophys. 423, 200–212. https://doi.org/10.1016/j.abb.2003.12.018.

Orru, K., Nordin, S., Harzia, H., Orru, H., 2018. The role of perceived air pollution and health risk perception in health symptoms and disease: a population-based study combined with modelled levels of PM_{10}. Int. Arch. Occup. Environ. Health 91, 581–589. https://doi.org/10.1007/s00420-018-1303-x.

Perrone, M.G., Zhou, J., Malandrino, M., Sangiorgi, G., Rizzi, C., Ferrero, L., Dommen, J., Bolzacchini, E., 2016. PM chemical composition and oxidative potential of the soluble fraction of particles at two sites in the urban area of Milan, Northern Italy. Atmos. Environ. 128, 104–113. https://doi.org/10.1016/j.atmosenv.2015.12.040.

Pietrogrande, M.C., Bacco, D., Ferrari, S., Ricciardelli, I., Scotto, F., Trentini, A., Visentin, M., 2016. Characteristics and major sources of carbonaceous aerosols in PM2.5 in Emilia Romagna Region (Northern Italy) from four-year observations. Sci. Total Environ. 553, 172–183. https://doi.org/10.1016/j.scitotenv.2016.02.074.

Pietrogrande, M.C., Perrone, M.R., Manarini, F., Romano, S., Udisti, R., Becagli, S., 2018. PM_{10} oxidative potential at a Central Mediterranean Site: association with chemical composition and meteorological parameters. Atmos. Environ. 188, 97–111. https://doi.org/10.1016/j.atmosenv.2018.06.013.

Pryor, W.A., 1994. Mechanisms of radical formation from reactions of ozone with target molecules in the lung. Free Radic. Biol. Med. 17, 451–465. https://doi.org/10.1016/0891-5849(94)90172-4.

Rui-Wen, H., Shirmohammadi, F., Gerlofs-Nijland, M.E., Sioutas, C., Cassee, F.R., 2018. Pro-inflammatory responses to $PM_{0.25}$ from airport and urban traffic emissions. Sci. Total Environ. 640, 997–1003. https://doi.org/10.1016/j.scitotenv.2018.05.382.

Saffari, A., Daher, N., Shafer, M.M., Schauer, J.J., Sioutas, C., 2014. Seasonal and spatial variation in dithiothreitol (DTT) activity of quasi-ultrafine particles in the Los Angeles Basin and its association with chemical species. J. Environ. Sci. Health Part A 49, 441–451. https://doi.org/10.1080/10934529.2014.854677.

Shirmohammadi, F., Hasheminassab, S., Wang, D., Saffari, A., Schauer, J.J., Shafer, M.M., Delfino, R.J., Sioutas, C., 2015. Oxidative potential of coarse particulate matter ($PM_{10-2.5}$) and its relation to water solubility and sources of trace elements and metals in the Los Angeles Basin. Environ. Sci.: Process Impacts 17, 2110–2121. https://doi.org/10.1039/c5em00364d.

Shen, H., Anastasio, C., 2012. A comparison of hydroxyl radical and hydrogen peroxide generation in ambient particle extracts and laboratory metal solutions. Atmos. Environ. 46, 665–668. https://doi.org/10.1016/j.atmosenv.2011.10.006.

Shiraiwa, M., Selzle, K., Pöschl, U., 2012. Hazardous components and health effects of atmospheric aerosol particles: reactive oxygen species, soot, polycyclic aromatic compounds and allergenic proteins. Free Radic. Res. 46, 927–939. https://doi.org/10.3109/10715762.2012.663084.

Shuster-Meiseles, T., Shafer, M.M., Heo, J., Pardo, M., Antkiewicz, D.S., Schauer, J.J., Rudich, A., Rudich, Y., 2016. ROS-generating/ARE-activating capacity of metals in roadway particulate matter deposited in urban environment. Environ. Res. 146, 252–262. https://doi.org/10.1016/j.envres.2016.01.009.

Simonetti, G., Conte, E., Perrino, C., Canepari, S., 2018. Oxidative potential of size-segregated PM in an urban and an industrial area of Italy. Atmos. Environ. 187, 292–300. https://doi.org/10.1016/j.atmosenv.2018.05.051.

Steenhof, M., Mudway, I.S., Gosens, I., Hoek, G., Godri, K.J., Kelly, F.J., Harrison, R.M., Pieters, R.H.H., Cassee, F.R., Lebret, E., Brunekreef, B.A., Strak, M., Janssen, N.A.H., 2013. Acute nasal pro-inflammatory response to air pollution depends on characteristics other than particle mass concentration or oxidative potential: the RAPTES project. Occup. Environ. Med. 70, 341–348. https://doi.org/10.1136/oemed-2012-100993.

Strak, M., Janssen, N.A., Godri, K.J., Gosens, I., Mudway, I.S., Cassee, F.R., Lebret, E., Kelly, F.J., Harrison, R.M., Brunekreef, B., Steenhof, M., Hoek, G., 2012. Respiratory health effects of airborne particulate matter: the role of particle size, composition, and oxidative potential-the RAPTES project. Environ. Health Perspect. 120, 1183–1189. https://doi.org/10.1289/ehp.1104389.

Szigeti, T., Dunster, C., Cattaneo, A., Cavallo, D., Spinazzè, A., Saraga, D.E., Sakellaris, I.A., de Kluizenaar, Y., Cornelissen, E.J.M., Hänninen, O., Peltonen, M., Calzolai, G., Lucarelli, F., Mandin, C., Bartzis, J.G., Záray, G., Kelly, F.J., 2016. Oxidative potential and chemical composition of $PM_{2.5}$ in office buildings across Europe – the OFFICAIR study. Environ. Int. 92–93, 324–333. https://doi.org/10.1016/j.envint.2016.04.015.

Tuet, W.Y., Chen, Y., Fok, S., Gao, D., Weber, R.J., Champion, J.A., Ng, N.L., 2017. Chemical and cellular oxidant production induced by naphthalene secondary organic aerosol (SOA): effect of redox-active metals and photochemical aging. Sci. Rep. 7, 15157. https://doi.org/10.1038/s41598-017-15071-8.

Van der Vliet, A., O'Neill, C.A., Cross, C.E., Koostra, J.M., Volz, W.G., Halliwell, B., Louie, S., 1999. Determination of low-molecular-mass antioxidant concentrations in human respiratory tract lining fluids. Am. J. Physiol. Lung Cell Mol. Physiol. 276, L289–L296. https://doi.org/10.1152/ajplung.1999.276.2.L289.

Vidrio, E., Jung, H., Anastasio, C., 2008. Generation of hydroxyl radicals from dissolved transition metals in surrogate lung fluid solutions. Atmos. Environ. 42, 4369–4379. https://doi.org/10.1016/j.atmosenv.2008.01.004.

Visentin, M., Pagnoni, A., Sarti, E., Pietrogrande, M.C., 2016. Urban $PM_{2.5}$ oxidative potential: importance of chemical species and comparison of two spectrophotometric cell-free assays. Environ. Pollut. 219, 72–79. https://doi.org/10.1016/j.envpol.2016.09.047.

Wang, Y., Arellanes, C., Curtis, D.B., Paulson, S.E., 2010. Probing the source of hydrogen peroxide associated with coarse mode aerosol particles in Southern California. Environ. Sci. Technol. 44, 4070–4075. https://doi.org/10.1021/es100593k.

Weber, S., Uzu, G., Calas, A., Chevrier, F., Besombes, J.-L., Charron, A., Salameh, D., Jevzek, I., Movcnik, G., Jaffrezo, J.-L., 2018. An apportionment method for the Oxidative Potential of atmospheric particulate matter sources: application to a one-year study in Chamonix. France. Atmos. Chem. Phys. 18, 9617–9629. https://doi.org/10.5194/acp-18-9617-2018.

Weichenthal, S.A., Lavigne, E., Evans, G.J., Godri-Pollitt, K.J., Burnett, R.T., 2016. Fine particulate matter and emergency room visits for respiratory illness effect modification by oxidative potential. Am. J. Respir. Crit. Care Med. 194, 577–586. https://doi.org/10.1164/rccm.201512-2434OC.

Weichenthal, S., Crouse, D.L., Pinault, L., Godri-Pollitt, K., Lavigne, E., Evans, G., van Donkelaar, A., Martin, R.V., Burnett, R.T., 2016. Oxidative burden of fine particulate air pollution and risk of cause-specific mortality in the Canadian Census Health and Environment Cohort (CanCHEC). Environ. Res. 146, 92–99. https://doi.org/10.1016/j.envres.2015.12.013.

Yang, A., Hellack, B., Leseman, D., Brunekreef, B., Kuhlbusch, T.A.J., Cassee, F.R., Hoek, G., Janssen, N.A.H., 2015. Temporal and spatial variation of the metal-related Oxidative potential of $PM_{2.5}$ and its relation to $PM_{2.5}$ mass and elemental composition. Atmos. Environ. 102, 62–69. https://doi.org/10.1016/j.atmosenv.2014.11.053.

Yu, H., Wei, J., Cheng, Y., Subedi, K., Verma, V., 2018. Synergistic and antagonistic interactions among the particulate matter components in generating reactive oxygen species based on the dithiothreitol assay. Environ. Sci. Technol. 52, 2261–2270. https://doi.org/10.1021/acs.est.7b04261.

atmosphere

MDPI

Review

Review of PM Oxidative Potential Measured with Acellular Assays in Urban and Rural Sites across Italy

Maria Chiara Pietrogrande *, Mara Russo and Elisa Zagatti

Department of Chemical and Pharmaceutical Sciences, University of Ferrara, 44121 Ferrara, Italy; rssmra1@unife.it (M.R.), elisa.zagatti@unife.it (E.Z.)

* Correspondence: mpc@unife.it

Received: 11 September 2019; Accepted: 11 October 2019; Published: 16 October 2019

Abstract: This work is an overview of the oxidative potential (OP) values up to date measured in Italy, with the aim to provide a picture of the spatial and seasonal variability of OP in the various geographical areas across Italy. The summarized works used the common acellular assays-based dithiothreitol (OP^{DTT}), ascorbic acid (OP^{AA}), glutathione (OP^{GSH}), and 2',7'-dichlorodfluorescein (OP^{DCFH}) assays. The paper describes the association of OP responses with PM chemical composition, the sensitivity of various acellular OP assays to PM components and emission sources, and PM size distribution of the measured OP values. Our synthesis indicates that crustal and transition metals (e.g., Fe, Ni, Cu, Cr, Mn, Zn, and V), secondary ions and carbonaceous components (elemental carbon, EC, organic carbon, OC and water soluble carbon, WSOC) show significant correlations with OP across different urban and rural areas and size ranges. These chemical species are mainly associated with various PM sources, including residual/fuel oil combustion, traffic emissions, and secondary organic aerosol formation. Although the OP assays are sensitive to the same redox-active species, they differ in the association with PM chemical components. The DDT assay is mainly sensitive to the organic compounds that are mostly accumulated in the fine PM fraction, i.e., tracers of burning sources, and redox active organics associated with other markers of photochemical aging. In contrast, OP^{AA} and OP^{GSH} were mostly responsive to metals, mainly those related to non-exhaust traffic emissions (Cu, Zn, Cr, Fe, Ni, Mn, Sn, Cd, Pb), that are mainly accumulated in the coarse PM. Among the investigated sites, our synthesis shows larger OP values in Trentino region and the Po Valley, that may be explained by the high density of anthropogenic sources, and the orographic and meteorological characteristics, that favor the pollutants accumulation and aerosol photo-oxidative aging.

Keywords: PM oxidative potential; acellular assays; Italy sites; PM chemical composition; PM sources; PM size

1. Introduction

In recent years, the oxidative potential (OP) of particulate matter (PM) has been proposed as a biologically relevant metric to be associated with a number of health endpoints and biomarkers of toxic effects in humans [1–7]. It is based on the increasing consensus that the oxidative stress is an important mechanism of human toxicity related to exposure to atmospheric aerosols. OP measures the capacity of inhaled PM to induce a redox imbalance generated by the interaction of redox-active species present in PM with physiological species undergoing Fenton reactions and redox cycling [6,8–11]. A range of acellular assays have been developed for measuring OP, having the advantages of low price, speed, practicality, and high data throughput, when compared to cellular assays [12–18]. Among them, the most commonly used are based on dithiothreitol as a proxy of cellular reductants (DTT assay, OP^{DTT}), or endogen antioxidant species, such as ascorbic acid (AA assay,

OP^{AA}) and glutathione (GSH assay, OP^{GSH}). The acellular version of the 2',7'-dichlorodfluorescein (DCFH) assay uses the enzymatic production of the fluorescent probe largely used for the evaluation of oxidative stress in living cells.

The present work summarizes the PM oxidative properties up to date measured in Italy using OP acellular assays, with the aim of giving a general insight of PM OP across the Italian territory, that has not been reported yet, in spite of the increasing number of OP measurements carried out in Europe [6,19–22]. In addition, the study reviews the association described in previous studies between OP from different assays with several inorganic ad organic components, that effect PM oxidative properties, i.e., metals, ions, and carbonaceous components. The aim is to give a picture of the spatial and seasonal variability of different contributions to OP in the various geographical areas across Italy. The relevance of such an investigation is based on the large variability in the chemical composition of different PM size fractions in various locations across Italy, as a consequence of the strong differences in the density of anthropogenic sources and the orographic and meteorological characteristics [23,24].

As the reviewed papers use different acellular OP assays, an additional outcome of our synthesis is the comparison among the sensitivities of various acellular OP assays to PM composition, emission sources, and particle size.

2. Methodology

2.1. PM Sampling and Filter Extraction

In general, daily PM_{10} or $PM_{2.5}$ samples were collected by using low-volume samplers to sample an air volume of about 55 m^3 per day. The particles were collected on Teflon membranes on quartz filters to be submitted to different instrumental analysis for chemical characterization.

In most studies, filter-collected PM samples were extracted with high-purity Milli-Q water using continuous agitation or ultra-sonication at room temperature, followed by filtering through polypropylene syringe filters. Therefore, the water-soluble fraction was investigated, to represent the bioavailable PM component [25,26]. Otherwise, some papers also investigated the PM insoluble fractions by skipping filtration of water suspension [17] or extraction with microwave-assisted acid digestion [27,28].

2.2. Quantification of PM Oxidative Potential Using Acellular Assays

Overall, the reported studies applied 4 of the most common acellular methods typically used in this field: The dithiothreitol (DTT), the ascorbic acid (AA), the glutathione (GSH), and the 2',7'-dichlorofluorescin (DCFH) assays. Details of the experimental protocols used for OP measurement is reported in each reviewed paper. A summary of the methods is provided below.

2.2.1. DTT Assay

DTT is a surrogate for the cellular oxidant NADPH, which reduces oxygen to the superoxide anion. OP is measured by the rate at which DTT is consumed, which is proportional to the concentration of redox-active species in the PM sample. Specifically, solvent-extracted (e.g., in water or methanol) PM samples are incubated with DTT and a potassium phosphate buffer under controlled conditions (T = 37 °C and pH = 7.4) for times varying from 15–90 min. A small aliquot is removed from the mixture at designated times and mixed with 1% w/v Trichloraoacetic acid (TCA) to quench DTT reactions. The aliquot is mixed with 0.5 mL 5,5'-dithiobis (2-nitrobenzoic acid) (DTNB) to form 2-nitro-5-mercaptobenzoic acid (TNB) by reacting with the residual DTT, which is then measured at the wavelengths of 4 using a UV/Vis spectrometer [8,13,26].

An alternative method has been proposed for measuring the superoxide anion produced by DTT, or by tris (2-carboxyethyl) phosphine (TCEP), based on the determination of the cytochrome c (cyt-c) reduction rate [29]. It uses two alternative analytical methods, i.e., a spectrophotometric

measure of cyt-c light absorption at 550 nm, and an amperometric assay, based on self-assembled Cyt-c immobilized monolayers on modified gold electrodes.

2.2.2. AA and GSH Assays

The chemical OP^{AA} protocol is very similar to the OP^{DTT} protocol. After controlled incubation of the antioxidant AA in the aqueous extract, the measurement of AA depletion over time is directly followed by the decrease of UV-Vis absorbance of the ascorbic ion at the wavelengths of 265 nm [23,24].

Modified AA procedures have also been used, performed in a synthetic surrogate respiratory tract lining fluid (RTLF), containing endogenous antioxidants at physiological levels, which is more indicative of realistic lung conditions, i.e., reduced glutathione (GSH), uric acid (UA), and citrate (Cit), in addition to ascorbate (Asc) [30]. In some OP protocols, the remaining concentrations of antioxidants in SLF is quantified at specific time intervals, using reversed-phase HPLC with electrochemical detection and/or enzyme-linked assay for total glutathione and GSH [17,19,31,32].

2.2.3. DCFH Assay

The 2′,7′-dichlorofluorescin (DCFH) assay is a direct detection method performed by a fluorescence technique using a specific florigenic probe, that is widely applied also for the ROS determination in biological assays. The nonfluorescent DCFH is oxidized to the fluorescent dichlorofluorescein (DCF) by ROS in the presence of horseradish peroxidase (HRP). The formed DCF can be easily measured by fluorescence at the excitation and emission wavelengths of 485 and 530 nm, respectively. The ROS concentration may be then calculated in terms of H_2O_2 equivalent [21,25,26,33].

2.3. Analytical Methodologies for Chemical Characterization

Macro-elements, soluble and insoluble fractions of micro-elements, inorganic ions and organic components—elemental carbon (EC), organic carbon(OC), water soluble carbon (WSOC)—were determined in most of the investigated PM samples (Table 1). Details of the experimental procedures are reported in each reviewed paper. A summary of the methods is provided below.

Major elements (Al, Si, Fe, Ca, Cr, and Ti) were determined using X-ray fluorescence (XRF, e.g., [34]). Trace elements—such as B, Cd, Ce, Co, Cs, Cu, La, Mn, Mo, Ni, Pb, Rb, Sb, Se, Sn, Sr, Tl, V, Zn, and Zr—were determined using inductively coupled plasma mass spectroscopy (ICP-MS), [23,24]. Ion Chromatography was used to quantify cations (Na^+, NH_4^+, K^+, Mg^{2+}, Ca^{2+}) and anions, namely Cl^-, NO_2^-, NO_3^-, SO_4^{2-} and ions of low weight (LW) carboxylic acids, i.e., oxalate, acetate, glycolate, proponiate, formate, and pyruvate chromatography [23,34]. Also sugars and anidrosugars, were determined by high-performance anion exchange chromatography combined with pulsed amperometry detection [24].

In general, organic carbon (OC) and elemental carbon (EC) concentrations were quantified using a thermo-optical analyser (Sunset Laboratory OC/EC analysers) [18,30], and water-soluble organic carbon (WSOC) was analyzed with a total carbon analyzer instrument [23]. From these values, the contribution of prima (POC) and secondary organic species (SOC) to OC was estimated [24, 34].

Table 1. Relevant information reported in the reviewed studies, grouped according to particulate matter (PM) dimensional fractions: Site location, period, and duration of PM samples collection, acellular assay used for oxidative potential (OP) measurement, analyzed species for chemical characterization. (TSP: total suspended particles, DTT: dithiothreitol, AA: ascorbic acid, GSH: glutathione, DCFH: 2',7'-dichlorofluorescin, EC: elemental carbon, OC: organic carbon, WSOC: water soluble organic carbon, POC: primary organic carbon, SOC: secondary organic carbon, LW: low weight, TC: total carbon, WSTC: water soluble total carbon, PAH: polycyclic aromatic hydrocarbon, BC: black carbon.)

PM fraction	Ref.	Location	Sampling Period	Sampling Duration	OP Assay	Chemical Characterization
TSP	[28]	Milan	January, June, October 2013	24 h	DTT, DCFH	EC, OC, inorganic ions, metals, trace organic compounds
PM_{10}	[23]	Trento	April–May 2016	24 h	DTT, AA	WSTC, ions, metals, sugars
	[34]	Lecce	December 2014–October 2015	24 h	DTT, AA	metals, ions, EC, OC, POC, LW carboxylic acids
	[29]	Milan	Winter 2009	24 h	DTT (cit-c)	OC, metals, quinones
PM_{10} and $PM_{2.5}$	[24]	Lecce	December 2014–October 2015	24 h	DTT, AA	metals, ions, EC, OC, POC, LW carboxylic acids
	[27]	Lecce	Fall/Winter 2013–2016	24 h	DTT	OC, EC, POC, SOC, TC
	[35]	Milan	December 2009–November 2010	24 h	DCFH	OC, EC, WSOC, ions, metals, levoglucosan, PAHs, hopanes, alkanes
$PM_{2.5}$	[18]	Bologna	February–July 2013	24 h	DTT, AA	metals, EC, OC
	[30]	Bologna	mar 2018	24 h	AA	metals, EC, OC
	[20]	Rome	January 2010–January 2011	24h	DTT	OC, EC, PAH, hopanes
	[21]	Rome	January–February 2017	24 h	DCFH	OC, EC, BC, WSOC, water soluble BrC, metals, levoglucosan, PAH
	[19]	Turin	February 2010–January 2011	24 h	AA, GSH	metals, NO_2
	[17,32]	Milan, Florence	Summer/Winter 2012–2013	24 h	AA, GSH	OC, EC, ions, metals
	[31]	Turin, Pavia	June–December 2000	24 h	AA, GSH	metals
PM_3–PM_{3-7}–PM_7	[16]	Milan	April–July 20	3–4 days	DTT, DCFH	metals, ions
9 PM fractions 0.18–18 μm	[25]	Ferrara, Rome	February–March 2017	24 h	DTT, AA, DCFH	ions, metals
50 μm dust	[26,33]	specific sources	-	-	DTT, AA, DCFH	OC, EC, WSOC, ions, metals

3. Results and Discussion

3.1. Study Overview

The relevant studies concerning Italian sites published up to May 2019 were searched in the Web of Science database, using as inclusion criteria that they report OP data of PM samples collected in Italian sites measured using cell-free systems. In total, 19 independent studies were identified. Among these, 11 papers were detailed investigations specifically devoted to locations in Italy, while 8 were general studies in European cities also including Italian sites.

Overall, nine sites have been investigated located in different regions to cover the main geographical areas across the Italian peninsula, even if their spatial distribution is rather inhomogeneous, with Northern Italy, mainly the Po Valley, quite extensively monitored and other areas, especially Southern Italy, still lacking data (Figure 1). The monitoring stations include urban, industrial, traffic, and semi-rural sites, so that they may give information on the impact of anthropogenic sources on PM oxidative property.

The reviewed studies were based on four of the most commonly used OP acellular assays, often using two or more OP assays in combination, i.e., 11 studies measured OP^{DTT}, 11 studies OP^{AA}, 3 studies OP^{GSH}, and 6 studies OP^{DCFH}.

Table 1 summarizes the relevant information on the studies considered in our synthesis, by grouping the data according with PM dimensional fractions. The table reports the characteristics of PM samples collection, i.e., site location, period and duration of PM sampling, the acellular assays used for OP measurement, and the chemical species analyzed for PM characterization.

Figure 1. Location of the studied sites across the Italian peninsula. Symbols indicate different PM size fractions investigated in each site, i.e., black points: PM_{10}; red points: $PM_{2.5}$; blue points: Other PM size fractions.

Different particle size fractions were investigated, including total suspended particles, PM_{10}, $PM_{2.5}$, and size-aggregated fractions, even if most of the studies concerned fine $PM_{2.5}$ fraction.

OP of total suspended particles (TSP) were measured in Milan, the biggest Italian city in Northern Italy (~1,400,000 inhabitants). Three campaigns were conducted in January, July, and October 2013. The OP^{DTT} and OP^{DCHF} responses were measured at two sites with different traffic loads, i.e., low emission zone and busy traffic site, giving comparable data [28].

Oxidative properties of PM_{10} samples were investigated in Trentino region (Alpine valley in Northern Italy) in April–May 2016, at an urban background and industrial sites, in order to characterize the impact of local emission sources, including a Zn coating factory [23]. OP^{DTT} and OP^{AA} of PM_{10} particles were measured also in Lecce, an urban background site in Southern Italy over a whole year, from December 2014 to October 2015, so that it was possible to investigate seasonal trend (autumn–winter, AW, vs. spring–summer, SS) [34]. In the same campaign, also $PM_{2.5}$ granulometric fraction was simultaneously collected and analyzed to investigate the variation of the OP^{DTT} and OP^{AA} activity in relation with the particle size and chemical composition [24]. At the same site, an independent study was conducted by Chirizzi et al. to measure OP^{DTT} of the water-soluble $PM_{2.5}$ and PM_{10} particles, with the specific concern of characterizing the impact of Saharan dust outbreaks [27]. For both coarse PM_{10} and fine $PM_{2.5}$ particles, OP^{DCHF} was investigated in Milan on a weekly basis in a year-long period (December 2009 to November 2010) and related to PM chemical properties [35].

Oxidative properties of fine particles were investigated at an urban site (Bologna, 400,000 inhabitants) and a rural location (SPC, san Pietro Capofiume, 30 km far from Bologna) located in the Emilia Romagna region, in the Eastern side of Po Valley, one of the most polluted areas in Europe. One monitoring campaign was conducted in February–July 2013 [18] and the other one in March 2018 [30]. OP of $PM_{2.5}$ samples in some Italian cities were also measured as a part of more general studies concerning different locations over Europe. Rome was included in a study that measured OP^{DTT} in 2010 [20] and also in a work carried out in February 2017 to measure OP^{DCHF} of particles collected using PILS system [21]. Two studies measured OP^{AA} and OP^{GSH} of fine PM at Turin, a big industrial city (~900,000 inhabitants) located on the Western side of the Po Plain [19,31] and one of them, concerning 20 European sites over one year, also included smaller city Pavia (~70,000 inhabitants) [31].

In addition, some studies measured OP in size-resolved PM fractions. One included PM samples collected in April–July 20 in Milan, among six cities and three rural sites across Europe [16]. Three PM size classes ($PM_{>7}$, $PM_{3–7}$, PM_{3}) were characterized for OP^{DTT} and for total elements. Others were performed on PM sampled in Rome and Ferrara, eastern Po valley, and also on PM from specific sources [25,26,33]. They used DTT, AA, and DCFH assays to measure OP of nine size-segregated PM fractions, i.e., cut-sizes: 0.18, 0.32, 0.56, 1.0, 1.8, 3.2, 5.6, 10, and 18 μm.

Finally, two papers concern oxidative properties of indoor air. They are general studies concerning several European cities, within the European Union project OFFICAIR, including Milan and Florence, a big city (~1,000,000 inhabitants) located in the center of Italy [17,32]. $PM_{2.5}$ particles were collected in mechanically ventilated offices and their OP was measured by using the ascorbate and glutathione assays.

Overall, the operative protocols used by the Authors varied widely by study for each of the four assays. The extraction procedures changed in terms of the used solvent (water, phosphate buffer at pH7.4, or methanol), duration time, and temperature of agitation or ultra-sonication operations and also different reagent concentrations were employed.

In addition, the units for expressing the OP responses varied by assay and study: They are based on time rate-of-change, expressed as nmol or % depletion per min. They may be volume-based values (nmol or % depletion per min per m^3 of air) or mass-based data (nmol or % depletion per min per μg of PM; sometimes referred as intrinsic OP). However, the conversion between the volume- and mass-based metrics (OP_V and OP_m, respectively) was not always possible, since data on PM mass concentration was not always reported in the papers.

It is evident that such a protocol variability strongly affects the magnitude of the measured responses, with the consequence that not reliable and conclusive results are reported within every study, that can make comparisons across studies difficult.

3.2. Association of Oxidative Potential with PM Chemical Composition

Most of the reviewed studies performed the characterization of the chemical composition of the PM samples and investigated the association of OP responses with PM components (Table 1). In

general, the papers concern volume-based OP, as mostly relevant metric for epidemiologic studies, since it reflects the actual exposure to redox-active PM upon inhalation, being a combination of the intrinsic PM oxidative potential with the total PM concentration [6,8–16]. Therefore, in the following OP indicates volume-based OP, OP_V, when not specified.

The aim of the correlation analysis is to single out the PM components that drive OP responses from different assays and also to estimate the contribution of each individual species to OP. Table 2 summarizes the results from correlation analysis reported in the reviewed studies, grouped according with PM dimensional fractions. Most of the analyses were based on Pearson or Spearman correlations, assuming statistically significant relationships at $p < 0.01$ or $p < 0.05$ levels. The table reports the PM components having the highest association with OP responses from different assays.

Table 2. Association among the measured OP and chemical composition reported in the reviewed studies, grouped according with PM dimensional fractions: Site location of PM samples collection, correlation analysis used for association at p level, acellular assay used for OP measurement, chemical species showing significant correlation to OP.(;

PM fraction	Ref.		Correlation	Assay	Chemical Species
TSP	[28]	Milan	Spearman $p < 0.01$	DTT	Solar Radiation
				DCFH	TSP mass, OC, TC, SO_4^{2-}, NO_3^-, NH_4^+, Ca, Mn, Co, Zn, As
PM_{10}	[23]	Trento	Pearson $p < 0.01$	DTT	SO_4^{2-}, NH_4^+, NO_3^-, Cl^-, Ca, Mg, K, Mn, Cu, Rb, and Zn, Fe, Ni, Pb, Sr, V, WSOC, sugars, levoglucosan
				AA	SO_4^{2-}, NH_4^+, NO_3^-, Cl^-, Ca, Mg, K, Mn, Cu, Rb and Zn, Fe, Ni, Pb, Sr, V, WSOC, sugars
	[34]	Lecce	Pearson $p < 0.01$	DTT	***AW:*** K^+,Ca^{2+}, Ba, Cd, Ce, Cr, Cu, Fe, Mn, OC, EC, POC;
					SS: NO_3^-, NH_4^+,Cu, OC, EC, POC, LW carboxylic acids
				AA	***AW***: K^+, Ca^{2+}, Ba, Ce, Cr, Cu, Fe, Mn, OC, EC, POC;
					SS*:* NH_4^+, nss-K^+, nss-Mg^{2+}, nss-Ca^{2+}, nss-SO_4^{2-}, Cu, Mn, P, Pb, LW carboxylic acids
PM_{10} and $PM_{2.5}$	[24]	Lecce	Pearson $p < 0.01$	DTT	***AW***: K^+, NO_3^-, Ba, Cd, Cu, Fe, Mn, P, V, OC, EC, carboxylic acids;
					SS: NO_3^-, SO_4^{2-}, OC, EC, TC, POC
				AA	***AW***: NO_3^-, Ba, Cd, Cu, Fe, Mn, P, V, OC, EC;
					SS: NO_3^-, SO_4^{2-}, OC, EC, TC, POC
$PM_{2.5}$	[27]	Lecce	Pearson $p < 0.05$	DTT	OC, EC

	[35]	Milan	Spearman $p < 0.05$	DCFH	Ni, Cr, Cu, OC
	[18]	Bologna	Pearson $p < 0.01$	DTT	Mn, Fe, Cu, Cr, Zn, OC, EC
				AA	Mn, Cu, OC, EC
	[30]	Bologna	Pearson $p < 0.01$	AA	Mn, Fe, Cu, Cr, Zn, OC, EC
	[20]	Rome	linear regression	DTT	OC, EC Levoglucosan, ∑PAHs
	[21]	Rome	linear regression	DCFH	equivalent Black Carbon, ∑PAHs
	[19]	Turin	Pearson $p < 0.05$	AA	$PM_{2.5}$ mass, NO_2, Cu, Fe
				GSH	NO_2, Cu, Fe
	[17]	Milan, Florence	Spearman $p < 0.01$	AA	***Indoor***: Cu, Mo, OC;
					Outdoor: Fe, Cu, Cr, Ni, Cd, Sn, Sb, K^+
				GSH	***Indoor***: Cu, Mo, OC;
					Outdoor: Cu, Sn, OC
	[31]	Turin, Pavia	Pearson	AA	Fe, Cu, Zn
				GSH	Cu, Al
PM_3, $PM_{3–7}$, PM_7	[16]	Milan	Spearman $r > 0.70$	DTT	< 3 μm: -
					3–7 μm: Fe, Sn, Cu, Sb, Ba
					> 7 μm: As, Al, Ti, Sr, Li

AW: Autumn–winter: December to March data; ***SS:*** Spring–summer: April to October data.

In the following, the results of such associations will be compared among the different studies, with the aim to give a picture of different species contributing to OP in the various geographical areas across Italy.

In general, three main classes of inorganic and organic species showed the highest associations with OP from different assays, in agreement with literature data [8,19,36–40]:

- Metals. The major PM components, such as alkali (Na, K) and hearth metals (Ca, Mg, Ba, Al) can be originated from resuspension of road dust, road abrasion, and soil dust emissions. Trace elements are several transition metals (i.e., Fe Cu, Zn, Pb, Cr, Ni, Mn, Sn, Cd) associated with non-tail pipe traffic emissions, mainly related to brake and tire wear [11,25,39,41–44]. Finally, K and Rb can be considered as tracers of the biomass burning [23,26].
- Carbonaceous components. They include elemental, EC, organic, OC, and water soluble organic carbon, WSOC. OC may be discriminated between primary (POC) and secondary organic species (SOC), based on the quantification of individual compounds, as tracers of specific sources, i.e., sugars, levoglucosan—widely used tracer of biomass burning [22,31,37,43];

n-alkane and PAHs—tracers of tail pipe traffic emissions [20]; carboxylic acids and quinones—markers of photochemical formation of SOA [45–52].

- Ions. Mostly associated ions are Cl^- and Na^+, components of sea-salt particles, and SO_4^{2-}, NO_3^-, NH_4^+, which are the main constituents of the secondary inorganic particles [25,34].

3.2.1. Association with Metals

Several studies across Italy reported that the volume-normalized OP^{AA} data are widely correlated with both soluble and total fractions of several elements, i.e., Mn, Fe, Cu, Cr, Zn, Ni, Al, K, Mg, Ca, Cd, Ba, and Rb. This has been found for ambient PM_{10} particles at Trento [23] and Lecce [34], for $PM_{2.5}$ at Bologna [18] and Lecce [24] and in general studies including Turin [19,31], Milan, and Florence [17,32]. Correlations with the same metals were also observed for OP^{DTT} responses for PM_{10} and $PM_{2.5}$ samples at Trento [23], Lecce [24,27,37] and Bologna [18], for TSP at Milan [28] and for size aggregated PM_3, PM_{3-7}, PM_7 particles at Milan [16]. OP^{GSH} showed significant correlations with some metals, including copper, tin, molybdenum, and aluminum in outdoor and indoor $PM_{2.5}$ particles [17,32]. By investigating outdoor and indoor (office buildings) $PM_{2.5}$ samples in Firenze and Milan, the correlation analysis revealed that indoor OP^{AA} and OP^{GSH} responses were significantly associated with fewer components (Cu and Mo) compared with outdoor OP. It is noteworthy that mean indoor OP values were substantially lower than the related outdoor data, with a mean indoor/outdoor ratio of 0.62. This suggests that the indoor air is generally less oxidatively dangerous than outdoors, even if the indoor air chemistry might involve complex formation of other redox-active species which alter the oxidative properties of PM.

3.2.2. Association with Organic Species

Many studies across Italy show that the OP assays are sensitive to organic species, described by WSOC, EC, and OC. In particular, some authors investigated the discrimination between primary and secondary OC in detail. They found that OP^{DTT} and OP^{AA} data at Lecce and Trento were mainly associated with POC [23,34], that is also confirmed by association of OP^{DTT} with anhydrosugras emitted from wood combustion [23]. Conversely, Chirizzi found that secondary organic species have a larger effect on OP^{DTT} with respect to primary OC, as OP^{DTT}_V is more strongly correlated with OC than with EC [27]. This result is consistent with the data of other authors, suggesting that photochemical aging is an important factor in determining PM redox properties. In fact, Perrone found a strong correlation of OP^{DTT} with global radiation, a proxy for secondary oxidizing organics [28], while others observed that OP^{DTT} and OP^{AA} values were strongly associated with secondary ions, such as SO_4^{2-}, NO_3^-, NH_4^+ and low weight carboxylic acids, produced by atmospheric photo oxidation of organics [24,34]. This correlation is the strongest in spring/summer at Lecce, characterized by highest solar irradiance values [24].

Also, OP^{DCFH} showed a positive correlation with OC in PM_{10} [28] and $PM_{2.5}$ particles [35].

3.2.3. Intercorrelation among Species

Some studies reported that the chemical components associated with PM-induced OP exhibited strong inter-correlations among them [23,34,37]. Consequently, the association of OP with each individual species is difficult, and monodimensional analysis may produce misleading results. In these cases, a multivariate approach has to be preferred to take such cross-correlations into account and also to evaluate the effects of possible multicomponent interactions, e.g., between metals and organics and/or emission sources.

As an example, Pietrogrande applied the cluster hierarchical analysis for investigating the associations of OP^{DTT} and OP^{AA} with several chemical markers [23]. Even if several species resulted cross-correlated from Pearson's analysis, the computed HA dendrograms clearly showed that OP^{DTT} values were closest to K^+ and Rb and then to a larger group formed by Mg^{2+}, Pb, SO_4^{2-}, WSTC, and Mn. This finding may indicate that the DTT activity is mainly driven by primary emissions, such as biomass burning (K^+, Rb, and WSTC) and traffic (Mg^{2+}, Pb, and Mn), and also by secondary particle

formation (SO_4^{2-}). Otherwise, in the HA dendrogram the species closest to OP^{AA} was Cu followed by Zn, and then to a wide group of chemical components, including Al, K, Rb, Ca, and Mg elements. This suggests that the OP^{AA} values are mainly dominated by contribution from industrial/agricolture activities and non-exhaust traffic emissions.

3.3. Comparison among Different Acellular Assays

3.3.1. Sensitivity of Different Acellular Assays

The reviewed studies confirmed the general finding that the various OP assays display different sensitivity towards the same redox-active PM components, because they capture the redox reactions of different species [4,6,8,10,12–15,37,46]. Overall, DTT mainly responded to the organic compounds, as traced by OC, EC, that represent burning sources, including fuel vehicular and biomass burning emissions—and redox active species such as quinones, associated with other markers of photochemical aging (SO_4^{2-}, NO_3^-). In addition, OP^{DTT} responses are also affected by traffic-related metals. In contrast, OP^{AA} and OP^{GSH} were mostly responsive to metals, mainly related to non-exhaust traffic emissions (Cu, Zn, Cr, Fe, Ni, Mn, Sn, Cd, Pb) [12,18,25,26–28,32–36].

Although both OP^{DTT_V} and OP^{AA_V} are sensitive to the same redox-active species, they show different sensitivity, as found in outdoor and indoor fine particles [22]. This point was investigated in detail by performing linear regression analysis on OP^{DTT} and OP^{AA} as a function of species concentration, and comparing the slope of best fitting lines, as a measure of each assay sensitivity to the investigated species [23,24]. Both assays showed similar sensitivity to the soluble fractions of K, Ca, Mn, Rb, and WSTC, while AA was six times more sensitive Zn and times to Cu compared with DTT [23].

Overall, it must be pointed out that association of volume-normalized OP^{DTT} with transition metals should be interpreted with caution, as it may be due to similar variations in metal and PM concentrations, and also to higher concentration of metals compared with that of quinones, that are more efficient than metals to DTT oxidation [48,49].

Finally, DTT and DCFH showed different sensitivity when applied to TSP samples at Milan, with OP^{DCFH} mainly associated with OC, TC, SO_4^{2-}, NO_3^-, NH_4^+ markers secondary aerosol [28].

3.3.2. Correlation between OP Responses from Different Acellular Assays

The paper summarized in this study describe contrasting results on the relationship between OP responses from the various assays, as reported in other literature references [4,6,8,10–15].

Concerning the most investigated comparison between OP^{DTT} and OP^{AA} responses, no significant correlation was found between the measurements on $PM_{2.5}$ at Bologna (Pearson correlation coefficient, $r < 0.4$), even if the values obtained with both assays were similarly correlated with metals, i.e., OP^{DTT} was found highly correlated with several metals (Cu, Zn, Cr, Fe, Ni, Mn), whereas OP^{AA} only moderately with Cu and Mn [18]. This result is consistent with other papers reporting that OP^{DTT}—similarly to OP^{DCFH}—is mostly sensitive towards the combustive and secondary compounds of PM, i.e., Mo, Ni, SO_4^{2-}, Cd, and WSOC, in contrast with OP^{AA}, that mainly responds to high concentrations of water soluble fractions of Mn, Sr, Rb, Se, P, and Ca, that are typical markers of pellet ash and also in brake dust [25,26,28,35–37,41,44].

In contrast, a significant correlation was found between OP^{DTT} and OP^{AA} responses measured on PM_{10} at an industrial site (Ala, Pearson correlation coefficient $r = 0.60$, $p < 0.01$), and at urban background site (Trento, $r = 0.71$, $p < 0.01$, [23]), and also at Lecce ($r = 0.52$, $p < 0.01$), where DTT and AA assays provide similar OP values within the same variability range [34]. This suggests that DTT and AA assays have similar associations with the chemical species in the studied PM samples, that are additionally strengthen by the inter-correlations among their concentrations.

In the alternative method proposed based on the cytochrome c (cyt-c) reduction rate, TCEP is more reactive towards quinones, in comparison to DTT, suggesting that it may be used as more sensitive device for measuring OP of low amount of ROS-generating compounds, such as quinines, in complex mixtures [29].

3.3.3. PM Size Distribution of OP Responses

The dimensional profile of redox activity of various PM size fractions has been investigated in several reviewed studies. Literature data suggest that the OP responses, both volume- and mass-based values, show a clear size distribution, as a consequence of the specific sensitivity of each OP assay used for measurement towards the redox-active components accumulated in the different PM fractions [4,6,8,13–16,21,45,50]. This is very relevant for its toxicological concern, since different size fractions may reach different parts of the lung, and therefore display different toxicological effects [1,6–8,11].

Accordingly, to literature, DTT has been found most reactive towards species accumulated in the fine fraction, such as tracers of burning sources, including fuel vehicular and biomass burning emissions—OC, EC, K, Rb, levoglucosan—and markers of secondary aerosol, such as quinones and ions (SO_4^{2-}, NO_3^-). In particular:

- Similar OP^{DTT}_V values were measured in Lecce for $PM_{2.5}$ and PM_{10} fractions (close to 0.20 ± 0.04 nmol min^{-1} m^{-3}), while the intrinsic OP^{DTT}_m value was larger for $PM_{2.5}$ than for PM_{10} [24];
- An average ratio of 0.86 (±0.10 standard deviation) was found between OP^{DTT}_V of $PM_{2.5}$ and PM_{10} particles in an independent study in Lecce, with the differences between the two fractions maximized for Saharan dust events and minimized for high carbon content samples [27];
- By investigating OP distribution of size-segregated PM samples collected in Rome and Ferrara, Simonetti found that OP^{DTT}_V, as well as OP^{DCFH}_V responses, shows a size distribution profile characterized by of a broad maximum in the 0.32–1.8 μm PM, that is similar to that of the markers of BB emissions [25];
- In a study concerning PM_3, PM_{3-7}, and $PM_{>7}$ in 17 sites in Europe, including Milan, Shafer found that OP^{DTT}_V is dominated by the PM_3 fraction, since it represents 76% of total OP activity, with the PM_{3-7} contributing on average 17% and $PM_{>7}$ 7%. Accordingly, PM_3 fraction showed a higher intrinsic OP^{DTT}_m in comparison with the larger particles. No chemical components were found associated with DTT activity (Spearman $r > 0.7$) in the PM_3 size cut, while tracers of biomass burning—K and Rb—and of non-tailpipe vehicle emission—Fe, Sn, Cu, Sb, and Ba—exhibited good correlations with OP^{DTT}_V in the PM_{3-7} size fraction [16].

The OP^{DCFH} responses showed a similar size profile as OP^{DTT} data, since the measured values tend to increase with decreasing aerosol median diameter (Rome, [21]).

Otherwise, the AA assay has been found more sensitive towards metals mainly accumulated in the coarse fraction, as tracers of re-suspended road dust and brake abrasion. Simonetti found a clear OP^{AA}_V size distribution profile with the maximum in the size range 3.2–5.6 μm, that is the same size particle distribution displayed by the tracers of brake abrasion to re-suspended road dust, i.e., Cu and Fe [25,26]. This conclusion has been also confirmed by the chemical composition of the insoluble fractions (microwave assisted digestion with HNO_3/H_2O_2 mixture) of the size-resolved PM samples. It mainly consists of particles belonging to the coarse mode (maximum in the 3.2–10 μm range), with the dominant contribution of soil re-suspended dust, together with break and tire wear, mainly traced by Ca, Al, Fe, Cu, Mo, Sb, and Sn. Consistently, Perrone found significantly higher OP^{AA}_V responses for PM_{10} than for $PM_{2.5}$ particles, i.e., 0.35 ± 0.06 vs. 0.21 ± 0.03 nmol min^{-1} m^{-3} in AW and 0.23 ± 0.04 vs. 0.09 ± 0.01 nmol min^{-1} m^{-3} in SS, respectively [24].

3.4. Spatial Variability of OP in Different Areas across Italy

Although several OP^{DTT} and OP^{AA} values have been up to date measured across Italy, the meaningful comparison among the data has to be restricted to the OP responses obtained with similar experimental assay protocols, to generate reliable and conclusive results within every study. Such a comparison across studies may give a picture of the spatial and seasonal variability of aerosol OP across the Italian peninsula to obtain insight into the contribution of sources, atmospheric processes, and meteorological conditions.

3.4.1. OP Responses of PM_{10} Particles

Four independent studies assessed the OP^{DTT} and OP^{AA} values of the PM_{10} particles in three different locations, i.e., Trentino region, Lecce, and Milan using close assay protocols [23,24,27,28,34]. The data are summarized in Figure 2a,b to describe spatial and seasonal variation among the three study sites.

Overall, we can observe a remarkable uniformity in OP^{DTT} values across Italy, since similar values were measured in the different sites, also independent of seasonality. Inside such a general uniformity, the OP^{DTT} levels were nearly triple in the northern Trentino region (0.61 ± 0.2 nmol min^{-1} m^{-3}) compared to the southern site of Lecce (0.24 ± 0.9 nmol min^{-1} m^{-3}). Such a trend is opposite to that of PM_{10} mass concentration, as PM_{10} mass is lower in Trentino (mean value 14 ± 10 μg m^{-3}) than at Lecce (mean value 37 ± 25 μg m^{-3}) and therefore it may be explained by variation in PM_{10} chemical composition, as reported in the reviewed papers [23,34]. As the DTT assay mainly responds to organic components, we can infer that the increase in OP^{DTT} in Trentino may be mainly related to the larger impact of carbonaceous particles released by combustion sources (road traffic and domestic heating). Such a hypothesis is supported by a similar high OP^{DTT} value of 0.72 ± 0.29 nmol min^{-1} m^{-3} measured at Lecce for a specific subset of PM_{10} samples characterized by high total carbon content [27]. This assumption can be associated with morphological and climatic differences among the different sites. In fact, Trentino is a pre-alpine region, close to the high mountain chain of the Alps, that is characterized by cold winters, low wind speed, and frequent stable atmospheric conditions, especially during winter. These conditions favor pollutant accumulation, that strengthens the impact from anthropogenic source emissions [23]. Otherwise, Lecce is a coastal site of the Central Mediterranean area, away from large sources of local pollution with high wind speed and high boundary layers that favor pollutant dispersion [51].

For comparison, the Figure 2a also reports the OP^{DTT} data of total suspended particles measured in Milan, although the comparison is weakened by the difference in particle size compared to PM_{10} [28]. Overall, we can observe a surprising low OP^{DTT} value close to 0.61 ± 0.2 nmol min^{-1} m^{-3} associated with a high mass concentration (up to 9 μg m^{-3} in the cold season). This may be likely explained by the different assay operative conditions, that used methanol instead of phosphate buffer as extraction solvent.

PM_{10} samples at Lecce and in Trentino region were also investigated with AA assay (data summarized in Figure 2b). As seen in the figure, inside the general homogeneity of the OP^{AA} values, the contrast across the two sites is still larger than that for OP^{DTT} data, with comparable values at Lecce (OP^{AA} ~ 0.24 nmol min^{-1} m^{-3}) and an increase up to 0.68 ± 0.42 nmol min^{-1} m^{-3} at Trento and further to 1.41 ± 0.4 nmol min^{-1} m^{-3} at the industrial site Ala.

As this difference corresponds to relatively small variation in PM concentrations across the study sites, it is likely explained by a contrasting mix of sources that can significantly change concentrations of the chemical drivers of oxidative activity. Based on the specific reactivity of AA towards metals, higher OP^{AA} in Trentino may be mainly associated with higher levels of AA-active metals. In fact, three main emission sources are present in the investigated region: Traffic in a congested major motorway (Fe, Pb, Ca, Mg, Mn), a zinc coating industry (Cl^-, NO_3^-, NH_4^+, Ca^{2+}, Cu, Zn) and the widespread pesticide use in the surrounding vineyards (Cu). Consequently, the concentrations of PM-associated airborne metals are higher at Ala in comparison with Lecce, in particularly Zn (24.5 ng m^{-3} at Ala vs. 7 ng m^{-3} at Lecce) and Cu (8.4 ng m^{-3} vs. 6.1 ng m^{-3}). This concentration trend explains the larger differences for OP^{AA} than for OP^{DTT}, on the basis of the specific sensitivity of the AA assay to these metals.

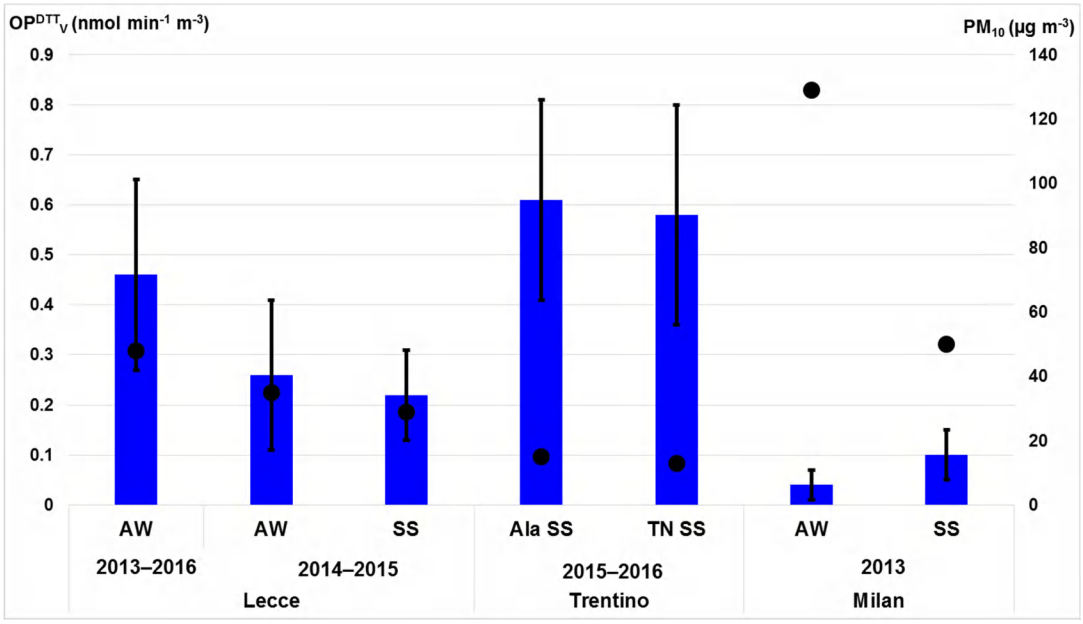

(a)

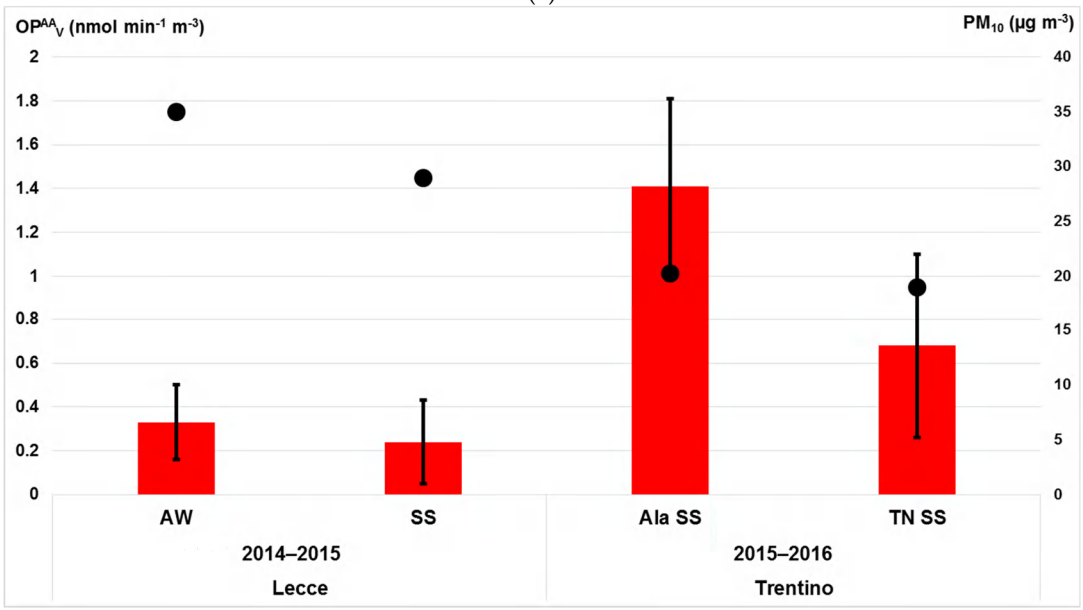

(b)

Figure 2. OP_V responses of PM_{10} samples measured using the same dithiothreitol (DTT) and ascorbic acid (AA) assay protocols: Mean values of each sampling campaign, standard errors are indicated by the bars. Points: Mean PM_{10} mass concentration values of each sampling campaign (right y-axis): (**a**) OP^{DTT}_V values of PM_{10} samples collected at Lecce (two independent studies), Trentino, and Milan (total suspended particles); (**b**) OP^{AA}_V values of PM_{10} samples collected at Lecce and Trentino.

3.4.2. OP Responses of $PM_{2.5}$ Particles

Among the reviewed papers, four studies reported OP^{DTT}_V responses measured with similar assay protocol for $PM_{2.5}$ samples collected at Lecce, Rome, and Bologna in both seasons, as summarized in Figure 3a [18,20,24,27]. Compared with PM_{10} particles, the location-dependence (or source-dependence) of PM oxidative potential is more evident for the $PM_{2.5}$ size, with values nearly 5 times higher at Bologna in AW (1.1 ± 0.2 nmol min^{-1} m^{-3}) than at Lecce in SS (0.2 ± 0.02 nmol min^{-1} m^{-3}). This variation can be explained by higher $PM_{2.5}$ concentrations at Bologna in wintertime (48 µg

m^{-3}) compared to those in all the investigates studies (14 to 25 μg m^{-3}) and also by the intrinsic redox reactivity, measured as mass-normalized OP^{DTT}_m value, that is higher at Bologna compared to Lecce i.e., 0.029 nmol min^{-1} μg^{-1} vs. 0.010 min^{-1} μg^{-1}. In addition, a clear seasonal trend is shown at both sites, with larger winter increase at Bologna (4 times higher) compared to Lecce (2 times).

Three studies measured OP^{AA} values of $PM_{2.5}$ samples collected at Bologna and Lecce in different seasons (data summarized in Figure 3b, [18,24,30]). The highest OP^{AA}_V responses were measured in Bologna, as their value was nearly triple (0.75 ± 0.2 nmol min^{-1} m^{-3}) compared to Lecce (~0.20 nmol min^{-1} m^{-3}) with a clear increase during cold season at both sites. As $PM_{2.5}$ mass concentrations were similar at both sites, the OP^{AA} variations can be mainly explained by differences in the intrinsic redox reactivity, as confirmed by higher OP^{AA}_m measured at Bologna than at Lecce, mainly during the warm season, i.e., 0.03 nmol min^{-1} μg^{-1} vs. 0.005 nmol min^{-1} μg^{-1}, respectively.

Considering that the OP^{DTT} values showed the higher spatial and temporal variations, compared to OP^{AA}, and that DDT assay is mostly sensitive to organic species, we can infer that the observed behavior for $PM_{2.5}$ OP is mainly associated with the contribution of secondary organics, especially highly oxidized organics traced by SOC concentration. In fact, significantly higher SOC concentrations have been found at Bologna compared to Lecce, mainly in the cold season, both as concentration values (on average, ≈ 3 vs. 1.5 μg m^{-3}) and relative contribution to $PM_{2.5}$ mass (~50% vs. 15%) [24,52]. The high contribution of secondary pollutants in the Po Plain has been motivated by the large impact of anthropogenic emissions, mainly wood combustion for domestic heating during winter, combined with the stable atmospheric conditions (H_{mix} ≈ 300 m), that promote pollutant accumulation in the atmosphere and therefore favor the photochemical aging of organic aerosol. In particularly, PAHs can be converted into large oxidized aromatic, e.g., DTT-active quinones, as strongly supported by chamber studies [48,49]. This explanation is also consistent with the positive correlation observed for PM samples in Milan between OP^{DTT}_m with global radiation and, to a lesser and low extent, also with T, O_3, and chemical components formed by photochemical reactions (SO_4^{2-} and oxalic acid) [28].

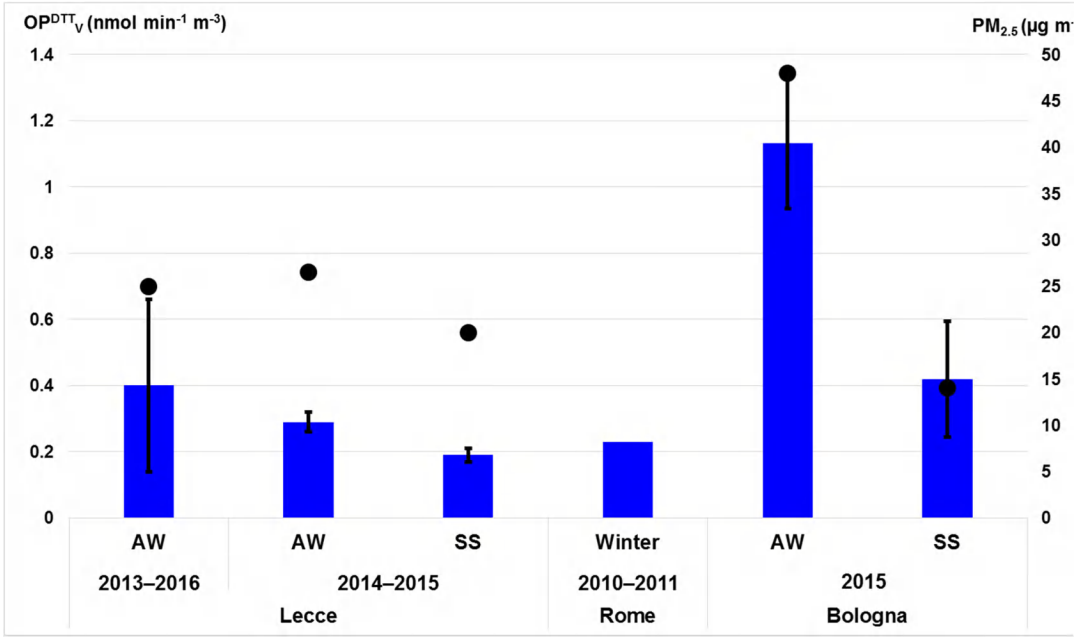

(a)

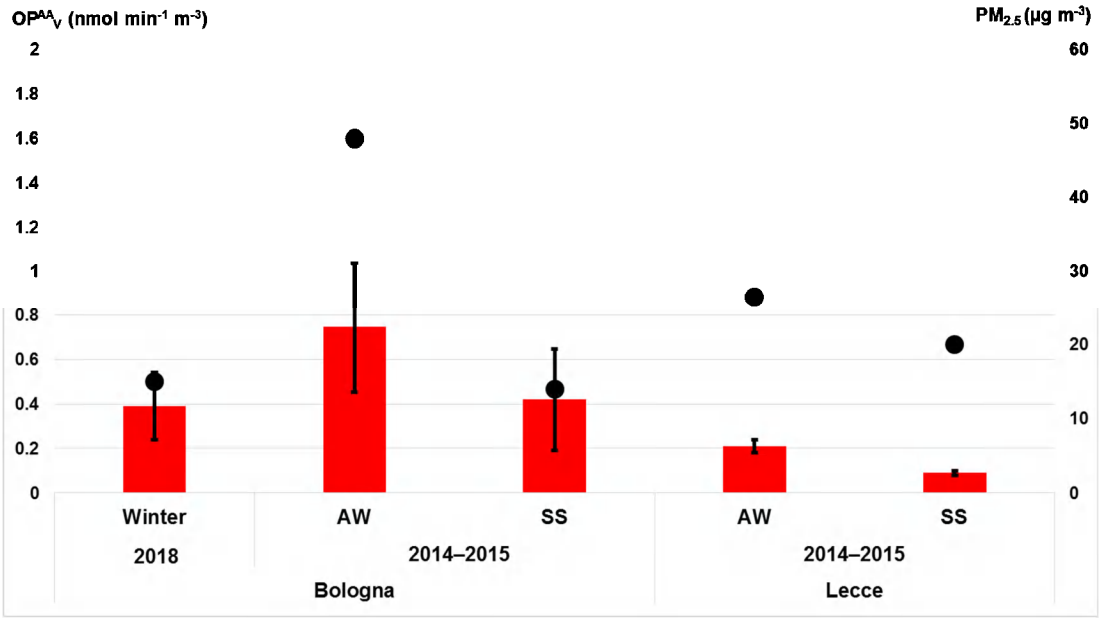

(b)

Figure 3. OP$_V$ responses of PM$_{2.5}$ samples measured using the same DTT and AA assay protocols: Mean values of each sampling campaign, standard errors are indicated by the bars. Points: Mean PM$_{2.5}$ mass concentration values of each sampling campaign (right y-axis): (**a**) OP$^{DTT}_V$ values of PM$_{2.5}$ samples collected at Lecce (two independent studies), Rome, and Bologna; (**b**) OP$^{AA}_V$ values of PM$_{2.5}$ samples collected at Bologna (two independent studies) and Lecce.

4. Conclusions

Our review based on 19 independent studies in 9 sites in Italy gives an insight on the spatial and seasonal variations of PM redox activity across the peninsula. The reviewed papers are based on the most common acellular assays, including the DTT, AA, GSH, and DCFH, for the simple, fast, and reliable measurement of OP. However, care should be taken when comparing OP results from different studies, as they often use varying operative protocols, since a unique standard method is still lacking. Future work should be needed to optimize and standardize the operative conditions of each OP acellular assay in order to provide consistent data for comparison between data of different locations and times.

The study supports the current literature highlighting that most OP assays respond to metals, mainly associated with vehicle traffic emission, and also to organics, from sources like biomass burning. In addition, DTT assay is especially sensitive to photochemically aged organics, as found in the Po Plain during winter. Inside a general similarity among different investigated sites, the OP$^{DTT}_V$ and OP$^{AA}_V$ responses show some differences, in particular between Northern and Southern regions. They may be explained by variation in PM chemical composition, as consequence of the different impact of emission sources and atmospheric conditions. However, to date, only a limited number of Italian locations has been investigated for OP: Further studies should to be continued in order to homogeneously cover the different geographical areas across the Italian peninsula.

Although the conclusions reached in this review are based on limited available studies, they clearly confirm that OP is a multipollutant parameter, that integrates the composition effects into just one measurement, rather than speciation of individual components requiring a suite of instrumental measurements. As OP captures the redox active components and sources that can be related to health end points, it can be used as predictor of adverse health impacts associated with an oxidative stress mechanism. Though the promising results for understanding what chemical species

and interactions drive OP, further investigations are needed for determining the underlying mechanism of the adverse health outcomes associated with PM exposure.

Author Contributions: The contribution of the authors is summarized as follows: Conceptualization, M.C.P., data curation, M.R. and E.Z.; writing—original draft, M.C.P.; writing—review and editing, M.R.

Funding: This research received no external funding.

Acknowledgments: This review was written to be presented at the International Workshop "PM Oxidative Potential: response of acellular assays to predict PM-induced oxidative stress activity" held in Ferrara on 3 July 2019. The Authors acknowledge the Italian Aerosol Society for organizing and financially supporting the Workshop.

Conflicts of Interest: The authors declare no conflict of interest.

References

1. Abrams, J.Y.; Weber, R.J.; Klein, M.; Samat, S.E.; Chang, H.H.; Strickland, M.J.; Verma, V.; Fang, T.; Bates, J.T.; Mulholland, J.A.; et al. Associations between Ambient Fine Particulate Oxidative Potential and Cardiorespiratory Emergency Department Visits. *Environ. Health Perspect.* **2017**, *5*, 10.
2. Antinolo, M.; Willis, M.D.; Zhou, S.; Abbatt, J.P.D. Connecting the oxidation of soot to its redox cycling abilities. *Nat. Commum.* **2015**, *6*, 68.
3. Crobeddu, B.; Aragao-Santiago, L.; Bui, L.C.; Boland, S.; Baeza Squiban, A. Oxidative potential of particulate matter 2.5 as predictive indicator of cellular stress. *Environ. Pollut.* **2017**, *230*, 5–133.
4. Janssen, N.A.H.; Strak, M.; Yang, A.; Hellack, B.; Kelly, F.J.; Kuhlbusch, T.A.J.; Harrison, R.M.; Brunekreef, B.; Cassee, F.R.; Steenhof, M.; et al. Associations between three specific a-cellular measures of the oxidative potential of particulate matter and markers of acute airway and nasal inflammation in healthy volunteers. *Occup. Environ. Med.* **2015**, *72*, 49–56.
5. Mittal, M.; Siddiqui, M.R.; Tran, K.; Reddy, S.P.; Malik, A.B. Reactive oxygen species in inflammation and tissue injury. *Antioxid. Redox Signal.* **2014**, *20*, 16–1167.
6. Saffari, A.; Daher, N.; Shafer, M.M.; Schauer, J.J.; Sioutas, C. Global Perspective on the Oxidative Potential of Airborne Particulate Matter: A Synthesis of Research Findings. *Environ. Sci. Technol.* **2014**, *48*, 7576–7583.
7. Strak, M.; Janssen, N.A.H.; Godri, K.J.; Gosens, I.; Mudway, I.S.; Cassee, F.R.; Lebret, E.; Kelly, F.J.; Harrison, R.M.; Brunekreef, B.; et al. Respiratory Health Effects of Airborne Particulate Matter: The Role of Particle Size, Composition, and Oxidative Potential-The RAPTES Project. *Environ. Health Perspect.* **2012**, *120*, 1183–1189.
8. Bates, J.T.; Fang, T.; Verma, V.; Zeng, L.; Weber, R.J.; Tolbert, P.E.; Abrams, J.; Sarnat, S.E.; Klein, M.; Mulholland, J.A.; et al. Review of acellular assays of ambient particulate matter oxidative potential: Methods and relationships with composition, sources, and health effects. *Environ. Sci. Technol.* **2019**, *53*, 4003–4019.
9. Delfino, R.J.; Staimer, N.; Tjoa, T.; Gillen, D.L.; Schauer, J.J.; Shafer, M.M. Airway inflammation and oxidative potential of air pollutant particles in a pediatric asthma panel. *J. Expo. Sci. Environ. Epidemiol.* **2013**, *23*, 466–473.
10. Sauvain, J.; Rossi, M.J.; Riediker, M. Comparison of three acellular tests for assessing the oxidation potential of nanomaterials. *Aerosol Sci. Technol.* **2013**, *47*, 218–227.
11. Spagnolo, A.M.; Ottria, G.; Perdelli, F.; Cristina, M.L. Chemical Characterization of the Coarse and Fine Particulate Matter in the Environment of an Underground Railway System: Cytotoxic Effects and Oxidative Stress—A Preliminary Study. *Int. J. Environ. Res. Public Health* **2015**, *12*, 4031–4046.
12. Jiang, H.; Ahmed, C.M.S.; Canchola, A.; Chen, J.Y.; Lin, Y.-H. Use of Dithiothreitol Assay to Evaluate the Oxidative Potential of Atmospheric Aerosols. *Atmosphere* **2019**, *10*, 571.
13. Fang, T.; Verma, V.; Bates, J.T.; Abrams, J.; Klein, M.; Strickland, M.J.; Sarnat, S.E.; Chang, H.H.; Mulholland, J.A.; Tolbert, P.E.; et al. Oxidative potential of ambient water-soluble PM2.5 in the southeastern United States: Contrasts in sources and health associations between ascorbic acid (AA) and dithiothreitol (DTT) assays. *Atmos. Chem. Phys.* **2016**, *16*, 3865–3879.
14. Hedayat, F.; Stevanovic, S.; Miljevic, B.; Bottle, S.; Ristovski, Z.D. Review—Evaluating the molecular assays for measuring the oxidative potential of particulate matter. *Chem. Ind. Chem. Eng. Q.* **2015**, *21*, 201–210.

15. Hellack, B.; Nickel, C.; Albrecht, C.; Kuhlbusch, T.A.J.; Boland, S.; Baeza-Squiban, A.; Wohlleben, W.; Schins, R.P.F. Analytical methods to assess the oxidative potential of nanoparticles: A review. *Environ. Sci. Nano* **2017**, *4*, 1920–1926.
16. Shafer, M.M.; Hemming, J.D.C.; Antkiewicz, D.S.; Schauer, J.J. Oxidative potential of size-fractionated atmospheric aerosol in urban and rural sites across Europe. *Faraday Discuss.* **2016**, *189*, 381–405.
17. Szigeti, T.; Dunster, C.; Cattaneo, A.; Cavallo, D.; Spinazzè, A.; Saraga, D.E.; Sakellaris, I.A.; de Kluizenaar, Y.; Cornelissen, E.J.M.; Hänninen, O.; et al. Oxidative potential and chemical composition of PM2.5 in office buildings across Europe—The OFFICAIR study. *Environ. Int.* **2016**, *92–93*, 324–333.
18. Visentin, M.; Pagnoni, A.; Sarti, E.; Pietrogrande, M.C. Urban PM2.5 oxidative potential: Importance of chemical species and comparison of two spectrophotometric cell-free assays. *Environ. Pollut.* **2016**, *219*, 72–79.
19. Gulliver, J.; Morley, D.; Dunster, C.; McCrea, A.; van Nunen, E.; Tsai, M.-Y.; Probst-Hensch, N.; Eeftens, M.; Imboden, M.; Ducret-Stich, R.; et al. Land use regression models for the oxidative potential of fine particles ($PM_{2.5}$) in five European areas. *Environ. Res.* **2018**, *160*, 247–255.
20. Jedynska, A.; Hoek, G.; Wang, M.; Yang, A.; Eeftens, M.; Cyrys, J.; Keuken, M.; Ampe, C.; Beelen, R.; Cesaroni, G.; et al. Spatial variations and development of land use regression models of oxidative potential in ten European study areas. *Atmos. Environ.* **2017**, *150*, 24–32.
21. Costabile, F.; Alas, H.; Aufderheide, M.; Avino, P.; Amato, F.; Argentini, S.; Barnaba, F.; Berico, M.; Bernardoni, V.; Biondi, R.; et al. First Results of the "Carbonaceous Aerosol in Rome and Environs (CARE)" Experiment: Beyond Current Standards for PM_{10}. *Atmosphere* **2017**, *8*, 249.
22. Sandrini, S.; Fuzzi, S.; Piazzalunga, A.; Prati, P.; Bonasoni, P.; Cavalli, F.; Bove, M.C.; Calvello, M.; Cappelletti, D.; Colombi, C.; et al. Spatial and seasonal variability of carbonaceous aerosol across Italy. *Atmos. Environ.* **2014**, *99*, 587–598.
23. Pietrogrande, M.C.; Dalpiaz, C.; Dell'Anna, R.; Lazzeri, P.; Manarini, F.; Visentin, M.; Toninandel, G. Chemical composition and oxidative potential of atmospheric coarse particles at an industrial and urban background site in the alpine region of northern Italy. *Atmos. Environ.* **2018**, *191*, 340–350.
24. Perrone, M.R.; Bertoli, I.; Romano, S.; Russo, M.; Rispoli, G.; Pietrogrande, M.C. $PM_{2.5}$ and PM_{10} oxidative potential at a Central Mediterranean Site: Contrasts between dithiothreitol—And ascorbic acid—Measured values in relation with particle size and chemical composition. *Atmos. Environ.* **2019**, *210*, 143–155.
25. Simonetti, G.; Conte, E.; Perrino, C.; Canepari, S. Oxidative potential of size-segregated PM in an urban and an industrial area of Italy. *Atmos. Environ.* **2018**, *187*, 292–300.
26. Simonetti, G.; Conte, E.; Massimi, L.; Frasca, D.; Perrino, C.; Canepari, S. Oxidative potential of particulate matter components generated by specific emission sources. *Atmos. Environ.* **2018**, *6*, 99–109.
27. Chirizzi, D.; Cesari, D.; Guascito, M.R.; Dinoi, A.; Giotta, L.; Donateo, A.; Contini, D. Influence of Saharan dust outbreaks and carbon content on oxidative potential of water-soluble fractions of $PM_{2.5}$ and PM_{10}. *Atmos. Environ.* **2017**, *163*, 1–8.
28. Perrone, M.G.; Zhou, J.; Malandrino, M.; Sangiorgi, G.; Rizzi, C.; Ferrero, L.; Dommen, J.; Bolzacchini, E. PM chemical composition and oxidative potential of the soluble fraction of particles at two sites in the urban area of Milan, Northern Italy. *Atmos. Environ.* **2016**, *8*, 104–113.
29. Ciriello, F.; Gualtieri, M.; Longhin, E.; Ruffo, R.; Camatini, M.; Parenti, P. A new method and tool for detection and quantification of PM oxidative potential. *Environ. Sci. Pollut. Res.* **2015**, *22*, 469–478.
30. Pietrogrande, M.C.; Bertoli, I.; Manarini, F.; Russo, M. Ascorbate assay as a measure of oxidative potential for ambient particles: Evidence for the importance of cell-free surrogate lung fluid composition. *Atmos. Environ.* **2019**, *211*, 103–112.
31. Künzli, N.; Mudway, I.S.; Götschi, T.; Shi, T.; Kelly, F.J.; Cook, S.; Burney, P.; Forsberg, B.; Gauderman, J.W.; Hazenkamp, M.E.; et al. Comparison of oxidative Properties, Light Absorbance, and Total and Elemental Mass Concentration of Ambient PM2.5 Collected at 20 European Sites. *Environ. Health Perspect.* **2006**, *114*, 684–690.
32. Mihucz, V.G.; Szigeti, T.; Dunster, C.; Giannoni, M.; de Kluizenaar, Y.; Cattaneo, A.; Mandin, C.; Bartzis, J.G.; Lucarelli, F.; Kelly, F.J.; et al. An integrated approach for the chemical characterization and oxidative potential assessment of indoor $PM_{2.5}$. *Microchem. J.* **2015**, *119*, 22–29.

33. Conte, E.; Canepari, S.; Frasca, D.; Simonetti, G. Oxidative Potential of Selected PM Components. In Proceedings of the 2nd International Electronic Conference on Atmospheric Sciences, Basel, Switzerland, 16–31 July 2017; Volume 2, doi:10.3390/ecas2017-04131.
34. Pietrogrande, M.C.; Perrone, M.R.; Manarini, F.; Romano, S.; Udisti, R.; Becagli, S. PM_{10} oxidative potential at a Central Mediterranean Site: Association with chemical composition and meteorological parameters. *Atmos. Environ.* **2018**, *188*, 97–111.
35. Daher, N.; Ruprecht, A.; Invernizzi, G.; De Marco, C.; Miller-Schulze, J.; Heo, J.B.; Shafer, M.M.; Shelton, B.R.; Schauer, J.J.; Sioutas, C. Characterization, sources and redox activity of fine and coarse particulate matter in Milan, Italy. *Atmos. Environ.* **2012**, *49*, 130–141.
36. Calas, A.; Uzu, G.; Martins, J.M.F.; Voisin, D.; Spadini, L.; Lacroix, T.; Jaffrezo, J.L. The importance of simulated lung fluid (SLF) extractions for a more relevant evaluation of the oxidative potential of particulate matter. *Sci. Rep.* **2017**, *7*, 2045–2322.
37. Fang, T.; Verma, V.; Guo, H.; King, L.E.; Edgerton, E.S.; Weber, R.J. A semi-automated system for quantifying the oxidative potential of ambient particles in aqueous extracts using the dithiothreitol (DTT) assay: Results from the Southeastern Center for Air Pollution and Epidemiology (SCAPE). *Atmos. Meas. Tech.* **2015**, *8*, 471–482.
38. Park, J.; Park, E.H.; Schauer, J.J.; Yi, S.-M.; Heo, J. Reactive oxygen species (ROS) activity of ambient fine particles ($PM_{2.5}$) measured in Seoul, Korea. *Environ. Int.* **2018**, *117*, 276–283.
39. Grigoratos, T.; Martini, G. Brake wear particle emissions: A review. *Environ. Sci. Pollut. Res.* **2015**, *22*, 2491–2504.
40. Lyu, Y.; Guo, H.; Cheng, T.; Li, X. Particle size distributions of oxidative potential of lung-deposited particles: Assessing contributions from quinones and water-soluble metals. *Environ. Sci. Technol.* **2018**, *52*, 6592–6600.
41. Shuster-Meiseles, T.; Shafer, M.M.; Heo, J.; Pardo, M.; Antkiewicz, D.S.; Schauer, J.J.; Rudich, A.; Rudich, Y. ROS-generating/ARE-activating capacity of metals in roadway particulate matter deposited in urban environment. *Environ. Res.* **2016**, *146*, 252–262.
42. Diapouli, E.; Manousakas, M.I.; Vratolis, S.; Vasilatou, V.; Pateraki, S.; Bairachtari, K.A.; Querol, X.; Amato, F.; Alastuey, A.; Karanasiou, A.A.; et al. AIRUSE-LIFE +: Estimation of natural source contributions to urban ambient air PM_{10} and PM2. 5 concentrations in southern Europe—Implications to compliance with limit values. *Atmos. Chem. Phys.* **2017**, *17*, 3673–3685.
43. Taghvae, S.; Sowlat, M.H.; Diapouli, E.; Manousakas, M.I.; Vasilatou, V.; Eleftheriadis, K.; Sioutas, C. Source apportionment of the oxidative potential of fine ambient particulate matter ($PM_{2.5}$) in Athens, Greece. *Sci. Total Environ.* **2019**, *653*, 1407–1416.
44. Charrier, J.C.; Anastasio, C. On dithiothreitol (DTT) as a measure of oxidative potential for ambient particles: Evidence for the importance of soluble transition metals. *Atmos. Chem. Phys.* **2012**, *20*, 9321–9333.
45. Samara, C. On the redox activity of urban aerosol particles: Implications for size distribution and relationships with organic aerosol components. *Atmosphere* **2017**, *8*, 205.
46. Bae, M.; Schauer, J.J.; Lee, T.; Jeong, J.; Kim, Y.; Ro, C.; Song, S.; Shon, Z. Relationship between reactive oxygen species and water-soluble organic compounds: Time-resolved benzene carboxylic acids measurement in the coastal area during the KORUS-AQ campaign. *Environ. Pollut.* **2017**, *231*, 1–12.
47. Decesari, S.; Sowlat, M.H.; Hasheminassab, S.; Sandrini, S.; Gilardoni, S.; Facchini, M.C.; Fuzzi, S.; Sioutas, C. Enhanced toxicity of aerosol in fog conditions in the Po Valley, Italy. *Atmos. Chem. Phys. Discuss.* **2017**, *17*, 7721–7731.
48. Jiang, H.H.; Jang, M.; Sabo-Attwood, T.; Robinson, S.E. Oxidative potential of secondary organic aerosols produced from photooxidation of different hydrocarbons using outdoor chamber under ambient sunlight. *Atmos. Environ.* **2016**, *131*, 382–389.
49. Tuet, W.Y.; Chen, Y.; Xu, L.; Fok, S.; Gao, D.; Weber, R.J.; Ng, N.L. Chemical oxidative potential of secondary organic aerosol (SOA) generated from the photooxidation of biogenic and anthropogenic volatile organic compounds. *Atmos. Chem. Phys.* **2017**, *17*, 839–853.
50. Velali, E.; Papachristou, E.; Pantazaki, A.; Choli-Papadopoulou, T.; Planou, S.; Kouras, A.; Manoli, E.; Besis, A.; Voutsa, D.; Samara, C. Redox activity and in vitro bioactivity of the water-soluble fraction of urban particulate matter in relation to particle size and chemical composition. *Environ. Pollut.* **2016**, *208*, 774–786.

51. Perrone, M.R.; Becagli, S.; Gracia Orza, J.A.; Vecchi, R.; Dinoi, A.; Udisti, R.; Cabello, M. The impact of long-range-transport on PM1 and PM2.5 at a Central Mediterranean site. *Atmos. Environ.* **2013**, *71*, 176–186.
52. Pietrogrande, M.C.; Bacco, D.; Ferrari, S.; Ricciardelli, I.; Scotto, F.; Trentini, A.; Visentin, M. Characteristics and major sources of carbonaceous aerosols in PM2.5 in Emilia Romagna Region (Northern Italy) from four-year observations. *Sci. Total Environ.* **2016**, *553*, 172–183.

Atmospheric Environment 221 (2020) 117085

Contents lists available at ScienceDirect

Atmospheric Environment

journal homepage: http://www.elsevier.com/locate/atmosenv

Ecotoxicity, genotoxicity, and oxidative potential tests of atmospheric PM10 particles

S. Romano [a,*], M.R. Perrone [a], S. Becagli [b], M.C. Pietrogrande [c], M. Russo [c], R. Caricato [d], M. G. Lionetto [d]

[a] Department of Mathematics and Physics, University of Salento, 73100, Lecce, Italy
[b] Department of Chemistry, University of Florence, 50019, Sesto Fiorentino, Florence, Italy
[c] Department of Chemical and Pharmaceutical Sciences, University of Ferrara, 44121, Ferrara, Italy
[d] Department of Biological and Environmental Sciences and Technologies, University of Salento, 73100, Lecce, Italy

HIGHLIGHTS

- Determination of ecotoxicity, genotoxicity, and oxidative potential of PM10 particles.
- Ecotoxicity and genotoxicity estimates by toxic unity and induction factor.
- Characterization of the PM10 chemical composition by about 30 chemical species.
- Chemical species driving ecotoxicity, genotoxicity and ROS activity in PM10 samples.
- The investigated toxicity tests contrasted in sensibility towards chemical species.

GRAPHICAL ABSTRACT

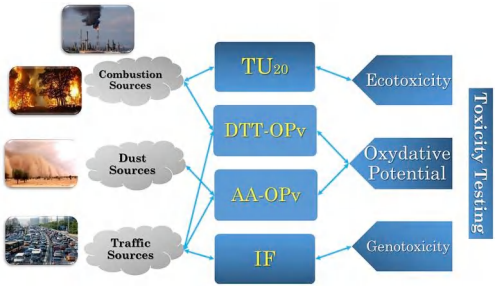

ARTICLE INFO

Keywords:
PM10
Vibrio fischeri
SOS chromotest
DTT assay
AA assay
Chemical composition

ABSTRACT

The aim of the present work was to investigate the likely toxicological impact of atmospheric PM10 particles by comparing different effect-based methodologies, namely the *Vibrio fischeri* bioluminescence inhibition bioassay to evaluate ecotoxicity, the SOS Chromotest assay to estimate genotoxicity, and the Dithiothreitol (DTT) and Ascorbic Acid (AA) acellular assays to assess oxidative potential. The chemical composition was characterized for about 30 species, to assess the potential health impact of specific chemical components. Atmospheric particles were collected from spring to summer at a coastal site of the Central Mediterranean, away from large sources of local pollution. The Toxicity Unit (TU) index, used to assess the ecotoxicity, showed that 33% of the samples were toxic. The Induction Factor (IF), generally used to assess particle's genotoxicity, varied from 0.3 to 1.5 that represents the threshold value for genotoxicity. The oxidative potential (OP) determined by the DTT and AA assay varied within the 4.9–34.5 and 4.8–140.6 nmol min^{-1} range, respectively. DTT-OP and TU values were significantly correlated with OC, EC, and nss-K^+, likely because the DTT and *Vibrio fischeri* responses were mainly associated with species from combustion sources. The IF factor was significantly correlated with some metals (Al, Ba, La, P, Sr, and Ti) likely from traffic sources and did not show any significant correlation with TU and OP values. Overall, paper's results proved the episodic occurrence of ecotoxicity and genotoxicity levels in PM10 particles sampled directly from their natural environment and away from strong pollution sources, highlighting

* Corresponding author.
E-mail address: salvatore.romano@unisalento.it (S. Romano).

https://doi.org/10.1016/j.atmosenv.2019.117085
Received 10 June 2019; Received in revised form 22 October 2019; Accepted 26 October 2019
Available online 31 October 2019

the role mainly of carbonaceous compounds and heavy metals. The impact of spurious correlations between DTT- and AA-OP_V and chemical species concentration has also been addressed.

1. Introduction

The atmospheric particulate matter (PM) consists of a complex mixture of substances and chemical compounds of natural and/or anthropogenic origin (e.g., Seinfeld and Pandis, 1998; Dulac and Hamonou, 2016). The PM10 fraction is widely used as air quality indicator (CEC, 2008). However, one must be aware that the chemical composition of these particles, and the associated toxicity, genotoxicity, and adverse health effects may significantly vary with sampling location, meteorological conditions, and long-range transported contributions (e.g., Roig et al., 2013; Pinter et al., 2017; Perrone et al., 2019a).

Toxicity testing using different biological systems, from cultured cells to test organisms, has advanced in recent years (Roig et al., 2013; Yang et al., 2016; Aammi et al., 2017; Abbas et al., 2018). Toxicity refers to the degree to which a substance can cause a negative effect on a living organism at biochemical, physiological or behavioural level (Lionetto et al., 2019). Toxicity testing provides useful information about the biological effects of chemical pollutants (single and in mixture) and their bioavailability, complementing in this way physical-chemical analyses of environmental matrices. Therefore, the requirement for an integrated chemical and biological approach in environmental monitoring has receiving growing attention. Great effort has been directed, in the last decades, toward developing *in vitro* alternatives to *in vivo* tests as a first step of toxicity analysis. Tissue culture assays are currently the most popular *in vitro* tests for evaluating acute toxicity. However, there is a great political intention to reduce animal experiments and replace them with alternatives. Currently, the bioassays using natural bioluminescent bacteria such as *Vibrio fischeri*, *Vibrio harveyi*, *Pseudomonas fluorescens*, and *Pseudomonas leiognathi* have widely been used for testing ecotoxicity, namely the potential toxicity level to which a toxic substance may affect biota in the environment (Girotti et al., 2008). Abbas et al. (2018) have recently overviewed the *V. fischeri* bioluminescence inhibition assay (Microtox® test) for ecotoxicity assessment, elucidating the biochemical and genetic basis of the bacterial bioluminescence and its regulatory mechanism. The natural bioluminescence is directly related to the respiratory activity of the bacteria and, therefore, it represents a good marker of the bacterial metabolic activity. The test responds to a wide range of chemicals (including organic and inorganic compounds) and is applicable to a broad array of matrices (pure compounds, metals, wastewater, river water, sewage sludge, landfill leachate, herbicides, treated wastewater, etc.). Only a limited number of studies exists in literature on the application of the *V. fischeri* assay to atmospheric particles sampled directly from their natural environment (Abbas et al., 2018). Commercialized as Microtox ® test, the *V. fischeri* bioluminescent inhibition assay has been widely used for assessing the toxicity of various contaminants in liquid and solid samples.

A number of studies have demonstrated a significant correlation between *in vivo* or *in vitro* toxicity tests using mammalian cells and *in vitro* test using *Vibrio fischeri* (Burton et al., 1986; Bruner et al., 1991; Bulich et al., 1990; Nałecz-Jawecki et al., 1997; Fort, 1992). The *V. fischeri* appeared to be more sensitive than the mammalian tissue culture assays for a number of tests and displayed few false negatives compared to standard toxicity tests (Burton et al., 1986; Bulich et al., 1990). Roig et al. (2013) used the Microtox ® assay to assess the toxicity of PM10 samples collected in various areas of Catalonia (Spain). They found that the *Vibrio fischeri* method, compared with *in vitro* toxicity tests based on the use of the human lung cell line A549, showed a better correlation with PM pollutants. Then, the authors proposed the *Vibrio fischeri* test as an excellent screening test for a first evaluation of the quality of air and able to provide indication on possible adverse effects on living organisms including humans. Chang et al. (2013) used the Microtox ® assay to evaluate the toxicity of fly ash samples. Aqueous extracts of coarse PM samples collected at several sites of Istanbul (Turkey) were instead analyzed with the *V. fischeri* Microtox ® by Aammi et al. (2017).

A number of studies has also shown that atmospheric particles are a reservoir of genotoxic chemicals because of the ability of both organic and metallic components of the PM to react with the cell genetic material causing changes and alterations (e.g., Dhawan et al., 2009; Traversi et al., 2015; Aammi et al., 2017). Among the organic components, polycyclic aromatic hydrocarbons and their nitro-, chloro- and oxy-derivatives have generally considered the most genotoxic species (Claxton et al., 2004). The DNA alterations due to the PM exposure can cause increased levels of DNA strand breaks, oxidative base damage, DNA adducts formation, and increased mutation frequency and genetic rearrangement (André et al., 2011; Lepers et al., 2013). The Comet and the SOS chromotest assays represent two reliable tools for the assessment of the DNA damage of environmental mixtures according to Dhawan et al. (2009) and Aammi et al. (2017). Therefore, in order to properly investigate the likely impact of PM on the health, toxicity testing should be deepened with the analysis of the genotoxicity of the airborne particulate (Aammi et al., 2017).

Although the mechanisms of PM-associated toxicity are still not fully understood, there is an increasing scientific consensus on pathophysiological mechanisms involving the production of reactive oxygen species (ROS). In fact, they can activate a number of redox sensitive pathways, triggering a cascade of events associated with inflammation and potential cell apoptosis (e.g., Antiñolo et al., 2015; Crobeddu et al., 2017; Ghio et al., 2012; Piao et al., 2018; Quintana et al., 2015; Shiraiwa et al., 2012; Verma et al., 2015). Therefore, the oxidative potential (OP), defined as the capacity of PM to cause damaging oxidative reactions, has been suggested as an additional PM indicator that would encompass the PM toxicological response (Ayres et al., 2008; Hedayat et al., 2015; Janssen et al., 2015; Pietrogrande et al., 2018a). Among the several assays developed to quantify PM OP, abiotic and cell free methods are chemical assays that measure OP as the capacity of the PM components to oxidize biologically relevant chemicals in operative conditions simulating the PM-cell interactions. They are most commonly used, since they have the advantages of requiring less controlled variability factors with respect to cellular assays and providing faster readouts (Bates et al., 2019; Calas et al., 2018; Fang et al., 2016; Hedayat et al., 2015; Hellack et al., 2017; Janssen et al., 2015). They are based on the consumption of endogenously antioxidants, such as ascorbic acid (AA, Crobeddu et al., 2017; Mudway et al., 2004) or surrogates for the cellular oxidant NADPH, e.g., dithiothreitol (DTT assay, Charrier and Anastasio, 2012). An extended study on the OP by the AA and DTT assays applied to PM10 particles collected at the monitoring site of this study has been reported in Pietrogrande et al. (2018b). They showed that the DTT- and AA-OP responses were very similar in the mean values and variability range, but differed in the association with PM10 chemical composition, as well as in seasonality of such association. Consequently, it is important to test different assays to better identify/quantify the PM potentiality to induce oxidative stress.

The present work aimed to evaluate the ecotoxicity, genotoxicity, and ability to generate ROS of airborne PM10 particles collected from their natural environment, at a costal site of the Central Mediterranean, away from large pollution sources. Nevertheless, one must be aware that, due to the specificities of the Mediterranean region (sunny, hot and dry climate mainly in spring-summer; long-range transport converging over the basin), air pollution in reactive compounds over the Mediterranean is often higher than in most European inland regions, according to Dulac and Hamonou (2016). Reactive gases are very diverse and

include surface ozone (O_3), carbon monoxide (CO), volatile organic compounds (VOCs), oxidized nitrogen compounds (NO_x, NO_y), and sulphur dioxide (SO_2). All of these compounds play a major role in the chemistry of the atmosphere and as such are heavily involved in inter-relations between atmospheric chemistry and climate, either through control of ozone and the oxidizing capacity of the atmosphere, or through the formation of aerosols (https://www.wmo.int/pages/prog/arep/gaw/reactive_gases.html). The dominant airflow over the Mediterranean basin in summertime is driven from north to south; therefore, the basin is exposed to air masses coming from European cities and industrialized areas. Consequently, transported pollution and local anthropogenic and biogenic activity can result in high loadings of atmospheric gases, particles and complex chemistry (Lelieveld et al., 2002; Zannoni et al., 2017). The total OH reactivity was investigated by Zannoni et al. (2017) at a coastal receptor site in the western Mediterranean Basin to evaluate the completeness of the measurements of reactive trace gases.

Even if several studies have been published on the chemical composition of the Mediterranean PM (e.g., Pandolfi et al., 2011; Mailler et al., 2016; Becagli et al., 2017), rather few studies are available on measurements of its ecotoxicity, genotoxicity, and ability to generate ROS, to the best of our knowledge.

The toxicity assessment of PM10 samples was performed by the *V. fischeri* Microtox assay and the analysis was deepened by the study of their genotoxicity, through the SOS Chromotest, a bacterial test based on a genetically engineered *Escherichia coli* strain. Then, the AA and DTT assays were applied to determine corresponding OP values. The study focused on aqueous extracts of sampled airborne PM. The choice of aqueous extracts arises from the need to resemble the physiological bioavailability conditions of chemical pollutants at the level of respiratory epithelium, where the apical side of the epithelial cells is entirely covered by a thin fluid layer. Any chemical pollutant present in the inspired air needs to be dissolved in this thin aqueous film before absorption by epithelial cells.

The relationships between ecotoxicity and genotoxicity levels, DTT- and AA-OP values and chemical composition of the airborne PM10 particles have also been investigated to contribute to the understanding of the variety of adverse health impacts of atmospheric aerosols.

2. Experimental and analytical methods

2.1. Site description and PM sampling

The study site is located in a suburban area (40.3°N; 18.1°E) of the flat Salento's peninsula, in the Central Mediterranean. More specifically, the PM sampler was located at the Mathematics and Physics Department of the University of Salento (~10 m above ground level). Sampling was performed with a (2.3 $m^3 h^{-1}$) HYDRA-FAI dual-sampler that allowed the simultaneous collection of PM10 particles on two 47-mm-diameter quartz filters (PALLFLEX, Tissuquartz), pre-heated for 1 h at 700 °C, using two independent sampling lines. The preheated filters were conditioned for 48 h (25 °C and 50% relative humidity) before and after sampling and the PM mass concentrations were determined by the gravimetric measurements of the filters before and after sampling. Uncertainties on mass concentrations were lower than 5%. In total, 16 samples were collected from May to July 2017 by performing 24- or 48-h samplings. One of the two PM10 loaded filters was divided in four punches for the determination of inorganic ions and methanesulfonate, metals, organic and elemental carbon, and the oxidative potential. The other PM10 filter was used for Microtox bioassay and SOS Chromotest analyses.

2.2. Ions, metals, and organic and elemental carbon analyses

Loaded as well as blank PM10 filters were subjected to different analyses to characterize their chemical composition by using the methods described in detail in Perrone et al. (2014) and Pietrogrande et al. (2018a, 2019). In particular, anions (Cl^-, NO_2^-, NO_3^-, SO_4^{2-}, MSA^-, oxalate, and glycolate) and cations (Na^+, NH_4^+, K^+, Mg^{2+}, Ca^{2+}) mass concentrations were determined by a Flow Analysis Ion Chromatography (FA-IC). An Inductively Coupled Plasma Atomic Emission Spectrometer was used to determine the mass concentration of Al, Ba, Cd, Cu, Fe, La, Mn, Ni, P, Pb, Sr, Ti, and V (Becagli et al., 2017). The Sunset Carbon Analyzer Instrument with the EUSAAR-2 temperature program protocol (Cavalli et al., 2010) was used to determine the organic and elemental carbon (OC and EC, respectively) mass concentrations.

2.3. Assessment of the PM oxidative potential

The oxidative potential of the collected PM10 samples was assessed with the DTT (DTT-OP) and AA (AA-OP) acellular methods. The OP response was measured as the antioxidant depletion rate of known quantity of DTT and AA, following the experimental procedure described in Pietrogrande et al. (2018a, 2018b). In particular, both the assays were performed on 3 mL of the aqueous extract of a quarter of the sampled filters (extracted for 15 min in an ultrasonic bath using 10 mL of 0.1 M buffer at pH 7.4). The extract was filtered on a regenerate cellulose syringe filter (13 mm, 0.22 μm, Kinesis) to remove the suspended solid particles and then introduced into an amber vial at a constant temperature of 37 °C using a dry bath. The DTT and AA depletion rates (in nmol min^{-1}) were determined by linear fitting of five experimental points of the reagents concentration versus time (5, 10, 15, 25, and 40 min) plot. In general, a good linearity of the concentration-time relationship was found with correlation coefficient $R \geq 0.98$ (Visentin et al., 2016). For both methods, the laboratory blank filter response was determined by measuring the depletion rates of DTT or AA on the extract of a quarter of blank quartz filters. Sample and blank assays were run in duplicate. The average filter blank responses were subtracted from the depletion rates of the collected PM samples.

2.4. Ecotoxicity testing by the Microtox® assay

The Microtox® Model 500 (M500) analyzer (Azur Environmental) was used for measuring the ecotoxicity of PM10 particles. Freezed dried luminescent bacteria were reconstituted before use. The salinity of the sample was osmotically adjusted to the NaCl content of 2%. The test was performed according to the manufacturer's operational procedure (Microtox manual, 1995) on aqueous extracts of quartz filters. The extraction procedure was performed for 80 min in an ultrasonic bath using 8 ml of ultrapure water (SIGMA, W4502). The toxicity of the samples was firstly evaluated by the bioluminescence inhibition percentage:

$$\%\text{Inhibition} = 100 \cdot (Io - It)/Io \quad (1)$$

where *Io* is the initial bacterial luminescence and *It* is the luminescence after exposure of the bacterial suspension to the extract. In particular, the %Inhibition was evaluated after 5, 15, and 30 min of exposure of the bacteria to serial dilutions of the extracts. The %Inhibition values were corrected using the value measured for the blank sample (aqueous extract prepared from a cleaned filter). A standard phenol solution (100 mg/l in water) was used to confirm the test protocol. Then, the percentages of sample concentration causing 20% (EC_{20}) and 50% (EC_{50}) of light inhibition on the test organisms were calculated to estimate the sample ecotoxicity. More specifically, EC_{20} and EC_{50} values were calculated from the regression analysis of the concentration-effect curves on serial dilutions (6.25%, 12.5%, 25%, 50%, and 100%) of the extracts. EC values decrease with the increase of the sample toxicity. More specifically, the EC_{20} and EC_{50} values were calculated for non-hormetic samples utilizing the 30 min exposure values and were transformed in Toxicity Units (TU), which are defined as follows (Aammi et al., 2017):

$$TU_{20} = 100\% / EC_{20} \quad (2)$$

$$TU_{50} = 100\% / EC_{50} \quad (3)$$

TU is unitless and its value increases with the sample ecotoxicity. Samples with $TU_{50} < 1$ are considered non toxic, while samples with $1 < TU_{50} < 10$ are considered toxic, according to Kahru et al. (2000). Very toxic and extremely toxic samples are characterized by TU_{50} values varying within the 10–100 range and $TU_{50} > 100$, respectively.

2.5. Genotoxicity by SOS chromotest ® assay

The PM10 genotoxicity effects were evaluated by means of the SOS Chromotest ®, a bacterial test based on a genetically engineered *Escherichia coli* (strain PQ37). The test is based on the measurement of the ability of bacterial cells in repairing DNA damages induced by contaminants by the induction of the SOS repair system. The SOS system of this *E. coli* strain is linked to lacZ, the reporter gene encoding a β-galactosidase (β-gal), used for genotoxicity activity quantification. The parallel measure of the activity of alkaline phosphatase (AP) was used for the assessment of bacterial survival. The test was performed according to methodologies previously validated by Quillardet and Hofnung (1985) using EBPI SOS-ChromoTest™ kit. Serial dilutions of the extracts were dissolved in DMSO and used for the assay. 4-Nitroquinoline-N-oxide was used as a positive genotoxic standard to test the validity of the assay. Genotoxicity activity was expressed as Induction Factor (IF) and calculated as follows:

$$IF = R(c)/Ro \quad (4)$$

where $R(c) =$ β-gal/AP with β-gal expressing the β-galactosidase activity at a given concentration c of the tested sample and AP indicating alkaline phosphatase activity, while Ro represents the same ratio measured for a blank sample. IF values > 1.5 are considered genotoxic according to Quillardet and Hofnung (1985). More specifically, samples are marginally genotoxic if the IF ranges between 1.5 and 2, while they are strongly genotoxic for IF > 2 (Aammi et al., 2017).

3. Results and discussion

3.1. PM10 mass concentration and chemical composition results

Sampling date and time of the 16 collected PM10 samples are reported in Table S1 of the Supplementary Information (SI) file, in addition to corresponding PM10 and chemical species mass concentrations, and volumes of the sampled air. Table 1 reports the statistics for the measured parameters, including means, standard deviations (SD), medians, 25th and 75th percentiles, minima and maxima values, skewness, and data representativeness (REPR). The K^+, Mg^{2+}, Ca^{2+}, and SO_4^{2-} mass concentrations have been split into sea-salt (ss-) and non-sea-salt (nss-) mass concentrations to infer the corresponding anthropogenic contributions. Assuming that all measured Na^+ ions were of marine origin, the sea salt contribution to K^+, Mg^{2+}, Ca^{2+}, and SO_4^{2-} was estimated as measured Na^+ times 0.038, 0.119, 0.038, and 0.242, respectively (Pio et al., 2007). Then, the nss-mass concentrations were calculated by subtracting the ss-contribution to their corresponding total mass concentration. With the exception of nss-Mg^{2+}, La, Mn, and P, all parameters showed mean values larger than the corresponding median values and, therefore, were characterized by positive skewness values spanning the 0.2–2.6 range, for which almost normal distributions (skewness

Table 1
Mean values of PM10 and chemical species mass concentration of the 16 analyzed samples with the corresponding standard deviation (SD), median, minimum and maximum values (Min and Max, respectively), 25th and 75th percentiles, skewness, and representativeness (REPR).

Parameters	Mean	SD	Median	Min	Max	Percentiles	75	Skewness	REPR
(μg m^{-3})						25			
PM10	25	7	25	13	41	21	29	1.35	0.70
OC	4.7	2.2	4.0	2.5	9.2	3.2	5.6	1.03	0.83
EC	1.3	0.6	1.3	0.6	2.5	0.7	1.7	0.34	0.73
Na^+	0.9	0.6	0.7	0.2	2.1	0.3	1.2	0.83	0.77
NH_4^+	0.8	0.3	0.8	0.3	1.5	0.6	1.0	0.77	0.82
K^+	0.35	0.20	0.30	0.16	0.96	0.21	0.39	2.05	0.70
ss-K^+	0.03	0.02	0.03	0.01	0.08	0.02	0.05	0.83	
nss-K^+	0.32	0.21	0.27	0.12	0.95	0.17	0.37	1.89	
Mg^{2+}	0.15	0.06	0.13	0.08	0.30	0.10	0.16	1.56	0.60
ss-Mg^{2+}	0.10	0.08	0.09	0.03	0.25	0.04	0.14	0.92	
nss-Mg^{2+}	0.05	0.03	0.05	0.01	0.08	0.03	0.07	−0.21	
Ca^{2+}	1.07	0.44	1.04	0.37	1.98	0.73	1.42	0.29	0.80
ss-Ca^{2+}	0.03	0.02	0.03	0.01	0.08	0.02	0.05	0.83	
nss-Ca^{2+}	1.04	0.43	1.02	0.33	1.96	0.72	1.34	0.30	
Cl^-	0.4	0.4	0.2	0.0	1.1	0.1	0.6	0.72	0.93
NO_3^-	1.1	0.6	0.9	0.2	2.5	0.7	1.3	1.10	0.93
SO_4^{2-}	3.8	0.7	3.7	2.7	4.7	3.1	4.5	0.04	0.72
ss-SO_4^{2-}	0.2	0.2	0.2	0.1	0.5	0.1	0.3	0.83	
nss-SO_4^{2-}	3.6	0.7	3.4	2.6	4.6	2.9	4.3	0.16	
Oxalates	0.23	0.08	0.22	0.09	0.39	0.14	0.30	0.19	
Glycolates	0.003	0.002	0.004	0.001	0.009	0.002	0.004	1.81	
MS^-	0.011	0.007	0.010	0.005	0.027	0.007	0.012	1.84	
Al	0.3	0.2	0.2	0.1	0.8	0.2	0.3	1.65	0.90
Ba	0.008	0.004	0.008	0.002	0.020	0.006	0.009	1.30	
Cd	0.0002	0.0001	0.0002	0.0001	0.0003	0.0001	0.0002	0.68	
Cu	0.009	0.006	0.007	0.004	0.027	0.006	0.010	2.41	0.83
Fe	0.3	0.1	0.3	0.1	0.6	0.2	0.4	0.06	0.88
La	0.0008	0.0003	0.0008	0.0003	0.0012	0.0010	0.0011	−0.17	
Mn	0.008	0.002	0.008	0.003	0.011	0.007	0.010	−0.59	0.83
Ni	0.002	0.001	0.002	0.001	0.005	0.002	0.003	2.02	
P	0.03	0.01	0.03	0.02	0.04	0.02	0.03	−1.13	
Pb	0.006	0.003	0.007	0.000	0.012	0.004	0.008	0.25	
Sr	0.003	0.001	0.003	0.002	0.007	0.002	0.004	1.27	
Ti	0.010	0.006	0.008	0.003	0.026	0.006	0.012	1.42	0.72
V	0.005	0.003	0.004	0.003	0.016	0.003	0.005	2.57	0.73

close to zero) were observed. The representativeness of PM10 and chemical species mass concentrations has been tested using the methodology proposed by Ganesan et al. (2016), which allowed calculating the representativeness parameter (denoted as REPR) reported in Table 1. REPR values close to zero indicate that the selected subset cannot represent the global dataset, while REPR values close to 1 indicate that subset and global dataset present a similar frequency distribution. We calculated REPR values by comparing the PM10 and chemical species dataset of this study, based on samples collected in spring-summer 2017, with those related to spring-summer 2012 (reported in Perrone et al., 2018) and spring-summer 2015 (reported in Perrone et al., 2019a, 2019b; Pietrogrande et al., 2018b). The REPR values calculated for the chemical species common to the three data sets (Table 1) were all larger than 0.70 (with the exception of Mg^{2+}) indicating that the analyzed PM10 and chemical species mass concentrations were all characterized by a high representativeness with respect to the selected global dataset. Therefore, we believe that the data set of this study can be considered as representative of the spring-summer PM10 particles at the study site.

Concerning organic components, OC and EC were the main components of PM10 because they totally accounted nearly 25% of the PM10 total mass. Fig. 1 shows the mass percentage contribution of the tested species in the 16 PM10 samples, where MET represents the mass percentage due to all metals (Al, Ba, Cd, Cu, Fe, La, Mn, Ni, P, Pb, Sr, Ti, and V), which varied within the 1.5–4.5% range. UM represents the undetermined mass percentage.

Although the small number of PM10 samples of this study prevents a source apportionment analysis, in order to describe the source contribution to the PM10 mass, we can use the main results on the sources identified by Positive Matrix Factorization (PMF) in a recent study concerning PM10 samples collected in the year 2015 at the same site of this work (Perrone et al., 2019a). The REPR values of Table 1 support the above hypothesis. A 6-factor PMF solution was considered to be the most reliable by Perrone et al. (2019a) and the apportionment of the resolved sources to the PM10 mass was in Spring-Summer (March–August) as follows: sulphate (27%), mixed anthropogenic source (26%), soil dust (25%), reacted dust (12%), sea-salt (7%), and heavy oil/secondary marine (2%). Note that the mixed anthropogenic source was characterized by the presence of markers from both traffic (e.g., EC, OC, Cu, Fe, Ba) and biomass burning (e.g., K^+, OC, EC). The reacted dust source had signatures from crustal particles mixed with secondary species like nitrate and sulphate, while the soil dust source showed soil related elements in high percentages (e.g., Al, Ca^{2+}, Sr, Ti, Fe).

3.2. Oxidative potential results

The DTT- and AA-OP responses were measured for 15 PM10 samples, since it was not possible to assess the OP response of sample S7 because of technical reasons. The oxidative potential (OP) determined by the DTT and AA assay varied within the 4.9–34.5 and 4.8–140.6 nmol min^{-1} range, respectively. Then, the OP depletion rate was normalized by the volume of sampled air (DTT-OP_V and AA-OP_V, expressed as nmol min^{-1} m^{-3}) as an exposure metrics accounting for inhaled air (Table S1 for each tested sample). Fig. 2a shows the DTT- and AA-OP_V responses for each sample, in addition to the corresponding PM10 mass concentration. The DTT- and AA-OP_V varied within the 0.05–0.33 and the 0.05–1.36 nmol min^{-1} m^{-3} range, respectively. The mean DTT- and AA-OP_V value ± SD, calculated by averaging the DTT- and AA-OP_V responses of the 15 PM10 samples, was equal to 0.17 ± 0.10 and 0.35 ± 0.34 nmol min^{-1} m^{-3}, respectively. These values are in good accordance, within ±SD, with the corresponding spring-summer mean values reported by Pietrogrande et al. (2018b, Table 2), which were equal to 0.22 ± 0.09 and 0.24 ± 0.19 nmol min^{-1} m^{-3} for the DTT- and AA-OP_V assay, respectively. These OP_V values were calculated from the DTT- and AA-OP_V responses of the 25 PM10 samples collected at the study site from May to October 2015. Therefore, the results of this study have furthermore shown that the study-site DTT- and AA-OP_V values are in the lower end of the typical ranges observed for ambient particles at other sites. In fact, values spanning the ~0.2–2 nmol min^{-1} m^{-3} and ~0.3–4 nmol min^{-1} m^{-3} for the DTT and AA assay, respectively, have been reported (Janssen et al., 2014; Perrone et al., 2016; Calas et al., 2018; Shafer et al., 2016; Szigeti et al., 2016; Weber et al., 2018). The particular location of the study site, which is in a suburban site of the flat Salento's peninsula, in the Central Mediterranean, away from large sources of local pollution, was likely responsible for these results, as discussed in Pietrogrande et al. (2018b) and Perrone et al. (2019a).

The role of chemical components on the oxidation activity assessed by both AA and DTT assay was firstly identified and apportioned by computing the linear regression between the OP responses and the detected species concentrations. Table S2 of the Supplementary Information file shows the Pearson's correlation coefficients r among all tested parameters. Significant r-values at p-level < 0.10, 0.05, and 0.01, for a two-tailed t-test, are marked in bold and with *, **, and ***, respectively. DTT-and AA-OP_V values were weakly correlated ($r = 0.52$) suggesting that DTT and AA assays can have different association with chemical species. In fact, DTT-OP_V showed significant positive correlation at p-level < 0.01 with OC, EC, NH_4^+, nss-K^+, nss-Mg^{2+}, and Cu. It

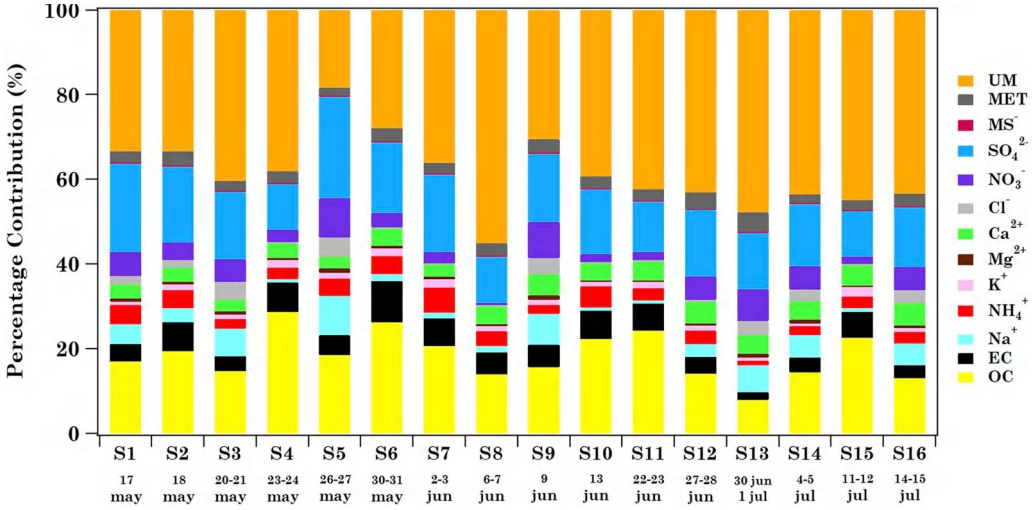

Fig. 1. Percentage contribution of all the tested chemical species in the 16 analyzed PM10 samples. OC and EC represent the organic and elemental carbon, respectively. MET and UM indicate all the sampled metals (Al, Ba, Cd, Ce, Co, Cr, Cu, Fe, La, Mn, Mo, Ni, P, Pb, Sr, Ti, V, and Zn) and the undetermined mass, respectively.

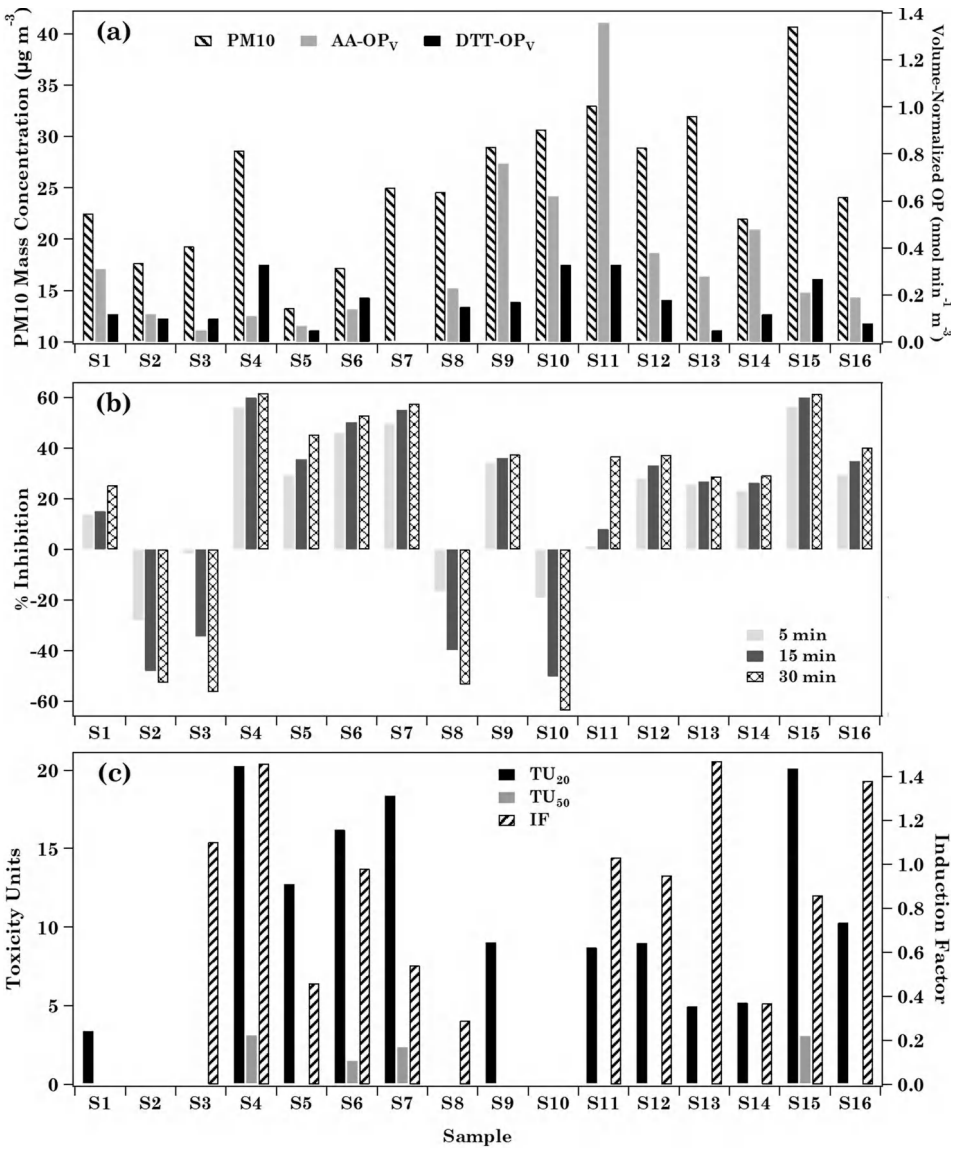

Fig. 2. (a) AA- and DTT-OP$_V$ (volume-normalized ascorbic acid- and dithiothreitol-oxidative potential, respectively) response as a function of the 16 analyzed samples, in addition to the corresponding PM10 mass concentration. (b) Percentage (%) of bioluminescence Inhibition from Microtox assay under 5, 15, and 30 min exposure time for the 16 tested samples. (c) Toxicity Units (TU$_{20}$) calculated from EC20 for the 16 tested samples (black bars). The TU$_{50}$ values (grey bars) are also reported when available. Marked bars represent the genotoxicity activity by the Induction Factor.

also showed significant positive correlation at p-level < 0.05 and 0.10 with nss-Ca^{2+}, and Glycolates, Mn, and P mass concentrations, respectively. Therefore, the contribution to DTT-OP$_V$ of primary carbon components and Cu in ambient PM10 samples was observed. In contrast, AA-OP$_V$ showed a strong (p-level < 0.01) and a weak (p-level < 0.10) correlation with Cu, and nss-Ca^{2+}, nss-SO_4^{2-}, Ba, and Mn mass concentrations, respectively, as shown in Table S2. The correlation of AA-OPv with Cu, and nss-Ca^{2+}, nss-SO_4^{2-}, Ba, and Mn may be mainly related to the soil dust source, which is driven either by the vehicular traffic (Bates et al., 2019; Pietrogrande et al., 2018a) and/or by the long-range transport of Saharan dust particles (e.g., Calzolai et al., 2015). The Pearson's correlation coefficients between AA- and DTT-OPv and the monitored chemical species are summarized in Table 2. The Spearman's rank correlation test, which is a non-parametric test generally used to measure the degree of association between two variables, was also used to further contribute to the assessment of redox active species. Correlation coefficients (ρ) from the Spearman's test are reported in brackets in Table 2 and one observes that they are in reasonable accordance with the corresponding Pearson's correlation coefficients. The correlation of AA-OPv with Oxalates, Fe, La, Ni, Sr, and V, which may be related to traffic sources (Lin et al., 2015), was also highlighted by the Spearman's ρ-values at the p-level < 0.10, in accordance with previous studies (Perrone et al., 2019b; Calas et al., 2018; Weber et al., 2018).

Table 2 shows that the DTT-OPv is negatively correlated with Na^+ and Cl^-, as it was found in Pietrogrande et al. (2018b) and Perrone et al. (2019b). The negative correlation between Na^+ and/or Cl^- and the main chemical species driving the DTT-OPv was likely responsible for these last results. Therefore, it is important looking for cross-correlations (Table S2) to better identify redox active species, as well as to explain contrasting results (Pietrogrande et al., 2018b; Perrone et al., 2019b). To further test the correlation between the analyzed chemical species and the oxidative potential and identify possible spurious correlations, we also calculated the corresponding partial correlation coefficients (r_P). In fact, a partial correlation coefficient measures the strength of a linear relationship between two variables after "adjusting" for the relationships involving all the other variables of a selected dataset (e.g., Freund et al., 2010; Ruiz et al., 2014). The partial correlation coefficients for DTT- and AA-OPv with the corresponding highly-correlated chemical species concentrations have been reported in Tables 3b–4b, respectively. These r_P values are also compared with the corresponding linear (Pearson's) correlation coefficients (r) extracted from Table S2 and reported in Tables 3a–4a to perform a proper comparison for DTT- and AA-OP$_V$, respectively. By comparing Tables 3a–3b, one can observe that DTT-OPv assumes a high partial correlation only with OC ($r_P = 0.88$)

Table 2
Relationships between volume-normalized AA- and DTT-OP_V (ascorbic acid- and dithiothreitol-oxidative potential), toxicity units TU_{20}, induction factor IF, and mass concentration of OC, EC, ions, and metals by means of the Pearson's correlation coefficient (r). The corresponding Spearman's correlation coefficient is reported in brackets. The number of samples (N), on which the statistics is based, is also reported in the table. Significant r-values at the p-level < 0.10, 0.05, and 0.01, according to the parametric two-tailed *t*-test (non-parametric rank correlation test in brackets), are marked in bold and with *, **, and ***, respectively.

Parameters		Oxidative Potential (N = 15)		Toxicity Units (N = 12)	Induction Factor (N = 12)
		AA-OP_V	DTT-OP_V	TU_{20}	IF
Chemical Species	OC	0.40 (0.37)	**0.92***** (**0.93*****)	**0.62**** (**0.54***)	0.20 (−0.01)
	EC	0.39 (0.34)	**0.92***** (**0.92*****)	**0.69**** (**0.54***)	0.04 (−0.11)
	Na^+	−0.05 (−0.15)	**−0.68***** (**-0.79*****)	**−0.65**** (−0.43)	0.25 (0.11)
	NH_4^+	0.32 (0.35)	**0.71***** (**0.71*****)	0.47 (0.36)	−0.27 (−0.31)
	nss-K^+	0.15 (0.22)	**0.70***** (**0.83*****)	**0.72***** (**0.65****)	0.08 (0.17)
	nss-Mg^{2+}	0.17 (0.26)	**0.76***** (**0.83*****)	**0.76***** (**0.68****)	−0.14 (−0.20)
	nss-Ca^{2+}	**0.50*** (**0.69*****)	**0.52**** (**0.50***)	0.03 (−0.10)	0.29 (0.21)
	Cl^-	−0.08 (−0.01)	**−0.68***** (**-0.70*****)	**−0.62**** (**-0.57***)	0.29 (0.41)
	NO_3^-	0.08 (0.13)	−0.43 (**-0.49***)	**−0.59**** (**-0.49***)	0.46 (0.38)
	nss-SO_4^{2-}	**0.48*** (**0.62****)	0.40 (0.38)	−0.10 (−0.15)	0.11 (0.16)
	Oxalates	0.30 (**0.48***)	0.30 (0.27)	0.22 (0.14)	0.33 (0.24)
	Glycolates	0.15 (0.40)	**0.49*** (0.40)	0.27 (−0.14)	0.17 (0.24)
	MS^-	0.25 (0.41)	−0.16 (−0.17)	−0.46 (**-0.51***)	−0.06 (0.17)
	Al	0.14 (0.43)	0.05 (0.31)	−0.19 (−0.06)	**0.49*** (0.44)
	Ba	**0.45*** (**0.51***)	0.37 (0.40)	0.01 (0.08)	**0.60**** (**0.50***)
	Cd	0.24 (0.23)	0.41 (**0.56****)	0.35 (0.31)	0.29 (0.39)
	Cu	**0.93***** (**0.66*****)	**0.69***** (**0.79*****)	−0.02 (0.25)	0.12 (0.03)
	Fe	0.41 (**0.50***)	0.38 (0.36)	−0.06 (−0.04)	0.31 (0.27)
	La	0.37 (**0.51***)	0.31 (0.31)	−0.18 (−0.16)	**0.78***** (**0.69****)
	Mn	**0.45*** (**0.54****)	**0.46*** (0.37)	−0.06 (−0.16)	0.45 (0.46)
	Ni	0.14 (**0.49***)	−0.07 (0.10)	0.14 (−0.16)	−0.01 (0.24)
	P	0.30 (0.33)	**0.50*** (**0.56****)	0.06 (−0.02)	**0.78***** (**0.66****)
	Pb	0.34 (0.33)	0.40 (0.43)	0.06 (0.22)	0.29 (0.19)
	Sr	0.23 (**0.51***)	0.02 (0.15)	−0.33 (−0.36)	**0.62**** (**0.57***)
	Ti	0.14 (0.42)	0.12 (0.38)	−0.14 (−0.05)	**0.57**** (**0.49***)
	V	0.07 (**0.49***)	−0.18 (0.01)	0.15 (−0.20)	−0.16 (−0.07)

and nss-Ca^{2+} ($r_P = 0.69$) confirming the high correlation with combustion sources, as also pointed out by Table 2. Conversely, the low values of r_P indicate that the linear correlation of DTT-OPv with EC, nss-K^+, and nss-Mg^{2+} can be considered spurious probably due to the common correlation of EC, nss-K^+, and nss-Mg^{2+} with OC. The comparison between Tables 4a and 4b shows that the high linear correlation between AA-OPv and Cu (r = 0.93) is also confirmed by the corresponding high partial correlation coefficient ($r_P = 0.90$), both at a p-level < 0.01. In contrast, the linear correlations of AA-OPv with nss-Ca^{2+}, nss-SO_4^{2-}, Ba, and Mn could be considered spurious because of the low r_P. The high Cu correlation with nss-Ca^{2+}, nss-SO_4^{2-}, Ba, and Mn likely contributed to this last result.

We are aware that these last results are based on a low amount of samples (15) and that further investigations are needed to better identify the main relationships between OP and chemical species at the study site.

3.3. Results on the PM10 toxicity assessed by the Microtox assay

The toxicity of the 16 PM10 samples was first assessed as percentage of bioluminescence inhibition (%Inhibition) exerted by the undiluted aqueous extracts under 5, 15, and 30 min of exposure time, as reported in Fig. 2b. In 75% of the samples, we measured a positive %Inhibition, ranging from 25% to 62% after 30 min of exposure, because of the effect exerted by the PM10 extract exposure to the bacterial suspension. In contrast, the %Inhibition was negative (the light emission of the extract exposure was higher than that of the blank sample) for the S2, S3, S8, and S10 samples (Fig. 2b and Table S1). Negative values of the %Inhibition can be due to the hormesis widespread phenomenon. Hormesis consists in a biphasic dose-response to an environmental agent with a low dose stimulation and a high dose inhibition of a biological function (Calabrese et al., 2007; Shi et al., 2016). The stimulatory effect of low concentrations of toxic chemicals on organismal metabolism has been found to be common in luminescent bacteria utilized for toxicity bioassays (Shen et al., 2009). In particular, hormesis has been described as a frequent response to the exposure to low metal concentrations (Shen et al., 2009) or to low dose complex mixtures (Zou et al., 2013) with likely antagonistic or synergistic responses, although the underlying mechanisms need to be further clarified. In fact, even if hormesis has been found to be common in bioluminescent bacteria, it has rarely been mentioned and accepted in mainstream toxicology, since it was always a minor effect and it has often been considered as an experimental error or distortion of results, according to Shen et al. (2009). Shi et al. (2016) pointed out that, due to an incomplete understanding of the mechanism of hormesis, quantitative research has progressed slowly. Therefore, hormesis requires further elucidation also in view of a proper assessment of the anthropogenic pollution toxicity (Abbas et al., 2018). Most of the studies available in literature on the PM toxicity mainly focused on heavy polluted PM samples (Papadimitriou et al., 2006; Turòczi et al., 2012; Roig et al., 2013; Aammi et al., 2017). In that experimental conditions, the detection of a hormetic effect was likely prevented by the high pollutant concentrations.

In the present work, the use of PM samples collected at a coastal site away from large pollution sources has likely allowed detecting this phenomenon in 25% of the samples, highlighting the sensitivity of the Microtox test to different degrees of the PM toxicity.

Fig. 2b shows that the %Inhibition increased with the exposure time in all samples and varied from sample to sample likely because of the changes of the sample chemical composition. Sample S11 showed a rapid temporal increase of the %Inhibition, which was close to 0% after 5 min and reached the value of 37% after 30 min of exposure. As reported by Petala et al. (2005) and Yang et al. (2016), organic contaminants kept the same level in different exposure times, while the heavy metal toxicity to *V. fischeri* increased along with the exposure time. In particular, they found a marked time-dependence of the toxicity effect for Cd, Cu, Cr, Zn, and Ni. Accordingly, we found a strong temporal increase of the %Inhibition mainly in sample S11, which was characterized by the highest Cu mass concentration in this study (Table S1). These results likely suggest that exposure times longer than 30 min should be used in future studies.

In 25% of the samples, the %Inhibition was above 50% after 30 min of exposure (Fig. 2b), suggesting the presence of a toxic effect, as shown by the calculated TU_{50} values in Fig. 2c (grey bars) and in Table S1. We found that the TU_{50} values varied within the 1.5–3.1 range. The %

Table 3
Relationships between volume-normalized DTT-OP_V (dithiothreitol-oxidative potential) and mass concentration of the corresponding highly correlated chemical species by means of (a) the Pearson's correlation coefficient (r) and (b) the partial correlation coefficient (r_P). Significant r and r_P values at the *p*-level < 0.10, 0.05, and 0.01, according to the parametric two-tailed *t*-test are marked in bold and with *, **, and ***, respectively.

(a)	linear correlation coefficient matrix											
	DTT-OP_V	OC	EC	NH_4^+	nss-K^+	nss-Mg^{2+}	nss-Ca^{2+}	Glycolates	Cu	Mn	P	Na^+	Cl^-
DTT-OP_V	1.00												
OC	**0.92****	1.00											
EC	**0.92****	**0.94****	1.00										
NH_4^+	**0.71****	**0.64****	**0.72****	1.00									
nss-K^+	**0.70****	**0.88****	**0.84****	**0.49***	1.00								
nss-Mg^{2+}	**0.76****	**0.73****	**0.84****	**0.54****	**0.75****	1.00							
nss-Ca^{2+}	**0.52****	**0.62****	**0.57****	0.37	**0.70****	**0.60****	1.00						
Glycolates	**0.49***	**0.72****	**0.68****	**0.58****	**0.83****	**0.56****	**0.73****	1.00					
Cu	**0.69****	**0.63****	**0.60****	0.40	0.38	0.30	**0.52****	0.28	1.00				
Mn	**0.46***	**0.47***	**0.47***	0.25	**0.48***	**0.56****	**0.81****	**0.50***	**0.47***	1.00			
P	**0.50***	**0.51***	0.44	0.29	0.34	0.21	0.40	0.41	0.43	**0.53****	1.00		
Na^+	**−0.68****	**−0.61****	**−0.67****	**−0.68****	**−0.51***	**−0.59****	−0.08	−0.32	−0.22	0.02	0.05	1.00	
Cl^-	**−0.68****	**−0.61****	**−0.68****	**−0.71****	**−0.54****	**−0.65****	−0.17	−0.35	−0.23	−0.08	0.07	**0.97****	1.00

(b)	partial correlation coefficient matrix											
	DTT-OP_V	OC	EC	NH_4^+	nss-K^+	nss-Mg^{2+}	nss-Ca^{2+}	Glycolates	Cu	Mn	P	Na^+	Cl^-
DTT-OP_V	1.00												
OC	**0.89****	1.00											
EC	0.31	−0.43	1.00										
NH_4^+	0.23	−0.04	**0.62****	1.00									
nss-K^+	**−0.56****	**0.76****	**0.78****	**−0.53****	1.00								
nss-Mg^{2+}	0.10	0.11	**0.84****	**−0.66****	**−0.52***	1.00							
nss-Ca^{2+}	**0.53****	**−0.61****	**−0.78****	0.42	**0.81****	**0.57****	1.00						
Glycolates	**−0.80****	**0.72****	0.33	0.36	−0.34	−0.07	**0.55****	1.00					
Cu	−0.14	0.40	**0.86****	**−0.57****	**−0.72****	**−0.87****	**0.73****	−0.28	1.00				
Mn	−0.18	0.08	−0.05	−0.06	−0.12	0.28	0.32	−0.06	0.16	1.00			
P	0.40	−0.09	0.29	−0.28	−0.13	**−0.53****	−0.03	0.26	−0.44	**0.56****	1.00		
Na^+	0.12	−0.32	**−0.59****	**0.49***	**0.55****	**0.53****	−0.40	0.08	**0.55***	0.14	0.18	1.00	
Cl^-	−0.31	0.44	**0.68****	**−0.60****	**−0.70****	**−0.56****	**0.59****	−0.18	**−0.59****	−0.20	0.00	**0.92****	1.00

Table 4
Relationships between volume-normalized AA-OP_V (ascorbic acid-oxidative potential) and mass concentration of the corresponding highly correlated chemical species by means of (a) the Pearson's correlation coefficient (r) and (b) the partial correlation coefficient (r_P). Significant r and r_P values at the *p*-level < 0.10, 0.05, and 0.01, according to the parametric two-tailed *t*-test are marked in bold and with *, **, and ***, respectively.

(a)	linear correlation coefficient matrix					
	AA-OP_V	nss-Ca^{2+}	nss-SO_4^{2-}	Ba	Cu	Mn
AA-OP_V	1.00					
nss-Ca^{2+}	**0.50***	1.00				
nss-SO_4^{2-}	**0.48***	**0.62*****	1.00			
Ba	**0.45***	**0.63*****	**0.66*****	1.00		
Cu	**0.93*****	**0.52****	**0.47***	**0.48***	1.00	
Mn	**0.45***	**0.81*****	**0.53****	**0.66*****	**0.47***	1.00

(b)	partial correlation coefficient matrix					
	AA-OP_V	nss-Ca^{2+}	nss-SO_4^{2-}	Ba	Cu	Mn
AA-OP_V	1.00					
nss-Ca^{2+}	−0.03	1.00				
nss-SO_4^{2-}	0.14	0.29	1.00			
Ba	−0.11	0.02	**0.45***	1.00		
Cu	**0.90*****	0.11	−0.07	0.15	1.00	
Mn	0.07	**0.66*****	−0.12	0.32	−0.05	1.00

Inhibition was in the 20–50% range in half of the analyzed samples, highlighting a lower toxicity than the previous samples. Consequently, it was possible to calculate only the TU_{20} values for these last samples. The TU_{20} values calculated for 12 samples are shown in Table S1 and Fig. 2c (black bars). They varied within the 3.4–20.3 range and were greater than 16 in the samples for which TU_{50} values were also available (S4, S6, S7, and S15). Aammi et al. (2017) used the Microtox bioassay to evaluate the toxicity of the coarse (PM10-PM2.5) PM, collected on Teflon filters, using a passive sampling method on a monthly basis. The coarse PM fraction was extracted into both the lipophilic and the hydrophilic phases using dimethyl sulfoxide (DMSO) and ultra-pure water, respectively. They observed that the lipophilic extracted samples showed a greater toxicity response than the hydrophilic ones and that the threshold levels for the urban background and episodic occurrence of toxicity levels were identified to be 1.11 and 8.73 TU_{50}, respectively, for lipophilic extracts. These results are in reasonable accordance with the ones of this study, where ultra-pure water extracts were tested.

The impact of the chemical components on the %Inhibition and TU_{20} values was assessed by computing the linear regression coefficients between the chemical component mass concentrations and the measured toxicity parameters of the 12 samples not affected by hormesis (Table S3). Table 2 shows the Pearson's correlation coefficients *r* among the TU_{20} values and the mass concentration of the tested chemical species. The TU_{20} values showed significant positive correlations at *p*-level < 0.05 with OC, EC, nss-K^+, and nss-Mg^{2+}. Since OC, EC, and nss-K^+ are the main species of combustion sources (e.g., Perrone et al., 2019a, 2019b), this last result likely indicates that the *V. fischeri* Microtox assay was sensitive to species generated by combustion processes in our study. Correlation coefficients from the Spearman's test, which are reported in Table 2, are in reasonable accordance with the corresponding Pearson's correlation coefficients.

The larger contribution of the carbon component to the ecotoxicity of PM10 assessed by *V. fischeri* assay is in agreement with previous experimental evidences, showing the ecotoxicological potential of the PM carbonaceous fraction (e.g., Túroczi et al., 2012; Pintér et al., 2017; Abbas et al., 2018). In particular, Abbas et al. (2018) pointed out that the relatively inadequate sensitivity of the *V. fischeri* assay to heavy metals has diminished its applicability as a screening test in ecotoxicological assessment studies. In contrast, the Microtox® assay was identified as an excellent screening test to perform a first evaluation of air quality, as it presented very significant correlation values with metals, according to Roig et al. (2013). They applied the Microtox® assay to

PM10 samples collected at industrial, urban, and rural locations of Catalonia (NE Spain) in different seasons. Besides suggesting the need to perform further studies, the obtained contrasting results likely highlight the strong dependence of the pollution toxicity at the monitoring site.

We also found that the TU_{20} values showed significant positive correlations at p-level < 0.05 ($r = 0.62$) with the DTT-OP_V values, being both assays significantly correlated with species generated by combustion processes (Table 2). In contrast, TU_{20} did not show any significant correlation with AA-OP_V.

3.4. PM10 genotoxicity results

The genotoxicity of the samples was assessed by the SOS Chromotest assay in 12 PM10 samples (S3, S4, S5, S6, S7, S8, S11, S12, S13, S14, S15, and S16) because of technical reasons. The determined IF values spanned the 0.3–1.5 range and the threshold IF value (1.5) was reached in two samples (S4 and S13), as reported in Table S1 and shown in Fig. 2c (marked bars). Aammi et al. (2017) also used the SOS Chromotest assay to monitor the genotoxicity of coarse PM particles collected at several sites of the Istanbul (Turkey) megacity. They found that 87.5% of the total water-extracted samples werenon-genotoxic (their IF values were below 1.5), while the others were considered marginally toxic since the IF values spanned the 1.5–1.9 range, in reasonable accordance with the results of this study.

By considering the two analyzed samples (S4 and S13) characterized by the highest value of IF, the PM10 mass concentration was comparable in both samples (Table S1). In more detail, the (OC + EC) mass percentage reached the highest and the smallest value in S4 and S13, respectively, while the mass percentage due to all metals reached larger values in both samples. The last column of Table 2 and Table S4 show the Pearson's correlation coefficients r among the IF values and the mass concentration of the tested chemical species, in order to highlight the chemical species impact on genotoxicity. Any significant relationship was found between carbonaceous compounds and IF values. The IF was only correlated with some metals (Al, Ba, La, P, Sr, and Ti), which have on average been associated with a "traffic source" responsible for the resuspension of road dust generated by abrasion of vehicle-parts and pavement, according to Viana et al. (2006). Spearman's test correlation coefficients are in reasonable accordance with the corresponding Pearson's correlation coefficients (Table 2). Table S4 also shows that on average Al, Ba, La, P, Sr, and Ti were significantly inter-correlated, supporting the hypothesis that they were due to a common pollution source. Aammi et al. (2017) found that the highest IF values were observed at the site where the main source of PM was heavy local traffic and industrial activity, in reasonable accordance with the results of this study. One must be aware that, even if the monitoring site of this study is away from large pollution sources, it can be significantly affected by long-range transported polluted particles from the surrounding countries, as outlined in Dulac and Hamonou (2016) and Perrone et al. (2019a).

Concerning the sensitivity of the SOS Chromotest to metal compounds, a clear evidence of genotoxicity has been previously demonstrated for chromium (VI), tin (II), cadmium, copper, mercury, nickel, and zinc (e.g., Codina et al., 1995; Lantzsch and Gebel, 1997). In our samples, we did not observe any significant correlation between the IF and the above mentioned metals, which are mainly related to industrial activities. The geographical location of the monitoring site, which is away from large pollution sources, likely contributed to this last result. On the other hand, we observed a significant correlation with some metals related to traffic sources, increasing the knowledge on the SOS Chromotest sensitivity to the metal components of the PM.

High SOS Chromotest IF values were also associated with high concentrations of organic compounds emitted in sites with intense traffic, according to Aammi et al. (2017). However, in our samples, the correlation between the IF and the PM carbonaceous components was lacking. Presumably, the organic content of our PM samples did not allow inducing detectable DNA damages, even if it was able to induce toxic effects at the metabolic *V. fischeri* level.

We did not find any significant correlation of IF with TU_{20} and OP_V values. In fact, TU_{20} and OP_V values showed a rather weak correlation with most of the chemical compounds correlated with IF (Table 2). Consequently, Fig. 2 shows that, even if IF reached the highest value in S4 and S13, the TU_{20} and DTT-OP_V values reached one of the highest and smallest values in sample S4 and S13, respectively, since the (OC + EC) mass percentage reached the highest and smallest value in S4 and S13, respectively. In contrast, AA-OP_V reached a small and high value in S4 and S13, respectively (Fig. 2a).

4. Summary and conclusion

PM10 particles were sampled from May to July 2017 at a suburban area (40.3°N; 18.1°E) of the Central Mediterranean, away from large pollution sources, to evaluate both ecotoxicity and genotoxicity levels, and investigate the relationships with the PM chemical composition and its ability to generate reactive oxygen species.

- The DTT- and AA-OP_V varied within the (0.05–0.33) and (0.05–1.36) nmol min^{-1} m^{-3} range, respectively. The DTT-OP_V responses were mainly associated with water-soluble chemical species likely from combustion sources, while the AA-OP_V responses were likely driven by traffic sources.
- The *Vibrio fischeri* bioassay responses showed that the %Inhibition increased with the exposure time of the PM extracts, suggesting that exposure times should be longer than 30 min, mainly in metal-rich samples. They were likely driven by species from combustion processes and, consequently, were significantly correlated with DTT-OP_V. Any significant correlation with AA-OP_V was not found.
- The widespread hormesis phenomenon, which has been found to be common in bioluminescent bacteria, was observed in 25% of the PM10 samples.
- The SOS chromotest responses were likely driven by metals from traffic sources and did not show any significant relationship with OP_V and *V. fischeri* responses.
- Overall, the paper results proved the *V. fischeri* and SOS chromotest sensitivity for ecotoxicity and genotoxicity monitoring, respectively, for PM10 particles sampled directly from their natural environment and away from large pollution sources. Consequently, their responses were towards the lowest end of the range of values retrieved from samples collected at heavily polluted areas.
- Concerning the still open question on the ability of acellular OP assays to represent biological responses, our results showed an experimental evidence that DTT-OP_V responses were positively correlated with TU_{20} values, being both driven by combustion-generated chemical species. In contrast, the AA-OP_V activity did not show any significant correlation with both biological tests.

For the first time in this study, to the best of our knowledge, ecotoxicity, genotoxicity, and OP tests of PM10 particles were simultaneously investigated. We found that OP, *V. fischeri,* and SOS Chromotest responses on average contrasted in sensibility towards individual chemical species/pollution sources, highlighting that different methods are required to better identify chemical species with potential health impacts and, hence, that they are likely sensitive to different PM composition. Besides providing complementary information, the use of multiple bioassays allows acquiring a more comprehensive valuation of the potential harmful effects associated with PM.

We believe that the paper's results have contributed to the understanding of the toxicological impact of the Mediterranean PM10 particles and should be considered helpful to design regulatory strategies for mitigating the PM toxicity. The small number of tested samples can represent a fault of this study, even if the paper results are supported by previous studies. However, further studies are underway to support

achieved results.

Declaration of competing interest

The authors declare that they have no known competing financial interests or personal relationships that could have appeared to influence the work reported in this paper.

Acknowledgments

S. Romano has carried out this work with the support of a post-doctoral fellowship from the Consorzio Nazionale Interuniversitario per le Scienze Fisiche della Materia (CNISM). The financial support of EARLINET as part of the ACTRIS Research Infrastructure Project by the European Union's Horizon 2020 research and innovation programme under grant agreement no. 654109 and 739530 (previously under grant agreement no. 262254) in the 7th Framework Programme (FP7/2007–2013) is gratefully acknowledged.

Appendix A. Supplementary data

Supplementary data to this article can be found online at https://doi.org/10.1016/j.atmosenv.2019.117085.

References

Aammi, S., Karaca, F., Petek, M., 2017. A toxicological and genotoxicological indexing study of ambient aerosols ($PM_{2.5-10}$) using in vitro bioassays. Chemosphere 174, 490–498. https://doi.org/10.1016/j.chemosphere.2017.01.141.

Abbas, M., Adil, M., Ehtisham-Ul-Haque, S., Munir, B., Yameen, M., Ghaffar, A., Shar, G. A., Asif Tahir, M., Iqbal, M., 2018. Vibrio fischeri bioluminescence inhibition assay for ecotoxicity assessment: a review. Sci. Total Environ. 626, 1295–1309. https://doi.org/10.1016/j.scitotenv.2018.01.066.

André, V., Billet, S., Pottier, D., Le Goff, J., Pottier, I., Garçon, G., Shirali, P., Sichel, F., 2011. Mutagenicity and genotoxicity of PM2.5 issued from an urbano-industrialized area of Dunkerque (France). J. Appl. Toxicol. 31, 131–138. https://doi.org/10.1002/jat.1572.

Antiñolo, M., Willis, M.D., Zhou, S., Abbatt, J.P., 2015. Connecting the oxidation of soot to its redox cycling abilities. Nat. Commun. 6, 6812. https://doi.org/10.1038/ncomms7812.

Ayres, J.G., Borm, P., Cassee, F.R., Castranova, V., Donaldson, K., Ghio, A., Harrison, R. M., Hider, R., Kelly, F., Kooter, I.M., 2008. Evaluating the toxicity of airborne particulate matter and nanoparticles by measuring oxidative stress potential – a workshop report and consensus statement. Inhal. Toxicol. 20, 75–99. https://doi.org/10.1080/08958370701665517.

Bates, J.T., Fang, T., Verma, V., Zeng, L., Weber, R.J., Tolbert, P.E., Abrams, J.Y., Sarnat, S.E., Klein, M., Mulholland, J.A., Russel, A.G., 2019. Review of acellular assays of ambient particulate matter oxidative potential: methods and relationships with composition, sources, and health effects. Environ. Sci. Technol. 53, 4003–4019. https://doi.org/10.1021/acs.est.8b03430.

Becagli, S., Anello, F., Bommarito, C., Cassola, F., Calzolai, G., Di Iorio, T., di Sarra, A., Gómez-Amo, J.-L., Lucarelli, F., Marconi, M., Meloni, D., Monteleone, F., Nava, S., Pace, G., Severi, M., Sferlazzo, D.M., Traversi, R., Udisti, R., 2017. Constraining the ship contribution to the aerosol of the central Mediterranean. Atmos. Chem. Phys. 17, 2067–2084. https://doi.org/10.5194/acp-17-2067-2017.

Bruner, L.H., Kain, D.J., Roberts, D.A., Parker, R.D., 1991. Evaluation of seven in vitro alternatives for ocular safety testing. Fundam. Appl. Toxicol. 17, 136–149. https://doi.org/10.1016/0272-0590(91)90246-Z.

Bulich, A.A., Tung, K.K., Scheibner, G., 1990. The luminescent bacteria toxicity test: its potential as an in vitro alternative. J. Biolumin. Chemilumin. 5, 71–77. https://doi.org/10.1002/bio.1170050202.

Burton, S.A., Petersen, R.V., Dickman, S.N., Nelson, J.R., 1986. Comparison of in vitro bacterial bioluminescence and tissue culture bioassays and in vivo tests for evaluating acute toxicity of biomaterials. J. Biomed. Mater. Res. 20, 827–838. https://doi.org/10.1002/jbm.820200613.

Calabrese, E.J., Bachmann, K.A., Bailer, A.J., Bolger, P.M., Borak, J., Cai, L., et al., 2007. Biological stress response terminology: integrating the concepts of adaptive response and preconditioning stress within a hormetic dose-response framework. Toxicol. Appl. Pharmacol. 222, 122–128. https://doi.org/10.1016/j.taap.2007.02.015.

Calas, A., Uzu, G., Kelly, F.J., Houdier, S., Martins, J.M.F., Thomas, F., Molton, F., Charron, A., Dunster, C., Oliete, A., Jacob, V., Besombes, J.L., Chevrier, F., Jaffrezo, J.L., 2018. Comparison between five acellular oxidative potential measurement assays performed with detailed chemistry on PM10 samples from the city of Chamonix (France). Atmos. Chem. Phys. 18, 7863–7875. https://doi.org/10.5194/acp-18-7863-2018.

Calzolai, G., Nava, S., Lucarelli, F., Chiari, M., Giannoni, M., Becagli, S., Traversi, R., Marconi, M., Frosini, D., Severi, M., Udisti, R., di Sarra, A., Pace, G., Meloni, D., Bommarito, C., Monteleone, F., Anello, F., Sferlazzo, D.M., 2015. Characterization of PM10 sources in the central Mediterranean. Atmos. Chem. Phys. 15, 13939–13955. https://doi.org/10.5194/acp-15-13939-2015.

Cavalli, F., Viana, M., Yttri, K., Genberg, J., Putaud, J., 2010. Toward a standardized thermal-optical protocol for measuring atmospheric organic and elemental carbon: the EUSAAR protocol. Atmos. Meas. Tech. 3, 79–89. https://doi.org/10.5194/amt-3-79-2010.

CEC (Commission of the European Communities), 2008. CEC directive 2008/50/EC of the European parliament and of the council of 21 may 2008 on ambient air quality and cleaner air for Europe. Off. J. Eur. Union L152, 1–44.

Chang, S.C., Wang, Y.F., You, S.J., Kuo, Y.M., Tsai, C.H., Wang, L.C., Hsu, P.Y., 2013. Toxicity evaluation of fly ash by Microtox®. Aerosol Air Qual. Res. 13, 1002–1008. https://doi.org/10.4209/aaqr.2012.10.0267.

Charrier, J.G., Anastasio, C., 2012. On dithiothreitol (DTT) as a measure of oxidative potential for ambient particles: evidence for the importance of soluble transition metals. Atmos. Chem. Phys. 12, 11317–11350. https://doi.org/10.5194/acpd-12-11317-2012.

Claxton, L.D., Matthews, P.P., Warren, S.H., 2004. The genotoxicity of ambient outdoor air, a review: Salmonella mutagenicity. Mutat. Res. 567 (2–3), 347–399. https://doi.org/10.1016/j.mrrev.2004.08.002.

Codina, J.C., Pérez-Torrente, C., Pérez-García, A., Cazorla, F.M., de Vicente, A., 1995. Comparison of microbial tests for the detection of heavy metal genotoxicity. Arch. Environ. Contam. Toxicol. 29, 260–265. https://doi.org/10.1007/BF00212978.

Crobeddu, B., Aragao-Santiago, L., Bui, L.-C., Boland, S., Squiban, A.B., 2017. Oxidative potential of particulate matter 2.5 as predictive indicator of cellular stress. Environ. Pollut. 230, 125–133. https://doi.org/10.1016/j.envpol.2017.06.051.

Dhawan, A., Bajpayee, M., Parmar, D., 2009. Comet assay: a reliable tool for the assessment of DNA damage in different models. Cell Biol. Toxicol. 25 (1), 5–32. https://doi.org/10.1007/s10565-008-9072-z.

Dulac, F., Hamonou, E., 2016. Air quality and climate in the Mediterranean region. In: book: The Mediterranean Region under Climate Change, a scientific update. Jean-Paul Moatti et Stéphane Thiébault (dir.). IRD Editions. https://doi.org/10.4000/books.irdeditions.24600.

Fang, T., Verma, V., Bates, J.T., Abrams, J., Klein, M., Strickland, M.J., Sarnat, S.E., Chang, H.H., Mulholland, J.A., Tolbert, P.E., Russell, A.G., Weber, R.J., 2016. Oxidative potential of ambient water-soluble PM2.5 in the southeastern United States: contrasts in sources and health associations between ascorbic acid (AA) and dithiothreitol (DTT) assays. Atmos. Chem. Phys. 16, 3865–3879. https://doi.org/10.5194/acp-16-3865-2016.

Fort, F., 1992. Correlation of microtox EC with mouse LD. In: Vitro Toxicol, vol. 5, pp. 73–82.

Freund, R., Mohr, D., Wilson, W., 2010. Statistical Methods, third ed. Academic Press. https://doi.org/10.1016/C2009-0-20216-9.

Ganesan, A., Oates, T., Schmill, M., 2016. Finding Representative Points in Multivariate Data Using PCA. ArXiv preprint, arXiv: 1610.05819.

Ghio, A.J., Carraway, M.S., Madden, M.C., 2012. Composition of air pollution particles and oxidative stress in cells, tissues, and living system. J. Toxicol. Environ. Health B Crit. Rev. 15, 1–21. https://doi.org/10.1080/10937404.2012.632359.

Girotti, S., Ferri, E.N., Fumo, M.G., Maiolini, E., 2008. Monitoring of environmental pollutants by bioluminescent bacteria. Anal. Chim. Acta 608 (1), 2–29. https://doi.org/10.1016/j.aca.2007.12.008.

Hedayat, F., Stevanovic, S., Miljevic, B., Bottle, S., Ristovski, Z.D., 2015. Review-Evaluating the molecular assays for measuring the oxidative potential of particle matter. Chem. Ind. Chem. Eng. Q. 21, 201–210. https://doi.org/10.2298/ciceq140228031h.

Hellack, B., Nickel, C., Albrecht, C., Kuhlbusch, T.A.J., Boland, S., Baeza-Squiban, A., Wohlleben, W., Schins, R.P.F., 2017. Analytical methods to assess the oxidative potential of nanoparticles: a review. Environ. Sci.: Nano 4, 1920–1934. https://doi.org/10.1039/C7EN00346C.

Janssen, N.A.H., Yang, A., Strak, M., Steenhof, M., Hellack, B., Gerlofs-Nijland, M.E., Kuhlbusch, T., Kelly, F., Harrison, R., Brunekreef, B., Hoek, G., Cassee, F., 2014. Oxidative potential of particulate matter collected at sites with different source characteristics. Sci. Total Environ. 472, 572–581. https://doi.org/10.1016/j.scitotenv.2013.11.099.

Janssen, N.A.H., Strak, M., Yang, A., Hellack, B., Kelly, F.J., Kuhlbusch, T.A.J., Harrison, R.M., Brunekreef, B., Cassee, F.R., Steenhof, M., Hoek, G., 2015. Associations between three specific a-cellular measures of the oxidative potential of particulate matter and markers of acute airway and nasal inflammation in healthy volunteers. Occup. Environ. Med. 72, 49–56. https://doi.org/10.1136/oemed-2014-102303.

Kahru, A., Pollumaa, L., Reiman, R., Ratsep, A., Liiders, M., Maloveryan, A., 2000. The toxicity and biodegradability of eight main phenolic compounds characteristic to the oil-shale industry wastewaters: a test battery approach. Environ. Toxicol. 15, 431–442. https://doi.org/10.1002/1522-7278(2000)15:5<431::AID-TOX11>3.0.CO;2-T.

Lantzsch, H., Gebel, T., 1997. Genotoxicity of selected metal compounds in the SOS chromotest. Mutat. Res. 389 (2–3), 191–197. https://doi.org/10.1016/S1383-5718(96)00146-5.

Lelieveld, J., Berresheim, H., Bormann, S., Crutzen, P.J., Dentener, F.J., et al., 2002. Global air pollution crossroads over the Mediterranean. Science 298, 794–799. https://doi.org/10.1126/science.1075457.

Lepers, C., André, V., Dergham, M., Billet, S., Verdin, A., Garçon, G., Dewaele, D., Cazier, F., Sichel, F., Shirali, P., 2013. Xenobiotic metabolism induction and bulky DNA adducts generated by particulate matter pollution in BEAS-2B cell line: geographical and seasonal influence. J. Appl. Toxicol. 34, 703–713. https://doi.org/10.1002/jat.2931.

Lin, Y.-C., Tsai, C.-J., Wu, Y.-C., Zhang, R., Chi, K.-H., Huang, Y.-T., Lin, S.-H., Hsu, S.-C., 2015. Characteristics of trace metals in traffic-derived particles in Hsuehshan Tunnel, Taiwan: size distribution, potential source, and fingerprinting metal ratio. Atmos. Chem. Phys. 15, 4117–4130. https://doi.org/10.5194/acp-15-4117-2015.

Lionetto, M.G., Caricato, R., Giordano, M.E., 2019. Pollution biomarker in environmental and human biomonitoring. Open Biomark. J. 9, 1–9. https://doi.org/10.2174/1875318301909010001.

Mailler, S., Menut, L., di Sarra, A.G., Becagli, S., Di Iorio, T., Bessagnet, B., Briant, R., Formenti, P., Doussin, J.-F., Gómez-Amo, J.L., Mallet, M., Rea, G., Siour, G., Sferlazzo, D.M., Traversi, R., Udisti, R., Turquety, S., 2016. On the radiative impact of aerosols on photolysis rates: comparison of simulations and observations in the Lampedusa island during the ChArMEx/ADRIMED campaign. Atmos. Chem. Phys. 16, 1219–1244. https://doi.org/10.5194/acp-16-1219-2016.

Mudway, I.S., Stenfors, N., Duggan, S.T., Roxborough, H., Zielinski, H., Marklund, S.L., Blomberg, A., Frew, A.J., Sandström, T., Kelly, F.J., 2004. An in vitro and in vivo investigation of the effects of diesel exhaust on human airway lining fluid antioxidants. Arch. Biochem. Biophys. 423, 200–212. https://doi.org/10.1016/j.abb.2003.12.018.

Nałecz-Jawecki, G., Rudz, B., Sawicki, J., 1997. Evaluation of toxicity of medical devices using Spirotoxand Microtox tests: I. Toxicity of selected toxicants in various diluents. J. Biomed. Mater. Res. 35, 101–105. https://doi.org/10.1002/(SICI)1097-4636(199704)35:1<101:AID-JBM10>3.0.CO;2-M.

Pandolfi, M., Gonzalez-Castanedo, Y., Alastuey, A., de la Rosa, J.D., Mantilla, E., Sanchez de la Campa, A.S., Querol, X., Pey, J., Amato, F., Moreno, T., 2011. Source apportionment of PM10 and PM2.5 at multiple sites in the strait of Gibraltar by PMF: impact of shipping emissions. Environ. Sci. Pollut. Res. 18, 260–269. https://doi.org/10.1007/s11356-010-0373-4.

Papadimitriou, C., Evagelopoulos, V., Samaras, P., Triantafyllou, A.G., Zoras, S., Albanis, T.A., 2006. Toxicity of atmospheric particulate matter using aquatic bioassays. In: Kungolos, A.G., Brebbia, C.A., Samaras, C.P., Popov, V. (Eds.), Environmental Toxicology. WIT Press, Southampton, USA, pp. 31–40.

Perrone, M.R., Dinoi, A., Becagli, S., Udisti, R., 2014. Chemical composition of PM1 and PM2.5 at a suburban site in southern Italy. Int. J. Environ. Anal. Chem. 94, 127–150. https://doi.org/10.1080/03067319.2013.791978.

Perrone, M.G., Zhou, J., Malandrino, M., Sangiorgi, G., Rizzi, C., Ferrero, L., Dommen, J., Bolzacchini, E., 2016. PM chemical composition and oxidative potential of the soluble fraction of particles at two sites in the urban area of Milan, Northern Italy. Atmos. Environ. 128, 104–113. https://doi.org/10.1016/j.atmosenv.2015.12.040.

Perrone, M.R., Romano, S., Genga, A., Paladini, F., 2018. Integration of optical and chemical parameters to improve the particulate matter characterization. Atmos. Res. 205, 93–106. https://doi.org/10.1016/j.atmosres.2018.02.015.

Perrone, M.R., Vecchi, R., Romano, S., Becagli, S., Traversi, R., Paladini, F., 2019. Weekly cycle assessment of PM mass concentrations and sources, and impacts on temperature and wind speed in Southern Italy. Atmos. Res. 218, 129–144. https://doi.org/10.1016/j.atmosres.2018.11.013.

Perrone, M.R., Bertoli, I., Romano, S., Russo, M., Rispoli, G., Pietrogrande, M.C., 2019. PM2.5 and PM10 oxidative potential at a Central Mediterranean Site: contrasts between dithiothreitol- and ascorbic acid-measured values in relation with particle size and chemical composition. Atmos. Environ. 210, 143–155. https://doi.org/10.1016/j.atmosenv.2019.04.047.

Petala, M., Tsiridis, V., Kyriazis, S., Samaras, P., Kungolos, A., Sakellaropoulos, G.P., 2005. Evaluation of toxic response of heavy metals and organic pollutants using microtox acute toxicity test. In: Proceedings of the 9th International Conference on Environmental Science and Technology, pp. 1200–1205.

Piao, M.J., Ahn, M.J., Kang, K.A., Ryu, Y.S., Hyun, Y.J., Shilnikova, K., Zhen, A.X., Jeong, J.W., Choi, Y.H., Kang, H.K., Koh, Y.S., Hyun, J.W., 2018. Particulate matter 2.5 damages skin cells by inducing oxidative stress, subcellular organelle dysfunction, and apoptosis. Arch. Toxicol. 92 (6), 2077–2091. https://doi.org/10.1007/s00204-018-2197-9.

Pietrogrande, M.C., Dalpiaz, C., Dell'Anna, R., Lazzeri, P., Manarini, F., Visentin, M., Tonidandel, G., 2018. Chemical composition and oxidative potential of atmospheric coarse particles at an industrial and urban background site in the alpine region of northern Italy. Atmos. Environ. 191, 340–350. https://doi.org/10.1016/j.atmosenv.2018.08.022.

Pietrogrande, M.C., Perrone, M.R., Manarini, F., Romano, S., Udisti, R., Becagli, S., 2018. PM10 oxidative potential at a Central Mediterranean Site: association with chemical composition and meteorological parameters. Atmos. Environ. 188, 97–111. https://doi.org/10.1016/j.atmosenv.2018.06.013.

Pietrogrande, M.C., Bertoli, I., Manarini, F., Russo, M., 2019. Ascorbate assay as a measure of oxidative potential for ambient particles: evidence for the importance of cell-free surrogate lung fluid composition. Atmos. Environ. 211, 103–112. https://doi.org/10.1016/j.atmosenv.2019.05.012.

Pintér, M., Utry, N., Ajtai, T., Kiss-Albert, G., Jancsek-Turóczi, B., Imre, K., Palágyi, A., Manczinger, L., Vágvölgyi, C., Horváth, E., Kováts, N., Gelencsér, A., Szabó, G., Bozóki, Z., 2017. Optical properties, chemical composition and the toxicological potential of urban particulate matter. Aerosol Air Qual. Res. 17, 1515–1526. https://doi.org/10.4209/aaqr.2016.09.0395.

Pio, C.A., Legrand, M., Oliveira, T., Afonso, J., Santos, C., Caseiro, A., Fialho, P., Barata, F., Puxbaum, H., Sanchez-Ochoa, A., Kasper-Giebl, A., Gelencsér, A., Preunkert, S., Schock, M., 2007. Climatology of aerosol composition (organic versus inorganic) at nonurban sites on a west-east transect across Europe. J. Geophys. Res. A Space Phys. 112 (23), D23S02. https://doi.org/10.1029/2006JD008038.

Quillardet, P., Hofnung, M., 1985. The SOS Chromotest, a colorimetric bacterial assay for genotoxins: procedures. Mutat. Res. 147 (3), 65–78. https://doi.org/10.1016/0165-1161(85)90020-2.

Quintana, R., Alfaro-Moreno, E., García-Cuéllar, M.C., Gomez, V., Vázquez-López, I., de Jesús Salmón-Salazar, M., Rosas, I., Vargas, O.A., 2015. Evaluation of the oxidative potential of urban PM and its relation to in vitro induced DNA damage: a spatial and temporal comparison. Rev. Int. Contam. Ambient. 31, 145–154.

Roig, N., Sierra, J., Rovira, J., Schuhmacher, M., Domingo, J.L., Nadal, M., 2013. *In vitro* tests to assess toxic effects of airborne PM_{10} samples. Correlation with metals and chlorinated dioxins and furans. Sci. Total Environ. 443, 791–797. https://doi.org/10.1016/j.scitotenv.2012.11.022.

Ruiz, F., González-Regalado, M.L., Muñoz, J.M., Abad, M., Toscano, A., Prudencio, M.I., Dias, M.I., 2014. Distribution of heavy metals and pollution pathways in a shallow marine shelf: assessment for a future management. Int. J. Environ. Sci. Technol. 11, 1249–1258. https://doi.org/10.1007/s13762-014-0576-1.

Seinfeld, J.H., Pandis, S.N., 1998. Atmospheric Chemistry and Physics: from Air Pollution to Climate Change. J. Wiley &Sons, INC.

Shafer, M.M., Hemming, J.D.C., Antkiewicz, D.S., Schauer, J.J., 2016. Oxidative potential of size-fractionated atmospheric aerosol in urban and rural sites across Europe. Faraday Discuss 189, 381–405. https://doi.org/10.1039/c5fd00196j.

Shen, K., Shen, C., Lu, Y., Tang, X., Zhang, C., Chen, X., Shi, J., Lin, Q., Chen, Y., 2009. Hormesis response of marine and freshwater luminescent bacteria to metal exposure. Biol. Res. 42, 183–187. https://doi.org/10.4067/S0716-97602009000200006.

Shi, J., Huber, M., Wang, T., Dali, W., Lin, Z., Chun-Sheng, Y., 2016. Progress in the studies on hormesis of low-dose pollutants. Environ. Dis. 1, 58–64. https://doi.org/10.4103/2468-5690.185296.

Shiraiwa, M., Selzle, K., Pöschl, U., 2012. Hazardous components and health effects of atmospheric aerosol particles: reactive oxygen species, soot, polycyclic aromatic compounds and allergenic proteins. Free Radic. Res. 46 (8), 927–939. https://doi.org/10.3109/10715762.2012.663084.

Szigeti, T., Dunster, C., Cattaneo, A., Cavallo, D., Spinazzè, A., Saraga, D.E., Sakellaris, I. A., de Kluizenaar, Y., Cornelissen, E.J.M., Hänninen, O., Peltonen, M., Calzolai, G., Lucarelli, F., Mandin, C., Bartzis, J.G., Záray, G., Kelly, F.J., 2016. Oxidative potential and chemical composition of PM2.5 in office buildings across Europe – the OFFICAIR study. Environ. Int. 92–93, 324–333. https://doi.org/10.1016/j.envint.2016.04.015.

Traversi, D., Festa, E., Pignata, C., Gilli, G., 2015. Aero-dispersed mutagenicity attributed to particulate and semi volatile phase in an urban environment. Chemosphere 124, 163–169. https://doi.org/10.1016/j.chemosphere.2014.12.033.

Turóczi, B., Hoffer, A., Tóth, Á., Kováts, N., Ács, A., Ferincz, Á., Kovács, A., Gelencsér, A., 2012. Comparative assessment of ecotoxicity of urban aerosol. Atmos. Chem. Phys. 12, 7365–7370. https://doi.org/10.5194/acp-12-7365-2012.

Verma, V., Fang, T., Xu, L., Peltier, R.E., Russel, A.G., Ng, N.L., Weber, R.J., 2015. Organic aerosols associated with the generation of reactive oxygen species (ROS) by water-soluble PM2.5. Environ. Sci. Technol. 49, 4646–4656. https://doi.org/10.1021/es505577w.

Viana, M., Querol, X., Alastuey, A., Gil, J.I., Menendez, M., 2006. Identification of PM sources by principal component analysis (PCA) coupled with wind direction data. Chemosphere 65, 2411–2418. https://doi.org/10.1016/j.chemosphere.2006.04.060.

Visentin, M., Pagnoni, A., Sarti, E., Pietrogrande, M.C., 2016. Urban PM2.5 oxidative potential: importance of chemical species and comparison of two spectrophotometric cell-free assays. Environ. Pol. 219, 72–79. https://doi.org/10.1016/j.envpol.2016.09.047.

Weber, S., Uzu, G., Calas, A., Chevrier, F., Besombes, J.-L., Charron, A., Salameh, D., Ježek, I., Močnik, G., Jaffrezo, J.-L., 2018. An apportionment method for the oxidative potential of atmospheric particulate matter sources: application to a one-year study in Chamonix, France. Atmos. Chem. Phys. 18, 9617–9629. https://doi.org/10.5194/acp-18-9617-2018.

Yang, X., Yan, J., Wang, F., Xu, J., Liu, X., Ma, K., Hu, X., Ye, J., 2016. Comparison of organics and heavy metals acute toxicities to Vibrio fischeri. J. Serb. Chem. Soc. 81, 697–705. https://doi.org/10.2298/JSC151124011Y.

Zannoni, N., Gros, V., Sarda Esteve, R., Kalogridis, C., Michoud, V., Dusanter, S., Sauvage, S., Locoge, N., Colomb, A., Bonsang, B., 2017. Summertime OH reactivity from a receptor coastal site in the Mediterranean Basin. Atmos. Chem. Phys. 17, 12645–12658. https://doi.org/10.5194/acp-17-12645-2017.

Zou, X., Lin, Z., Deng, Z., Yin, D., 2013. Novel approach to predicting hermetic effects of antibiotic mixtures on Vibrio fischeri. Chemosphere 90, 2070–2076. https://doi.org/10.1016/j.chemosphere.2012.09.042.

Chemosphere 240 (2020) 124746

Contents lists available at ScienceDirect

Chemosphere

journal homepage: www.elsevier.com/locate/chemosphere

Proinflammatory properties and oxidative effects of atmospheric particle components in human keratinocytes

Franco Cervellati [a], Mascia Benedusi [a], Francesco Manarini [b], Brittany Woodby [c], Mara Russo [b], Giuseppe Valacchi [a, b, c, d, *], Maria Chara Pietrogrande [b, **]

[a] Department of Medical and Surgical Sciences and Neurosciences, University of Siena, NC State University, Siena, Italy
[b] Department of Chemical and Pharmaceutical Sciences, University of Ferrara, Ferrara, Italy
[c] Plants for Human Health Institute Animal Science Dept., NC Research Campus, Kannapolis, NC, 28081, USA
[d] Department of Food and Nutrition, Kyung Hee University, Seoul, South Korea

HIGHLIGHTS

- Comparison between AA and DDT and in vivo cells oxidation in the presence of PM components.
- Activation of the redox transcription factor NFκB on keratinocytes treated with PM components.
- Cu (II) and quinones increased the activities and expression of IL8, SOD1 and GPX genes.
- Keratinocytes mitochondrial alteration and apoptosis was increased after treatment.
- Exposure of skin to air pollutants can modifies the redox equilibrium of keratinocytes.

GRAPHICAL ABSTRACT

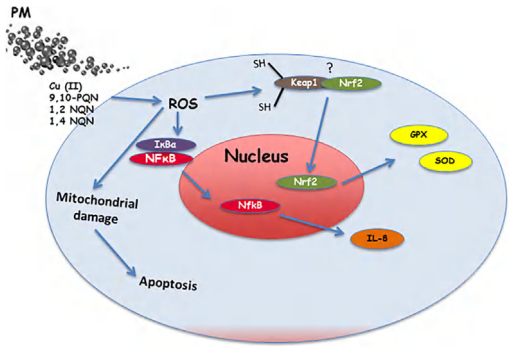

ARTICLE INFO

Article history:
Received 29 May 2019
Received in revised form
22 August 2019
Accepted 3 September 2019
Available online 13 September 2019

Handling Editor: Andreas Sjodin

Keywords:
Cu 9,10 phenanthrenequinone
Naphthoquinone isomers 1,2
Airborne particulate matter
Redox-active chemicals
Cutaneous tissues
Oxidative damage

ABSTRACT

The skin is one of the main organs exposed to airborne particulate matter (PM), which may contain various pollutants linked to a wide range of adverse health endpoints. In the present work, we analyzed the proinflammatory and oxidative effects of some PM components leading to inflammatory responses, cell proliferation or cell death. We investigated four redox-active chemicals, such as Cu (II) metal and quinones generated from polycyclic aromatic hydrocarbons (PAHs), i.e., 9,10 phenanthrenequinone and isomers 1,2 and 1,4 naphthoquinone. We performed *in vitro* biological tests on human keratinocyte (HaCaT) cells and also acellular assays based on the oxidation of dithiothreitol and ascorbic acid, antioxidants to assess the oxidative potential (OP).

We found that treated keratinocytes showed increased activation of the redox-sensitive transcription factor NFκB and increased transcript levels of the NFκB-dependent gene IL8. Moreover, the treatment with Cu(II) and quinones increased the activities and the expression of genes involved in the redox response, SOD1 and GPX, suggesting that PM components induced cellular damage due to redox imbalances. Finally, we found alteration of the mitochondrial ultrastructure and increased apoptosis after 24 h of treatment. The results presented suggest that all of the analyzed pollutant components are able to

* Corresponding author. Plants for Human Health Institute Animal Science Dept., NC Research Campus, Kannapolis, NC, 28081, USA.
** Corresponding author.
E-mail address: franco.cervellati@unife.it (F. Cervellati).

https://doi.org/10.1016/j.chemosphere.2019.124746

modulate similar signal transduction pathways, resulting in activation of inflammatory processes in the skin, followed by oxidative damage.

Altogether these observations indicate that exposure of skin to air pollutants modifies the redox equilibrium of keratinocytes, which could explain the increased skin damage observed in populations that live in high-pollution cities.

1. Introduction

Numerous studies have linked exposure to airborne particulate matter (PM) to a wide range of adverse health endpoints, including cardiovascular diseases, respiratory problems, skin damage, and adverse neurodevelopmental effects (Delfino et al., 2010; Ghio et al., 2012, Piao MJ et al., 2018; Mohan Kumar et al., 2008). Due to the fact that the skin is the largest organ in our body and its particular location, these facts make the skin a potential route by which outdoor contaminants (organisms, pollutants, etc.) can enter in our body (Valacchi et al., 2012; Drakaki et al., 2014). In fact, a recent study demonstrated that the amount of pollutants taken up from the air either by inhalation or transdermally in human subjects was similar (Weschler, 2015). Our group has also recently demonstrated that PM can enter the stratum corneum and reach the proliferating keratinocytes in the lower layers (Magnani, 2016).

Although the mechanisms of PM-associated health problems are still incompletely understood, oxidative stress has been proposed as one of the main mechanisms for PM toxicity in recent years (Delfino, 2010; Kelly, 2003). In fact, it has been suggested that PM exposure stimulates the endogenous production of O_2^- through the reduction of oxygen by biological reducing agents, such as nicotinamide adenine dinucleotide (NADH) and nicotinamide adenine dinucleotide phosphate (NADPH) (Dellinger et al., 2001; Squadrito et al., 2001). This process contributes to the induction of oxidative stress by both depleting antioxidant species in the cell and generating reactive oxygen species (ROS). Furthermore, increased cutaneous levels of ROS can activate the release of several inflammatory cytokines, stimulating tissue infiltration of activated neutrophils and phagocytic cells leading to OxInflammation feedback (Valacchi et al., 2017). It has also been suggested that ROS may be present in the atmosphere on particles to which we are daily exposed, due to the high adsorption capacity of these particles (Hasson and Paulson, 2003; Venkatachari et al., 2007).

Regardless of the mechanism, it is clear that PM exposure increases oxidative stress, resulting in an inflammatory response. However, most of these studies have focused on the effects of particulate matter exposure on organs other than skin, such as the lung (Biswal et al., 2002, Psarras et al., 2005), nervous system (Mortamais et al., 2017, Chen et al., 2017), and the heart (Cohen et al., 2017, Zeng et al., 2017, Liu et al., 2018); thus, studies on the effects of PM exposure on the skin are still limited. However, our group has shown that concentrated ambient particles (CAPs, in the dimensional range between 0.1 and 2.5 μm) are able to damage the skin by altering redox homeostasis and inducing a pro-inflammatory status, as demonstrated by increased levels of 4-HNE and the activation of NF-kB and IL-1α production respectively (Romani et al., 2018).

In order to assess the possible mechanisms involved in this process, in this paper we evaluate the role of oxidative stress in mediating PM-induced skin damage by investigating the effects of specific redox-active species that have been demonstrated mostly responsible for PM-induced ROS generation. They are transition metals like iron (Fe), copper (Cu), chromium (Cr), cobalt (Co), which can undergo Fenton reaction or bind to intracellular thiols (Yang et al., 2014). In addition, surface-bound organic compounds, such as quinones and polycyclic aromatic hydrocarbons (PAH) are able to consume antioxidants in a catalytic cycle to produce ROS in biological systems (Crobeddu et al., 2017). Among these species, our study investigated Cu (II), 9,10 phenanthrenequinone (9,10-PQN) and naphthoquinone isomers 1,2 and 1,4- NQNs, which have been found the most redox-active components present in PM (Fang et al., 2016; Mudway et al., 2011; Verma et al., 2015).

The biological responses of Hacat cells after treatment with these PM components was evaluated by cellular morphological alterations and the biochemical effects analyzing genic and protein expression (Hedayat et al., 2014). In addition, acellular assays were applied to measure the oxidative potential (OP), which addresses the intrinsic capacity of the individual PM components to generate reactive oxygen species (ROS) (Antiñolo et al., 2015; Ayres et al., 2008; Crobeddu et al., 2017; Janssen et al., 2014; Saffari et al., 2015).

2. Materials and methods

2.1. Cell culture

HaCaT cells, established by Boukamp et al., (1988), were purchased from ATCC (Rockville, MD). Cells were cultured using Ham's F-12, fetal bovine serum, DMEM high glucose, penicillin/streptomycin, and L-glutamine, which were obtained from Lonza (Milan, Italy). Cells were incubated at 37 °C for 24 h in 95% air/5% CO2 until 80% confluency. 1,2-NQN and 1,4-NQN, 9,10-PQN and CuSO4 were purchased from Analytical chemistry laboratory, University of Ferrara.

2.2. Measurement of oxidative potential

The Oxidative Potential of species standard solutions was measured with the acellular dithiothreitol (DTT) and ascorbic acid (AA) assays. The kinetics of the oxidation reactions was investigated according to the experimental procedure described elsewhere for the depletion rate of DTT (Charrier and Anastasio, 2012; Li et al., 2009; Pietrogrande, 2018a, 2018b), and for the AA assay (Janssen et al., 2014; Yang et al., 2014).

2.3. Cytotoxicity determination

Cytotoxicity studies were performed on HaCaTs treated with 1 μM or 10 μM of 1,2-NQN and 1,4-NQN, 9,10-PQN and CuSO4 after 24 h measuring LDH (lactate dehydrogenase) release, according to the manufacturer's protocol (EuroClone, Milan, Italy).

2.4. RNA extraction and gene expression analysis

Total RNA was isolated from confluent cells using TRIzol Reagent (Invitrogen, Carlsbad, California, USA), as previously described (Canella et al., 2019). Gene-specific primers and housekeeping in Table 1.

Table 1
Q-PCR Primer sequences and PCR conditions.

Gene	Primer sequence	T_a °C	Product length (bp)	QPCR Amplification Efficiency* (%)	n° of cycles	Ref. Primer Bank
IL-8	F: 5′- ggtgcagttttgccaaggag -3′ R: 5′-atccagctgtgcaactccaa -3′	59.9	183	98.4	39	GenBank Accession NM_000584.3
SOD1	F: 5′- acaaagatggtgtggccgat -3′ R: 5′- aacgacttccagcgtttcct -3′	59.7	162	94.5	39	GenBank Accession NM_000454.4
GPX1	F: 5′-cttgagtctctggacccctc-3′ R: 5′- cagctcgttcatctgggtgt -3′	60.2	152	94.8	39	GenBank Accession M21304.1
RPL13A	F: 5′-cctaagatgagcgcaagttgaa- 3′ R: 5′-ccacaggactagaacacctgctaa-3′	60.2	203	97.3	39	
RPL11A	F: 5′- tgcgggaacttcgcatccgc-3′ R: 5′- gggtctgccctgtgagctgc-3′	60.1	108	96.5	39	GenBank Accession NM 000975.2
GAPDH	F: 5′- tgacgctggggctggcattg -3′ R: 5′- ggctggtggtccaggggtct -3′	60	134	94.6	39	GenBank Accession NM 002046.3

2.5. Total protein extraction

After treatment, 1.5×10^6 cells were detached and washed twice with 1X ice-cold PBS, and total cell lysates were extracted as previously described (Romani et al., 2018). Protein concentrations were determined using the Bio-Rad protein assay kit (Bio-Rad, Milan, Italy).

2.6. Immunofluorescence

Hacat cells were grown on coverslips at a density of 1×10^5 cell/ml, and, after treatment was fixed in 4% paraformaldehyde in PBS for 30 min at 4 °C. The sc-372 primary antibody NFκB and the FITC-conjugated anti-rabbit secondary antibodies were Santa Cruz. Nuclei were stained with DAPI (Molecular Probes). Samples were examined by the Zeiss Axioplan2 light microscope equipped with epifluorescence at 40 × magnification. Images were acquired and analyzed with Axio Vision Release 4.6.3 software.

2.7. Nuclear-cytosolic protein extractions

Nuclear, cytosolic and membrane fractions of HaCaT cells were extracted as previously described (Muresan XM, 2018). Protein concentration was determined by Bradford analysis (Biorad protein assay; Biorad, Milan, Italy).

2.8. Superoxide dismutase (SOD) polyacrylamide activity assay

MnSOD and CuSOD activity was assayed by an active gel method (Cervellati et al., 2015).

2.9. Glutathione peroxidase (Gpx) activity assay

Gpx was assayed by an indirect spectrophotometric assay, (Cervellati et al., 2015).

2.10. Transmission electron microscopy

For ultrastructural analysis, treated Hacat cells were treated as previously described (Magnani ND, 2016) and examined in a Philips CM100 transmission electron microscope.

2.11. Muse millipore cytofluorimetric assay

The levels of total apoptosis cells were detected by Muse Caspase-3/7 Assay Kit. 1×10^5 cells treated for 24 h with different pollutants, according to the manufacturer's protocol (Kitagawa et al. 2016).

2.12. Statistical analysis

All the results were expressed as means ± SEM. Treatments, sampling time, and their interaction were tested by parametric (one-way ANOVA) and non-parametric (Mann-Whitney and Kruskal-Wallis tests) tests. Bonferroni's Multiple Comparison Test was applied as a post-hoc test. p values < 0.05 were considered statistically significant. Data were analyzed using the software GraphPad Prism 4.0 (GraphPad Software, Inc., La Jolla, CA).

3. Results

3.1. Responses assays of DTT and AA assays to PM redox active

In this work, we used two *in vitro* acellular methods for measuring the OP of PM components. They are inexpensive and user-friendly methods based on low-cost UV–Vis spectrophotometric measurements of simple molecular probes, which mimic the consumption of cellular antioxidants catalyzed by redox-active species. One assay uses dithiothreitol (DTT) as a surrogate for biological reducing agents owing to its two sulfhydryl and measures the ability of redox-active compounds to transfer electrons from the dithiol to oxygen, generating superoxide, that subsequently comproportionates to hydrogen peroxide and oxygen (Cho et al., 2005; Li et al., 2009; Charrier and Anastasio, 2012). The ascorbic acid assay uses ascorbic acid (AA), as a simplified model describing the synthetic respiratory tract lining fluids, as the most abundant physiological antioxidant, which has a vital role in oxidant production from redox-active species. AA is oxidized to dehydroascorbic acid, while redox active species are reduced by promoting the formation of ROS (Janssen et al., 2014; Mudway et al., 2011).

To more fully understand the ROS reactivity of the individual species, we measured OP^{DTT} and OP^{AA} for different concentrations ranging from 0.25 to 2 μM, as environmentally relevant levels. For each component, the relationships between OP^{DTT} and OP^{AA} response and concentration are plotted in Fig. 1A. In general, the OP responses are proportional to the species concentration, and the slope of each computed regression line is a measure of the species reactivity toward DTT or AA oxidation. The only exception is OP^{DTT} response for 9,10-PQN, as the response-concentration function is linear only in a limited concentration range up to 1 μM, as found by other Authors (Charrier and Anastasio, 2012).

Although all the investigated quinones and Cu are reactive to both assays, they show different sensitivity. Based on our results on DTT assay (Fig. 1a), we can observe that, of the investigated species, 9,10-PQN is by far the most reactive species, as the slope computed in the 0.25–1 μM range is nearly 10 times higher than that of the

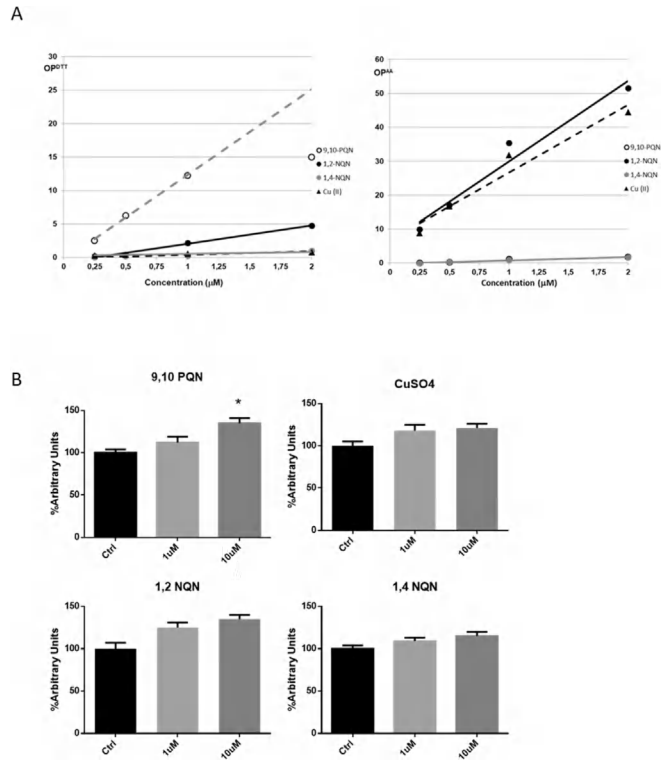

Fig. 1. A) **PM components oxidize DTT and AA**. The oxidative potential of 9, 10 Phe, 1, 4 NPQ, 1,2 NPQ, and Cu were measured using the DTT or AA assays, respectively. The consumption of 9, 10 Phe and 1,4 NPQ is similar in the AA assay, so the curves in that graph are superimposed. The red arrows indicate the points corresponding to the concentration of 1 μM that coincides with the concentration used for cell treatments. B) **Effects of PM constituents on LDH release levels in human keratinocytes**. HaCaTs were treated with either 1 μM or 10 μM doses of 9, 10 Phe (a), CuSO4 (b), 1,2 NPQ (c) or 1,4 NPQ (d), and LDH released was assessed after 24 h of treatment.

other species, that display similar reactivity. Then, the relative reactivities follow the order:

$$9,10\text{-PQN} \gg 1,2\text{-NQN} > 1,4\text{-NQN} \sim \text{Cu}$$

Otherwise, 1,2-NQN and Cu are the most active species towards the AA assay, across the entire range of concentrations tested, followed by 1,4-NQN and 9,10-PQN, that show lower reactivity with similar values (Fig. 1b). Then, the relative reactivities of the AA assay are the following:

$$1,2\text{-NQN} \sim \text{Cu} \gg 1,4\text{-NQN} \sim 9,10\text{-PQN}$$

3.2. Effects of PM constituents on LDH release

To determine the optimum concentration of PM components to use for our *in vitro* assays, we employed an LDH release assay to assess cell damage after 24 h of treatment. As shown in Fig. 1B, neither 1 μM nor 10 μM concentrations of any of the compounds resulted in a large increase in LDH release. However, we did detect a significant increase in LDH release in response to a 10 μM concentration of 9, 10-PQN. Thus, in the subsequent experiments, we used a 1 μM concentration to assess the effects of these PM components on keratinocytes.

3.3. PM components induce NFκB nuclear translocation

Since we observed that these components of PM were capable of oxidizing DTT and/or AA (Fig. 1A), we wanted to see whether these compounds could induce oxidative stress in human keratinocytes. As a readout of oxidative stress, we assessed whether these compounds could affect nuclear translocation of the redox-sensitive transcription factor NFκB. As shown in Fig. 2A–B and 3A-3B, we observed a significant increase in the levels of nuclear NFκB within 30 min of treatment with CuSO4 (Fig. 3A), 9,10-PQN (Figs. 3B), 1 and 2NQN (Figs. 4A) and 1,4-NQN (Fig. 4B) by immunofluorescence assay. We also observed that the levels of nuclear NFκB continued to increase after 60 min of treatment with 1,4-NQN, while the levels of nuclear NFκB in response to the other compounds started to decrease, as compared with the 30 min time point.

3.4. PM components induce NFκB-dependent transcription

Since we observed an increase in nuclear NFκB levels in response to treatment with these compounds, we also tested whether treatment resulted in an increase in NFκB-dependent gene transcription. We examined the levels of the NFκB-responsive gene Interleukin 8 (IL8) (Elliot 2001). As shown in Fig. 4, the gene expression of IL-8 is markedly increased following treatment with 1 μM 9,10-PQN and with the treatment of both quinones (1,2-NQN and 1,4-NQN). Treatment with CuSO4 induced a rapid increase in

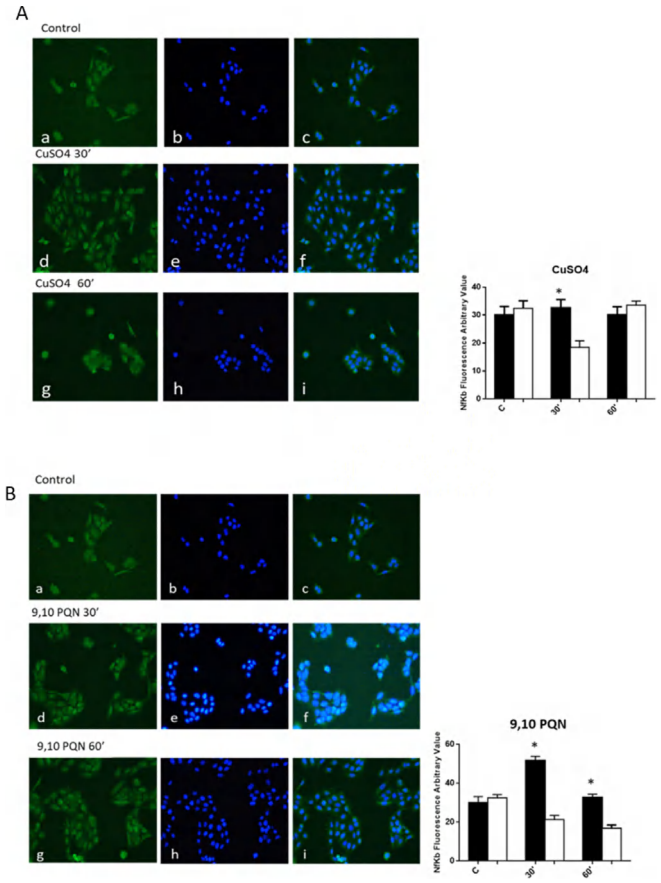

Fig. 2. PM components induce NFκB nuclear translocation. A) Nuclear translocation of NFκB was assessed in HaCaT cells treated with 1 μM of CuSO4 after 30 min (d–f) or 60 min (g–i). B) Nuclear translocation of NFκB was assessed in HaCaT cells treated with 1 μM of 9,10 Phe after 30 min (d–f) or 60 min (g–i). Black Bar: nucleus; White Bar: Cytoplasms.

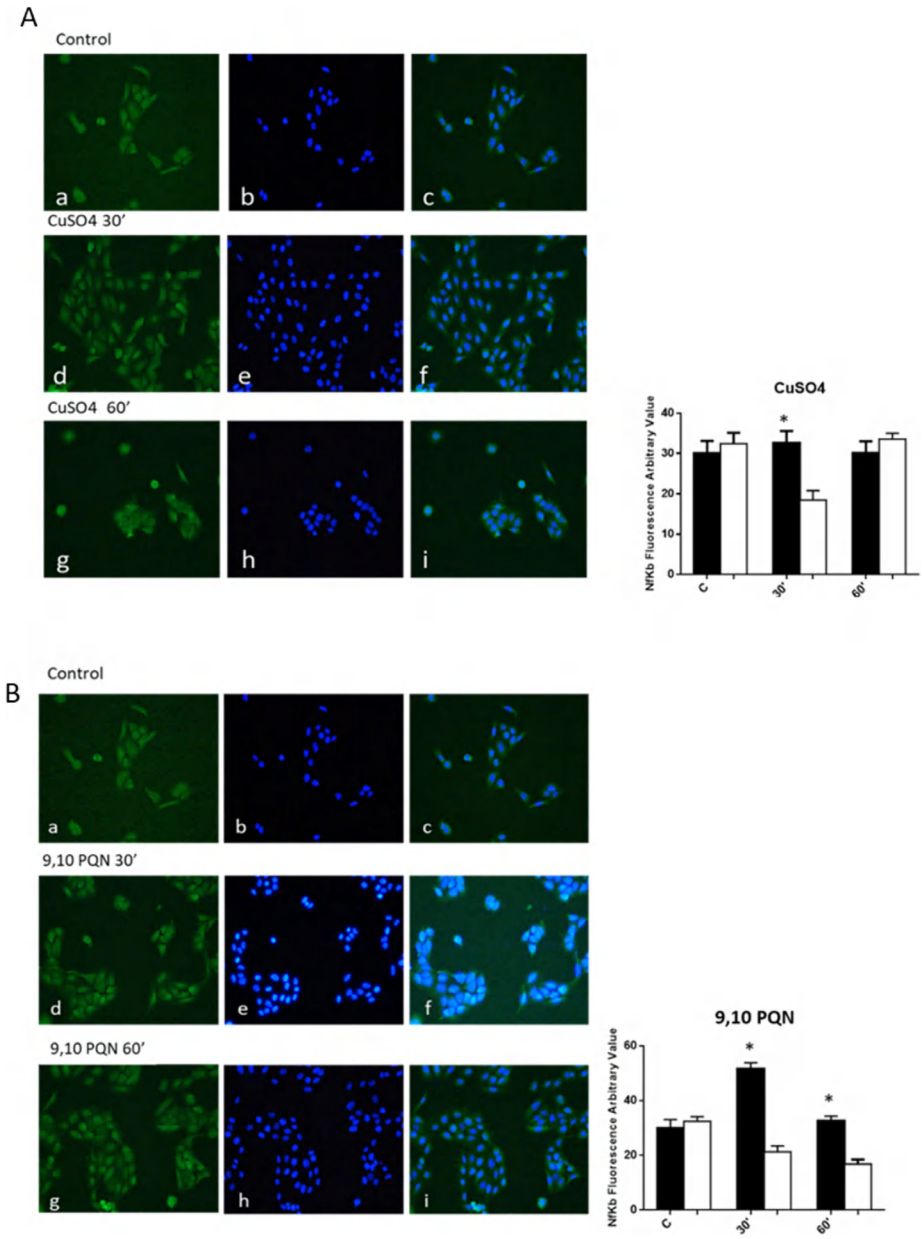

Fig. 3. A) Nuclear translocation of NFκB was assessed in HaCaT cells treated with 1 μM of 1,2 NPQ Phe after 30 min (d–f) or 60 min (g–i). B) Nuclear translocation of NFκB was assessed in HaCaT cells treated with 1 μM of 1, 4 NPQ Phe after 30 min (d–f) or 60 min (g–i). Black Bar: nucleus; White Bar: Cytoplasms.

IL8 transcript levels, which is then lost after 2 h.

3.5. Oxidative stress is increased in keratinocytes after treatment with PM constituents

NFκB has been well-characterized as being responsive to changes in redox homeostasis (Byun, 2002), so we also measured whether treatment with the PM components altered transcription of genes involved in maintaining the cellular redox balance. We examined transcript levels of superoxide dismutase-1 (SOD-1) and observed that transcript levels of SOD-1 significantly increased after 12–24 h of treatment with all of the different PM constituents (Fig. 5A). We also examined transcript levels of glutathione peroxidase (GPX) and observed that treatment with 9,10- PQN and 1,2-NQN significantly increased transcript levels at all time points (Fig. 5B). However, treatment with CuSO4 and 1,4-NQN only resulted in significant increases of GPX transcripts after 6–12 h of treatment.

Since we observed that treatment with the PM components increased transcript levels of SOD-1 and GPX, we next wanted to evaluate whether the treatment also resulted in increased enzymatic activity of these enzymes. Therefore, we evaluated the enzymatic activity of SOD-1 and GPX from cytoplasmatic protein extracts with two specific ELISA kits after 24 h of treatment. As shown in Fig. 5C both SOD-1 and GPX enzymatic activity were significantly increased in response to all of the tested compounds, due to redox cellular imbalances induced by the pollutants.

3.6. Treatment of keratinocytes with PM components results in mitochondrial stress

We believe that the altered redox imbalance induced by these

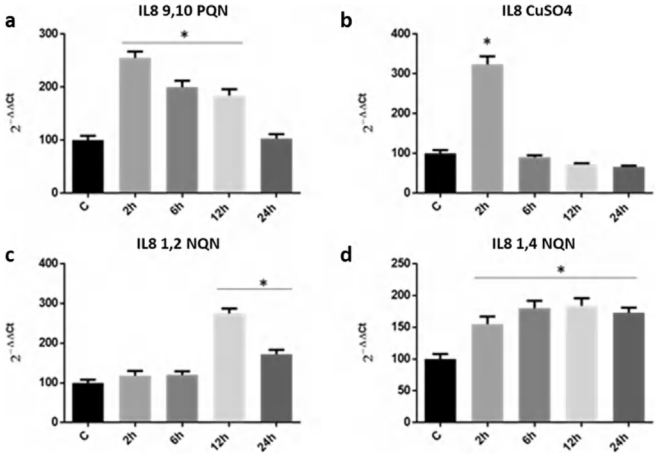

Fig. 4. PM components induce NFκB-dependent transcription. RT-qPCR analysis of IL-8 transcripts in HaCaT cells treated with 1 μM of (a) 9,10 Phe, (b) CuSO4, (c) 1,2 NPQ, and (d) 1,4 NPQ were analyzed after 2, 6, 12, and 24 h of treatment. *p < 0.05 vs C.

pollutants was due to mitochondrial dysfunction, so we used TEM to morphologically assess the effects of the pollutants on the mitochondria. As shown in Fig. 6A, we observed alteration of the mitochondrial ultrastructure with respect the control. In particular, CuSO4 and 9,10-PQN induced mitochondrial dilation, vacuolization, and loss of cristae, while 1,2- and 1,4-NQNs induced mitochondrial thickness and shrinking.

3.7. Oxidative stress induced by PM constituents results in apoptosis

Because the structural alterations observed in the mitochondria in response to the different treatments the induction of apoptosis was also determined.

Caspases are a family of enzymes that play a central role in the apoptotic process. Once activated, these enzymes cause degradation of many key cellular proteins and influence chromatin condensation and DNA damage during apoptosis. Activation of caspase-3/7 is thus a hallmark of apoptosis. We used the Muse™ Caspase-3/7 to quantify the percentage of apoptotic cells. As shown in Fig. 6B, after 24 h of treatment with the PM components, we detected an increase in the number of both apoptotic cells in response to all of the different treatments.

4. Discussion

In developing countries and industrialized regions, air quality has an important impact on the health of people and society. Pollution that consists of fine and ultrafine particulate matter (PM) is a current issue of great concern. It is often referred to as atmospheric aerosol, being composed of a complex mixture of inorganic and organic particles, liquid and solids suspended in the atmosphere; (Hinds, 1999). PM is currently one of the most studied pollutants, due to its complex nature and the variety of chemical distributions, dimensions, and compositions (Colbeck and Lazaridis, 2014).

One of the main toxicological mechanisms resulting from atmospheric PM exposure is believed to be the deregulation of redox homeostasis, by depleting the antioxidant cellular defense and also generating reactive oxygen species (ROS). The generation of ROS during multiphase interactions between air pollutants and the human cells is closely related to the PM chemical composition, since the combination of various pollutants may influence chemical

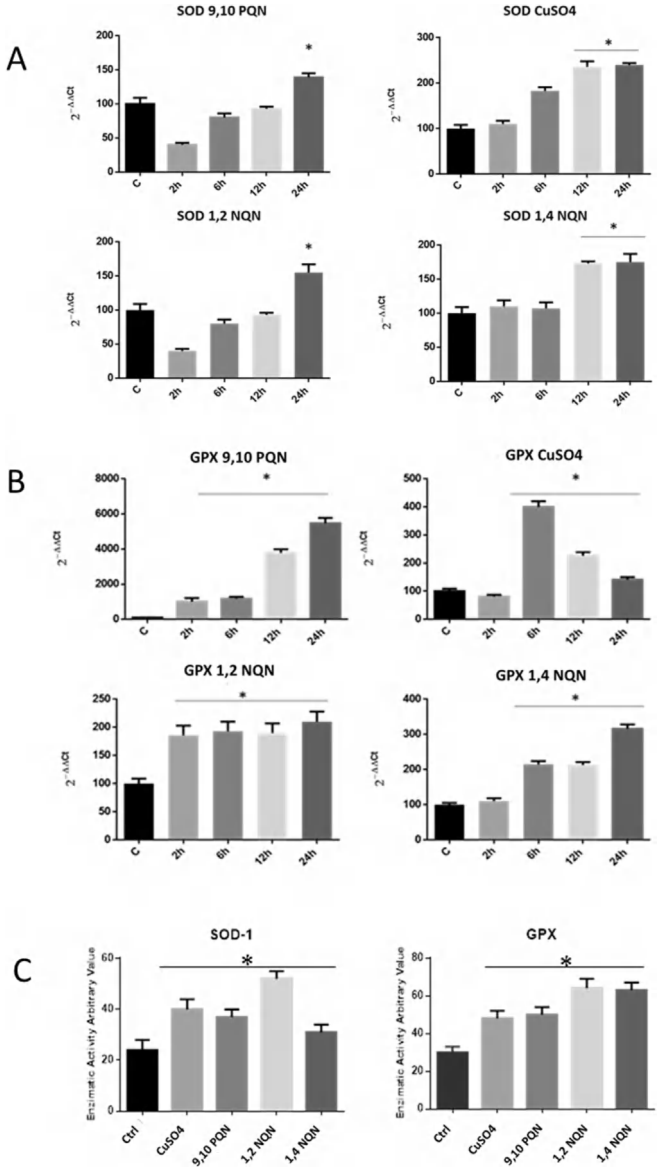

Fig. 5. PM constituents increase SOD transcript levels in keratinocytes. A) RT-qPCR analysis of SOD transcript levels HaCaT cells treated with 1 μM of 9, 10 Phe, (CuSO4, 1,2 NPQ, and 1,4 NPQ were analyzed after 2, 6, 12, and 24 h of treatment. *p < 0.05 vs C. **B) PM components increase GPX transcript levels in keratinocytes.** RT-qPCR analysis of GPX transcript levels HaCaT cells treated with 1 μM of 9,10 Phe, CuSO4, 1,2 NPQ, and 1,4 NPQ was analyzed after 2, 6, 12, and 24 h of treatment. *p < 0.05 vs C. **C) Treatment of keratinocytes with PM components increases SOD-1 and GPX enzymatic activity**. Enzymatic activity of SOD1 and GPX in after 24 h of treatment. Data are expressed as averages of five different experiments, *p < 0.05 vs control.

reactivity as well as bioavailability of PM while having synergistic or nonlinear influences on its oxidative properties (Antiñolo et al., 2015; Fang et al., 2016). Constituents of PM that have been shown as active redox cycling catalysts include black carbon from diesel particles (Shinyashiki et al., 2009), transition metals (Charrier and Anastasio, 2012), humic-like substances (Lin and Yu, 2011; Verma et al., 2015), and quinones (Kumagai et al., 2002).

Among them, the most efficient redox-cycling agents have been identified as the transition metals, mainly Cu (II) and quinones, in particular, the small soluble quinones, such as 1,2-naphthoquinone, 1,4-naphthoquinone, and 9,10 phenanthrenequinone (Charrier and Anastasio, 2012; Kelly, 2003; Lin and Yu, 2011). Although quinones are minor PM constituents, their formation from PAH precursors in

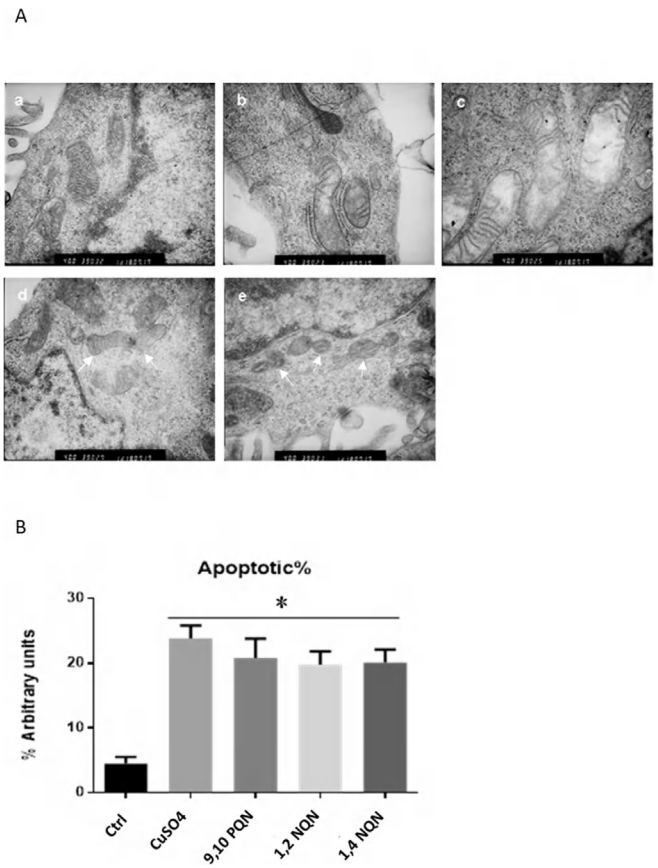

Fig. 6. A) Treatment of keratinocytes with PM components results in structural alterations in mitochondria. a) Ctrl; b) CuSO4; c) 9,10 PQN; d) 1,4 NQN; e) 1,2 NQN. Magnification 40 k. **B): Oxidative stress induced by PM results in apoptosis and cell death. Percentage of apoptotic cells.** Cytofluorimetric Analysis of HaCaT cells 24 h of treatment with1 μM of CuSO4, 9,10 PQN, 1,2 NQN, and 1,4 NQN.

the atmosphere could increase the redox activity of ambient particles during photochemical aging in locations with PAH emission sources, as also confirmed from chamber controlled oxidation studies (Verma et al., 2015).

Therefore, for investigating PM toxicity, we focused on the effects of these most redox active PM components on a line of human keratinocytes. Concerning 9,10-PQN, some authors have shown that it imposes strong oxidative stress conditions in neutrophils after treatment (Wang et al., 2004), inhibits cytochrome P450 functionality (Shimada et al., 2009), and converts T regulatory cells into Th2 helper T cells (Liu et al., 2013). Furthermore, exposure to PQN has been suggested as an important risk factor for developing esophageal squamous cell carcinoma in many populations (Roshandel et al., 2012). Transition metals present in PM, including Cu (II), have also been implicated in inducing DNA strand breakage by promoting ROS generation (Solomon et al., 2014). Further, a study on the effects of Cu (II) exposure on fibroblasts demonstrated its ability to increase lipid peroxidation and decrease the levels of reduced glutathione (GSH) and superoxide dismutase (SOD), leading to cell death (Campo et al., 2004). However, few reports have examined the adverse effects of other oxidized PAHs on the cellular redox balance. Especially, little is known about how exposure to quinones affects NFκB activation in human cells, even exposure to PAHs has been shown to promote inflammation through inducing transcription of IL-8 with an NFκB-dependent mechanism in BEAS-2B cells (Sunazuka et al., 1999).

In this study, we observed that treating human keratinocytes with Cu (II), 9,10-PQN, 1,2- and 1,4-NQNs stimulates the inflammatory response, resulting in NFκB activation and increased levels of NFκB-dependent transcription of IL8 in HaCaT cells. Increased IL-8 transcription correlates with the inflammatory state induced by treatment with pollutants (Ushio et al. 1999; Li et al. 2017). Since alterations in the cellular inflammatory state can result in oxidative stress, we investigated whether treatment with the PM constituents altered transcript levels of genes involved in the cellular redox balance. We observed that transcript levels for SOD-1 and GPX were increased in response to treatment with all of the tested PM components as well as their enzymatic activity. This results is most likely a consequences of NRF2 activation, a transcription factor redox sensitive inolve in the cellular responses to oxidative insults (Schäfer M and Werner S, 2015). Indeed the activation of NRF2 by pollution has been recently demonstrated by several group (Magnani N et al., 2016; Marrot, 2018; Valacchi et al., 2015) and it is possible to hypothesize that an important aspect in cell response to pollution is a consenquence of the cross-talk between NFKB and NRF2, both transcriptors factors sensitive to altered cellular redox homeostasis (Wardyn et al., 2015).

Next, we tested whether this treatment-induced redox imbalance could also cause ultrastructural damage to the exposed cells and observed structural alterations of mitochondria. In particular, we found that treatment with Cu (II) and with 9,10-PQN induced dilatation and vacuolization with consequent loss of mitochondrial cristae, while treatment with 1,2- and 1,4-NQNs was able to induce mitochondrial shrinkage and condensation. In parallel, increased apoptosis and cell death in keratinocytes were also noticed.

Altogether, our results consistently indicate that all of the tested PM components induce inflammation and a redox-imbalance. Therefore, although PM particles vary in size, mass, number, shape, aggregation status, surface area, as well as chemical composition, these differences may not be as biologically relevant as previously thought, if exposure to all of the different components results in the same biological consequence.

In addition, the oxidative potential of each investigated species was measured in order to quantify the intrinsic of capacity to oxidize target molecules inside the human body. Up to date, a number of different *in vitro* acellular assays have been used for assessing OP of aerosol particles, all with varying sensitivity, detection limits and technical requirements. They are based on different probes mimicking the consumption of antioxidants (e.g. ascorbic acid (AA), reduced glutathione (GSH) or surrogates (e.g. dithiothreitol (DTT)), or hydroxyl radical formation in the presence of H_2O_2, or the application of electron spin resonance (ESR) to quantify ROS production. In comparison with cellular methods *in vitro,* cell-free assays have the advantages of requiring less-controlled environments and providing faster readouts for the screening of toxicity in airborne PM and nanoparticles. Among them, in this paper, we applied both dithiothreitol and ascorbic acid assays. Most of the current literature indicates that the two assays respond differently to various redox-active species. In particular, the DTT assay is known to be strongly sensitive to organic species, such as polycyclic aromatic hydrocarbons (PAHs) and quinones (Charrier and Anastasio, 2012; Cho et al., 2005; Chung et al., 2006; Li et al., 2009; Guin et al., 2011; Dai et al., 2017), and only recently it has been characterized to be sensitive also to standard solutions of transition metal ions, such as Cu (II) and Zn (II), (Charrier and Anastasio, 2012; Lin and Yu, 2011). In contrast, it is well known that the presence of transition metals promotes oxidation reaction of ascorbic acid (Ayres et al., 2008; Buettner and Jurkiewicz, 1996; Xu and Jordan, 1990), and quinones have been discovered able to oxidize ascorbic acid (Mudway et al., 2011; Roginski et al., 1999).

In accordance with these literature data, our results showed that

9,10-PQN is the most effective in the DTT test, followed by 1,2-NQN (Fig. 1a), while 1,2-NQN, and Cu (II) are the most reactive to the AA assay (Fig. 1b). 1,4-NQN showed small responses in both tests. Indeed, since each of the existing OP assays is somewhat specific to the precise structure of ROS-inducer (Yang et al., 2014), a standard methodology should most probably include a combination of different antioxidant probes, in order to provide complementary information on the ability of generating ROS through a combination of different processes (Janssen et al., 2014). However, such a combination has not emerged yet, since the link between OP and chemical composition of PM is not fully understood.

As an additional outcome of the present paper, we tried to investigate possible associations of OP responses with cellular endpoints, inside the general consistency among the results indicating that all of the tested species reactive to OP assays produce a redox-imbalance. In particular, we can observe that 9, 10 PQN, which is the species with the highest OP^{DTT} response, is the only one which significantly increased LDH release (at 10 μM concentration, Fig. 2) and also induced dilatation and vacuolization of mitochondria, together with Cu (II), with an high OP^{AA} response, while 1, 2 NQN, with the highest OP^{AA}, induced mitochondrial shrinkage and condensation (Fig. 6A). Indeed, these are partial and preliminary results, that require further experimental evidence to highlight the possible associations of the acellular assay responses with biological findings elicited by exposure to redox-active species.

In conclusion, our data showed that, although chemically different, all the investigated redox-active PM components were able to induce a proinflammatory status and the activation of the cellular defensive system, suggesting a common mechanism of action among these species. Finally, the present results can further support the idea that exposure to PM can lead to skin conditions observed in populations that live in areas with high levels of pollution (Drakaki et al., 2014).

References

Antiñolo, M., Willis, M.D., Zhou, S., Abbatt, J.P.D., 2015. Connecting the oxidation of soot to its redox cycling abilities. Nat. Commun. 79, 271–285, 6. Atmos. Environ.

Ayres, J.G., Borm, P., Cassee, F.R., Castranova, V., Donaldson, K., Ghio, A., Harrison, R.M., Hider, R., Kelly, F., Kooter, I.M., Marano, F., Maynard, R.L., Mudway, I., Nel, A., Sioutas, C., Smith, S., Baeza-Squiban, A., Cho, A., Duggan, S., Froines, J., 2008. Evaluating the toxicity of airborne particulate matter and nanoparticles by measuring oxidative stress potential—a workshop report and consensus statement. Inhal. Toxicol. 20, 75–99.

Biswal, S., Acquaah-Mensah, G., Datta, K., Wu, X., Kehrer, J.P., 2002. Inhibition of cell proliferation and AP-1 activity by acrolein in human A549 lung adenocarcinoma cells due to thiol imbalance and covalent modifications. Chem Res Toxicol. Feb 15 (2), 180–186.

Boukamp, P., Petrussevska, R.T., Breitkreutz, D., Hornung, J., Markham, A., Fusenig, N.E., 1988. Normal keratinization in a spontaneously immortalized aneuploid human keratinocyte cell line. J. Cell Biol. 106 (3), 761–771, 1988 Mar.

Buettner, G.R., Jurkiewicz, B.A., 1996. Catalytic metals, ascorbate and free radicals: combinations to avoid. Carcinogenesis. Jan;21 Radiat. Res. 145 (1), 532–541, 87-92.

Byun, M.S., Jeon, K.I., Choi, J.W., Shim, J.Y., Jue, D.M., 2002 Nov 30. Dual effect of oxidative stress on NF-kappa B activation in HeLa cells. Exp. Mol. Med. 34 (5), 332–339.

Campo, G.M., D'Ascola, A., Avenoso, A., Campo, S., Ferlazzo, A.M., Micali, C., Zanghì, L., Calatroni, A., 2004. Glycosaminoglycans reduce oxidative damage induced by copper (Cu+2), iron (Fe+2) and hydrogen peroxide (H2O2) in human fibroblast cultures. Glycoconj. J. 20 (2), 133–141.

Canella, R., Martini, M., Cavicchio, C., Cervellati, F., Benedusi, M., Valacchi, G., 2019. Involvement of the TREK-1 channel in human alveolar cell membrane potential and its regulation by inhibitors of the chloride current. J. Cell Physiol. 25 https://doi.org/10.1002/jcp.28396. Feb.

Cervellati, C., Sticozzi, C., Romani, A., Belmonte, G., De Rasmo, D., Signorile, A., Cervellati, F., Milanese, C., Mastroberardino, P.G., Pecorelli, A., Savelli, V., Forman, H.J., Hayek, J., Valacchi, G., 2015. Impaired enzymatic defensive activity, mitochondrial dysfunction and proteasome activation are involved in RTT cell oxidative damage. Biochim. Biophys. Acta 1852 (10 Pt A), 2066–2074. https://doi.org/10.1016/j.bbadis.2015.07.014. Epub 2015 Jul 17.

Charrier, J.G., Anastasio, C., 2012. On dithiothreitol (DTT) as a measure of oxidative potential for ambient particles: evidence for the importance of soluble transition metals. Atmos. Chem. Phys. 12, 11317–11350.

Chen, M., Li, B., Sang, N., 2017. Particulate matter (PM2.5) exposure season-dependently induces neuronal apoptosis and synaptic injuries. J. Environ. Sci. (China) 54, 336–345. https://doi.org/10.1016/j.jes.2016.10.013.

Cho, A.K., Sioutas, C., Miguel, A.H., Kumagai, Y., Schmitz, D.A., Singh, M., Eiguren-Fernandez, A., Froines, J.R., 2005. Redox activity of airborne particulate matter at different sites in the Los Angeles Basin. Environ. Res. 99, 40–47.

Chung, M.Y., Lazaro, R.A., Lim, D., Jackson, J., Lyon, J., Rendulic, D., Hassom, A.S., 2006. Aerosol-borne quinones and reactive oxygen species generation by particulate matter extracts. Environ. Sci. Technol. 40, 4880–4886.

Cohen, G., Levy, I., Yuval, Kark, J.D., Levin, N., Broday, D.M., Steinberg, D.M., Gerber, Y., 2017. Long-term exposure to traffic-related air pollution and cancer among survivors of myocardial infarction: a 20-year follow-up study. Eur. J. Prev. Cardiol. 24 (1), 92–102.

Colbeck, Lazaridis, 2014. Aerosol Science: Technology and Applications.

Crobeddu, B., Aragao-Santiago, L., Bui, L.C., Boland, S., Baeza Squiban, A., 2017 Nov. Oxidative potential of particulate matter 2.5 as predictive indicator of cellular stress. Environ. Pollut. 230, 125–133. https://doi.org/10.1016/j.envpol.2017.06.051. Epub 2017 Jun 22.

Dai, F., Yan, W.J., Du, Y.T., Bao, X.Z., Li, X.Z., Zhou, B., 2017. Structural basis, chemical driving forces and biological implications of flavones as Cu (II) ionophores. Free Radic. Biol. Med. 108, 554–563. https://doi.org/10.1016/j.freeradbiomed.2017.04.023.

Delfino, R.J., Sioutas, C., Malik, S., 2005. Potential role of ultrafine particles in associations between airborne particle mass and cardiovascular health. Environ. Health Perspect. 113, 934–946.

Dellinger, B., Pryor, W.A., Cueto, R., Squadrito, G.L., Hegde, V., Deutsch, W.A., 2001. Role of free radicals in the toxicity of airborne fine particulate matter. Chem. Res. Toxicol. 14, 1371–1377.

Drakaki, E., Dessinioti, C., Antoniou, C.V., 2014. Air pollution and the skin. Front. Environ. Sci. 15. https://doi.org/10.3389/fenvs.2014.00011.

Fang, T., Verma, V., Bates, J.T., Abrams, J., Klein, M., Strickland, M.J., Sarnat, S.E., Chang, H.H., Mulholland, J.A., Tolbert, P.E., Russell, A.G., Weber, R.J., 2016. Oxidative potential of ambient water-soluble PM2:5 in the southeastern United States: contrasts in sources and health associations between ascorbic acid (AA) and dithiothreitol (DTT) assays. Atmos. Chem. Phys. 16, 3865–3879.

Ghio, Carraway M.S., Madden, M.C., 2012. Composition of air pollution particles and oxidative stress in cells, tissues, and living system. J. Toxicol. Environ. Health B Crit. Rev. 15, 1–21.

Guin, P.S., Das, S.,2, Mandal, P.C., 2011. Electrochemical reduction of quinones in different media: a review. Int. J. Electrochem. 2011, 22. Article ID 816202. https://doi.org/10.4061/2011/816202.

Hasson, A.S., Paulson, S.E., 2003. An investigation of the relationship between gas-phase and aerosol-borne hydroperoxides in urban air. J. Aerosol Sci. 34, 459–468.

Hedayat, F., Stevanovic, S., Miljevic, B., Bottle, S., Ristovski, Z.D., 2014. Review-evaluating the molecular assays for measuring the oxidative potential of particulate matter. Chem. Ind. Chem. Eng. Q. 21, 201–210.

Hinds, William C., 1999. Aerosol Technology: Properties, Behavior, and Measurement of Airborne Particles, second ed. In: Aerosol Technology. A Wiley-Interscience Publication John Wiley & Sons, Inc, California. Department of Environmental Health Sciences Center for Occupational and Environmental Health UCLA School of Public Health Los Angeles.

Janssen, N.A.H., Yang, A., Strak, M., Steenhof, M., Hellack, B., Gerlofs-Nijland, M.E., Kuhlbusch, T., Kelly, F., Harrison, R., Brunekreef, B., Hoek, G., Cassee, F., 2014. Oxidative potential of particulate matter collected at sites with different source characteristics. Sci. Total Environ. 472, 572–581.

Kelly, F.J., 2003. Oxidative stress: its role in air pollution and adverse health effects. Occup. Environ. Med. 60, 612–616.

Kitagawa, N., Morikawa, T., Motai, C., Ninomiya, K., Okugawa, S., Nishida, A., Yoshikawa, M., Muraoka, O., 2016. The antiproliferative effect of chakasaponins I and II, floratheasaponin A, and epigallocatechin 3-O-gallate isolated from camellia sinensis on human digestive tract carcinoma cell lines, 2016 Nov 26 Int. J. Mol. Sci. (12), 17. pii: E1979.

Kumagai, Y., Koide, S., Taguchi, K., Endo, A., Nakai, Y., Yoshikawa, T., Shimojo, N., 2002. Oxidation of proximal protein sulfhydryls by phenanthraquinone, a component of diesel exhaust particles. Chem. Res. Toxicol. 15, 483–489.

Li, Q., Wyatt, A., Kamens, R.M., 2009. Oxidant generation and toxicity enhancement of aged-diesel exhaust. Atmos. Environ. 43, 1037–1042.

Li, Q., Kang, Z., Jiang, S., Zhao, J., Yan, S., Xu, F., Xu, J., 2017 Jan 12. Effects of ambient fine particles PM2.5 on human HaCaT cells. Int. J. Environ. Res. Public Health (1), 14. https://doi.org/10.3390/ijerph14010072 pii: E72.

Lin, P., Yu, J.Z., 2011. Generation of reactive oxygen species-mediated by humic-like substances in atmospheric aerosols. Environ. Sci. Technol. 45, 10362–10368.

Liu, J., Zhang, L., Winterroth, L.C., Garcia, M., Weiman, S., Wong, J.W., Sunwoo, J.B., Nadeau, K.C., 2013. Epigenetically mediated pathogenic effects of phenanthrene on regulatory T cells. J. Toxicol. 967029. https://doi.org/10.1155/2013/967029, 2013.

Liu, H., Tian, Y., Xiang, X., Sun, K., Juan, J., Song, J., Cao, Y., Xu, B., Hu, Y., 2018. Air pollution and hospitalization for acute myocardial infarction in China, 2017 Sep. 1 Am. J. Cardiol. 120 (5), 753–758. https://doi.org/10.1016/j.amjcard.2017.06.004.

Magnani, N.D., Muresan, X.M., Belmonte, G., Cervellati, F., Sticozzi, C., Pecorelli, A., Miracco, C., Marchini, T., Evelson, P., Valacchi, G., 2016. Skin damage

mechanisms related to airborne particulate matter exposure. Toxicol. Sci. 149 (1), 227–236. https://doi.org/10.1093/toxsci/kfv230. Epub 2015 Oct 26.
Marrot, L., 2018. Pollution and sun exposure: a deleterious synergy. Mechanisms and opportunities for skin protection. Curr. Med. Chem. 25 (40), 5469–5486. https://doi.org/10.2174/0929867324666170918123907.
Mohan Kumar, S.M.J., Campbell, A., Block, M., Veronesi, B., 2008. Particulate matter, oxidative stress and neurotoxicity. Neurotoxicology (Little Rock) 29, 479–488.
Mortamais, M., Pujol, J., van Drooge, B.L., Macià, D., Martínez-Vilavella, G., Reynes, C., Sabatier, R., Rivas, I., Grimalt, J., Forns, J., Alvarez-Pedrerol, M., Querol, X., Sunyer, J., 2017. Effect of exposure to polycyclic aromatic hydrocarbons on basal ganglia and attention-deficit hyperactivity disorder symptoms in primary school children. Environ. Int. 105, 12–19. https://doi.org/10.1016/j.envint.2017.04.011. Epub 2017 May 5.
Mudway, I.S., Fuller, G., Green, D., Dunster, C., Kelly, F.J., 2011. Quantifying the London Specific Component of PM_{10} Oxidative Activity. UK Department for Environment. Food & Rural Affair. http://uk-ait.defra.gov.uk/library/reports?report_id1/4649.
Muresan, X.M., Sticozzi, C., Belmonte, G., Cervellati, F., Ferrara, F., Lila, M.A., Valacchi, G., 2018. SR-B1 involvement in keratinocytes in vitro wound closure, 2018 Nov 15 Arch. Biochem. Biophys. 658, 1–6. https://doi.org/10.1016/j.abb.09.014. Epub 2018 Sep. 18.
Piao, M.J., Ahn, M.J., Kang, K.A., Ryu, Y.S., Hyun, Y.J., Shilnikova, K., Zhen, A.X., Jeong, J.W., Choi, Y.H., Kang, H.K., Koh, Y.S., Hyun, J.W., 2018. Particulate matter 2.5 damages skin cells by inducing oxidative stress, subcellular organelle dysfunction, and apoptosis. Arch. Toxicol. 2018 Mar 26.
Pietrogrande, M.C., Perrone, M.R., Manarini, F., Romano, S., Udisti, R., Becagli, S., 2018a. PM10 oxidative potential at a Central Mediterranean Site: association with chemical composition and meteorological parameters. Atmos. Environ. 188, 97–111.
Pietrogrande, M.C., Dalpiaz, C., Dell'Anna, R., Lazzeri, P., Manarini, F., Visentin, M., Tonidandel, G., 2018b. Chemical composition and oxidative potential of atmospheric coarse particles at an industrial and urban background site in the alpine region of northern Italy. Atmos. Environ. 191, 340–350.
Psarras, S., Caramori, G., Contoli, M., Papadopoulos, N., Papi, A., 2005. Oxidants in asthma and in chronic obstructive pulmonary disease (COPD). Curr. Pharmaceut. Des. 11 (16), 2053–2062 (submitted for publication).
Roginski, V.A., Barsukova, T.K., Stegmann, H.B., 1999. Kinetics of redox interaction between substitutes quinones and ascorbate under aerobic conditions. Chem-Bio Interact. 121, 177–197.
Romani, A., Cervellati, C., Muresan, X.M., Belmonte, G., Pecorelli, A., Cervellati, F., Benedusi, M., Evelson, P., Valacchi, G., 2018. Keratinocytes oxidative damage mechanisms related to airbone particle matter exposure. Mech. Ageing Dev. 172, 86–95. https://doi.org/10.1016/j.mad.2017.11.007. Epub 2017 Nov 8.
Roshandel, G., Semnani, S., Malekzadeh, R., Dawsey, S.M., 2012. Polycyclic aromatic hydrocarbons and esophageal squamous cell carcinoma, 2012 Nov Arch. Iran. Med. 15 (11), 713–722. doi: 0121511/AIM.0013. (submitted for publication).
Saffari, A., Hasheminassab, S., Wang, D., Shafer, M.M., Schauer, J.J., Sioutas, C., 2015. Impact of primary and secondary organic sources on the oxidative potential of quasi-ultrafine particles (PM0.25) at three contrasting locations in the Los Angeles Basin. Atmos. Environ. 120, 286–296.
Schäfer, M., Werner, S., 2015. Nrf2–A regulator of keratinocyte redox signaling. Free Radic. Biol. Med. 88 (Pt B), 243–252, 2015 Nov.
Shimada, T., Tanaka, K., Takenaka, S., Foroozesh, M.K., Murayama, N., Yamazaki, H., Guengerich, F.P., Komori, M., 2009. Reverse type I binding spectra of human cytochrome P450 1B1 induced by flavonoid, stilbene, pyrene, naphthalene, phenanthrene, and biphenyl derivatives that inhibit catalytic activity: a structure-function relationship study. Chem. Res. Toxicol. 22 (7), 1325–1333. https://doi.org/10.1021/tx900127s, 2009 Jul.
Shinyashiki, M., Eiguren-Fernandez, A., Schmitz, D.A., Di Stefano, E., Li, N., Linak, W.P., Cho, S.H., Froines, J.R., Cho, A.K., 2009. Electrophilic and redox properties of diesel exhaust particles, 2009 Apr Environ. Res. 109 (3), 239–244. https://doi.org/10.1016/j.envres.2008.12.008. Epub 2009 Feb 6.
Solomon, E.I., Heppner, D.E., Johnston, E.M., Ginsbach, J.W., Cirera, J., Qayyum, M., Kieber-Emmons, M.T., Kjaergaard, C.H., Hadt, R.G., Tian, L., 2014. Copper active sites in biology. Chem. Rev. 114 (7), 3659–3853. https://doi.org/10.1021/cr400327t, 2014 Apr 9.
Squadrito, G.L., Cueto, R., Dellinger, B., Pryor, W.A., 2001. Quinoid redox cycling as a mechanism for sustained free radical generation by inhaled airborne particulate matter, 2001 Nov 1 Free Radic. Biol. Med. 31 (9), 1132–1138 (submitted for publication).
Sunazuka, T., Takizawa, H., Desaki, M., Suzuki, K., Obata, R., Otoguro, K., Omura, S., 1999. Effects of erythromycin and its derivatives on interleukin-8 release by human bronchial epithelial cell line BEAS-2B cells. J. Antibiot. (Tokyo) 52 (1), 71–74, 1999 Jan.
Ushio, H., Nohara, K., Fujimaki, H., 1999. Effect of environmental pollutants on the production of pro-inflammatory cytokines by normal human dermal keratinocytes. Toxicol. Lett. 105 (1), 17–24, 1999 Mar 8.
Valacchi, G., Sticozzi, C., Pecorelli, A., Cervellati, F., Cervellati, C., Maioli, E., 2012. Cutaneous responses to environmental stressors. Ann. N. Y. Acad. Sci. 1271, 75–81. https://doi.org/10.1111/j.1749-6632.2012.06724.x. Review, 2012 Oct.
Valacchi, G., Sticozzi, C., Belmonte, G., Cervellati, F., Demaude, J., Chen, N., Krol, Y., Oresajo, C., 2015. Vitamin C compound mixtures prevent ozone-induced oxidative damage in human keratinocytes as initial assessment of pollution protection. PLoS One 10 (8), e0131097, 2015 Aug 13.
Valacchi, G., Pecorelli, A., Cervellati, C., Hayek, J., 2017. 4-hydroxynonenal protein adducts: key mediator in Rett syndrome oxinflammation, 2017 Oct Free Radic. Biol. Med. 111, 270–280. https://doi.org/10.1016/j.freeradbiomed.2016.12.045. Epub 2017 Jan 5. Review.
Venkatachari, P., Hopke, P.K., Brune, W.H., Ren, X., Lesher, R., Mao, J., Mitchell, M., 2007. Characterization of wintertime reactive oxygen species concentrations in Flushing, New York. Aerosol Sci. Technol. 41, 97–111.
Verma, V., Fang, T., Xu, L., Peltier, R.E., Russel, A.G., Ng, N.L., Weber, R.J., 2015. Organic aerosols associated with the generation of reactive oxygen species (ROS) by water-soluble $PM_{2.5}$. Environ. Sci. Technol. 49, 4646–4656.
Wang, Q., Dubé, D., Friesen, R.W., LeRiche, T.G., Bateman, K.P., Trimble, L., Sanghara, J., Pollex, R., Ramachandran, C., Gresser, M.J., Huang, Z., 2004. Biochemistry 43 (14), 4294–4303.
Wardyn, J.D., Ponsford, A.H., Sanderson, C.M., 2015. Dissecting molecular cross-talk between Nrf2 and NF-κB response pathways. Biochem. Soc. Trans. 43 (4), 621–626.
Weschler, C.J., Bekö, G., Koch, H.M., Salthammer, T., Schripp, T., Toftum, J., Clausen, G., 2015. Transdermal uptake of diethyl phthalate and di(n-butyl) phthalate directly from air: experimental verification. Environ. Health Perspect. 123 (10), 928–934. https://doi.org/10.1289/ehp.1409151, 2015 Oct.
Xu, J., Jordan, R.B., 1990. Kinetics and mechanism of the reaction of aqueous copper (II) with ascorbic acid. Inorg. Chem. 29, 2933–2936.
Yang, A., Jedynska, A., Hellack, B., Kooter, I., Hoek, G., Brunekreef, B., Kuhlbusch, T.A.J., Cassee, F.R., Janssen, N.A.H., 2014. Measurement of the oxidative potential of PM2.5 and its constituents: the effect of extraction solvent and filter type. Atmos. Environ. 83, 35–42.
Zeng, Q., Li, P., Ni, Y., Li, G.X., Wang, D.Z., Pan, X.C., Jiang, G.H., 2017. [Research on the relationship between atmospheric inhalable particulate matter and cardiovascular diseases burden in Tianjin]. Zhonghua Xinxueguanbing Zazhi 46 (1), 50–55. https://doi.org/10.3760/cma.j.issn.0253-3758.2018.01.009. Chinese, 2018 Jan 24.

atmosphere

MDPI

Article

Oxidative Potential Sensitivity to Metals, Br, P, S, and Se in PM10 Samples: New Insights from a Monitoring Campaign in Southeastern Italy

Salvatore Romano [1,*], Silvia Becagli [2], Franco Lucarelli [3], Mara Russo [4] and Maria Chiara Pietrogrande [4]

1 Department of Mathematics and Physics, University of Salento, 73100 Lecce, Italy
2 Department of Chemistry, University of Florence, 50019 Sesto Fiorentino, Florence, Italy
3 Department of Physics, University of Florence, 50019 Sesto Fiorentino, Florence, Italy
4 Department of Chemical and Pharmaceutical Sciences, University of Ferrara, 44121 Ferrara, Italy
* Correspondence: salvatore.romano@unisalento.it

Received: 15 March 2020; Accepted: 7 April 2020; Published: 9 April 2020

Abstract: Different analytical techniques were used in this work to investigate the relationships between oxidative potential (OP) and metal, Br, P, S, and Se concentration in PM10 samples. Dithiothreitol and ascorbic acid acellular assays were used to determine the oxidative potential (OP) in PM10 samples. The particle-induced X-ray emission technique was used to estimate the mass concentration of specific chemical elements. PM10 samples were collected in Lecce, a coastal site of the Central Mediterranean away from large sources of local pollution. Both winter and spring samples were analyzed to study the seasonal dependence of the relationships between OP values and chemical element concentrations. The Redundancy Discriminant Analysis (RDA) was applied to (volume- and mass-normalized) OP values as response variables and metal, Br, P, S, and Se concentrations as explanatory variables. RDA triplots allowed to visualize the main relationships between PM10 OP values and corresponding chemical element concentrations. Spearman correlation coefficients were also used to investigate the relationships between OP values and metal, Br, P, S, and Se concentrations, besides comparing RDA outcomes. The integrated approach based on two different techniques allowed to better highlight the potentially harmful effects associated with specific metals and other chemical elements in PM10 samples.

Keywords: PM chemical composition; air pollution; air quality observations; seasonal variations; oxidative potential; metals; redundancy discriminant analysis; Spearman correlation coefficient

1. Introduction

Particulate matter (PM) is a complex mixture of particles with different characteristics (e.g., mass, size, shape, surface area, solubility, acidity, and number) and different chemical components. Metals come from impurities derived from fuel additives and/or brakes and tires attrition, and they can be generally found adhered to PM particles [1,2]. Iron (Fe), nickel (Ni), vanadium (V), chromium (Cr), and copper (Cu) are the most studied and analyzed transition metals due to their potential to produce reactive oxygen species (ROS) in biological systems [3]. Fe, Cu, Ni, and V in fine PM have been found to be associated with cardiovascular and respiratory hospital admissions and mortality [4,5], as well as increased heart rate and decreased lung function [6]. Heavy metals such as cadmium (Cd), lead (Pb), and mercury (Hg) are generally produced by industrial, combustion, extraction, and processing activities. They are also able to exert their toxic effects by the production of ROS [1]. These toxic effects are generally quantified by oxidative potential (OP), which is a measure of the capacity of PM to

deplete certain antioxidant molecules such as ascorbic acid (AA) or dithiothreitol (DTT) in synthetic airway fluid and to generate ROS ([7,8] and references therein). OP has been proposed as a more relevant exposure metric that is closely related to biological responses to PM exposure compared to PM mass concentration [9,10]. In fact, oxidative stress is considered to be the main link between PM exposure and associated diseases [11–13]. PM OP was found to contribute to oxidative stress and inflammation in cultured human lung carcinoma cells [14]. Significant variations in PM OP levels were reported in the Netherlands and Belgium [15,16], London (UK) [17], Hungary [18], Chamonix (France) [19,20], and Canada [21,22]. Daher et al. [23] explained that the differences in the OP levels of PM samples are mostly related to transition metal content. In fact, the measurement of OP involves the redox activity of transition metals and organic chemicals, and it reflects interactions between different metals in the reaction [2].

In this study, two common acellular techniques based on low-cost spectrophotometric UV–Vis measurements, dithiothreitol ([24]) and ascorbic acid ([25]) assays were used to determine PM OP responses and study their relationships with metal, Br, P, S, and Se mass concentrations. Several studies have been devoted to the analysis of the relationships between the main features of the PM OP values and specific metals ([23] and references therein). Liu et al. [22] performed an explanatory study in Toronto (Canada) and proved that the metal constituents in ambient PM may have partially contributed to the generation of OP and its adverse effects like systemic inflammation, oxidative stress, the perturbation of neural function, and physiological stress. Nishita-Hara et al. [26] carried out a continuous sampling of both fine and coarse PM particles in spring 2016 in Fukuoka (Japan) to study the effects of the main chemical components of Asian dust on PM OP. In particular, they investigated the contributions of both total and water-soluble metals to the OP determined by the DTT assay activity. They found a significant increase of OP during the analyzed Asian dust events, but the water-soluble transition metals were only responsible for 37% and 60% of the measured OP of the fine and coarse PM fraction, respectively. Saffari et al. [27] performed a year-long sampling campaign of quasi-ultrafine particles (with an aerodynamic diameter of less than 0.25 μm) at 10 distinct sites with different characteristics near Los Angeles (USA). They observed, particularly during winter, a strong correlation between DTT activity and transition metals (Cr, Mn, V, Fe, Cu, Cd, and Zn) generally associated with the vehicular traffic source. Calas et al. [20] reported the main findings related to the seasonal OP variations from both the DTT and AA acellular assays, as well as their correlations with PM chemical composition over a one-year period in seven French urban background sites. They also found that correlation between volume-normalized OP and metal mass concentration was strongly seasonal-, assay-, and location-dependent.

Two previous works defined the main features of PM OP over Southeastern Italy at the same site of this study. First, Pietrogrande et al. [8] investigated the OP measured with both the AA and DTT assays in PM10 samples collected from December 2014 to October 2015 in order to highlight the sensitivity of both acellular methods. The seasonal dependence of the PM10 OP responses was also analyzed in relation to chemical composition and meteorological parameters. Then, Perrone et al. [28] simultaneously evaluated the OP responses of both PM10 and PM2.5 samples. They compared the DTT- and AA-OP responses to associate changes in the OP activity with particle size and the concentration of the redox-active species in PM10 and PM2.5 fractions. Being carried out at the center of the Mediterranean area, the main results of these last works could be considered representative of Mediterranean coastal sites away from large sources of local pollution [29]. With respect to the two previous works related to OP characterization over Southeastern Italy, this study is mainly related to the association of OP response sensitivity with several metal and Br, P, S, and Se mass concentrations by using two different analytical techniques: the Redundancy Discriminant Analysis (RDA) and Spearman correlation coefficients. To the best of our knowledge, this study was the first to apply RDA to relate PM OP responses with specific metal and Br, P, S, and Se mass concentrations. The RDA outcomes were compared with Spearman correlation coefficients to highlight benefits and limits of both used methodologies. The seasonal variations of the relationships between (volume- and mass-normalized)

OP and chemical element concentration were also evaluated since the PM10 samples were collected both in winter and in spring.

2. Experiments

2.1. Site Description and Sample Collection

The measurements analyzed in this study were performed at the Aerosol and Climate Laboratory of the Mathematics and Physics Department of the Salento University in Lecce (40.33° N, 18.11° E, 30 m a.s.l.) in Southeastern Italy. The monitoring site is located in a flat peninsular area, about 6 km away from the city center of Lecce, 20 km away from both the Ionian and Adriatic seas, and 100 and 800 km away from the Balkan and North African coasts, respectively. Therefore, the study site could be considered as representative of coastal sites of the Central Mediterranean, away from large sources of local pollution [30,31].

A low volume (2.3 m^3 h^{-1}) Hydra dual-sampler (FAI Instruments, Fonte Nuova, Rome, Italy) was used to simultaneously collect 72-h winter and 48-h spring PM10 samples on two different 47-mm-diameter filters. Polytetrafluoroethylene (PTFE) filters (TEFLO W/RING 2 μ from VWR International, Radnor, Pennsylvania, USA) and quartz filters (Tissuquartz from PALLFLEX, Putnam, Connecticut, USA) were used to determine the chemical element mass concentrations and the OP responses, respectively. Both filters are characterized by an excellent aerosol collection efficiency [32]. Ten PM10 samples were collected, approximately once a week, both in winter (from January to March 2018) and in spring (from May to June 2018) to study the seasonal impact on the analyzed parameters. The PM10 mass concentrations of this study (Supplementary Table S1) were in reasonable agreement with previous data [8,33] and, therefore, could be considered as representative of PM10 measurements at the study site.

2.2. Chemical Element Mass Concentrations and Oxidative Potential Acellular Assays

Metal (Al, As, Ba, Ca, Cd, Cr, Cu, Fe, K, Mn, Mo, Ni, Pb, Rb, Si, Sr, Ti, V, Zn, and Zr) and Br, P, S, and Se mass concentrations in each PM10 sample (Supplementary Table S1) were determined by the particle-induced X-ray emission (PIXE) technique at the INFN (Istituto Nazionale di Fisica Nucleare) LABEC (LAboratorio di tecniche nucleari applicate ai BEni Culturali) laboratory in Florence, Italy [34,35]. Each sample was irradiated with a 3.0 MeV proton beam (10–150 nA intensity) for 90 s. The beam was collimated to ~2 mm^2, and filter scanning was carried out to analyze most of the deposit area. Elemental concentrations were obtained by a calibration curve from a set of thin standards. Measurement accuracy was tested by the use of a NIST RM 8785 (National Institute of Standards and Technology, USA) standard. The minimum detection limits (MDLs) were of the order of few ng m^{-3} for the low Z elements, down to a minimum value of 0.2 ng m^{-3} for Cu–Zn. The total uncertainties on elemental concentrations were determined by the sum of independent uncertainties on sample thickness (5%), deposition area (2%), air flow (2%), and X-ray counting statistics (2%–20%). The uncertainties increased when concentrations approached minimum detectable limits (MDLs). More details about the used methodology can be found in [34,35].

The oxidative potential responses of the collected PM10 samples were determined by the DTT and AA acellular assays (Supplementary Table S1). Both the assays were performed on 3 mL of the aqueous extract of a quarter of the sampled filters (extracted for 15 min in an ultrasonic bath using 10 mL of a 0.1 M buffer at pH 7.4). The extract was filtered on a regenerate cellulose syringe filter (13 mm and 0.22 μm, Kinesis) to remove the suspended solid particles, and then it was introduced into an amber vial at a constant temperature of 37 °C using a dry bath. The OP response was evaluated as the antioxidant depletion rate of a known quantity of DTT and AA, according to the experimental procedure described in [8]. In more detail, both DTT and AA depletion rates were determined by linear fitting the reagent concentration as a function of time using five experimental points (at 5, 10, 15, 25, and 40 min). A good linearity was, on average, found with correlation coefficient $R^2 \geq 0.98$ [36]. Both DTT and AA depletion

rates were also determined for blank quartz filters (Table S1) and subtracted from the response of each real PM10 sample in order to estimate the detection limits of the two used methods. The obtained OP values were then normalized to the total volume of sampled air, i.e., volume-normalized OP_V (expressed in nmol min^{-1} m^{-3}), and to the PM10-sampled mass, i.e., mass-normalized OP_m (expressed in nmol min^{-1} μg^{-1}), as reported in Table S1. In particular, the volume-normalized OP_V provides a measure of the atmospheric concentration of PM OP response, while the mass-normalized OP_m represents a measure of the intrinsic OP of the overall PM10 contribution [8] (i.e., an indication of the PM10 "toxicity" in terms of OP). Therefore, the OP_V response is an extensive parameter depending on the PM10 mass concentration, as proven by [8,28], while the intrinsic OP_m can also provide insight on contributions of specific sources to the overall PM oxidative potential.

2.3. Data Analysis

The Redundancy Discriminant Analysis represents a widespread chemometric procedure to compare different types of data as chemical species or meteorological parameters [37,38]. The RDA could be considered as the multivariate extension of a simple linear regression applied to some sets of variables [39]. More specifically, the application of RDA needs the combination of two datasets: "species data" as response (or dependent) variables and "environmental variables" as explanatory (or predictive) variables [40]. In this work, the RDA technique was used to investigate the relationships between oxidative potential as "species data" and metal, Br, P, S, and Se mass concentrations as "environmental variables." The RDA analysis was applied to the selected datasets using the Fathom Toolbox for MATLAB [41]. In particular, the selected datasets were first standardized and then used as input (samples as rows and variables as columns) of the function *f_rda* included in the Fathom Toolbox estimating all the statistical parameters needed for the RDA triplot. As described by [38], Monte Carlo tests were also used by setting 499 unrestricted permutations as input for the *f_rda* function. Then, the structure of outputs from *f_rda* function, the datasets of the transformed response variables, the weighted average scores, and a selected scaling factor (optimized to better visualize data) represented the inputs of the *f_rdaPlot* function. This latter was used to plot two RDA outputs on the same graphical framework: the sample and the OP datasets represented the response variables in the first and in the second plot, respectively, while the chemical dataset represented the predictive variables in both plots. This overlap of two plots representing three variables (in this work, sample dataset as points, OP and chemical species dataset as arrows) is generally called an RDA triplot.

The regression analyses performed on the parameters used in this study were based on the non-parametric Spearman correlation coefficients, which are strictly related to rank and not dependent on data distribution. The thresholds of the *p*-value were 10%, 5%, and 1% for the statistical tests (Supplementary Table S2).

3. Results and Discussion

The main features of the metal, Br, P, S, and Se mass concentrations and DTT and AA volume- and mass-normalized oxidative potential responses (OP_V and OP_m, respectively) were analyzed in this Section. RDA and Spearman correlation coefficients were the tools used to analyze major relationships between chemical element mass concentrations and oxidative potential responses. The changes of the relations between the winter and spring PM10 samples were also investigated.

3.1. Metal, Br, P, S, and Se Mass Concentration Characterization

Figure 1 shows the percentage mass concentrations of the analyzed chemical elements in winter and spring PM10 samples. Al, Ca, Fe, K, S, and Si were the most abundant elements in the analyzed samples. All the other chemical components were characterized by a not significant relative abundance of, in total, less than 3%. In particular, among the analyzed chemical elements, S, Ca, and Si showed the highest relative abundance (28%, 19%, and 16%, respectively, in winter and 35%, 21%, and 18%, respectively, in spring). According to [42], the most abundant chemical elements in this study (S, Ca,

and Si) can be associated with the "Agriculture Soil" and the "Natural Soil" sources characterized by respective abundancies larger than 1% in both sources (Table 1). Anthropogenic contributions were likely significant, since Al, Ca, Fe, K, S, and Si can also be associated with the "Paved Road Dust," "Unpaved Road Dust," and "Construction" sources (Table 1). Road dust typically consists of particles deposited over the street pavement and resuspended into the atmosphere by passing vehicles [43]. Road dust represents one of the main components of anthropogenic coarse-mode PM [44], as also proven at the study site [29]. Al, Ca, Fe, K, S, and Si can also be related to the "Motor Vehicle," "Coal-Fired Boiler," and "Oil Fired Power Plant" sources (Table 1), but with a lower percentage contribution, according to [42].

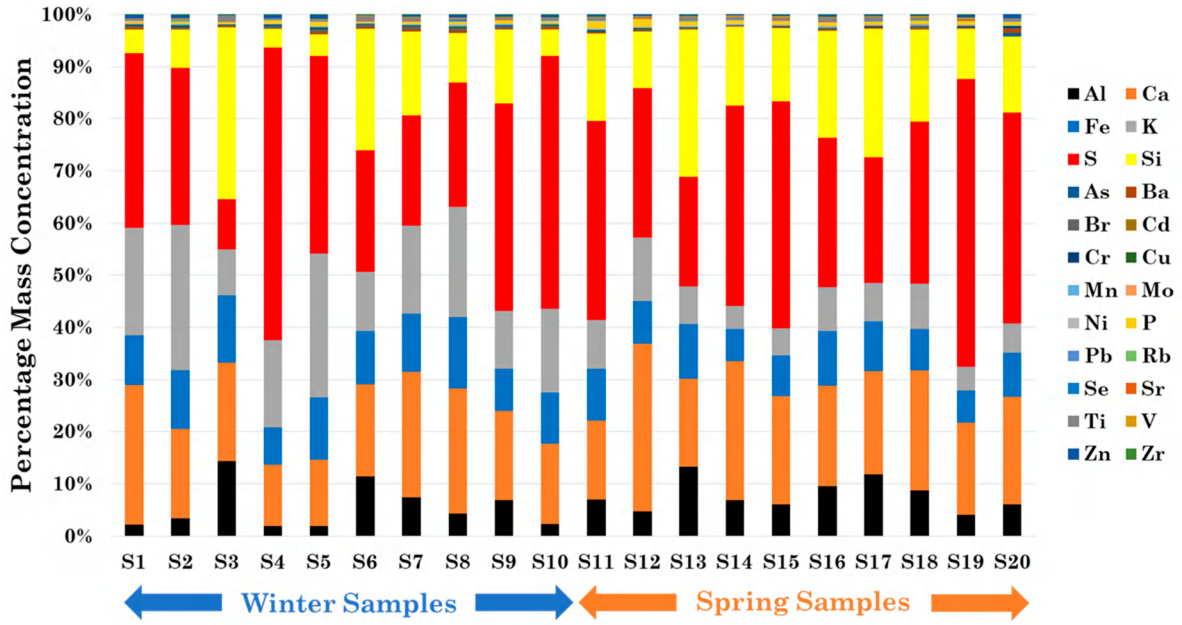

Figure 1. Bar plot of the mass concentration percentages of the investigated chemical elements in the 20 analyzed samples (S1–S10 in winter and S11–S20 in spring). The reported percentages are referred to the total sampled mass of all the 24 analyzed chemical elements.

Table 1. Clustering of the 20 PM10 samples analyzed in this study, according to Romano et al. [45]. Main pollution sources and corresponding chemical fingerprints (according to the Chow [42] classification) are also reported.

Cluster	Samples	PM Sources	Chemical Fingerprints
Anthropogenic	S1, S2, S10	Road Dust, Construction, Motor Vehicle, Coal-Fired Boiler, Oil Fired Power Plant	Al, Ca, Fe, K, Pb, S, Si
Heavy Rain	S5, S9, S11, S13		
Desert Dust	S3, S6, S12	Natural Soil	Al, Ca, Fe, K, Mg, P, S, Si, Ti
Marine	S4, S7, S8	Marine	Al, Ba, Ca, Cu, Fe, K, Si, Zn
Late Spring	S14, S15, S16, S17, S18, S19, S20	Natural Soil, Agricultural Soil, Vegetative Burning	Al, Ca, Fe, K, Mg, P, S, Si, Ti

According to [45], the PM10 samples analyzed in this study can be associated with five different clusters, which are listed in Table 1. Main pollution sources contributing to each identified cluster are also given in Table 1, in addition to the main chemical fingerprints of each source [42]. Romano et al. [45] identified the sample clusters listed in Table 1 by mainly using the four-day

analytical air mass back-trajectories (Figures SI9–SI23 of their paper). They used the HYbrid Single-Particle Lagrangian Integrated Trajectory (HYSPLIT) model version 4.8 from NOAA/ARL (https://www.ready.noaa.gov/; [46]). They identified a "desert dust" cluster composed of samples S3, S6, and S12 that were mainly characterized by a high concentration of elements associated with the "Natural Soil" source (Table 1). Samples S4, S7, and S8 represented the "marine" cluster (Table 1), characterized by Al, Ca, Fe, K, and Si abundances larger than 1%, as well as a reduced S abundance, according to [42]. Then, the "continental" cluster composed of samples S1, S2, and S10 was also characterized by significant abundances of Al, Ca, Fe, K, S, and Si, all generally associated with anthropogenic-related pollution sources. The "late spring" cluster was mainly composed of chemical components typically associated with the "Natural Soil," "Agricultural Soil," and "Vegetative Burning" PM sources (Table 1). A "heavy rain" cluster was also identified by [45] during the analyzed monitoring campaign (Table 1).

Significant seasonal variations of the investigated chemical element mass concentrations can be observed from Figure 1: the winter samples (S1–S10) were clearly characterized by a larger variability with respect to the spring samples (S11–S20). In fact, in winter, low air temperatures associated with cloudy, wet, and stormy days likely contributed to the marked changes of the chemical species' mass concentrations in the collected samples. In contrast, the meteorological conditions occurring in spring all over the Mediterranean basin favored the air mass aging, enhanced natural and anthropogenic dust resuspension, and limited the removal of atmospheric particles by wet deposition. Therefore, the spring meteorological conditions contributed to a decrease of the PM chemical composition variability. Different previous works related to the PM main features at the study site proved the above-reported comments [28,33,47].

3.2. Oxidative Potential Characterization and Relationships with Metal, Br, P, S, and Se Total Concentration

Figure 2 shows the temporal evolution of the DTT and AA volume- and mass-normalized OP responses during the analyzed period from January to June 2018. Observe from Figure 2 that OP_VDTT and OP_VAA values largely varied among the analyzed samples, both in winter and in spring. Such a large variability was probably due to the specific characteristics of the study site, where both the PM concentration and chemical composition were characterized by a high variability. The impact of long-range transported air masses from Northern and/or Eastern Europe (likely characterized by high anthropogenic pollution contributions) and from desert regions and the Mediterranean Sea (all surrounding Southeastern Italy) could be considered responsible for these results [29,31,48–50]. Figure 2 also shows that the OP_VAA response was, on average, significantly larger than the corresponding OP_VDTT response (with mean values ± standard deviation (SD) equal to 0.35 ± 0.11 and 0.17 ± 0.05 nmol min^{-1} m^{-3}, respectively, as reported in Table 2). Perrone et al. [28] found a similar result when investigating autumn–winter PM10 OP_V values. They explained that the larger OP_VAA values compared to those of OP_VDTT were mainly related to a different sensitivity of the two assays to some chemical species. In particular, they demonstrated by multi-linear regression analyses that the OP_VAA sensitivity to K^+ was significantly greater than that of OP_VDTT. In this study, a significant seasonal variation was found only for the OP_VAA values (mean value equal to 0.32 ± 0.08 in winter and to 0.38 ± 0.13 in spring; Table 2). Different results were found by the authors of [51], who investigated the seasonal variability of OP_VDTT and OP_VAA values for PM10 samples monitored in Chamonix (France). They observed OP_VAA values that were significantly greater in winter than in summer, in contrast with the finding of this study. Note also from Figure 2 that the OP_m assumed a lower variability range than OP_v, both for DTT and for AA assays.

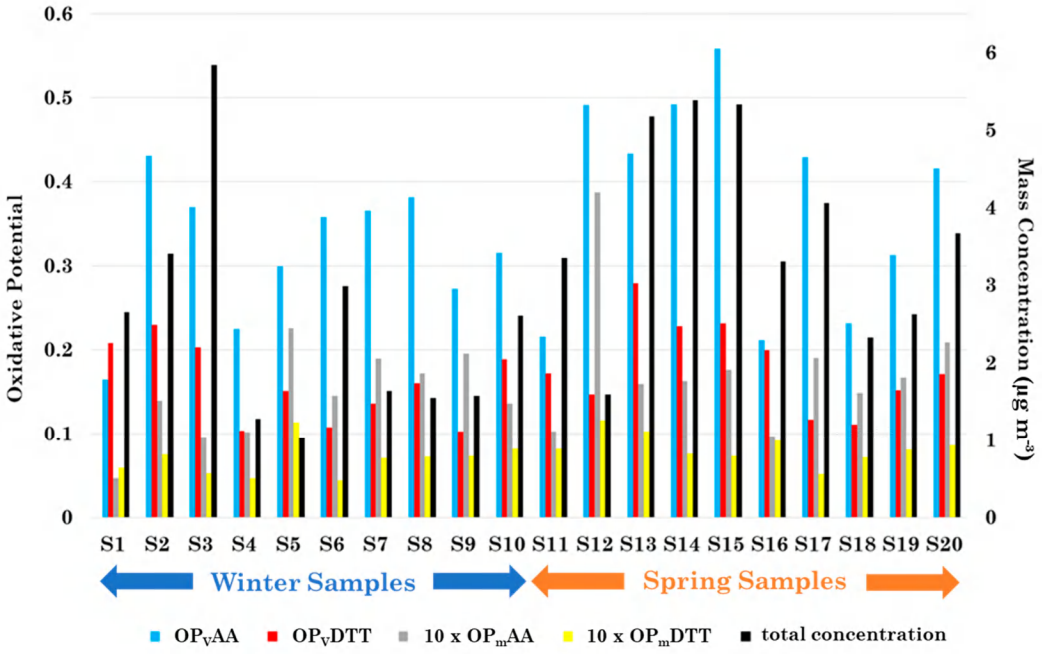

Figure 2. Temporal evolution of volume-normalized ascorbic acid- and dithiothreitol-oxidative potential (OP_VAA and OP_VDTT, respectively, expressed in nmol min^{-1} m^{-3}), mass-normalized ascorbic acid- and dithiothreitol-oxidative potential (OP_mAA and OP_mDTT, respectively, expressed in nmol min^{-1} μg^{-1}), and the total mass concentration of all the analyzed chemical elements. OP_mAA and OP_mDTT values were multiplied by 10 to better visualize data.

Table 2. Mean values and standard deviations (SD) of PM10 volume- and mass-normalized oxidative potential responses (OP_V and OP_m, respectively) obtained from ascorbic acid (AA) and dithiothreitol (DTT) assays and total mass concentration of all the analyzed metals (Al, As, Ba, Ca, Cd, Cr, Cu, Fe, K, Mn, Mo, Ni, Pb, Rb, Si, Sr, Ti, V, Zn, and Zr) and Br, P, S, and Se. The data related to the total analyzed period, the 10 winter samples (from January to March 2018), and the 10 spring samples (from May to June 2018) are reported. Values with a significant seasonal difference (with p-value < 0.10) are marked in bold.

Oxidative Potential	TOTAL		WINTER		SPRING	
	Mean	SD	Mean	SD	Mean	SD
OP_VAA ($nmol^{AA}$ min^{-1} m^{-3})	0.35	0.11	**0.32**	0.08	**0.38**	0.13
OP_VDTT ($nmol^{DTT}$ min^{-1} m^{-3})	0.17	0.05	0.16	0.05	0.18	0.05
OP_mAA ($nmol^{AA}$ min^{-1} μg^{-1})	0.016	0.007	0.014	0.005	0.018	0.008
OP_mDTT ($nmol^{DTT}$ min^{-1} μg^{-1})	0.008	0.002	0.007	0.002	0.008	0.002
Total Mass Concentration (μg m^{-3})	3.1	1.5	**2.5**	1.4	**3.7**	1.3

The main features of OP_V and OP_m previously described in this section were consistent with those reported by [8,28] at the same site. In particular, Pietrogrande et al. [8] investigated the OP_V and OP_m seasonal trend in relation to the meteorological and atmospheric conditions and the PM10 chemical composition over a full year (from November 2014 to October 2015). They also proved that the OP_V values from the DTT and AA assays had a similar association with the distinct chemical

species analyzed in the PM10 samples, as also found by [15,52]. The two previous works on the OP characterization at the same site also demonstrated that the OP_V response is an extensive parameter depending on the PM10 mass concentration, since high OP_V responses were associated with high PM10 mass concentrations, according to [52]. Consequently, it is also particularly interesting to compare the OP_V relationships with the total mass concentration of all analyzed chemical elements (black bars in Figure 2), which were also characterized by high variability during the analyzed period, as previously discussed in Section 3.1. In detail, the seasonal variation of the total mass concentration of all analyzed chemical components between winter and spring analyzed samples could be considered significant, as also proven by its corresponding mean values (2.5 and 3.7 μg m^{-3}, respectively, as shown in Table 2). The larger mean value of the chemical element mass concentration found in spring was mostly due to the larger occurrence of desert dust outbreaks that were responsible for the transport of crustal matter during the sampling time [8,29,31]. The seasonal variation of the total mass concentration was in agreement with the corresponding average increase of OP_VAA from winter to spring, as previously reported. In fact, observe from Figure 2 that the spring samples characterized by the highest total mass concentration (more than 5 μg m^{-3} for S13, S14, and S15) also presented larger values of OP_VAA and OP_VDTT responses. Romano et al. [45] grouped S13, S14, and S15 as a "late spring sample" cluster (Table 1). S3 and S12, which were identified as "desert dust" samples by [45], assumed the largest value of the total mass concentration of the analyzed elements (5.8 μg m^{-3}) and the largest value of OP_mAA (0.039 nmol min^{-1} μg^{-1}). The "marine samples" S4, S7, and S8 (Table 1) assumed the lowest values of total mass concentration (less than 2 μg m^{-3}), but they were also characterized by larger values of OP_VAA. Conversely, the "continental samples" S1, S2, and S10 presented the highest value of total mass concentration of all analyzed chemical elements and the highest value of OP_VDTT among the winter samples. A similar variability between "desert dust" and "continental" PM10 samples was also found by the authors of [28], who analyzed the main features of OP_VAA, OP_VDTT, and PM chemical composition at the same site.

3.3. Relationships between Metal, Br, P, S, and Se Concentration and Oxidative Potential by RDA

A graphical view of the chemical element mass concentration–oxidative potential relationships is provided by the RDA triplot shown in Figure 3. As described in Section 2.3, this technique was applied to the metal, Br, P, S, and Se concentration dataset as predictive variables and the oxidative potential dataset as dependent variables. More specifically, Figure 3 shows the RDA triplot relating the AA and DTT OP_V and OP_m responses (green arrows, dependent variables) to chemical element mass concentrations (red arrows, predictive variables) in (a) winter and (b) spring. Note that the arrow length and direction are strictly related to the variance that can be explained by analyzed variables [40]. Stronger correlations between two parameters involve a greater absolute value of the cosine of the angle between the two corresponding arrows. Arrows in the same and in the opposite direction suggest a positive and a negative correlation, respectively, among the corresponding variables [53].

Figure 3 shows that the red arrows associated with the analyzed chemical elements were, on average, spread in the canonical axis plane over a wider area in spring than in winter. The typical spring–summer air mass aging over the Mediterranean favored the mixing of particles of different types/sources [29,50] and, therefore, likely contributed to this result. In contrast, OP green arrows were spread over a similar area of the canonical axis plane in winter and in spring (Figure 3a,b, respectively). Both OP response and chemical element arrow lengths were, on average, similar among winter and spring samples likely because the corresponding variables assumed a similar value of the explained variance among the two analyzed seasons. Conversely, OP responses (mainly for the AA assay) experienced a larger explained variance with respect to the analyzed chemical species concentrations, both in winter and in spring, as proven by their larger arrow length. In addition, note from Figure 3 that the OP_V and the OP_m arrows are located in a different region of the RDA triplot, proving their different features in relation to the metal, Br, P, S, and Se concentrations. In fact, as reported in Section 2.2, OP_V represents an extensive parameter depending on the total mass concentration of the analyzed chemical

elements, and, hence, this can likely be responsible for the lower angles between OP_V and chemical element arrows in the RDA triplot. Conversely, OP_m represents an intrinsic sample parameter that is not dependent on the total mass concentration of the analyzed chemical species, and, therefore, the corresponding arrows are located in a different area of the RDA triplot. Note also that the lower OP_m variability range with respect to OP_v, both for the DTT and AA assays (as shown in Figure 2 and discussed in Section 3.2), could also have contributed to this last result. The angles between OP_VAA and OP_VDTT arrows and the angles between OP_mAA and OP_mDTT arrows are small and, likely, they highlight similar characteristics in relation to metal, Br, P, S, and Se concentrations. It is worth observing that these last relations are not dependent on the season, since they were similar both in winter and in spring (Figure 3a,b, respectively).

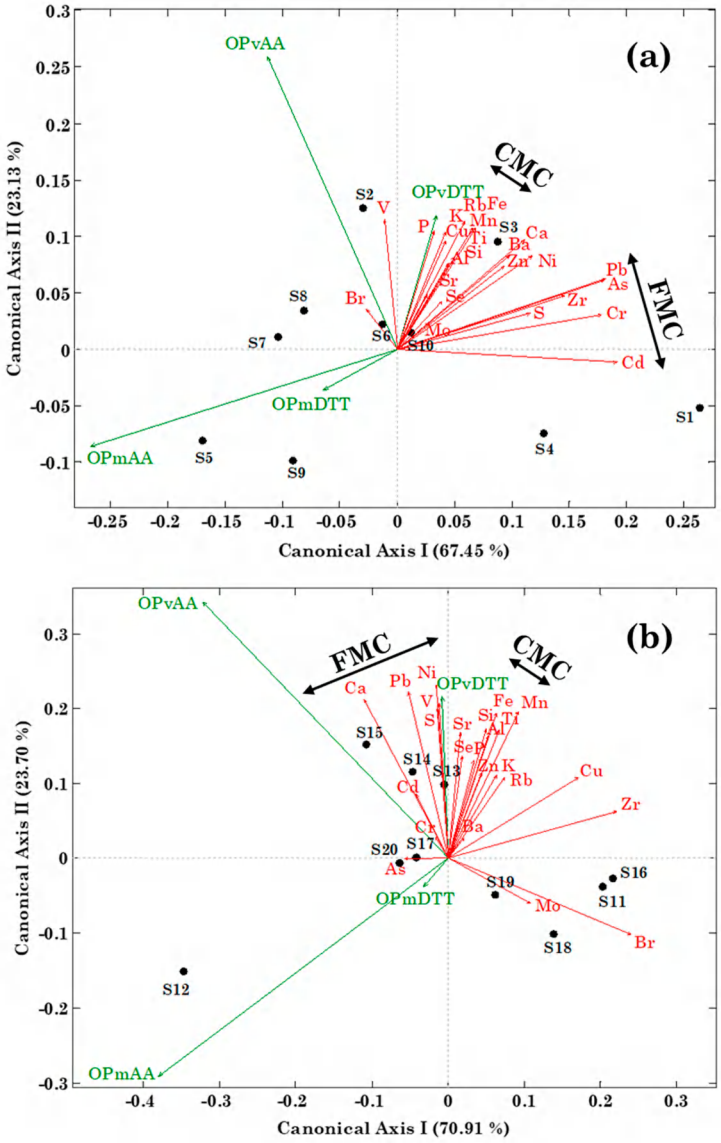

Figure 3. Ordination triplot based on the Redundancy Discriminant Analysis (RDA) between the mass concentrations of all analyzed chemical elements as predictive variables (red arrows), ascorbic acid and dithiothreitol volume-normalized oxidative potential (OP_VAA and OP_VDTT, respectively) and mass-normalized oxidative potential (OP_mAA and OP_mDTT, respectively) as response variables (green arrows), and detected samples (black full dots) in (**a**) winter and (**b**) spring. Black arrows indicate the two identified clusters (coarse-mode cluster (CMC) and fine-mode cluster (FMC)) based on the sources associated with the analyzed chemical elements. The total variance explained by the two RDA axes is also reported in parentheses.

The RDA triplots reported in Figure 3 also allowed for the identification of some clusters of chemical species that could be associated with different pollution sources according to [42] and Table 1. In particular, both in winter and in spring, two main clusters of chemical components can be clearly identified: a cluster related to both natural and anthropogenic sources mainly composed of Al, Fe, Mn, Si, and Ti (metals generally associated with coarse-mode crustal matter and/or road dust, denoted as CMC in Figure 3) and an anthropogenic source-related cluster that consists of As, Cd, Cr, Pb, and S (generally associated with fine-mode PM, denoted as FMC in Figure 3). According to the classification reported in [42], the main components of the metal coarse-mode cluster are included in the sources "Agriculture Soil," "Natural Soil," "Paved Road Dust," and "Unpaved Road Dust". Conversely, the chemical components of the fine-mode cluster are mainly associated with the sources "Smelter Fine," "Motor Vehicle," and "Oil Fire Power Plant". The selected clustering can be considered consistent with those reported in previous studies related to the characterization of PM sample chemical composition [54,55].

Winter and spring PM10 samples are also reported in Figure 3a,b, respectively, by black full dots. Only two main sample clusters could be identified in the winter RDA triplot (Figure 3a), according to the classification reported by [45]: the "marine" cluster composed of S7 and S8 and the "heavy rain" cluster composed of S5 and S9 (Table 1). The samples S7 and S8 were associated with air masses that crossed the Atlantic and the Mediterranean Sea before reaching the study site, according to [45]. In particular, the location of S7 and S8 is, on average, close to the OP_VAA arrow, which assumed higher values in the corresponding days, as previously discussed in Section 3.2. In fact, note that the location of the samples in the RDA triplot is close to the arrows associated with the metals and/or the other chemical elements that reached the highest concentrations in that sample and/or with the arrows related to the OP responses that assumed the highest values in that sample. Consequently, the winter sample S3, associated with the "desert dust" cluster by [45], is located very close to the arrows related to the "crustal matter" metals (Al, Fe, Mn, Si, and Ti). Analogously, Figure 3a shows that the winter sample S1 (classified among the "continental" samples by [45]) is close to the "anthropogenic source-related" metals (As, Cd, Cr, Pb) and S. In contrast, Figure 3b shows a larger variability in the location of the spring samples. As reported in Section 3.2, S13, S14, and S15 were the spring samples characterized by the highest total mass concentration of all the analyzed elements and also presented larger values of OP_VAA and OP_VDTT responses. As a consequence, the location of S13, S14, and S15, all grouped by [45] as "late spring samples" (Table 1) and characterized by a larger occurrence of desert dust advections, is close to the "crustal matter" metal, OP_VAA, and OP_VDTT arrows. The highest value of OP_mAA measured during the day of the "desert dust" sample S12 explains its location in the RDA triplot. Note that the impact of long-range transported air masses on the ion and metal speciation of PM samples collected at the study site has been widely reported/discussed in several previous works [29,31,56].

The oxidative potential response association with specific chemical elements represents one of the main outcomes of the RDA triplot. As previously discussed, the metals Al, Fe, Mn, Si, and Ti were strongly correlated with each other, ultimately defining a coarse-mode cluster CMC, while the strong correlation among As, Cd, Cr, Pb, and S defined an anthropogenic source-related fine-mode cluster FMC. The RDA triplot reported in Figure 3 shows that the OP_VDTT arrow was located near the arrows related to the elements associated with the CMC (both in winter and in spring). The highest values of OP_VDTT associated with the highest values of the total mass concentration of the tested elements (S1, S2, and S10 in winter and S13, S14, and S15 in spring) could have contributed to this last result. Conversely, the location of OP_VAA in the RDA triplot is in a different area with respect to the chemical elements associated with the CMC and FMC clusters in winter (Figure 3a). In fact, the winter OP_VAA arrow is close to the "marine" cluster composed of S7 and S8 that is characterized by low concentrations of metals, Br, P, S, and Se. In spring, the OP_VAA arrow is close to the FMC arrows, probably strictly related to higher OP_VAA values associated with higher total mass concentration of the tested chemical elements (in particular, samples S13, S14, and S15), as shown in Figure 2. Different relationships

between OP_m and specific chemical elements, with similar seasonal features, can be observed in the RDA triplot. In fact, both OP_mAA and OP_mDTT arrows are located in opposite directions with respect to both metal CMC and FMC clusters (Figure 3), showing out an anti- correlation between OP_m responses and the analyzed chemical element concentrations. Note that, as previously discussed, OP_m is an intrinsic parameter that is not related to the mass concentration of specific chemical species. In conclusion, Figure 3 and the above reported comments show that the clustering of some chemical elements in the analyzed PM10 samples allowed for the inference of the main pollution sources and, hence, their association with OP values.

3.4. Relationships between Metal, Br, P, S and Se Concentration and Oxidative Potential by Spearman Correlation Coefficients

The relationships between oxidative potential responses and chemical element concentrations were also analyzed by Spearman correlation coefficients (r) for both winter and spring samples. The main goals of this section are to highlight the relationship strengths, identify the main elements responsible for the relationships, and compare the results from the correlation coefficient analysis with corresponding RDA results. Table 3 summarizes significant positive and negative relationships between OP responses and metal, Br, P, S, and Se mass concentrations for both winter and spring samples. The Spearman correlation coefficients, with values significant at *p*-levels of <0.01 and 0.05 in bold and in bold–italic, respectively, are reported in Table S2 for all the analyzed parameters.

Table 3. AA and DTT volume- and mass-normalized oxidative potential responses (OP_V and OP_m, respectively) positively and negatively correlated with total (all analyzed chemical elements) and PM10 mass concentration for the 10 winter samples and the 10 spring samples. Spearman correlation coefficients are reported in brackets (values significant at *p*-levels of < 0.01 and 0.05 are in bold and in italics, respectively).

	WINTER	**SPRING**
OP_VAA		OP_mAA (*0.67*), Br (*−0.65*)
OP_VDTT	PM10 (*0.67*), Ba (*0.68*), Cr (**0.85**), Ni (**0.85**), Pb (*0.70*), P (**0.85**), K (**0.97**), Ca (*0.73*), Mn (*0.65*), Fe (*0.69*), Cu (**0.94**), Zn (**0.85**), Rb (**0.84**), Zr (*0.67*)	PM10 (**0.82**), Pb (*0.80*), P (*0.76*), Ca (*0.72*), Fe (*0.63*), Zn (*0.66*)
OP_mAA	PM10 (*−0.77*), As (**−0.87**), Cd (**−0.86**), Pb (**−0.92**), S (*−0.63*), Zn (*−0.70*)	OP_VAA (*0.67*)
OP_mDTT		

According to the Spearman correlation coefficients reported in Table 3, different relationships between OP responses and specific chemical element concentrations could be found in winter and in spring. The OP_VDTT values were correlated with a larger number of elements in winter than in spring. More specifically, the winter OP_VDTT values were characterized by strong correlations with metals associated with the anthropogenic sources (such as Cr, Ni, Cu, and Zn) and chemical elements associated with the natural sources (such as K and P), according to [42]. This last result is consistent with those reported by [8,28] at the study site. The previous results outlined from the Spearman correlation coefficients appear to contrast with the RDA outcomes, indicating strong correlations of winter OP_VDTT, but only with some elements related to natural sources and/or road dust. Significant winter OP_VDTT-related Spearman correlation coefficients with lower *p*-values were also found with other metals generally associated with some natural sources and/or road dust (such as Ca, Mn, and Fe) and metals characterized by very low concentrations (such as Ba, Rb, and Zr). As one can observe from Table 3, a smaller amount of chemical elements (Pb, P, Ca, Fe, and Zn) was correlated with OP_VDTT in spring. Nishita-Hara et al. [26] sampled both fine and coarse PM particles in spring 2016 in Fukuoka (Japan). According to the results of this study, they found a significant correlation of OP_VDTT with Fe in the PM coarse-mode fraction, which they mainly associated with mineral dust events. They also

found that OP_VDTT was associated with Pb in PM fine-mode fraction, likely due to anthropogenic combustion sources. Calas et al. [19] also reported a strong correlation between OP_VDTT response and Fe mass concentration (r = 0.71, significant with a *p*-level < 0.01) in PM10 samples monitored in Chamonix (France). The latter results from Spearman correlation coefficients are not consistent with the previously reported RDA outcomes (Figure 3), thus indicating relationships between spring OP_VDTT and several element concentrations, related to both natural and anthropogenic sources. Note also from Table 3 that OP_VDTT was correlated with PM10 mass concentration both in winter and in spring, since it represents an extensive parameter (Section 2.2). Accordingly, the highest values of OP_VDTT were associated with the highest values of the total mass concentration of all the analyzed chemical elements (S1, S2, and S10 in winter and S13, S14, and S15 in spring), as shown in Figure 2. Janssen et al. [52] also found a strong correlation between OP_VDTT and PM10 mass concentration (r = 0.75, significant with *p*-level < 0.01) when analyzing some PM10 samples from March to October 2009 in different sites of the Netherlands.

The main results from Spearman correlation coefficient analysis on the winter OP_VAA relationships with chemical components were in reasonable accordance with the corresponding ones from RDA. In fact, OP_VAA response did not present any correlations with specific element concentrations in winter. The higher values of OP_VAA found in relation to the "marine" cluster composed of S7 and S8 that was characterized by low chemical element mass concentrations could have likely contributed to this last result. In spring, OP_VAA assumed an inverse correlation with Br, which is generally associated with anthropogenic sources according to [42]. Accordingly, the RDA outcomes indicated a strong relation between OP_VAA and the anthropogenic cluster in spring (Figure 3b).

The winter OP_mAA was anti-correlated with the mass concentration of some chemical species generally associated with anthropogenic sources (As, Cd, Pb, S, and Zn), in agreement with the RDA outcomes (Figure 3a). OP_mDTT did not present correlations with any element concentrations, both in winter and in spring. The corresponding small length of the OP_mDTT arrow in the RDA triplot is consistent with this result, indicating a reduced variance explained by OP_mDTT in the analyzed samples.

Table 3 showed that the relations of a given OP response with a specific chemical element presented some seasonal characteristics, in accordance with RDA results. To further investigate these mean seasonal variations among the analyzed parameters, Figure 4a,b shows the OP_V responses, and Figure 4c,d shows the OP_m responses as a function of the total mass concentration of the analyzed chemical elements for both the winter (blue circles) and spring (red circles) samples. OP_VDTT assumed the largest correlation coefficients with respect to the total mass concentration due to all chemical species (r = 0.58 in winter and r = 0.75 in spring, both significant at a *p*-level < 0.05), as suggested by the large number of specific mass concentrations correlated with OP_VDTT responses (Table 3). As shown in Figure 2, the highest values of OP_VDTT associated with the highest values of chemical species mass concentration (S1, S2, and S10 in winter and S13, S14, and S15 in spring) also likely contributed to this last result. OP_VAA also showed an increasing trend as a function of total mass concentration (Figure 4a), but it was characterized by a not significant correlation coefficient (r = 0.34 in winter and r = 0.49 in spring). The higher winter values of OP_VAA were found in relation to the "marine" samples S7 and S8 that were characterized by low total mass concentrations, and, therefore, this could have probably contributed to the low r value in winter. The low number of specific elements correlated with OP_VAA also confirmed the results of Figure 4a. A slight decreasing trend of OP_m response as a function of the total mass concentration was found (Figure 4c,d). Only the correlation coefficient between OP_mAA and total concentration in winter (r = −0.52) was significant (at a *p*-level < 0.10), in agreement with the larger number of specific element concentrations anti-correlated with OP_mAA (Table 3).

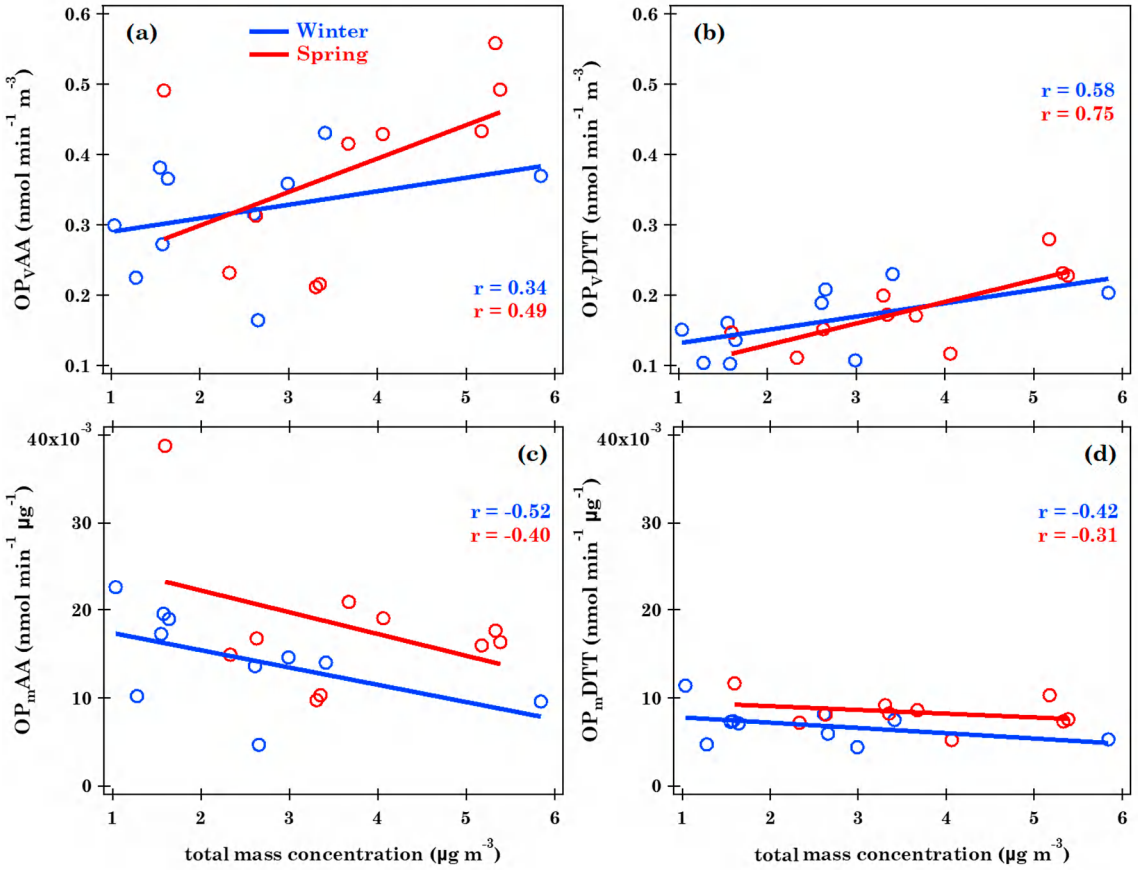

Figure 4. Scatterplot of the (**a**) ascorbic acid and (**b**) dithiothreitol volume-normalized oxidative potential (OP_VAA and OP_VDTT, respectively) and the (**c**) ascorbic acid and (**d**) dithiothreitol mass-normalized oxidative potential (OP_mAA and OP_mDTT, respectively) as a function of the mass concentration of all the analyzed chemical elements (Al, As, Ba, Br, Ca, Cd, Cr, Cu, Fe, K, Mn, Mo, Ni, P, Pb, Rb, S, Se, Si, Sr, Ti, V, Zn, and Zr) for the 10 winter samples (blue circles) and the 10 spring samples (red circles). The correlation coefficients r and the corresponding fitting lines are also reported in each plot.

The results previously reported in this section showed some contrasting results between the analysis of Spearman correlation coefficients and RDA about the determination of relationship strengths and the identification of the main chemical elements responsible for the relationships with oxidative potential responses. The discrepancies between Spearman coefficient results (Table 3) and RDA triplots (Figure 3) were likely due to the fact that the location of a specific arrow in the RDA triplot is dependent on more factors (mainly the sample location in the plot, the chemical element relationships with other elements, and the relationships of OP values with chemical elements) that may contrast among them. Conversely, Spearman correlation coefficients link the relationship between two specific parameters.

4. Conclusions

Redundancy Discriminant Analysis and Spearman correlation coefficients were used in this work to investigate the oxidative potential sensitivity to the mass concentration of specific chemical elements (metals, Br, P, S, and Se) in PM10 samples. The monitoring was performed from January to June 2018 in an Italian coastal site of the Central Mediterranean away from large sources of local pollution. Dithiothreitol and ascorbic acid acellular assays and the particle-induced X-ray emission technique were used to estimate oxidative potential responses and mass concentrations of 24 specific chemical elements, respectively. The main results of this study are reported below.

Al, Ca, Fe, K, S, and Si were the most abundant chemical elements among those analyzed in the detected samples, both in winter and in spring. They were associated both with natural

sources like soil and/or desert dust and with anthropogenic sources like road dust. Total and specific mass concentrations assumed significant seasonal variations: winter samples were clearly characterized by a larger variability with respect to spring samples, mainly because of the different meteorological conditions.

OP_VDTT and OP_VAA were both characterized by a large variability among the analyzed samples, both in winter and in spring, a variability that was, in turn, related to the large variability of PM concentration and chemical composition. The OP_VAA response was, on average, significantly larger than the corresponding OP_VDTT response, and its significant seasonal variation was consistent with that of the total mass concentration of all the analyzed chemical elements. OP_m assumed a lower variability range than OP_v, both for the DTT and AA assays.

The RDA—which was applied to oxidative potential responses as dependent variables and metal, Br, P, S, and Se concentrations as explanatory variables—allowed to visualize main relations between PM10 oxidative potential and the corresponding concentration of specific chemical elements. A coarse-mode cluster related to both natural and anthropogenic sources (such as desert dust and road dust, respectively) and a fine-mode cluster related only to anthropogenic sources were identified by RDA. OP_VDTT was mainly related to the chemical elements associated with the coarse-mode cluster (both in winter and in spring), while OP_VAA was associated with the fine-mode cluster only in spring.

Spearman correlation coefficients were used to compare the main RDA results contributing to the evaluation of benefits and limits of both used techniques. According to Spearman correlation coefficients, winter OP_VDTT was characterized by strong correlations with metals associated with anthropogenic sources (such as Cr, Ni, Cu, and Zn) and with chemical elements related to natural sources (such as K and P). Conversely, less element mass concentrations (Pb, P, Ca, Fe, and Zn) were correlated with OP_VDTT in spring. OP_VAA response did not present any correlations with specific element mass concentrations. Both RDA triplots and Spearman coefficients suggested an anti-correlation between OP_m responses and specific chemical element concentrations.

In conclusion, this work has contributed to the validation of the main results from previous studies related to the OP characterization over Southeastern Italy. In addition, it represents the first work relating PM OP responses and specific chemical elements (metals, Br, P, S, and Se) by the RDA technique. Its main results have demonstrated that the integrated approach based on both RDA and Spearman correlation coefficients can provide new insights about the relations between OP responses and chemical element concentrations. We are aware that the RDA technique can be affected by different factors (e.g., sample location in the plot, chemical element relationships with other elements, OP relationships with all the analyzed chemical elements), while the Spearman correlation coefficients depend only on the relations between two specific parameters. However, their integration can contribute to the better evaluation of harmful effects associated with specific chemical components in PM samples.

Supplementary Materials: The following are available online at http://www.mdpi.com/2073-4433/11/4/367/s1, Table S1: Dataset of PM10 mass concentration, ascorbic acid and dithiothreitol volume- and mass-normalized oxidative potential, and mass concentration of all analyzed chemical elements, Table S2: Spearman correlation coefficients between PM10 mass concentration, ascorbic acid and dithiothreitol volume- and mass-normalized oxidative potential, and mass concentration of all analyzed chemical elements.

Author Contributions: Conceptualization, S.R.; methodology, S.R., S.B., F.L., and M.R.; software, S.R.; formal analysis, S.R.; investigation, S.R.; measurements, S.B., F.L., and M.R.; writing—original draft preparation, S.R.; supervision, S.R. and M.C.P. All authors have read and agreed to the published version of the manuscript.

Funding: S. Romano has carried out this work with the support of a Temporary Researcher position financed by the Italian "Programma Operativo Nazionale (PON) Ricerca e Innovazione 2014–2020 (Azione I.2—Attrazione e Mobilità dei Ricercatori)". The work was partially supported by the PON project "PER-ACTRIS-IT—Potenziamento della componente italiana dell'Infrastruttura di Ricerca Aerosol, Clouds and Trace Gases Research Infrastructure" and by the Italian INFN (Istituto Nazionale Fisica Nucleare), in the frame of the projects TRACCIA (Time Resolved Aerosol Characterisation: Challenging Improvements and Ambitions) and IS-ABS (Integrated System for Aerosol and Bioaerosol Studies at the Pierre Auger Observatory).

Conflicts of Interest: The authors declare no conflict of interest. The funders had no role in the design of the study; in the collection, analyses, or interpretation of data; in the writing of the manuscript; or in the decision to publish the results.

References

1. Kelly, F.J.; Fussell, J.C. Size, source and chemical composition as determinants of toxicity attributable to ambient particulate matter. *Atmos. Environ.* **2012**, *60*, 504–526. [CrossRef]
2. Fortoul, T.I.; Rodriguez-Lara, V.; Gonzalez-Villalva, A.; Rojas-Lemus, M.; Colin-Barenque, L.; Bizarro-Nevares, P.; García-Peláez, I.; Ustarroz-Cano, M.; López-Zepeda, S.; Cervantes-Yépez, S.; et al. Health Effects of Metals in Particulate Matter. *Curr. Air Qual. Issues* **2015**. [CrossRef]
3. Englert, N. Fine particles and human health—A review of epidemiological studies. *Toxicol. Lett.* **2004**, *149*, 235–242. [CrossRef] [PubMed]
4. Lippmann, M.; Chen, L.-C.; Gordon, T.; Ito, K.; Thurston, G.D. National Particle Component Toxicity (NPACT) Initiative: Integrated epidemiologic and toxicologic studies of the health effects of particulate matter components. *Res. Rep. Health Eff. Inst.* **2013**, *177*, 5–13.
5. Zhou, J.; Ito, K.; Lall, R.; Lippmann, M.; Thurston, G. Time-Series Analysis of Mortality Effects of Fine Particulate Matter Components in Detroit and Seattle. *Environ. Health Perspect.* **2011**, *119*, 461–466. [CrossRef]
6. Cakmak, S.; Dales, R.; Kauri, L.M.; Mahmud, M.; Van Ryswyk, K.; Vanos, J.; Liu, L.; Kumarathasan, P.; Thomson, E.; Vincent, R.; et al. Metal composition of fine particulate air pollution and acute changes in cardiorespiratory physiology. *Environ. Pollut.* **2014**, *189*, 208–214. [CrossRef]
7. Ayres, J.G.; Borm, P.; Cassee, F.R.; Castranova, V.; Donaldson, K.; Ghio, A.; Harrison, R.M.; Hider, R.; Kelly, F.; Kooter, I.M.; et al. Evaluating the Toxicity of Airborne Particulate Matter and Nanoparticles by Measuring Oxidative Stress Potential—A Workshop Report and Consensus Statement. *Inhal. Toxicol.* **2008**, *20*, 75–99. [CrossRef]
8. Pietrogrande, M.C.; Perrone, M.R.; Manarini, F.; Romano, S.; Udisti, R.; Becagli, S. PM10 oxidative potential at a Central Mediterranean Site: Association with chemical composition and meteorological parameters. *Atmos. Environ.* **2018**, *188*, 97–111. [CrossRef]
9. Borm, P.J.A.; Kelly, F.; Künzli, N.; Schins, R.P.F.; Donaldson, K. Oxidant generation by particulate matter: From biologically effective dose to a promising, novel metric. *Occup. Environ. Med.* **2007**, *64*, 73–74. [CrossRef]
10. Janssen, N.A.H.; Strak, M.; Yang, A.; Hellack, B.; Kelly, F.J.; Kuhlbusch, T.A.J.; Harrison, R.M.; Brunekreef, B.; Cassee, F.R.; Steenhof, M.; et al. Associations between three specific a-cellular measures of the oxidative potential of particulate matter and markers of acute airway and nasal inflammation in healthy volunteers. *Occup. Environ. Med.* **2015**, *72*, 49–56. [CrossRef]
11. Brook, R.D.; Rajagopalan, S.; Pope, C.A.; Brook, J.R.; Bhatnagar, A.; Diez-Roux, A.V.; Holguin, F.; Hong, Y.; Luepker, R.V.; Mittleman, M.A.; et al. Particulate Matter Air Pollution and Cardiovascular Disease: An Update to the Scientific Statement From the American Heart Association. *Circulation* **2010**, *121*, 2331–2378. [CrossRef] [PubMed]
12. Nel, A. Air Pollution-Related Illness: Effects of Particles. *Science* **2005**, *308*, 804–806. [CrossRef] [PubMed]
13. Weichenthal, S.A.; Godri Pollitt, K.; Villeneuve, P.J. PM2.5, oxidant defence and cardiorespiratory health: A review. *Environ. Health* **2013**, *12*, 40. [CrossRef] [PubMed]
14. Crobeddu, B.; Aragao-Santiago, L.; Bui, L.-C.; Boland, S.; Baeza Squiban, A. Oxidative potential of particulate matter 2.5 as predictive indicator of cellular stress. *Environ. Pollut.* **2017**, *230*, 125–133. [CrossRef] [PubMed]
15. Yang, A.; Jedynska, A.; Hellack, B.; Kooter, I.; Hoek, G.; Brunekreef, B.; Kuhlbusch, T.A.J.; Cassee, F.R.; Janssen, N.A.H. Measurement of the oxidative potential of PM2.5 and its constituents: The effect of extraction solvent and filter type. *Atmos. Environ.* **2014**, *83*, 35–42. [CrossRef]
16. Yang, A.; Wang, M.; Eeftens, M.; Beelen, R.; Dons, E.; Leseman, D.L.A.C.; Brunekreef, B.; Cassee, F.R.; Janssen, N.A.H.; Hoek, G. Spatial Variation and Land Use Regression Modeling of the Oxidative Potential of Fine Particles. *Environ. Health Perspect.* **2015**, *123*, 1187–1192. [CrossRef] [PubMed]
17. Kelly, F.; Armstrong, B.; Atkinson, R.; Anderson, H.R.; Barratt, B.; Beevers, S.; Cook, D.; Green, D.; Derwent, D.; Mudway, I.; et al. The London low emission zone baseline study. *Res. Rep. Health Eff. Inst.* **2011**, *163*, 3–79.

18. Szigeti, T.; Óvári, M.; Dunster, C.; Kelly, F.J.; Lucarelli, F.; Záray, G. Changes in chemical composition and oxidative potential of urban PM2.5 between 2010 and 2013 in Hungary. *Sci. Total Environ.* **2015**, *518–519*, 534–544. [CrossRef]
19. Calas, A.; Uzu, G.; Kelly, F.J.; Houdier, S.; Martins, J.M.F.; Thomas, F.; Molton, F.; Charron, A.; Dunster, C.; Oliete, A.; et al. Comparison between five acellular oxidative potential measurement assays performed with detailed chemistry on PM $_{10}$ samples from the city of Chamonix (France). *Atmos. Chem. Phys.* **2018**, *18*, 7863–7875. [CrossRef]
20. Calas, A.; Uzu, G.; Besombes, J.-L.; Martins, J.M.F.; Redaelli, M.; Weber, S.; Charron, A.; Albinet, A.; Chevrier, F.; Brulfert, G.; et al. Seasonal Variations and Chemical Predictors of Oxidative Potential (OP) of Particulate Matter (PM), for Seven Urban French Sites. *Atmosphere* **2019**, *10*, 698. [CrossRef]
21. Weichenthal, S.; Crouse, D.L.; Pinault, L.; Godri-Pollitt, K.; Lavigne, E.; Evans, G.; van Donkelaar, A.; Martin, R.V.; Burnett, R.T. Oxidative burden of fine particulate air pollution and risk of cause-specific mortality in the Canadian Census Health and Environment Cohort (CanCHEC). *Environ. Res.* **2016**, *146*, 92–99. [CrossRef] [PubMed]
22. Liu, L.; Urch, B.; Szyszkowicz, M.; Evans, G.; Speck, M.; Van Huang, A.; Leingartner, K.; Shutt, R.H.; Pelletier, G.; Gold, D.R.; et al. Metals and oxidative potential in urban particulate matter influence systemic inflammatory and neural biomarkers: A controlled exposure study. *Environ. Int.* **2018**, *121*, 1331–1340. [CrossRef] [PubMed]
23. Daher, N.; Saliba, N.A.; Shihadeh, A.L.; Jaafar, M.; Baalbaki, R.; Shafer, M.M.; Schauer, J.J.; Sioutas, C. Oxidative potential and chemical speciation of size-resolved particulate matter (PM) at near-freeway and urban background sites in the greater Beirut area. *Sci. Total Environ.* **2014**, *470–471*, 417–426. [CrossRef] [PubMed]
24. Charrier, J.G.; Anastasio, C. On dithiothreitol (DTT) as a measure of oxidative potential for ambient particles: Evidence for the importance of soluble transition metals. *Atmos. Chem. Phys.* **2012**, *12*, 9321–9333. [CrossRef]
25. Mudway, I.S.; Stenfors, N.; Duggan, S.T.; Roxborough, H.; Zielinski, H.; Marklund, S.L.; Blomberg, A.; Frew, A.J.; Sandström, T.; Kelly, F.J. An in vitro and in vivo investigation of the effects of diesel exhaust on human airway lining fluid antioxidants. *Arch. Biochem. Biophys.* **2004**, *423*, 200–212. [CrossRef]
26. Nishita-Hara, C.; Hirabayashi, M.; Hara, K.; Yamazaki, A.; Hayashi, M. Dithiothreitol-Measured Oxidative Potential of Size-Segregated Particulate Matter in Fukuoka, Japan: Effects of Asian Dust Events. *GeoHealth* **2019**, *3*, 160–173. [CrossRef]
27. Saffari, A.; Daher, N.; Shafer, M.M.; Schauer, J.J.; Sioutas, C. Seasonal and spatial variation in dithiothreitol (DTT) activity of quasi-ultrafine particles in the Los Angeles Basin and its association with chemical species. *J. Environ. Sci. Health A* **2014**, *49*, 441–451. [CrossRef]
28. Perrone, M.R.; Bertoli, I.; Romano, S.; Russo, M.; Rispoli, G.; Pietrogrande, M.C. PM2.5 and PM10 oxidative potential at a Central Mediterranean Site: Contrasts between dithiothreitol- and ascorbic acid-measured values in relation with particle size and chemical composition. *Atmos. Environ.* **2019**, *210*, 143–155. [CrossRef]
29. Perrone, M.R.; Romano, S.; Orza, J.A.G. Columnar and ground-level aerosol optical properties: Sensitivity to the transboundary pollution, daily and weekly patterns, and relationships. *Environ. Sci. Pollut. Res.* **2015**, *22*, 16570–16589. [CrossRef]
30. Basart, S.; Pérez, C.; Cuevas, E.; Baldasano, J.M.; Gobbi, G.P. Aerosol characterization in Northern Africa, Northeastern Atlantic, Mediterranean Basin and Middle East from direct-sun AERONET observations. *Atmos. Chem. Phys.* **2009**, *9*, 8265–8282. [CrossRef]
31. Perrone, M.R.; Romano, S.; Orza, J.A.G. Particle optical properties at a Central Mediterranean site: Impact of advection routes and local meteorology. *Atmos. Res.* **2014**, *145–146*, 152–167. [CrossRef]
32. Burton, N.C.; Grinshpun, S.A.; Reponen, T. Physical collection efficiency of filter materials for bacteria and viruses. *Ann. Occup. Hyg.* **2007**, *51*, 143–151. [CrossRef] [PubMed]
33. Perrone, M.R.; Romano, S.; Genga, A.; Paladini, F. Integration of optical and chemical parameters to improve the particulate matter characterization. *Atmos. Res.* **2018**, *205*, 93–106. [CrossRef]
34. Lucarelli, F.; Calzolai, G.; Chiari, M.; Giannoni, M.; Mochi, D.; Nava, S.; Carraresi, L. The upgraded external-beam PIXE/PIGE set-up at LABEC for very fast measurements on aerosol samples. *Nucl. Instrum. Methods B* **2014**, *318*, 55–59. [CrossRef]
35. Lucarelli, F.; Calzolai, G.; Chiari, M.; Nava, S.; Carraresi, L. Study of atmospheric aerosols by IBA techniques: The LABEC experience. *Nucl. Instrum. Methods B* **2018**, *417*, 121–127. [CrossRef]

36. Visentin, M.; Pagnoni, A.; Sarti, E.; Pietrogrande, M.C. Urban PM2.5 oxidative potential: Importance of chemical species and comparison of two spectrophotometric cell-free assays. *Environ. Pollut.* **2016**, *219*, 72–79. [CrossRef]
37. Wang, T.; Cai, G.; Qiu, Y.; Fei, N.; Zhang, M.; Pang, X.; Jia, W.; Cai, S.; Zhao, L. Structural segregation of gut microbiota between colorectal cancer patients and healthy volunteers. *ISME J.* **2012**, *6*, 320–329. [CrossRef]
38. Innocente, E.; Squizzato, S.; Visin, F.; Facca, C.; Rampazzo, G.; Bertolini, V.; Gandolfi, I.; Franzetti, A.; Ambrosini, R.; Bestetti, G. Influence of seasonality, air mass origin and particulate matter chemical composition on airborne bacterial community structure in the Po Valley, Italy. *Sci. Total Environ.* **2017**, *593–594*, 677–687. [CrossRef]
39. Van den Wollenberg, A.L. Redundancy analysis an alternative for canonical correlation analysis. *Psychometrika* **1977**, *42*, 207–219. [CrossRef]
40. Paliy, O.; Shankar, V. Application of multivariate statistical techniques in microbial ecology. *Mol. Ecol.* **2016**, *25*, 1032–1057. [CrossRef]
41. Jones, D.L. *Fathom Toolbox for MATLAB: Software for Multivariate Ecological and Oceanographic Data Analysis*; College of Marine Science, University of South Florida: St. Petersburg, FL, USA, 2017; Available online: https://www.marine.usf.edu/research/matlab-resources/ (accessed on 2 December 2019).
42. Chow, J.C. Measurement Methods to Determine Compliance with Ambient Air Quality Standards for Suspended Particles. *J. Air Waste Manag. Assoc.* **1995**, *45*, 320–382. [CrossRef] [PubMed]
43. Amato, F.; Pandolfi, M.; Escrig, A.; Querol, X.; Alastuey, A.; Pey, J.; Perez, N.; Hopke, P.K. Quantifying road dust resuspension in urban environment by Multilinear Engine: A comparison with PMF2. *Atmos. Environ.* **2009**, *43*, 2770–2780. [CrossRef]
44. Lyamani, H.; Olmo, F.J.; Alados-Arboledas, L. Physical and optical properties of aerosols over an urban location in Spain: Seasonal and diurnal variability. *Atmos. Chem. Phys.* **2010**, *10*, 239–254. [CrossRef]
45. Romano, S.; Di Salvo, M.; Rispoli, G.; Alifano, P.; Perrone, M.R.; Talà, A. Airborne bacteria in the Central Mediterranean: Structure and role of meteorology and air mass transport. *Sci. Total Environ.* **2019**, *697*, 134020. [CrossRef]
46. Stein, A.F.; Draxler, R.R.; Rolph, G.D.; Stunder, B.J.B.; Cohen, M.D.; Ngan, F. NOAA's HYSPLIT Atmospheric Transport and Dispersion Modeling System. *Bull. Am. Meteorol. Soc.* **2015**, *96*, 2059–2077. [CrossRef]
47. Perrone, M.R.; Vecchi, R.; Romano, S.; Becagli, S.; Traversi, R.; Paladini, F. Weekly cycle assessment of PM mass concentrations and sources, and impacts on temperature and wind speed in Southern Italy. *Atmos. Res.* **2019**, *218*, 129–144. [CrossRef]
48. Becagli, S.; Anello, F.; Bommarito, C.; Cassola, F.; Calzolai, G.; Iorio, T.D.; di Sarra, A.; Gómez-Amo, J.-L.; Lucarelli, F.; Marconi, M.; et al. Constraining the ship contribution to the aerosol of the central Mediterranean. *Atmos. Chem. Phys.* **2017**, *17*, 2067–2084. [CrossRef]
49. Chirizzi, D.; Cesari, D.; Guascito, M.R.; Dinoi, A.; Giotta, L.; Donateo, A.; Contini, D. Influence of Saharan dust outbreaks and carbon content on oxidative potential of water-soluble fractions of PM2.5 and PM10. *Atmos. Environ.* **2017**, *163*, 1–8. [CrossRef]
50. Romano, S.; Perrone, M.R.; Pavese, G.; Esposito, F.; Calvello, M. Optical properties of PM2.5 particles: Results from a monitoring campaign in southeastern Italy. *Atmos. Environ.* **2019**, *203*, 35–47. [CrossRef]
51. Calas, A.; Uzu, G.; Martins, J.M.F.; Voisin, D.; Spadini, L.; Lacroix, T.; Jaffrezo, J.-L. The importance of simulated lung fluid (SLF) extractions for a more relevant evaluation of the oxidative potential of particulate matter. *Sci. Rep.* **2017**, *7*, 1–12. [CrossRef]
52. Janssen, N.A.H.; Yang, A.; Strak, M.; Steenhof, M.; Hellack, B.; Gerlofs-Nijland, M.E.; Kuhlbusch, T.; Kelly, F.; Harrison, R.; Brunekreef, B.; et al. Oxidative potential of particulate matter collected at sites with different source characteristics. *Sci. Total Environ.* **2014**, *472*, 572–581. [CrossRef] [PubMed]
53. Sun, Y.; Xu, S.; Zheng, D.; Li, J.; Tian, H.; Wang, Y. Effects of haze pollution on microbial community changes and correlation with chemical components in atmospheric particulate matter. *Sci. Total Environ.* **2018**, *637–638*, 507–516. [CrossRef] [PubMed]
54. Okuda, T.; Kato, J.; Mori, J.; Tenmoku, M.; Suda, Y.; Tanaka, S.; He, K.; Ma, Y.; Yang, F.; Yu, X. Daily concentrations of trace metals in aerosols in Beijing, China, determined by using inductively coupled plasma mass spectrometry equipped with laser ablation analysis, and source identification of aerosols. *Sci. Total Environ.* **2004**, *330*, 145–158. [CrossRef] [PubMed]

55. Gao, J.; Tian, H.; Cheng, K.; Lu, L.; Zheng, M.; Wang, S.; Hao, J.; Wang, K.; Hua, S.; Zhu, C.; et al. The variation of chemical characteristics of PM2.5 and PM10 and formation causes during two haze pollution events in urban Beijing, China. *Atmos. Environ.* **2015**, *107*, 1–8. [CrossRef]
56. Perrone, M.R.; Becagli, S.; Garcia Orza, J.A.; Vecchi, R.; Dinoi, A.; Udisti, R.; Cabello, M. The impact of long-range-transport on PM1 and PM2.5 at a Central Mediterranean site. *Atmos. Environ.* **2013**, *71*, 176–186. [CrossRef]

Zagatti, E., Russo, M., Pietrogrande, M. C. (2020). On-Site Monitoring Indoor Air Quality in Schools: A Real-World Investigation to Engage High School Science Students. Journal of Chemical Education. 97(11), 4069-4072. https://doi.org/10.1021/acs.jchemed.0c00065

JOURNAL OF CHEMICAL EDUCATION

pubs.acs.org/jchemeduc

Activity

On-Site Monitoring Indoor Air Quality in Schools: A Real-World Investigation to Engage High School Science Students

Elisa Zagatti, Mara Russo, and Maria Chiara Pietrogrande*

Cite This: https://dx.doi.org/10.1021/acs.jchemed.0c00065

Read Online

ACCESS | Metrics & More | Article Recommendations | Supporting Information

ABSTRACT: This article describes the on-site monitoring of indoor air quality (IAQ) in school classrooms and laboratories. The students were personally involved in the monitoring experience, by using low-cost IAQ sensors, and then in evaluation and interpretation of the measured values. The joint school–university project, which provides lessons, equipment, and support to high school classes, is a model of how to engage students in real-world science research and learning. The obtained results pointed out two alerts: unacceptable high levels of fine particle matter ($PM_{2.5}$)—mainly entered into indoor environments from highly polluted outdoor air—and uncomfortably high CO_2 levels—due to classroom crowding and inadequate ventilation.

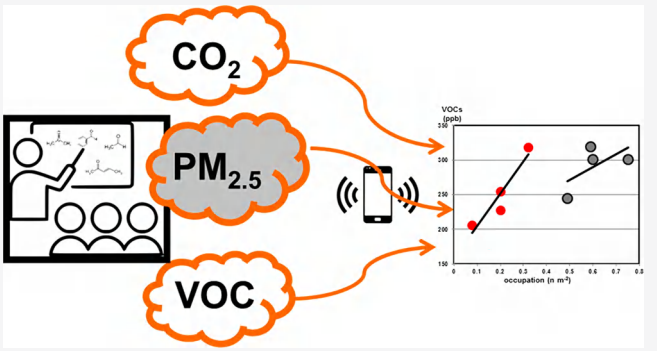

KEYWORDS: *High School/Introductory Chemistry, Environmental Chemistry, Hands-On Learning/Manipulatives, Atmospheric Chemistry, Analytical Chemistry*

INTRODUCTION

Nowadays, there is increasing concern about the impact of indoor air quality (IAQ) on human health. This may generate long-term adverse effects, as most of the air exposure occurs indoors, where people spend a large fraction of their lives.[1,2] This is particularly critical in school buildings, considering that young people spend more than 60% of their time in schools and they are very sensitive to indoor pollutants, also including a significant decrease in the efficiency of student learning processes and cognitive performances.[3−7] Accordingly, it may be useful to develop new subjects related to these topics in the curricula of different school degrees in sciences and technology, in order to raise student awareness about the quality of the environment where they learn and live.[3,6,8−11]

With this is mind, the activity presented here is focused on indoor air quality monitoring in schools, in order to provide students with direct knowledge of the quality of the air they breathe. The students were actively involved in the teaching–learning activity, since they personally used low-cost sensors, based on the modern sensor technology, that are able to collect high-density temporal and spatial data in a broader range of households.[11−15] In addition, the students were given instructions to elaborate the IAQ data measured in their own classroom/laboratory, in order to analyze their dependence on different environment conditions.[7,10,13,14]

The project was developed as part of the "Piano Lauree Scientifiche" project (Italian Educational and Research Minister, MIUR) linking university and high schools. Such a school–university collaboration may generate benefit in the teaching–learning processes and enhance student interest in the proposed subjects.[8−11] Finally, this study is a further contribution to the characterization of the indoor air quality in Italian schools.[1,3,13,16−18]

The activity was designed to work with the basic contents of chemistry, physics, math, and computing sciences learned in the first classes of Italian high schools. The project integrated lecture-based teaching on IAQ concepts with experimental hands-on activity, as a Project-Based Learning approach particularly applicable to environmental chemistry.[8−11]

The educational objectives of this activity were as follows:

- exposing student to basic information on indoor air quality, with specific concern for the parameters responsible of indoor air pollution;
- approaching on-site modern sensor technology as the basis for developing high-density networks of low-cost instruments that may provide reliable information to citizens on air quality;
- enhancing awareness on the impact of personal behavior on air pollution and promote more responsible actions.

Received: January 23, 2020
Revised: September 23, 2020

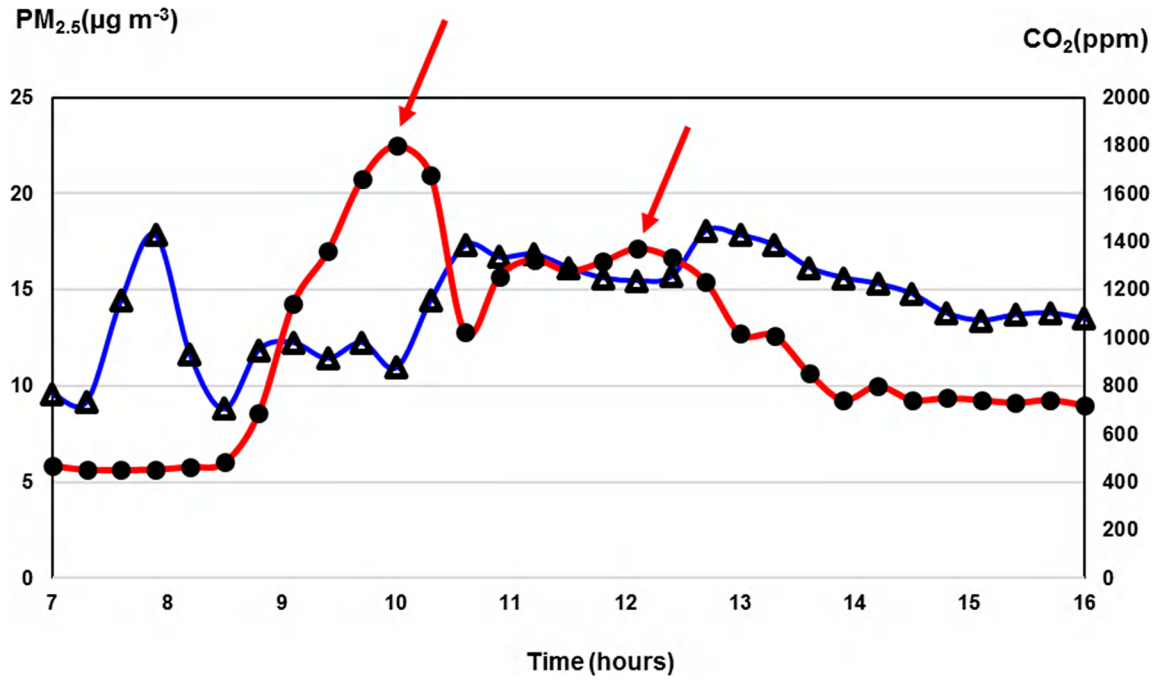

Figure 1. Temporal evolution of the monitored indoor $PM_{2.5}$ and CO_2 concentrations through the occupation hours monitored in classroom Cl3 during Feb. 14, 2019. Black points, indoor CO_2 level; empty triangles, indoor level. Red arrows indicate windows opening.

MATERIALS AND METHODS

The activity was performed during February−March 2019 in two secondary schools in the Emilia-Romagna region (Northern Italy) and involved nearly 200 students (details are reported in the Supporting Information).

The project was performed in different steps: presentation at the high school classes, monitoring of the IAQ parameters, data collection and analysis, and final presentation of the results to the students.

Phase 1: Presentation at the High School

The activity started with a presentation given by a university researcher at each participating class, introducing students to concepts of indoor air quality, covering the main indoor air pollutants, their sources, and also information about the threshold levels for alert conditions.[1,3,7,12] In addition, the monitoring sensors were described, highlighting their capability of continuous on-site monitoring of the IAQ parameters.[12−14,19]

Phase 2: Monitoring of IAQ Parameters

In each school environment the IAQ parameters were on-site measured using monitoring sensors operating 24 h continuously. The investigated parameters were temperature, relative humidity (RH%), concentration of fine particle matter ($PM_{2.5}$) and concentration of volatile organic compounds (VOCs), ubiquitous compounds with significant impact on the environment and human health, and CO_2, a surrogate for the quality of ventilation in the indoor environment.[1,4,7,13,18,19]

Measurements were performed with Foobot sensors purchased from Foobot (AirBoxLab, Luxembourg). The sensor measures 0.3−2.5 μm particles using light scattering technology and total VOCs, through a metal oxide semiconductor, from which a CO_2 equivalent concentration is estimated by an algorithm conversion.[12,19] In each school, the monitors operated in four rooms of at the same time. The devices communicated the real-time measurements via Wi-Fi to the manufacturer Web site (https://partner.foobot.io/), from which data can be downloaded using a smartphone application.

Phase 3: Data Collection and Analysis

The sensors were placed at the side of each room in a location that minimized disruption to classroom activities. For each day, two students were asked to register any classroom event, such as lesson/laboratory activity, lesson changing, and windows and doors opening/closing. Each school teacher was provided with continuous access to the remote server where IAQ raw data were saved (at 5 min intervals). At the end of each monitoring campaign, hourly data of each IAQ parameter were discharged and shared with the students for visualization and investigation.

Phase 4: Final Presentation of Results

At the end of the two sampling campaigns, the university researchers presented the whole data set to each participating class. Thus, all of the data were available to the students for comprehensive analysis and interpretation of the results. A classroom activity was performed consisting of an open discussion where the students were actively involved to comment on the measured IAQ values, with specific focus on the impact of the different environmental conditions.

RESULTS AND DISCUSSION

Classroom Activity on IAQ Parameters of Individual Classroom/Laboratory

After 2 weeks of saving data, the students gathered the IAQ values in the classroom/laboratory where they spent school time. They worked in groups of 4−6 participants with the support of school teachers to report and analyze the data. The students were given instructions to elaborate single parameters, temporal profiles, different time averages, summary tables, and correlations between parameters. Excel files were used to report the temporal evolution of the IAQ levels through the occupation hours. As an example, Figure 1 reports the variation of $PM_{2.5}$ mass and CO_2 concentrations in the most crowded classroom

https://dx.doi.org/10.1021/acs.jchemed.0c00065
J. Chem. Educ. XXXX, XXX, XXX−XXX

Cl3 (occupancy, 0.75 m^{-2}; Table S1 in the Supporting Information). It was related to any event that occurred during the lesson/laboratory and registered by the students in order to highlight its effects on room air quality. From the plot, it is clear that the indoor CO_2 (black points in the figure) and $PM_{2.5}$ values (empty triangles) largely changed throughout the occupation hours, mainly depending on windows opening (arrows in the figure). In fact, we can see that CO_2 started to increase with the lesson beginning after 8 AM to reach a maximum value at 10 AM, when the windows were opened to introduce fresh air. Then, CO_2 was nearly constant (≈13,000 ppm) until a further air exchange performed at 12 PM, before the last lesson. In contrast, the window opening generated a significant increase in the indoor $PM_{2.5}$ concentration up to 17 $\mu g\ m^{-3}$. In fact, the $PM_{2.5}$ concentration was the highest close to 8 AM, when windows were opened before lesson beginning, and at 10.30 AM and 12.30 PM, when the windows were opened again for air changing (Figure 1).

In addition, for each monitored IAQ parameter, the students computed the median daily values using only the data collected during occupation time, to be representative of their exposure time. They also related indoor (I) to outdoor (O) $PM_{2.5}$ levels by computing the indoor to outdoor I/O ratio in order to quantify the contribution of particles incoming from outside.[13,14,16,18]

Classroom Activity on the Whole Data Set of IAQ Parameters

In each participating class, a meeting was organized, where the university supervisor invited the students to present and comment on the results of the IAQ parameters measured in their classroom/laboratory. Such student presentations demonstrated that the performed activity enhanced students' knowledge on the modern sensor technology and its ability to provide reliable information on the real-world characteristics.

Then, the university researcher gave a summary of the whole set of IAQ values measured in the monitoring periods, also reporting two additional parameters, such as outdoor $PM_{2.5}$ concentrations and room occupancy, quantified as the number of students on a room surface (reported in Table S1 in the Supporting Information). On the basis of such information, the students were invited to discuss the data collected in their classroom/laboratory and compare them with the other data, with specific focus on indoor $PM_{2.5}$ and CO_2 concentrations, that were found the most critical parameters in all of the investigated environments. Examples of the problems posed to the students are the following:

- evaluate the indoor air quality in own classroom/laboratory in relation with threshold levels imposed by Italian legislation;[1]
- compare the IAQ levels in own classroom/laboratory with those of other classrooms/laboratories in the same and other schools;
- analyze the evolution of indoor $PM_{2.5}$ levels in relation with the outdoor $PM_{2.5}$ during the study days;
- evaluate the relationship of CO_2 concentration with the student occupancy in the different rooms;
- elaborate a hypothesis on the possible influence of outdoor $PM_{2.5}$ pollution, based on the indoor to outdoor ratio of $PM_{2.5}$ levels in the monitored classes.

The students actively participated in the discussion and elaborated interesting conclusions, so proving that they achieved a deep understanding of the IAQ characteristics and the parameters responsible for indoor air pollution. Given the educational context of this work, the obtained experimental results are only briefly discussed here, and more detailed information are reported in the Supporting Information.

Overall, the mean indoor $PM_{2.5}$ concentrations measured in each room were close to the WHO threshold value (25.0 $\mu g\ m^{-3}$)[1], as they ranged from 20.7 ± 9.8 $\mu g\ m^{-3}$ (Lab3) to 25.0 ± 17.0 $\mu g\ m^{-3}$ (Lab2 and Cl2) (Table S2 and Figure S1). A clear dependence was found between indoor and outdoor $PM_{2.5}$ concentrations, with significant correlation ($p < 0.05$) for most of the investigated rooms (Table S3). This suggests that indoor $PM_{2.5}$ values are mainly dominated by the contribution of outdoor $PM_{2.5}$, which may enter indoor environments by natural ventilation when windows are opened, by penetration through cracks in building envelopes, and through the operation of mechanical ventilation systems.[2,7,13,14,16,17] The computed I/O values were close to 0.8, ranging from 0.67 ± 0.17 (Lab3) to 0.86 ± 0.43 (Cl2) (Table S2). These values always below 1 indicate that the penetration through building physical barriers can remove particles, so that the particle concentration experienced by persons inside the schools is lower than outdoors. This result is very relevant from the toxicological point of view, mainly when outdoor $PM_{2.5}$ concentration is too high.[14,16−18]

Another critical IAQ parameter discussed in detail was the indoor CO_2 concentration, as it is of relevant health concern in schools.[3,4,7,13,17,20] Overall, the mean CO_2 levels measured in the study pointed out critical situations, since half of the surveyed rooms showed CO_2 levels exceeding the limit of 1,000 ppm imposed by legislation[1] (Table S2). A deep insight into the evolution of CO_2 concentration in each investigated room (example in Figure 1) clearly showed that the indoor CO_2 accumulated during the teaching time until reaching high levels, and then it decreased by opening the windows to introduce fresh air.

The measured data showed that the CO_2 concentration is significantly correlated with the student occupancy (Pearson r, 0.72; $p > 0.01$), with a general increase in more densely crowded rooms (Tables S1 and S2). This is consistent with literature that reports that the CO_2 concentration in closed spaces mainly depends on emission from the human body of occupants through breathing and correlates with human metabolic activity.[2,4,7,13] Another reason for CO_2 accumulation may be an inadequate air exchange, as the investigated school buildings were lacking mechanical ventilation systems.[13,17,20] In general, high indoor CO_2 values have been commonly encountered in previous studies in Italian schools, as a consequence of inadequate ventilation.[3,13,16−18] Under such limitations, the window opening is the only way to intake fresh air and cycle pollutants out.

Final Results

On the basis of this information, the university researcher promoted a student concluding discussion to design an operative protocol for reducing the indoor levels of pollutants. The strategies suggested by the students included a proper window opening−closing behavior as well as more breaks and recesses between classes. This conclusion was proof that the students achieved a good awareness of the indoor pollution as well as they have been stimulated toward healthier and environmentally friendly behavior.

https://dx.doi.org/10.1021/acs.jchemed.0c00065
J. Chem. Educ. XXXX, XXX, XXX−XXX

CONCLUSIONS AND IMPLICATIONS FOR PRACTICE

The main outcomes of this school activity were very appreciated and interesting for the students, namely, the availability of IAQ monitoring sensors for on-site continuous measurements, the possibility to obtain information on IAQ in the room where they live, the identification of the most effective conditions that may mitigate indoor air pollution, the participation of university researchers, and the fact that such measurements had never been made in their schools. The obtained results pointed out two health alerts in the investigated schools: unacceptably high levels of $PM_{2.5}$ particles, mainly related to polluted outdoor air, and uncomfortably high CO_2 levels, due to the classroom crowding and inadequate ventilation.

ASSOCIATED CONTENT

Supporting Information

The Supporting Information is available at https://pubs.acs.org/doi/10.1021/acs.jchemed.0c00065.

Detailed description of the activity including investigated laboratories and classrooms and sensors used for IAQ monitoring; additional information on the results obtained (PDF, DOCX)

AUTHOR INFORMATION

Corresponding Author

Maria Chiara Pietrogrande − *Department of Chemical and Pharmaceutical Sciences, University of Ferrara, I-44100 Ferrara, Italy;* orcid.org/0000-0003-1865-6959; Email: mpc@unife.it

Authors

Elisa Zagatti − *Department of Chemical and Pharmaceutical Sciences, University of Ferrara, I-44100 Ferrara, Italy*

Mara Russo − *Department of Chemical and Pharmaceutical Sciences, University of Ferrara, I-44100 Ferrara, Italy*

Complete contact information is available at: https://pubs.acs.org/10.1021/acs.jchemed.0c00065

Notes

The authors declare no competing financial interest.

ACKNOWLEDGMENTS

This was conducted as part of the "Piano Lauree Scientifiche" project, which was supported and financed by the Italian Educational and Research Minister (MIUR). We are very thankful to the teachers of Secondary Schools for making the study possible with their active participation, i.e., Liceo Scientifico Roiti (Claudio Mantovani, Maria Petresi, and Sara Tamburini) and Istituto di Istruzione Superiore Bassi -Burgatti (Paola Aleotti, Beatrice Lelli, Marzia Maccaferri, and Maria Chiara Poggioli).

REFERENCES

(1) Settimo, G.; Manigrasso, M.; Avino, P. Indoor Air Quality: A Focus on the European Legislation and State-of-the-Art Research in Italy. *Atmosphere* **2020**, *11*, 370.

(2) Abbatt, J. P. D.; Wang, C. The Atmospheric Chemistry of Indoor Environments. *Environ. Sci.: Processes Impacts* **2020**, *22*, 25−48.

(3) De Gennaro, G.; Farella, G.; Marzocca, A.; Mazzone, A.; Tutino, M. Indoor and Outdoor Monitoring of Volatile Organic Compounds in School Buildings: Indicators Based on Health Risk Assessment to Single out Critical Issues. *Int. J. Environ. Res. Public Health* **2013**, *10* (12), 6273−6291.

(4) Bluyssen, P. M. Health, comfort and performance of children in classrooms − new directions for research. *Indoor Built Environ.* **2017**, *26* (8), 1040−1050.

(5) Savelieva, K.; Marttila, T.; Lampi, J.; Ung-Lanki, S.; Elovainio, M.; Pekkanen, J. Associations between indoor environmental quality in schools and symptom reporting in pupil-administered questionnaires. *Environ. Health* **2019**, *18* (1), 115.

(6) Temprano, J. P.; Eichholtz, P.; Willeboordse, M.; Kok, N. Indoor environmental quality and learning outcomes: protocol on large-scale sensor deployment in schools. *BMJ Open* **2020**, *10* (3), No. e031233.

(7) Becerra, J. A.; Lizana, J.; Gil, M.; Barrios-Padura, A.; Blondeau, P.; Chacartegui, R. Identification of potential indoor air pollutants in schools. *J. Cleaner Prod.* **2020**, *242*, 118420.

(8) Adams, E.; Smith, G.; Ward, T. J.; Vanek, D.; Marra, N.; Jones, D.; Henthorn, M.; Striebel, J. Air Toxics under the Big Sky: A Real-World Investigation To Engage High School Science Students. *J. Chem. Educ.* **2008**, *85* (2), 221−224.

(9) Diaz-de-Mera, Y.; Notario, A.; Aranda, A.; Adame, J. A.; Parra, A.; Romero, E.; Parra, J.; Munoz, F. A Research Study of Tropospheric Ozone and Meteorological Parameters To Introduce High School Students to Scientific Procedures. *J. Chem. Educ.* **2011**, *88* (4), 392−396.

(10) Quattrucci, J. G. Problem-Based Approach to Teaching Advanced Chemistry Laboratories and Developing Students' Critical Thinking. *J. Chem. Educ.* **2018**, *95* (2), 259−266.

(11) Delaloye, N.; Blank, L.; Ware, D.; Hester, C.; Ward, T.; Holian, A.; Adams, E. Evaluating the Impact of Authentic Research on Secondary Student Self-efficacy and Future Scientific Possible Selves. *Int. J. Environ. Sci. Educ.* **2018**, *13* (9), 737−746.

(12) Chojer, H.; Branco, P. T. B. S.; Martins, F. G.; Alvim-Ferraz, M. C. M.; Sousa, S. I. V. Development of low-cost indoor air quality monitoring devices: Recent advancements. *Sci. Total Environ.* **2020**, *727*, 138385.

(13) Schibuola, L.; Tambani, C. Indoor environmental quality classification of school environments by monitoring PM and CO2 concentration levels. *Atmos. Pollut. Res.* **2020**, *11* (2), 332−342.

(14) Chen, L-W.A.; Olawepo, J. O.; Bonanno, F.; Gebreselassie, A.; Zhang, M. School children's exposure to PM2.5: a student club-based air quality monitoring campaign using low-cost sensors. *Air Qual., Atmos. Health* **2020**, *13* (5), 543−551.

(15) Schieweck, A.; Uhde, E.; Salthammer, T.; Salthammer, L. C.; Morawska, L.; Mazaheri, M.; Kumar, P. Smart homes and the control of indoor air quality. *Renewable Sustainable Energy Rev.* **2018**, *94*, 705−718.

(16) Rovelli, S.; Cattaneo, A.; Nuzzi, C. P.; Spinazzè, A.; Piazza, S.; Carrer, P.; Cavallo, D. M. Airborne particulate matter in school classrooms of northern Italy. *Int. J. Environ. Res. Public Health* **2014**, *11* (2), 1398−1421.

(17) Stabile, L.; Massimo, A.; Canale, L.; Russi, A.; Andrade, A.; Dell'Isola, M. The Effect of Ventilation Strategies on Indoor Air Quality and Energy Consumptions in Classrooms. *Buildings* **2019**, *9* (5), 110.

(18) Ruggieri, S.; Longo, V.; Perrino, C.; Canepari, S.; Drago, G.; L'Abbate, L.; Balzan, M.; Cuttitta, G.; Scaccianoce, G.; Minardi, R.; Viegi, G.; Cibella, F.; et al. Indoor air quality in schools of a highly polluted south Mediterranean area. *Indoor Air* **2019**, *29* (2), 276−290.

(19) Moreno-Rangel, A.; Sharpe, T.; Musau, F.; McGill, G. Field evaluation of a low-cost indoor air quality monitor to quantify exposure to pollutants in residential environments. *J. Sens. Sens. Syst.* **2018**, *7* (1), 373−388.

(20) Fisk, W. J. The ventilation problem in schools: literature review. *Indoor Air* **2017**, *27*, 1039−51.